The membrane attack complex drives the thrombotic microangiopathy in complement mediated atypical haemolytic uraemic syndrome

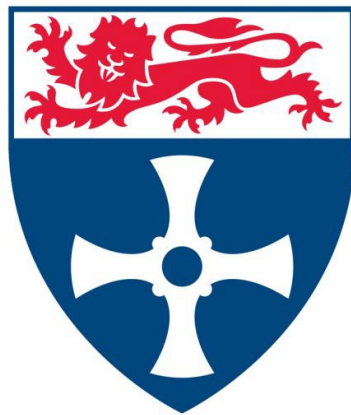Kate Smith-Jackson

Submitted for the degree of Doctor of Philosophy

Newcastle University

Faculty of Medical Sciences

November 2024

Abstract

Complement mediated atypical haemolytic uraemic syndrome (c-aHUS), is an ultra-rare but important cause of kidney disease. The discovery of the role of the alternative pathway in disease has revolutionised the clinical management of this ultra-rare kidney disease, but also sparked a complement therapeutics revolution, that has led to the introduction of new complement inhibiting agents into clinical practice.

The golden standard treatment of c-aHUS is life-long C5 inhibiting therapy, that said, our clinical practice is likely to evolve, becoming disease driven rather than continuous lifelong therapy. The seismic revolution in complement therapeutics will present to us alternative complement inhibiting agents. In tandem, with the real time advancement in complement therapeutics, we must advance our understanding of the pathogenesis of c-aHUS to see if therapy can be refined.

In this thesis, I show a novel *C3p.L1109V* variant to be associated with the development of c-aHUS through an inability of FH to regulate the protein at the C terminus. Next, we engineered a mouse model of c-aHUS around a point mutation in *C3p.D1115N* associated with c-aHUS in man from a local Newcastle family. This mouse model fully recapitulates the clinical disease and is rescued through C5 genetic deletion or therapeutic inhibition.

Backcrossing our model onto *C7* deficient and *C5aR1* deficient mice enabled us to determine the roles of the C5a-C5aR1 axis and C5b-9 (the membrane attack complex) on c-aHUS. *C7* deficiency completely abolished both clinical and histological evidence of disease. We found that removing *C5aR1* (CD88, and therefore C5a mediated signalling) significantly attenuated the risk of developing clinical disease, but 29% of mice could still develop a thrombotic microangiopathy. An oral C5aR1 antagonist when used before detectable clinical disease prevented hC5aR1.C3^{D1115N} mice from succumbing to acute disease.

Our data suggest that whilst C5aR1 inhibition can significantly attenuate disease penetrance, C5b-9 plays the dominant role in the development of the conditions required for sustenance of a TMA in the kidney. Consequently, as well as the requirement for AP dysregulation, membrane attack complex within the kidney is critical to drive disease pathology in c-aHUS.

Authors Declaration

The candidate confirms that the work submitted is her own work under the guidance of supervisors, Professor Kevin Marchbank and Professor David Kavanagh. Except for commonly held perceptions, and where specific reference is made to the work of others, the content of the thesis is original.

The work in this thesis was performed from 2016-2024 in the Immunity and inflammation laboratory, Translational and Clinical Research Institute, Newcastle University.

No part of this thesis has been submitted for the award of any other degree.

Acknowledgement

Firstly, I would like to thank my supervisors Kevin and David for their unwavering support over the last eight years. From my time as an academic clinical fellow, through the fellowship applications and then through to the fruition of this PhD. I recognise I have taken the scenic route through my clinical academic training and none of this work would have been possible without your support, guidance and mentorship. I will forever be indebted to David for his ten-year PowerPoint life plan.

The content of this thesis would not be possible without Isabel's assistance with the mice crossing, monitoring and home office licence navigating. Thank you for all your work throughout the years allowing me to work flexibly and for managing the mice during my maternity leaves.

Harriet, thank you for all your advice and lab assistance you have kindly provided over the years.

Yi, your protein expertise was invaluable and helped to elevate the understanding of the molecular mechanisms of the $C3^{D1115N}$ mouse. Your patience and assistance in teaching me chromatography was greatly appreciated.

Tom H, thank you for sharing your Biacore expertise so we could functionally analyse the *C3p.L1109V* variant.

Beth, thank you for your ubiquitous presence over the last 5 years for fruitful discussion, debriefing and general advice and navigation in completing this thesis.

To everyone else in the Complement therapeutic research group thank you for creating a fun, enjoyable and helpful working environment.

Attributed work

I would like to express my thanks to the following mentors and collaborators who helped in generating data for the thesis and for publication:

Dr Thomas Hallam (formerly of Newcastle University) for his expert guidance and assistance with the Biacore experiments in Chapter 3

Dr P Walsh for his development of the reticulocyte and platelet count assays.

Mrs Harriet Denton for her assistance in developing the FH and C5 ELISA assays

Professor T H Cook for his Histological expertise in the analysis of the $B6.C3^{D1115N}$ and $B6.C3^{D1115N}.C5^{-/-}$ mice.

Dr Yi Yang (formerly of Newcastle University) for his assistance with murine C3 purification, fluid phase assays and Biacore experiments in Chapter 4

Dedication

To Frankie & Margot

Table of contents

xi

Table of figures

Abbreviations

AC = Affinity Chromatography

AKI = Acute kidney injury

AMD = Age-related macular degeneration

AP = Alternative pathway

AWERB = Animal welfare and ethics review board

BCS = Body condition score

bME- Beta mercaptoethanol

BUN = Blood urea nitrogen

C3 = Complement component 3

C3G = C3 Glomerulopathy

c-aHUS = Complement mediated atypical HUS

CCP = Complement control protein

CFB = Complement factor B

CFH = Complement factor H

CFI = Complement factor I

CHO = Chinese Hamster Ovarian cells

ciGMVECS = conditional immortalised human glomerular endothelial cells

ConKI = Conditional knock-in

Crry = Complement receptor 1-related gene/protein Y

CV = Column volumes

DAB = 3,3'-Diaminobenzidine

DAF = Decay accelerating factor

DAPI = 4'6-diamidino-2-phenylinodole

DMEM-F12 = Dulbecco's modified eagle medium nutrient mixture F12

DMSO = Dimethyl sulfoxide

ECL = Electrochemiluminescence

EDC = N-3-dimethylaminopropyl-N-ethlcarbodimide

EDTA = Ethylenediaminetetraacetic acid

ELISA = Enzyme-linked immunoassay

EM = Electron microscopy

EMA = European medicines agency

ESKD = End stage kidney disease

FB = Factor B

FD = Factor D

FDA = Food and Drug administration

FH = Factor H

FHRP = Factor H Related proteins

FI = Factor I

FLFH = Full length Factor H

FSC = Forward scatter

GEC = Glomerular endothelial cells

GEnCs = Glomerular endothelial cells

GPI = Glycosylphosphatidylinositol anchored proteins

HBS = HEPES - Buffered saline

HDMEC-1 = Human dermal microvascular endothelial cells

HEPES = 4-(2-hydroxyethyl)-1-piperazineethanesulfonic acid

His-tag = 6-10x Histidine sequence tag

HMEC-1 = Human microvascular endothelial cell

HRP = Horseradish peroxidase

HUS = Haemolytic uraemic syndrome

IL-8 = Interleukin 8

IMAC = Immobilised metal ion affinity chromatography

IVC = Individually ventilated cages

K_D = Calculated affinity

M = Molar

MA = Methylamine

MAC = Membrane attack complex

MAHA = Microangiopathic haemolytic anaemia

MAT I/II = Methionine adenosyltransferase

MCP = Membrane cofactor protein

MCP-1 = Monocyte chemoattractant protein-1

mFH = Mouse Factor H

$MgCL_2$ = Magnesium Chloride

MSB = Martius Scarlet Blue

MWCO = Molecular weight cut off

NaCL = Sodium Chloride

NHS = N-hydroxysuccinimide

nM = Nanomolar

NRCTC = National Renal Complement Therapeutic Centre

OD = Optical density

PAS = Periodic Acid Schiff

PBS = Phosphate Buffered Saline

PBST = Phosphate buffered saline with 0.1% TWEEN®20

PCR = Polymerase chain reaction

PEG = Polyethylene Glycol

PNH = Paroxysmal nocturnal haemoglobinuria

RU = Resonance units

sC5b-9 = soluble C5b-9

SDS = Sodium dodecyl-sulfate

SDS-PAGE = Sodium dodecyl-sulfate polyacrylamide gel electrophoresis

SPR = Surface plasmon resonance

SRBC = Sheep red blood cell

SSC = Side scatter

STEC-HUS = Shiga toxin-HUS

TED = Thioester containing domain

TMA = Thrombotic microangiopathy

TMB = Tetramethylbenzidine substrate solution

TMC = Trimolecular complex

TNF-α = Tumour Necrosis Factor

vWF = von Willebrand factor

WT CHOs = Wild type Chinese Hamster ovary cells

μM = Micromolar

Chapter1   Introduction

1.1   Introduction

Haemolytic uraemic syndrome (HUS) is a clinical condition, which comprises of the triad of microangiopathic haemolytic anaemia (MAHA), thrombocytopenia and acute kidney injury (AKI) (1). The term 'Haemolytic uraemic syndrome' was first employed in 1955 describing a case series of five children who had thrombocytopenia, a coombs negative haemolytic anaemia and small vessel renal thrombi.   Following the intervening decades, the syndrome was re-classified into diarrhoeal associated HUS and non-diarrhoeal/sporadic/familial HUS. The latter being more common in adults and associated with a poorer prognosis.

In 1998, a seminal paper published the role of complement in 'non-diarrhoeal HUS' (2). Over the last two decades as our understanding of the aetiologies and pathophysiology of this condition has evolved, the nomenclature has been re-defined to accurately reflect this; shiga toxin-HUS (STEC-HUS) (diagnosed by isolation of shiga toxin producing bacteria), secondary HUS, and complement mediated atypical HUS (c-aHUS) (3). The commonest type of HUS being STEC-HUS, which is predominantly seen in the paediatric population, and follows an infection with shiga-toxin producing E.coli (4, 5). Secondary HUS is typically associated with a coexisting disease which could be; autoimmune, following transplantation, in the setting of cancer, infection or particular cytotoxic drugs (6). Common infections are streptococcus pneumonia (7) and HN1N influenza (8). In secondary HUS the infection or coexisting disease is hypothesised to be the cause rather than a trigger of disease.   c-aHUS is a disease of complement dysregulation, with a complement gene mutation identified in approximately 60% -70% of patients (9-12).   Although the terminology is based upon the molecular underpinnings of disease, many patients with an underlying complement risk factor often require a secondary trigger for c-aHUS to manifest (13).

Pathologically, the defining feature of STEC-HUS, secondary HUS, and c-aHUS is a thrombotic microangiopathy (TMA). To date the specific role of complement dysregulation and potential of complement inhibiting therapy in STEC-HUS and secondary HUS, largely remains unknown (figure 1).
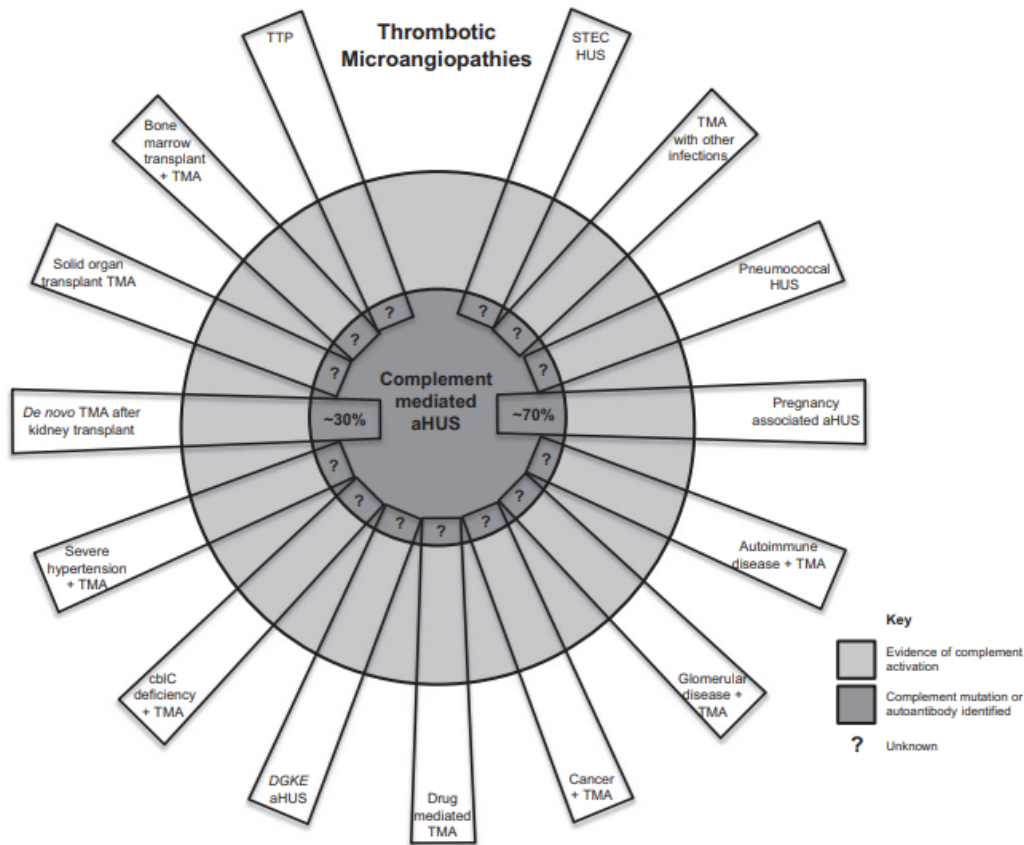
Figure 1 Classification of Thrombotic Microangiopathies.

The term 'Thrombotic microangiopathy'(TMA) defines a spectrum of diseases that all lead to endothelial injury. The role of transient complement activation in the TMAs which are not due to a pathogenic variant in complement genes (i.e. complement mediated aHUS) remains to be determined as does the role of complement inhibiting therapy. Taken from Brocklebank & Kavanagh, 2017 (14)

1.2   Thrombotic microangiopathy

This pathological feature (histological pattern of injury) is found irrespective of the aetiology and occurs due to severe endothelial cell injury (14). The term TMA is the histological appearance associated with the clinical phenotype of MAHA, thrombocytopenia and acute organ injury that reflects the underlying endothelial injury. It is possible to have a renal limited TMA, i.e. histological evidence of a TMA but no circulating MAHA or thrombocytopenia. In 'HUS' the glomerular capillary wall becomes thickened with swelling and detachment of the endothelial cell from the basement membrane, allowing accumulation of flocculent material within the sub-endothelial space (15). Platelet and fibrin rich thrombi can then accumulate in the vascular lumen leading to partial or total occlusion, although a proportion of patients with

2

endothelial injury presents with microangiopathy without thrombi (15). This disruption in the microvasculature results in, mechanical haemolysis due to the increased sheer stress and end organ ischaemia leading to infarction (16).

1.3   Current treatment strategy for Thrombotic microangiopathies

Although, TMA is a hallmark, which unifies the conditions under the historical umbrella term of 'HUS' it does not translate into a standardised treatment for all. Whilst Eculizumab (a humanised monoclonal antibody that functionally blocks C5) has revolutionised the treatment for patients with c-aHUS in native disease (17, 18) and enabling successful renal transplantation (19), its role in STEC-HUS and secondary HUS remains unproven. Following *in vitro* work showing activation of complement by shiga toxin (20), case reports and observational data regarding the potential therapeutic value of Eculizumab for STEC-HUS were also published (21, 22). However, a recent placebo controlled trial (ECULISHU from France) has found no improved renal outcomes during acute phase of the disease (no difference in duration of renal replacement therapy),but at 1 year follow up, Eculizumab treated patients had lower renal sequela (23). We await the double-blinded placebo controlled trial ECUSTEC from the UK to inform us further (4). In spite of the successful treatment revolution for c-aHUS; practically it is onerous with having to be given intravenously on a fortnightly schedule. This is then coupled with the heavy burden of immunosuppression for patients, in view of the risk of encapsulated bacterial infection due to terminal pathway inhibition. Vaccination and lifelong prophylactic antibiotics do not fully mitigate against this risk, with patients on Eculizumab therapy carrying a 550 times increased risk of meningococcal disease (18), which is pertinent given Eculizumab is currently licensed for lifelong use in patients with c-aHUS. In the UK, access to Eculizumab is granted through the National aHUS Service (Newcastle Upon Tyne, UK). The National service provides a complete diagnostic toolkit to assess potential cases of c-aHUS and offer timely treatment to reduce morbidity and mortality from c-aHUS. Evolving treatment from lifelong therapy to disease driven requires a detailed understanding of the complement system to ascertain potential sites for therapeutic intervention.

3
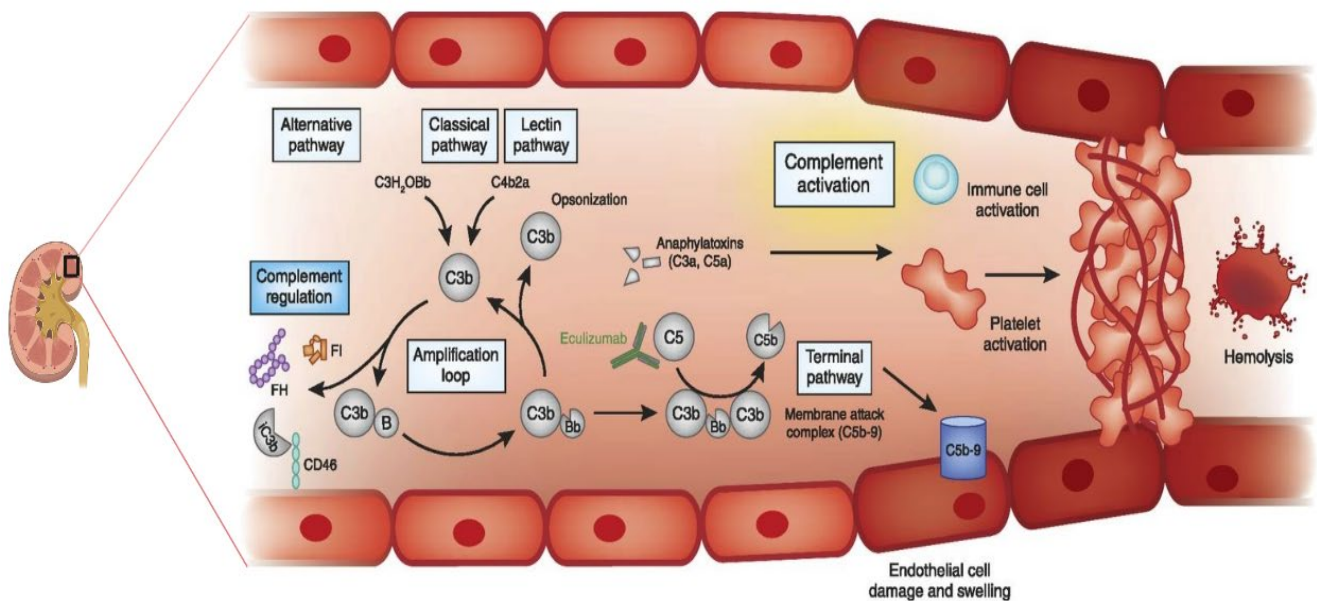
Figure 2 Thrombotic Microangiopathy.

A schematic illustrating the thrombotic microangiopathy process upon the glomerular endothelium. In the resting state, the endothelium exhibits a thromboresistant phenotype. Following complement activation the endothelium becomes activated; vWF is exocytosed to the luminal surface, with expression of P-selectin and tissue factor. Immune cells are recruited and activated as are platelets. Activated platelets in turn can provide a source of complement and an assembly platform for further alternative pathway activation. This series of events results in a pro-thrombotic environment upon the luminal surface of the endothelium, leading to platelet aggregation and fibrin deposition. As the red blood cells flow across the damaged endothelium, they can become fragmented, accounting for the mechanical haemolysis, which is evidenced as schistocytes upon a blood film. Adapted from Brocklebank et al (3)

1.4 The Complement system

The complement system was first identified in the late 19th century by microbiologist's who identified that serum had the capacity to kill microorganisms and 'complement' the role of antibodies in our immunological defence (24). Over the last century it has become clear the complement system acts as a critical innate immune responder (25) and provides essential links to our adaptive immunity (25). To date over 30 plasma proteins or membrane bound regulators/receptors have been identified that once activated via one of the three pathways; classical, lectin and alternative pathway, ignite an enzymatic cascade (26). All of which converge in the cleavage of Complement component 3 (C3). The cleavage of C3 (185 kDa) into

C3b (177 kDa) and C3a (8 kDa) is the central activating step of the complement cascade (27). C3 cleavage leads to the key complement effector functions; deposition of C3b onto the surface of microbes (opsonisation), release of pro-inflammatory anaphylactic products C3a, and initiation of the terminal pathway leading to the release of C5a (potent anaphylatoxin) and the formation of the membrane attack complex C5b-9 (capable of cell lysis) (25, 26). The cleavage of C3 into C3b, results in a conformational change of C3b revealing the highly reactive thioester domain site, which is capable of binding to hydroxyl groups of carbohydrates and amino groups of proteins (28). Surface bound C3b can then be sequentially cleaved to C3d that then enhances our B cell response through interaction with Complement receptor 2 (29). In addition to this, complement communicates with key biological systems, preventing the spread of infection through potentiating of the coagulation system, and recruitment of hematopoietic stem-progenitor cells from the bone marrow to replenish the immune system cell stocks (25). The overall purpose of the complement system is to provide host defence, maintain homeostasis and consequently health. The classical and lectin pathways are activated through binding of recognition proteins to specific targets (antigen-antibody immune complexes and mannose binding lectins and ficolins) (30, 31). The alternative pathway is initiated through an activating surface (a surface that does not have complement regulation or sufficient complement regulation to control complement), it recognizes and eliminates foreign pathogens and self-tissue that has become damaged i.e. 'altered self'(32). Mutations in the regulatory proteins and activating proteins of the alternative pathway are those found to be associated with the development of c-aHUS (33, 34).
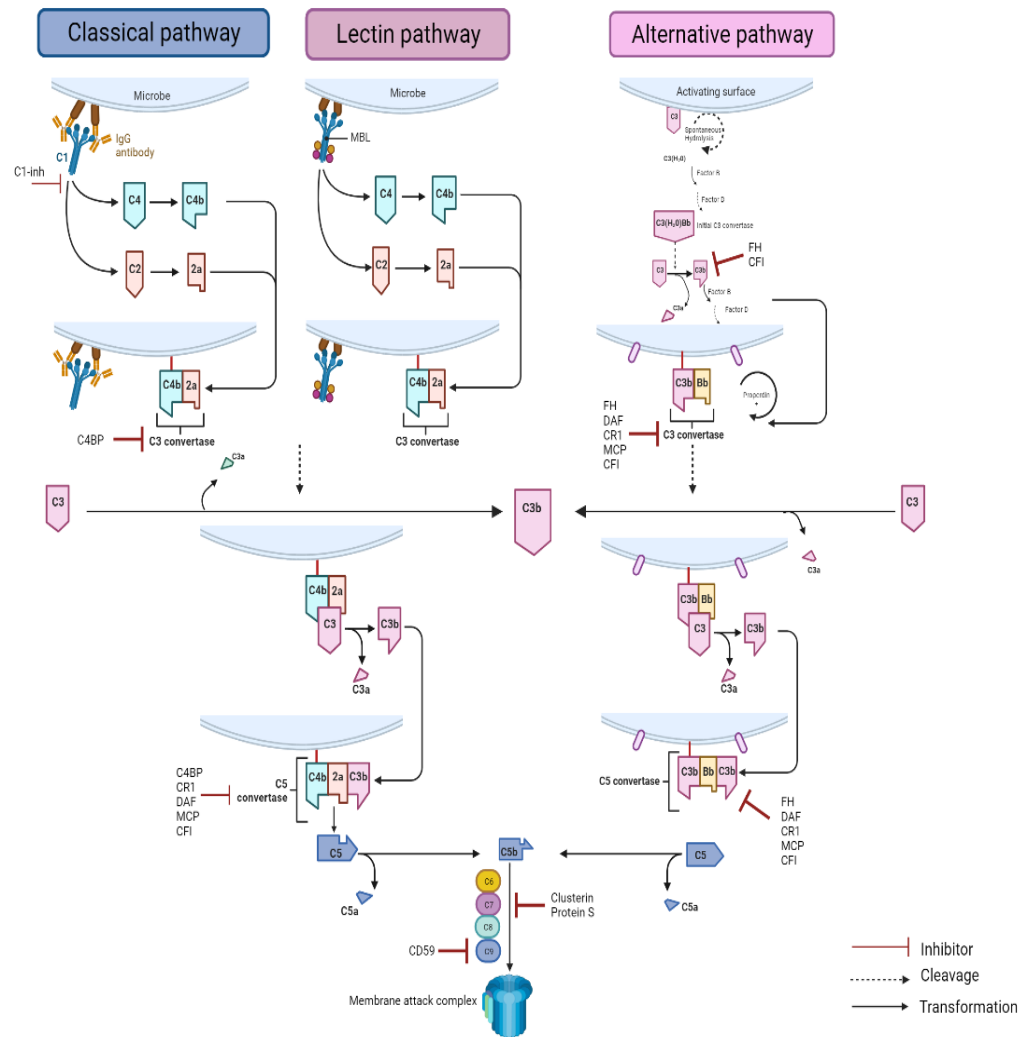
Figure 3 The Complement cascade.

The complement cascade can be activated through one of three pathways: classical, lectin and alternative. The classical pathway is activated through binding of C1q to antibody-antigen complexes. The lectin pathway is activated through mannose-binding lectin in complex with MASP. The classical and lectin pathways create a C3-convertase (C4b,2b). The alternative pathway is activated on an activating surface (one with insufficient complement regulation), C3 is spontaneously hydrolysed to $C3b(H_2O)$, this can then be cleaved by Factor B in the presence of Factor D to C3b, this C3b can then bind with Factor B following cleavage by Factor D, to the alternative pathway convertase C3bBb. All three pathways converge on C3 convertase formation. The C3 convertase can then associate with an additional C3b molecule to form the C5 convertase. The C5 convertase can then cleave C5 into C5a and C5b-9. C5b-9 then sequentially binds to C6, C7, C8 and multiple C9 molecules to form the Membrane attack complex. Red lines show inhibitors at the various steps of the cascade, dashed arrows shows where cleavage occurs and full arrows indicate a transformation step.

1.5 The Alternative pathway

In contrast to the classical and lectin pathway, the alternative pathway uniquely auto-activates, through a tick over process. At a rate of 1% per hour, native (relatively inert) C3, undergoes spontaneous hydrolysis to C3 (H_2O), which then allows binding of Factor B (FB) followed by cleavage of Factor D (FD) (35). This generates the 'initial C3 convertase' C3(H_2O)Bb, this reaction is slow and only generates a low level of convertase, but nonetheless, it cleaves C3 into C3a and C3b. This C3b can then bind to any surface within the vicinity through its exposed thioester domain or can associate with FB, followed by cleavage of FD, thus generating the 'amplification C3 convertase' (C3bBb), and the chain reaction ensues (35). In contrast to the initial reaction, the amplification reaction is rapid and exponential (36). The spontaneous tick over mechanisms enables the alternative pathway to be in a constant primed state, so upon activation from fixed C3b from the classical or lectin pathway, there is rapid amplification and elimination of pathogens. Regardless of the initial triggering pathway, the alternative pathway contributes to 80-90% of Complement component 5 (C5) complement activation (31, 37). Given the constant activation, it is therefore necessary to have constant regulation, ensuring control of complement, so homeostasis and 'health' are maintained.
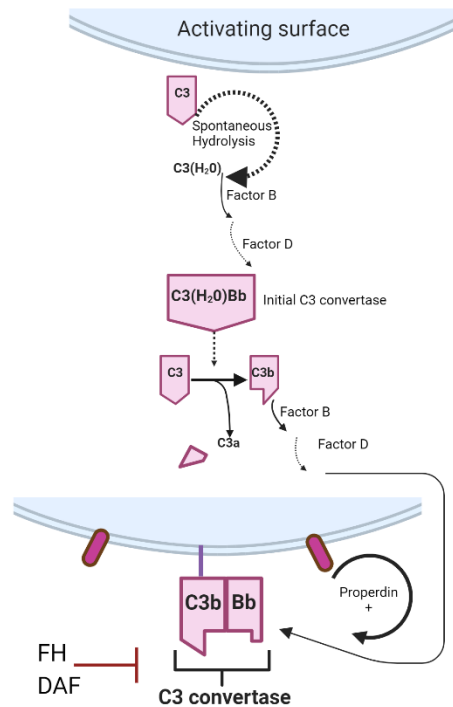
Figure 4 'Tick over' mechanism of Alternative Pathway.

C3 undergoes spontaneous hydrolysis to form C3(H$_2$0)Bb which is the 'initial convertase', this can then cleave C3 to C3b, followed by binding of Factor B and cleavage of Factor D, to form C3bBb 'alternative pathway convertase' which is then able to cleave further C3 molecules within the vicinity and go forward to form the C5 convertase, cleaving C5 and activating the terminal pathway.

.

1.6   Regulators of the Alternative pathway

Many soluble (in plasma) and membrane-associated proteins function to regulate and inactive C3 (26, 32). Together these protect healthy host cells and tissues from unwanted complement activation while unprotected surfaces rapidly become coated in C3b molecules. Collectively, the regulators inhibit the assembly of active C3, inactivate a surface deposited with C3b, and inactivate any assembled C3 convertase, thus terminating the cascade and preventing further amplification (38). Regulators can be subdivided into those found on the surface of host cells including; CR1 (CD35), Membrane cofactor protein (MCP,CD46) , Decay-accelerating factor (DAF, CD55) , CD59 and those found in the fluid phase; Factor H (FH), Factor H Related proteins (FHRP) and Factor I (FI) (26).

 FH is the most abundant regulator of the alternative pathway and regulates both in the fluid phase and on the cell surface (39). It is a single polypeptide chain glycoprotein (155kda),

comprising of 20 complement control proteins (CCP), with CCPs 1-5 important for fluid phase regulation (i.e. co-factor activity and decay-accelerating activity) and CCPs 19-20 for surface regulation (i.e. essential for cell binding)(39). FH competes with FB for C3b binding to inhibit the assembly of the alternative pathway C3 and C5 convertase, it orchestrates the disassembly of the C3 and C5 convertases by displacing bound Bb (decay accelerating activity) and acts as a cofactor for FI (serine protease) mediated cleavage and inactivation of C3b (co-factor activity)(38). FH also controls complement activation on cell surfaces; glycosaminoglycans and sialic acid increase the affinity for FH to C3b on the surface of molecules and CCPs 19-20 allow binding of FH to host cells to hinder complement activation upon the cell surface (40)
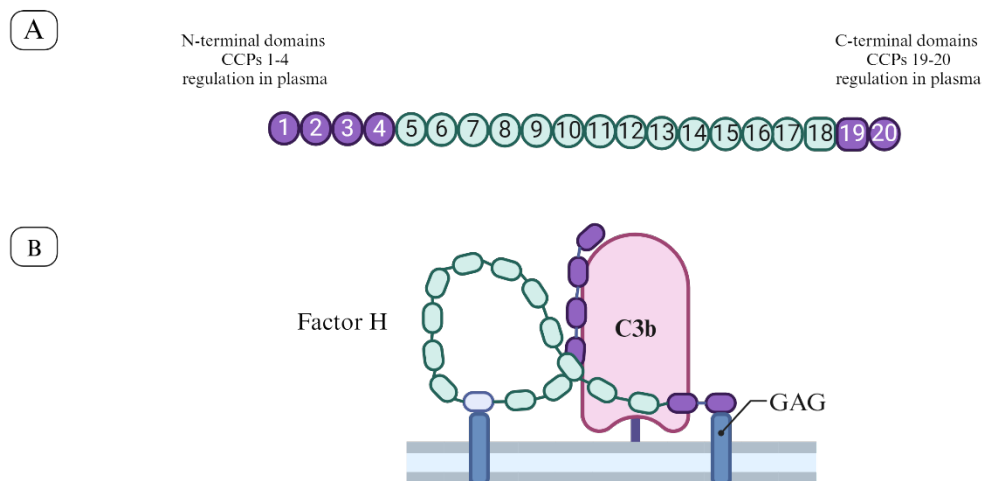
Figure 5. Factor H regulation.

Schematic showing Factor H (FH) molecule (A), illustrating the N-terminal domains, CCPs 1-4 which are critical for regulation in the fluid phase and C terminal domains CCPs 19-20 which regulates on the cell surface. (B) Illustrates its dynamic interaction with C3b, with CCP 1-5 capturing fluid phase C3b, and through CCP 19-20 cell surface regulation.

1.7 An imbalance between activation and regulation

Abnormalities in the complement system, derived by genetic or acquired means, are associated with a variety of pathologies (41). Health is maintained through a delicate balance of complement regulation; disease develops when the balance is disturbed and the threshold of regulatory ability is breached (see figure 6). Paroxysmal nocturnal haemoglobinuria (PNH) clearly shows the effect of an imbalance of complement activation and regulation. In PNH, mutations in the *PIG-A* gene leads to a lack of glycosylphosphatidylinositol (GPI)-anchored proteins (42). Consequently, the absence of the GPI- anchored complement regulatory proteins CD55 and CD59 on the surface of red blood cells leads to intravascular haemolysis due to complement mediated lysis. Before 2007, treatment options were limited to supportive therapy with red blood cell transfusions and anticoagulation or possible stem cell transplantation (42). The latter carrying high-treatment related morbidity and mortality. Phase three clinical trials showed the benefit of Eculizumab treatment in reducing haemolysis, transfusion requirements and thromboses (43-45). PNH was the first disease successfully treated with complement inhibiting therapy, proving proof of concept and paving the way for treatment of c-aHUS. The kidney and eye are particularly vulnerable to dysregulation of the alternative pathway evidenced through the prototypical complement mediated diseases aHUS/C3 Glomerulopathy (C3G) in the kidney (15) and age-related macular degeneration (AMD) in the eye (46). Genomic studies coupled with animal models over the last two decades have provided invaluable insight into the pathophysiology of these complement mediated diseases. Why the kidney and the eye appear so vulnerable to alternative pathway dysregulation remains to be fully elucidated.
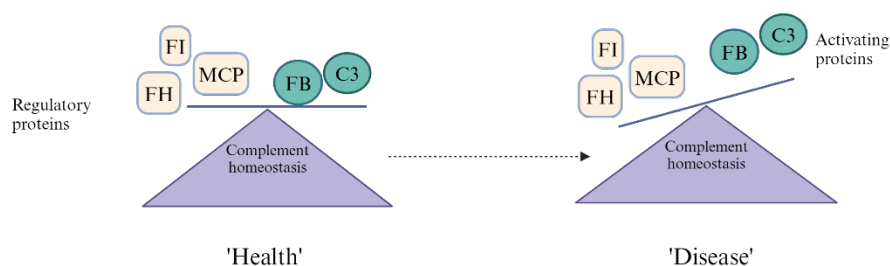
Figure 6 Complement Homeostasis.
Complement Homeostasis and health is maintained through a balance of regulation of the activating proteins. If this balance is disrupted, then the complement regulatory ability is breached, and increased complement activation ensues leading to disease.

1.8 Dysregulation at the 'Cell surface'

Dysregulation of the alternative pathway of the complement system at the cell or extracellular matrix surface is a major factor in susceptibility to c-aHUS (47). An imbalance between the activators and regulators of the alternative pathway results in complement-mediated damage to the endothelium (48, 49). Approximately 60-70% of individuals with c-aHUS have at-risk mutations in their complement genes (9-12, 18). Mutations occur either in the genes encoding complement-regulatory proteins such as *CFH*, *CFI* and *MCP* or in genes encoding complement-activating proteins *C3* and *CFB (13)*. In general, it has been observed that disease-linked mutations in regulators result in a loss of function, while disease-linked mutations in activators results in a gain of function (50, 51). It is well accepted that the genetic mutation predisposes the patient, but a trigger (such as infection or pregnancy in 39-70% of individuals) is needed in order for disease penetrance and the complement mediated TMA to clinically manifest (13).

The most frequently mutated gene in c-aHUS cohorts is *CFH,* occurring in 24-27% of sporadic cases, however, mutations are also found in *C3* at a rate of 2-8%, in *CFI* at 4-8%, in *MCP* at 5-9%, and in *FB* at <1-4% (13, 51). The nature of the genetic complement abnormality has a significant impact on the clinical phenotype. Mutations in *MCP* have the best prognosis (only 12.5% reach end stage kidney disease (ESKD)) while mutations in *CFH* have historically been associated with the worst prognosis, including earlier disease onset and higher risk of relapse (18). Interestingly, mutations in *C3* have varied outcomes with 63-75% of adult patients progressing to ESKD, some of which can take a more chronic process (18, 52, 53). This is a similar renal prognosis as seen with the *CFH* mutations (83% reached ESKD within 5 years if untreated in the UK cohort) (18) (1).

1.9 'Loss of function' mutations leading to c-aHUS

CFH mutations tend to cluster in the CCPs 19-20, but not exclusively (1). This led to an eloquent mouse model of c-aHUS by Pickering *et al*, which showed through expression of a truncated FH protein (FHΔSCR16-20), transgenic mice, which lacked the terminal four CCPs domains of the C terminus of FH, developed a phenotype akin to c-aHUS in man. This suggested the pathogenesis of c-aHUS to be complement dysregulation on the cell surface through defective FH regulation, resulting in endothelial injury, whilst preserving regulation in the fluid phase (co-factor and decay accelerating) as CCPs 1-5 remained functionally intact (54). The animals were backcrossed onto the C5 deficient mice, which rescued the phenotype

(55). More recently, a mouse model of c-aHUS was engineered through a single point mutation in *CFH* associated with c-aHUS in man (W1206R), whilst this model did exhibit a renal TMA, it also developed extra renal manifestations with macrovascular thromboses found in multiple organs, which is not commonly seen in the clinical presentation of c-aHUS (<20% of patients) (13). Nonetheless, it consolidated the earlier work in proving the impaired interaction of FH with the surface of host cells leads to complement dysregulation and disease, with the preservation of plasma complement regulating activity within the fluid phase (56). A summary of mouse models of c-aHUS engineered from complement dysregulation are detailed below (mouse models of STEC-HUS and secondary TMAs are not included). To date no 'Gain of function' mutation have been modelled *in vivo*, although occurring less frequent than *CFH*, *C3* mutations do carry a significant clinical risk of ESKD (63-75%).

Table 1Animal models of TMA engineered around complement dysregulation. Taken and adapted from Ueda et al (57)

Animal Model	Pathology	Clinical Features	Strain	Reference
FH^{-/-}.FH▲16-20	aHUS	Glomeruli microthrombi, double contours of GBM, mesangiolysis	C57BL/6-CBA	(54)
FH^{R/R} **p.*CFH.W1206R***	aHUS	TMA & Macrovascular thrombosis	C57BL/6	(56)
Anti-FH autoantibody to WT mouse	aHUS	Crescent formation tubulointerstitial inflammation acute tubular injury	C57BL/6	(58)

1.10 *C3* Gain of function mutations in c-aHUS

In 2008, Freemeaux-Bacchi et al described nine novel *C3* mutations associated with c-aHUS from two independent cohorts (France and UK) (59). Seven variants were recombinantly produced and functional studies undertaken. Five of the seven variants had decreased MCP binding and decreased cofactor activity, allowing the authors to hypothesis that these variants in heterozygosity were gain of function mutations associated with c-aHUS in patients. 3/7 of the mutants were located in the thioester containing domain (TED) of C3d.
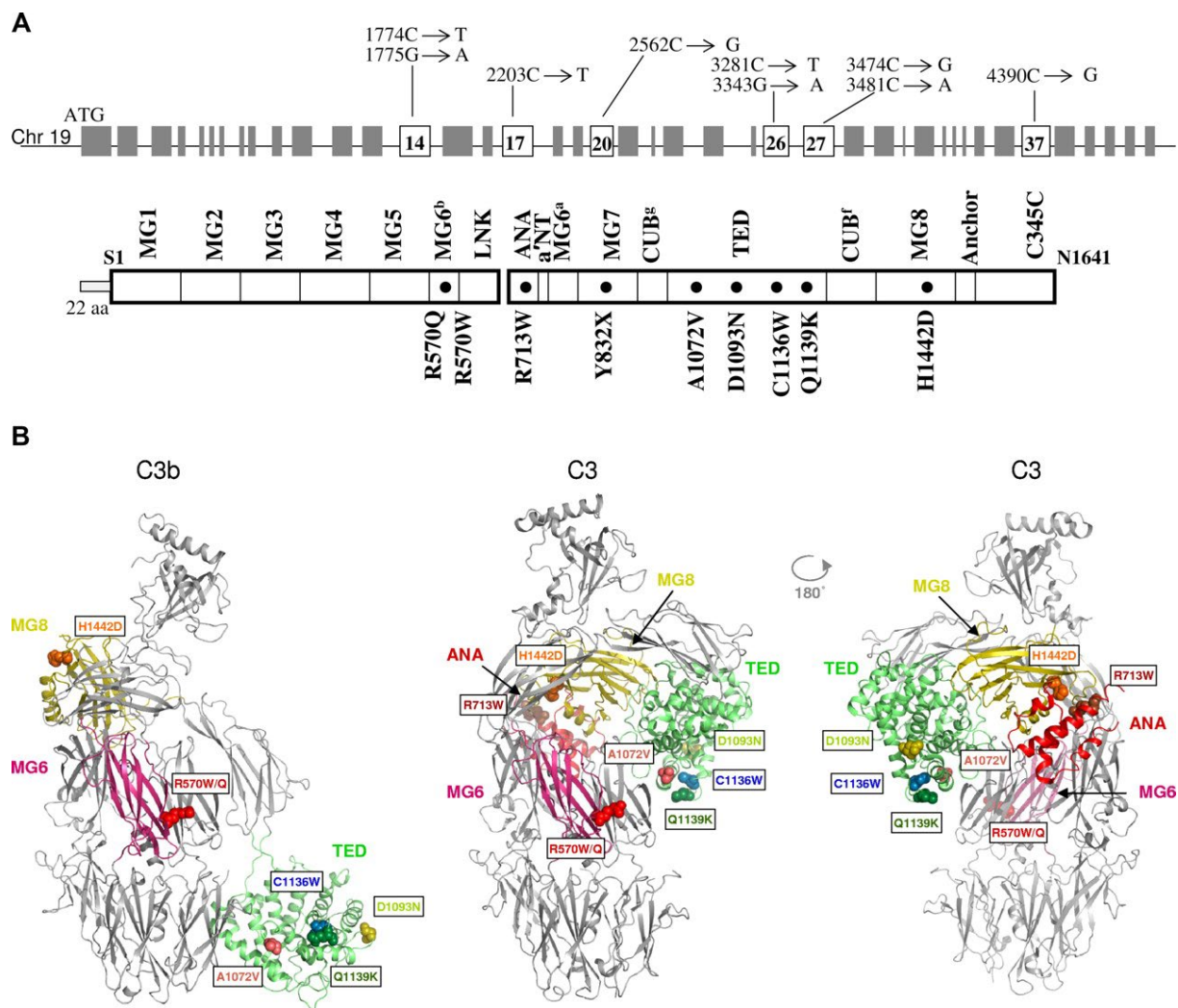
Figure 7 Location of C3 mutations associated with c-aHUS.
*A Schematic shows the gene structure of C3 and the position of the mutations. **B** Ribbon structure of C3b and C3 and the location of the C3 mutations (labelled spheres) identified in c-aHUS patients. Taken from (59).*

The mutations within the TED domain of C3d mirror the cluster of mutations in *CFH* CCPs 19-20 that are associated with c-aHUS (see figure 8). Structural crystallography of the C3d-FH CCPs 19-20 complex has shown how mutations in FH and potentially C3b may perturb the affinity of FH, voiding its functional regulation (60).
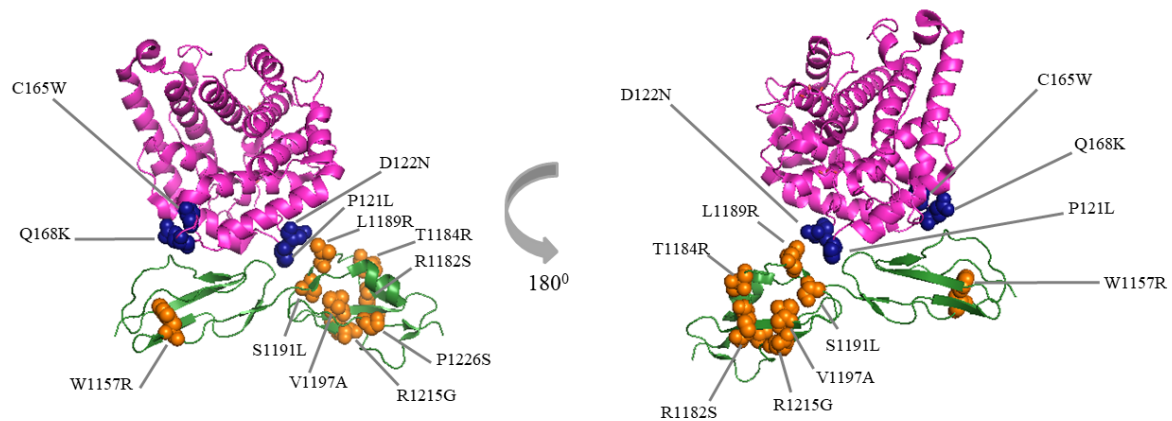
Figure 8 Pymol figure showing interaction of C3d with FH CCPs 19-20
A schematic showing C3d (pink ribbons) with FH CCPS 19-20 (green ribbon). FH associated mutations
are shown in orange spheres with C3 mutations shown in blue spheres. Figure created in Pymol with
the 3OXU structure taken from (60).

Further work by Schramm and colleagues, mapped 27 *C3* mutations associated with c-aHUS, finding they cluster around FH binding sites of FH CCPs 1-4 or FH CCPs 19-20 on C3b (61). 23 recombinant mutants were produced, and using surface plasmon resonance (SPR), showed that 17 mutants displayed reduced binding to one or more of the complement regulators (FH, MCP) compared to wild type C3(61). This *in vitro* study of recombinant mutants further substantiated the functional consequences of *C3* mutations associated with c-aHUS.

FB gain of function mutations offer a complementary view on the pathophysiology of c-aHUS. *FB* variants are much rarer (<1-4% of variants from c-aHUS cohorts) than *C3* associated variants. Nonetheless, *in vitro* work with recombinant produced *FB* mutants shows increased alternative pathway activation and enhancing C3b generation, i.e. dysregulated alternative pathway complement activation (62). The generation of C3b is enhanced through increases in the activity of C3bB proenzyme and an increase in its ability to resist functional decay and disassembly by DAF and FH. Thus, in addition to cell surface dysregulation of FH CCPs 19-20 at the C3d interface, *FB* gain of function mutations are associated with c-aHUS through their augmentation in activity of the alternative pathway C3 convertase (62).

1.11 C5 functional blockade is not a paneaca

The *in vivo* modelling of the truncated FH protein and complement dysregulation coupled with the successful use of C5 functional blockade in patients with c-aHUS has led to the current

understanding of disease pathogenesis and the clinical rational of C5 inhibiting treatment (FDA and EMA approved since 2011).

Whilst C5 functional blockade with Eculizumab and, latterly, Ravulizumab has revolutionised the treatment of a c-aHUS (17, 63), its role in C3G and non-complement mediated TMAs is yet to be proven. Nonetheless, its use is extending beyond c-aHUS and PNH with approval now for myasthenia gravis and neuromyelitis optica (64-66).

The use of Eculizumab has undoubtedly revolutionised the lives of patients, however, this is not without risks. There is an increased risk of meningococcal infection, additionally, in those patients who have a renal transplant, whom are already receiving standard immunosuppression, this coupled with the complete complement terminal pathway blockade provided by Eculizumab increases the burden of immunosuppression and enhances their vulnerability to infection. Finally, the sheer cost of Eculizumab (£328,000 per patient per annum in the UK) in a world where health economics is increasingly important prevents access for many. Eculizumab withdrawal strategies are now being trialled to identify if we can safely withdraw during remission, monitor and initiate prompt rescue therapy for a clinical relapse.

The risk of relapse following Eculizumab withdrawal is thought to rely upon the underlying genetic mutation, severity at presentation and a previous history of relapse causing organ failure (i.e. loss of transplant). A series of prospective trials were undertaken to assess if Eculizumab can be safely withdrawn. The first to report was STOPECU study, this study consisted of 55 patients all of whom had Eculizumab withdrawn (mean treatment duration was 16.5 months), 13/55 patients relapsed. Moreover, of those, 2 had a deterioration in their pre-existing chronic kidney disease and a further patient progressed to ESKD despite restarting Eculizumab. The risk of relapse in carriers of complement gene variants was ̃50% compared to <5% in those patients with no rare variant detected. Thus, the authors concluded it is both safe and feasible to withdraw Eculizumab, based upon the patients complement genetics and shared decision-making. Interestingly, being female (but, not pregnant) increased risk of relapse as did elevated levels of circulating sC5b-9 (67). Next, CUREiHUS reported the safe withdrawal from 18 patients, with 4 patients having a relapse. No clinical deterioration in renal function was observed following prompt reintroduction of Eculizumab in this study. CUREiHUS therefore confirms the STOPECU findings that Eculizumab withdrawal was safe after 3 months of therapy in native kidneys (68). The authors also provided a cost benefit analysis for Eculizumab withdrawal. We await the outcome of the SETS-AHUS trial (National aHUS service, UK) to

inform us further, on how we safely make that clinical transition from lifelong complement inhibiting therapy to an intermittent disease driven therapy (69).

One limitation faced by clinicians is the absence of a biomarker to accurately identify those individuals with a complement mediated TMA from secondary TMAs (genetic analysis is not possible within the immediate days of clinical presentation), and to enable prompt diagnosis, therapeutic monitoring and to assist in therapy withdrawal. Variability of complement profiles exists among c-aHUS patients, both in the active disease state and those who are clinically in remission with or without C5 inhibiting therapy (70),(71),(72). Volokhina *et al* (70) showed normal C3, C5a and soluble C5b-9 (sC5b-9) in patients in remission from c-aHUS, Noris *et al* *(73)* showed elevated sC5b-9 levels irrespective of disease activity, finally, Wehling *et al* (72)showed reduced C3d and a reduction in sC5b-9 in a proportion of aHUS patients on Eculizumab therapy. Interestingly, it took 6 months of therapy for C5a levels to return to normal ranges (remained normal or elevated compared to healthy donor controls and did not correlate with inhibition of CH50 and AH50), suggesting that Eculizumab may not silence the C5a axis as originally thought. The authors postulated alternative cleaving events through interaction with the coagulation system. There are confounders within these individual study groups that could explain the differing results in addition to the variability of assays and challenges with the vulnerability of complement to freeze thaw when collecting and analysing. In Volokhina *et al* (70) 9/11 patients in remission had ESKD, and within the acute phase of disease only 1/6 patients received Eculizumab with the others having had plasma exchange. In Noris *et al*,(73) only 4/14 in the acute aHUS group had a complement variant detected. Despite no robust biomarker signature to discriminate between acute disease or remission, it was shown from the Noris group that serum-induced endothelial C5b-9 deposits normalised after Eculizumab treatment in 8/14 patients. Serum from patients with active c-aHUS resulted in an increased amount of C5b-9 deposition on both resting and activated endothelial cells, which normalised after Eculizumab treatment. Interestingly, patients in clinical remission and carriers with a pathogenic variant had serum induced increased C5b-9 deposition on activated endothelium (but not resting). Postulating, that the assay may aid in the diagnostic process before the availability of genetic screening results. This has led the group to develop the *ex vivo* assay using human dermal microvascular endothelial cells (HDMEC-1), aiming to monitor disease activity, to individualise treatment and potentially predict relapse (73). Unfortunately, a recent study using this assay in kidney transplant has questioned its clinical utility, with 3 c-aHUS patients and 4 controls showing elevated C5b-9 deposits on resting cells, but no clinical

characteristics of a TMA. Thus, the authors advised caution in adopting this assay within the clinical setting of monitoring disease following kidney transplantation due to its heterogeneous results and by extension its low specificity (74).

In addition to the variability of results using the *ex vivo* complement assay, the individual roles of C5a and C5b-9 upon endothelial activation remains unknown. Recently, the same group used the human microvascular endothelial cell (HMEC-1) line to investigate the effects of c-aHUS patient serum on cell phenotype. After demonstrating increased platelet aggregation on HMEC-1 exposed to patient serum, they demonstrated that adding C5a to normal human serum was sufficient to recapitulate the prothrombotic effects of c-aHUS serum. Again, using the HMEC-1 model, therapeutic inhibition of C5aR1 (using CCX168 or Avacopan) reduced platelet aggregates to background level whilst use of a goat anti-C7 polyclonal antibody, previously confirmed to prevent C5b-9 formation on HMEC-1 in this context (71), was only partially effective in restricting platelet aggregation on the HMEC-1 (75).

Recently, Stevens *et al* (76)have attempted to develop an assay to model complement activation *ex vivo* using conditionally immortalised human glomerular endothelial cells (ciGMVECS), given the specific vulnerability of the glomerular endothelium to complement dysregulation, it was proposed this cell line may more accurately mimic *in vivo* conditions. The authors concluded the assay could measure complement C5b-9 deposition, with serum from patients with acute c-aHUS showing an increase in C5b-9 deposition when compared to normal human serum controls, furthermore, the increased C5b-9 deposition could be dose-dependently inhibited following the addition of Eculizumab(76). The effect of unaffected carriers and patients in clinical remission remains to be tested within this assay and it does not evaluate the possible causative role of C5a in disease either as highlighted by the HMEC-1 study detailed above.

Despite the lack of a biomarker or complement assay, discriminating clearly between acute disease and clinical remission, it is clear that terminal pathway activation is critical to the development of c-aHUS, evidenced through the pre-clinical models, successful C5 inhibitor clinical trials and latterly with relapse off C5 inhibiting therapy in the withdrawal trials.

What we do not yet know is the independent roles of C5a and the membrane attack complex (MAC) complex in driving the disease. Understanding this, will enable us to potentially

rationalise the application of emerging complement therapeutics (such as the C5aR antagonist), providing a targeted therapy for patients (77).

1.12 The terminal pathway

Regardless of the initial activating step of complement, the classical, lectin and alternative pathway unite with the C3 convertase that directly leads to activation of the terminal pathway, initiating the effector phase of complement activation. The C5 convertase (either the classical/lectin C4b2a3b or alternative pathway C3bBb3b) cleaves C5, releasing the potent anaphylatoxin C5a and C5b. C5b can then sequentially bind to C6, followed by C7, C8, then multiple C9 molecules to form C5b-9, otherwise known as 'MAC'(78). The detection of C5a and C5b-9 in plasma from patients with various diseases may represent spill over and the breakthrough of the inflammatory response from localized tissue (79). Eculizumab prevents the cleavage of C5, therefore preventing the release of C5a and C5b-9. Avacopan is an orally administered small molecule that selectively blocks the effects of C5a through the C5aR1 and has been proven to be effective in a phase 3 trial in patients with ANCA-associated vasculitis (80). There was no reported cases of N.meningitidis infection given it does not block C5b but abnormal liver function test occurred in 5.4% of patients (80). As well as the oral C5aR1 antagonists being introduced into clinical practice, C7 inhibitors are being developed (81) and tested in pre-clinical models (82). The advantages of targeting C7 as compared to targeting C5 is that C7 is not an acute phase protein, potentially meaning that lower doses of an anti-C7 agent would be required for functional blockade and of course targeting C7 leaves the C5a axis functionally intact. Given these novel agents and their potential benefits to patients with c-aHUS compared to C5 inhibiting therapy, there is a need to ascertain the roles of C5a and C5b-9 upon disease pathogenesis; to determine if there is a clinical rationale to justify a change from gold standard treatment.
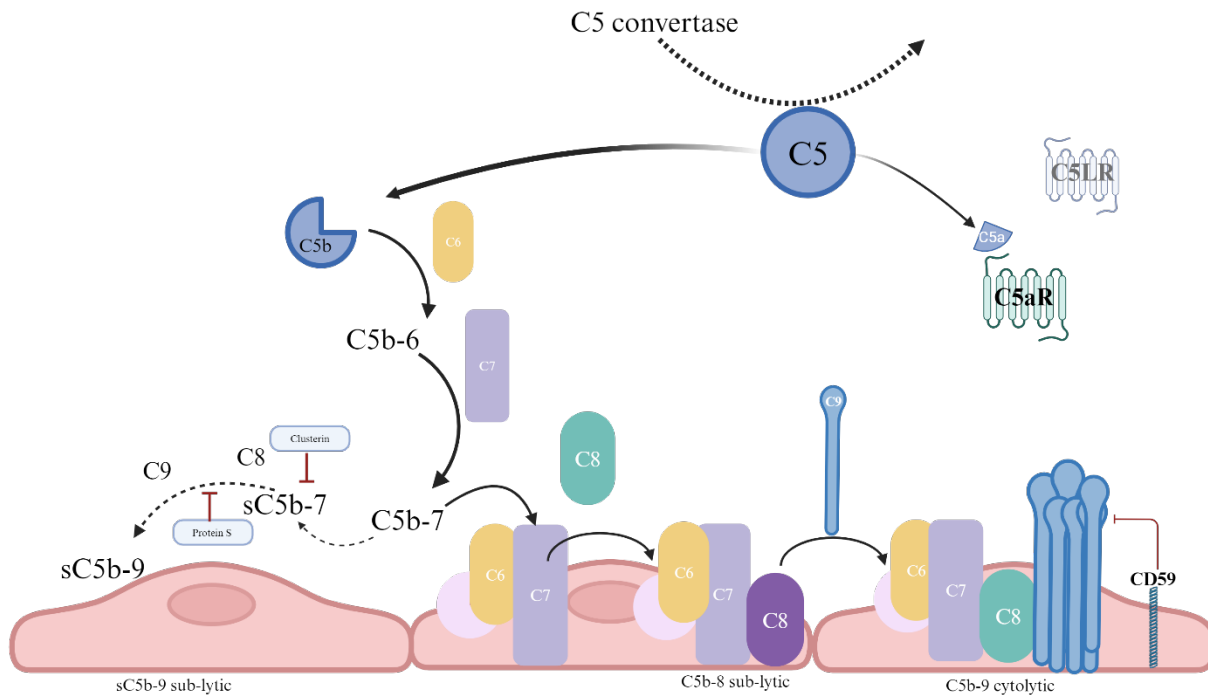
Figure 9 Terminal pathway activation.

The C5 convertase cleaves C5, releasing the potent anaphylatoxin C5a and C5b-9. C5b-9 then sequentially binds to C6 and C7. C5b-7 forms a stable trimeric complex which exposes the lipid binding to enable the complex to bind to the cell membrane. C8 then binds followed by multiple C9 molecules to form C5b-9, or the membrane attack complex which can lyse cells directly. C5b-9 can also induce sub-lytic effects. The regulators of the terminal pathway are CD59, Clusterin and protein S. The former prevents MAC insertion through binding C5b-8, whilst the latter two prevent C5b-7 from binding to the cell membrane, thus preventing the formation of MAC.

1.13 C5a and its thrombotic effects

C5a is a potent anaphylatoxin, which possesses chemoattractive, inflammatory and immune-modulatory functions through binding of C5aR1 and C5L2 (83). C5aR is expressed on numerous cell types, including, neutrophils, macrophages, and endothelial cells (83). C5a mediated signaling leads to a series of events which aims to produce a localized and proportionate acute inflammatory response that includes vasodilatation, increased blood flow, smooth muscle contraction and oedema (79, 83). C5a primes neutrophils to achieve an enhanced phagocytic response, enhancing the functional ability of neutrophils to kill bacteria and resist apoptosis (84-86). Similarly, in the presence of C5a, macrophages have a potentiated response (79). Upon the endothelium, C5a induces expression of C5aR1 (87). Under

inflammatory conditions endothelial cells become activated, which in turn facilitates neutrophil adhesion through upregulation of leukocyte adhesion molecules such as p-selectin (88-90), these adherent neutrophils then subsequently become activated, thus propagating the ongoing inflammatory milieu. Following C5a stimulation there is increased production of IL-6 and IL-8 and the generation of tissue factor, which pro-thrombotic action leads to intravascular coagulation (79, 91, 92). Finally, whilst C5a may not directly affect platelets, it can influence platelet activation through its activation of leukocytes (93).

1.14 C5b-9 and its thrombotic effects

C5b is released from C5 following cleavage by the C5 convertase, this then binds with C6 to become C5b-6. The binding of C7, results in the stable trimeric C5b-7, this complex is then able to bind to the cell membrane through its exposure of the lipid binding site (94, 95). C8 then binds to C5b-7 resulting in the tetrameric complex, C5b-8, this then enables binding and polymerization of C9, resulting in C5b-9 (94, 95). C5b-9 creates a pore to enable an influx of water via osmosis, until the cell 'bursts' and is thus lysed (96). Protein S binds to C5b-7 and prevents the polymerization of C9, similarly, clusterin prevents the insertion of C5b-7 into the cell membrane, both of which are present in the fluid phase (94). CD59 on the cell surface prevents the polymerization of C9 (97, 98). The effects of C5b-9 are not limited to its lytic ability; its sub-lytic ability upon endothelial cells is well established (98, 99). The presence of MAC leads to the expression of p-selectin upon the luminal side of the endothelium and enhances the tumour necrosis factor alpha (TNF-α) induced expression of leukocyte adhesion molecules (100, 101). The release of monocyte chemoattractant protein-1 (MCP-1), interleukin-8 (IL-8) and platelet activation factor, collectively orchestrate the pro-inflammatory effects of MAC upon the endothelial cells (102-104). MAC also triggers the coagulation process through stimulation of endothelial cell expression of tissue factor (105). Finally, MAC induces structural changes to the endothelium creating interendothelial gaps and modifying vascular tone through the release of vasodilators and vasoconstrictors (103, 106, 107). In addition to its effects upon the endothelial cell, MAC is able to induce the formation of phosphatidylserine exposing micro vesicles, which leads to the formation of the prothrombinase complex (108). Furthermore, platelets, p-selectin and secreted von Willebrand factor (vWF) can serve as a scaffold for the assembly of alternative pathway components, propagating complement activation (99, 108, 109).

Figure 10 Terminal pathway activation in TMA.

A summary of the individual and shared functional effects of C5a and C5b-9 and how these may contribute to a thrombotic microangiopathy upon the glomerular endothelium.

1.15 Dissecting the role of the terminal pathway in complement mediated aHUS

We know c-aHUS is caused by alternative pathway dysregulation that initiates terminal pathway activation, with C5 inhibition being the gold standing of treatment. What remains to be elucidated are the specific roles of C5a and C5b-9, and how they lead to the development of a glomerular thrombotic microangiopathy.

Collectively, or individually, C5a and C5b-9 possess the ability to activate and transform the glomerular endothelium from a resting state of thromboresistance to pro-thrombotic phenotype. Determining a greater understanding of their roles may enable a refined treatment approach to the current standard of overt terminal pathway blockade. C5aR1 oral inhibitors have progressed through clinical trials with limited adverse effects and C7 inhibitors are being trialed in pre-clinical models. As our treatment strategy will likely evolve to a disease driven rather than continuous therapy, in tandem, so may our choice of complement inhibiting agent.

1.16 Research Aims

To date, our understanding of the pathogenesis of c-aHUS has evolved from *in-vitro* assays using recombinant proteins coupled with pre-clinical models based upon changes within *CFH*. I seek to investigate the role of a gain of function change in *C3*. I aim to determine the significance of an unknown *C3* variant identified within our patient cohort at the National Renal Complement Therapeutics Centre (NRCTC), model a *C3* change in mouse to determine the effects of a hyperfunctional C3 *in vivo*, and finally, dissect the role of C5a and C5b-9 through genetic deletion. With the overall aim of contributing to and advancing, the scientific field of c-aHUS.

1.17 Hypotheses

- C3 L1109V leads to c-aHUS due to lack of regulation by FH at the cell surface due to the mutations location in the thioester domain of C3d.

- The C3 D1115N point mutation from man can be transferred to mouse and recapitulate the clinical disease akin to man i.e. c-aHUS.

- C5aR1 genetic deletion or oral administration of a C5aR1 antagonist will not prevent a renal TMA in the $C3^{D1115N}$ mouse model of c-aHUS.

- $C7^{-/-}$ will rescue the B6-$C3^{D1115N}$ and prevent the development of a complement mediated TMA.

Chapter2   Methodology

2.1   Methods

2.1.1   Protein purification

2.1.2   Principles of Ion exchange chromatography

Ion exchange chromatography separates proteins based upon their net charge at a particular pH. The protein charge is determined by the number and type of functional groups and the amino acid composition. Anion exchange columns bind negatively charged proteins whilst cation exchange columns bind positively charged proteins. First, the isoelectric point (pI) is needed to know the pH at which the protein carries no net charge (i.e. the overall number of –ve and +ve charge equates to zero). This can be calculated here https://web.expasy.org/protparam using the amino acid sequence of the protein (which can be found here, https://www.uniprot.org). Therefore, in buffered solution, the protein is negatively charged if the pH >pI, and positively charged if pH <pI. Once the protein has bound to the ion exchanger, it can then be eluted, by changing the ionic strength using a linear salt gradient, with the bound proteins being displaced by the chloride or sodium ion.

Table 2 Buffers required for ion exchange chromatography for Human and mouse C3

Protein	pI	Anion exchange buffer	Cation exchange buffer
Human C3	6.02	**Buffer A**: 10mM Potassium phosphate (KH_2PO_4), 5mM EDTA, pH 7.8 in dH_20.	**Buffer A**: 50mM Sodium phosphate (NaH_2P0_4), 5mM EDTA, pH 6 in dH20
		Buffer B: 10mM Potassium phosphate (KH_2PO_4), 5mM EDTA, 1 M sodium chloride (NaCl) pH 7.8 in dH_20.	**Buffer B**: 50 mM Sodium phosphate (NaH_2P0_4), 5mM EDTA, 1 M NaCl, pH 6 in dH_20.
Mouse C3	6.29	**Buffer A**: 20mM Tris base, 5mM EDTA pH7.5	**Buffer A**: 20mM Tris base, 5mM EDTA, 70mM NaCl, pH5.5
		Buffer B:500mM NaCl, 20mM Tris base, 5mM EDTA, pH7.5	**Buffer B**: 20mM Tris base, 5mM EDTA, 700mM NaCl, pH5.5

2.1.3   Human C3 protein purification

2.1.3.1   Plasma preparation and protein precipitation of Human C3^{WT} and C3 ^{L1109V}

The method for C3 purification was adapted from 'Purification and characterisation of human and mouse complement C3' Ruseva & Heurich 2014 (110). In brief, Na_2SO_4 removes high-molecular weight compounds, then the anion exchange isolates C3, the cation exchange removes hydrolysed C3, finally, the gel filtration process removes C3 aggregates. The patient carrying the C3^{L1109V} variant was consented in clinic and blood withdrawn. Alternatively, a healthy volunteer donated blood following the protocol and ethics of the 'Understanding mechanisms of immune mediated disease study' (Newcastle University). 9mls of blood was collected from both donors into Ethylenediaminetetraacetic acid (EDTA) coated tubes, placed on ice then immediately centrifuged at 2,000xg for 15 mins at 4°C. The plasma supernatant was then carefully removed from the cell pellet. To the plasma, 10% (w/v) Na_2SO_4 was slowly added whilst the solution was undergoing continuous stirring. This solution was stirred at 4°C for 2hrs, and then centrifuged at 26,892xg for 30 mins (Sorval Ultacentrifuge). The supernatant was transferred to 23.8mm dialysis Tubing (Medicall membranes Ltd, UK) and dialysed overnight at 4°C into Anion exchange Buffer A (10mM KH_2PO_4, 5mM EDTA, pH 7.8 in dH_2O). The dialysate underwent a final centrifuge 2,602xg for 15mins at 4°C (to remove any precipitate). The supernatant was then filtered through a 0.45μM filter (Whatman™, Cytiva).

2.1.3.2   Anion and cation exchange and gel filtration

The filtered solution from 2.1.3.1 was then applied to a 1ml HiTrap™ Q HP column (GE Healthcare, UK) using an AKTA START™ (GE Healthcare, UK). A salt gradient (Anion exchange Buffer B) was applied to elute the proteins bound into 1ml fractions (using the automated fraction collector). The elution was tracked via the integral ultraviolet probe and optical density at 280 nM plotted. A small aliquot of the peak OD 280nm fractions were run via SDS PAGE to confirm uniformity (see below). Selected fractions were then pooled and dialysed into Cation exchange Buffer A (50mM NaH_2PO_4 pH 6.0) for 2 hours at 4°C. This solution was then applied to a 1ml HiTrap™ SP HP column (GE Healthcare, UK). This was eluted and again, the peak fractions were confirmed on using SDS PAGE. Selected fractions were pooled, and then finally underwent gel filtration chromatography using a HiLoad® 16/600 Superdex® 200pg column (GE Healthcare, UK) using an AKTA Purifier which simultaneously buffer exchanged the C3 fractions into Phosphate Buffered Saline pH 7.0 (PBS).

2.1.4   SDS-PAGE and Western Blotting

Running samples via sodium dodecyl sulphate -polyacrylamide gel electrophoresis (SDS-PAGE) enables proteins to be separated by their mass and conformation. The gel acts as a size-selective sieve during separation, the gel structure allows smaller proteins to travel more quickly than larger ones. C3 has a molecular weight of 185 kDa, which contains two disulphide linked chains, thus under reducing conditions, reveals a 110kDa C3b α-chain and a 75kDa C3b β chain. Generally, samples were diluted in PBS (1:10, 20µl volume) followed by the addition of 2µl of 10x reducing buffer (containing 5% beta-2-mercaptoethanol (bME)). The resulting 22µl volume was then boiled for 95^0C for 5 mins then loaded into individual lanes of a Novex WedgeWell™ 10-20% Tris-Glycine gel alongside 5µl a PageRuler™ Plus pre-stained protein ladder. Electrophoresis was then performed in an XCELL SureLock™ Electrophoresis Cell, filled with 500ml of SDS running buffer (see section Table 13 Buffers) and run for˜45 minutes at 200V.

For Coomassie staining, gels were extracted from the XCELL Surelock™ cell, washed in dH_20, then incubated at room temperature for 1 hour in 1% Coomassie Brilliant Blue™ R-250 on a rocker. Gels were then rinsed in 1x PBS with 0.1% TWEEN®20 (PBST) and placed in de-stain solution (10% acetic acid, 50% methanol, 40% dH_20) for 1 hour at room temperature on a rocker. Gels were then imaged using an HP Scanjet™ G0450 scanner (Hewlett Packard, Palo Alto, CA, USA).

For Western blotting, SDS-PAGE gels were then assembled in a standard cassette to allow proteins to be transferred onto a Protran™ Nitrocellulose Western blotting membrane. The system was run at 100V for 1.5 hours with cool water running through the cell to dissipate heat. The membrane was then removed and placed in PBST. This was replaced with 5% whole milk-PBST and incubated for 1 hour at room temperature to block the membrane. The membrane was then incubated with 1:10,000 goat anti- C3 horseradish peroxidase (HRP) in 5% whole milk-PBST for 1 hour. The membrane then underwent 3x 10mins washing with PBST. Finally, the nitrocellulose was 'developed' using the Pierce™ electrochemiluminescence (ECL) Western Blotting Substrate Kit as per manufacturer instructions (ThermoScientific, UK), followed by imaging on the LI-COR Fc imaging system (LI-COR Biosciences, Lincoln, Nebraska, USA).

Protein concentration was calculated using a NanoDrop One[C] (ThermoScientific, UK) using an extinction coefficient of 178430 and a molecular weight of 187.148. The purified C3 was aliquoted and stored at -80°C for future use.

2.1.5 Mouse C3 purification

2.1.5.1 Plasma preparation and protein precipitation from B6-C3[WT] and B6-C3[D1115N] mice

Mouse C3 for biochemical analysis was purified from mouse plasma (either B6-C3[WT] or B6-C3[D1115N]) adapted from (110) and (111). Mouse plasma was collected into Eppendorf's containing 10mM EDTA following terminal cardiac puncture and centrifuged at 12,470xg for 15 mins at 4^0C. The supernatant was collected, and to this, 50% (w/v) Polyethylene Glycol 4000 (PEG 4000) (dissolved in PBS, 5mM EDTA) was added to achieve a 4% PEG cut. The PEG cut is used as a method of fractional precipitation, so that proteins can be separated by their solubility, with an increase in PEG concentration, decreasing the proteins solubility (112). The PEG solution was continuously stirred for 1h at 4^0C then transferred to a sterile centrifuge rube and centrifuged at 16,900xg for 15 mins at 4^0C using a J25-50 rota. The pellet was discarded and a further 50% PEG 4000 solution was added to the supernatant whilst undergoing continuous stirring to achieve a 16% pegylation, this solution was stirred for 1 hour at 4^0C then centrifuged at 16,900xg for 15 mins at 4^0C. This time, the supernatant was discarded, and the pellet suspended to the original plasma volume in Anion exchange Buffer A (20mM Tris, 5mM EDTA pH 7.5) and 5% Anion exchange Buffer B (20mM Tris base, 500mM Sodium Chloride (NaCL), 5mM EDTA pH 7.5)

2.1.5.2 Anion and cation exchange and gel filtration

The prepared solution was then flowed over a 1ml HiTrap™ Q anion exchange column using an AKTA START. Fractions were eluted using a 20-column volume (CV) linear NaCl gradient (0-500mM NaCl). Potential C3 containing fractions were assessed via SDS-PAGE. Selected fractions were then pooled and dialysed for 2h into 500mls of cation exchange Buffer A (20mM Tris base, 70mM NaCl, 5mM EDTA, pH 5.5) with the addition of 10% Cation buffer B (20mM Tris base, 700mM NaCl, 5mM EDTA, pH 5.5), replacing the dialysis buffer after the first hour of dialysis. This was then flowed over a 1ml HiTrap™ SP HP column using the AKTA START. The column was eluted using a linear gradient from 0-50% of Cation exchange Buffer B over 30 CV. 1ml fractions were collected. Aliquots of the peak fractions were then subjected to SDS-PAGE. Those suspected to contain C3 were pooled and underwent gel filtration using a

HiPrep™ Sephacryl® 16/60 S100 column equilibrated in PBS, which eluted the purified samples into PBS.

As for purified human C3, SDS-PAGE and Western blotting were performed to confirm uniformity of purified mouse C3 (*see Figure 63*). Mouse C3 Protein concentration was calculated by NanoDrop One^C (ThermoScientific, UK) using an extinction coefficient of 181410 and a molecular weight of 186.484. Samples were aliquoted then stored at -80^{0}C until required.

2.1.6   Mouse Factor H, recombinant murine FH CCPs 1-5 and recombinant human FH CCPs 19-20

Mouse Factor H (mFH) was purified by Dr Yi Yang, from 20ml of mouse plasma using a previously generated 2a5 (anti-mouse FH, gift from Prof C. Harris, Newcastle, UK) affinity column following standard protocols using an AKTA START followed by gel filtration column on a HiPrep™ Sephacryl® 16/60 S100. The recombinant murine FH CCPs 1-5 and recombinant human FH SCRs 19-20 were produced in house using Chinese Hamster Ovary (CHO) cell culture by Dr Yi Yang (formerly of Complement therapeutics research group).

2.1.7   Recombinant CR1-related gene/protein Y (Crry) protein production.
2.1.7.1   Transfection of a Crry containing vector into CHO cells.

Transfection delivers exogenous nucleic acids (DNA or RNA) into eukaryotic cells, enabling the production of recombinant proteins. Jet polyethylenimic (jetPEI®, Polyplus) is a stable cationic polymer that condenses DNA into positively charged particles that bind to anionic cell surfaces so the DNA:PEI complex is endocytosed by the cell.

In house wild type Chinese hamster ovary cells (WT CHOs) were grown in Dulbecco's modified eagle medium nutrient mixture F12 (DMEM-F12) (Invitrogen, UK) with 10% heat inactivated foetal calf serum (Gibco, UK) and 1% l-glutamine-penicillin-streptomycin solution (Sigma, UK). Cells were grown in T25 flasks (incubator conditions; 37^{0}C, 5% carbon dioxide) and passaged 3 times then seeded (~70,000 cells/well) onto a 24 well plate (in 1 ml of selection medium; DMEM-F12 and 0.6mg/ml of hygromycin B (Sigma, UK). The cells were then transfected with a Crry vector (VB170925-1194cwd, see figure 11) (previously designed in house by Prof K Marchbank and made via VectorBuilder) using jetPEI® DNA transfection reagent and their transfection procedure for adherent cells. The inclusion of hygromycin resistance gene in the vector enables the selection of successfully transfected mammalian cell lines with selection media containing hygromycin.
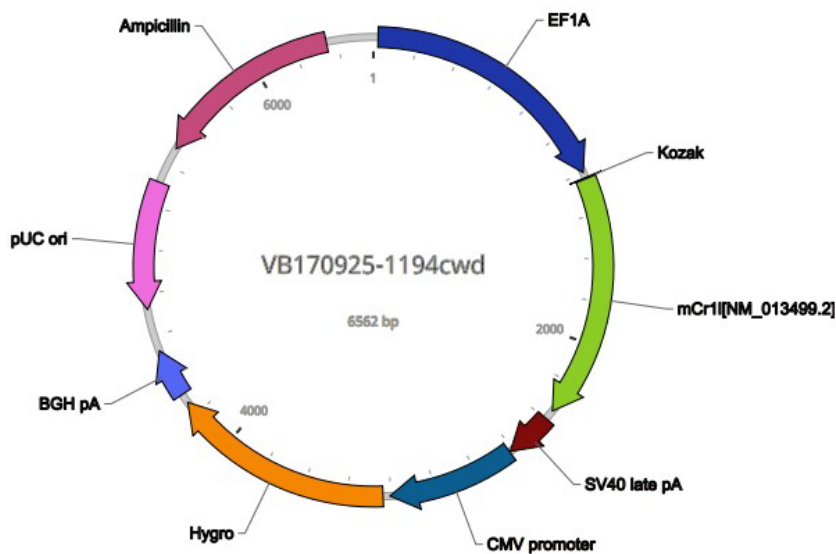
Figure 11 Crry vector design.

Schematic showing the plasmid map of the Crry vector than was used for transfection into CHOs cells in order to produce the recombinant Crry. EF1A (Human eukaryotic translation elongation factor 1 α1 promoter). Kozak (Kozak translation initiation sequence), mCR1 (murine Crry), SV40 late pA (Simian virus 40 late polyadenylation signal), CMV promoter (Human cytomegalovirus immediate early enhancer/promoter), Hygro (Hygromycin resistance gene), BGH pA (Bovine growth hormone polyadenylation signal), pUC ori (pUC origin of replication), Ampicillin (Ampicillin resistance gene) From the VectorBuilder website (www.vectorbuilder.com), ID VB170925-1194cwd

Briefly, per well, 1μg of DNA was diluted in 150mM NaCl to a final volume of 50μl, vortexed gently then spun down. Next, 2μl of jetPEI® reagent was diluted into 150mM NaCl to a final volume of 50μl, vortexed and spun down. Then the 50μl jetPEI® solution was added to the 50μl DNA solution. The mixture was immediately vortexed and then spun down. Following 30 minutes of incubation at room temperature, 100μl of jetPEI®/DNA mixture was added to the cells (per well) in a drop wise manner and the plate gently swirled before being placed back into the cell incubator.   The selection media was replaced every 48 hours over a period of 14 days. Surviving colonies were removed using trypsin solution, counted and then a limiting clone dilution was undertaken across a 96 well plate. Colonies were allowed to establish over 14 days in selection media. Following this, 200μl of cell culture media was harvested (and replaced with fresh selection media) to identify a high Crry expressing clone.

2.1.7.2 Identification of a high expressing recombinant Crry CHO cell clone

Nunc Maxisorb 96 well enzyme linked immunosorbent assay (ELISA) plates were coated with 50µl of harvested supernatant in 50µl of 0.2M Carbonate buffer overnight. The following day, plates were repetitively washed with PBST then blocked with 2% BSA-PBST for 1 hour at room temperature. Following washing, the plate was then incubated with mouse anti-polyhistidine antibody (1:3000) for 1 hour at room temperature, followed by further repetitive washing (3x 5min) with PBST. The plates were then incubated with a sheep anti mouse-HRP conjugated antibody (1:5000 in PBST). A final wash step was performed before the plate was developed by adding 100µl tetramethylbenzidine substrate solution (TMB, Leinco Technologies™, Inc, UK) to each well. The reaction was terminated after 5 minutes with 100µl/well of 10% sulphuric acid and the absorbance was immediately read at 450nM using a FLOUstar Optima Microplate Reader (BMG Labtech, Aylesbury, UK). Clones with an OD>0.2 were re-seeded and scaled up using a 24 well culture plate and DMEM-F12 with 0.2mg/ml of hygromycin B (modified selection media). The selection ELISA was then repeated with freshly harvested cell culture supernatant and the five clones with the highest absorbance (OD) were taken into T25 flasks (1ml of cells and 4 ml of selection media). After confirmation by SDS-PAGE and Western Blotting as per SDS-PAGE and Western Blotting above, and use of 1:1000 rat anti-mouse E1E10 Crry antibody (gift from Prof C Harris), followed by incubation of donkey anti-rat HRP 1:3000 Clone B4 was selected for large-scale purification, with all remaining cell stocks frozen down (see 2.1.7.3).

2.1.7.3 Cryopreservation of transfected Crry CHO cell lines

From selected high expression clones in T25 flasks, cell media was first removed and centrifuged at 2000xg for 5 minutes at room temperature to remove debris and the supernatant stored to extract protein, as needed. The flask was briefly washed with PBS to remove residual media and then cells were liberated from T25 flasks surface using 1% trypsin-EDTA (Sigma-Aldrich ,UK) in 5ml PBS. The trypsin-PBS cell solution was then centrifuged at 300xg for 5 minutes and the resulting pellet re-suspended in freezing media (standard DMEM-F12 with 10% dimethyl sulfoxide (DMSO) in Nalgene™ general long-term storage cryogenic tubes and frozen at -80⁰C for 48 hours then transferred to liquid nitrogen for long-term storage.

2.1.7.4 Large scale Crry recombinant production

Clone B4 was continuously scaled up from T25, T75, then finally into 10x T175 flasks, grown in DMEM-F12 media with 0.2mg/ml of hygromycin B. 250ml of cell culture/media was placed into a 2L roller flasks (4x2L flasks prepared) and left to equilibrate by incubating with loosened lids and rolling at ~1 rpm at 37°C. The supernatant was harvested on day 8 and replenished with fresh media with a final harvest on day 16. Once the supernatant was collected, the cells and any debris were removed from the supernatant by centrifugation at 8000xg for 20 minutes before being filtered using a 0.44µM Whatman filter (GE Healthcare), ready for purification.

2.1.7.5 Recombinant Crry purification

The Crry vector was designed such that the recombinant Crry produced would include a 10x histidine sequence tag (His-tag) in frame before the stop codon. The inclusion of this feature enabled purification via immobilised metal ion affinity chromatography (IMAC). A His-tag contains six or more consecutive histidine residues. Given its small size (0.84 kDa) and uncharged properties at physiological pH, it does not typically affect protein folding, thus it is unlikely to interfere with the structure and function (113). IMAC is based on affinity of histidine residues for immobilised metal ions. Ni^{2+} metal ions are immobilised on chromatographic matrices by chelating ligand (i.e. His trap excel®) column, which can be eluted using imidazole, as imidazole competes with the His-tag for binding to the Ni^{2+} charged resin (113).

Imidazole was added to the filtered supernatant (20mM final concentration to act as a block for weak affinity binding non-specific histidine residue containing proteins), this was then, using an AKTA START, slowly run through a 5ml HisTrap™ excel® column overnight at 4^0C (flow rate 1.5ml/minute) until complete. Buffer A was then applied to the column for ~4 column volumes (CV), or until the OD 280nM trace had stabilised (~0 relative units). The protein was then eluted from the column using a concentration gradient to 100% Buffer B (containing 500mM Imidazole) over 20mls and collected in 1mL fractions. Aliquots of the peak OD280nm fractions were then analysed on SDS PAGE. Selected fractions were concentrated using a Vivaspin® 6 molecular weight cut off (MWCO) 10kDa centrifugal concentrator (Sartorius, UK) and stored at -80^0C until future use.

2.1.8 Human C3MA conversion

Purified $C3^{WT}$ and $C3^{L1109V}$ were activated to their respective C3MA forms by incubation with 2.0 M methylamine (MA) at 1:10 (C3:MA) at 37ºC for 2 hours. The C3MA was then buffer exchanged into PBS using a PD10 desalting column (Cytiva, UK) following the standard gravity protocol as per manufacturer's instructions. The C3MA was then ready to be used for functional studies i.e. co factor activity assays and SPR experiments. The MA treatment reduces native C3 into a $C3(H_20)$ like molecule, which has the ability to bind FB and form an initial alternative pathway convertase or renders it susceptible to proteolytic cleavage by FI when served by its co factor, FH (114). C3MA binds the same ligands as C3b and is inactivated by the same regulatory proteins(115).
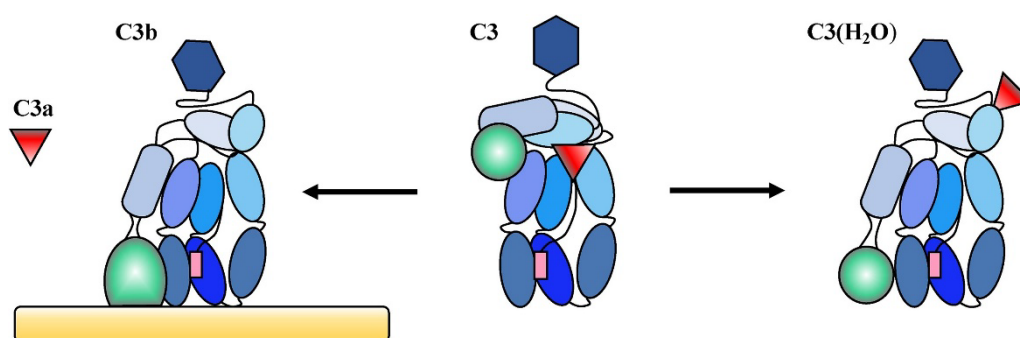
Figure 12 C3 conformation
Conformational changes in C3, taken from (116)

2.1.9 Co factor assays in the fluid phase for a human C3 variant.

The co factor assay is used to detect the ability of FH to act as a co-factor to the serine protease FI, in the proteolytic inactivation of C3b into iC3b in solution, a.k.a, the fluid phase. In order

to determine the regulatory co-factor activity of FH on $C3^{L1109V}$ in the fluid phase, co factor assays were ran. Reactions were set up with either $C3^{WTMA}$ (1µg) or $C3^{L1109VMA}$ (1µg) and incubated with FI 50ng (CompTech, USA), and FH 1-4 250ng (provided by Dr T Hallam) or full length FH (FLFH) 250ng (CompTech, USA). The final reaction volume was 30µl following the addition of PBS and this was then incubated at 37°C in the water bath. At serial time points; 0, 5, 15, 30 minutes the reaction was terminated following the addition of 2x SDS-PAGE reducing buffer and incubated at 95ºC for 5min. The samples were subjected to SDS-PAGE (using a 10% gel). The gel was stained Coomassie blue for 1 hour and then de-stained for a further 1h and imaged as above (SDS-PAGE and Western Blotting2.1.4). Densitometry analysis was performed using Image Studio v5 on the breakdown of the C3b α chain (standardised for loading consistency using the C3b Beta chain), and this data was then imported into Graph pad v9.0 for statistical analysis.
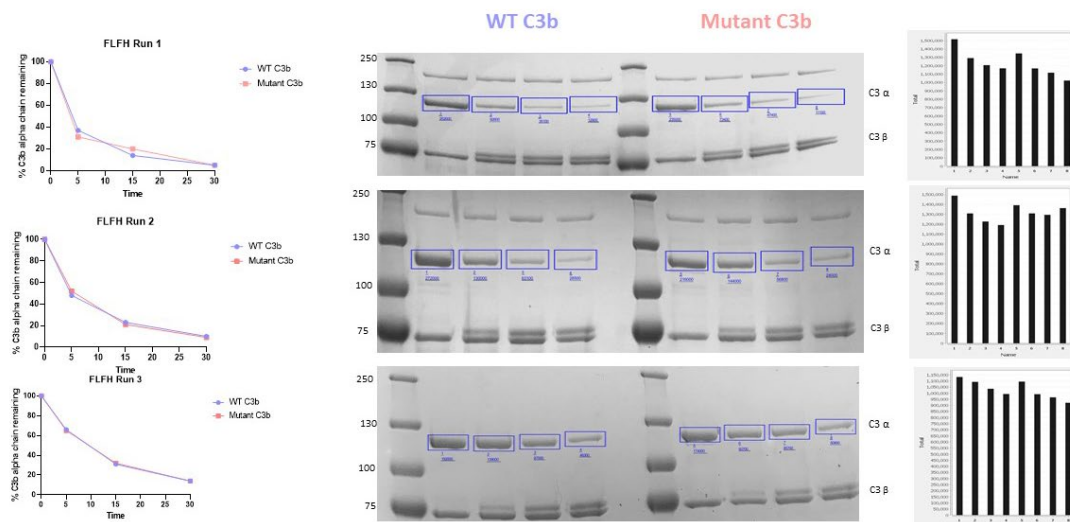
Figure 13 Example of Densitometry analysis.

An example of the co-factor activity assay run with either $C3^{WTMA}$ or $C3^{L1109VMA}$ when incubated with full-length factor H with time points taken at 0,5,15 and 30 minutes. The C3bα chain is demarcated by the blue outline and within the Licor studio this was ascribed a value (number in blue). The percent of C3b α remaining at the individual time points is the value at that time point divided by the value ascribed to the C3bα at time point 0mins.

2.1.10 Mouse fluid phase co-factor activity assays

Murine proteins were purified as above. 30µl reactions were set up to convert either purified $C3^{WT}$ or $C3^{D1115N}$ to C3b following the in-house protocol developed by Dr Yi Yang (formerly

34

Complement Therapeutics Group). Briefly, 3μg of either murine C3 was incubated with 1μg of human FB and 0.01μg of human FD in the presence of 5 mM Magnesium Chloride (MgCl$_2$) at 37 °C for 1 hour. After the reaction was stopped by the addition of 10 mM EDTA, plasma purified murine FH and human FI were added to the concentration at 200nM and 20nM respectively. The 35μl breakdown reaction was maintained at 37 °C, 4μl sample was taken at 0, 5, 10, 20, 30, 40 and 60 mins and analysed by anti-murine C3 Western blotting, and densitometry analysis performed on the breakdown of the C3b α chain as per the human C3 co-factor fluid phase assays as above.

2.1.11 Surface Plasmon Resonance

Surface plasmon resonance (SPR) enables quantification of molecular interactions in real time assessing the binding, kinetics and affinity of molecular interactions.
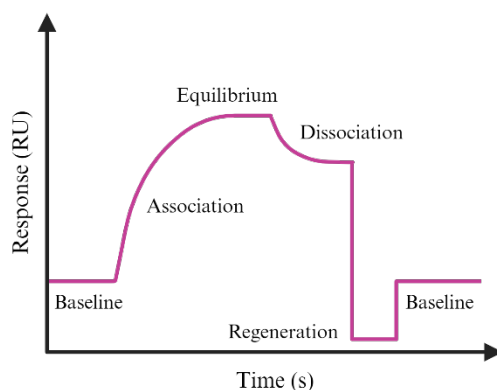
Figure 14 Surface Plasmon Resonance profile of a Biacore™ sensogram.
The sensogram measures the interaction between two molecules in real time.

2.1.11.1 Amine coupling of C3^{WTMA} or C3^{L1109VMA} onto CM5 chip and affinity assays

Purified C3$^{WT\ MA}$ or C3$^{L1109V\ MA}$ was immobilised onto two flow cells (one for C3MA binding and one blank) of a CM5 chip on the BIAcore™ S200 (GE healthcare). Firstly, the CM5 sensor chip was activated by flowing N- (3-dimethylaminopropyl)-N'-ethlcarbodimide (EDC) and N-hydroxysuccinimide (NHS) over the surface of the specific flow cell on the chip. This creates a negatively charged surface for the C3MA to covalently bind. The C3MA proteins were then flowed across at 5ug/ml diluted in 50mM sodium acetate pH 4.5, repeatedly for 20 second cycles at 20µl/min until the 1000 Resonance units (RU) of C3MA was immbolised onto the required flow cell (C3$^{WT\ MA}$ 991.7 RU, C3$^{L1109V\ MA}$ 1025.1 RU). After the RU was achieved, further active sites were blocked by an injection of 1M ethanolamine. Additional protein analytes (FH CCP 1-4 20µM, FH CCP 19-20 20µM (both gifted from Dr T Hallam) and FLFH 2.5µM (CompTech, USA) were then flown over the immobilised C3MA to measure the SPR of each analyte. Sensorgrams could then be produced using the BIAcore™ S200 BIAevaluation software, steady state responses were plotted as a function of time against RU for each

concentration, following subtraction of the RU from the blank flow cell, and the software then calculated affinity (K_D).

2.1.11.2 Alternative pathway regulatory Trimolecular complex building on a CM5 chip

A novel method developed by Dr T Hallam (formerly Complement Therapeutic Group) was used to analyse the differences between $C3^{WT\ MA}$ and $C3^{L1109V\ MA}$ in their ability to build the Alternative pathway (AP) regulatory trimolecular complex (C3b:FI:FH) (ref). In brief, inactive FI (developed by Dr Tom Cox, formerly Complement Therapeutic Group) was injected with FLFH flown across the $C3^{WTMA}$ or $C3^{L1109V\ MA}$ coupled CM5 chip. The inactive FI enables the binding of the components of the AP regulatory TMC without cleaving the C3MA on the chip surface. This assay allows us to measure the building of the AP regulatory TMC in real time (117).

2.1.11.3 Murine SPR studies

All experiments were conducted on a BIAcore™ S200 by Dr Yi Yang (formerly, Complement therapeutic Group). Each version of murine C3 was converted to C3b, via incubation with purified human FB and FD as described above in the fluid phase co factor activity. The incubated samples were gel filtrated using a Superdex 200 10/300 GL column; C3b-containing fractions were pooled and concentrated. Each version of murine C3b (i.e. $C3b^{WT}$ and $C3b^{D1115N}$) was immobilized (930 ± 10 RU) on separate flow cells of a CM5 chip using standard amine coupling. A 2-fold dilution series of purified murine FH (10µM to 0µM), recombinant murine FH CCPs 1–5 (14.6µM to 0µM), recombinant human FH CCPs 19–20 (20µM to 0 µM), or recombinant Crry (10µM to 0µM) was made in HBST buffer (10mM Hepes-buffered saline (HBS), 150 mM NaCl, and 0.005% Tween-20, pH 7.4) and flowed across either chip surface in the same buffer. All analytes were injected in duplicate (30µl/minutes for 200 seconds), followed by running buffer for 300 seconds and a regeneration phase involving injection of regeneration buffer (10 mM sodium acetate, 1 M NaCl, pH 4.5) for 60 seconds. The equilibrium dissociation constant, KD, and standard error were calculated using the steady-state model in BIAcore™ S200 Evaluation Software.

2.1.12 Mice

2.1.12.1 Mouse husbandry

All mice were housed in the Comparative Biology Centre (Newcastle University, UK). They were housed in same sex, individually ventilated cages (IVC). Standard housing conditions were employed with a 12 hour light/dark cycle and *ad libitum* access to food, water, bedding and enrichment. Mice at risk of developing kidney disease were monitored with daily weighing, urine analysis and general conditions scores, reducing to weekly weighing and urinalysis monitoring from 2 months of age in the absence of any detectable disease or clinical concern.

2.1.12.2 Clinical monitoring Table.

Table 4 Mouse clinical monitoring table

Characteristic	Grading guidance – for use in moderate and severe protocols				Score
Activity	Normal, stands upright, explores, climbs	Active but avoids being upright on hind legs or displays altered gait (ataxia)	Inactive, moves around bottom of cage only Or transient fit (<1 min)	No activity, only moves when provoked Or prolonged fit, or 3 transient fits in 24hr	
	0	1	2[b]	3[b]	
Appearance	Normal, well groomed	Patches of piloerection covering >25 but <50% of body	>50 but less than 75% of back showing piloerection Or possible hydrocephaly	Mouse appears puffy, >75% piloerection Or distinct hydrocephaly	
	0	1	2	3[b]	
*Body condition score (BCS)	BCS of 3 or 4	Change in BCS	BCS of 2; or 5.	BCS of 1	
	0	1[a]	2[b]	3[b]	

*Body weight change	Weight change of up to 5%	Weight change of 5-12%	Weight change of 13-19%	Weight change >20 < 30%	
	0	1ᵃ	2ᵇ	3ᵃ	
Hydration	Normal skin turgor	Skin folds on back but returns to normal within 2 seconds	Skin fold remains > 2 seconds but returns to normal after 5 seconds	Skin fold on back remains > 5 seconds or does not resolve	
	0	1ᵃ	2ᵃ	3ᵇ	
Faeces	Normal	Soft, but formed	Soft, wet in appearance	Watery, v. loose (diarrhoea)	
	0	1	2ᶜ	3ᵃ	
Respiration	Normal rapid mouse breathing	Periods of laboured breathing for 5-10 secs,	Laboured breathing for >10 secs and/or abdominal breathing, no gasping	Laboured and/or abdominal breathing with gasps >1s between breaths	
	0	1	2ᶜ	3ᵇ	
Proteinuria (mg/dl)	Normal (0-30)	>31	>100	>800	
	0	1	2ᶜ	3ᵇ	
Haematuria (Ery/µl)	Normal (0)	>10	>50	>100	
	0	1	2ᶜ	3ᵇ	

TOTAL SCORE		

Notes: 1ᵃ – add soaked diet to cage.

1ᵇ- treat affected area with green clay or Vetericyn spray twice daily for 3 days and trim nails

2ᵃ- give subcutaneous fluids, reassess in 1 hour, can be given up to 3 times then consult NACWO/VET

2ᵇ - consult NACWO/vet – interventions maybe available;

2ᶜ –increase monitoring or for **moderate protocols refer to 3ᵇ**

3ᵃ- if associated with BCS of 2 this finding may require humane killing, consult NAWCO/NVS, ensure you have checked correct protocol;

3ᵇ- arrange to humanely kill a.s.a.p.; preferably - Terminal exsanguination via Cardiac Puncture followed by schedule 1 technique.

Guide to cumulative score and suggested outcome – severe protocols
0-6 Continue normal monitoring
7-11 Examine and rescore daily; treat animals; use soaked diet if not already used. Consult with NACWO/NVS as needed, **particularly if moderate severity study**.
ǂ12-15 Treat animals ASAP or Consult NACWO/NVS (with view to humane killing).
>15 Humanely Kill.
N.B. * compared to baseline evaluation and please see below for BCS diagrams
ǂ**in moderate severity protocols if score is >11 – arrange to humanely kill (as per 3ᵇ).**

BC1 - Mouse is emaciated.

- Skeletal structure extremely prominent; little or no flesh cover.
- Vertebrae distinctly segmented

BC2 - Mouse is underconditioned.

- Segmentation of vertebral column evident.
- Dorsal pelvic bones are readily palpable.

BC3 - Mouse is well-conditioned.

- Vertebrae and dorsal pelvis not prominent; palpable with slight pressure.

BC4 - Mouse is overconditioned.

- Spine is a continuous column.
- Vertebrae palpable with only firm pressure.

BC5 - Mouse is obese.

- Mouse is smooth and bulky.
- Bone structure disappears under flesh and subcutaneous fat.

A "+" or "−" can be added to the body condition score if additional increments are necessary (i.e. ...2+, 2, 2 −...)

Body condition scoring is a quick and easy methodology that is useful in assessing animal health. It is particularly helpful when body weight might not reflect body condition (e.g. presence of tumors, ascites, organomegaly, pregnancy). Simply run your finger over the sacral area and score the animal according to the chart.

Figure 15 Mouse Body condition score.

Scoring system to assess mouse body condition, to aid in clinical monitoring of mice. Taken from (118).

2.1.12.3 Generation of the B6.C3^{Tm1(D1115N)Oz/NCL} (C3^{D1115N}) mice

B6.C3$^{Tm1(D1115N)Oz/NCL}$ (C3^{D1115N}) were generated using standard knock-in technology under contract by Ozgene (Perth, Australia) and back crossed onto constitutive Cre recombinase expressing mice (B6^{OZCre} Ozgene, Perth, Aus). These F1 C3$^{D1115N.Cre}$ mice were deemed healthy and mice were shipped to Newcastle University and intercrossed to provide homozygous C3^{D1115N} expressing mice.
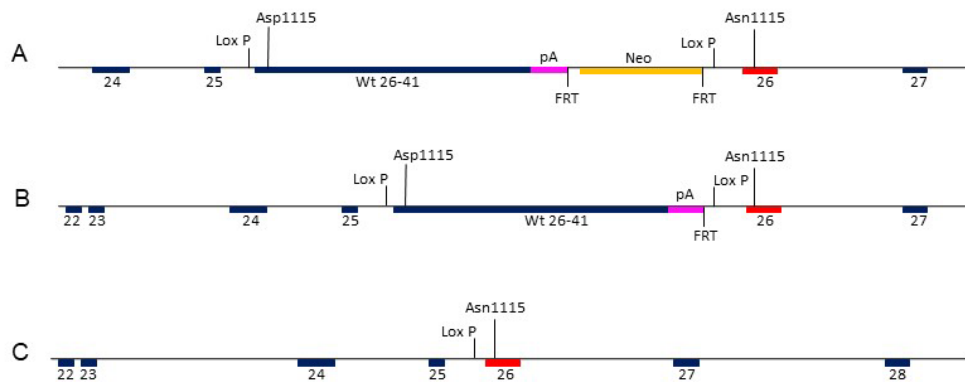
Figure 16 Construction of the C3^{D1115N} and constitutive KI mice
*A schematic map of the genetic organisation of the conditional knock-in (ConKI) construct which was transfected into embryonic stem cells. **B** shows the genetic reorganisation after crossing with the Flpe mice (C3-ConKI-Flp). Finally, **C** shows the final genetic organisation of the C3 KI mice after cross breeding with the OzCre mouse and the introduction of the Asn1115 mutation.*

2.1.12.4 Generation of the B6.C3^{D1115N}.C5^{-/-}

B6-C3^{D1115N} mice were maintained in house (119) and the B6.C5$^{-/-}$ mice were provided by Prof M Pickering (Imperial College London)(55).

2.1.12.5 Generation of the Balb/c.C3^{D1115N}.C5aR1^{-/-} and Balb/c.C3^{D1115N}

B6-C3^{D1115N} mice were maintained in house (119). RRID:IMSR_JAX:006845 (*C5ar1^{tm1Cge}* or Balb/c-*C5aR1$^{-/-}$*) were purchased from the Jackson Laboratory (JAX Lab, Bar Harbour, Maine, USA)(120). B6-C3^{D1115N} were backcrossed for 4 generations onto the Balb/c-C5aR1$^{-/-}$. Resulting mice, heterozygous for C3^{D1115N}, were then intercrossed to produce the homozygous Balb/c-C3^{D1115N}.*C5aR1$^{-/-}$*. Additionally, Balb/c-C3^{D1115N}.*C5aR1$^{-/-}$* mice were subsequently

backcrossed onto wild type Balb/c to produce a Balb/c-C3^{D1115N}.C5aR1$^{+/+}$ line (Balb/c-C3^{D1115N}.)

2.1.12.6 Generation of the B6.C5aR1tm2$^{(hC5aR1)Idor}$ mice

A humanized C5aR1 receptor mouse was generated by Cyagen Biosciences (under contract from Idorsia; B6.C5aR1$^{tm2(hC5aR1)Idor}$) and this was crossed onto the C3^{D1115N} background for 4 generations producing C3^{D1115N}.hC5aR1$^{+/+}$.
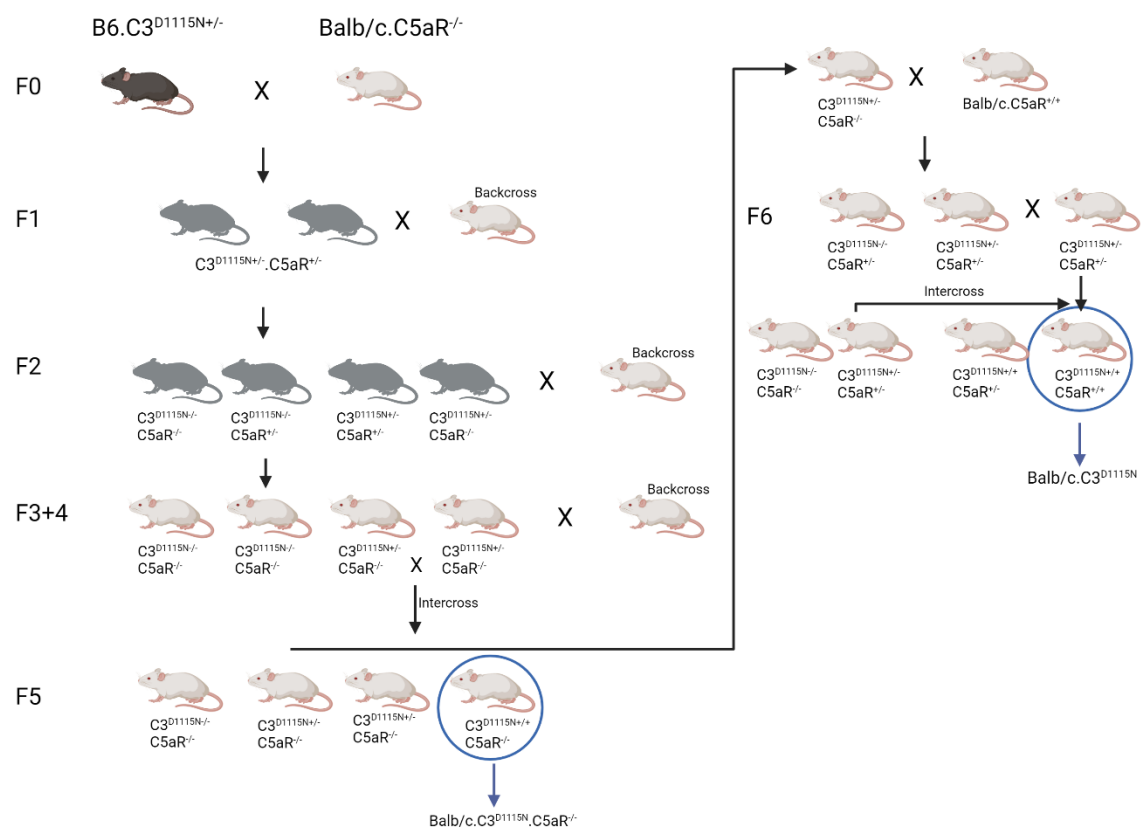
Figure 17 Backcross of the B6.C3$^{D1115N+/-}$ onto the Balb/c.C5aR$^{-/-}$.
Generation of the C3^{D1115N}.C5aR$^{-/-}$ and the Balb/c.C3^{D1115N}.

2.1.12.7 Generation of the B6-C3^{D1115N}.C7$^{-/-}$

B6-C3^{D1115N} mice were maintained in house and RRID:MMRRC_042133-MU (C57BL/6N-C7$^{em1(IMPC)J}$/J or C7$^{-/-}$) were purchased from the Jackson Laboratory (JAX Lab, Bar Harbour, Maine, USA). B6-C3^{D1115N} were backcrossed for 4 generations onto the B6-C7$^{-/-}$ background. Resulting mice, heterozygous for C3^{D1115N}, were then intercrossed to produce the homozygous B6-C3^{D1115N}.C7$^{-/-}$ line.
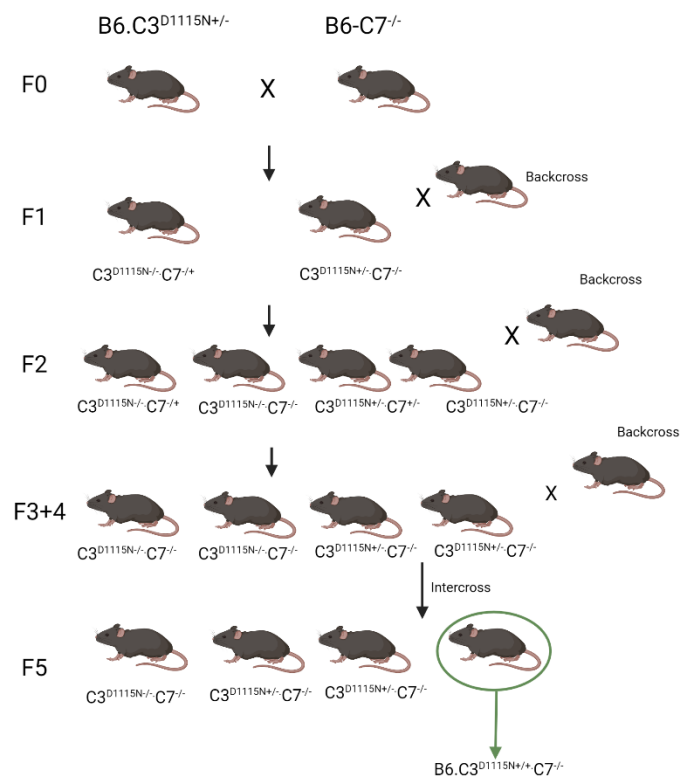
Figure 18 Mice backcross onto the B6-C7$^{-/-}$ line.
Backcrossing the B6.C3D1115N$^{+/-}$ onto the B6-C7$^{-/-}$ line.

2.1.12.8 Genotyping of mice

Genotyping was performed by polymerase chain reaction (PCR) on digested ear notch tissue. Generally, pups were ear notched at 14 days post-partum, for identification and genotyping purposes. The ear tags were placed into 100µL of ear digest buffer and boiled in 0.6mL Eppendorfs for 30 mins. Following a freeze/thaw cycle, the PCR reaction was set up (see table 5) and run on a BioRad T100™ Thermal Cycler. Following completion of the PCR reaction, 10µL of sample was run on a 2% agarose gel (with the addition of 5µl SYBR™ Safe DNA gel stain) to separate the products by standard gel electrophoresis (100V for 90 mins) in TAE buffer. Gels were imaged using the 600 laser channel on the LI-COR Odyssey Fc Imaging System (LI-COR Biosciences ,USA).

2.1.12.9 PCR reaction

Table 5 shows the PCR volume of reagents required per reaction to perform genotyping of the mice from digested ear notches. Primer pairs are listed in table 2.4.2.

Table 5 PCR reaction mix

PCR mix	Reagent
7.4µL	H_2O
10µL	Immomix™
0.8 µL	Forward primer
0.8µL	Reverse primer
1µL	DNA (ear digest)
20µL	Reaction total

2.1.12.10   PCR cycling protocol

The PCR thermo cycling programmes to identify the different mouse genotypes for $C3^{D1115N}$, $C5aR1$ and $C7$ are detailed in the below tables.

2.1.12.10.1   C3 D1115N

Table 6 PCR programme for the C3^{D1115N} gene

Stage	Temperature	Time	Number of cycles
Denaturing	95^{0}C	5 minutes	
Denaturing	95^{0}C	30 seconds	x 35 cycles
Annealing	58^{0}C	30 seconds	
Extension	68^{0}C	1 minute 45 seconds	
Extension	68^{0}C	10 minutes	
Final Hold	4^{0}C	∞	

2.1.12.10.2   C5aR1

Table 7 PCR programme for the C5aR1 gene

	Stage	Temperature	Time	Number of cycles
	Denaturing	95^{0}C	10 minutes	
Stage 1	Denaturing	95^{0}C	20 seconds	x 10 cycles
	Annealing	65^{0}C	15 seconds	
	Extension	68^{0}C	10 seconds	
Stage 2	Denaturing	94^{0}C	15 seconds	x 28 cycles
	Annealing	60^{0}C	15 seconds	
	Extension	72^{0}C	10 seconds	
	Final Extension	72^{0}C	5 minutes	
	Final Hold	4^{0}C	∞	

2.1.12.10.3   C7

Table 8 PCR programme for the C7 gene

Stage	Temperature	Time	Number of cycles
Denaturing	95^0C	2 minutes	
Denaturing	95^0C	1 minutes	
Annealing	64.8^0C	30 seconds	x 30 cycles
Extension	72^0C	1 minutes	
Extension	72^0C	5 minutes	
Final Hold	10^0C	∞	

2.1.14 Assessment of murine renal function

Mouse urine was collected following spontaneous voiding during daily weighing. Proteinuria and haematuria were measured by pipetting 10 µL of urine onto the corresponding section of the urinalysis dipstick (Hema-Combistix, Siemens, Berlin, Germany), following the manufactures instruction, the urinalysis was read after 1 minute and a value assigned which was then imported into GraphPad v9.0 and graphically presented.
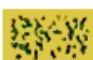
Figure 19 Urine parameters tested using the urinalysis dipsticks.
Proteinuria and Haematuria highlighted by the pink arrow.

2.1.15 Collection of murine blood

Whole blood was collected from animals through terminal exsanguination. Practically, mice were deeply anaesthetised using isoflurane inhalation. Blood was collected via terminal cardiac puncture into 2.7ml lithium heparinised coated tube (SARSTEDT, Germany).

2.1.16 Mouse haemoglobin count and blood urea nitrogen levels

100 µl of whole murine heparinised blood was then placed into a Chem8+ cartridge and run on an i-STAT analyzer as per manufacturer instruction (Abbott, UK) to obtain haemoglobin and blood urea nitrogen (BUN) levels. An aliquot of whole blood was placed on ice for platelet and reticulocyte count, and the remaining blood centrifuged at 2.5xg following the addition of EDTA to achieve a final concentration of 2.5mM. The plasma was then stored in aliquots at -80^0C for further work.

2.1.17 Reticulocyte count

The method to measure the reticulocyte count was developed in house by Dr P Walsh (Complement therapeutics group). BD Retic-count™ (BD Biosciences) contains thiazole orange, which acts as an intercalating DNA/RNA dye, enabling binding to nucleated reticulocytes, but not mature anuclear erythrocytes. Generally, 10µl of heparinised blood was added to 1 ml of BD Retic-count (a background control was run simultaneously, with 10µl of blood added to 1ml of Dulbecco phosphate buffered saline). Both samples were incubated for 1 hour at room temperature (protected from light) with data then acquired using flow cytometry.
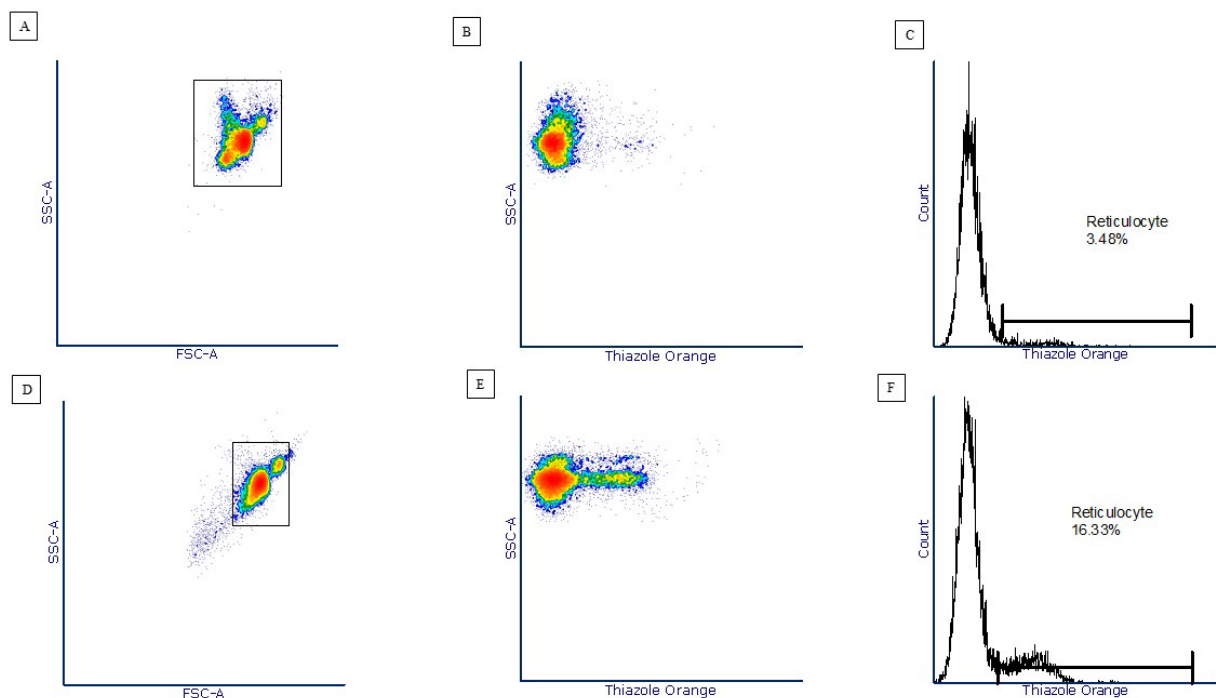
Figure 20 Reticulocyte count analysis.

A scatter plot showing side scatter against forward scatter (A,D). Next, cells are identified with thiazole orange staining, reflecting reticulocytes (B, E). C & F are the histogram showing the cell count of the cells staining positive with thiazole orange, C being a healthy mouse and F illustrating an unwell mouse with a high reticulocyte count

2.1.18 Platelet count

10µl of heparinised blood was added to 400µl of Flow buffer. Of this 5µl was taken into 200µl of staining buffer (Flow buffer containing Rat Anti-mouse CD41 PE, 1:400). The sample was incubated on ice and protected from light for 30 mins. 50µl of CountBright™ Plus Absolute Counting beads (ThermoFisher, UK) were added immediately before analysis. Data was acquired using flow cytometry. The platelet count method was developed in house by Prof K Marchbank and Dr P Walsh (Complement therapeutics group). Data was acquired and presented using side scatter (SSC) and forward scatter (FSC) plotted on a log scale. Platelets were identified based upon the positivity of CD41-PE and the counting beads allowed for a quantitative platelet count.

Overlay #	Filename	Gate	# of Events	X Geometric Mean	Y Geometric Mean	% of gated cells	% of all cells
1	Specimen_001_12651_031.fcs compensated	None	96522	n/a	n/a	100.00	100.00
1	Specimen_001_12651_031.fcs compensated	Platelets	33264	1581.22	1069.80	34.46	34.46
1	Specimen_001_12651_031.fcs compensated	CD41+ Platelets	27476	1621.97	1023.95	28.47	28.47
1	Specimen_001_12651_031.fcs compensated	Beads	9914	15050.90	104007.48	10.27	10.27

Figure 21 Example of Platelet count flow analysis.

(A)Forward and side scatter plots of the data showing the total cell population and the bead population.
(B). Data then gated for CD41 PE positive cells. Data captured was for 10,000 Beads.

1. $\dfrac{\text{Platelet Count} * \text{volume of beads}}{(\text{Bead Count} * \text{volume of cells}) * (\text{Bead concentration/ volume of beads})}$

2. $\dfrac{\text{Platelet Count}}{\text{Dilution Factor}}$ - - - - - - - - - → First dilution (uL of blood) * Second dilution (uL of first dilution in final flow buffer suspension

3. Platelet count in uL * 1000 = Platelet count/ml

$\dfrac{\text{Volume of blood from first dilution (uL)}}{(\text{Final volume of cells \& beads uL + Volume of blood from first dilution})}$

Figure 22 Algorithm devised by Dr P Walsh to calculate platelet count/ml.

The number of events of CD41+ve platelets was taken as the initial 'Platelet count', the bead count was incorporated to allow an accurate cell number to be obtained, this count was then corrected for the dilution factors from the original sample that was taken from the whole blood and for correction following the flow buffer volume.

2.1.19 Histological analysis

2.1.19.1 Light microscopy

Kidneys were harvested and fixed in 10% neutral buffered formalin solution pots (Genta Medical, York). Following fixation (a minimum of 48 hours), the tissues were embedded in paraffin via The Newcastle Hospital NHS foundation trust laboratories, and 4µm sections were cut. Sections were then stained for using periodic acid Schiff (PAS) and Martius scarlet blue (MSB) staining protocols (by The Newcastle Hospital NHS foundation trust pathology department). Stained sections were then examined by light microscopy using an Olympus X microscope.

2.1.19.2 Freezing and cryosectioning of murine kidneys

Mouse kidneys were placed in base moulds (VWR, UK), immersed in OCT, then immediately frozen on dry ice and stored at -80°C until analysis. 5µM cryosections from mouse kidneys were mounted onto a SHANDON Colourfrost Plus microscope slide (ThermoFisher, UK), and stored at -80°C for future use.

2.1.19.3 Immunofluorescence identifying Glomerular C3 deposition

Immunofluorescence enables detection of proteins within tissues using antibody that are fluorescently labelled. This enables the identification, deposition and localisation of proteins within tissues and cell cultures. Kidney sections were thawed at room temperature then fixed in ice-cold acetone for 10mins, blocked for 1 hour with 60μl of 20% goat serum in PBS, then incubated with 60μl of FITC-conjugated goat polyclonal anti-mouse C3 Ab (MP Biomedicals, Santa Ana, 1 in 100) for 1 hour (protected from light). After repetitive washes with PBS, the tissue sections were stained with mounting medium with DAPI (4',6-diamidino-2-phenylindole; Abcam) and covered with glass coverslips. Fluorescent images were taken at ×20 magnification on a Leica DM2000 LED using a Leica DFC 7000 T camera.

2.1.19.4 Immunofluorescence identifying Glomerular C9 deposition

For C9 immunofluorescence, sections were fixed in ice cold acetone for 10 mins, blocked with Rat anti-mouse CD16/CD32 Fc block (BD Pharmingen 1:100) in 2% BSA/PBS for 1 hour followed by blocking in 20% goat serum in PBS at room temperature for 30 minutes. After washing, sections were then incubated with rabbit-anti rat C9 (1:100, gift from Prof Morgan) overnight at 4^OC. The next day sections were washed then incubated with goat-anti rabbit Alexa 594 (1:200, Thermofisher). Finally, the sections were washed, mounted in DAPI and imaged as above.

2.1.19.5 Immunofluorescence identifying Glomerular Fibrin Deposition

For glomerular fibrin deposition, sections were fixed in ice-cold acetone for 10 mins, blocked with 20% rabbit serum for 30 minutes, then incubated with a sheep anti-human fibrinogen for 1 hour (1:100). After repetitive washing, sections were incubated with an alexa 594 conjugated rabbit anti-sheep IgG (1:100) for 1 hour, washed and then mounted in DAPI and imaged as above

2.1.19.6 Quantification of immunofluorescence

Tiff images were exported from LAS X software and imported into image J. Images were converted to 8 bit, and the region of interest (glomerulus) demarcated and the signal measured using the standard image J algorithm for 'mean grey value'. This is graphically presented as mean glomerular intensity, and is the average pixel intensity on the grey scale within the defined area.

2.1.20 Immunohistochemistry

Immunohistochemistry is akin to immunoflourescence, however, instead of using a fluorochrome, DAB (3,3'-Diaminobenzidine) is used as a chromogen. Using HRP conjugated antibodies, DAB is oxidised by HRP and forms brown precipitate at the location of the antibody.

For F4/80 and Ly6-G staining, frozen sections were fixed in acetone then blocked in 3% hydrogen peroxide (to reduce nonspecific background staining). After repetitive washing, sections were blocked in 20% normal goat serum then incubated in rabbit-recombinant F4/80 (Abcam, 1:100) or rat anti mouse Ly6-G 9 (R&D systems, 1:50) followed by goat-anti rabbit HRP (Abcam, 1:200) or goat-anti rat HRP (Abcam,1:200) for Ly6-G. Following further washing, sections were incubated with DAB, counterstained with Meyers haemotoxylin and then dehydrated through graded alcohols and mounted in DPX Mountant (Sigma-Aldrich, UK). Images were then taken on an Olympus X microscope at x20 and analysed using a freely available macro plug in for image J (Immunohistochemistry (IHC) Image Analysis Toolbox, open source available online)

Tiff picture   IHC tool> H-DAB> colour   Process> binary   Analyse>set measurements
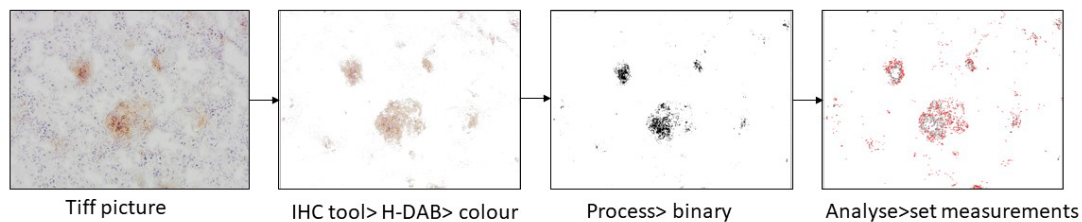
Figure 23 Quantification of IHC figures.

Process of quantifying DAB. Tiff images were imported into image J, and converted using the IHC tool. The image was then processed into a binary image, and then the number of pixels measured and presented as % area of positivity of staining.

2.1.21 Electron Microscopy

Small pieces of cortical tissue (~1mm^3) were fixed in 2% glutaraldehyde in 0.1M carbonate buffer and processed by EM research services, Newcastle University. Briefly, tissues were post-fixed in osmium tetroxide, dehydrated in a graded series of acetone and embedded in Taab epoxy resin. Ultrathin sections (70nm) were picked up on copper grids, stained with uranyl

acetate and lead citrate, and examined using a Philips CM100 transmission electron microscope (EM Research Services, Newcastle University).

2.1.22 ELISA.

ELISA is an assay that can measure antigens, antibodies and proteins in biological samples. Typically, a 96 well-specialised absorbent plate is used to ensure the antibody adheres to the surface. For Sandwich ELISA, the plate is coated overnight with a capture antibody (raised against the antigen of interest), the following day the plate is washed to remove unbound antibody, blocked (to prevent non-specific binding of the sample to the plastic plate), then incubated with the sample of interest (in triplicate to enable statistical analysis). Following incubation, the plate is washed and incubated with a detection antibody that binds to the target antigen with an enzyme labelled antibody. Following this, a substrate is added, resulting in a chromogenic reaction and enabling the change in colour to be measured using a plate reader.
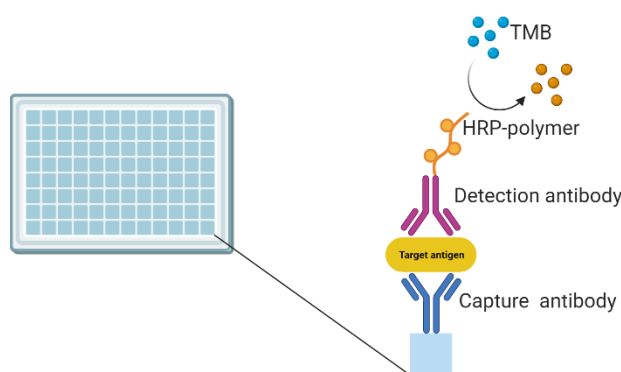
Figure 24 Sandwich ELISA methodology.
Schematic showing the antigen-antibody interactions inside an individual well of a 96 well ELISA plate.

2.1.22.1 Murine C3 ELISA

To determine mouse C3 levels, 50µl of the diluted plasma sample (1 in 800, diluted in PBST,2mM EDTA) was used for analysis. 20 ng/well of mAb 11H9 (Hycult Biotech via Cambridge Bioscience, UK) dilute in 0.2M Carbonate buffer were coated on a NUNC Maxisorp flat-bottom ELISA plate to capture mouse C3. Following overnight incubation, plates were washed and blocked with 2% BSA at room temperature for 1 hour. Plasma samples were then incubated for 1 hour (samples ran in triplicate), plates washed, then detected by an HRP-conjugated goat polyclonal anti-mouse C3 antibody (1 in 25000, MP Biomedicals). Plasma

from $C3^{-/-}$ animals were used as negative controls and 3 wells incubated with no plasma only carbonate buffer. The average of the triplicate wells taken from the negative controls was assumed to be the background and this was subtracted from the OD of the plasma samples. The ELISA was developed with TMB (50μl/well) and stopped with 10% sulphuric acid (50μl/well). The C3 concentrations were interpreted based on a standard curve generated using purified wild type mouse C3 (1mg/ml, purified in house, or, purchased from CompTech, USA).

2.1.22.2 Murine FH ELISA

To measure FH present in mouse plasma, ELISA plates (Nunc Maxisorp) were coated with monoclonal anti-FH (2A5, gift from Prof C Harris) at 1μg/ml (Protocol generated by Mrs H Denton, Complement therapeutics research group). After overnight incubation at 4°C, plates were blocked with 1% BSA at room temperature for 1 hour. After washing, plates were incubated with diluted mouse plasma (1 in 1000) for 1 hour at room temperature. Plates were washed and then incubated with sheep anti-mouse FH (1 in 5000, Abcam Ab8842) for 1 hour at room temperature and detected by adding donkey anti-sheep HRP conjugated antibody (1 in 5000, Jackson,) for 1 hour at room temperature. A standard curve using known concentration of purified mouse factor H (provided by Dr Yi Yang) was used to calculate the concentration of factor H in the mouse samples.

2.1.22.3 Murine C5 ELISA

To measure C5 present in mouse plasma ELISA plates were coated with 1ug/ml BB5.1 (Anti-C5, Hycult Biotech). After overnight incubation at 4°C, plates were blocked with 1% BSA at room temperature for 1hour then washed. Plates were then incubated with diluted mouse plasma (1 in 1000) for 1 hour, washed and then incubated with goat anti-human C5 (1/1000, Quidel A306, 073139). Plates were then incubated with donkey anti-goat HRP conjugated antibody (1/5000, Jackson). A final wash followed then the plate was developed with TMB. Samples were standardized to a wildtype control.

2.1.23 Study Approval

2.1.23.1 Patient consent and ethical approval

Patients or healthy donors provided fully informed consent. Ethical approval from Newcastle University.

2.1.23.2 Animal ethics

All animal experiments were approved by the animal welfare and ethics review board (AWERB) of Newcastle University and the UK Home office under the auspices of animal procedure licences PD86B3678 and PP2560803. Furthermore, individual experiments were fully reviewed by named animal welfare staff prior to their commencement.

2.2 Statistics

All statistical analysis were undertaken using GraphPad prism v9.0 (GraphPad Software, San Diego, CA; www.graphpad.com). Kaplan Meier was used for survival analysis. For statistical test between two or more groups, a test of normality (Kolmogorov-Smirnov) was undertaken, and when met, an unpaired students T test was performed. If unmet, then a Mann-Whitney test used. Welch's correction was applied if two groups were not assumed to have the same SD. Two-way ANOVA with Tukey's multiple comparison test was used to establish significance between groups and across time. A P value <0.5 was taken as statistically significant. P values are identified as follow, ns = non-significant, * = p <0.05, ** = p<0.01, *** = p<0.005, **** = p<0.0001. Data is shown as Mean ±SEM.

2.3 Figure assembly

Figures were created using Biorender (www.Biorender.com), Graphpad Prism 9.0 (Graphpad Software, USA) or PyMOL 2.5.5 (www.pymol.org).

2.4 Materials

2.4.1 Antibodies

2.4.1.1 Primary antibodies

Table 9 Primary antibodies

Antibody target	Conjugation, Application	Target species	Host species	Working dilution	Source	Code or clone
C3	HRP,WB/ELISA	Mm	Goat	1:10,000, 1:25,000	MP Biomedical	55557
C3, C3b, iC3b, C3d, C3dg	Elisa	Mm	Rat	1:25,000	Hycult	HM1045
C3	FITC, IF	Mm	Goat	1:100	MP Biomedical	0855500
C9	IF	Mm	Rat	1:100	Gift from Prof BP Morgan	n/a
Fibrinogen	IF	Hs & Mm	Sheep	1:200	Abcam	Ab118533
C5	Th , ELISA	Mm	Mm IgG1	40mg/kg or 1ug/ml	Hycult	BB5.1, HM1073
Crry	WB	Mm		1:1000	Gift from Prof C Harris	E1E10
polyhistidine	HRP, ELISA	n/a	Mm	1:3000	Sigma	A7058-1VL
FH	ELISA, AC	Mm	Mm	1ug/ml	Prof C Harris	2a5
Gr-1	IHC	Mm	Rat	1:20	R&D Systems	MAB1037
F4/80	IHC	Mm	Rb	1:50	Abcam	ab300421
mouse IgG$_1$/PBS	Th	Mm	-	40mg/kg	Inhouse	

Wb- Western blot, IF-Immunofluorescence, FC- Flow cytometry, IHC- immunohistochemistry, ELISA- Enzyme-linked immunosorbent assay, AC-Affinity Chromatography, Th- therapeutic , HRP – FITC -

Hs- homo sapiens (Human), Mm – mus musculus (Mouse), Rb-Rabbit

2.4.1.2 Secondary antibodies

Table 10 Secondary antibodies

Secondary antibody	Target species	Host species	Working dilution	Source
Goat anti-rat IgG Alexa Fluro ®594	Rat	Goat	1:200	Abcam
Alexa rabbit anti-sheep IgG 594	Sheep	Rabbit	1:200	Abcam
Goat anti-rat IgG HRPO	Rat	Goat	1:100	Abcam
Goat anti-rabbit IgG HRPO	Rabbit	goat	1:100	Abcam
Sheep anti- mouse IgG	Mouse	Sheep	1:5000	Abcam
Sheep Anti-FH antibody	FH	Sheep	1:5000	Abcam
Donkey Anti-Sheep IgG HRP	Sheep	Donkey	1:5000	Jackson
Goat anti-human C5	Human	Goat	1:1000	Quidel
Donkey Anti-Goat IgG HRP	Goat	Donkey	1:5000	Jackson

2.4.2 Primers

Table 11 Primers

Gene	Application	Species	Forward	Reverse
$C3^{D1115N}$	PCR	Mm	CCTTCTCTTTCTGGAATTT GCCTG	CTTTGGTGACCCTGTCTGTT CC
$C5$	PCR	Mm	CACGATAATGGGAGTCAT CTGCG	AAGTTGGAGTGTGGTCTTTG GGCC
$C5aR1$	PCR	Mm	GGT CTC TCC CCA GCA TCA TA Wild type	GGC AAC GTA GCC AAG AAA AA
			GCC AGA GGC CAC TTG TGT AG Mutant	
$C7$	PCR	Mm	ATG GCT CTT CCT CTC AT C TCC	CTG CAG CTC TCT GAA TGA AAG T

60

2.4.3 Reagents

Table 12 General reagents and consumables used

Reagent	Application	Source
Novex™ WedegWell™ 10-20% Tris-Glycine Gel	SDS Page gels	ThermoFisher
PageRuler™ Plus pre-stained protein ladder	SDS page gels, WB, co factor activity assays	ThermoFisher
Coomassie Brilliant Blue™R-250	SDS page gels	ThermoFisher
Protran™ Nitrocellulose Western Blotting membranes	WB	Amersham Biosciences
Pierce™ ECL Western Blotting Substrate	WB	Thermo Scientfic
Phosphate-Buffered Saline tablets	Multiple	Gibco
Thermo Scientific GeneRuler 1	DNA gels	Thermofisher
Eppendorf	Mulitple	Corning
UltraPure™ Agarose	PCR	Invitrogen
SYBR™ Safe DNA Gel Stain	PCR	Invitrogen
Chem8+ Istat cartridges	ISTAT	Abbott
Dialysis tubing	AC	Medicell Membranes Ltd
Dulbecco's Modified Eagle's Medium	Cell culture	Sigma-Aldrich
Fetal Bovine Serum (Ultra low IgG <5µg/ml)	Cell culture	Gibco
Bovine Serum Albumin	Elisa	Sigma-Aldrich
TMB Substrate solution	Elisa	LeincoTechnologies,INC
Mounting Medium with DAPI-Aqueous Fluroshield	IF	Abcam
DAB substrate kit	IHC	Abcam
BD Retic Count™	Reticulocyte count	BD Biosciences
OCT™	Tissue processing	Tissue-Tek®

2.4.4 Consumables

Product	Application	Source
T25, T75, T175	Cell culture	
Nunc maxisorp 94 well plates	Elisa	
Eppendorfs	Multiple	Starlab
S-Monovette Lithium-Heparin Gel blood collection tubes 2.7ml	Terminal cardiac puncture	SARSTEDT
Superfrost™Plus Adhesion Microscope slides	IHC/IF/Blood films	Epredia
10% Neutral Buffered Formalin Pots	Tissue processing	Genta Medical
1.5ml Microtubes (Maxymum Recovery)	AC	Axygen, Inc
NUNC-IMMUNO Maxisorp Plate	ELISA	ThermoScientific

AC- Affinity Chromatography

2.4.5 Buffers

Table 13 Buffers

Buffer	Ingredients	Stock solution	Working concentration
SDS (sodium dodecyl sulphate) buffer	60.6 g Trisbase, 288.2g glycine, 20g SDS	20x	1x
Transfer buffer	3g Trisbase, 14.4g glycine, 20% methanol	1x	1x
De-stain solution	10% acetic acid, 50% methanol, 40% water	-	-
Size exclusion/gel filtration	Phosphate-buffered saline (PBS) pH 7	1x	1x
Ear tag digest buffer	0.1 mM EDTA (20µl 0.5M EDTA), 10 mM Sodium Hydroxide		
Tris-acetate-EDTA (TAE)	242g Trisbase, 100ml 0.5 M EDTA, 57.2 ml acetic acid, pH 8.0	50	1
2% agarose gel	2g of agarose powder made up in 100ml of 1 x TAE buffer with 4µL SYBR™ Safe DNA Gel stain	-	-
1x PBS	2x Phosphate buffered saline tablets, 1000ml deionised water.	1x	1x
1x PBST	2x Phosphate buffered saline tablets, 1000ml deionised water, 1 ml TWEEN® (0.1% Tween)	1x	1x
5% Whole milk- PBST	5 grams of Marvels Milk Powder, 100mls of PBST	5%	-
0.2M Carbonate Buffer	2ml 0.2M Sodium Carbonate, 4.25ml of 0.2 Sodium Bicarbonate, 6.25mls of dH_2O	0.2 M	0.2 M
BSA	2 grams of Bovine serum albumin, 100mls of PBST	2x	2x
50% Polyethylene Glycol	10 grams of Polyethylene Glycol 4000, 20mls of 1x Phosphate Buffered Saline	4% and 16%	50%
DMEM/F12	Dulbecco's Modified Eagle Medium Nutrient Mixture F-12	-	-
Foetal Bovine Serum	Fetal Bovine Serum	100%	10%
1x Trypsin-EDTA solution	1ml of 10x Trypsin-EDTA Solution into 9mls of PBS	10x	1x

Selection media for transfection	500mls of DMEM F12, 10% FBS, 1% L-glutamine- penicillin-streptomycin, 0.6mg/ml of Hygromycin B	-	-
Selection media for sustaining transfected CHO cells to produce recombinant Crry	500mls of DMEM F12, 10% FBS, 1% L-glutamine- penicillin-streptomycin, 0.2mg/ml of hygromycin B	-	-
HBST	10 mM HEPES, 150 mM NaCl, and 0.005% Tween-20, pH 7.4	10mM	10mM
Flow buffer	1L PBS, 5% BSA, 1mM EDTA, 0.1% Sodium azide	1x	1x

Chapter3 Functional Characterisation of C3,p.L1109V

3.1 Introduction

A 9 year old girl (IM) was referred to the National aHUS Service having presented with c-aHUS at the age of 16 months. Following initial treatment with plasma exchange she had been commenced on Eculizumab and remained on this treatment. Genetic analysis had identified homogeneity of a point mutation in *C3*,p.L1109V (c.3325C>G:p.Leu1109Val). Her parents were unaffected heterozygous carriers (consanguineous). No other family members were affected and the mutation is not found on the genome aggregation database.

In addition to this, she had been identified to carry a mutation in Methionine adenosyltransferase I/III (MAT I/III) which was detected on newborn screening. There is no published mechanistic data on the effect of the p.L1109V change; and with the underlying MATI/III mutation, it was important to determine the significance of p.L1109V. It would be an exceedingly rare event for a patient to have two distinct rare conditions. Functional characterisation of L1109V would allow us to determine if IM had presented with c-aHUS and provide the clinical rational for continuation of Eculizumab treatment and debate the risk of relapse if it were to be withdrawn.

3.2 Hypothesis

- Due to its location in the thioester domain of C3d, *C3,p.*L1109V leads to c-aHUS due to lack of binding of FH via CCP 19-20.

3.3 Aims of Chapter

- To purify $C3^{L1109V}$ and healthy donor C3 control ($C3^{WT}$).

- To undertake functional characterisation of $C3^{L1109V}$ and compare to $C3^{WT}$ control.

3.4 Results

3.4.1 C3,p.L1109V modelled within the Trimolecular complex

The published trimolecular complex (TMC) crystal structure (5o32) enabled us to map the location of the *C3*,p.L1109V variant (along with another C3 mutation associated with c-aHUS, *C3*,p.D1115N). The pymol structure showed both C3 variants sit snugly within the TED and are at the binding interface of FH CCP 19-20. They mirror the cluster of *CFH* variants within FH CCP 19-20 associated with c-aHUS. Based upon the location of *C3*,p.L1109V and previous published work using recombinant C3 variants, we hypothesised that L1109V would have reduced binding affinity to FH CCP 19-20. Given its location, we did not expect to detect reduced cofactor activity of FH to L1109V given binding of FH CCP 1-4 to C3b appears unaffected.
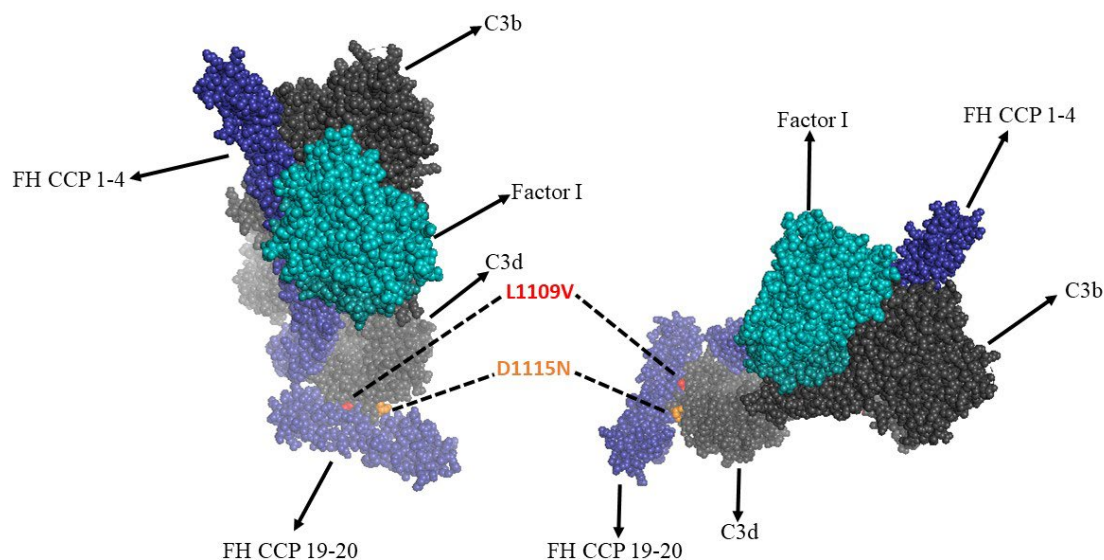
Figure 25 Trimolecular complex modelled in Pymol

The crystal structure 5o32 modelled in Pymol shown in two orientations. FH CCP 1-4 and CCP 19-20 (blue), Factor I (cyan), C3b (grey), C3d (lighter grey). The two C3 mutations identified in patients referred to the National aHUS service, C3,p.L1109V (red spheres), C3,p.D1115N (orange spheres).

3.4.2 Purification of C3^WT

IM carried the *C3*,p.L1109V in homogeneity, enabling us to purify the C3 protein directly from blood. 9mls of whole blood was collected into EDTA coated tubes and purified as per method

section 2.1.2.1. The chromatography graphs for each step of the purification process are shown below, for both, C3^{WT} and C3^{L1109V}.

A.i Anion exchange

A.ii
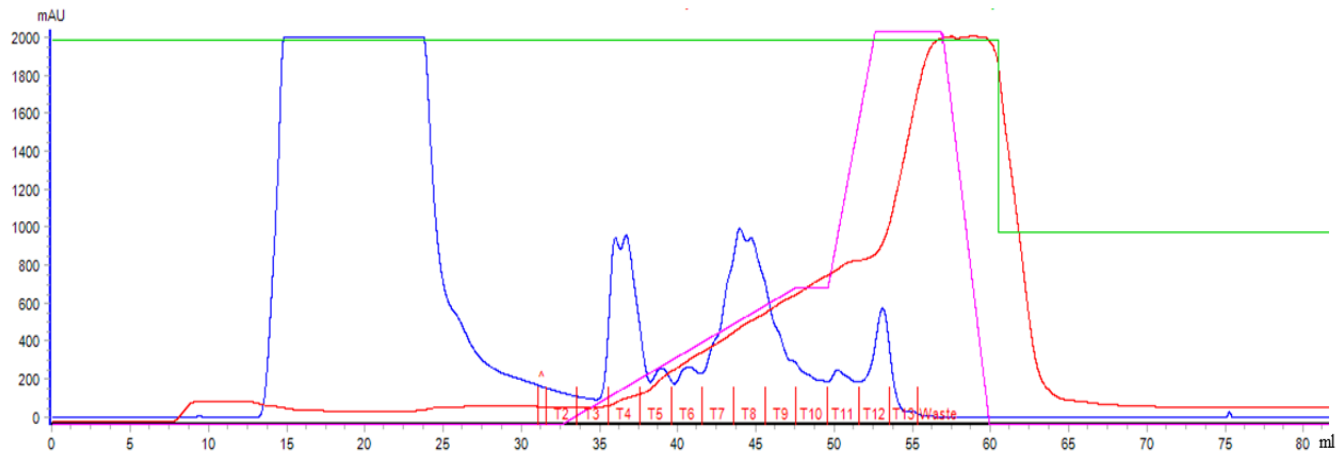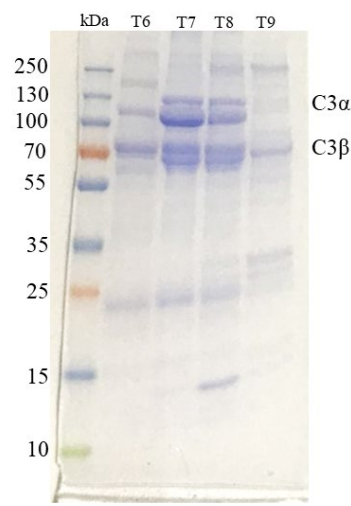
B.I Cation exchange
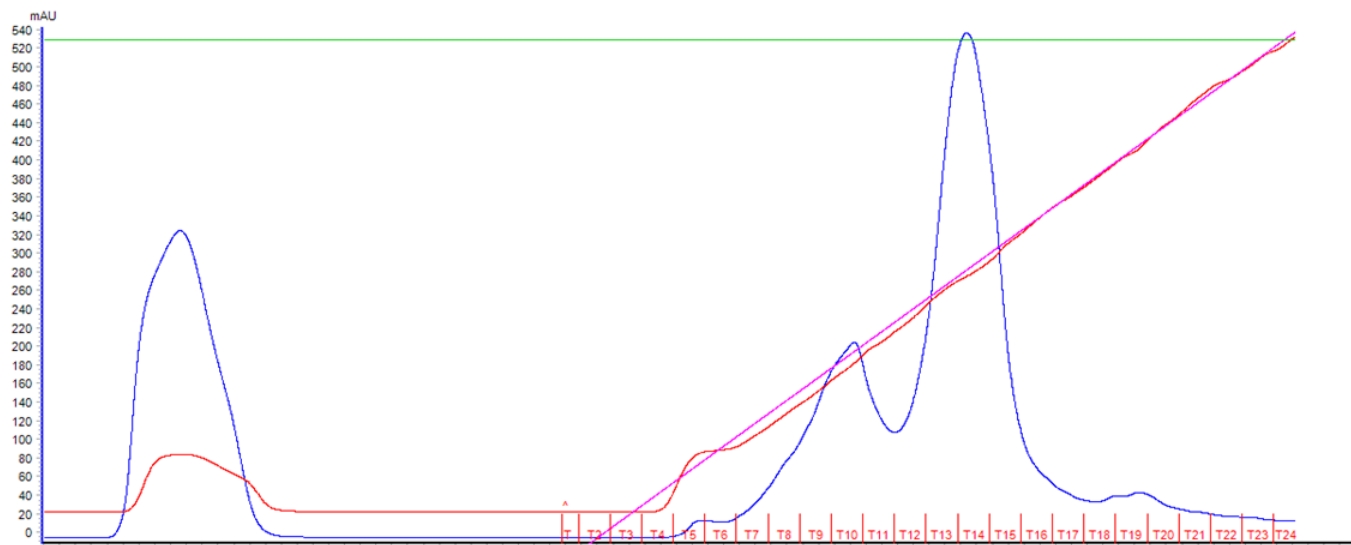
B.ii
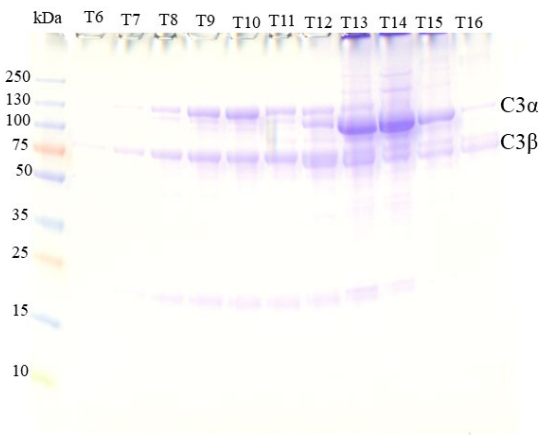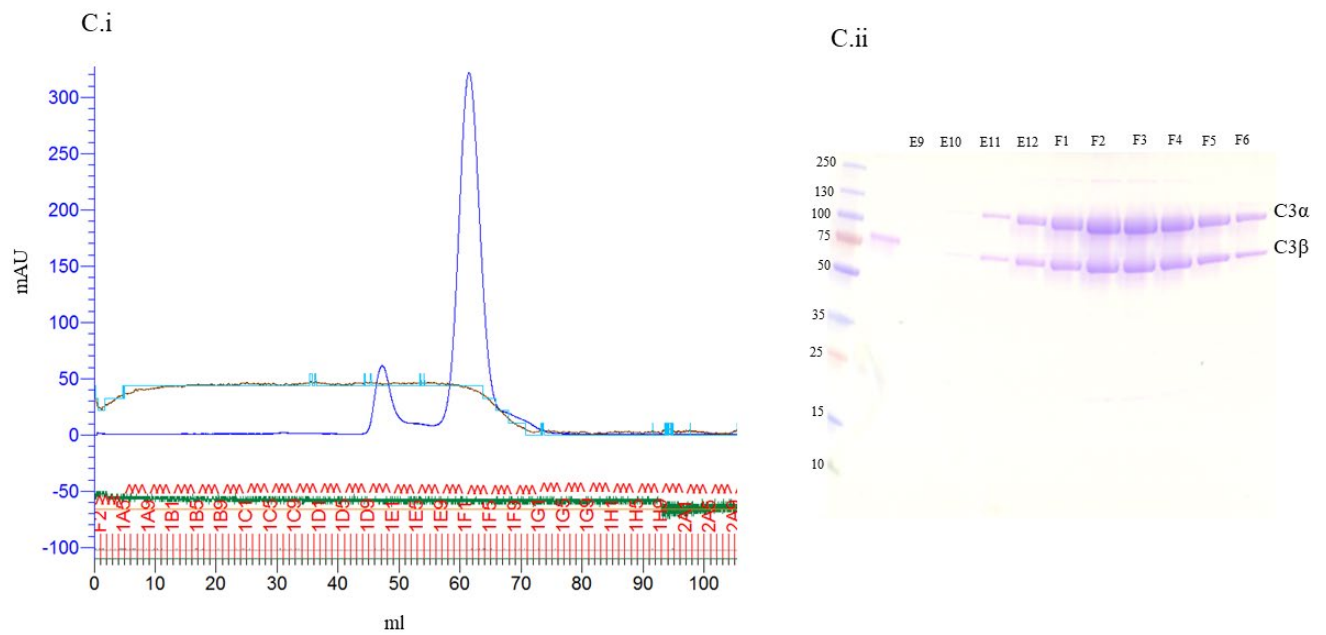
Figure 26 Purification of C3^{WT} protein.

Displayed are the Chromatographs (A.I), (B.I), (C.I) of the three stage C3^{WT} purification process. The Chromatograph display the uV peak (solid blue line, measured as mAU, red line shows conductivity, pink line shows gradient concentration). The peak fractions were ran on the corresponding 10% SDS Page gels (A.II, B.II,C.II) and Coomassie stained to visualise the fraction. Purified C3^{WT} can be seen in C.II.

3.4.3 Purification of C3^{L1109V}

A.I Anion exchange

A.ii
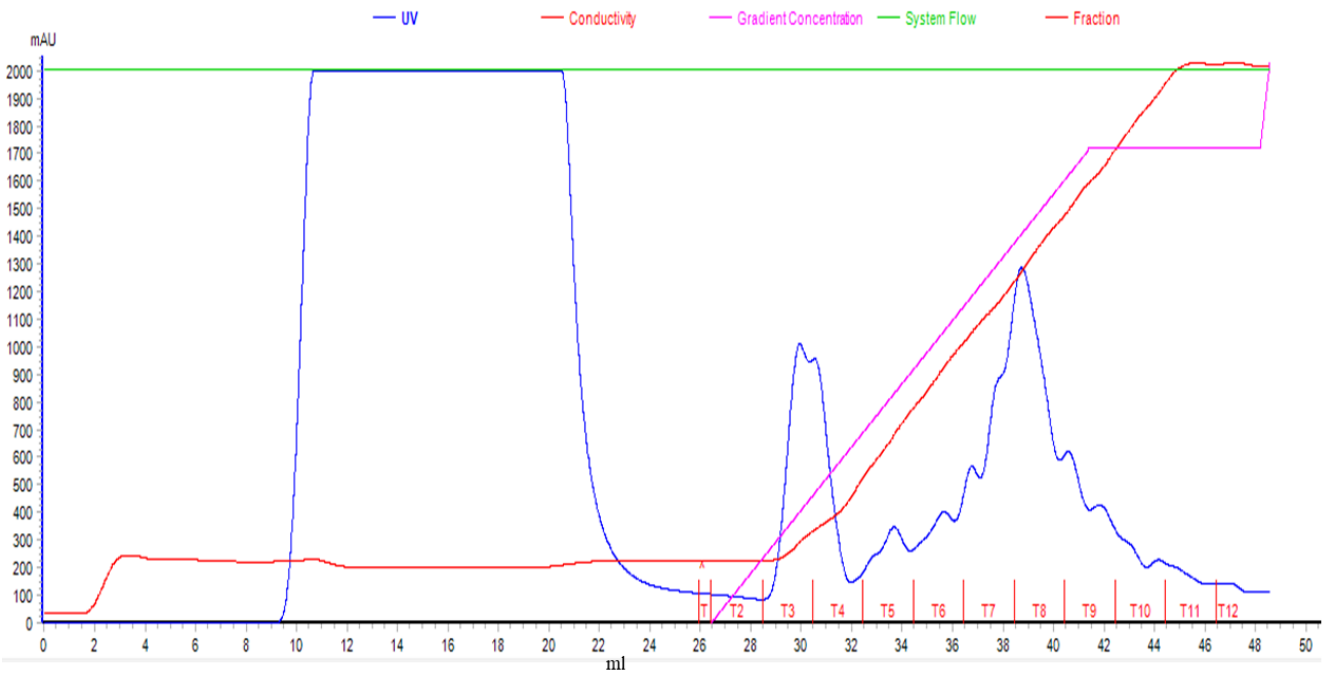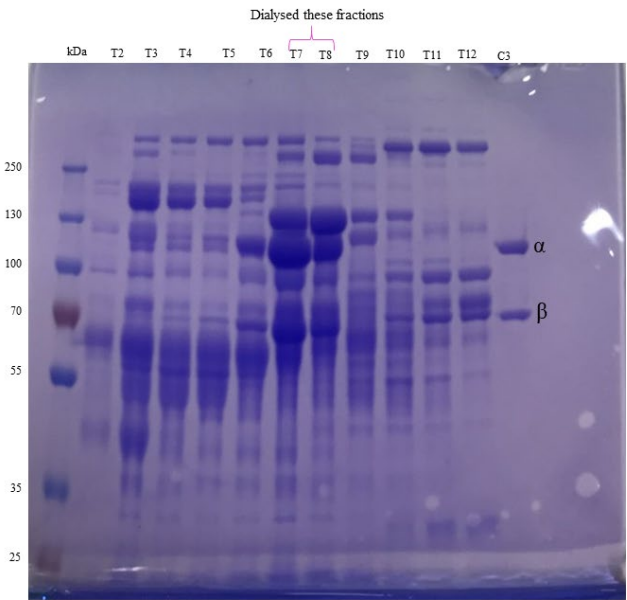
B.I Cation exchange
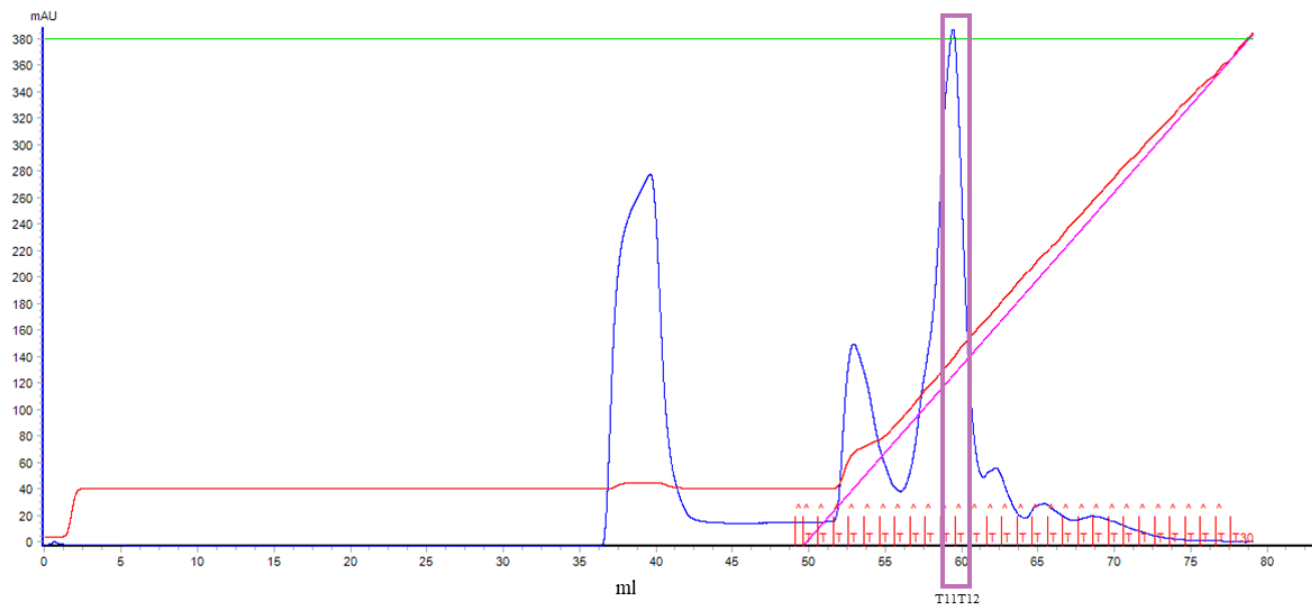
B.ii

Took these 2ml over Size exclusion column
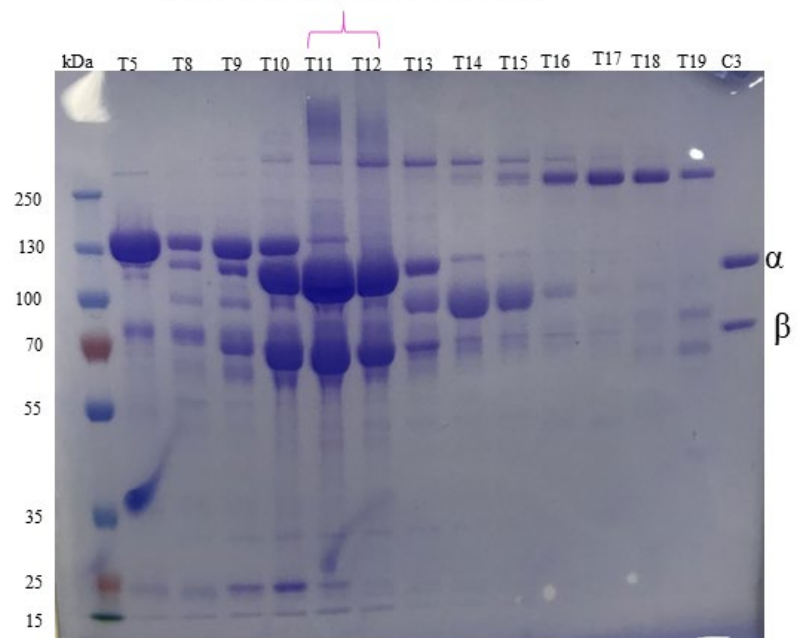
C.I Size exclusion chromatography
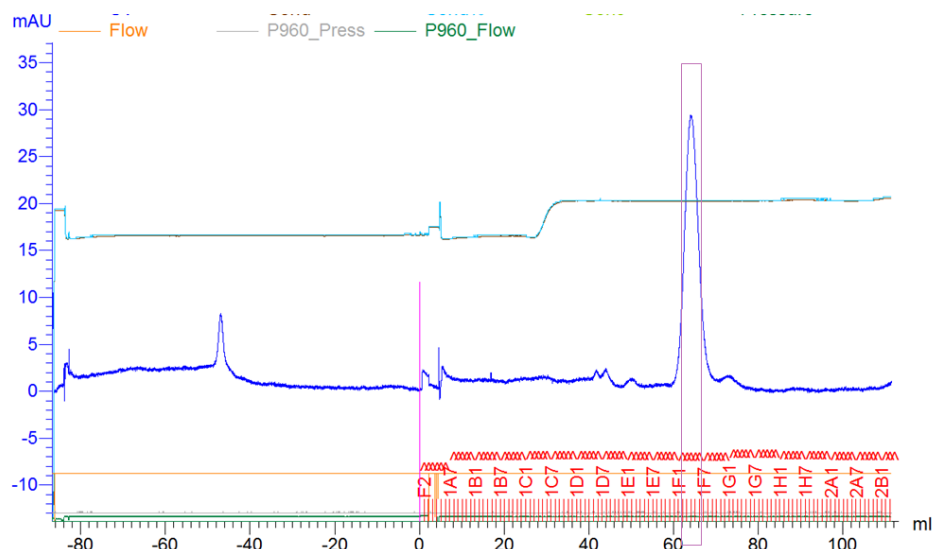
C.ii

Figure 27 Purification of C3 ^{L1109V} protein.

*9mls of whole blood was collected into EDTA and centrifuged at 2,000g for 15 minutes at 4°C. The C3 was then plasma purified as per methods section (**Human C3 protein purification**) Displayed are the Chromatographs (A.I), (B.I), (C.I) of the three stage C3^{L1109V} purification process. The Chromatograph*

72

display the uV peak (solid blue line, measured as mAU, red line shows conductivity, pink line shows gradient concentration). The peak fractions were ran on the corresponding 10% SDS Page gels (A.II, B.II,C.II) and Coomassie stained to visualise the fraction. Purified C3^{L1109V} can be seen in C.II.

3.4.4 Purified C3WT and C3 L1109V protein.

The sequential chromatography steps (anion exchange > cation exchange>gel filtration) resulted in purified $C3^{WT}$ (from healthy donor control) and $C3^{L1109V}$ as shown on the SDS page gel below. The purified protein then underwent methylamine treatment (see methods section 2.1.4) so it could be used for functional assays.
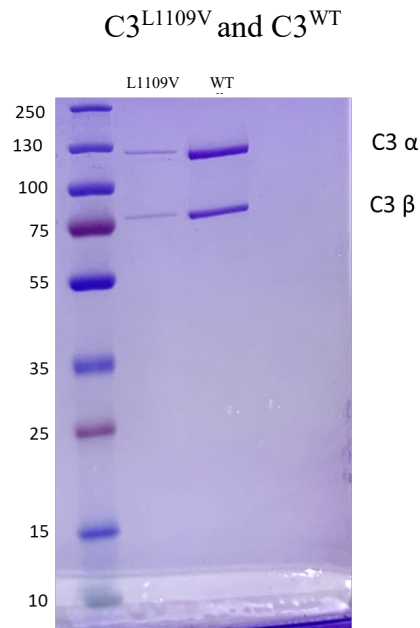
Figure 28: Purified C3 protein.
A 10% SDS-page gel is shown of purified C3L1109V and C3WT with no visible contaminants. The protein was reduced under standard reducing conditions to show C3b α (120kDa) and C3b β chains (75kDa) and stained with Coomassie reagent. A protein plus ladder was ran for reference with the size (kDa) of each fragment note on the left.

3.4.5 Co-factor activity assays
3.4.5.1 Co-factor activity assays using FH CCPs 1-4

First, we sought to test FH CCPs 1-4 co-factor activity. In this reaction, FH serves as a cofactor for FI mediated cleavage and inactivation of C3b. The assay sought to determine if $C3MA^{L1109V}$ showed a resistance to regulation by FH when functioning in the 'fluid phase' akin to its function in plasma *in vivo*. $C3MA^{WT}$ (1µg) or $C3MA^{L1109V}$ (1µg) were incubated with FI 50ng, and FH 1-4 250ng. The final reaction volume was made up to 30µl following the addition of PBS and this was then incubated at 37 °C in the water bath. At serial time points, 0, 5, 15, 30

minutes the reaction was terminated by the addition of 2xbME. The samples were reduced by boiling for 5 min, ran on a 10% SDS page gel and imaged following 1 hour of Coomassie staining and 1hr of de-staining. Densitometry analysis on the breakdown of the C3bα chain enables us to quantify and compare the % of C3b alpha chain remaining.
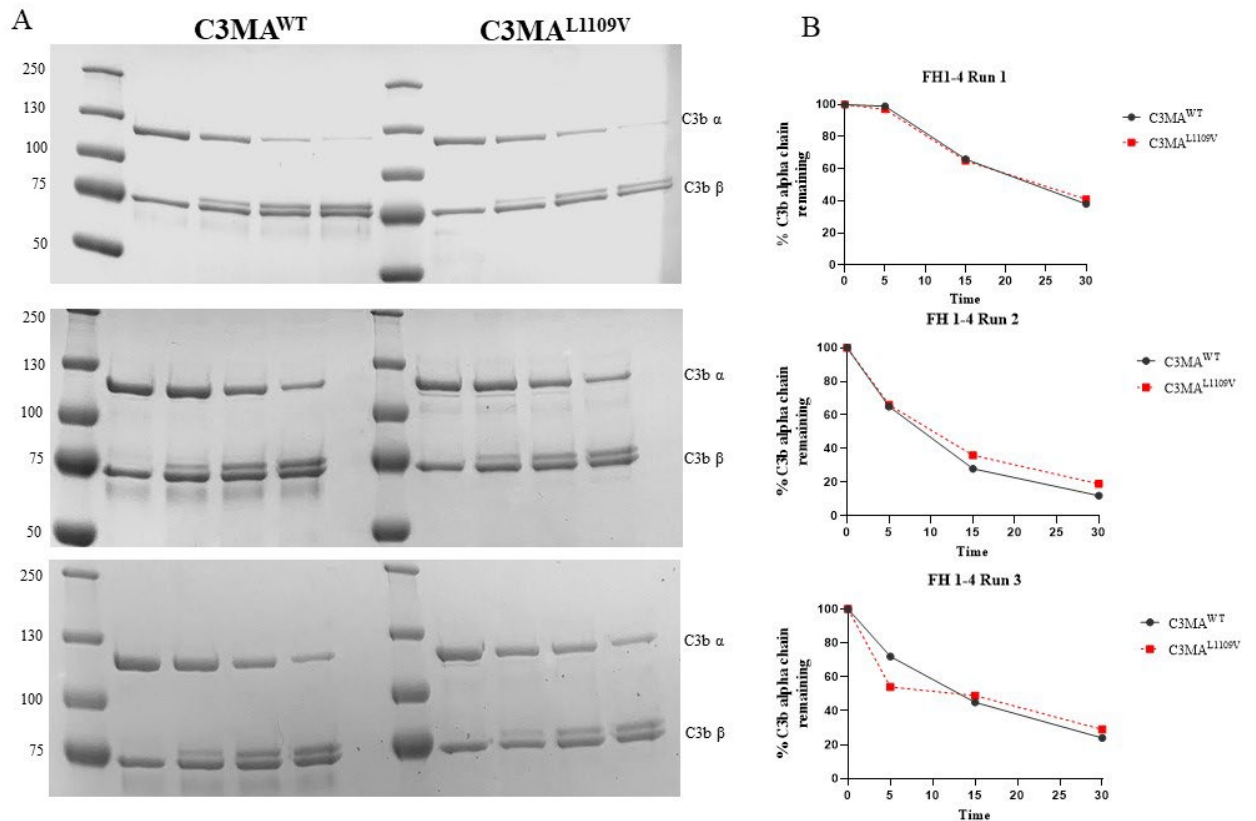
Figure 29: Co-factor fluid phase assays.

(A) 10% SDS page gel is shown and displays the terminated reaction at each set time point (0, 5, 15 and 30 minutes). (B) Densitometry analysis (measuring breakdown of the C3b α chain) of the co-factor activity of FH 1-4 was performed using Licor software (image studio) after import of gel images. Statistical analysis of the results was then carried out using Graph pad v.9

3.4.5.2 Average of Cofactor activity assays using FH CCPs 1-4

Following three repeats, the mean of each time point of the co-factor activity assay was taken, and directly compared for C3MA^{WT} and C3MA^{L1109V}. No statistical difference was found between C3MA^{WT} and C3MA^{L1109V}. This was as expected given the location of *C3*,p.L1109V and the assumption that binding of FH CCPs 1-4 would be unaffected.
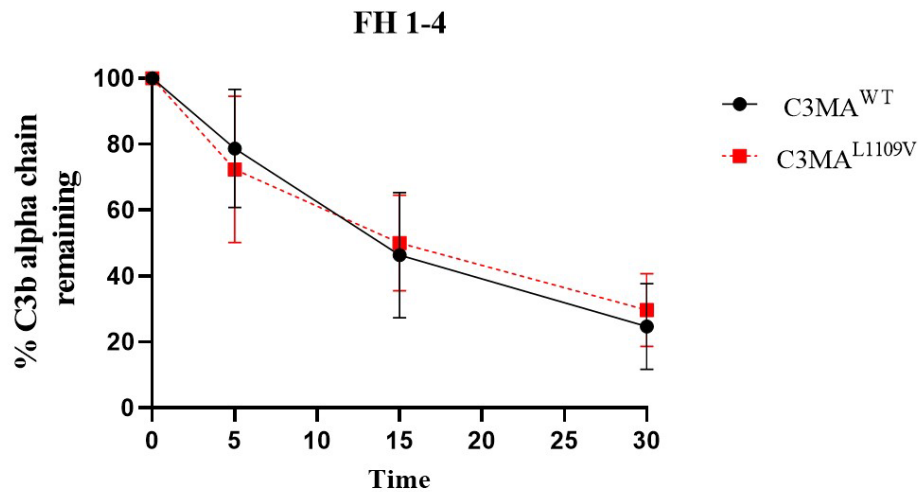
Figure 30. Average of the Cofactor activity assays using FH CCPs 1-4.
The cofactor activity assays were run three times using FH CCPs 1-4, and the mean densitometry of the 3 experiments of each time point are shown above with no significant difference between C3MA^{WT} and C3MA^{L1109V} when using FH CCPs 1-4 within the cofactor activity assay.

3.4.5.3 Co-factor activity assays using Full length FH

We next examined FLFH, to see if there were any differences between the ability of this to serve as a regulator in the fluid phase in concert with FI to regulate and inactivate $C3MA^{L1109V}$. As expected, there was no difference in the fluid phase co-factor assays using FLFH. This supports the FH CCP 1-4 data and is logical given we know FH fluid phase regulation is centred around its ability of CCPs 1-4 to bind to C3b and the L1109V variant is not located at this specific binding interface.
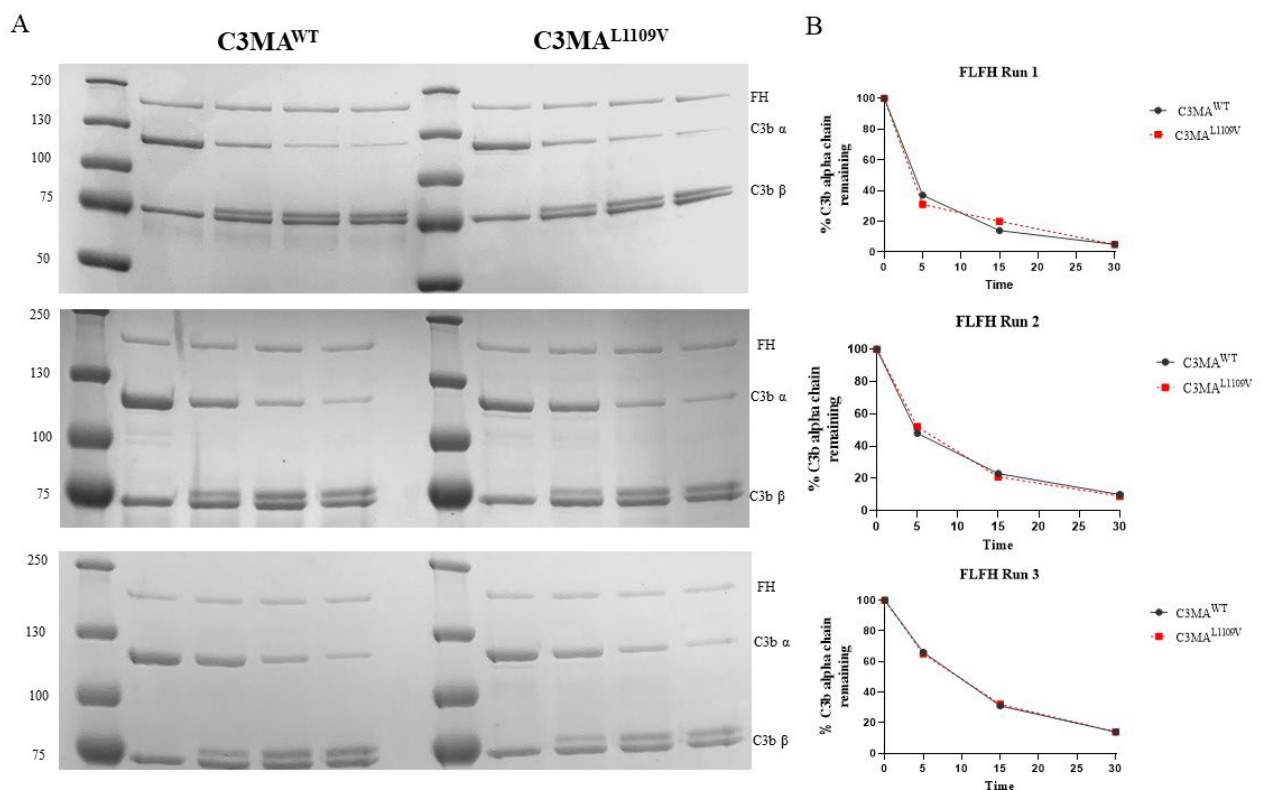
Figure 31 Cofactor activity assays using full length FH.
(A). 10% SDS page gel is shown, and displays the terminated reaction at each set time point (0,5,15,30 minutes).(B)Densitometry analysis (measuring breakdown of the C3b α chain) was undertaken in Licor image software studio after the gel images were imported and statistically analysed using Graph pad v.9 All 3 independent repeats of the assay are shown.

3.4.5.4 Average of cofactor activity assays using Full length FH

The mean densitometry of the three experiments for both C3MA^{WT} and C3MA^{L1109V} were directly compared, with no difference found in the breakdown of the C3b α between WT or the L1109V variant. Allowing us to assume, that C3MA^{L1109V} undergoes appropriate regulation by FH in the fluid phase when compared to healthy donor control.
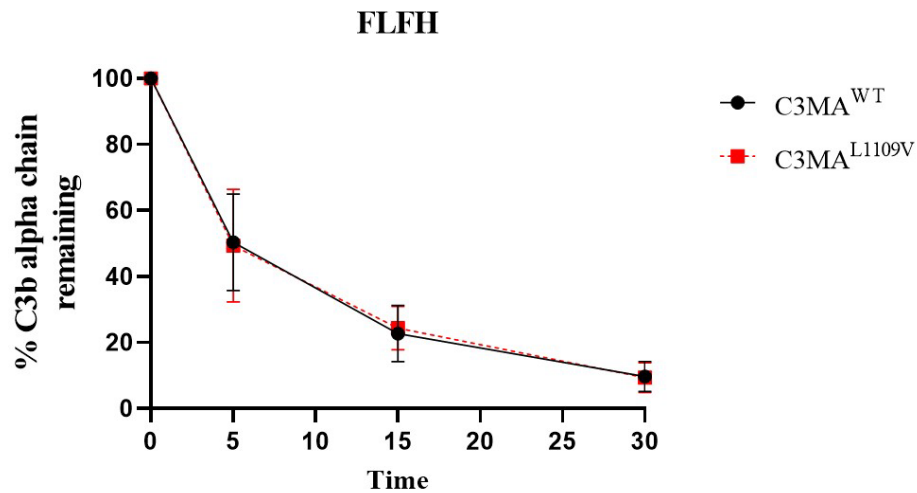
Figure 32 Average cofactor activity assay using Full length Factor H.

The mean densitometry of the cofactor activity assays of C3MAWT and C3MAL1109V with FLFH. The cofactor activity assays were run three times using FLFH, and the mean densitometry of the 3 experiments of each time point are shown above with no significant difference between C3MAWT and C3MAL1109V when using FLFH as a cofactor for Factor I mediated cleavage of C3b.

3.4.6 Evaluating cell surface regulation using Surface Plasmon Resonance

Given, C3MA^{L1109V} appears to undergo efficient regulation by FH in the *in vitro* fluid phase assays (binding of FH CCPs 1-4 appears unhindered), we next used SPR to mimic the *in vivo* interaction and regulation at the cell surface. This allows us to measure the binding affinity of FH CCPs 1-4, FLFH and FH CCPs 19-20, following the immobilisation of C3MA onto a CM5 chip.

3.4.6.1 Amine coupling of C3MAWT to CM5 chip.

Both C3MA^{WT} and C3MA^{L1109V} were immobilised onto a CM5 chip using the amine coupling method as described in methods (section 2.1.11)
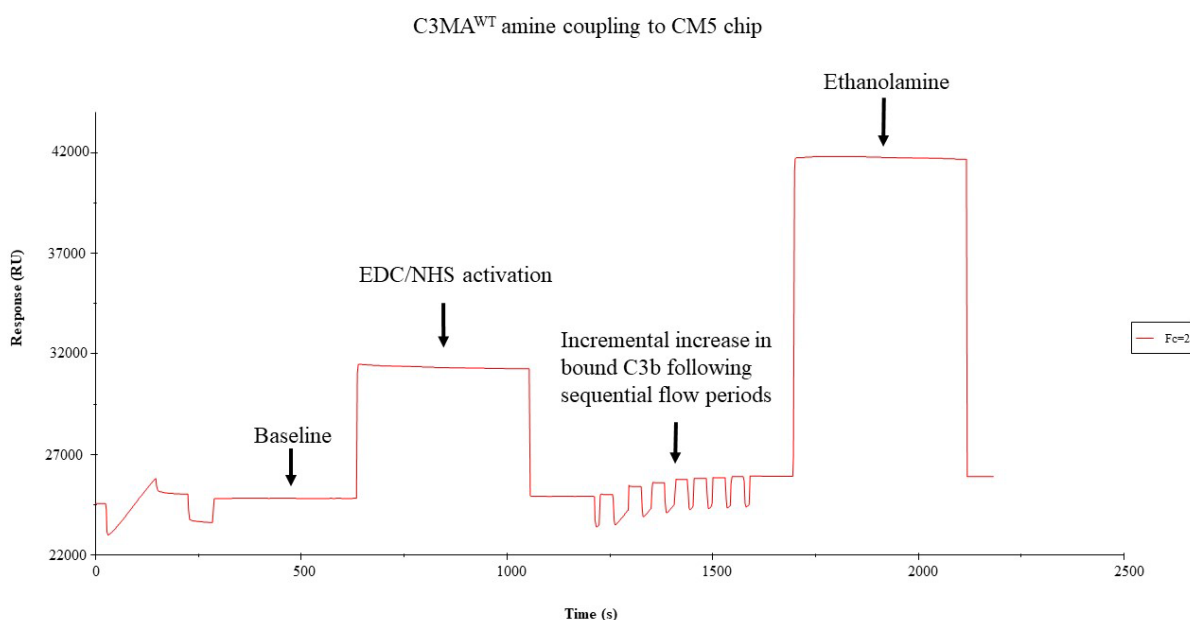
Figure 33: Amine coupling of C3MA^{WT} to a CM5 chip.

A sensorgram from BIAcore S200 BIAevaluation software showing immobilisation of C3MA^{WT} onto a CM5 chip through amine coupling. The RU is expressed on the y-axis and is calculated following the subtraction of the blank flow cell which is run simultaneously whilst the C3 is being immobilised onto the chip.

C3MA^{L1109V} amine coupling to CM5 chip
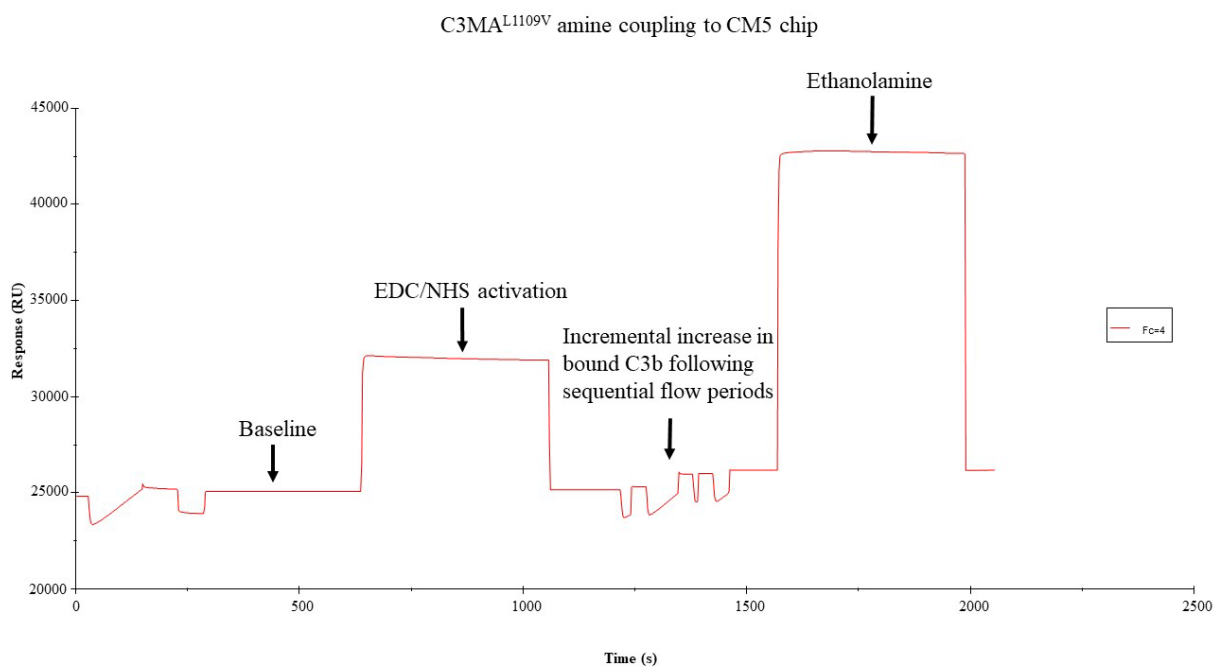
Figure 34 Amine coupling of C3MA^{L1109V} to a CM5 chip

A sensorgram from BIAcore S200 BIAevaluation software showing immobilisation of C3MA^{L1109V} onto a CM5 chip through amine coupling. The RU is expressed on the y axis following the subtraction of the blank flow cell.

3.4.6.2 Summary of RU achieved through amine coupling.

The 'response units' reflects the amount of ligand (C3MA^{WT} or C3MA^{L1109V}) that has been covalently bound to the CM5 chip. This was comparative for both ligands. We were then able to flow and measure the affinity of FH CCPs 1-4, FH CCPs 19-20 and FLFH to the immoblised C3MA on the chip, aiming to measure their affinity.

Table 14 Response units of bound C3MA^{WT} and C3MA^{L1109V} to the CM5 chip

C3MA^{WT}	1081.4
C3MA^{L1109V}	1104.1

80

3.4.6.3 Factor H CCPs 1-4 affinity with C3MA^{WT} and C3MA^{L1109V}

FH CCPs 1-4 was flowed across the immobilised C3MA, starting at a concentration of 20μM then followed by a serial dilution series (1:2), represented by each colour line displayed in the sensorgram graphs below. The K_D (measure of affinity) could be measured by the affinity calculation curve produced in the BIAevaluation (S200) software, with the K_D in μM being read at 50% of RU max (IC50). FH CCPs 1-4 had slightly lower affinity for C3MA^{L1109V} when compared to C3MA^{WT} (8.7μM vs 7.9μM, respectively), potentially this could translate into increased residency time on C3b that is deposited on a cell surface, diminishing the capacity of FH to release and interact with additional C3b/convertase molecules.

C3MA^{WT} FH CCP 1-4
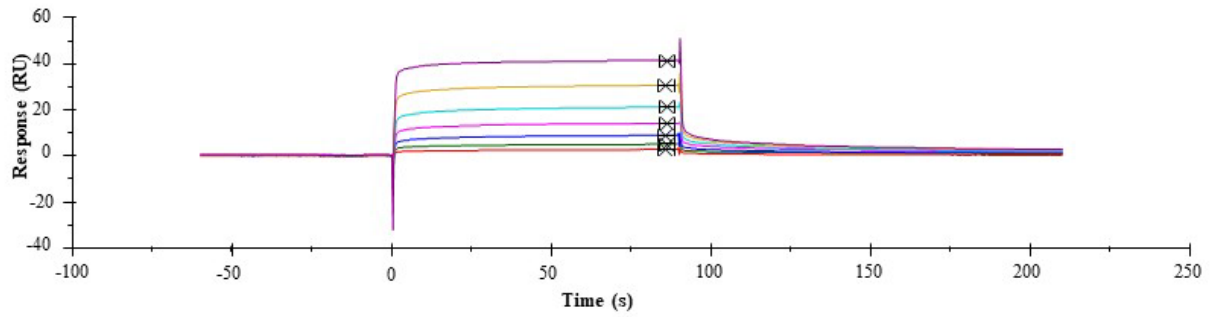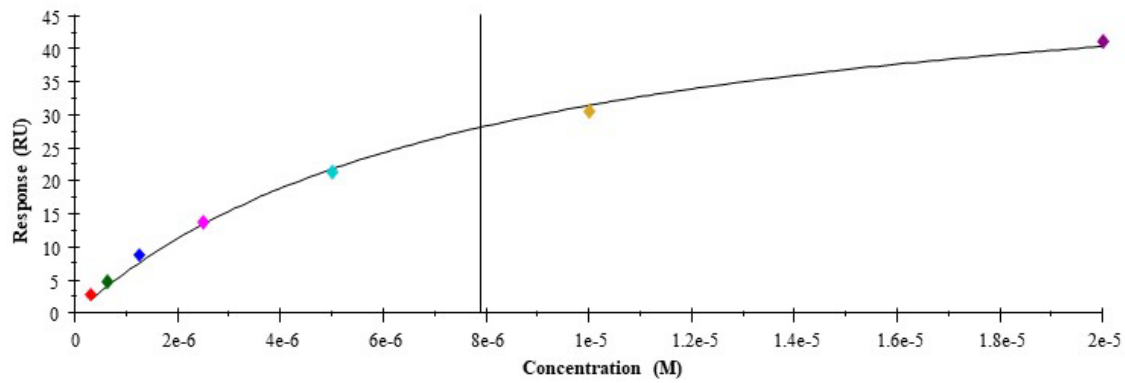
C3MA^{L1109V} FH CCP 1-4
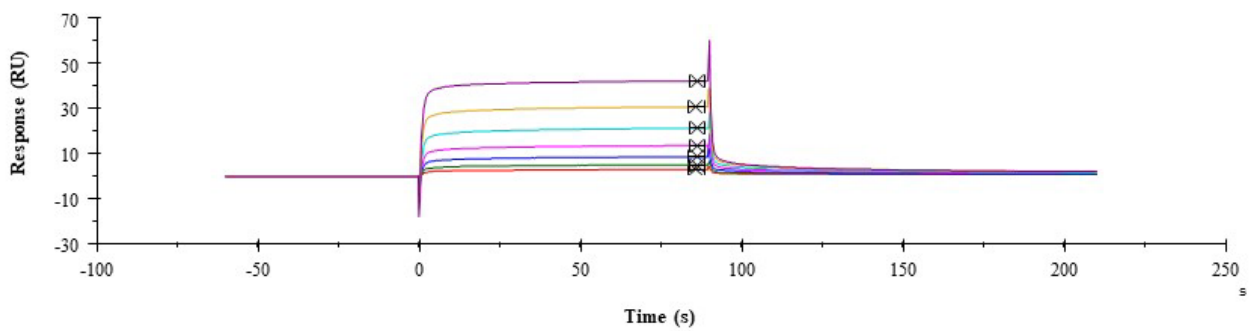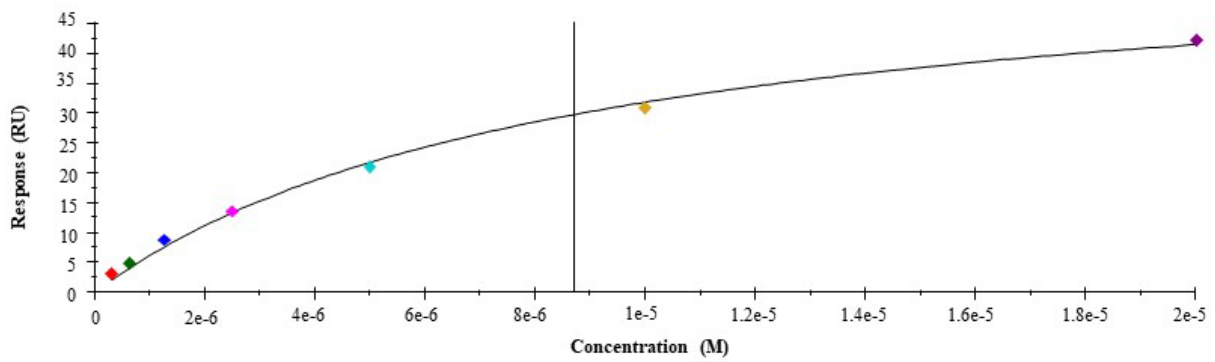
Figure 35 Factor H CCP 1-4 affinity with C3MA^{WT} and C3MA^{L1109V}

The 1st and 3rd graphs display Concentration (M) vs Response (RU) curves which calculates the dissociation constants at 50% maximal response within the BIAevaluation S200 software. The y axis shows the response (RU) after each injection of the serial dilution concentrations (M) on the x axis. The 2nd and 4th graphs are sensorgrams of steady state affinity of FH CCP 1-4 with C3MA^{WT} and C3MA^{L1109V}. FH CCP 1-4 were flowed across the immobilised C3MA CM5 chip, starting at a concentration of 20μM then followed by a serial dilution series (1:2), represented by each colour line on the sensorgram with the highest concentration giving the largest RU.

3.4.6.4 Factor H CCPs 19-20 affinity with C3MA^{WT} and C3MA^{L1109V}.

Based upon the current understanding of the pathogenesis of c-aHUS being due to impaired cell surface regulation, and given the mapped location of *C3*p.L1109V, we hypothesised that binding of FH CCPs 19-20 could be impaired. FH CCPs 19-20 was flowed across the immobilised C3MA (WT or L1109V) and we attempted to calculate binding affinity. This was achieved when measuring the K_D for C3MA^{WT} (10.1μM), but was not possible for C3MA^{L1109V} due to the absence of binding (estimated K_D 37.8μM). This key experiment shows that FH is therefore unlikely to bind efficiently to and regulate C3MA^{L1109V} at the cell surface due to the loss of binding at CCPs 19-20, consistent with current literature and confirming *C3*,p.L1109V to be a pathogenic variant associated with c-aHUS.
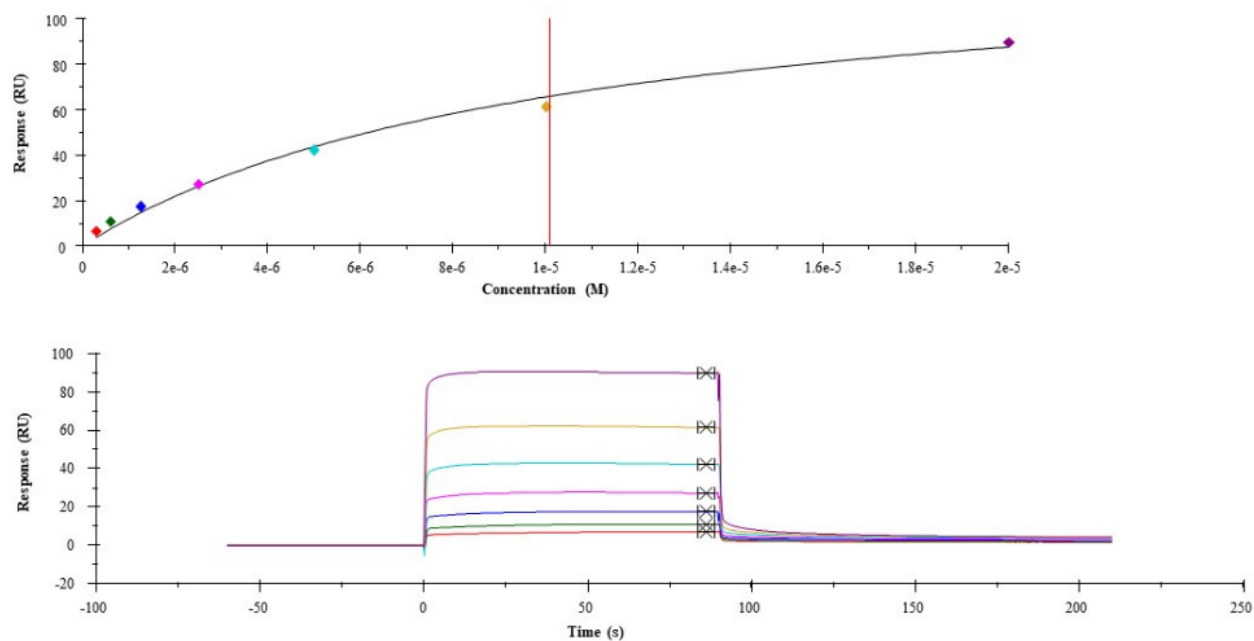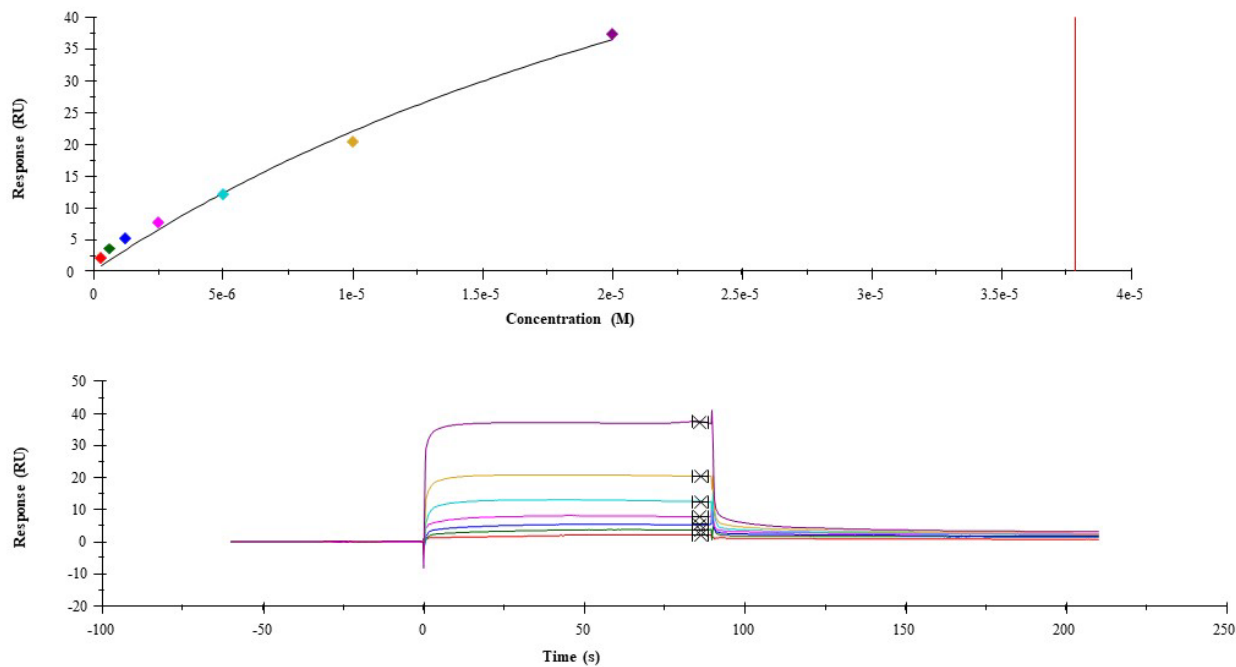
Figure 36 Factor H SCR 19-20 affinity with C3MA and L1190V C3MA.

The 1st and 3rd graphs display Concentration (M) vs Response (RU) curves which calculates the dissociation constants at 50% maximal response within the BIAevaluation S200 software. The y axis shows the response (RU) after each injection of the serial dilution concentrations (M) on the x axis. The

KD (measure of affinity) could be measured by the affinity calculation curve produced in the BIAevaluation (S200) software for C3MA^{WT}, but, not for C3MA^{L1109V} as the estimated KD was higher than the maximum concentration injected. The 2nd and 4th graphs are sensorgrams of steady state affinity of FH SCR 19-20 with C3MA^{WT} and C3MA^{L1109V}.

3.4.6.5   Full- length FH affinity with C3MA^{WT} and C3MA^{L1109V}.

To confirm the assertion, we measured the affinity of FLFH to both forms of C3MA. Given the two binding sites (CCPs 1-4 & CCPs 19-20), only an estimate of affinity can be calculated, as the reaction is not considered to be at a steady state. As anticipated, the higher K_D of C3MA^{L1109V} (2.17 µM compared to 1.44 C3MA$^{WT)}$) with FLFH reflects the loss of the binding avidity of FH CCPs 19-20. Additionally, the sensorgram visually depicts the lack of secondary binding with the tempered slope of the tail reflecting the more rapid dissociation to baseline RU in C3MA L1109V. This is further emphasised when directly comparing to FH CCPs 19-20 with the slope of the sensorgrams displaying the pattern of 'fast on, fast off' interaction.

C3MA^{WT} FLFH
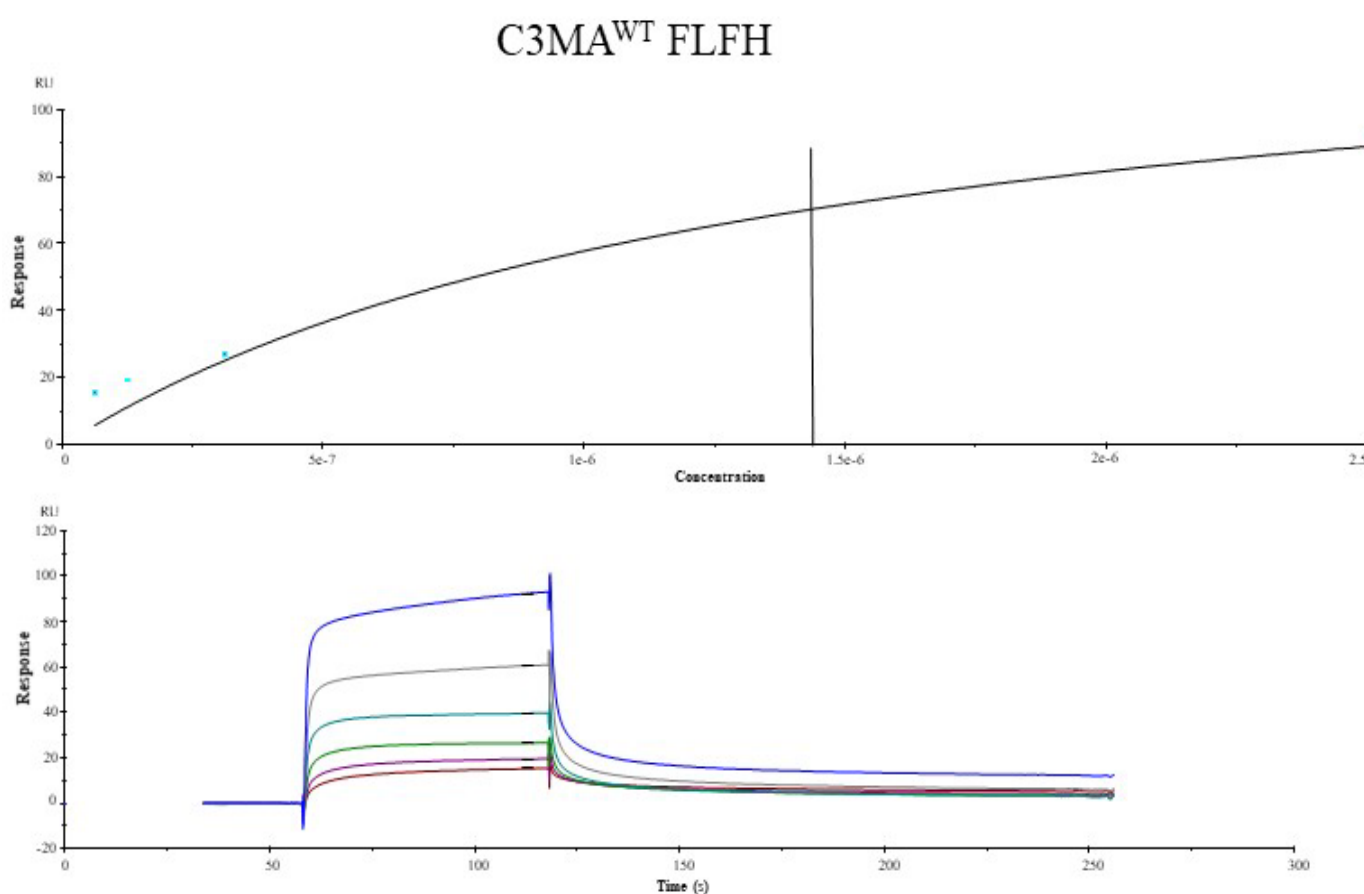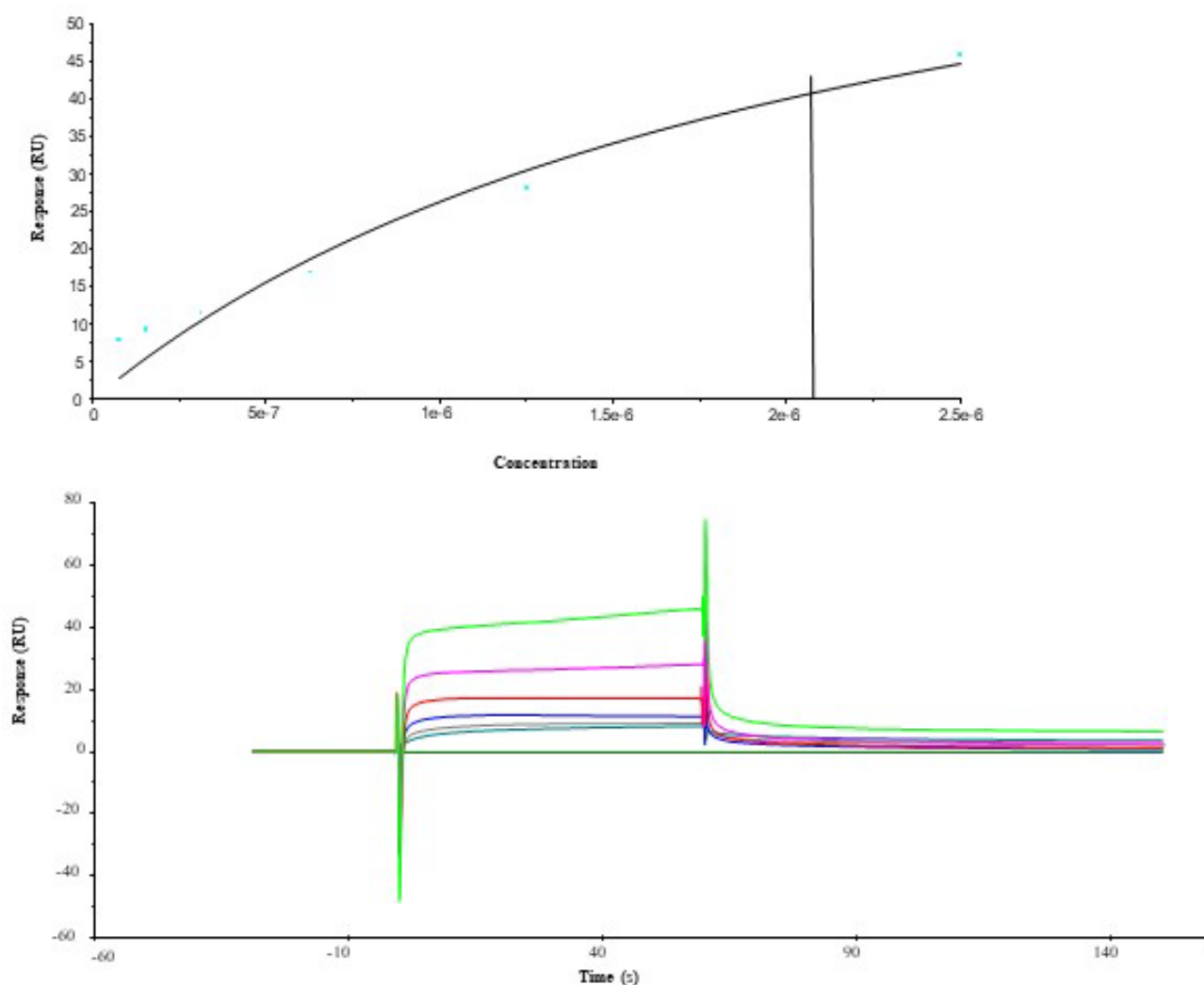
C3MA^{L1109V} FLFH

Figure 37 Full-length FH affinity with C3MA^{WT} and C3MA^{L1109V}.

The 1st and 3rd graphs display Concentration (M) vs Response (RU) curves which calculates the dissociation constants at 50% maximal response within the BIAevaluation S200 software. The y axis shows the response (RU) after each injection of the serial dilution concentrations (M) on the x axis. The K_D (measure of affinity) could be measured by the affinity calculation curve produced in the BIAevaluation (S200) software. The 2nd and 4th graphs are sensorgrams of the binding affinity of FLFH with C3MAWT and C3MAL1109V. The sensorgram shows the response on the y axis with time during the flow period on the x axis, with the highest concentration giving the highest response. Each concentration is represented by each individual colour line.

86

3.4.6.6 Building of the Alternative pathway regulatory Trimolecular complex

A novel method developed by Dr T Hallam allows the measurement of the alternative pathway regulatory trimolecular complex (TMC) building in real time (117). This assay incorporates FH, inactive FI and C3b and allows testing of FH, FI or C3 variants to enable functional characterisation of unknown variants. As shown in figure 38, no difference was detected in the amount of TMC built and bound when FH CCPs 1-4 was used. However, following injection of FLFH and inactive FI onto the C3MA^{WT}, this did result in an increased amount of TMC bound, illustrated by the higher RU peaks at each given concentration when compared to the mutant.

3.4.6.6.1 Trimolecular complex building with FH CCPs 1-4

C3MA^{WT} TMC FH1-4   C3MA^{L1109V} TMC FH1-4
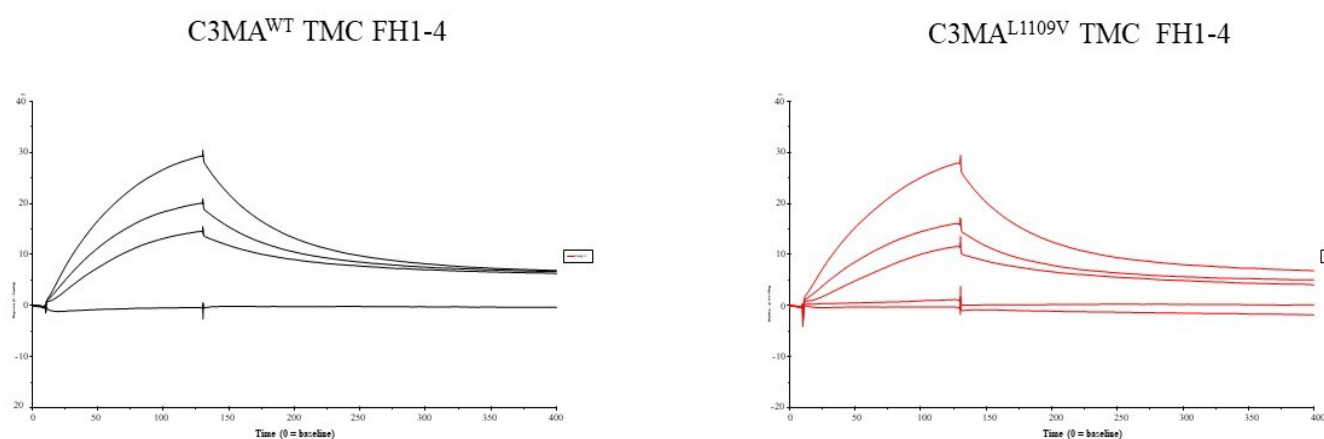
Figure 38 Trimolecular complex building using FH CCPs 1-4

Sensorgrams produced in the BIAevaluation S200 software following injection of decreasing concentrations of inactive FI and FH 1-4 CCPs onto a C3MA^{WT} or C3MA^{L1109V} coated chip. The highest concentration of inactive FI gives the largest response, reflecting the TMC being built and binding to the immobilised C3MA.

3.4.6.6.2 Trimolecular complex building with Full length FH
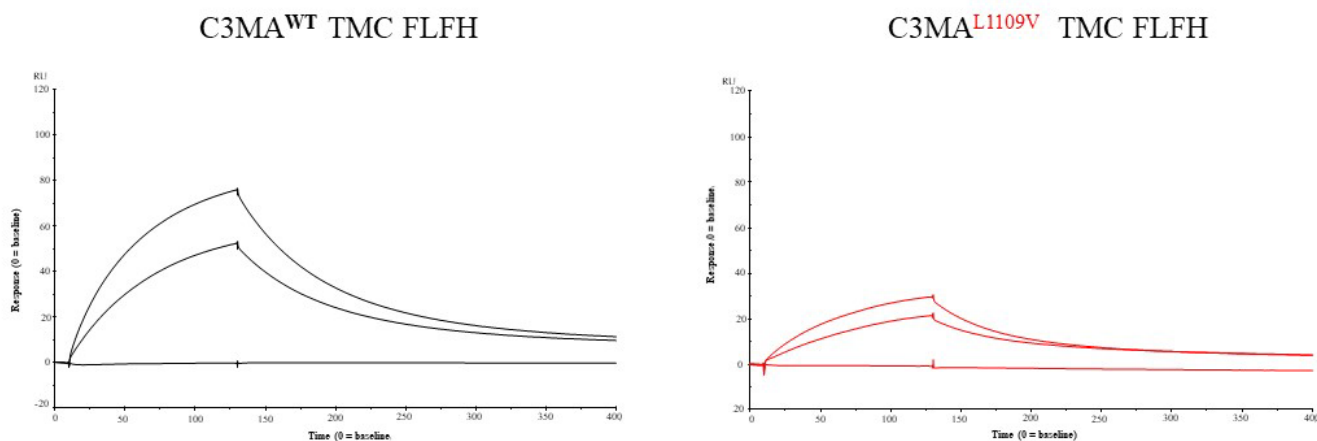
Figure 39Trimoelcular complex building with Full length Factor H

Sensorgrams produced in the BIAevaluation S200 software following injection of decreasing concentrations of inactive FI and FLFH onto a C3MA^{WT} or C3MA^{L1109V} coated chip. The highest concentration of inactive FI (125, 62.5, 31.25 nM) gives the largest RU response, reflecting the TMC being built and binding to the immobilised C3MA.

3.4.6.6.3 TMC building with C3MA^{WT} and C3MA^{L1109V} and FLFH

Overlaying the RU curves, clearly shows the C3MA^{L1109V} variant prevents the alternative pathway regulatory TMC domain from binding when compared to C3MA^{WT}, providing evidence that the variant would be resistant to inactivation by FI when FLFH is serving as its co-factor.
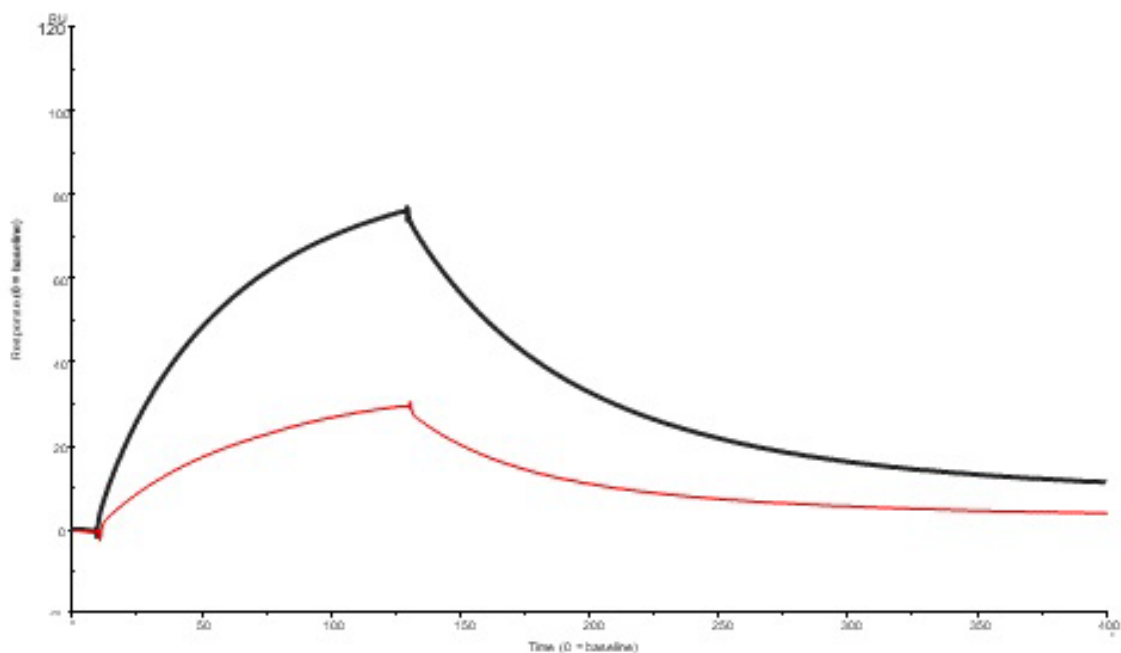
Figure 40 Alternative pathway regulatory TMC building on WT C3MA and L1109V C3MA amine coupled CM5 chip.
*Inactive FI and FLFH were injected onto a WT C3MA (**black line**) or L1109V C3MA (red line) coupled CM5 chip*

3.5 Discussion of Results

The location of the *C3*p.L1109V change in the thioester domain of C3d enabled us to hypothesise that fluid phase regulation would remain intact through normal binding of FH CCPs 1-4, but cell surface regulation would be impaired as the change is in the critical binding site of FH CCP 19 (as modelled in Figure 25 Trimolecular complex modelled in Pymol). The majority of FH variants associated with c-aHUS are located in the 'hot spots' of CCPs 19-20 (121), therefore the logic would imply that their mirrored counterparts in C3d would be pathogenic. Previous published work of recombinant C3 mutants located within the thioester-containing domain of C3b have consistently shown impaired FH regulation (59, 61) .

The co-factor assays support my hypothesis showing no difference in fluid phase regulation of C3MA^{L1109V} by FLFH or FH CCP 1-4 when compared to C3MA^{WT}, proving that binding of FH CCPs 1-4 in the fluid phase is unaffected by the point mutation in C3d.

I next modelled cell surface regulation in vitro using SPR and assessed real time binding of FLFH when C3MA is coupled to the cell surface. I was able to calculate the affinity to C3MA^{WT} of K_D 1.44 µM and C3MA^{L1109V} K_D 2.17 µM which is consistent with previous published work (122).

Interrogating this further, I examined binding of FH CCPS 1-4 and FH CCPs 19-20 separately. A marginal difference in FH CCPs 1-4 was observed (WT C3MA K_D 7.9 µM and L1109V C3ma K_D 8.7µM). In stark contrast, modelling cell surface regulation showed clear attenuation of binding of FH CCPs 19-20 to WT C3MA K_D 10.1 µM and L1109V C3MA estimated K_D 37.8µM. My FH CCPs 1-4 data reveals a slight increase in binding affinity (lower K_D) to C3MA compared to previous published work of FH CCPs 1-4 binding to human C3b (sourced from Comptech) (117, 122, 123).

Based upon previous crystollagropahy work, it is proposed that FH CCPs 19-20 can bind two C3d molecules simultaneously or one C3b and one C3d that are surface bound, with binding of C3d on the surface by CCP 20 a physiological substitution for binding to surface glycans when the density of C3b or C3d is high (60, 124). An absence of FH CCPs 19-20 binding to C3MA^{L1109V} would extend the actions of deposited C3b and prevent the inactivation and degradation of C3d, propagating ongoing complement activation and accelerating host tissue injury.

The attenuation of binding of FH CCPs 19-20 is further supported by the clear reduction in ability to build the TMC when FLFH is flown across the surface of C3MA^{L1109V} (35 RU) when compared to C3MA^{WT} (80 RU). The reduced efficacy (> 50%) to build the TMC implies that C3bL1109V would be protected from cleavage by FI as FH would not be available to serve as a co-factor on the cell surface. The resistance to complement regulation will result in a lack of C3b inactivation, increasing the chances of the C3 convertase formation and, thus complement activation on the endothelial cell.

The functional characterisation of L1109V clearly shows that FH does not bind this variant as well as wild type C3 and this will likely mean that the variant is resistant to regulation by FH.

3.6 Strength's and Limitations of Work

To our knowledge, this is the first functional study to demonstrate the rational for disease associated with L1109V and provide evidence as to why the variant could be resistant to complement regulation and thus a pathogenic variant in c-aHUS. Additionally, all functional assays were conducted from purified native proteins as compared to previous work on C3 mutations using recombinant protein, removing any doubt around potential altered glycosylation or structure that may arise from *in vitro* production methods (126). A limitation of this work is that we used C3MA as our 'C3b' like molecule. This is consistent with previously published work and C3MA still undergoes the same biological regulation as C3b. Whilst the SPR experiments are not affected by this as we measure K_D at 50% IC50 and we couple comparable amounts of C3MA onto the chip surface. The fluid phase assays maybe more susceptible as a proportion of the C3 prep may still have native C3 in the solution which will not interact with any ligand. To overcome this the native C3 was treated with methylamine to excess and both WT and L1109V were treated in identical conditions to enable consistency and relative comparability.

One limitation is that I did not assess the decay acceleration ability of FH upon C3 L1109V. The pathogenicity of this variant is surmised through binding analysis of my SPR experiments as we have shown no defect in decreased rate of C3b cleavage by FI, but it may lead to decreased dissociation *in vivo* by FH decay acceleration activity. We know FH forces Bb out from the bimolecular complex (C3b:FH) at a rapid rate whilst simultaneously binding to C3b.

In order to test the ability of it to irreversibly disassociate alternative pathway C3 convertase, I could measure on chip decay or SRBC (Sheep red blood cell) decay assays to prove the deficit in FH. Alternatively, we could use the purified C3 L1109V and incubate with GEnCs to see if the protein replicates the procoagulant phenotype produced akin to R139W.

3.7   Future Work

An alternative C3 mutation R138W found within the French cohort has interestingly shown that despite normal FH binding, pre-activated glomerular endothelial cells (GEnCs) incubated with R139W-C3 resulted in a hyperactive C3 convertase resulting in a procoagulant phenotype (hallmark signature of a TMA) of the GEnCs through increased release of C3a, C5a and higher expression of tissue factor (125). Future work using the GEnCs could determine if the C3 L1109V mutation affects the stability of the convertase and determine if it has an effect through an additional pathogenic mechanism.

From the data, we can confirm IM developed c-aHUS due to the C3 variant and withdrawal of complement inhibiting therapy carries a risk of relapse of disease. The patient has now entered the Stopping Eculizumab Treatment Safely in aHUS (SETS) trial.

In order to gain a greater understanding of how the effects of a hyperfunctional C3 acts *in vivo* we sought to model a point mutation in C3d in a mouse; investigating the effects of a gain of function mutation and enabling us to test targeted therapeutics.

Chapter 4   The $C3^{D1115N}$ mouse model of complement mediated- atypical Haemolytic Uraemic Syndrome

4.1   Introduction

Whilst previous mouse models of c-aHUS have been engineered around FH mutations and have therefore been loss of function, we sought to emulate disease based upon a C3 'gain of function' change. Whilst our *in vitro* work of *C3*,p.*L1109V* proposed a logical mechanism whereby disease could occur, an *in vivo* model would consolidate our findings and enable complement therapeutic testing. Whilst there are many C3 mutations linked to c-aHUS (59, 127), we opted for *C3*,p.D1115N. This was based upon a local family carrying the point mutation, its location within the C3 TED domain, and published work showing a reduction in the binding ability of MCP and FH (denoted previously as D1093N)(59). Previous work within the Complement therapeutics group had confirmed preservation between mouse and man and recombinant protein production proposed the variant to be pathogenic, thus we commissioned the mouse engineered using standard knock in techniques by Ozgene (Perth, Australia).

4.2   Hypothesis

- The *C3*,p.D1115N point mutation from man can be transferred to mouse and recapitulate the clinical disease found in man i.e. complement mediated atypical haemolytic uraemic syndrome.

4.3   Aims of chapter

- Characterise the phenotype of the *C3*,p.D1115N mouse (B6.C3^{D1115N}).

- If a thrombotic microangiopathy is identified, further validate the model by rescuing the phenotype with C5 genetic deletion or C5 therapeutic inhibition.

4.4 Results

4.4.1 C3^{D1115N} Newcastle Pedigree

The family carrying the *C3*p.D1115N had been cared for many years by the National aHUS Service. Interestingly, II.1 and II.3 had two distinct clinical courses. II.2 presented with End stage kidney disease at the age of 19, in the pre-Eculizumab era. During their third renal transplant (first two lost due to recurrent disease), Eculizumab became available. Unfortunately, they died aged 49 due to long standing complications of ESKD. II.3 presented with an AKI aged 43years, with a renal biopsy identifying a TMA upon the background of diabetic nephropathy. Unfortunately, they did not recover renal function and died most likely due to complications of longstanding diabetes. The family carried the change in heterozygosity. There was no identifiable trigger in either patient that pre-empted the clinical manifestation of disease.
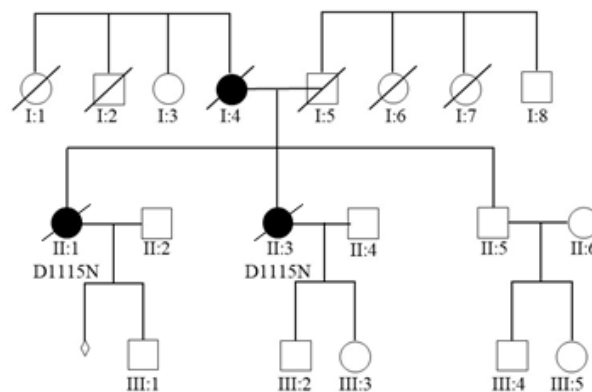
Figure 41 Pedigree of Newcastle family carrying the C3D1115N change.

A family pedigree with the solid black circles indicate the heterozygous carriers of the C3D1115N point mutation within the Newcastle family.
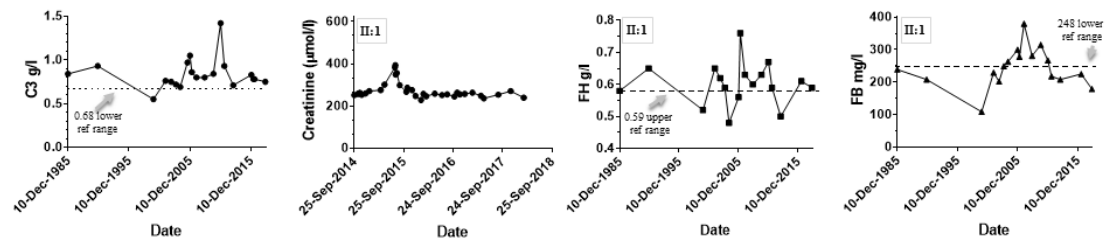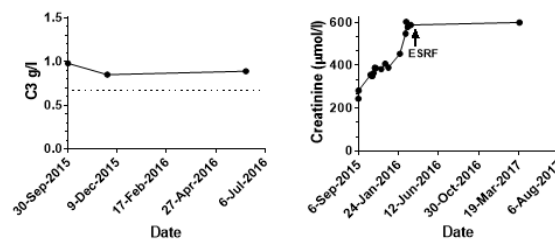
Figure 42 Complement levels and renal function of patients with C3,p.D1115N
Complement profiles and renal function of II:1 (top row) and II:3 (bottom row), as indicated and where available, dashed lines indicate upper or lower reference range as indicated on the graphs. Data obtained from routine clinical attendance and monitoring.

4.4.2 Crystal structure of FH CCP1-4, 19-20 and C3b illustrating the location of the C3^{D1115N} point mutation.

As with the *C3*,p.L1109V mutation, *C3*,p.D1115N sits snugly within C3d at the binding interface with FH CCP 19-20, illustrating this change may lead to a lack of binding of FH CCP 19-20 at the glomerular endothelial cell surface according to previously published results.
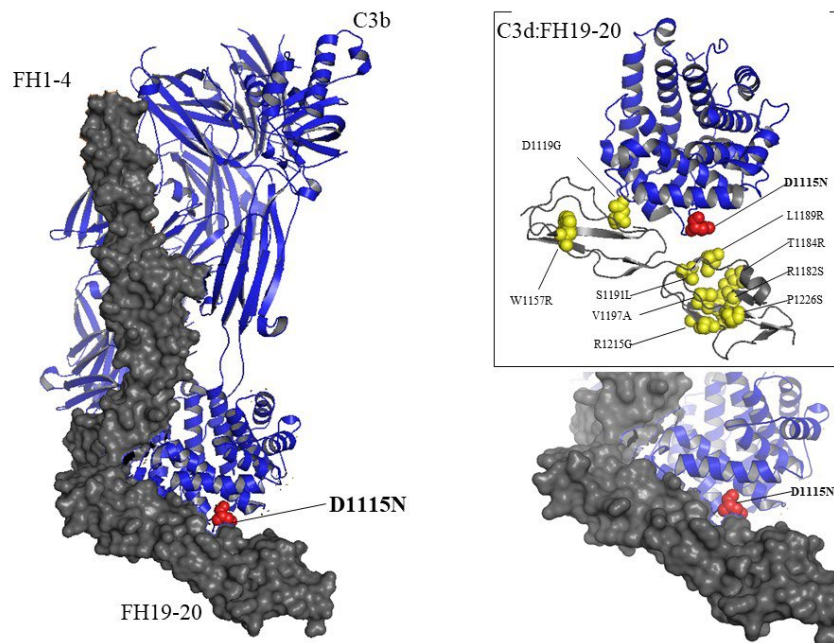
Figure 43 Location of the C3 mutation D1115N within C3b

A PyMOL figure of the crystal structure using 5o32 (CFI has been removed)(128). The structure show the complex of human C3b (blue ribbon) and human FH (CCPs 1-4 and CCPs 19-20 grey). The red spheres illustrate the location of *C3*,p.D1115N in the thioester domain of C3d. The boxed figure shows C3d(blue) with FH CCP 19-20 (grey)(figure generated in PyMOL using 3oXU (60) highlighting the *C3*,p.D1115N in red spheres and *CFH* mutations associated with c-aHUS in yellow spheres.

4.4.3 Genotyping of the B6.C3^{D1115N} mice

Mice were engineered under contract with Ozgene as per methods section and shipped to Newcastle, where heterozygote animals (B6.C3$^{D1115N+/-}$) were mated to generate the homozygote B6.C3^{D1115N}. Pups were ear clipped at weaning to enable identification and for genotyping. To begin with all B6.C3$^{D1115N+/-}$ and B6.C3^{D1115N} were monitored with daily weighing and clinical scoring to monitor for signs of disease.
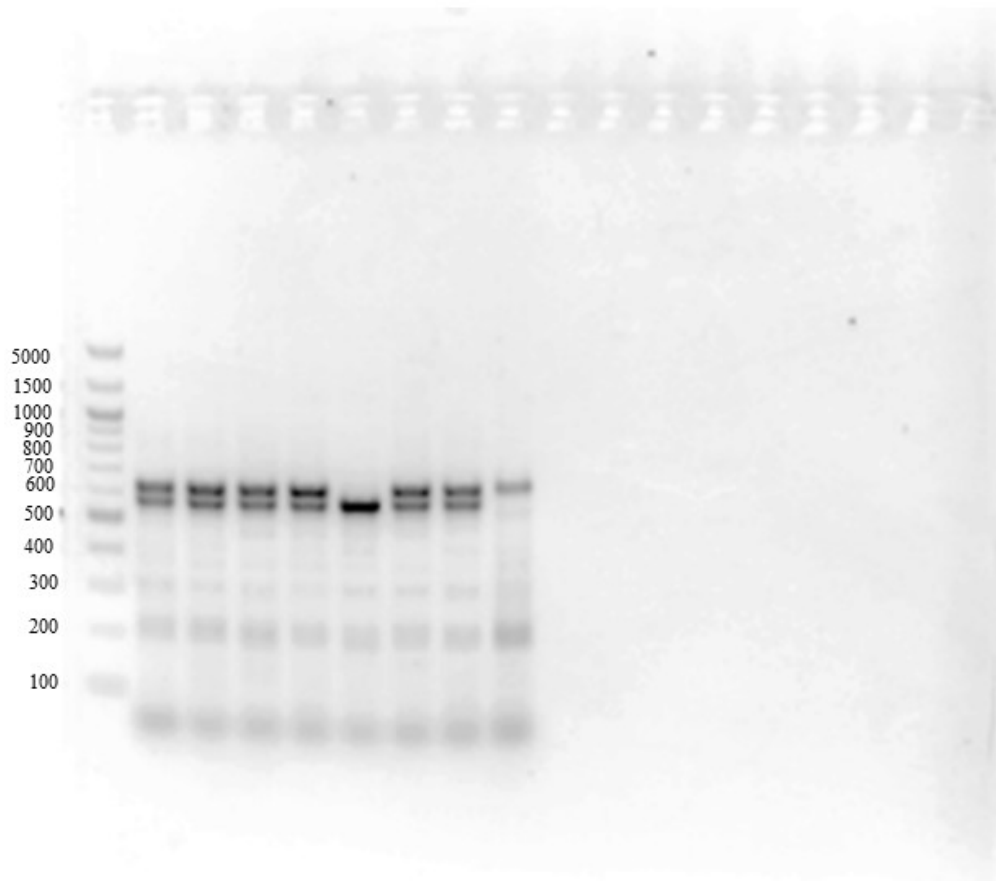
Figure 44. Genotyping of B6.C3^{D1115N} mice.

A representative 1.5% agarose gel with the PCR products obtained from the DNA of ear clipping. A 5KB DNA gene ruler is run on the first lane of the gel. B6.C3^{WT}(Wild type) mice showed a fragment at 574bp,B6.C3$^{D1115N+/-}$ (heterozygote) mice showed fragments 574 & 633bp and the B6.C3^{D1115N} (homozygote) mice a single fragment at 633bp.

4.4.4 Clinical evidence of renal disease measured through urinalysis

Typically, intrinsic kidney disease can present with an active urinary sediment (detection of proteinuria and haematuria on urinalysis). In a healthy state, the kidney should prevent protein from 'leaking' into the urine and no haematuria should be detectable. Evidence of either proteinuria or haematuria can be the first detectable evidence of kidney disease. We therefore collected the spontaneously voided urine from animals during daily weighing. I identified a proportion of the B6.C3^{D1115N} mice that spontaneously developed proteinuria and haematuria from approximately 21 days postpartum. On daily measuring, I found the proteinuria and haematuria could increment daily in combination with a reduction in the mouse's body weight. Following our clinical scoring system in methods (Figure 15 Mouse Body condition score)., the mice had to be euthanised once they reached a certain score as set out within our Home office licence.
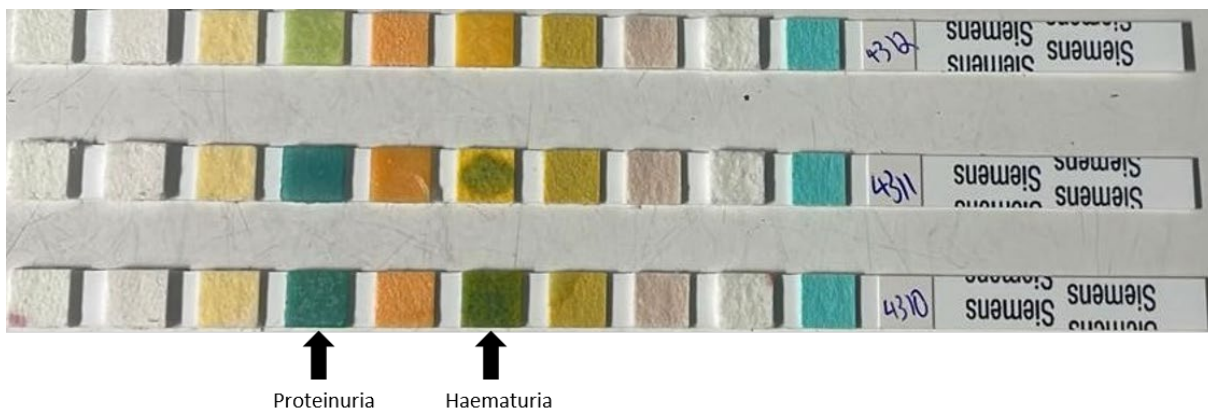
Figure 45 Siemens urinalysis strips of urine mice monitoring.

An example of three mice that had urinalysis monitoring, Mouse 4312 (top strip) showed no evidence of proteinuria or haematuria as per the green and yellow boxes. Mice 4310 and 431 show detectable proteinuria and haematuria. Other indicators on strip not routinely used.

4.4.5 Quantification of Proteinuria and Haematuria

I was able to quantify the proteinuria and haematuria and show the B6.C3^{D1115N} had significantly higher amounts of both proteinuria and haematuria on voided urine. This was our 'best' preliminary bench side test to show the animals were developing a spontaneous renal disease.
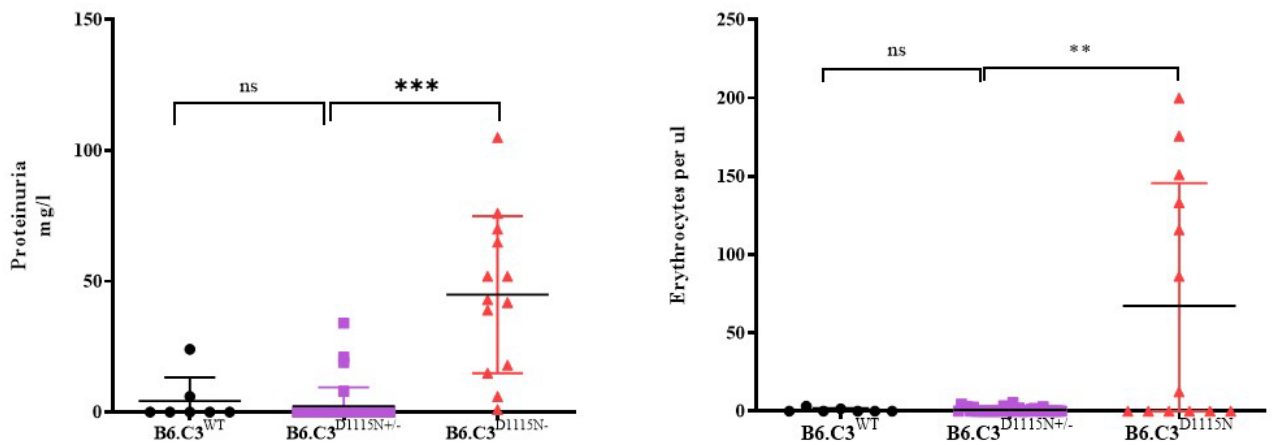
Figure 46 Quantification of proteinuria and haematuria in the B6.C3^{D1115N} mice.
Significant proteinuria and haematuria were detected in a proportion of the B6.C3^{D1115N} mice suggestive of glomerular disease. B6.C3^{WT} (wild type) N= 7, B6.C3$^{D1115N+/-}$ (heterozygote mice) N=36, B6.C3^{D1115}N (homozygote mice) N=13. Analysed using unpaired test with Welch's correction, Mean ± SEM, ns non significant, ** P<0.01, *** P<0.001.

4.4.6 Survival analysis of the B6.C3^{D1115N}

Our overall survival analysis found the B6.C3^{D1115N} had a significantly increased mortality compared to the B6.C3^{WT} and B6.C3$^{D1115N+/-}$. The increased mortality appeared most likely within the first 50 days of life, but animals could still succumb to disease as they aged.
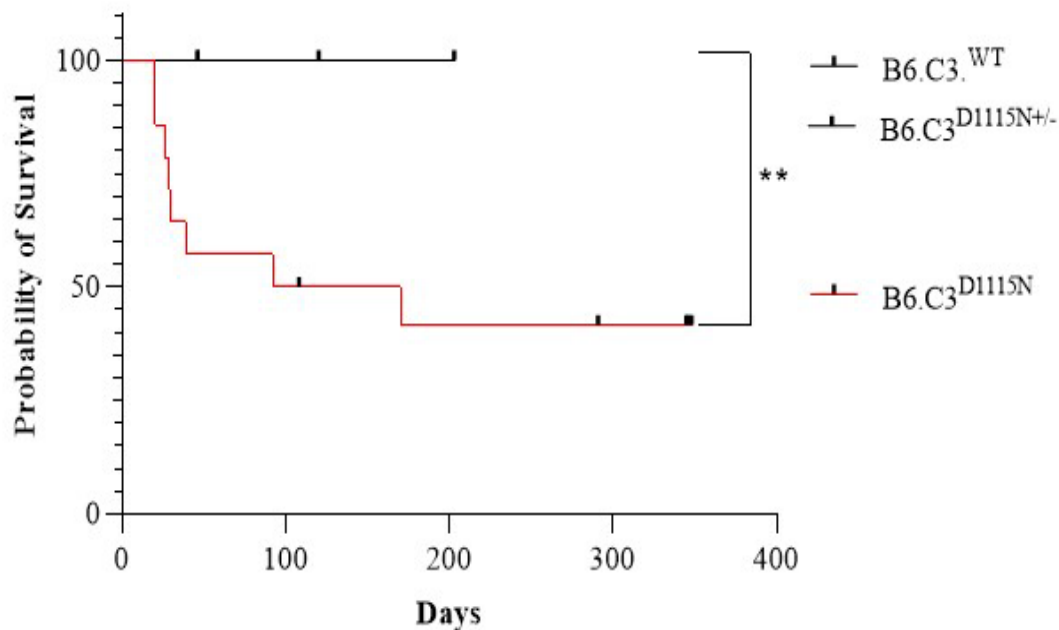
Figure 47 Survival curve for B6.C3^{D1115N} mice.
*The B6.C3^{D1115N} (N=14) showed a significantly increased mortality compared to their heterozygote (B6.C3$^{D1115N+/-}$ N=4) and wild type (B6.C3^{WT} N=10) counterparts. Kaplan-Meier survival curve analysis, ** P<0.01.*

4.4.7 Assessment of renal function in the B6-C3^{D1115N}

Following terminal cardiac puncture, we were able to analyse whole blood to measure BUN levels, which is a surrogate marker of kidney injury. Significantly, elevated levels of BUN were identified within the B6.C3^{D1115N} mice, substantiating that the detected proteinuria and haematuria were in keeping with a kidney disease.

BUN
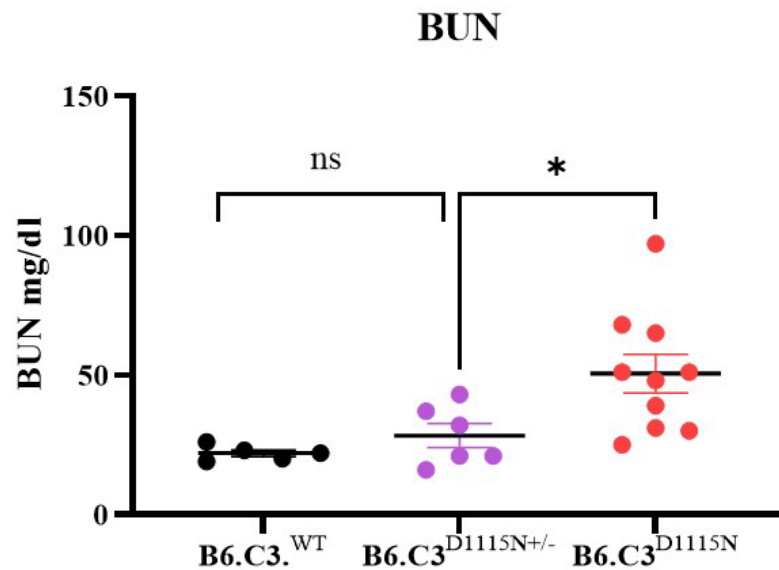
Figure 48 Assessment of renal function in B6.C3^{D1115N} mice.

BUN levels were significantly elevated in the B6.C3^{D1115N} mice when measured in whole blood (analysed on an iSTAT machine using a Chem8+ cartridge) following terminal cardiac puncture, reflecting an underlying renal impairment within the mice. B6.C3^{WT} (wild type) N=5, B6.C3$^{D1115N+/-}$ (heterozygote)N=6, B6.C3^{D1115N} (homozygote) N=10. Mean ±SEM. Analysed using unpaired t-test with Welch's correction.   ns non-significant, *P<0.05.

4.4.8   Evidence of MAHA in the B6-C3^{D1115N} mice

Given the B6.C3^{D1115N} mice were requiring euthanasia due to health concerns, and I had evidence of a kidney disease based upon an active urinary sediment and elevated BUN levels. I next sought to determine if the animals had a microangiopathic haemolytic anaemia. A clinical hallmark of c-aHUS. Haemoglobin level were measured from whole blood; whilst I did not achieve a statistical difference between the three groups of mice, I did identify that mice with higher BUN levels had lower Haemoglobin levels, suggesting the 'sickest' mice were anaemic i.e. BUN 97mg/dl, Haemoglobin 8.5g/dl.
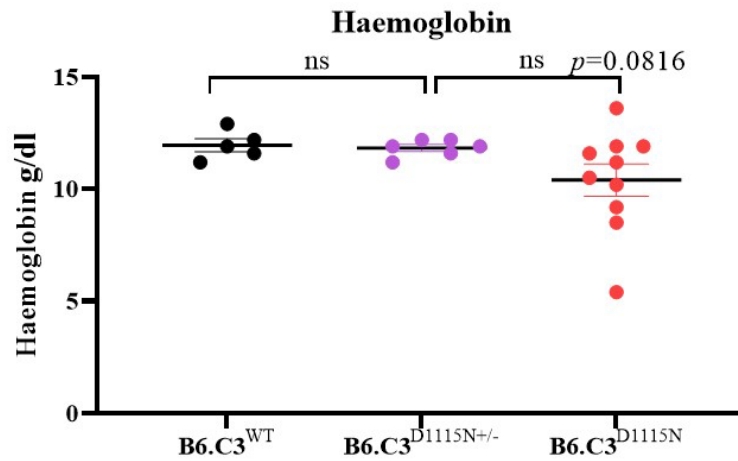
Figure 49 Haemoglobin levels in the B6.C3^{D1115N} mice.

Haemoglobin levels were measured from whole blood taken from mice during terminal cardiac puncture and analysed using a Chem8+ cartridge on an ISTAT device. B6.C3^{WT} (wild type) n=4, B6.C3$^{D1115N+/-}$ (heterozygote) n=6, B6.C3^{D1115N} (homozygote) n=10. Mean ±SEM. Analysed using unpaired t-test with Welch's correction.   ns non significant.
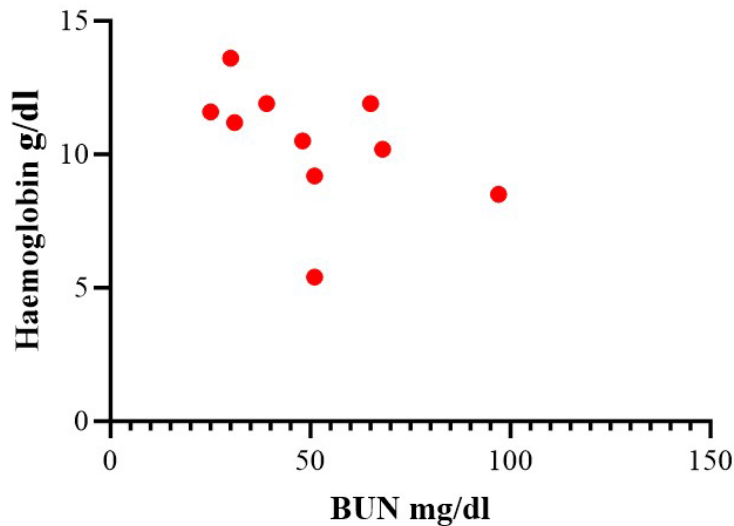
Figure 50 Correlation analysis between haemoglobin and BUN levels in the B6.C3^{D1115N} mice

A correlation analysis was undertaken finding a correlation coefficient of -0.5915 in keeping with one variable increasing (BUN) as the other decreases (Haemoglobin) in the B6.C3^{D1115N} N=10. Spearman R correlation analysis.

4.4.8.1 Evidence of schistocytes on peripheral blood film

I next examined a proportion of the B6.C3^{D1115N} that were anaemic and prepared peripheral blood films from mouse plasma. I found evidence of schistocytes (fragments) on the bloods films, suggesting the mice were haemolysing.
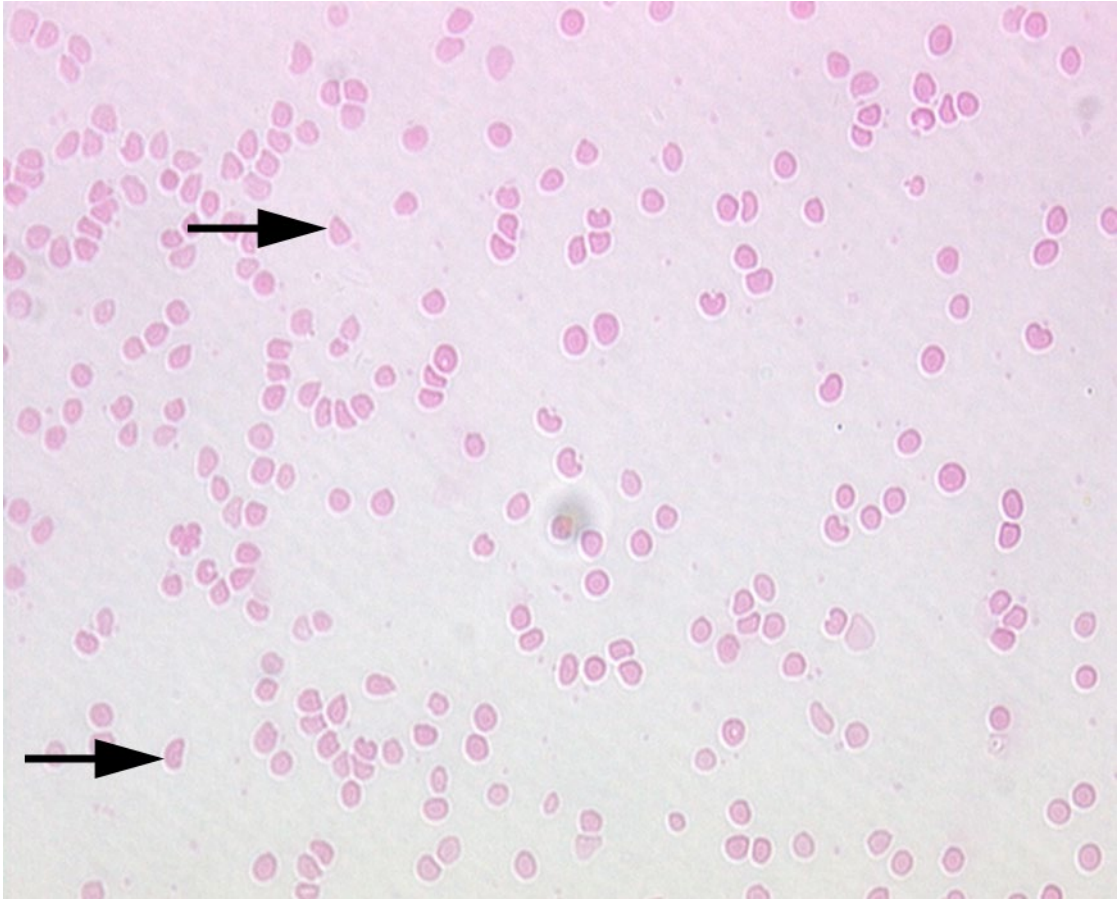
Figure 51 Evidence of haemolysis on blood film analysis in the B6.C3^{D1115N}.
Evidence of fragmented red blood cells (schistocytes) highlighted by the black arrows, indicating the red blood cells are sheared as they flow across the damaged glomerular endothelium. Representative of N=15 examined from the B6.C3^{D1115N} mice. Image taken at x40 magnification.
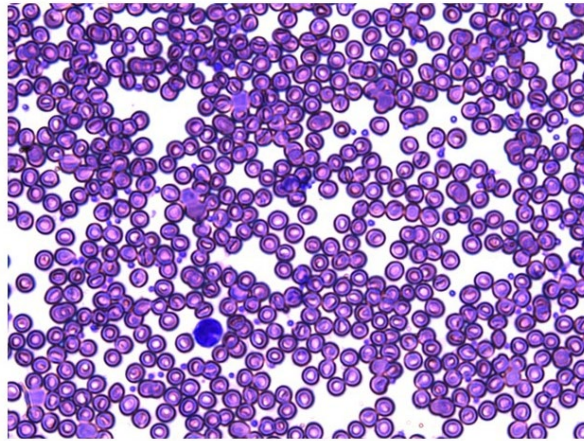
Figure 52 Blood film from a C57BL/6 mouse
Normal morphology of red blood cells shown. Small darker spots are platelets. Image taken at x40
Magnification.

4.4.8.2   Increased reticulocyte count in the B6.C3^{D1115N}

To further investigate, I measured the reticulocyte counts by an assay developed by Dr P Walsh (Complement therapeutics group). Reticulocytosis can help to differentiate the causes of anaemia, with a reduced count reflective of bone marrow failure or an increased count being an appropriate response to an anaemia. An increased reticulocyte count is in keeping with haemolytic anaemia and we did find evidence of this in the B6.C3^{D1115N} mice. Allowing me to surmise, that in a proportion of the B6.C3^{D1115N} mice that were anaemic, they had evidence of haemolysis on blood films and increased reticulocyte counts, collectively in keeping with a MAHA.
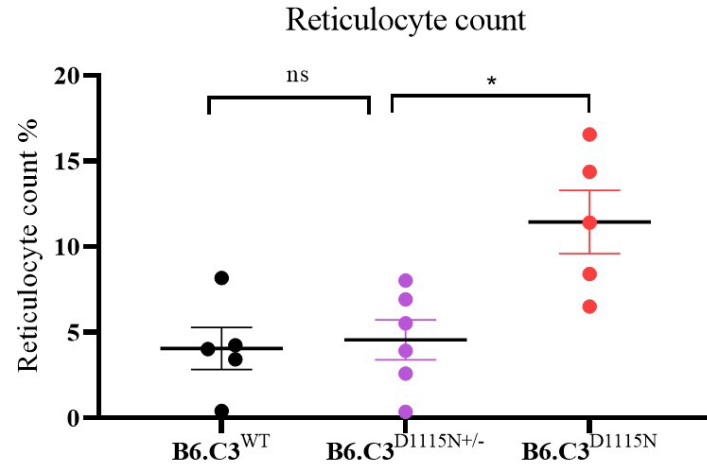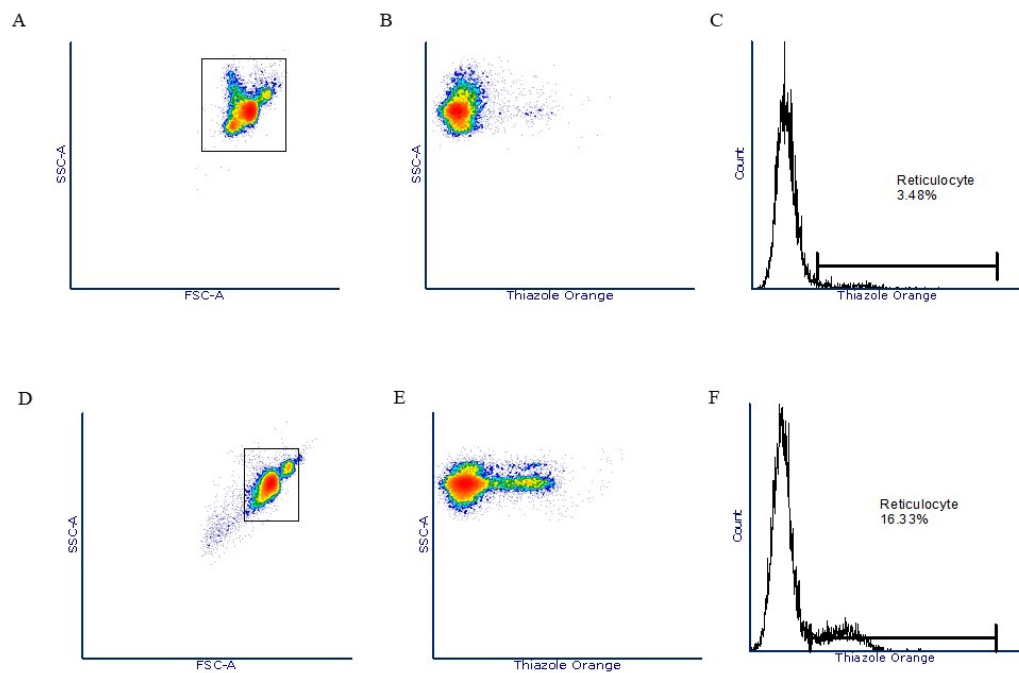
Figure 53 Increased reticulocyte count in the B6.C3$^{D1115N.}$ mice.

*Representative images of FACS analysis of a C57BL/6 wild type mouse (**A-C**) compared to an increased reticulocyte count in a B6-C3^{D1115N} (**D-F**). The B6.C3^{D1115N} had significantly higher reticulocyte count compared to B6.C3$^{D1115N+/-}$ as shown in the graph below the FACS analysis. . B6.C3^{WT} (wild type) n=5, B6.C3$^{D1115N+/-}$ (heterozygote) n=6, B6.C3^{D1115N} (homozygote) n=5. Mean ±SEM. Analysed using unpaired t-test with Welch's correction. ns non significant, *P<0.05.*

4.4.8.3 Reduced platelet counts in the B6.C3^{D1115N}

To complete the haematological assessment of the mice, I measured platelet counts from whole blood. As expected, B6.C3^{D1115N} had lower platelet counts compared to their control counterparts. The low platelet count is hypothesised due to consumption within the thrombi of theTMA.
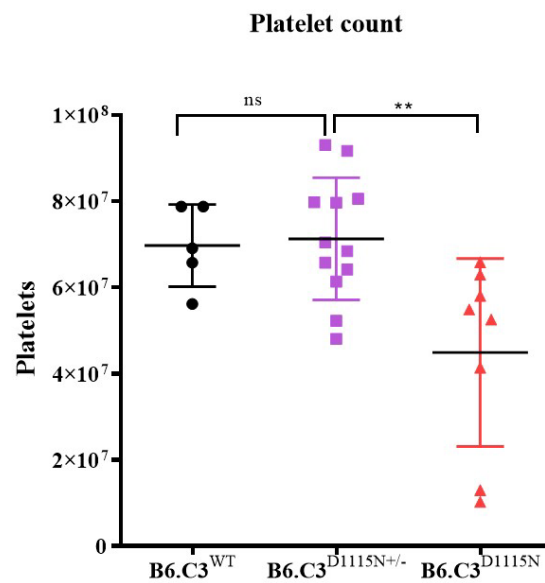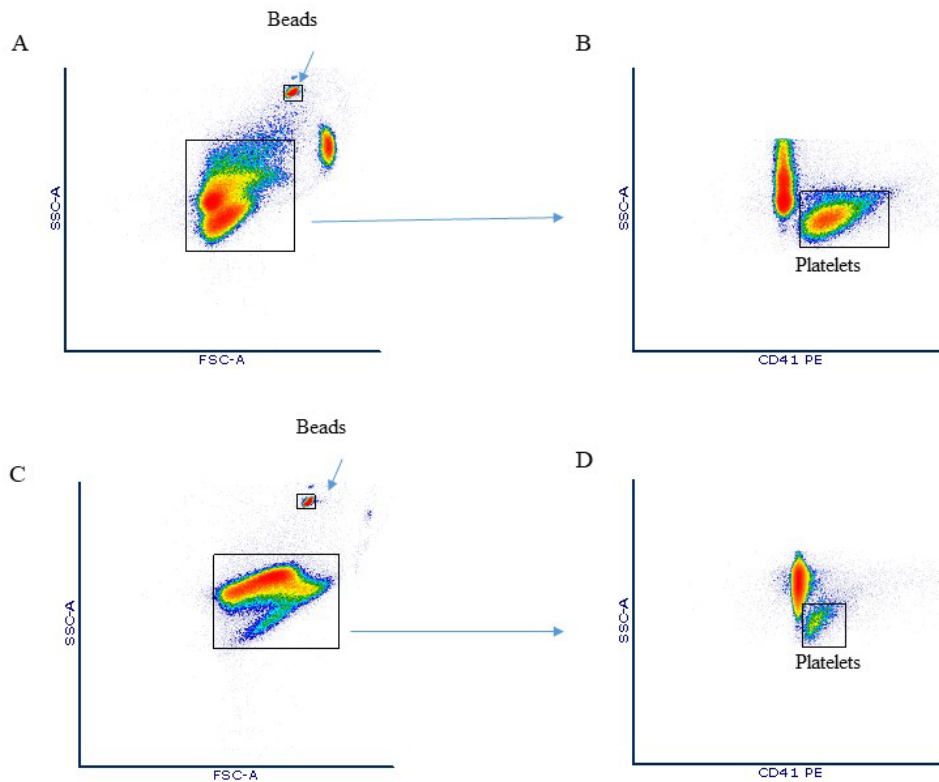
Figure 54 Thrombocytopenia in the B6.C3^{D1115N} mice.

Lower platelet counts were identified in the B6.C3^{D1115N} mice reflecting the consumptive thrombocytopenia as a consequence of the glomerular thrombotic microangiopathy. The top figure shows the FACS analysis of the Platelet count of a C57BL/6 wild type mouse, (**A-B**) and a B6.C3^{D1115N} (**C-D**). Platelets were confirmed by CD41 +ve stained cells with a reduced number in the B6.C3^{D1115N} (**D**) compared to a C57BL/6 wild type mouse (B). B6.C3^{WT} (wild type) n=4, B6.C3$^{D1115N+/-}$ (heterozygote) n=12, B6.C3^{D1115N} (homozygote) n=8. Mean ±SEM. Analysed using unpaired t-test with Welch's correction. ns non significant, ** P<0.01.

4.4.9 Histological analysis reveals a thrombotic microangiopathy

My data thus far, shows the B6.C3^{D1115N} have kidney impairment (as evidenced by proteinuria, haematuria and elevated BUN levels) coupled with evidence of a MAHA and thrombocytopenia. To complete the clinical triad and phenotypic characterisation, I examined the histology of the kidneys. I found histological evidence of a thrombotic microangiopathy on PAS and MSB stained sections. The mice glomeruli displayed mesangiolysis, microaneurysm formation, double contouring of the glomerular basement membrane and glomerular fibrin deposition with occasional intra-arterial thrombi. Thus, the phenotype of the B6.C3^{D1115N} mice recapitulated c-aHUS found in man.
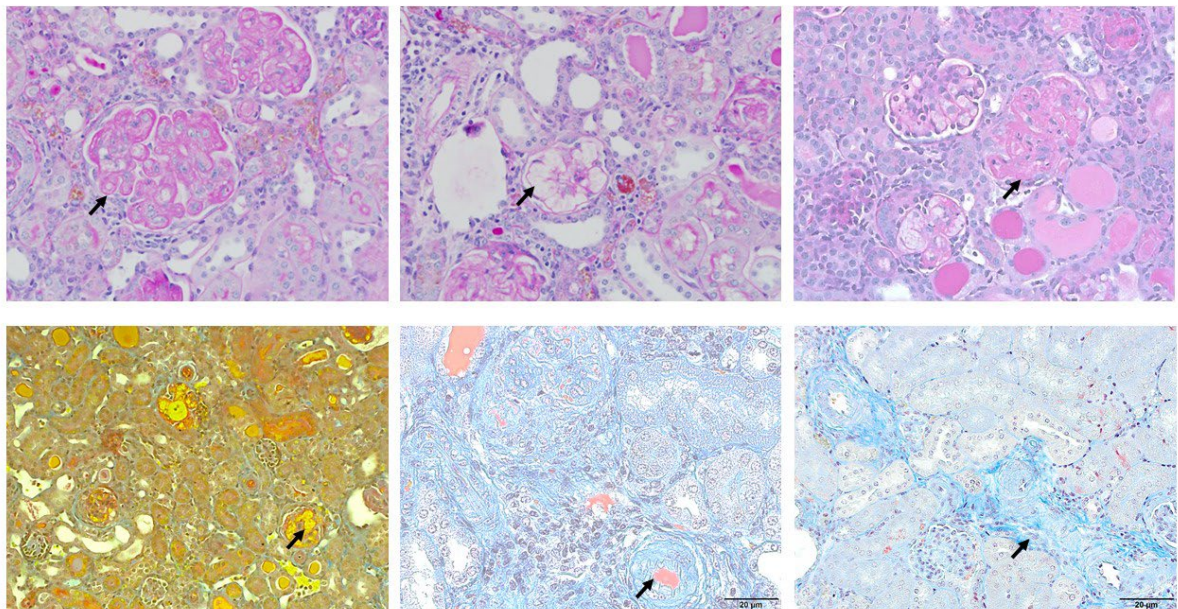
Figure 55 Histological analysis reveals a thrombotic microangiopathy.
The top panels show representative PAS stained sections of a B6.C3^{D1115N} mouse kidney illustrating, double contouring of glomerular basement membrane, microaneurysm formation and mesangiolysis.

The bottom panel shows martius scarlet blue stains showing microaneurysm formation and intrarterial thrombus.
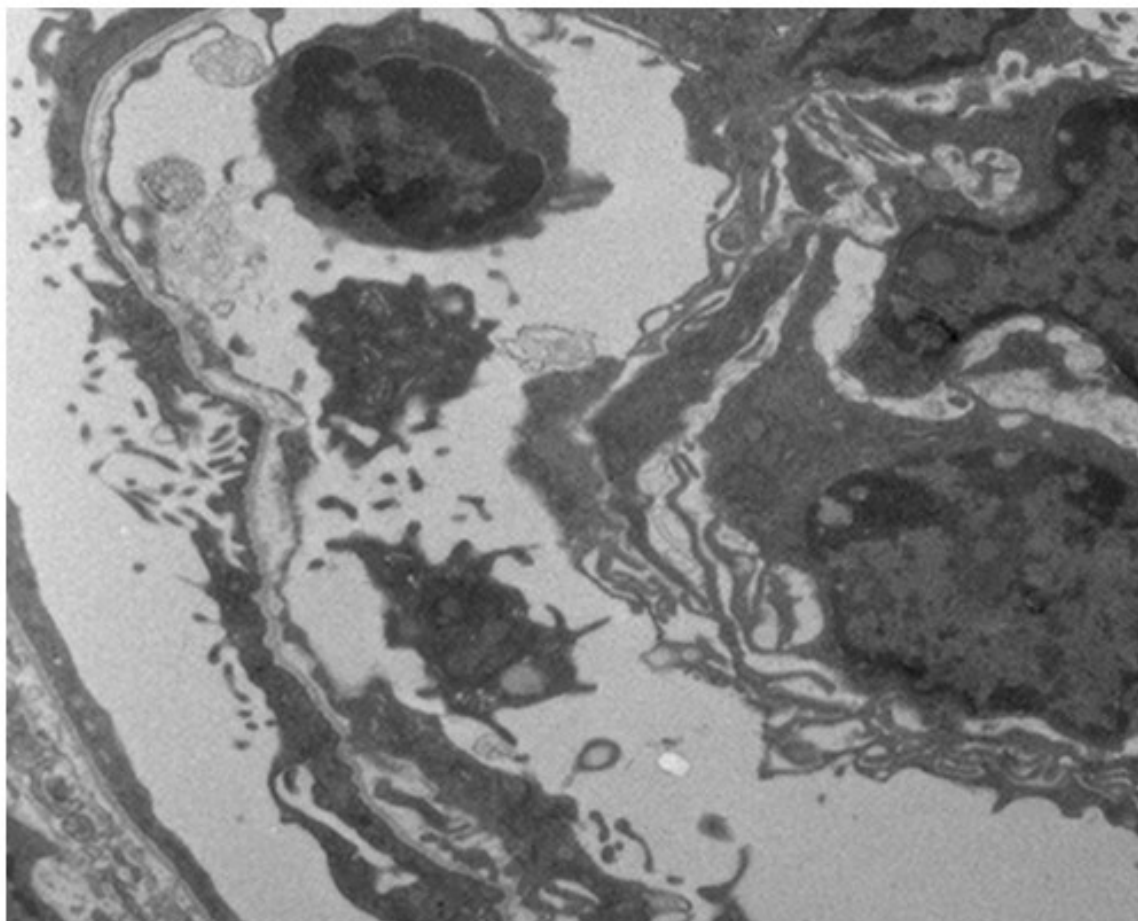
Figure 56 Electron microscopy of a B6.C3^{D1115N}

An electron microscopy image of a 21 day old B6.C3^{D1115N} mouse showing wrinkling of the glomerular basement membrane and subendothelial lucency which is consistent with ischaemic conditions precipitated by a TMA. Original magnification x7900

4.4.10 Complement dysregulation in the B6-C3^{D1115N} mice

Having confirmed the renal disease in the B6.C3^{D1115N}, in keeping with a TMA (akin to c-aHUS), I investigated the complement profile of the mice. Analysis of plasma from B6.C3$^{D1115N+/-}$ and B6.C3^{D1115N} mice showed the presence of intact mutant C3 protein and some evidence of C3 breakdown fragments, i.e. C3d, but not complete loss of intact C3. Interestingly, plasma FH levels in B6.C3^{D1115N} mice were elevated. This is consistent with a response to higher levels of complement activation or regulation (56). Additionally, plasma C5 levels were lower in B6.C3^{D1115N} mice.
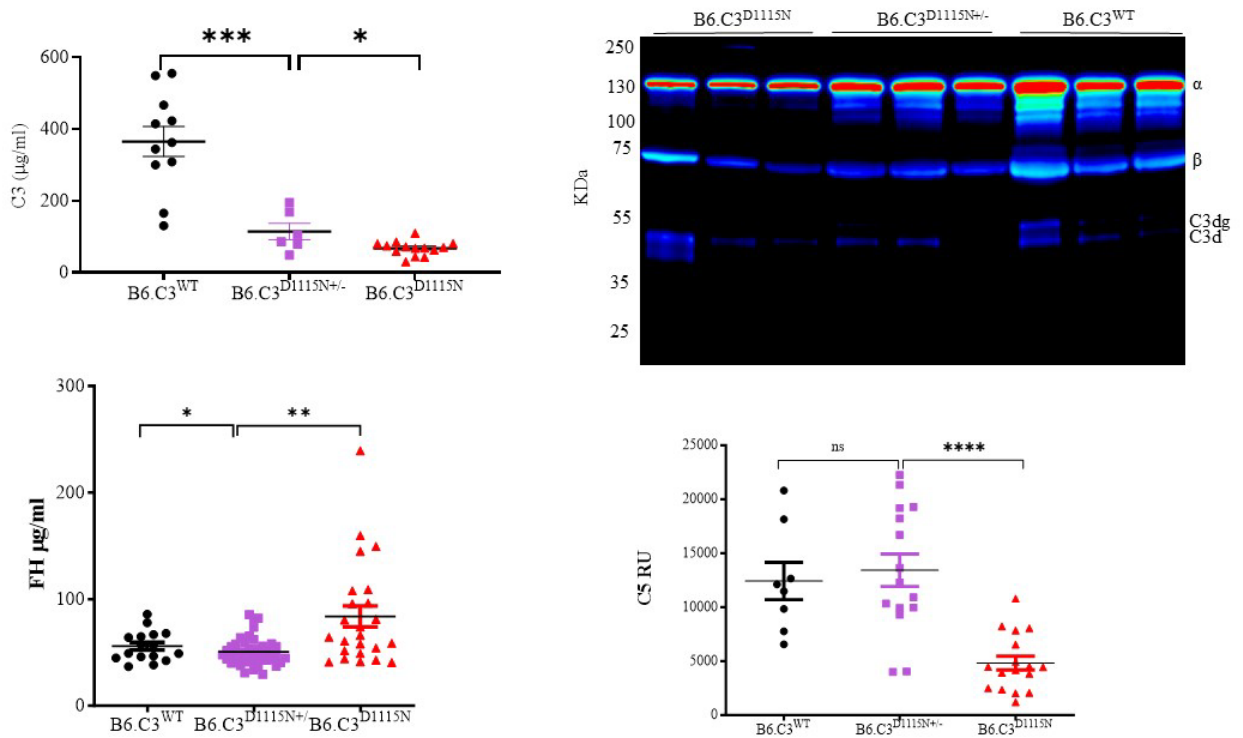
Figure 57 Complement profiles of B6.C3^{D1115N} mice.

Plasma murine C3 levels (Top left). Western blots of murine C3 derived from plasma (freshly collected into EDTA and run under reduced conditions). Complement FH (bottom left) and C5 levels (bottom right) in mice. B6.C3^{WT} (wild type), B6.C3$^{D1115N+/-}$ (heterozygote), B6.C3^{D1115N} (homozygote). Mean ±SEM. Analysed using unpaired t-test with Welch's correction. ns non significant, *P<0.05, ** P<0.01, *** P<0.001, ****P<0.0001.

4.4.11 Glomerular complement deposition in the B6-C3^{D1115N} mice

I next examined the glomerular complement deposition within the B6.C3^{D1115N} and found glomerular C3, C9 and fibrin deposition. Significant C3 deposition was identified with a granular staining pattern, largely confined to the mesangium and capillary walls of the glomerulus, in the B6.C3^{D1115N} mice. This was distinct from what was seen in the B6.C3$^{D1115N+/-}$ and B6.C3^{WT}, where tubulo-interstitial staining was observed (which is normal in murine kidneys (54, 56)). Detection of C9 in the glomeruli of B6.C3^{D1115N} mice, by immunofluorescent staining, suggested that terminal pathway activation and membrane-attack complex deposition contribute to disease. Similarly, glomerular fibrin deposition reflected the ongoing TMA.
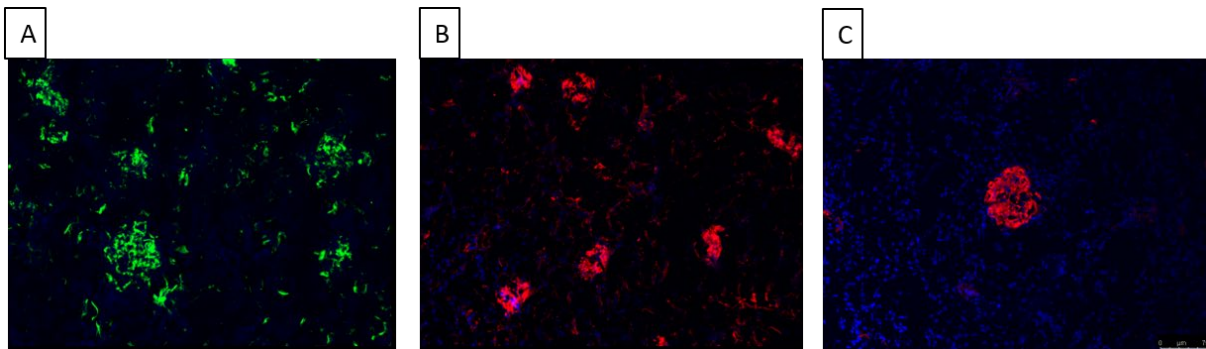
Figure 58 Glomerular complement deposition in the B6.C3^{D1115N} mice.
C3 (A), C9 (B), and fibrin (C) are all deposited within the glomerulus of the B6.C3^{D1115N} mice, illustrating glomerular complement activation. Representative images of N=20 examined. Taken at x20 Magnification.
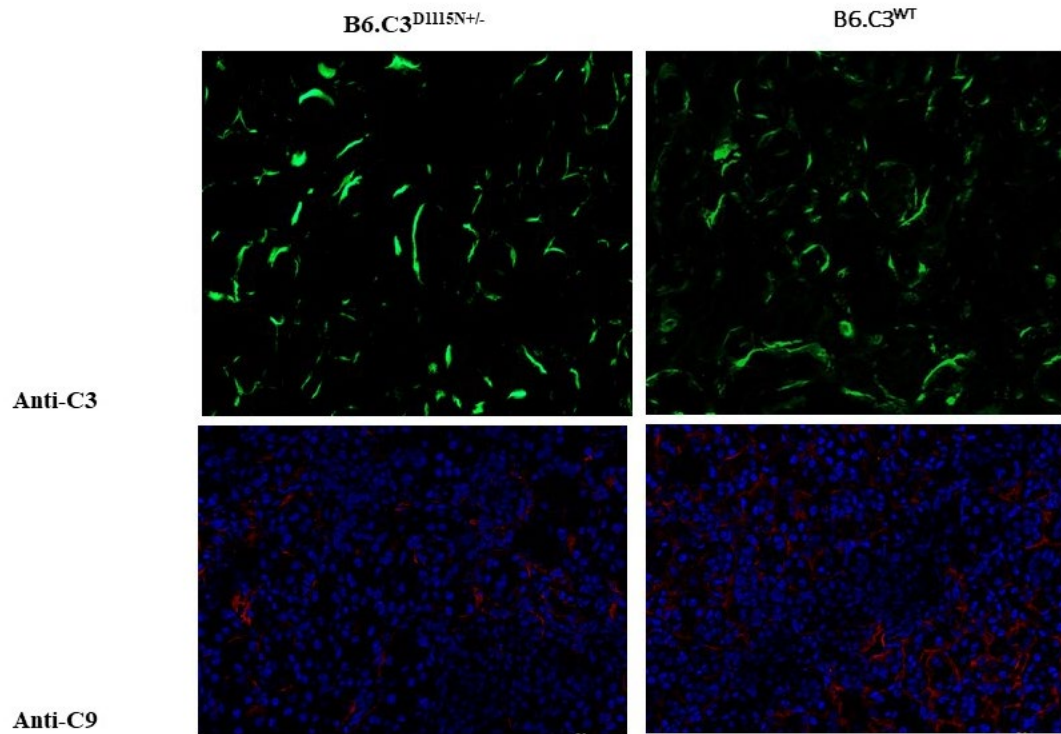
Figure 59 Glomerular complement deposition in the B6.C3$^{D1115N+/-}$ and B6.C3^{WT}
Tubulointerstitial C3 staining in B6.C3$^{D1115N+/-}$ and B6.C3^{WT}. No glomerular C9 staining seen.

No difference in glomerular complement deposition was seen in the B6.C3$^{D115N+/-}$ and the B6.C3^{WT}, indicating that in the heterozygote animals there is not an increase in glomerular complement activation and deposition compared to control. No glomerular C9 deposition was found in the kidney of B6.C3$^{D1115N+/-}$ and B6.C3^{WT} mice.

4.4.12 No histological evidence of disease in B6-C3$^{D1115N/WT}$

There was no histological evidence of TMA in any of the B6.C3$^{D1115N+/-}$ animals that I examined, up to 1 year of age.
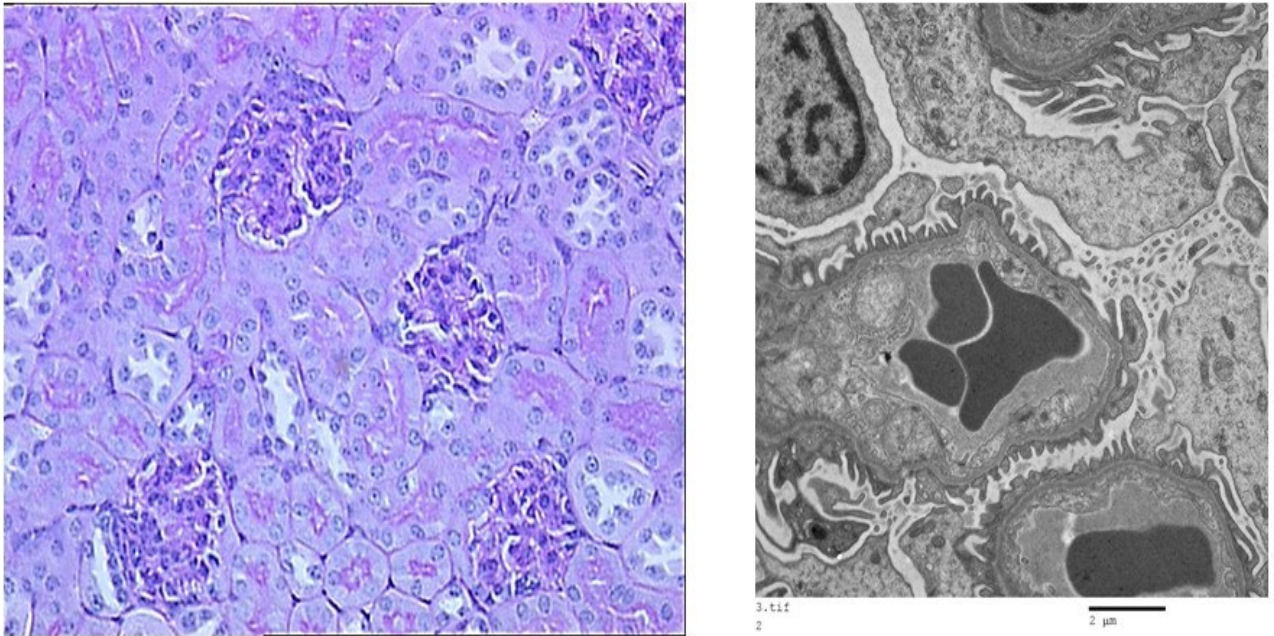
Figure 60 PAS and Electron microscopy of kidney sections from the B6.C3$^{D1115N+/-.}$
No histological evidence of disease was identified in the B6.$^{C3D1115N+/-}$ mice. The EM (top panel) and PAS stained section (bottom panel) show normal glomeruli within the mice heterozygote for the C3^{D1115N} point mutation at 12 months of age. EM original magnification x7900, PAS stained section imaged at x20 magnification.

4.4.13 Multisystem review of remaining organs

I sought a full histological evaluation from Charles River to identify any extra renal manifestations resulting from the *C3*,p.D1115N mutation. They examined the kidneys, spleen, stomach, cecum, brain, lung, heart, pancreas, bowel, lymph nodes, bone marrow and adipose tissue. They confirmed my findings within the kidney and identified extramedullary haematopoiesis within the spleen but all other organs and tissues were within normal limits.
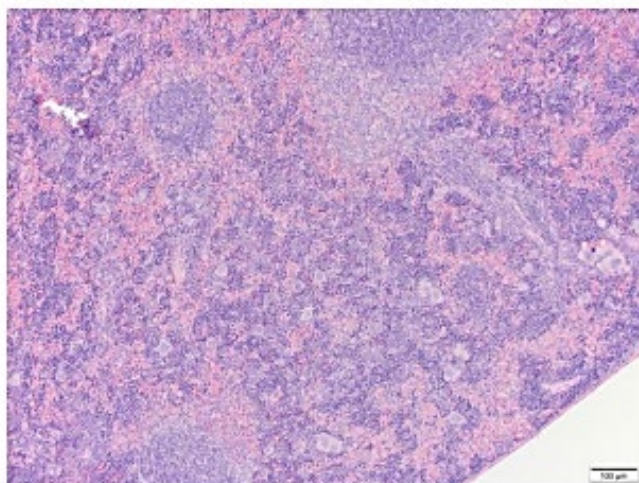
Figure 61 PAS stained section of a B6-C3^{D1115N} spleen.
Staining shows extramedullary haematopoiesis.

4.4.14 Molecular basis for complement dysregulation in the B6.C3^{D1115N} mice

I next examined the underlying mechanisms of how the single point mutation in *C3*, could lead to complement dysregulation. In keeping with previously published work and my analysis of *C3*,p.L1109V, I suspected impaired regulation and inactivation of C3b^{D1115N} by lack of binding of FH CCP 19-20 upon the endothelial cell surface. In order to prove my hypothesis I needed to purify murine FH, murine FH 1-5, Human FH 19-20, murine C3 (B6.C3^{WT} and B6.C3^{D1115N}) and recombinant Crry. This work was completed with the assistance of Dr Yi Yang (formerly of the Complement therapeutic research group) who provided the purified murine FH, murine FH 1-5, Human FH 19-20 and participated in the SPR experiments.

4.4.14.1 Murine C3 protein purification

Whole blood was collected from either B6.C3^{WT} or B6.C3^{D1115N} mice following terminal cardiac puncture and processed as per methods section 2.1.5 **Mouse C3 purification**, with the three-stage chromatography process shown below. Following isolation and purification of the murine C3^{D1115N} and murine C3^{WT} to homogeneity, it was incubated with human FB and FD to generate murine C3b to be used for functional studies.
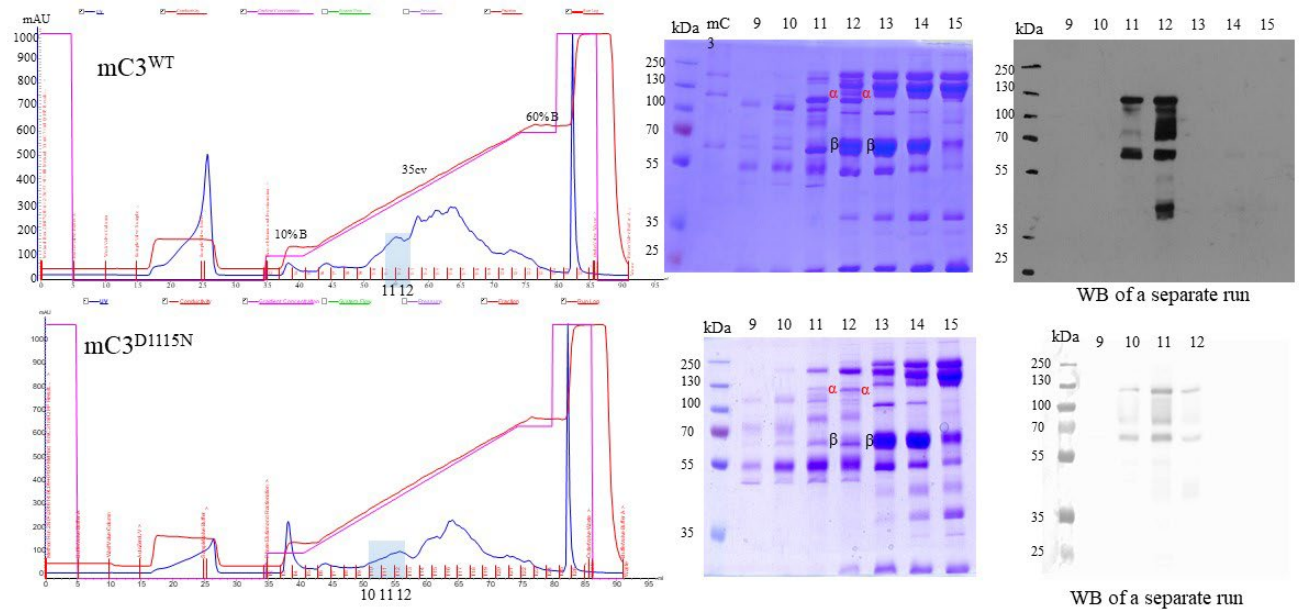
Figure 62 Anion exchange chromatography for the purification of murine C3^{WT} and C3^{D1115N}
The chromatography graphs are shown for mC3^{WT} and mC3^{D1115N} on the left, with the expected C3 uV
peak highlighted by the blue shadowed box. Blue line shows UV, Red line shows conductivity, and the
pink line shows gradient concentration. The fractions were run on the corresponding SDS page gel that
underwent Coomassie staining to visualise the fractions. A confirmatory western blot is then shown on
the right.
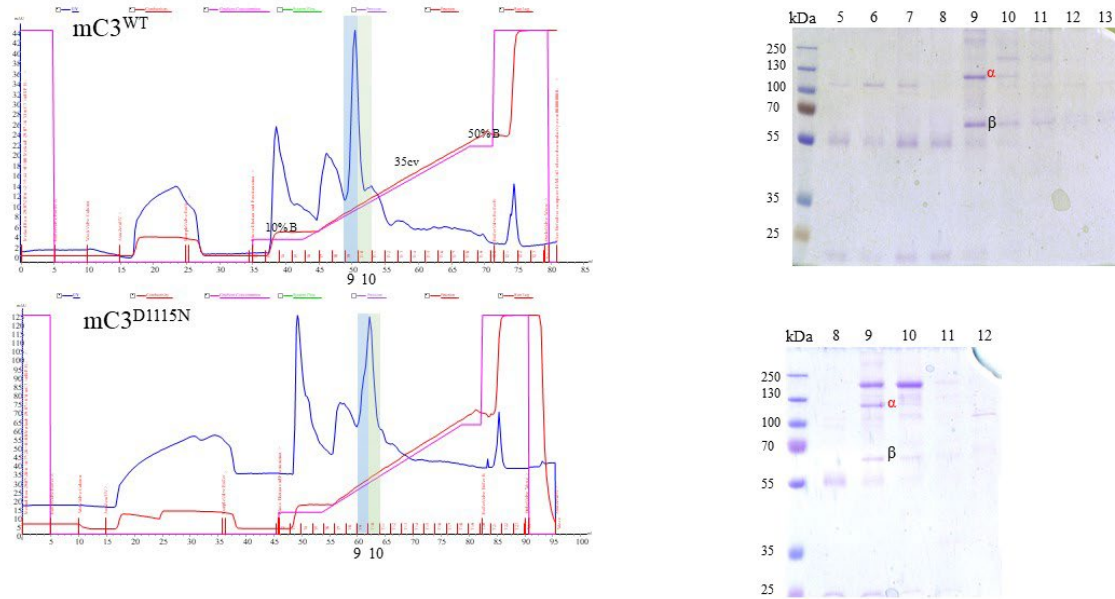
Figure 63 Cation exchange chromatography.

The chromatography graphs of the cation exchange with the expected C3 fractions are highlighted by the blue and green shaded boxes with the corresponding 10% SDS page gel on the right with the fractions visualised following Coomassie staining with a reference protein ladder run in well 1 starting at 250kDa. Blue line shows UV, Red line shows conductivity, and the pink line shows gradient concentration
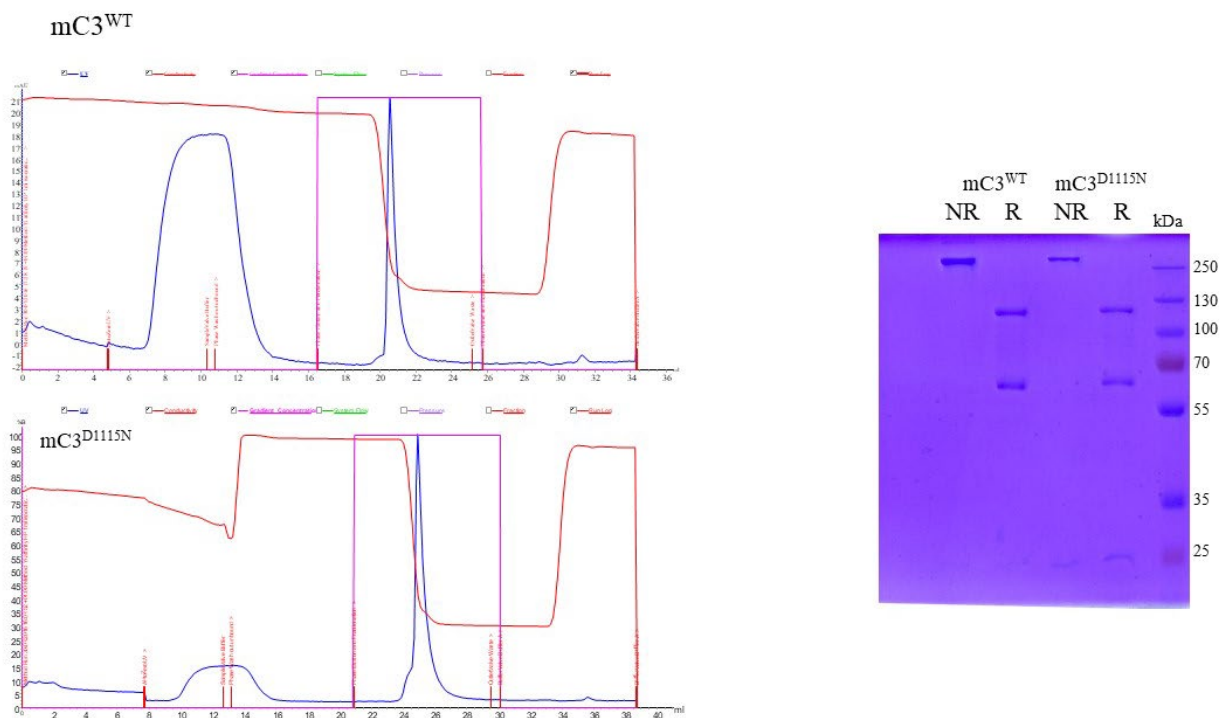
Figure 64 Size exclusion chromatography

The final step was to run the isolated C3 peaks from the cation exchange over the size exclusion column. Blue line shows UV, Red line shows conductivity, and the pink line shows gradient concentration The chromatograph shows the C3 peak fraction with the final purified mouse proteins mC3^{WT} and mC3^{D1115N} on the Coomassie stained 10% SDS page gel under non reduced and reducing conditions with a protein reference ladder ran in the final lane starting at 250kDa.

4.4.14.2 Transfection and Purification of recombinant Crry

One difference between mouse and man is that mice do not express Membrane cofactor protein (MCP). Instead, they express Complement receptor 1-related gene/protein Y(Crry) which provides a similar regulatory function to MCP and DAF (129, 130). I generated recombinant Crry in order to test the regulatory ability of both FH and Crry upon murine $C3b^{D1115N}$.

4.4.14.2.1.1 Clone selection for recombinant Crry

Firstly, I transfected a Crry containing vector into CHO cells as per methods section 2.1.7. A limiting dilution was undertaken and highly expressing clones were selected for large-scale purification. For confirmation of recombinant Crry protein production, a western blot was performed and probed with the anti-Crry antibody E1E10, with a media only sample used as a negative control. Clone B4 was selected and scaled up for large-scale production using roller flasks.
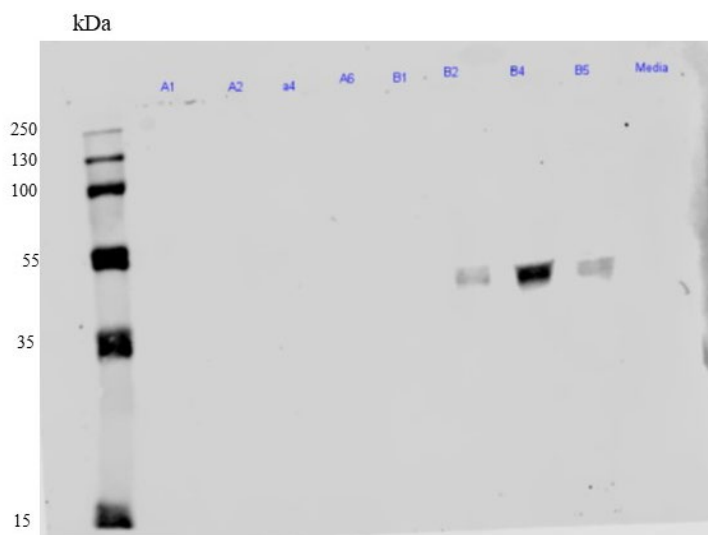
Figure 65 Clone selection for recombinant Crry.
CHO cells were transfected with Crry vector and a limiting clone dilution undertaken. Supernatant was taken and different clones tested (as indicated above each lane; media = fresh media with no transfected cells in) on a western blot using anti-Crry antibody E11.

The supernatant was run over a 5ml HisTrap Excel™ column and the peak fractions were ran on an SDS gel for confirmation.
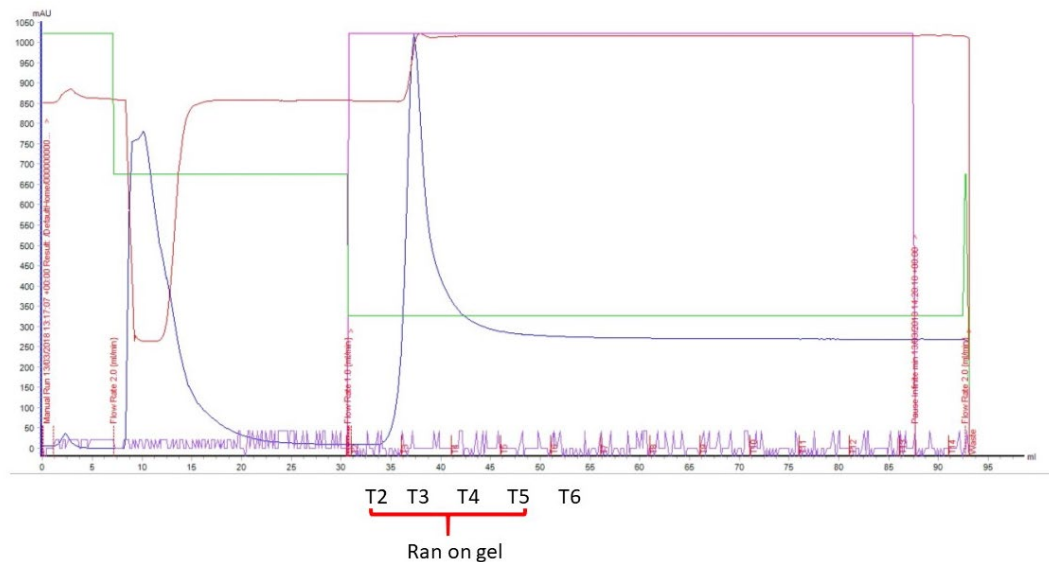
Figure 66 Chromatography graph of recombinant Crry purification

Chromatography graph showing harvested supernatant from Crry transfected CHO cells ran over a 5ml HisTrap Excel™. Blue line shows UV, Red line shows conductivity, the pink line shows gradient concentration and the green line shows the system flow.
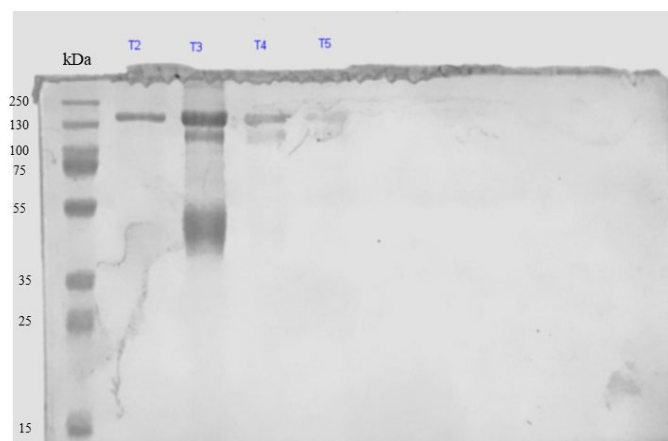
Figure 67 10% SDS page gel of peak fractions from the 5ml HisTrap Excel™ chromatography process above. Pre-stained markers run and size in kDa shown to the left of the image.

Fractions T3 and T4 were spin concentrated and then run over a 1ml HisTrap HP™ with the final chromatograph shown below.
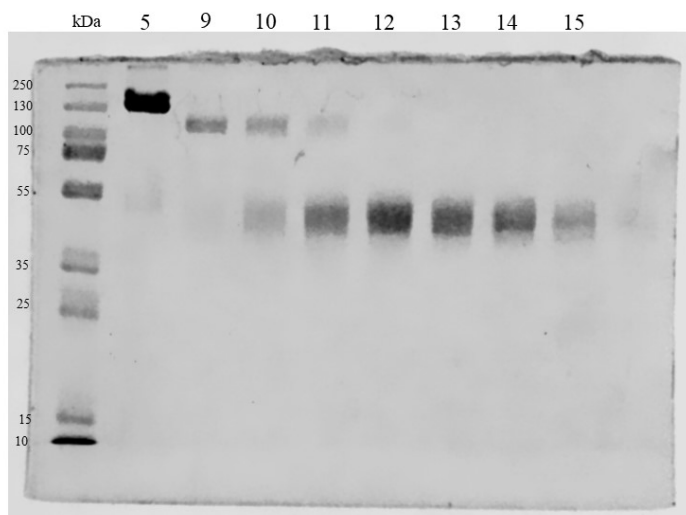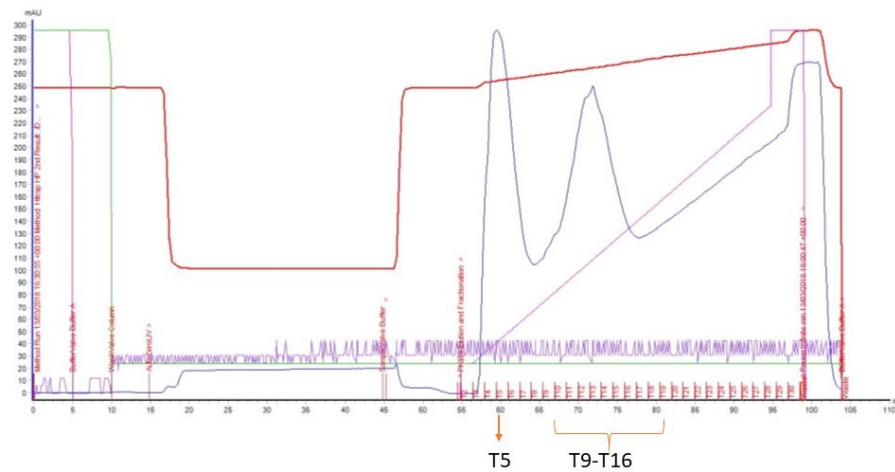
Figure 68 Step 2 recombinant Crry purification over a 1ml HisTrap™ column.
The chromatograph above showing the elution of the peak fractions with the corresponding SDS page gel below. The molecular weight of Crry being 53kDa. On the chromatograph the Blue line shows UV, Red line shows conductivity, the pink line shows gradient concentration and the green line shows the system flow

Fractions 12-15 were selected, spin concentrated and then stored ready to be used for functional assays.

4.4.14.3 SPR analysis of murine C3b wild type and D1115N

I used SPR to measure the interaction between murine C3b^{WT} and murine C3b^{D1115N} with the regulatory proteins; murine FLFH, recombinant murine FH 1-5, recombinant murine Crry and human FH CCP 19-20 (murine construct not available). Freeze-thawed C3 was attached (approximately 900 RUs) to a CM5 chip by amine coupling (as per methods sections), and then the various regulators were flowed across the immobilised C3b on the chip surface. Full-length mouse FH bound to murine C3^{WT} with an affinity of 1.4± 0.13μM, while it bound murine C3b^{D1115N} with a K$_D$ of 3.7 ± 0.25μM. Recombinant mouse FH1-5 bound to both murine C3b^{WT} and murine C3b^{D1115N} with equivalent affinity (2.9±0.24μM and 3.1±0.34μM respectively). These values are broadly similar to the affinity of full-length mouse FH binding to murine C3b^{D1115N}, and hence, taken together, these SPR data suggest the almost complete loss of binding between C3^{D1115N} and the C-terminus of FH. I confirmed this using SPR to measure the binding between human FH19-20 and the immobilised C3b (WT and D1115N). FH19-20 bound to murine C3b^{WT} with a K$_D$ of 9.4±1.2μM, whereas it attempted to bind to immobilised murine C3b^{D115N} but this was a much weaker K$_D$ of >17.4. To conclude, I evaluated Crry binding to murine C3b^{WT} and murine C3b^{D1115N}, and found that recombinant mouse Crry bound to C3b^{WT} and C3b^{D1115N} with essentially equivalent affinity (3.2 ± 0.03μM and 3.5 ± 0.06μM respectively).
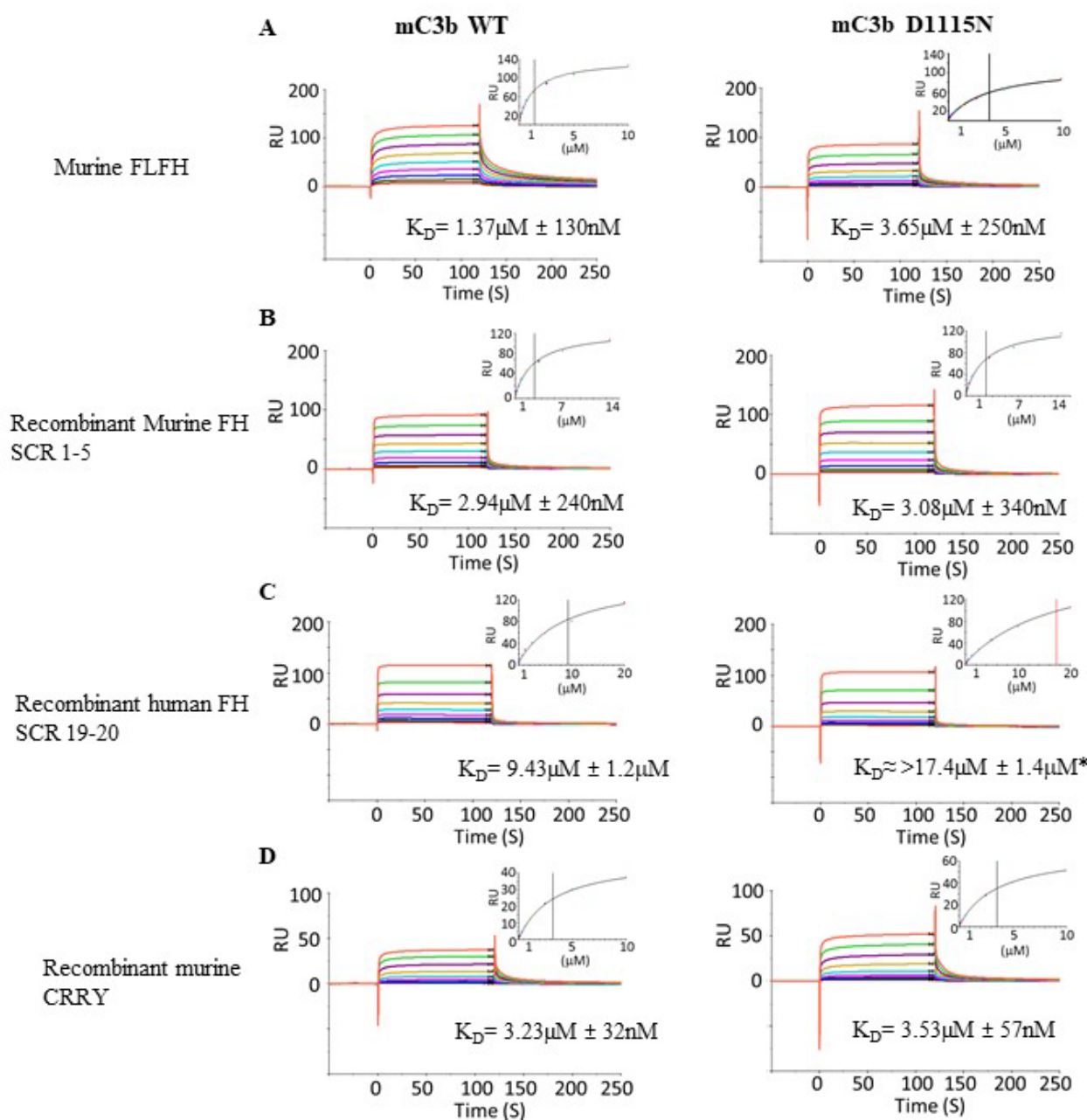
Figure 69 SPR analysis comparing murine C3b wild type and C3b D1115N.

*SPR analysis was performed using mouse C3b derived from WT plasma or mC3b^{D1115N} and amine coupled to the CM5 biosensor chip. Doubly diluted concentration series of **(A)** purified Murine FLFH (0 to 10 μM), **(B)** recombinant murine FH SCR 1-5 (0 to 14.6 μM), **(C)** recombinant human FH SCR 19-20 (0 to 20 μM) or **(D)** recombinant murine Crry (0 to 10 μM) were flowed across either chip surface. The equilibrium dissociation constant K_D was calculated using steady state model in Biacore evaluation package, indicated as the black vertical line. "*", at the concentration range assayed here, human FH 19-20 was not able to achieve saturated binding on the C3b^{D1115N} surface, thus a under estimated K_D was indicated by the red vertical line.*

4.4.15 Fluid phase co-factor activity assays comparing wild type murineC3b^{wt} and murineC3b^{D1115N}

Fluid-phase FI co-factor assays (performed by Dr Yi Yang), with purified reagents, indicated that murine C3b^{D1115N} was more resistant to cleavage by murine FH and human FI than was wild-type murine C3b (Figure 70 C-D). These data suggests that the D1115N substitution of murine C3b perturbs interactions with FH and hence the susceptibility of C3b^{D1115N} to regulation by FH and FI.
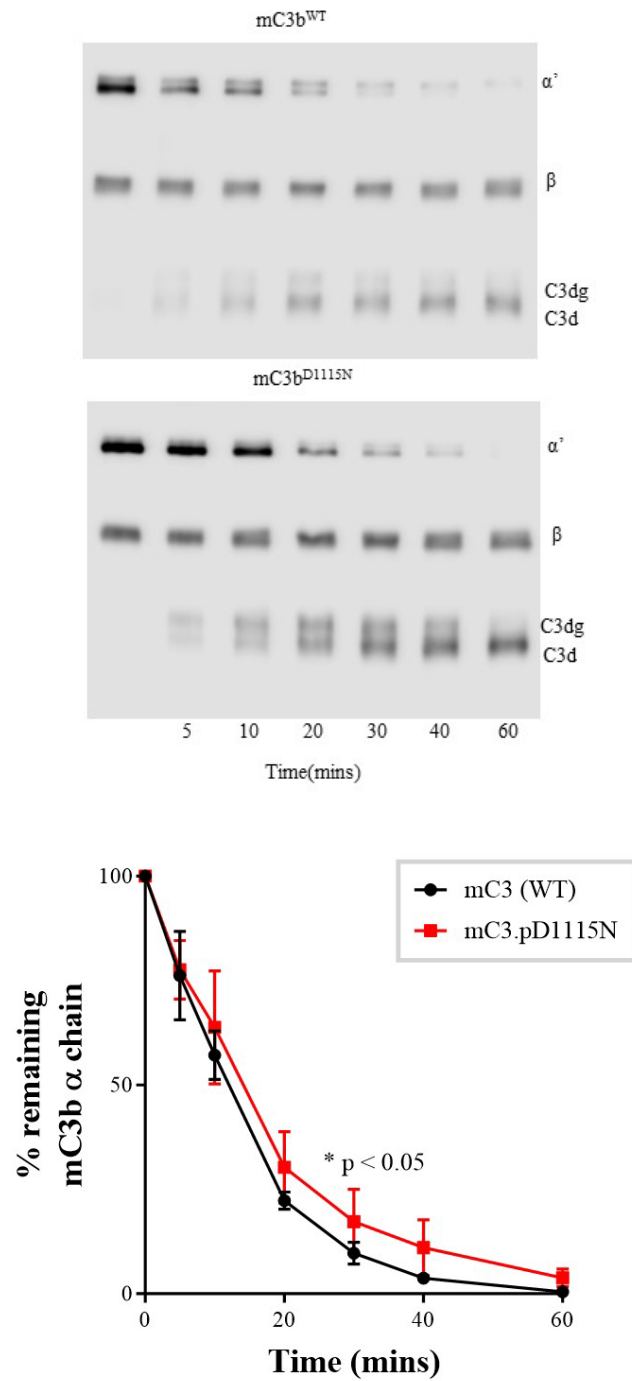
Figure 70 Fluid phase co-factor activity assays comparing wild type C3b and D1115N C3b

Co-factor activity assay of plasma purified murine C3 incubated with human FI and FH. Gel/western details. Densitometry analysis was undertaken on the remaining, intact alpha chain; with the average of three experiments +/- SEM shown and normalized for loading variations using the beta chain.. Each time point was analysed using unpaired t test.

4.4.16 Genetic deletion of C5 rescues the phenotype of the B6-C3^{D1115N}

To further validate the model and provide translational insight into long-term C5 blockade, I backcrossed the B6.C3^{D1115N} onto the C5 deficient mice (C5$^{-/-}$). As expected there was 100% survival of the B6.C3^{D1115N}.C5$^{-/-}$. Three cohorts of mice were tracked and culled at two, six and 12 months, respectively.

4.4.16.1 Survival curve of B6.C3^{D1115N}.C5$^{-/-}$
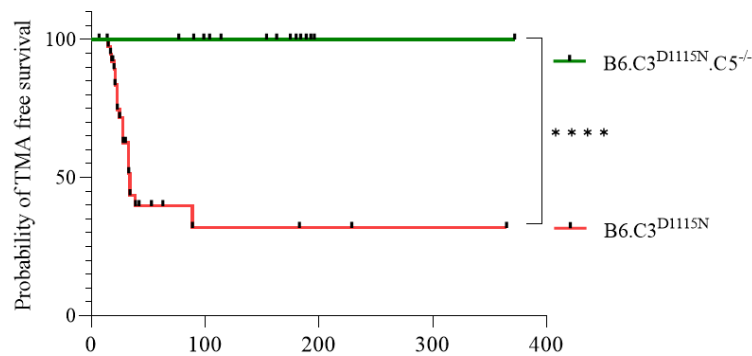
Figure 71 Genetic deficiency of C5 rescues the B6.C3^{D1115N} with 100% TMA free survival.
No B6.C3^{D1115N}.C5$^{-/-}$ N=38 succumbed to TMA for up to 1 year of age. Kaplan-Meier survival analysis.
****P<0.0001.

4.4.16.2 No renal injury in the B6.C3^{D1115N}.C5$^{-/-}$

No evidence of proteinuria or haematuria was detected in urine collected before mice were culled. Creatinine measurements (taken for 3 months and 6 month cohorts) were similar to age and litter mate-matched controls. No histological evidence of a thrombotic microangiopathy was identified in PAS and MSB stained sections. Collectively, these observations indicate a lack of evidence of a kidney disease.
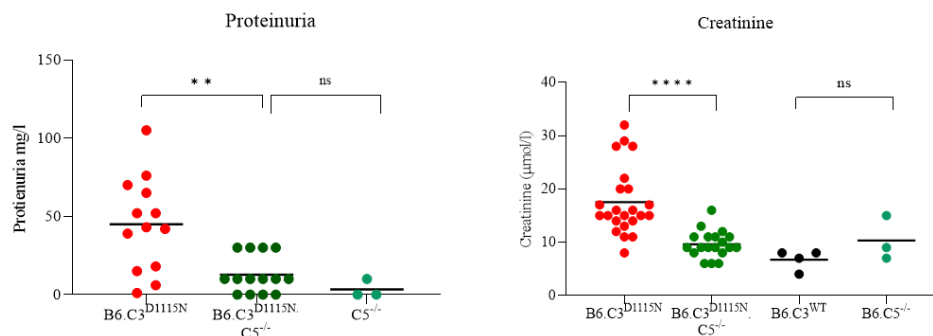
Figure 72 No evidence of renal disease in the B6.C3^{D1115N}.C5$^{-/-}$ mice.

*There was a significant reduction in proteinuria and creatinine in the B6.C3^{D1115N}.C5$^{-/-}$ showing no clinical or biochemical evidence of renal injury. Creatinine measurements taken from B6.C3^{D1115N} (homozygote) n=23. B6.C3^{D1115N}.C5$^{-/-}$ 3 months n=9, 6 months n=10. B6.C5$^{-/-}$ N=3. Mean ±SEM are displayed. Analysed using unpaired t-test with Welch's correction. ns no significant, ** P<0.01, ****P<0.0001.*

4.4.16.3 No TMA in the B6.C3^{D1115N}.C5$^{-/-}$ mice
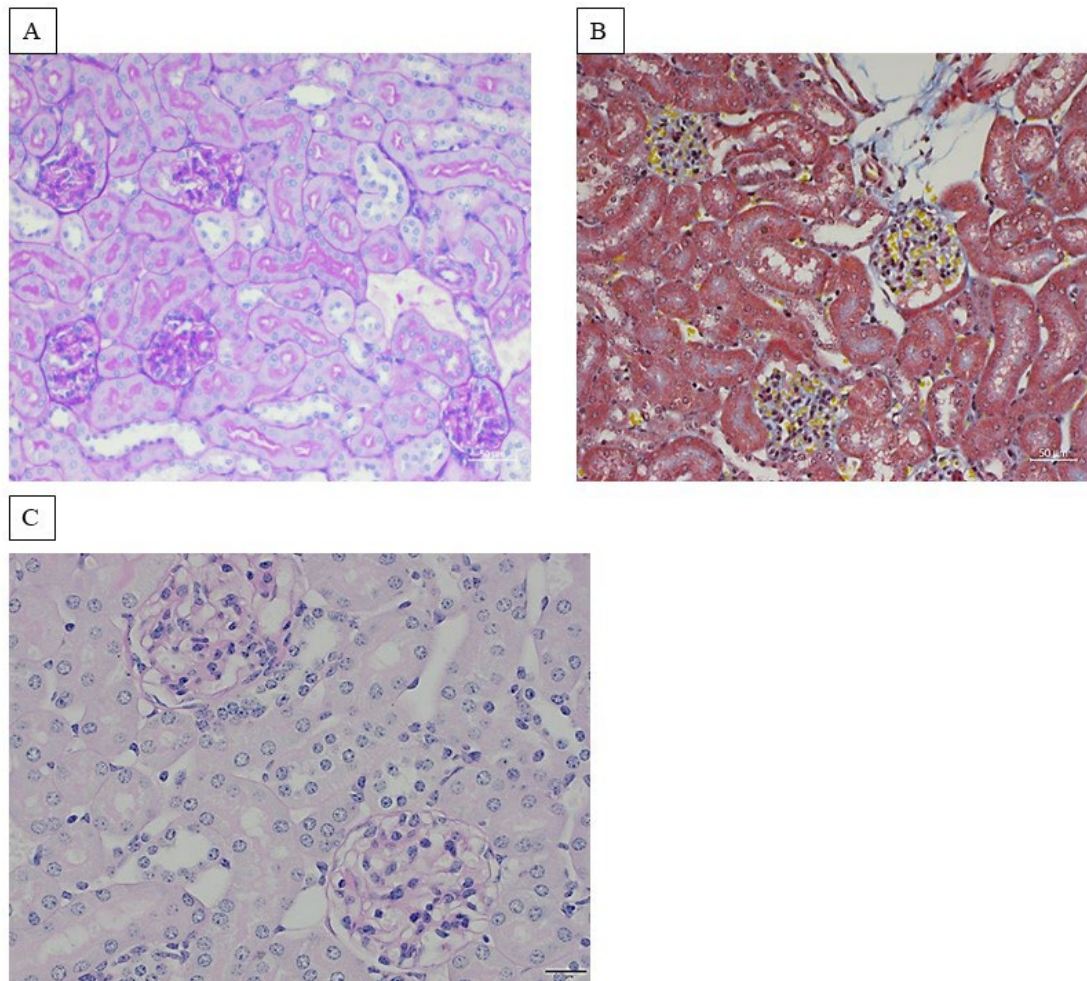
Figure 73 Histological analysis of B6.C3^{D1115N}.C5$^{-/-}$ mice
Representative images of a 6 month old B6.C3^{D1115N}.C5$^{-/-}$ mice. (A) & (C) PAS stained section and (B)
MSB stain. All show normal histology with normal glomeruli. Taken at Magnification x20 (A)& (B) with
(C) taken at magnification x40..

4.4.17 Glomerular complement C3 deposition in B6.C3^{D1115N}.C5$^{-/-}$

Glomerular C3 deposition was still evident in mice. Interestingly, I did see an increase in C3 deposition as the mice aged, but this did not appear to lead to morphological features of a C3 glomerulopathy as the MSB, PAS stained sections showed normal appearance of glomeruli at 12 months of age. This was probed further using electron microscopy within the 6-month cohorts, finding healthy glomeruli with no evidence of electron dense deposits in both the B6.C3^{D1115N}.C5$^{-/-}$ and aged matched wild type controls, which was in contrast to the 6-month B6.FH$^{-/-}$ animals, which show pathological features of C3 glomerulopathy.
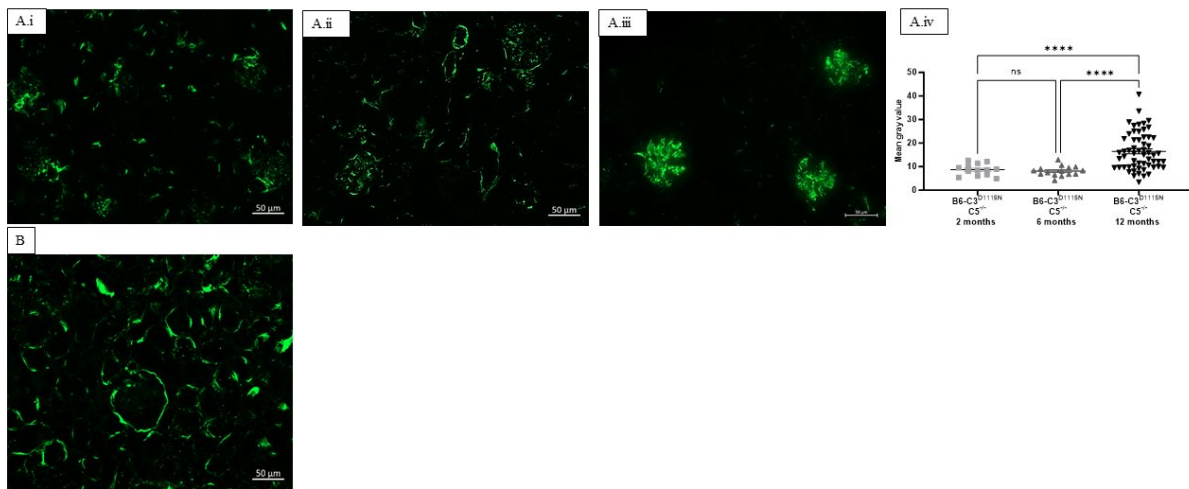
Figure 74 Glomerular complement C3 deposition in B6.C3^{D1115N}.C5$^{-/-}$.

*Glomerular C3 deposition in a B6.C3^{WT}.C5$^{-/-}$ (A), B6.C3^{D1115N} (B). B6.C3^{D1115N}.C5$^{-/-}$ 3months (A.i), B6.C3^{D1115N}.C5$^{-/-}$ 6 Months (A.ii), B6.C3^{D1115N}.C5$^{-/-}$ 12 months (A.iii). We do see an increase in glomerular C3 deposition as the B6.C3^{D1115N}.C5$^{-/-}$ age (A.iv). Glomerular C3 staining in B6.C3^{WT}.C5$^{-/-}$ (B). Taken at x20 magnification. Mean ±SEM. Analysed using unpaired t-test with *P<0.05, ** P<0.01, *** P<0.001, ****P<0.0001 Average number of glomeruli scored N=31.*
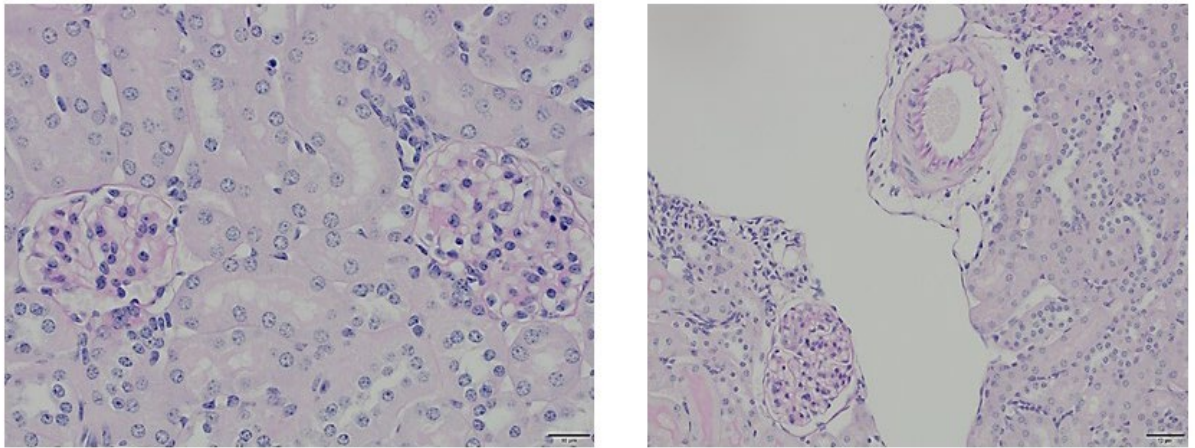
Figure 75 Normal glomeruli in the 12-month-old B6-C3^{D1115N}.C5$^{-/-}$ Mice
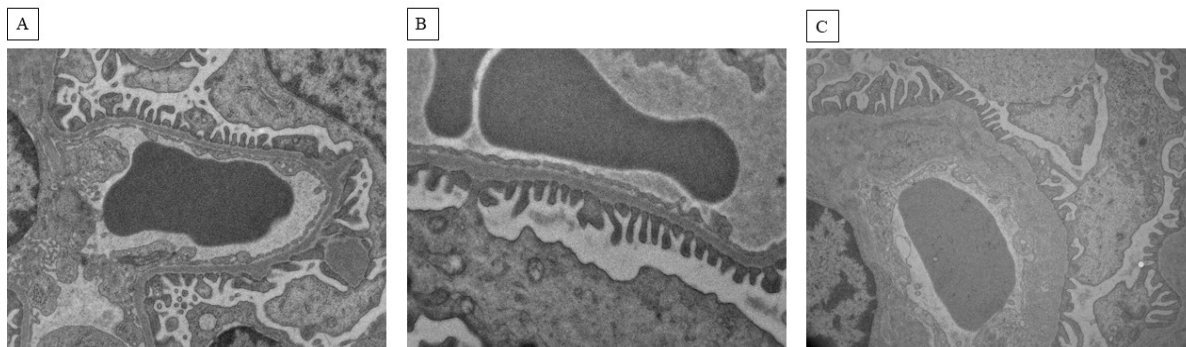
Figure 76 Electron Microscopy of 6-month-old mice

B6.C3^{D1115N}.C5$^{-/-}$, (B) B6.C3^{WT}.C5$^{-/-}$, (C) B6.FH$^{-/-}$. Both (A) and (B) illustrate a healthy glomerular basement membrane. (C) shows a thickened GBM, with sub endothelial deposits.

4.4.18 No schistocytes in the B6.C3^{D1115N}.C5$^{-/-}$

Peripheral blood smears showed no evidence of schistocytes in the B6.C3^{D1115N}.C5$^{-/-}$ mice.
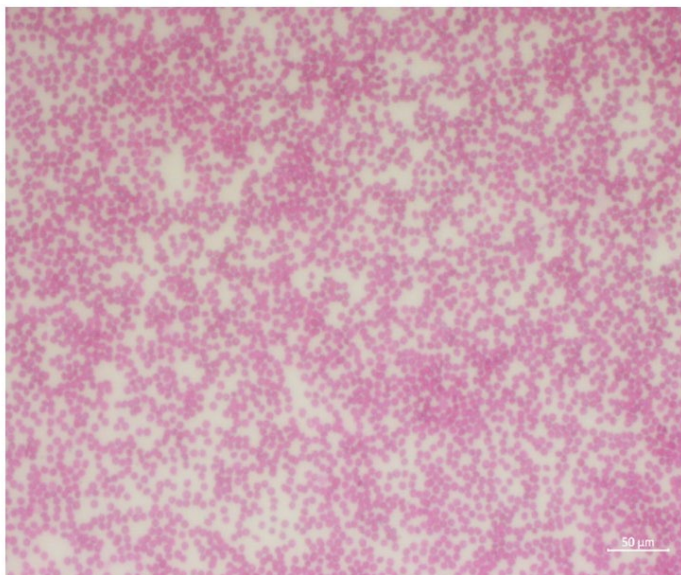
Figure 77 Normal blood film of a B6.C3^{D1115N}.C5$^{-/-}$.

No evidence of fragmented red blood cells on the blood film. Representative of N=10 examined.

4.4.19 Therapeutic C5 inhibition leads to 100% survival in B6.C3^{D1115N}

The data presented above suggest the B6.C3^{D1115N} is a novel model for c-aHUS in which the phenotype can be rescued through C5 genetic deletion. The novelty of the model is due to the disease arising from a gain-of-function mutation (in C3) rather than a loss-of-function (in FH). The current gold-standard treatment for c-aHUS in man is Eculizumab. I reasoned that treatment of B6.C3^{D1115N} mice with a C5-blocking monoclonal antibody should protect them from developing c-aHUS. Therefore, I injected C3^{D1115N} mice with active disease, with 50 μg/g of BB5.1 (a monoclonal antibody that inhibits C5[131, 132]), for up to two weeks and compared them to B6.C3^{D1115N} mice (again with active disease) dosed with isotype control antibody (mouse IgG$_1$/PBS). While 55% (6/11) of mice treated with the control antibody had to be removed from the study due to ill health, none of the mice treated with BB5.1 (0/8) succumbed to disease.
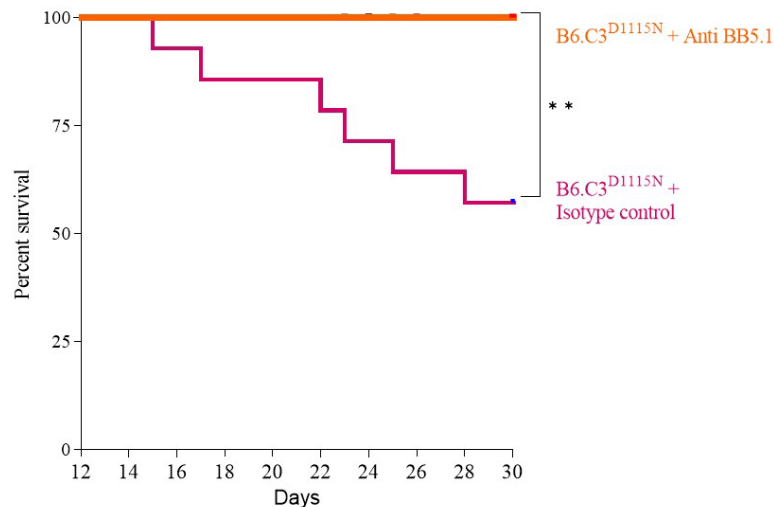
Figure 78 Anti C5 therapy rescues the B6.C3^{D1115N} mice.

100% survival was achieved when anti-C5 therapy was administered to B6.C3^{D1115N} mice that exhibited signs of clinical disease (cumulative clinical score based upon appearance, urinalysis, weight loss used to determine end point. B6.C3^{D1115N} + BB5.1 N=8, B6.C3^{D1115N} + Isotype control N=11. Kaplan-Meier survival curve analysis. ** P<0.01.

4.4.19.1 Improved platelet counts and renal function with Anti-C5 therapy

Creatinine values were lower in the BB5.1 treatment arm reflecting attenuation of renal injury, or else signs of renal recovery. Platelet counts were significantly higher in the animals treated with BB5.1, suggesting resolution of the consumptive thrombocytopenia.
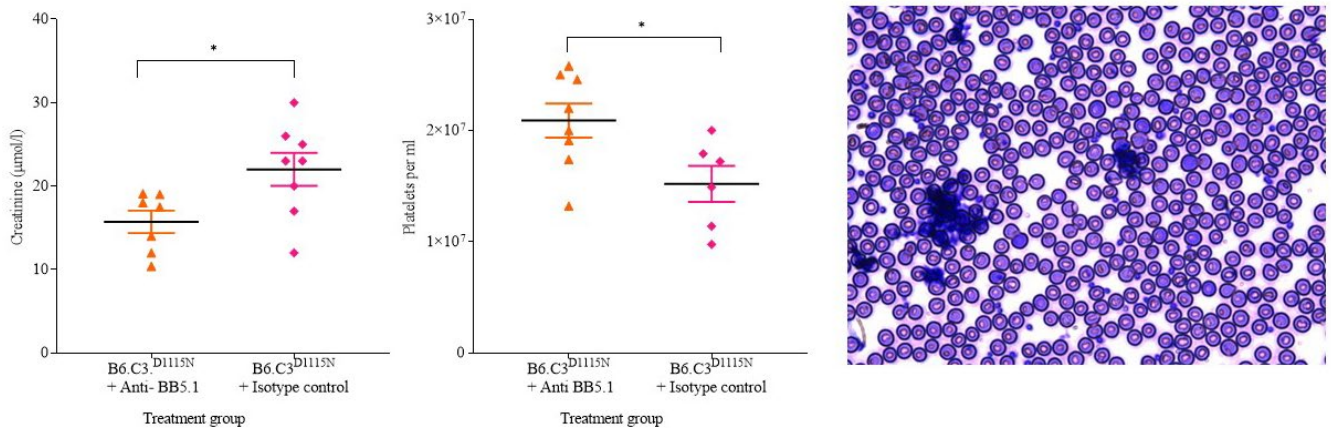
Figure 79 Improvement in platelet counts and renal function with anti-C5 therapy.

An increase in platelet counts was observed in terminal bleeds of mice treated with anti-C5 therapy (BB5.1), N=8, compared to mice treated with isotype control, N=6. Similarly, creatinine levels were lower (reflecting an attenuation in renal injury) in the mice treated with anti-C5 therapy, N=7, compared to isotype control, N=8. Blood film, on the right, is a B6.C3^{D1115N} mouse treated with BB5.1 showing normal shaped red blood cells. The platelets have clumped which is a known effect of EDTA. Mean ±SEM. Analysed using unpaired t-test with *P<0.05.

4.4.19.2 Reduction in glomerular C3 and C9 with Anti-C5 therapy

Both C3 and C9 glomerular deposition was lower in the BB5.1 treatment arm.
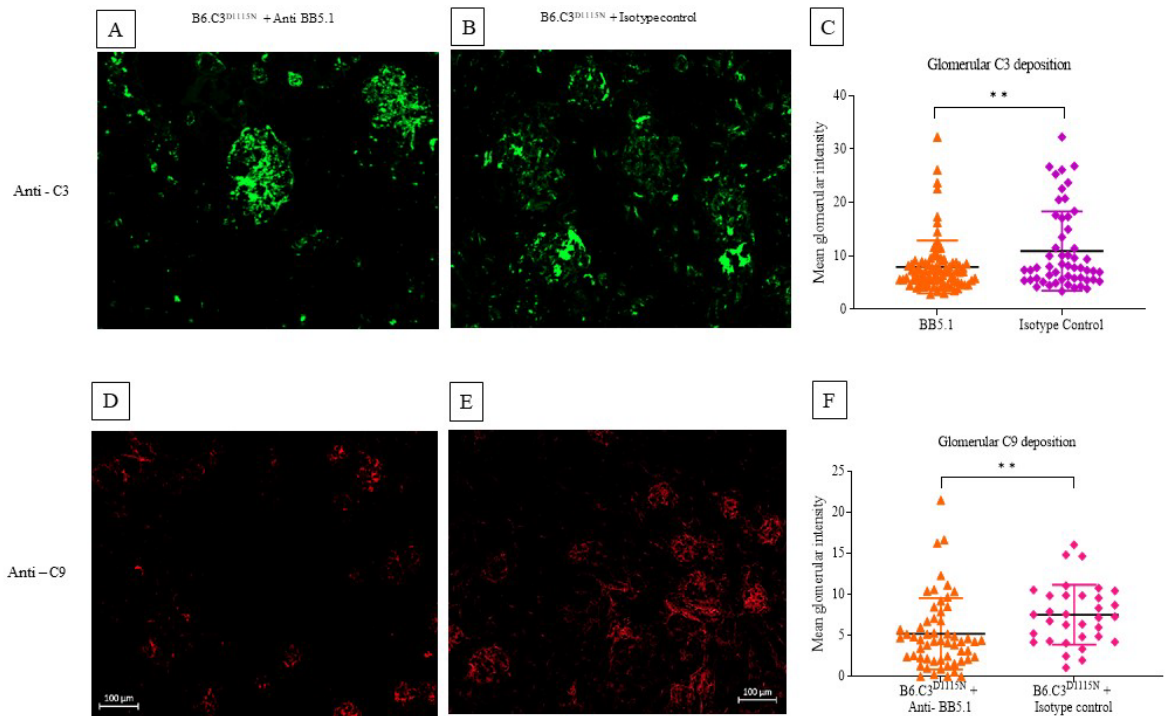
Figure 80 Reduction in glomerular C3 and C9 therapy with anti-C5 therapy.
*Mice treated with anti-C5 therapy had reduced C3 and C9 glomerular deposition. Average number of glomeruli scored in C3 deposition N=80, and C9 deposition N=34. Mean ±SEM. Analysed using unpaired t-test   ** P<0.01. Average number of glomeruli scored N=31.*

4.5   Discussion of Results

The above data demonstrates that transferring a disease-associated single-nucleotide substitution in *C3*, present in a family within the National aHUS service c-aHUS cohort, to murine *C3* faithfully recapitulated the salient features of the human disease. The data presented very strongly support the view that c-aHUS arises primarily due to deficient protection of host cellular and extracellular matrix surfaces from complement activation. The relative health of the heterozygous mice B6.C3$^{D1115N+/-}$ despite markedly increased complement turnover also offers potential to investigate how C3 activity shapes the progression of other complex genetic disorders, such as rheumatic and neurological conditions, including Age related macular degeneration.

The FHΔSCR16-20 transgenic mice (54) established that deletion of the FH C terminus and its self-surface-binding capabilities, combined with uncompromised FH-N terminus-mediated control of C3 depletion in fluid phase, allows development of a c-aHUS-like disease. This study was fully consistent with the discovery that most (although not all) disease-associated mutations in human FH cluster within SCRs 19-20, which are known to contain binding sites for C3d, the TED of C3b, and surface polyanions and to be crucial for distinguishing between self and non-self surfaces (133).

In contrast, my mouse model derives from a single mutation in a murine gene that maps directly to the equivalent disease-linked mutation in humans (59). The clear affinity reductions observed in SPR studies of the *ex vivo* purified murine C3b^{D1115N} are consistent with loss of an important C-terminal binding interaction but retention of the other FH (i.e. CCPs 1-5) binding sites. These data suggest that the D1115N substitution of murine C3b primarily perturbs interactions with the C-terminus of FH and hence the ability of deposited C3b^{D1115N} on the endothelial cell surface to be regulated by FH. This is somewhat surprisingly, based on the deficit in MCP binding noted with this change (59, 127). However, it is clear that the mutation has only subtle effects, if any, on the interaction of mouse C3b with Crry or the N-terminus of FH. This likely reflects differences in the contact residues/structures of mouse C3 in the context of Crry compared with human C3 in the context of MCP but it may give important information regarding the pathogenic burden of the loss of interaction with MCP versus FH. Clinically, MCP mutations rarely progress to end stage renal disease (ESRD) this is contrast to the poor renal prognosis associated with FH and C3 mutations (1, 47, 134). A failure of FH to engage

fully with the TED is expected to be particularly detrimental to protection of host-cell surfaces from excess complement activation. We also found evidence that C3b^{D1115N} is marginally more resistant than wild-type C3b to fluid-phase FH and FI-mediated cleavage. This, in concert with the MCP deficiency, apparently resulted in lower FB levels in one of the patients. Interestingly, we also detected an increase in FH levels in the plasma of B6-C3^{D1115N} mice. This suggests a compensatory up-regulation of *CFH* expression in an attempt to regulate the mutant C3b or that *CFH* expression can be modulated by the C3-driven inflammatory response. This observation is consistent with the mouse FH W1206R model of TMA in which elevated FH levels were also observed (56). Notably, both National aHUS service patients with the *C3*,p.D1115N mutation possessed plasma levels of FH above the normal range on the majority of readings, reaffirming the parallels of our model to that of the human disease.

It is clear from previous work with transgenic mice that more significant plasma C3 depletion than that seen in the B6-C3^{D1115N} mice may lead to the alternative phenotype of MPGN/C3G (135-137). Moreover, normal fluid-phase regulation is preserved in all of the mouse models of aHUS reported to date (54, 56, 138). The phenotype we obtain is that of aHUS, as evidenced by the histological features of a renal TMA rather than C3G. We therefore infer that any enhanced resistance to fluid-phase cleavage by FI of C3b^{D1115N} is not a major contributor to the disease-like symptoms observed in our model. Lower plasma C3 level are seen in many c-aHUS humans with C3 mutations (59, 127). The lower C3 levels in our murine model are fully consistent with previously published mouse models of a TMA (54, 56).

Thus I can conclude that in B6-C3^{D1115N} mouse, once C3b^{D1115N} is deposited on a surface, a positive-feedback process can operate that is neither controllable by FH nor restricted by a shortage of C3. This leads to extensive C3b deposition and activation of the terminal pathway, as evidenced from our observation of C5 consumption coupled with glomerular C9 deposition. Thus my data emphasize the delicate balance of complement regulation; disease develops when the balance is disturbed and the threshold of regulatory ability is breached. My B6-C3^{D1115N} animals retain the C3 'resources' to overwhelm complement regulation at the cell surface despite their plasma C3 levels being lower in comparison to their wild-type counterparts

My unique model of C3 convertase dysregulation has parallels with a study by the Song group in which the aHUS-linked single amino acid substitution W1206R was transferred from human FH into murine FH (56). Homozygous FH W1206R mice developed a renal phenotype consistent with aHUS but a significant proportion of animals also demonstrated an aggressive

TMA with significant thrombus found in multiple organs. Analysis of key organs in B6.C3^{D1115N} animals that required euthanasia due to ill health revealed no evidence of large or micro thrombi.

Given the successful use of C5 inhibition in aHUS patients (14, 17, 139-141) coupled with previous work showing that the disease is dependent on C5 (55) I sought to further validate our model through genetic deletion (C5$^{-/-}$) and the murine C5 inhibitor BB5.1. As predicted, this rescued the phenotype, with 100% survival in B6.C3^{D1115N} mice at 30 days post-partum. Whilst C3 deposition in the kidney of BB5.1-treated mice appeared unchanged, there was a reduction in glomerular C9 deposition. This suggests that C5a and/or MAC are critical to the endothelial dysfunction and subsequent development of a TMA.

Eculizumab has revolutionised the treatment of patients with aHUS, however, we do not yet know what the long-term effects of this drug will be in our patient population. Whilst inhibiting at the level of C5 arrests disease, it does not target the effect of a persisting dysregulated alternative pathway and subsequent upregulation of C3. This is a vital question to answer as it translates to all complement mutations associated with aHUS and could directly impact on longevity of treatment. It has been hypothesized that over time patients on C5 inhibiting therapy may revert to a C3 glomerulopathy due to sustained C3 activation. My 12 month mouse cohort provides us with the clearest evidence to date that long term C5 inhibition is unlikely to result in an alternative complement mediated renal disease, despite the presence of deposited C3 within the glomeruli. Extrapolating from a 12-month old mouse to man is the equivalent of 40 human years (142), thus my data highlights that C5 blockade in patients for this time frame will be unlikely to lead to an alternative disease process.

My C3 gain-of-function mouse model of aHUS will allow the dissection of the independent roles of C5a and MAC in the pathogenesis of disease with a clarity not achievable by other currently available models. Furthermore, the C3 gain-of-function model offers clear potential to assess therapies targeting the alternative pathway directly, such as homodimeric minimal-FH (143), CR2-FH (144) and anti-properdin (145) in the most realistic model of complement genetic alterations thus far conceived. One major aim of my studies is to help test therapeutics that can mitigate against the increased risk of infections posed by long-term use of Eculizumab (146-149).

In summary, my novel mouse model of aHUS, engineered by using a single point mutation in C3, recapitulates the clinical phenotype found in man. This C3 mutation results in systemic complement activation and endothelial dysfunction culminating in a renal TMA. The model provides the opportunity to investigate the roles played by various players downstream of C3 activation and is a test bed for future complement therapeutics. Developing a therapy to restore complement homeostasis would, in addition, be transferable to several other endothelial-damage mediated diseases for which therapy remains an unmet clinical need.

4.6 Strengths and limitations of work

Interestingly, only homozygotes mice develop spontaneous disease early in life while patients are heterozygous for *C3*,p.D1115N. This is consistent with the notion that the genetic change predisposes to the human disease, but an environmental trigger is needed for development of the disease (1, 15, 51). I have tracked our B6.C3$^{D1115N+/-}$ mice for 12 months and to date there is no evidence of the animals developing disease, consistent with the environmental trigger hypothesis. Whilst this absence of disease in the heterozygotes could be seen as a limitation of this study, we would argue that they represent an invaluable model to identify the factors beyond uncontrolled complement activation that drives aHUS i.e. the B6.C3$^{D1115N+/-}$ mice will be used to investigate a range of potential triggers to see if they can precipitate a c- aHUS. The spontaneous model will enable testing of a variety of complement inhibiting therapies, and importantly, test withdrawal of therapy and remission monitoring. This should culminate in a wealth of translation data that will directly inform future clinical trials and targeted therapies, with the overall aim of improving patient outcome from complement-mediated diseases.

4.7 Future work

My next steps to generate translational data were to backcross the B6-C3^{D1115N} mouse model of c-aHUS onto a C5aR$^{-/-}$, and C7$^{-/-}$ background. This will enable me to determine the specific roles of C5a and C5b-9. The model is rescued through C5 genetic deletion and therapeutic inhibition. What we do not know is if the predominant driver of pathology is C5a or C5b-9. By undertaking these genetic backcrosses, it will allow me to see if current complement inhibiting therapy can be refined. Currently, there is an oral C5a receptor inhibitor which has successfully progressed through clinical trials for ANCA associated vasculitis. Alternatively, targeting C7

(thus absence of C5b-9) could be favoured over C5, as it is not an acute phase protein, and would not require as large a dosing as C5, thus reduced production costs.

Chapter5 The Balb/c.C3^{D1115N}.C5aR1$^{-/-}$ & B6.C3^{D1115N}.hC5aR1$^{+/+}$ mice

5.1 Introduction

The C3^{D1115N} mouse model of c-aHUS enables us to explore the individual effect of C5a/C5aR mediated signalling upon disease development. I sought to determine both the effect of mouse strain and C5a by backcrossing onto the Balb/c strain. To mitigate for the potential strain effects, and in conjunction with Idorsia, a B6-C3^{D1115N}.hC5aR1$^{+/+}$ was generated to enable therapeutic oral C5aR1 inhibition upon the B6 strain. From previous published work using the FH^{W1206R} mouse, genetic deletion of C5aR1 did not rescue the renal phenotype. Although my mutation was in *C3*, given its intricate location with FH CCPs 19-20 I hypothesise our results would emulate that of the FH^{W1206R} mouse.

5.2 Hypothesis

C5aR1 genetic deletion or oral administration of a C5aR1 antagonist will not prevent a renal TMA in the C3^{D1115N} mouse model of c-aHUS.

5.3 Aims of Chapter

- Cross the B6.C3^{D1115N} mouse to generate the Balb/c.C3^{D1115N} and Balb/c.C3^{D1115N}.C5aR1$^{-/-}$

- Compare phenotypes of the B6.C3^{D1115N} and Balb/c.C3^{D1115N}

- Undertake histological and renal function analysis of the mice to see if there are features of TMA in the Balb/c.C3^{D1115N}.C5aR1$^{-/-}$.

- Validate the B6.C3^{D1115N}.hC5aR1$^{+/+}$ as a model of c-aHUS and test prophylactic administration of ACT-1014-6470 (oral C5aR1 antagonist).

5.4 Results

5.4.1 Characterisation and validation of Balb/c.C3^{D1115N}

5.4.1.1 Mouse genetic cross

The B6.C3^{D1115N} mouse was crossed onto the Balb/c.C5aR1$^{-/-}$, with the resultant Balb/c.C3^{D1115N}.C5aR1$^{-/-}$ then backcrossed onto the Balb/c.C5aR1$^{+/+}$ to generate the Balb/c.C3^{D1115N}.C5aR1$^{+/+}$. Phenotypic characterisation of both the Balb/c.C3^{D1115N}.C5aR1$^{-/-}$ and the Balb/c.C3^{D1115N}.C5aR1$^{+/+}$ was contemporaneous. For the purposes of the thesis, I show first the comparison of the C3^{D1115N} on the B6 and Balb/c strains then latterly compare the effect of C5aR1 genetic deletion.
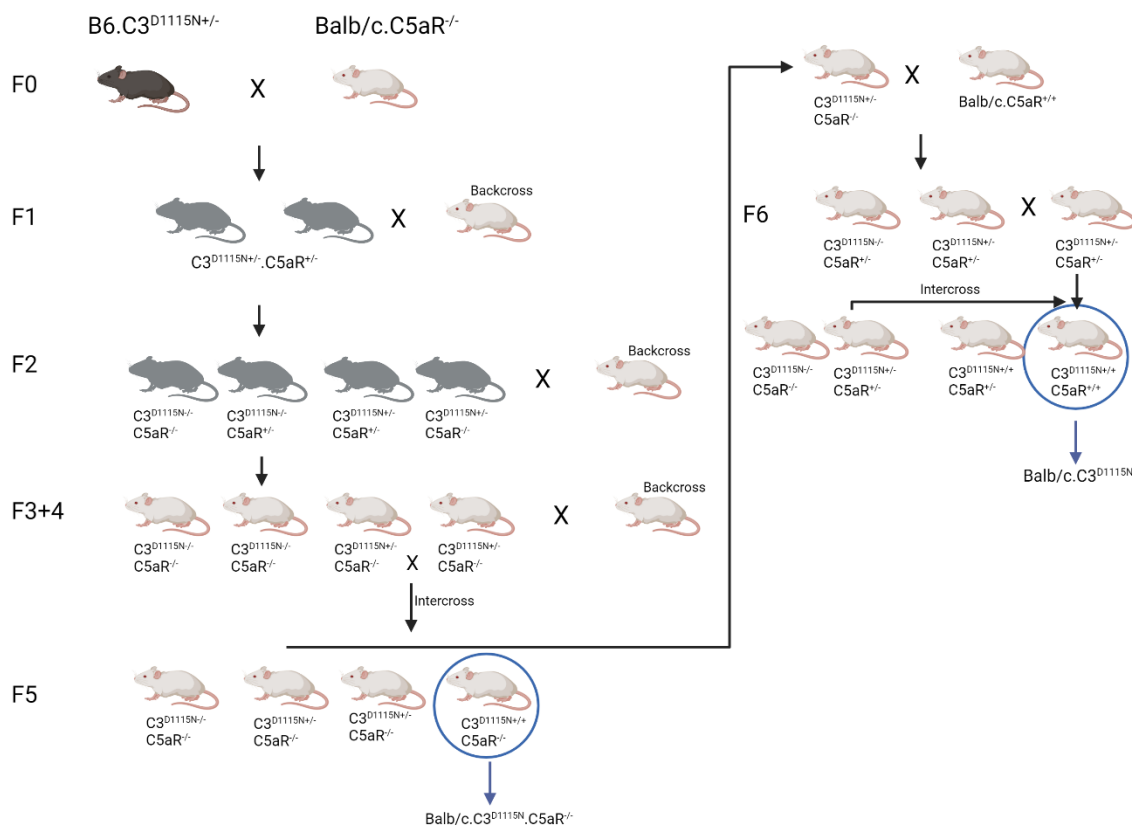
Figure 81 Backcrossing of the B6.C3^{D1115N} mice

Schematic showing the backcross undertaken to generate both the Balb/c.C3^{D1115N}.C5aR1$^{-/-}$ and Balb/c.C3^{D1115N}.C5aR1$^{+/+}$

5.4.1.2   B6.C3^{D1115N} and Balb/c.C3^{D1115N}

To determine the overall mortality both groups were aged to 12 months, with many mice succumbing to ill health before reaching the desired end point. Despite an observed higher mortality in the Balb/c.C3^{D1115N} this was not statistically different to the B6.C3^{D1115N} mice.
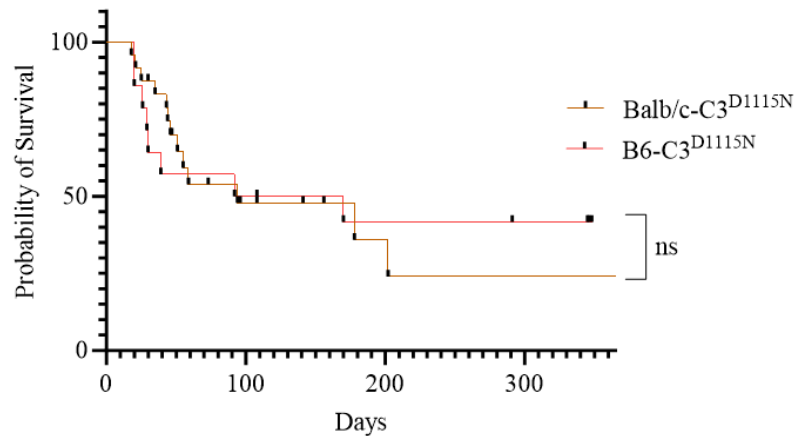
Figure 82 Balb/c.C3^{D1115N} and B6.C3D1115N overall survival
No difference in survival was observed between C3^{D1115N} on either the Balb/c (n= 16) or C57BL6 (n= 14) mouse strain. Kaplan-Meier survival curve analysis. ns=non significant.

5.4.1.3   Renal injury in the B6-C3^{D1115N} and Balb/c-C3^{D1115N}

As in my initial characterisation of the B6-C3^{D1115N}, I monitored spontaneously voided urine and identified a proportion of the mice exhibited proteinuria and haematuria. Renal injury was confirmed on terminal bleeds, which identified elevated BUN levels in the Balb/c.C3^{D1115N} that were similar to their B6.C3^{D1115N} counterparts.
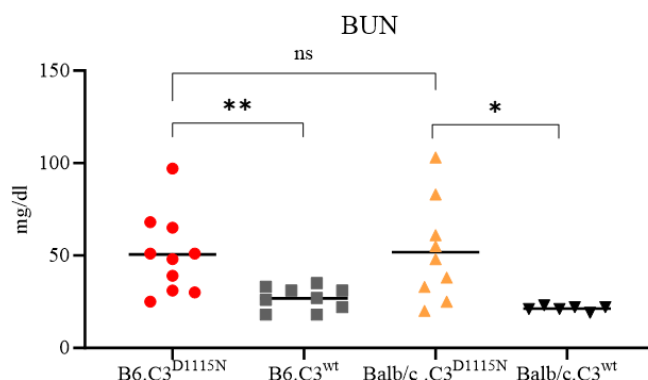
Figure 83 BUN analysis.

*Blood urea nitrogen levels of B6.C3^{D1115N} (n=10) and Balb/c.C3^{D1115N} (n=9) and their C3^{wt} controls (B6.C3^{wt} n=9, Balb/c.C3wt n=6). No significant difference observed between the two strains of C3^{D1115N} mice. Whole blood obtained from terminal cardiac puncture and analysed on the ISTAT using the Chem8$^+$ cartridge. Analysed using 2-way ANOVA with Tukey's multiple comparison. Mean ±SEM. ns= non significant, *P<0.05, ** P<0.01.*

5.4.1.4   Haemoglobin levels

Haemoglobin levels were lower as expected in the Balb/c.C3^{D1115N} cohort and in keeping with the B6.C3^{D1115N}, illustrating that the mice had evidence of anaemia.
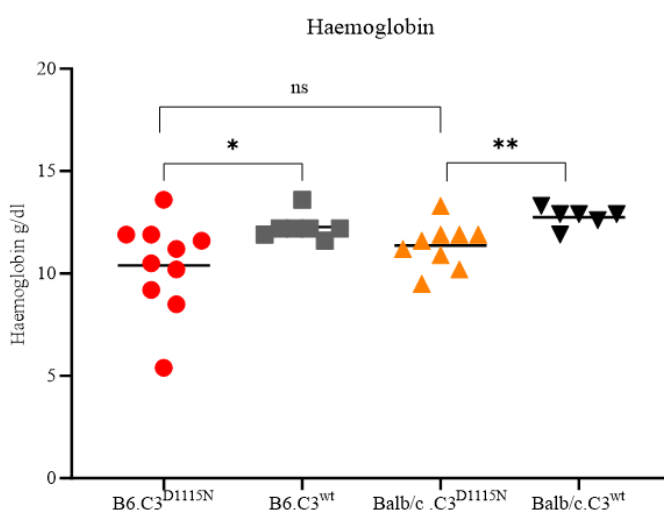
Figure 84 Haemoglobin levels in the B6.C3^{D1115N} and Balb/c.C3^{D1115N} and their C3^{wt} controls. No significant difference observed between the two strains of C3^{D1115N} (B6.C3^{D1115N} (n=10) and Balb/c.C3^{D1115N} (n=9)). Wild type Balb/c (n=9) and C57BL6 mice (n=9) had statistically higher

142

haemoglobin levels compared to their $C3^{D1115N}$ counterparts. Whole blood obtained from terminal cardiac puncture and analysed on the ISTAT using the Chem8+ cartridge. Analysed using 2-way ANOVA with Tukey's multiple comparison. Mean ±SEM. ns=non significant, *P<0.05, ** P<0.01.

5.4.1.5 Reticulocyte and Platelet count in the Balb/c.C3^{D1115N}

Reticulocyte counts were high in the Balb/c-C3^{D1115N} reflecting the appropriate reticulocytosis due to the haemolytic anaemia. Unfortunately, due to analyser error only three platelet samples could be processed, of which two had very low platelets in keeping with the thrombocytopenia.
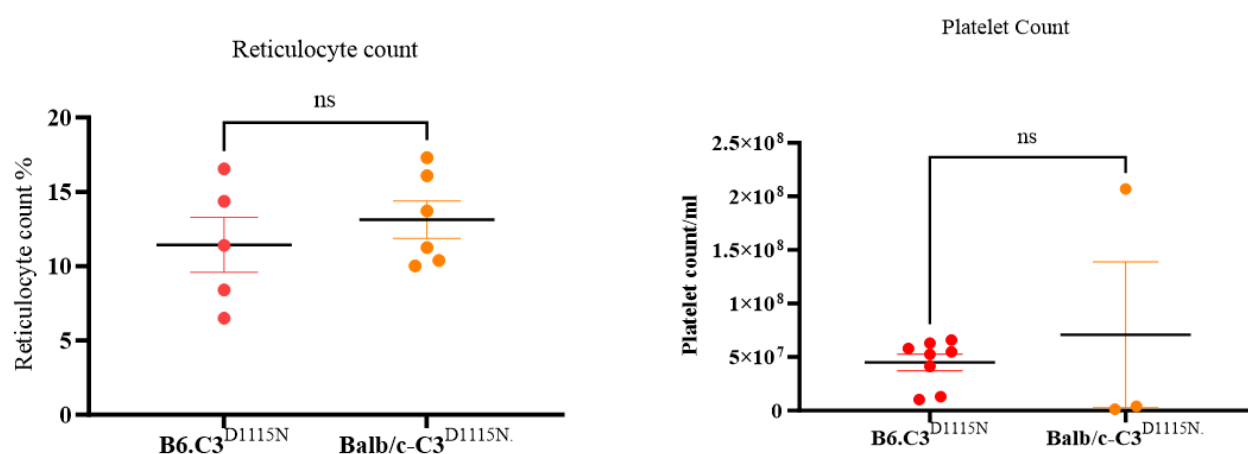
Figure 85 Reticulocyte and Platelet count in the Balb/c.C3^{D1115N} mice.
Reticulocyte count B6.C3^{D1115N} (n=5) and Balb/c.C3^{D1115N} (n=6), Platelet count B6.C3^{D1115N} (n=8) and Balb/c.C3^{D1115N} (n=3)). Analysed using unpaired t test. Mean ±SEM. ns=non-significant.

5.4.2 TMA on histological analysis of the Balb/c.C3^{D1115N}

Finally, the histological analysis confirmed that the Balb/c.C3^{D1115N} developed a renal TMA as expected.
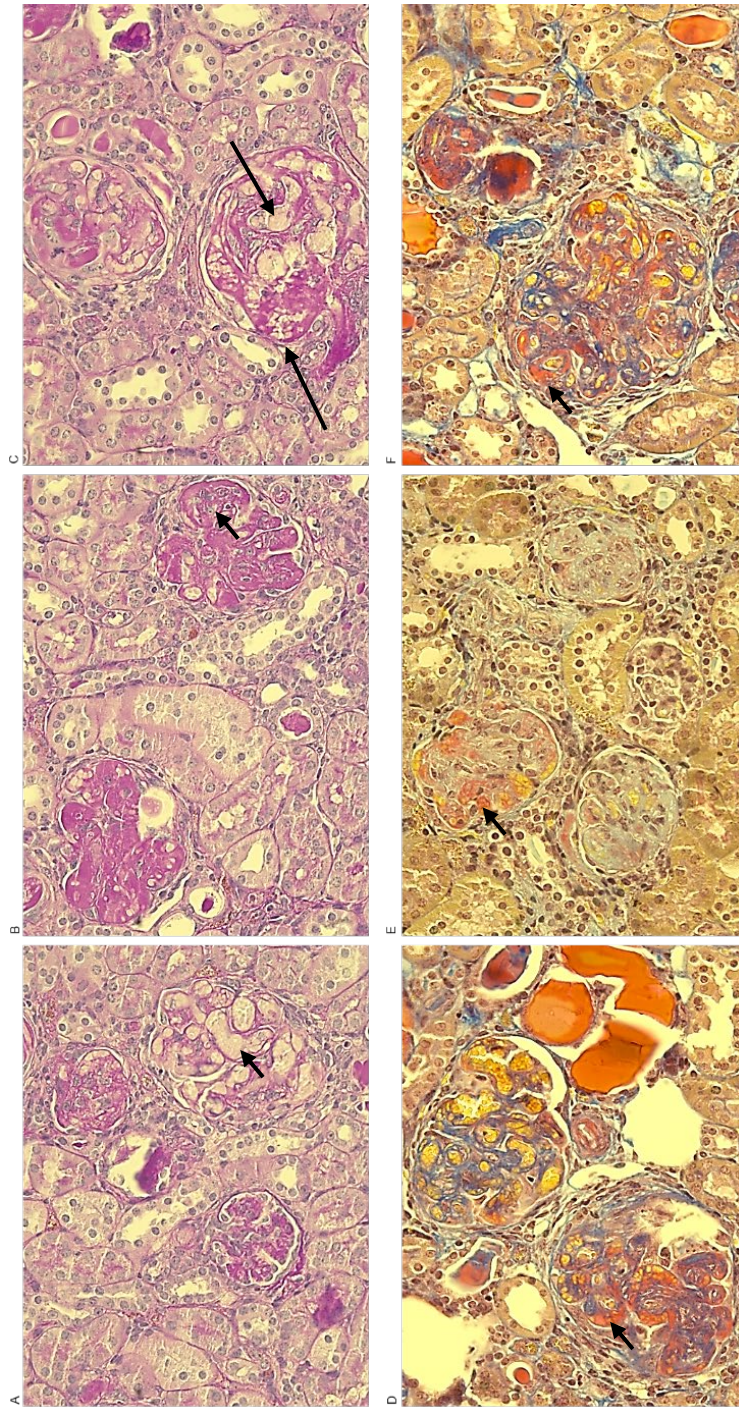
Figure 86 Histological analysis of Balb/c. C3^{D1115N} kidney.

(A-C) PAS stained section showing classical features of thrombotic microangiopathy. A- glomerular microaneurysms formation, B- double contouring of glomerular basement membrane. MSB stains (D-F) showing fibrin deposition and glomerulosclerosis. Pathology indicated by black arrows. All images taken at x40 magnification.

5.4.3 Immunofluorescence of Balb/c.C3^{D1115N}

Glomerular complement deposition was seen in the Balb/c.C3^{D1115N} mice and the pattern of mesangial deposition mirrored that seen in the B6.C3^{D1115N} mice.
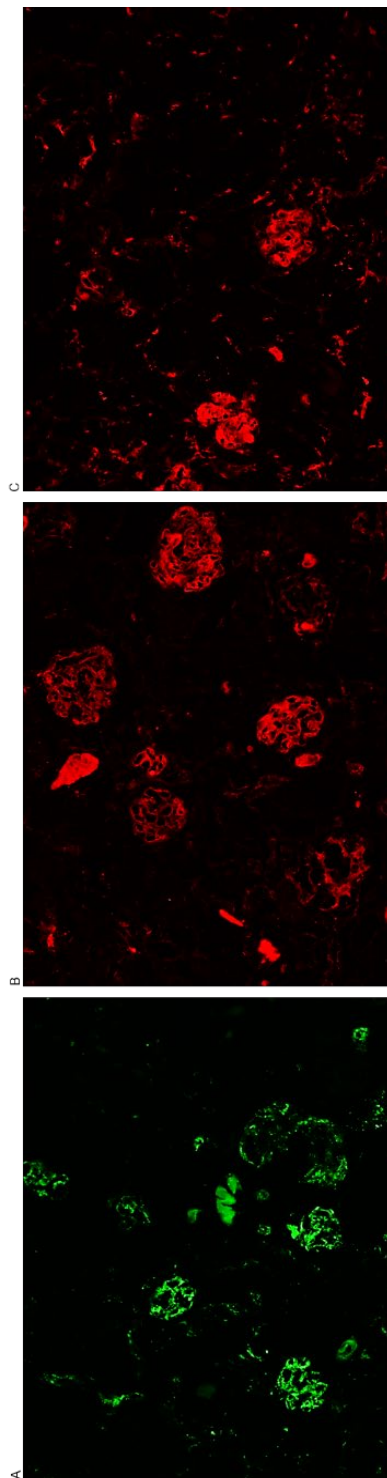
Figure 87 Immunofluorescence of Balb/c.C3^{D1115N} kidneys.
 *C3 glomerular deposition (**A**), C9 glomerular deposition (**B**), Fibrin glomerular deposition (**C**). All images taken at x20 magnification.*

5.4.4 Characterisation of the Balb/c.C3^{D1115N}.C5aR1$^{-/-}$

5.4.4.1 Genotyping of Balb/c.C3^{D1115N}.C5aR1$^{-/-}$

Genotyping of the mice confirmed the generation of Balb/c.C3^{D1115N}.C5aR1$^{-/-}$ pups, obtained from ear clips taken at 14 days post-partum. All mice underwent daily clinical monitoring as per the Home office license.
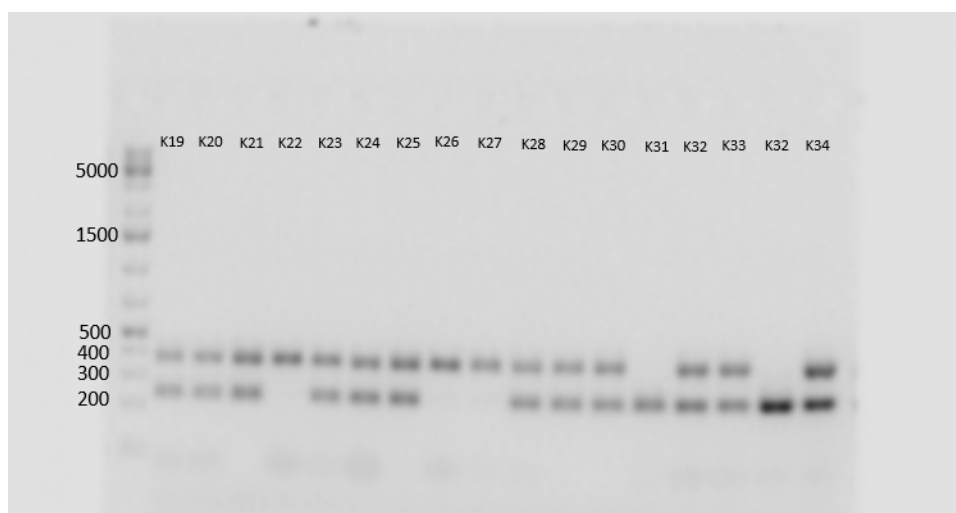
Figure 88 1.5% Agarose gel of PCR products of mice ear clips
A wild type fragment at 386bp (K22), a heterozygous C5aR1$^{+/-}$at 386bp and 244bp (K21) and homozygote C5aR1$^{-/-}$ (K32) ran with a 5kb Gene Ruler ladder for reference.

5.4.4.2 Survival benefit from all-cause mortality with C5aR1$^{-/-}$

Three cohorts of the Balb/c.C3^{D1115N}C5aR1$^{-/-}$ mice were tracked (3, 6 and 12 months) and analysed at each of their end points. I did see a significant improvement in survival following genetic deletion of C5aR1, yet these mice still had increased mortality compared to the Balb/c.C3^{WT}.C5aR1$^{-/-}$.
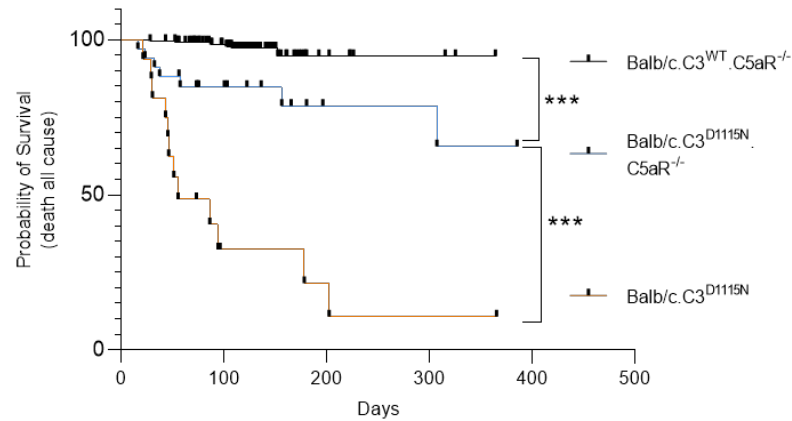
Figure 89 Kaplan Meier survival analysis of overall mortality in the Balb/c.C3^{D1115N} (n=16) compared to Balb/c.C3^{D1115N}.C5aR1$^{-/-}$ (n=34) and Balb/c.C3^{WT}.C5aR1$^{-/-}$ (n=239). ***P<0.001.

5.4.4.3 TMA free survival in the Balb/c. C3^{D1115N}.C5aR1$^{-/-}$

Interestingly, of the eight animals that required euthanasia due to health concern, three had an alternative cause of death. Therefore, whilst there was higher attrition in the Balb/c.C3^{D1115N}C5aR1$^{-/-}$ mice this was not always exclusively due to the development of a TMA. That said, a proportion of surviving mice in the 6 (3/7 mice) and 12 (3/5 mice) month cohorts had histological evidence of disease but this was only identified on post-mortem analysis.
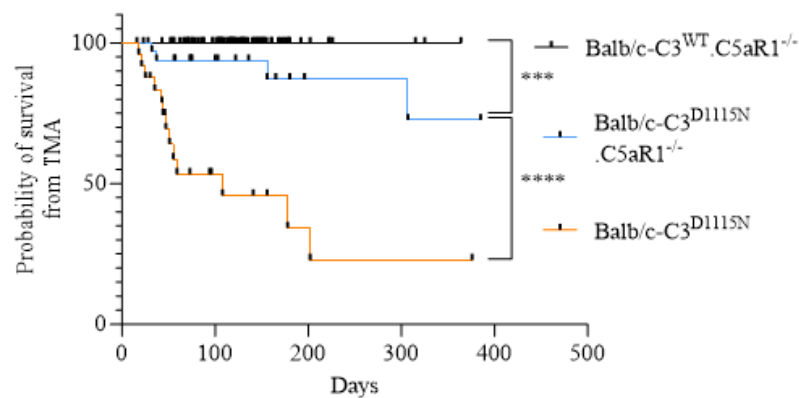
Figure 90 TMA free survival.

100% TMA free survival observed in the Balb/c. C3^{WT}.C5aR1$^{-/-}$. 3/8 animals in the Balb/c.C3^{D1115N}.C5aR1$^{-/-}$ had an alternative cause of death i.e. bad teeth, runt of litter, clear urinalysis with no histological evidence of disease. One animal was excluded from the analysis as no date of death was recorded. ***P<0.001.

5.4.4.4 Chronology of mice survival

The schematic below shows that the majority of the B6.C3^{D1115N} mice require euthanasia within the first month of life. In the Balb/c.C3^{D1115N}, although overall survival was similar, the mice appeared to succumb to disease typically after the first month of life. The Balb/c.C3^{D1115N}.C5aR1$^{-/-}$ had a higher attrition rate compared to Balb/c.C3^{WT}. The sequential aged cohorts were taken at 3, 6 and 12 months. Of the 8 animals that succumbed, 4/7 were attributed to renal disease, and 3 were attributed to alternative cause, with one excluded due to no data recorded.
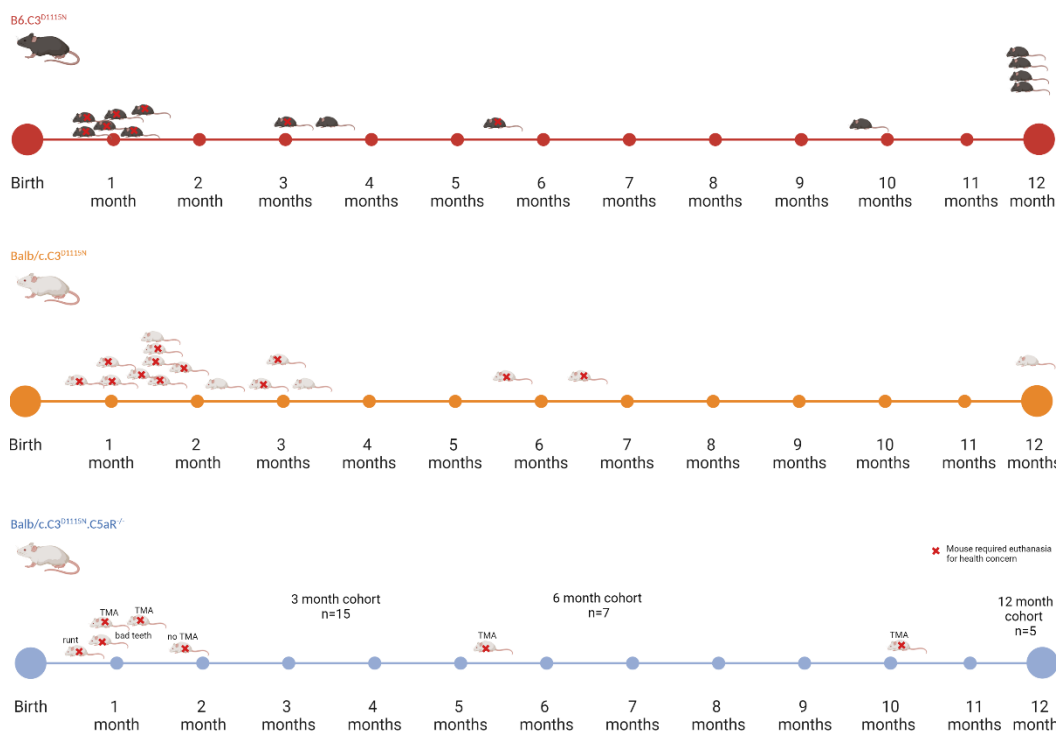
Figure 91 Schematic diagram detailing timeline of when the three (B6.C3^{D1115N}, Balb/c.C3^{D1115N}, Balb/c.C3^{D1115N}.C5aR1$^{-/-}$) different strains of mice succumbed to disease.

5.4.4.5   TMA in a Balb/c-C3^{D1115N}.C5aR1^{-/-} mice

Although there was an overall improvement in survival following genetic deletion of C5aR1, a small proportion of mice still did develop a TMA and required euthanasia due to this. Therefore, I can conclude that C5a/C5aR1 mediated signalling is not critical for the development of a TMA within the Balb/c-C3^{D1115N} mouse model of c-aHUS. That said C5a/C5aR1 removal clearly attenuates the disease penetrance.
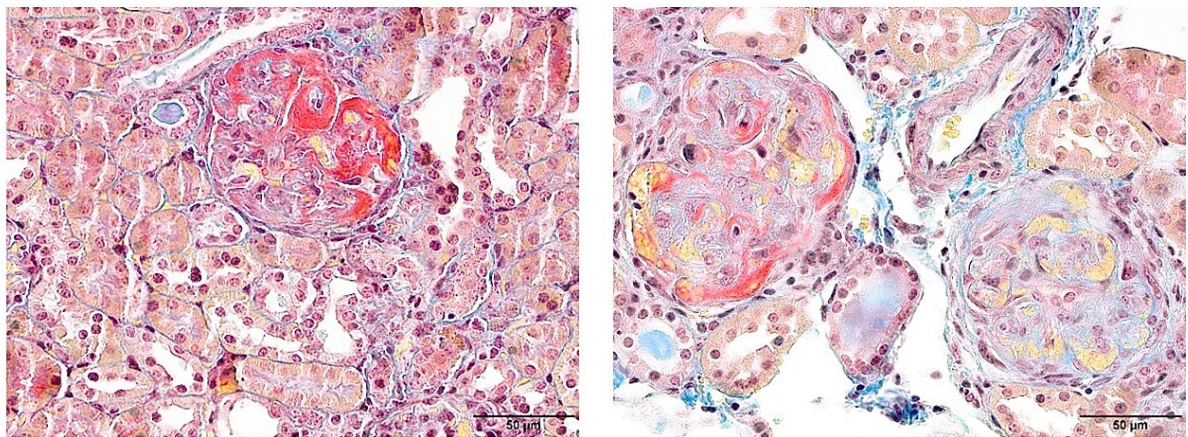
Figure 92 MSB stains showing thrombotic microangiopathy changes in two different Balb/c-C3^{D1115N}.C5aR1$^{-/-}$ mice that required euthanasia due to health concerns, thus their deaths were attributed to a renal TMA. Images taken at x40 magnification.

In an additional attempt to help explain the death of the remaining three animals, the Balb/c-C3^{D1115N}.C5aR1$^{-/-}$ underwent a further comprehensive histological review of brain, lung, heart, liver, spleen and bone marrow at Charles River research animal diagnostics but no significant pathology was identified. We know from the original publication of the C5aR$^{-/-}$ mice that they are immunocompromised evidenced through their vulnerability to lung infections (120).
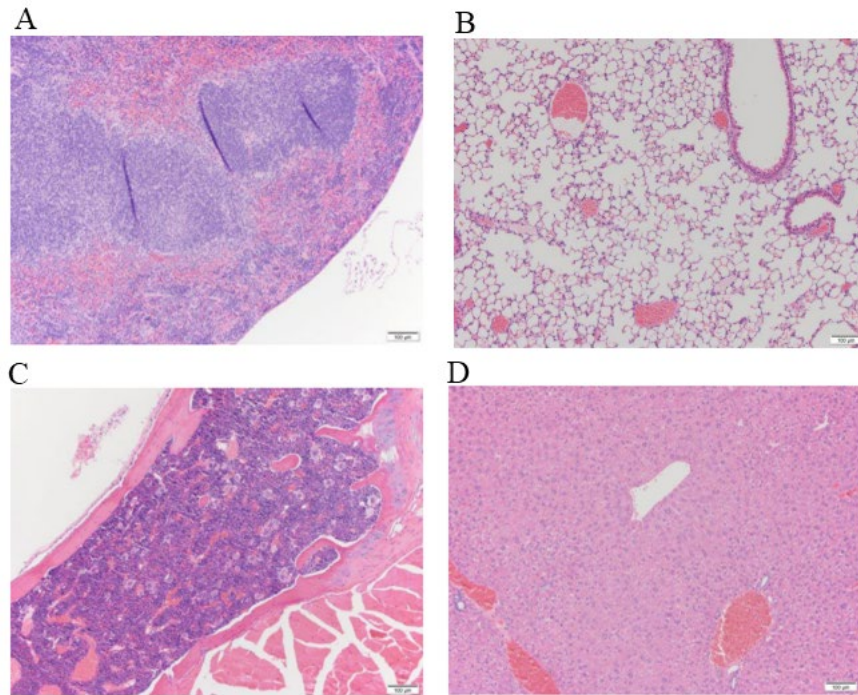
Figure 93 Review of the Balb/c.C3^{D1115N}.C5aR1$^{-/-}$ for extra renal manifestations.

An external pathology review of Spleen (A), Lung (B), Sternum, bone marrow (C), Liver (D) found all organs within normal limits.

5.4.4.6   Renal limited TMA in a proportion of the ageing Balb/c-C3^{D1115N}.C5aR1$^{-/-}$ mice

After analysis of the histology from the Balb/c-C3^{D1115N}.C5aR1$^{-/-}$ surviving mice (end point cohorts), it became clear that, a further 3/7 of the mice in the 6-month and 3/5 in the 12-month cohorts showed histological evidence of TMA. No mice (n =15) in the 3 month cohort showed evidence of TMA. The renal limited TMA identified in the aged cohorts by post-mortem histological analysis may represent a smouldering TMA, or recovery from a historical episode of TMA, which remained clinically undetectable during our clinical monitoring. Consequently, this suggests that removal of C5a-C5aR1 axis can attenuate the disease process
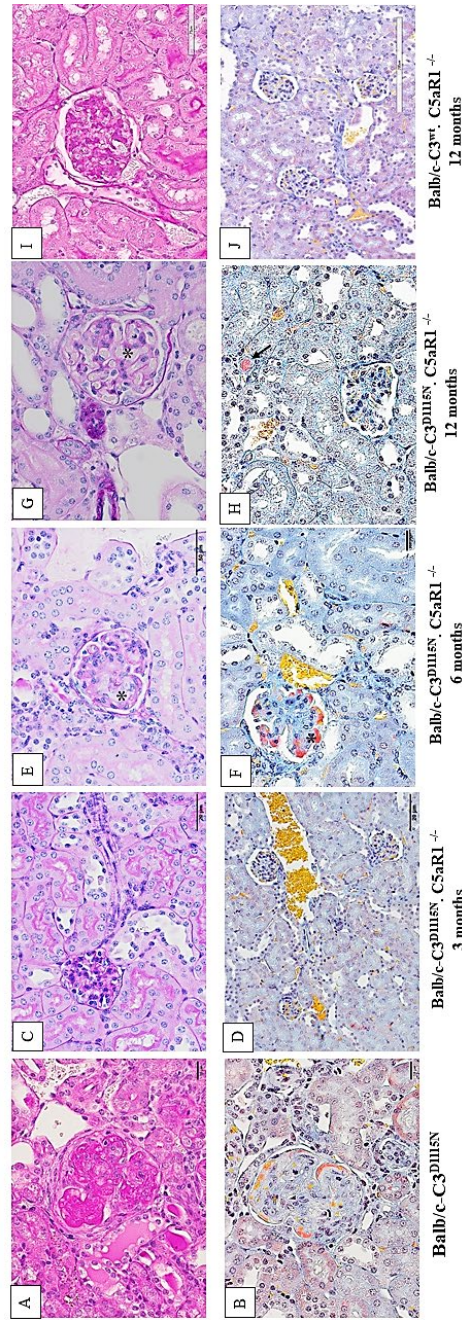
Figure 94 Histology of the 3, 6 and 12 month Balb/c-C3^{D1115N}.C5aR1$^{-/-}$cohorts.

(A) PAS stained section and (B) MSB stained section of a Balb/c-C3^{D1115N} control mouse. (C,E,G) PAS stained sections of 3, 6 and 12-month Balb/c-C3^{D1115N}.C5aR1$^{-/-}$ mice. (D,F,H) MSB stained sections of 3, 6 and 12-month Balb/c-C3^{D1115N}.C5aR1$^{-/-}$ mice. Histological changes in keeping with a TMA begin to appear in the 6 month cohort and are seen in the 12 month cohort marked by an asterisk. A-I taken at x40 magnification, H taken at x20 magnification.

5.4.4.7 No biochemical evidence of renal injury in the Balb/c-C3^{D1115N}.C5aR1$^{-/-}$ cohorts.

In the Balb/c-C3^{D1115N}.C5aR1$^{-/-}$ mice that remained clinically well until their allotted end point, I found no biochemical evidence of an impaired renal function as determined by normal BUN levels compared to age matched controls.
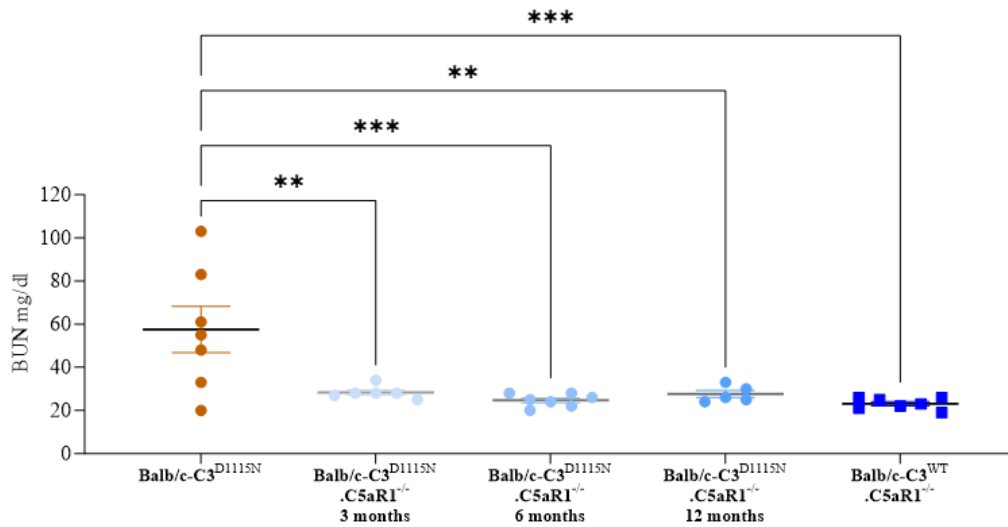
Figure 95 BUN levels in the Balb/c.C3^{D1115N}.C5aR1$^{-/-}$

*The surviving Balb/c-C3^{D1115N}.C5aR1$^{-/-}$ mice that reached their allotted time points had lower BUN levels reflecting a reduction in renal injury. Balb/c-C3^{D1115N} (n=6), Balb/c-C3^{D1115N}.C5aR1$^{-/-}$ 3 months (n=6), 6 months (n=7), 12 months (n=5), Balb/c-C3^{wt}.C5aR1$^{-/-}$ (n=7). Analysed using 2-way ANOVA with Tukey's multiple comparison. Mean ±SEM. ** P<0.01, *** P<0.001.*

5.4.4.8 Haemoglobin levels, reticulocyte and platelet count in the Balb/c-C3^{D1115N}.C5aR1$^{-/-}$ cohorts.

Furthermore, haemoglobin levels, platelet- and reticulocyte counts were within normal limits of the surviving mice. These results come with the caveat that in mice that succumbed to TMA and died acutely, no blood was available for real time analysis of renal function or MAHA parameters and so these results are inevitably skewed towards surviving mice.
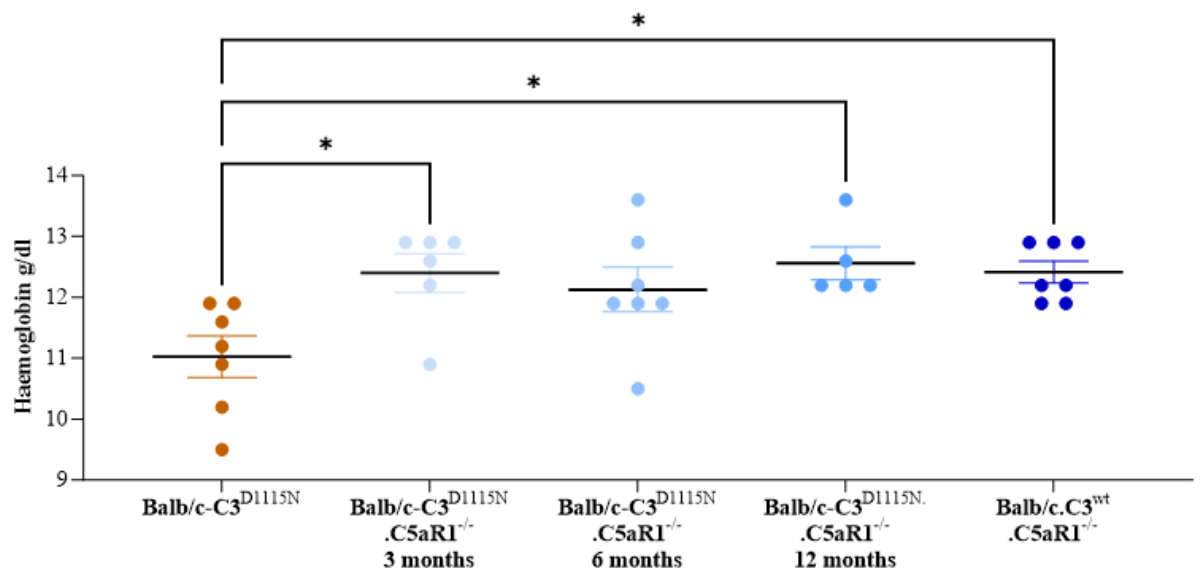
*Figure 96 Haemoglobin levels in the Balb/c-C3^{D1115N} (n=7) and the Balb/c-C3^{D1115N}.C5aR1$^{-/-}$ aged 3- (n=6), 6- (n=7) and 12-month (n=5) cohorts and Balb/c.C3^{WT}.C5aR1$^{-/-}$ control (n=7). Analysed using 2-way ANOVA with Tukey's multiple comparison. Mean ±SEM. *P<0.05.*
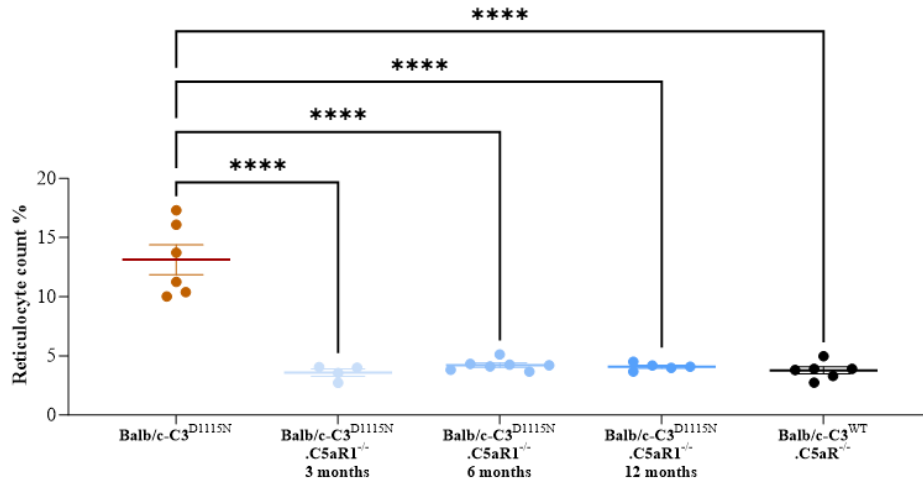
*Figure 97 Reticulocyte count in the Balb/c-C3^{D1115N} (n=6) and the Balb/c-C3^{D1115N}.C5aR1$^{-/-}$ aged 3- (n=4), 6- (n=7) and 12-month (n=5) cohorts and Balb/c.C3^{WT}.C5aR1$^{-/-}$ control (n=6). Analysed using 2-way ANOVA with Tukey's multiple comparison. Mean ±SEM. ****P<0.0001.*
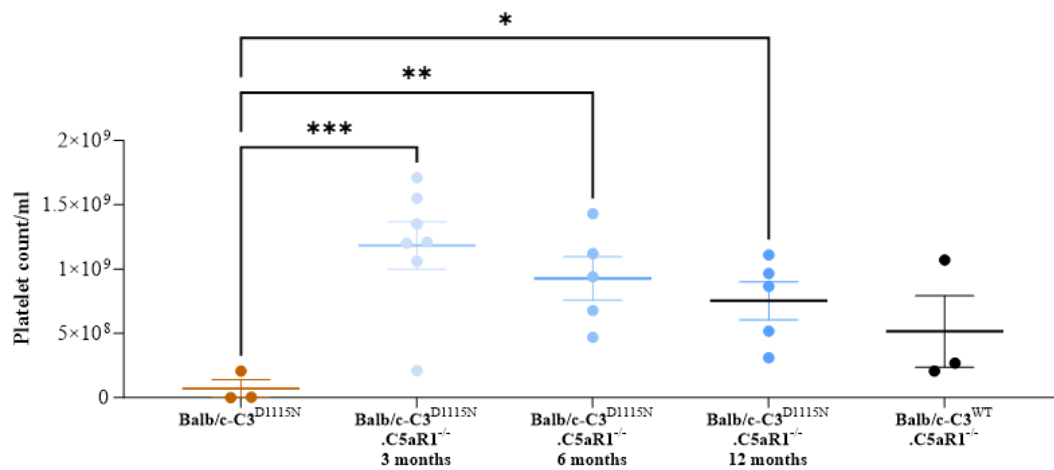
*Figure 98 Platelet count in the Balb/c-C3^{D1115N} (n=3) and the Balb/c-C3^{D1115N}.C5aR1$^{-/-}$ aged 3- (n=7), 6- (n=5) and 12-month (n=5) cohorts and Balb/c.C3^{WT}.C5aR1$^{-/-}$ control (n=3). Analysed using 2-way ANOVA with Tukey's multiple comparison. Mean ±SEM. *P<0.05, ** P<0.01, *** P<0.001.*

5.4.4.9 Immunofluorescence analysis of complement deposition in the Balb/c-C3^{D1115N}.C5aR1$^{-/-}$ mice

The evidence that C5aR1 deficiency attenuates the disease process is further substantiated through the significant reduction in C9 and fibrin deposits in the glomeruli of Balb/c-C3^{D1115N}.C5aR1$^{-/-}$ mice. Similar to what was observed in the B6-C3^{D1115N}.C5$^{-/-}$ mice, C3 glomerular deposits were increased in Balb/c-C3^{D1115N}.C5aR1$^{-/-}$ mice with advancing age.
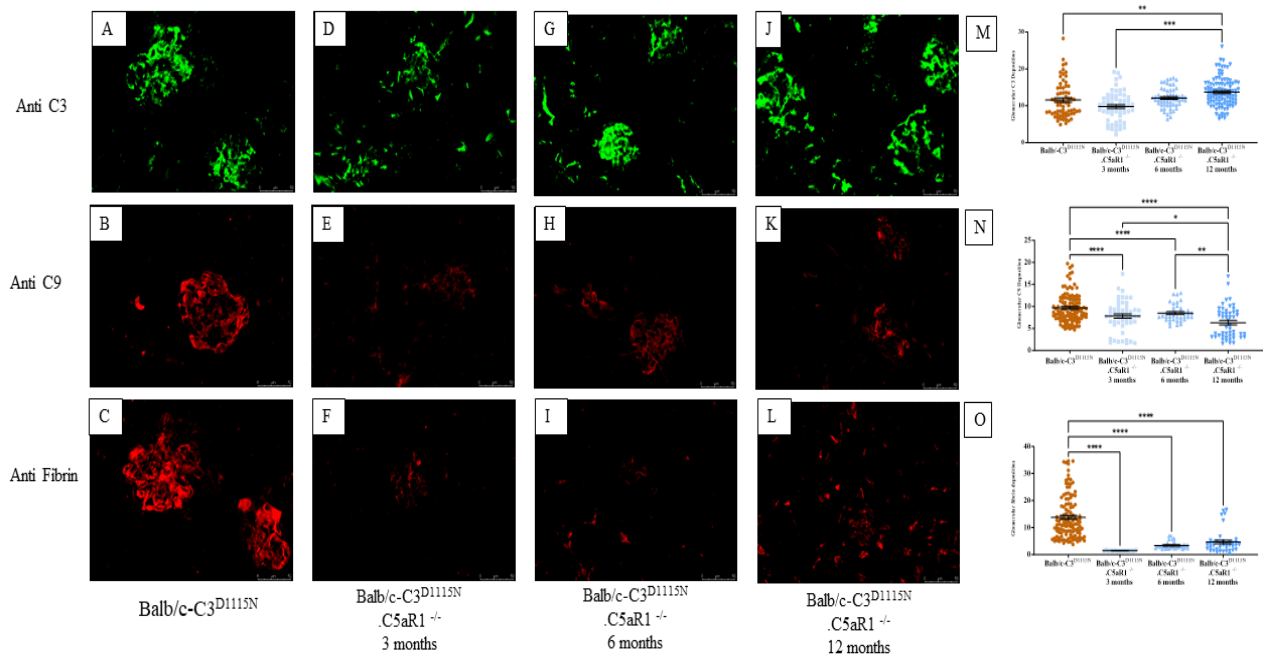
Figure 99 Glomerular complement deposition in the Balb/c-C3^{D1115N} and Balb/c-C3^{D1115N}.C5aR$^{-/-}$ cohorts

A,D,G,J show Glomerular C3 deposition, average number of glomeruli scored n=77, taken from an average of 6 mice. B,E,H,K show C9 deposition, average number of glomeruli scored in each group n=64, C,F,I,L Glomerular fibrin deposition, average number of glomeruli scored n=53. Densitometry analysis of glomerular C3 (M), Glomerular C9 (N), Glomerular Fibrin (O) Analysed using 2-way ANOVA with Tukey's multiple comparison. Mean ±SEM. *P<0.05, ** P<0.01, *** P<0.001, ****P<0.0001

5.4.5 Characterisation of the B6-C3^{D1115N}.hC5aR1$^{+/+}$ mice

To determine if pharmacological blockade of C5aR1 attenuates the disease process in the B6 background, I used an oral C5aR1 antagonist (ACT-1014-6470). To use the agent, which is only active on the human receptor, humanized C5aR1 mice were generated in which mouse C5aR1 was replaced with human C5aR1. A human C5aR1 (with knock out of the murine C5aR1) mouse was generated to order by Cygen Bioscience and provided to this study by Idorsia. After inter cross and generation of a new B6-C3^{D1115N}.hC5aR1$^{+/+}$ double knock-in line, I carried out standard analysis to confirm that the phenotype remained unchanged in the B6-C3^{D1115N}.hC5aR1$^{+/+}$ line. As expected, key features of a renal TMA were readily identified, validating the humanised model for therapeutic testing.
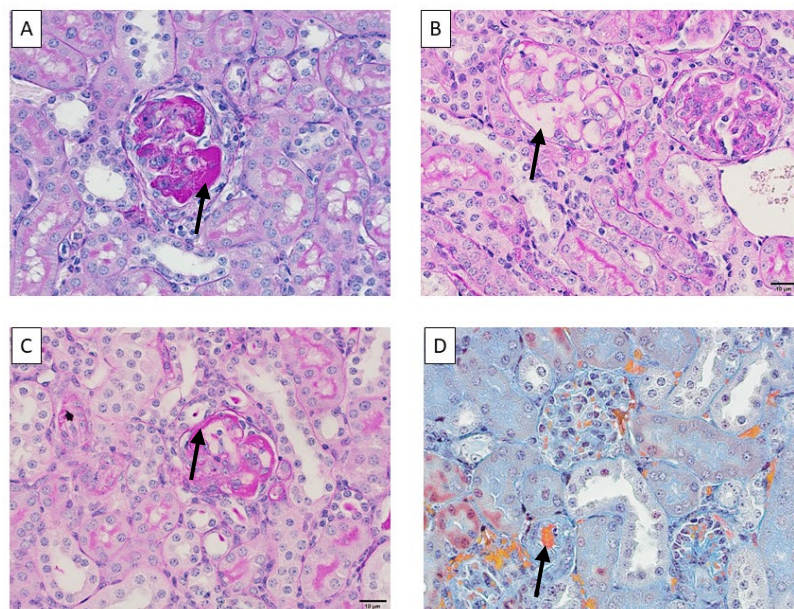
Figure 100 Histological stained sections of B6-C3^{D1115N}.hC5aR1$^{+/+}$ mice confirming the phenotype mirrors that of the B6-C3^{D1115N} with features of thrombotic microangiopathy highlighed by the arrows (A) Segmental sclerosis, (B) Microaneurysm formation, (C) Double contouring of the glomerular basement membrane, (D) Intraluminal thrombus. Images taken at x40 magnification.

5.4.6 Oral inhibition with a C5aR inhibitor (ACT-1014-6470) in the B6-C3^{D1115N}.hC5aR1$^{+/+}$

Mice receiving the C5aR1 antagonist ACT-1014-6470 (~45mg/per day) after weaning (for 8 weeks via diet) showed 100% survival compared to only 35% survival for B6-

C3^{D1115N}.hC5aR1$^{+/+}$ mice on a normal diet. However, there was evidence of renal disease (25ery/ul haem for at least 2 consecutive days) in 3 mice on the oral treatment (figure 102) with 6/12 animals exhibiting post- mortem histological evidence of TMA at the end of the study. Although there was histological evidence of a TMA the mice did not meet criteria necessitating euthanasia within the study duration. Indeed, only the 3 mice with renal disease detected by urine analysis showed a slight elevation in BUN levels in the treatment group (normal range 20 – 36 mg/dl, figure 102, G), reflecting improved renal function across the treatment cohort. When assessing markers of MAHA, normal parameters were observed in the mice receiving the C5aR1 antagonist, except for platelet numbers, which remained low in some of the treated animals (figure 102, H-J). The slightly elevated BUN and marginally lower platelets numbers in some treated mice compared to control may reflect the fact that we also found a spectrum of histological disease (figure 102 K-N). These findings are not surprising and mimic those seen in the Balb/c-C3^{D1115N}.C5aR1$^{-/-}$ strain where genetic knockout of C5aR1 did not prevent a TMA. So, whilst there was still histological evidence of renal disease, the mice did not breach the clinical health score necessitating euthanasia. Thus, this early intervention with therapeutic C5aR1 blockade ameliorated the phenotype in a similar manner to genetic knockout, appearing to clinically quiescent disease rather than abolish it. The persisting histological features seen in both the therapeutic inhibition and genetic deletion of C5aR, in spite of the difference in strains, suggests the disease is smouldering on rather than in full remission.
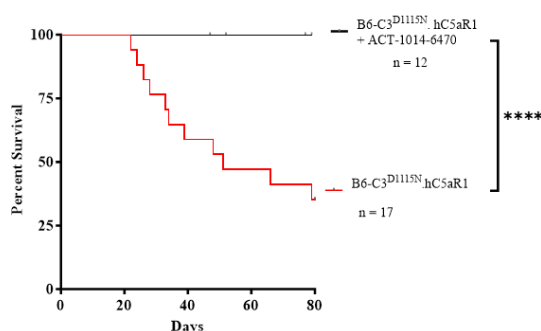
*Figure 101 A survival benefit is provided with the oral C5aR1 inhibitor added to the B6-C3^{D1115N}.hC5aR1$^{+/+}$ suggesting a therapeutic benefit with C5aR1 inhibitor B6-C3^{D1115N}.hC5aR1$^{+/+}$ + ACT-1014-6470 (n=12) vs B6-C3^{D1115N}.hC5aR1$^{+/+}$ (n=17). Kaplan Meier survival analysis, ****P<0.0001.*
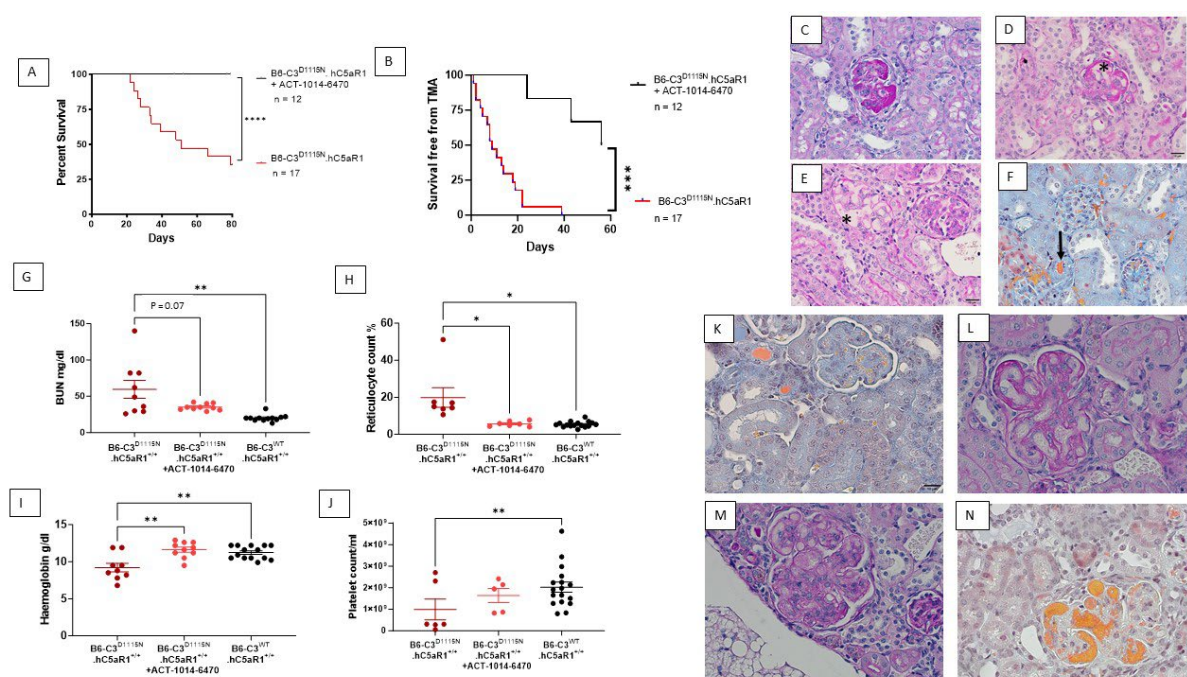
Figure 102 Oral C5aR1 inhibition in the B6-C3^{D1115N}.hC5aR1$^{+/+}$ mice

(A). Survival analysis shows B6-C3^{D1115N}.hC5aR1$^{+/+}$ mice succumb to a spontaneous renal TMA in a similar fashion to the B6-C3^{D1115N} parent strain – confirming full function of the hC5aR1 knock-in gene. The data also demonstrates that early therapeutic treatment of B6-C3^{D1115N}.hC5aR1$^{+/+}$ mice with ACT-1014-6470 (C5aR1 inhibitor) via diet is highly effective. (B) Oral hC5aR1 antagonism does not completely prevent renal disease in the mice, i.e. at least two consecutive days 25ery/ul of haematuria was detected in 3 mice, an indication of renal TMA and an additional 3 mice were found to have renal TMA on histological analysis after cull. Mantel-Cox was used to establish significance. (C,D,E) PAS stained sections showing histological features of TMA (*including double contouring and mesangiolysis) of C3^{D1115N}.hC5aR1 confirming the phenotype following the introduction of the hC5aR1. (F). MSB stain showing fibrin clot in a vessel in the C3^{D1115N}.hC5aR1$^{+/+}$ mouse. N=4 examined. (G). Blood urea nitrogen (plasma marker of kidney impairment) levels collected during terminal bleeds at the end of the study. (H) Mice receiving the C5aR inhibitor have higher levels of haemoglobin compared to untreated controls. (I). Reduced reticulocytosis in treated mice. (J). Improved platelet counts in treated mice. Two-way ANOVA was used for statistical analysis in Graphpad. Data shown as mean ± SEM. Only significant results between the multiple comparison are illustrated, * p <0.05, ** p<0.01, *** p<0.005, **** p<0.0001. Note that as around 50% of B6.C3^{D1115N}.hC5aR$^{+/+}$ died before we were able to collect blood the data in F thru I is skewed to surviving mice, indeed 2 mice show little or no evidence of disease at endpoint. (K-N), Histological analysis of C3^{D1115N}.hC5aR1$^{+/+}$ after 8 weeks of C5aR1 antagonist containing diet. Stained sections showing varied histology in the mice who received the C5aR1 inhibitor treatment, TMA was identified in 6/12 mice treated with a range of TMA. i.e. (K) Thrombi, (L) mesangiolysis/double contouring, (M) mesangiolysis and (N) fibrin deposits.

5.5 Discussion of Results

The Balb/c.C3^{D1115N} phenotype mirrors that seen in the B6.C3^{D1115N}, with a similar observed mortality. Histological evidence of TMA was identified, accompanied with the classical glomerular complement deposition of C3, C9 and fibrin. Renal injury, illustrated through elevated BUN levels, was equivalent, with accompanying lower haemoglobin levels confirming the mice to be anaemic. This proves the C3^{D1115N} mouse model of c-aHUS to be robust and independent of mouse strains, and, allowed me to then determine the effect of C5aR1$^{-/-}$ and thus lack of C5a mediated signalling upon disease development using the Balb/c.C3^{D1115N}.C5aR1$^{-/-}$

Genetic deficiency of C5aR1 confers a survival protection in the Balb/c.C3^{D1115N} mice. Despite this improved survival, 4/20 mice did require euthanasia due to a health concern and were found to have evidence of TMA with no other alternative cause for their health deterioration. Whilst this was typically seen within the first two months of life, two mice required culling at 5 and 10 months respectively. Examining the surviving mice that reached their aged cohorts found histological evidence disease begins to appear from 6 months. Despite the histological appearances, this did not translate into detectable clinical disease in any of the Balb/c.C3^{D1115N}.C5aR1$^{-/-}$ with normal BUN, haemoglobin, platelet and reticulocyte counts. This suggests it is a renal limited TMA and of a less severe endothelial injury as it does not lead to a biochemical renal injury or a detectable MAHA. Suggesting, C5a/C5aR1 signalling is involved in the development of a TMA, but that C5a is not a pre-requisite to the development of a TMA. Given the clinical benefit of C5aR1 deficiency, I next sought to evaluate an oral C5aR1 inhibitor to consolidate our findings.

The C3^{D1115N} mouse model of c-aHUS recapitulates the clinical phenotype both on the C57BL/6 and Balb/c strain, proving the model to be robust, reproducible and independent of the influence of background genetic traits in these mouse strains (150). Pharmacological inhibition through ACT-1014-6470 or *C5aR1* deficiency (removal of the C5a –C5aR1 axis) attenuates disease and prevents any detectable clinical disease in the majority of the mice. That said histological features of renal disease begin to appear in Balb/c-C3^{D1115N}.*C5aR1*$^{-/-}$ mice from 6 months of age. The data supports that excessive C5aR1 signalling in conjunction with dysregulated AP when given time, i.e. chronicity, can lead to TMA. Undoubtedly, this is a less

severe phenotype given it remains sub clinical and does not translate into a detectable renal injury on BUN measurements or a systemic MAHA.

Importantly, the normalisation of some of the clinical parameter in the B6-C3^{D1115N}.C5aR1$^{+/+}$ mice when prophylactically treated with a C5aR1 inhibitor almost completely recapitulates the outcome of the genetic deletion of the *C5aR1* on the Balb/c background. The persisting histological features seen in both the therapeutic inhibition and genetic deletion of C5aR1, in spite of the difference in strains, suggests disease is quiescent without the added 'pressure' of C5a mediated signalling.

My findings share some similarities with a previously published mouse model of renal thrombotic microangiopathy engineered around a FH point mutation (W1206R, FH$^{R/R}$) (151). In this model, C6 and C9 deficiency significantly improved survival and diminished renal TMA, suggesting C5b-8 and C5b-9 were the primary drivers of renal TMA. However, in contrast to my findings, they found no survival benefit with C5aR1 gene deficiency and that the renal TMA persisted (151). In addition to this, neither C6, C9, nor C5aR1 deficiency rescued the haemolytic anaemia or resolved the thrombocytopenia. It is important to highlight the differences in this model to our C3^{D1115N} model. Firstly, their model is built on a point mutation that principally affects the cell binding domain of the complement regulatory protein, FH in comparison to ours, which is a complement activating protein. Secondly, the FH$^{R/R}$ mice develop widespread macrovascular thromboses in multiple organs, which is not typical of the clinical syndrome in man. Interestingly, C5aR1 deficiency did rescue the macrovascular thromboses. The authors postulated the persisting thrombocytopenia was due to the C5aR1 dependent macrovascular thrombosis, but this does not explain why the thrombocytopenia was not rescued through C5aR1$^{-/-}$, nor does it account for the persisting anaemia in the C6 and C9 deficient mice. I would propose my model more accurately reflects the clinical disease in man with the microvascular glomerular thromboses and renal TMA being the dominant pathology. The next chapter will allow a comparison of C5a and C5b-9 following the characterisation of the B6-C3^{D1115N}.C7$^{-/-}$.

Whilst I recognise subtle features of TMA develop in the ageing, Balb/c-C3^{D1115N}.C5aR1$^{-/-}$ these histological features do not appear severe enough to cause significant red cell fragmentation and the systemic MAHA observed in the control animals. The protective effects of C5aR1 deficiency on the glomerular endothelium in our mice mirror that seen in an alternative mouse model of thrombotic microangiopathy induced by antiphospholipid

antibodies. In this study, the authors showed C5a-C5aR1 was a crucial step for glomerular injury induced by complement-activating antibodies in 7-8 week old mice (152, 153). C5aR1 deficiency undoubtedly protects from renal TMA in our mouse model akin to the Antiphospholipid model in 3 month aged mice. Advancing age diminishing this protective effect for reasons which remain to be elucidated. It has been shown that complement activity increases with reducing pH, if subtle features of TMA are developing in the animals this may lead to chronic kidney disease, this could result in a reduction in renal glomerular pH and thus exacerbating complement activation(154). Another possible explanation maybe the role of the C5L2 receptor. The specific role of this receptor remains controversial, but with advancing age, its expression may increase and C5adesArg (less potent form of C5a) binds at a greater affinity to it than C5aR1(155, 156). Literature appears to be conflicted with regards to the ability of the C5L2 receptor to bind C3adesArg/acylation stimulating protein(156, 157). We have not looked at circulating levels of C3adesArg in the Balb/c.C3^{D1115N} mice; we would hypothesise the levels to be increased due to the hyper functional effects of the mutant C3. If C5L2 is able to bind C3adesArg then the effects of this interaction remain speculative given the current inconsistencies regarding its role in health and disease (156, 157).

A recent study using *in vitro* and *ex vivo* assays further illustrates the protective effect of C5a inhibition upon the development of microvascular platelet aggregation (75). In the study, the authors used a human microvascular endothelial cell (HMEC-1) line to investigate the effects of c-aHUS patient serum on cell phenotype. After demonstrating increased platelet aggregation on HMEC-1 exposed to patient serum, they demonstrated that adding C5a to normal human serum was sufficient to recapitulate the prothrombotic effects of aHUS serum. Again, using the HMEC-1 model, therapeutic inhibition of C5aR1 (using CCX168 or Avacopan) reduced platelet aggregates to background level whilst use of a goat anti-C7 polyclonal antibody (previously confirmed to prevent C5b-9 formation on HMEC-1 in this context (71)) was only partially effective in restricting platelet aggregation on the HMEC-1 (75). Thus, these data are largely supportive of my findings in that loss of C5a/C5aR1 signalling reduces conditions that would sustain a renal TMA and prevention of MAC deposition restricts HMEC-1 activation/cell surface modulation. However, it was reported that blockade of C5aR1 did not alter C5b-9 deposition on the HMEC-1 in this context (75) which was not our experience in respect to analysis of the effects of deletion of C5aR1 on C5b-9/fibrin deposition *in vivo*. Obviously, these models are vastly different but arguable an *in vivo* study is more realistic than one based on an immortalised cell in static culture. My results do draw parallels to an observational study

finding that C5a levels did not correlate with Eculizumab treatment in patients with c-aHUS. Suggesting that despite clinical resolution with Eculizumab, the C5a axis is not fully silenced, and thus the C5a burden may not be critical to the development of clinically significant disease.

The B6-C3^{D1115N}.hC5aR1$^{+/+}$ mice clearly benefit from receiving the C5aR1 antagonist orally from weaning. However, despite the significant clinical improvement and survival advantage conferred by C5aR1 inhibition (i.e. 100% survival while on the drug), the histological analysis showed 50% of mice had underlying pathology. These data maybe partly a marker of the damage to the kidney before the mice receive the diet (i.e. embryo to weaning at postpartum day 21-24). I know from previous work that there is histological evidence of disease from 7 days post-partum, or, it may be low grade persisting disease. Interestingly, this study shows C5aR1 inhibition is sufficient to prevent acute disease from developing during an 8-week period. In order to gain further understanding of the effectiveness of C5a inhibition a longer study protocol would establish if grumbling histological changes will translate into clinically evident disease. Additionally, a rescue treatment strategy will rigorously test the utility of C5aR inhibition; identifying mice with active disease (haematuria and proteinuria) and commencing treatment at that stage to see if the active urinary sediment can be resolved. These translational studies are important as we await the report for of the terminated clinical trial (NCT02464891), testing CCX168 (Avacopan™) in patients with aHUS.

5.6   Strengths and limitations of work

The $C3^{D1115N}$ model of complement-mediated aHUS is robust and reproducible irrespective mouse strain. The efficacious findings of the ACT-1014-1670 on the $B6-C3^{D1115N}.hC5aR1^{+/+}$ consolidate the genetic findings on the $Balb/c-C3^{D1115N}.C5aR1^{-/-}$. Whilst I recognise the difference between mouse and man and particularly the complement regulatory proteins, my data offers a tangible insight into C5aR1 inhibition in complement mediated aHUS. It appears to attenuate disease but not entirely abolish it, whether, this is sufficient to induce disease remission in man remains to be elucidated. Unfortunately, the absence of blood parameters in the $Balb/c.C3^{D1115N}.C5aR1^{-/-}$ that acutely succumbed to TMA does skew my data. The study was ran during the Covid pandemic and was impacted due to my clinical redeployment at the time.

5.7   Future Work

The logical next step is to evaluate the efficacy of ACT-1014-1670 when used as a rescue therapy i.e. analyse the effectiveness of the drug when given to animals which have clinical evidence of disease measured through urinalysis and clinical scores. This will enable us to determine if the drug when challenged with active disease and if it is sufficient to attenuate disease. C5aR1 inhibition undoubtedly provides some protection from a TMA but this effect diminishes with advancing age. I will look at the role of the C5aR2 receptor to determine its expression within the mice and if this changes with advancing age. Finally, the specific role of C5a on TMA development still remains elusive, yes, removing C5a mediated signalling produces a milder phenotype, but we need to determine the mechanistic pathways through which it exerts its effects. I hypothesise it will be related to its role on recruitment of inflammatory cells but further work is needed to explore and substantiate this. My next step is to determine the role of C5b-9 upon disease development through crossing the $B6-C3^{D1115N}$ onto the $B6-C7^{-/-}$ mice.

Chapter6   Characterisation of the B6.C3^{D1115N}.C7$^{-/-}$ mouse.

6.1   Introduction

In order to determine the role of C5b-9 upon the development of complement mediated TMA, the B6-C3^{D1115N} mouse was crossed onto the B6-C7$^{-/-}$ background. C7 deficiency prevents the formation of both C5b-8 and C5b-9 [158], enabling us to examine for evidence of disease in the absence of both lytic and sublytic MAC [159, 160]. Based upon previous published preclinical models, the clinical success of C5 inhibiting treatment and the breakthrough renal TMA following C5aR1 deletion, I rationalised that C5b-9 was the culprit driving disease.

6.2   Hypothesis

C7$^{-/-}$ will rescue the B6-C3^{D1115N} and prevent the development of a complement mediated TMA.

6.3   Aims of chapter

- Cross the B6.C3^{D1115N} mouse onto the B6-C7$^{-/-}$ background to generate the B6.C3^{D1115N}.C7$^{-/-}$ mouse model.

- Undertake histological and renal function analysis of the mice to see if there are features of TMA in the B6.C3^{D1115N}.C7$^{-/-}$ mice.

- Perform age related studies to see if C7$^{-/-}$ transforms into a C3G-type phenotype akin to the FH^{W1206R} mouse

6.4 Results

6.4.1 Breeding strategy to generate B6.C3^{D1115N}.C7$^{-/-}$ mice.

B6.C7$^{-/-}$ mice were commercially available and purchased from The Jackson Laboratories and crossed with B6.C3$^{D1115N+/-}$ mice through 5 successful generations (F5; see figure 103), generating the B6.C3^{D1115N}.C7$^{-/-}$ mice and genetic equivalent controls (97% identical to parental B6.C7$^{-/-}$ mice).
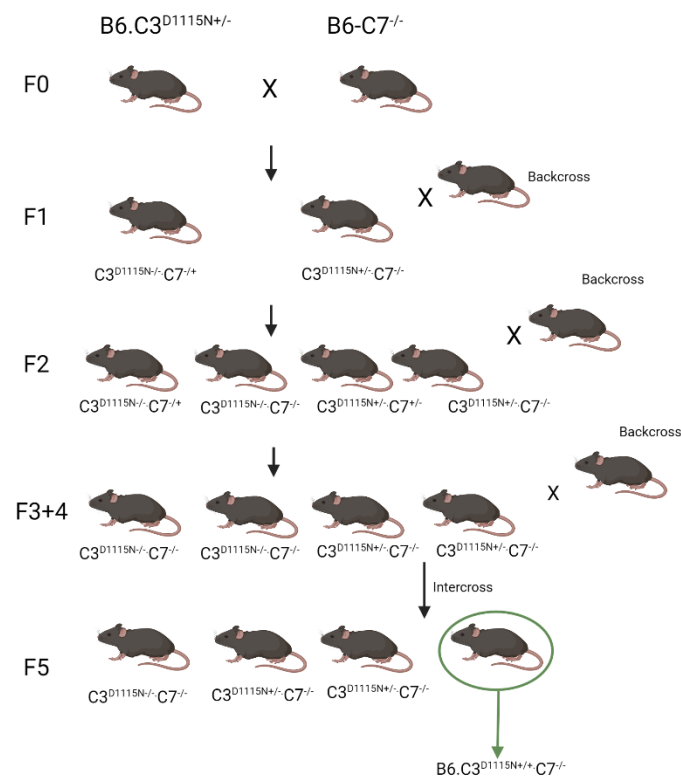
Figure 103 Schematic illustrating the mouse breeding strategy to derive the B6.C3^{D1115N}.C7$^{-/-}$ mice.

6.4.2   Confirmation of B6-C3^{D1115N}.C7$^{-/-}$

Pups were ear clipped and genotyped around 14 days post-partum and thereafter, mice homozygote for the C3^{D1115N} were monitored with daily weighing and urinalysis.
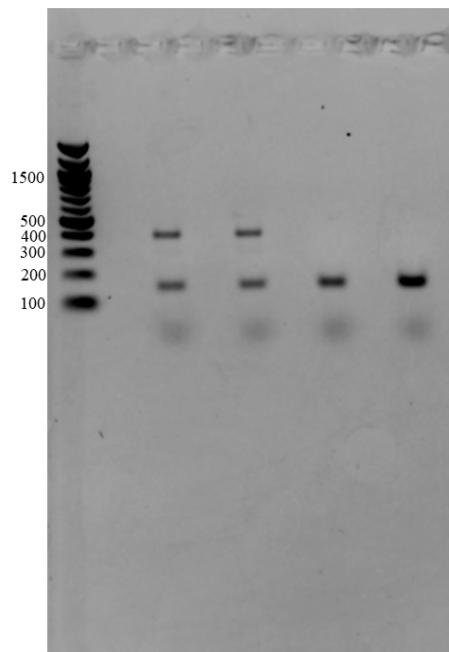
Figure 104 C7$^{-/-}$ Genotyping of mice.

A 1% agarose gel showing PCR products from DNA obtained from ear clips of mice pups taken at 14 days postpartum. WT 415bp, C7$^{-/-}$ 168 bp. Four mice shown, two B6.C3^{D1115N}.C7$^{+/-}$ (bands closest to gene ladder) and B6.C3^{D1115N}.C7$^{-/-}$ (latter two bands)

6.4.3 Overall survival in B6.C3^{D1115N}.C7$^{-/-}$ mice.

There was no increased attrition in the B6.C3^{D1115N}.C7$^{-/-}$ line compared to the B6.C3^{WT}.C7$^{-/-}$ mice.
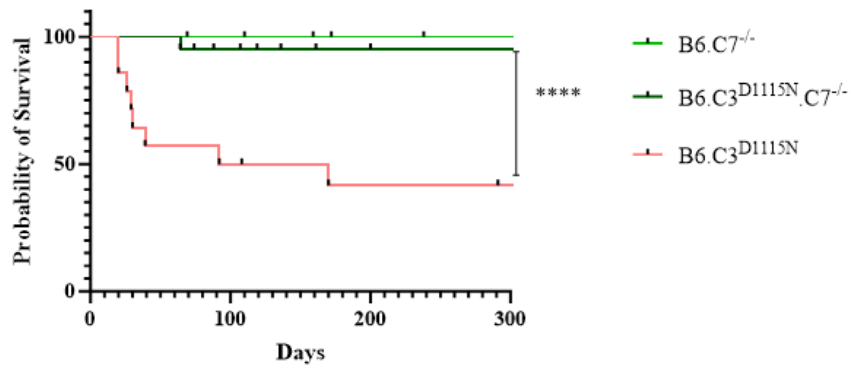
Figure 105 Overall Survival of B6.C3^{D1115N}.C7$^{-/-}$
C7 deficiency resulted in a significant survival advantage in the B6.C3^{D1115N} N=14. There was no significant difference in survival between the B6.C3^{D1115N}.C7$^{-/-}$ N=21 and the B6.C7$^{-/-}$ N=23. Kaplan-Meier survival analysis.

6.4.4 100% survival from renal TMA in B6.C3^{D1115N}.C7$^{-/-}$

I adopted the same strategy as the C5aR1 analysis, and tracked mice in 3, 6 and 12-month cohorts. All mice reached their allotted endpoints with none of the animals requiring euthanasia on health grounds.
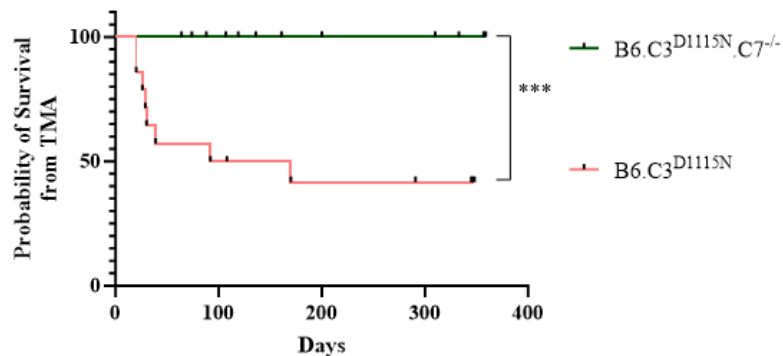
Figure 106 100% survival from renal TMA in the B6.C3^{D1115N}.C7$^{-/-}$.

None of the B6.C3^{D1115N}.C7$^{-/-}$ animals examined in the 3- (n=8), 6- (n=6) and 12- (n=7) month cohorts were euthanised due to health concerns.B6.C3^{D1115N} (n=14). Kaplan-Meier survival analysis. *** p<0.001.

One death occurred in the B6.C3^{D1115N}.C7$^{-/-}$. Terminal urinalysis found no abnormality and blood parameters were all within normal range. Histological analysis found no evidence of a TMA. Therefore, whilst the cause of death was inconclusive, I do not believe the mouse died due to a renal TMA.
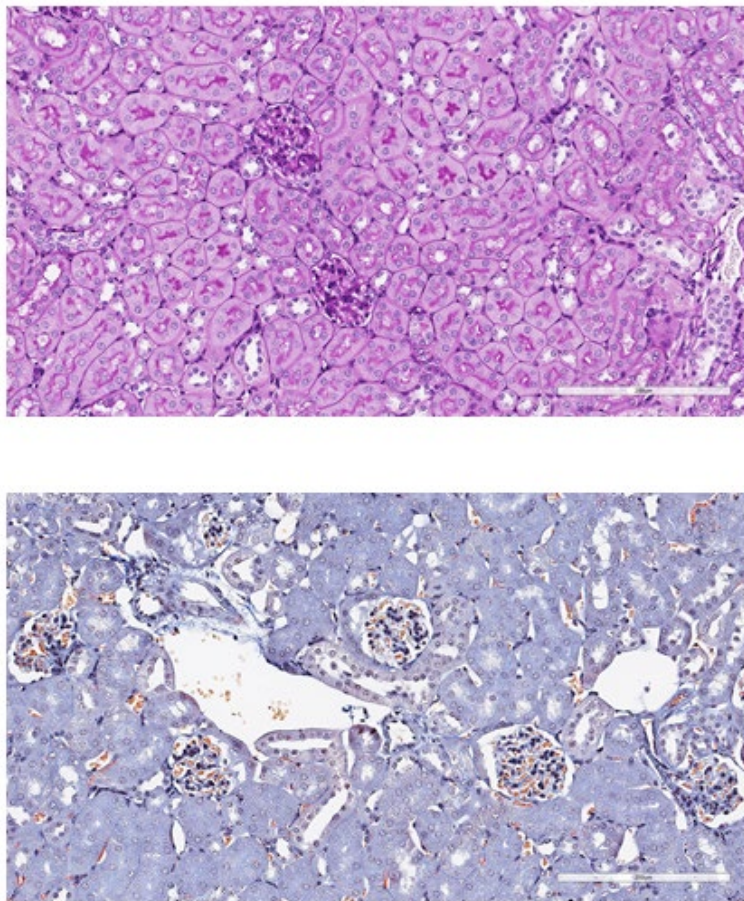
Figure 107 Histology of m21174 B6.C3^{D1115N}.C7$^{-/-}$.
PAS and MSB stained section of the B6. C3^{D1115N}.C7$^{-/-}$ that had to be culled due to a high clinical score. No convincing features of a renal TMA to account for the mouse having to be euthanised. Images taken at x20 magnification.

6.4.5   C7 deficiency protects against renal injury

Lower BUN levels were seen across all aged cohorts, illustrating that there was no biochemical renal injury detectable in the B6.C3^{D1115N}.C7$^{-/-}$.
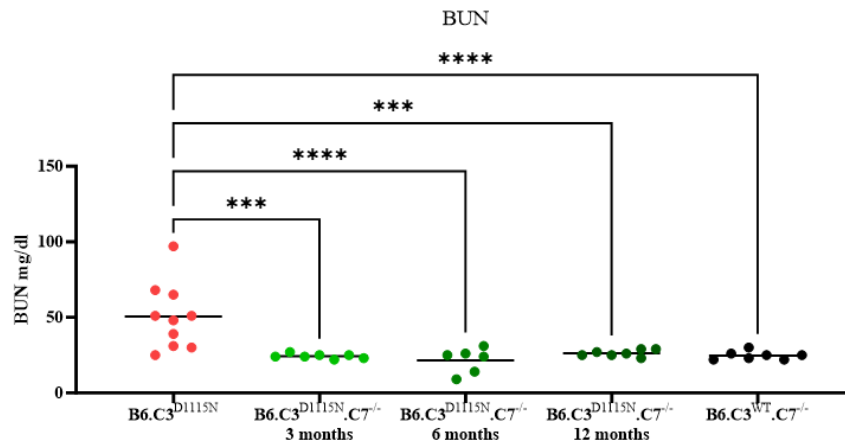
Figure 108 Lower BUN levels were observed in the B6.C3^{D1115N}.C7$^{-/-}$ cohorts at all ages, showing no biochemical evidence of renal injury. Analysed using 2-way ANOVA with Tukeys comparison. B6.C3^{D1115N} (n=10), B6.C3^{D1115N}.C7$^{-/-}$ (n=7), B6.C3^{D1115N}.C7$^{-/-}$ (n=6), B6.C3^{D1115N}.C7$^{-/-}$ (n=7), and B6.C3^{WT}.C7$^{-/-}$ (n=7). Mean ±SEM. *** P<0.001, ****P<0.0001.

6.4.6   C7 deficiency corrects anaemia and leads to resolution of MAHA

A significant increase in haemoglobin levels were seen in both the 3 and 12 month cohorts. One animal in the 12-month cohort had an unexplained low haemoglobin. There was a normalisation in reticulocyte count and an improvement in platelet count in all of the B6.C3^{D1115N}.C7$^{-/-}$ cohorts, showing C7 genetic deletion to be protective against developing a MAHA.
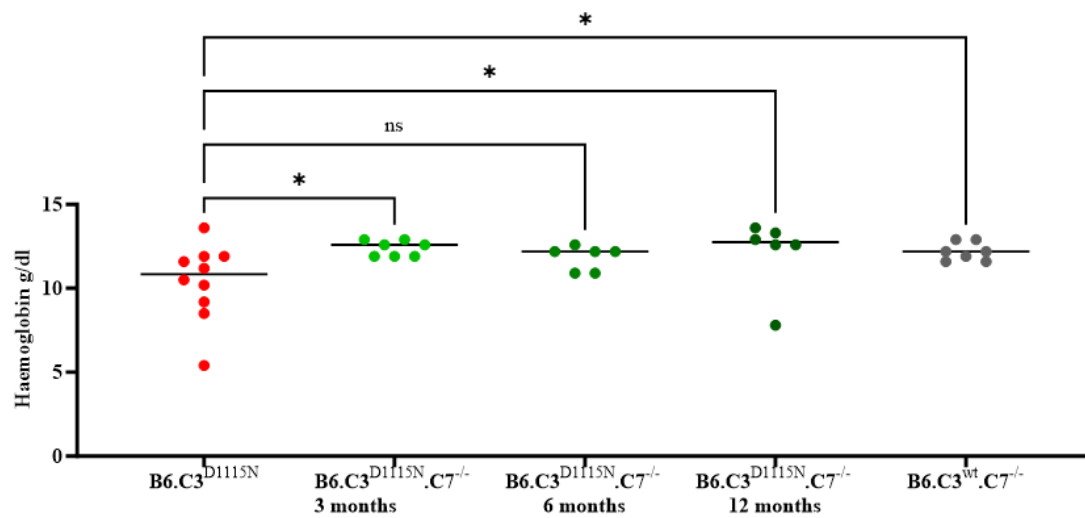
Figure 109 Haemoglobin levels in the B6-C3^{D1115N}.C7$^{-/-}$

Terminal blood taken and haemoglobin measured on the ISTAT Chem8+ cartridge. Haemoglobin levels were found to be to be higher in the majority of the mice at B6-C3^{D1115N}.C7$^{-/-}$ at 3 (n=7) and 12 (n=6) months of age. One 12 month old animal had an unexplained low haemoglobin. Analysed using Two-way ANOVA with Tukeys multiple comparison. Mean ±SEM. Ns non-significant, *P<0.05.
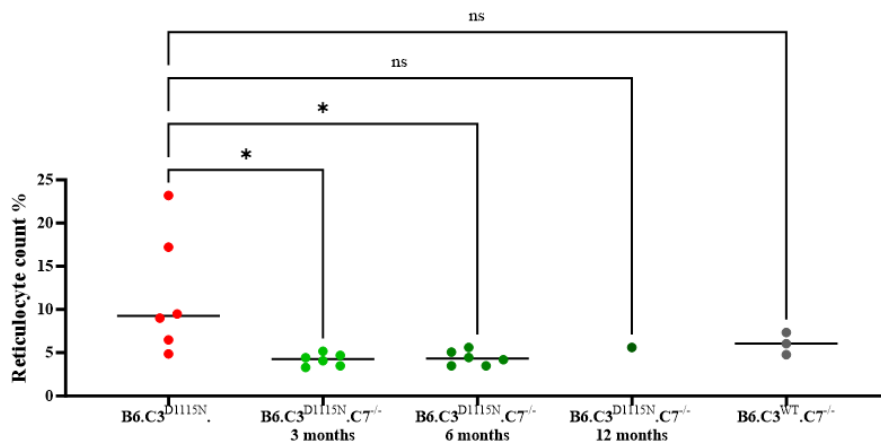
Figure 110 Reticulocyte count in the B6-C3^{D1115N}.C7$^{-/-}$

A normalisation in reticulocyte count is observed in the 3- (n=6) and 6- (n=6) month cohorts. Due to analyser failure we only obtained one result from the 12 month cohort. Analysed using Two-way ANOVA with Tukeys multiple comparison. Mean ±SEM. Ns non-significant, *P<0.05.
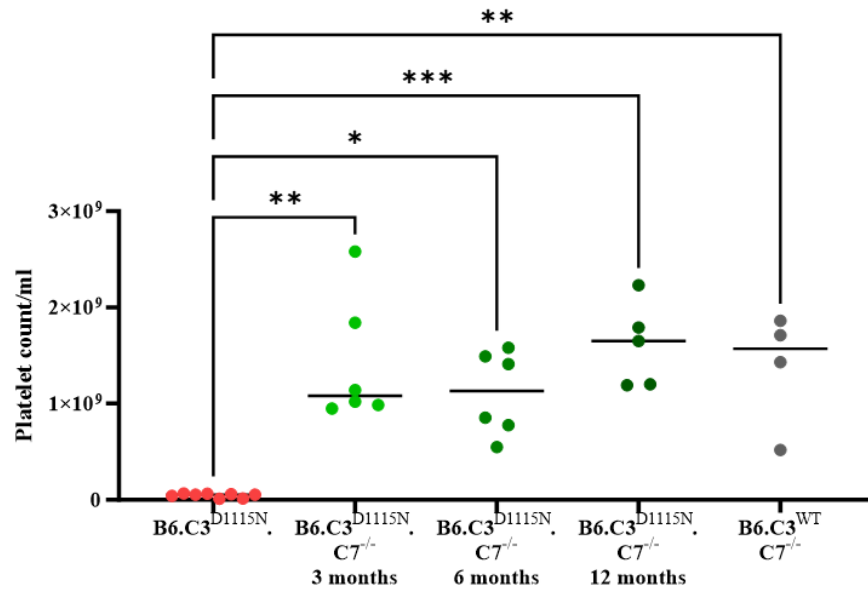
Figure 111 Platelet counts in the B6-C3^{D1115N}.C7$^{-/-}$

An improved platelet count was seen in the 3- (n=6), 6- (n=6) and 12- (n=5) month B6-C3^{D1115N}.C7$^{-/-}$
reflecting resolution of the MAHA. Analysed using Two-way ANOVA with Tukeys multiple comparison.
Mean ±SEM. *P<0.05, ** P<0.01, *** P<0.001.

6.4.7 C7 Deficiency prevents renal thrombotic microangiopathy in the B6-C3^{D1115N} mice up to 12 months of age

Histological analysis of the B6.C3^{D1115N}.C7$^{-/-}$ mice, up to 12 months of age, found no evidence of a renal TMA on the sections analysed and indeed, no detectable pathology following C7 genetic deletion. These data suggest that C5b-9 was the predominant driver of a TMA in the B6.C3^{D1115N} mouse model of c-aHUS.

B6-C3^{D1115N} B6-C3^{D1115N} . C7$^{-/-}$ 3 months   B6-C3^{D1115N} . C7$^{-/-}$ 6 months   B6-C3^{D1115N} . C7$^{-/-}$ 12 months
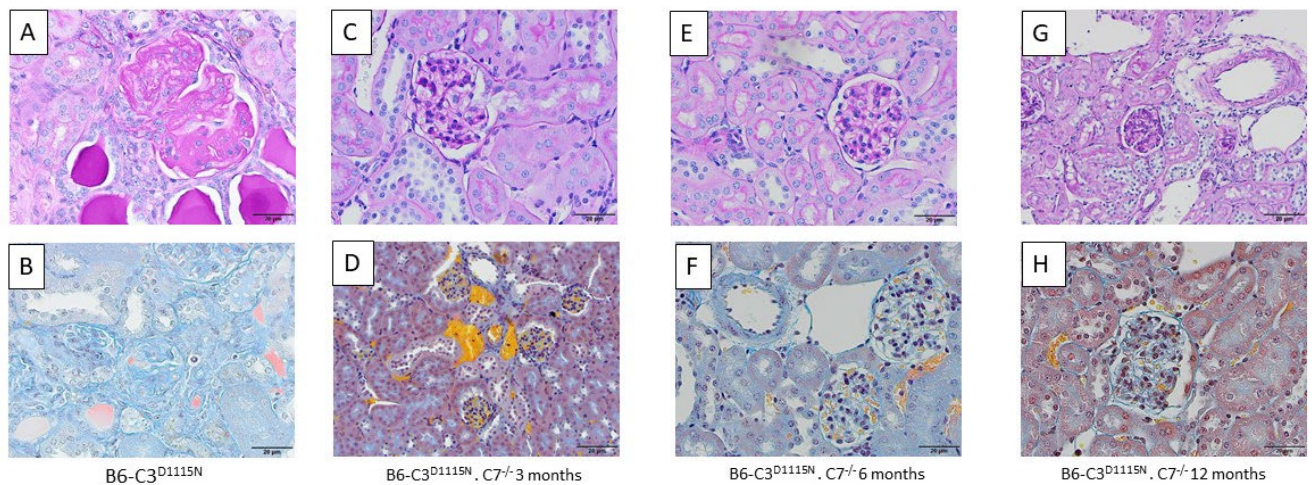
Figure 112 C7 deficiency prevents renal thrombotic microangiopathy in the B6-C3^{D1115N} mice. Periodic-acid-Shiff stained (A,C,E,G) and Martius scarlet blue stained sections (B,D,F,H) of B6-C3^{D1115N} and Balb/c-C3^{D1115N} C7$^{-/-}$ at 3-, 6- and 12-months of age. B6-C3^{D1115N} animals (A,B) show double contouring, segmental sclerosis, mesangiolysis and glomerular fibrin deposition (features of TMA). Normal glomeruli seen in the B6-C3^{D1115N}.C7$^{-/-}$ at 3- (C,D), 6- (E,F), and 12- (G,H) months of age. Light microscopy images were taken on the Olympus SC 50 at 40x magnification. Images were then exported as PNG files.
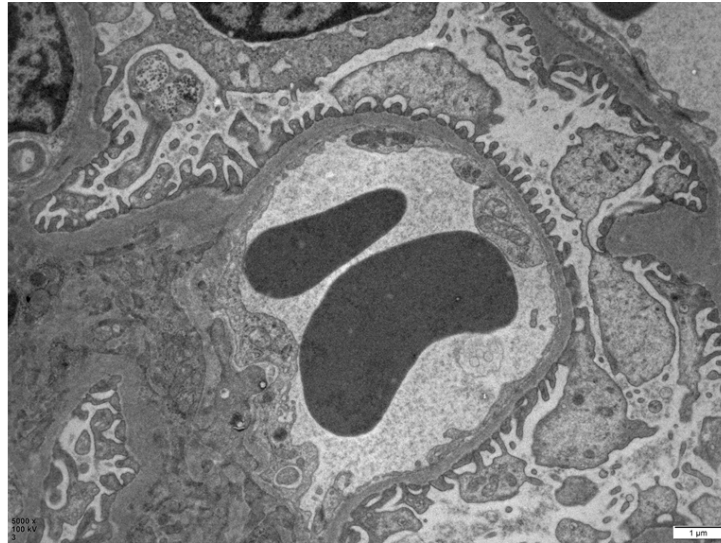
Figure 113 Electron Microscopy of a 12-month-old B6.C3^{D1115N}.C7$^{-/-}$

No obvious morphological features of a TMA or C3G in the glomerulus of a 12-month-old B6.C3^{D1115N}.C7$^{-/-}$

6.4.8   C7 Deficiency and the glomerular complement burden in the B6-C3^{D1115N} mice

Glomerular fibrin deposition was reduced in the 3-, 6- and 12-month B6.C3^{D1115N}.C7$^{-/-}$ cohorts. This expected finding supports the histology data above which found no evidence of a TMA, and in keeping with the haematological parameters showing no evidence of a MAHA. Interestingly, both C3 and C9 deposition increases with age. The C3 data is identical to that the B6.C3^{D1115N}.C5$^{-/-}$. The C9 was an unexpected finding and I hypothesise this was detecting an increased expression of native C9, which may be aggregated or polymerised given C9 can be detected in glomeruli of healthy 12 month old B6.C3^{WT}.C7$^{-/-}$ mice (figure 115) and the increased C9 staining is not overtly pathogenic.
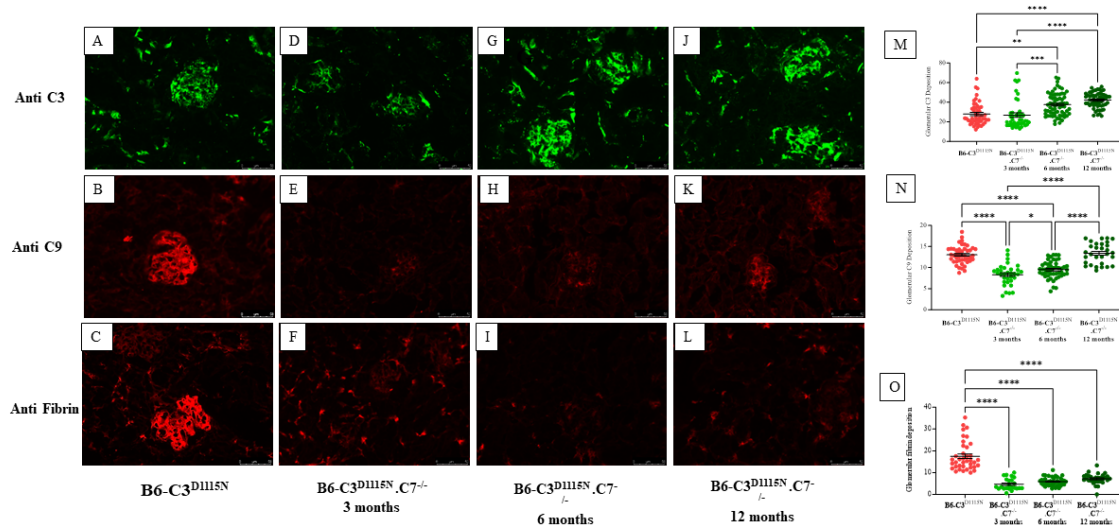
Figure 114 Glomerular complement deposition in the B6-C3^{D1115N}.C7^{-/-} mice.

A sequential increase in glomerular C3 was observed in the ageing B6-C3^{D1115N}.C7^{-/-} mice. An initial reduction in C9 staining was observed in the 3 and 6 months cohorts, but, no difference at 12 months of age. A significant reduction in glomerular fibrin deposition was observed in all cohorts. Analysed using Two-way ANOVA with Tukeys multiple comparison. Average number of glomeruli scored C3 n=60, C9 n=39, Fibrin n=33. Mean ±SEM. *P<0.05, ** P<0.01, *** P<0.001, ****P<0.0001.
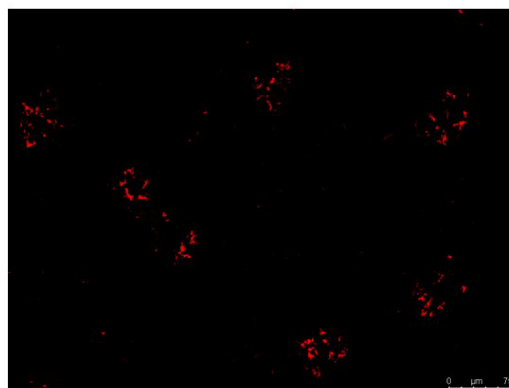
Figure 115 C9 staining in C6-C3^{WT}.C7^{-/-} mice 12 month old mice.

6.4.9   Rabbit anti Rat C9 antibody binds polymerised C9

Given the unexpected finding of detectable C9 in the B6.C3^{D1115N}.C7$^{-/-}$ mice, I polymerised commercially bought Comptech native C9 (incubated at 52^{0}C for 4 hours in Veronal-buffered saline) and detected this on a western blot probing with a control antibody (Rabbit anti Human C9, Abcam) and the Rabbit anti Rat C9 antibody gifted from Prof Morgan. As predicted the antibody bound to aggregated/polymerised C9, allowing me to hypothesise that this maybe occurring in the C7$^{-/-}$ which is providing the positive signal we are detecting in the glomerulus using immunofluorescence. We do not believe the detected and increased C9 to be nephrotoxic given there is no detectable renal pathology in the B6.C3^{D1115N}.C7$^{-/-}$ up to 12 months and suggest this is a phenomenon/artefact or sub clinical finding at this point. We are not aware of a reagent that can distinguish between C9 in MAC versus C9 monomers specifically and our attempts to find such a reagent have failed.
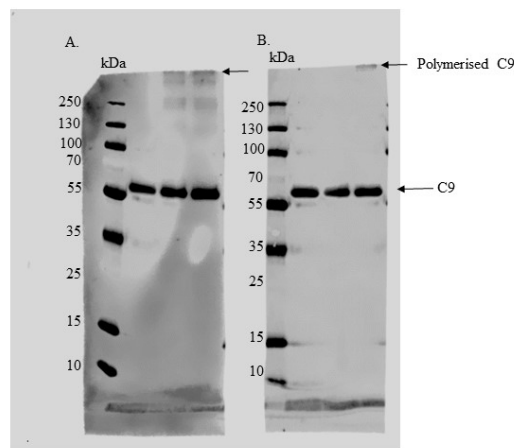
Figure 116 Detection of Polymerised C9 using the Rabbit anti rat C9 antibody

Native C9 was polymerised and ran on an SDS-PAGE gel, transferred onto a Western blot then probed with Rabbit anti Human C9 (A) and Rabbit anti Rat C9 (B). The detection of polymerised C9 can be seen at the top of the blot as identified with the labelled arrow.

6.4.10 Attenuation of inflammatory infiltration in the absence of C5aR1 or C7 in the C3^{D1115N} mice.

Our data to date has shown that the complement mediated TMA within the mice is initiated and driven by C5b-9; evidenced by the complete abolishment of clinical and histological disease in the B6-C3^{D1115N}.C7$^{-/-}$ cohorts. Renal TMA is associated with endothelial cell damage and immune cell infiltrates . To investigate for the presence of neutrophils and macrophages in the kidneys of both C7 and C5aR1 deficient animals, kidneys were stained with anti-Ly6-G

(neutrophils) and anti-F4/80 (macrophages). In C7 deficient animals, inflammatory cell infiltrates were significantly reduced compared to B6-C3^{D1115N} mice and remained equivalent to negative control animals at each time point analysed (figure 115 A-H). We see a similar reduction in staining of F4/80 and Ly6-G when examining the Balb/c-C3^{D1115N}.C5aR1$^{-/-}$ at 6 months of age (the time point when histological evidence of disease emerges on post-mortem review) (figure 115, I,J,M,N,L,P). However, at 12 months, neutrophil infiltrate in a proportion of the Balb/c-C3^{D1115N}.C5aR1$^{-/-}$ mice is like that observed in Balb/c-C3^{D1115N} mice. By removing C5a signalling through the absence of C5aR1 there is a reduction in complement induced inflammation, reducing inflammatory infiltrate, which translates into an attenuated disease process within the kidney
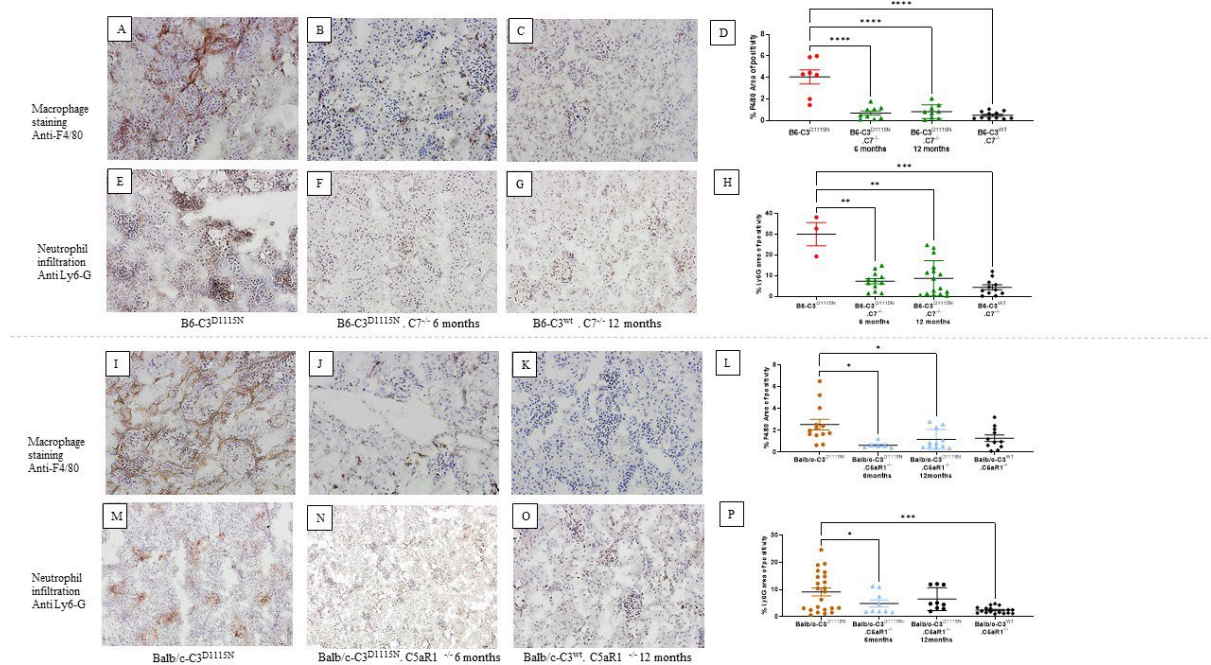
Figure 117Attenuation of inflammatory cell infiltrate in the absence of C5aR1 and C7 in the C3^{D1115N} mouse

*Positive F4/80 and Ly6-G staining is seen in both the B6-C3^{D1115N} (A, E), and Balb/c-C3^{D1115N} (I, M) mice. Reduced F4/80 and Ly6-G staining is seen in both the B6-C3^{D1115N}.C7$^{-/-}$ (B, F) and the Balb/c-C3^{D1115N}. C5aR1$^{-/-}$ at 6 months (J,N) or 12 months, with the exception of Neutrophils in the Balb/c-C3^{D1115N}. C5aR1$^{-/-}$ mice (O,P), where some mice showed similar infiltrate to the Balb/c-C3^{D1115N} mice. No difference in staining was noted when deficient mice were compared to their wild type controls - B6-C3^{wt}.C7$^{-/-}$ (D,H) and Balb/c-C3^{WT}.C5aR1$^{-/-}$ (L,P). Light microscopy images were taken on the Olympus SC 50 at 20x magnification. Images were then exported as TIFF files. Two-way ANOVA with Tukey's multiple comparison test was used to establish significance between groups and across time. Only significant results between the multiple comparison are illustrated, with * = p <0.05, ** = p<0.01, *** = p<0.005, **** = p<0.0001.*

6.5   Discussion of Results

No mouse succumbed to, or had evidence of TMA in the B6-C3^{D1115N}. $C7^{-/-}$ up to 12 months of age, suggesting C5b-9 (and possibly C5b-8) are the dominant pathogenic players in the development of a complement mediated TMA.   No renal injury could be detected on BUN measurements.   As MAHA arises due to erythrocyte fragmentation from the sheer stresses induced from the damaged glomerular endothelium and reticulocytosis is a compensatory mechanism in response to the reduction in circulating haemoglobin, the absence of anaemia in the C7 deficient B6.C3^{D1115N} animals likely reflects restoration of homeostasis to the glomerular endothelium and concomitantly less red blood cell fragmentation and platelet consumption. This is evidenced through normalisation of haematological parameters.

Fibrin deposition is significantly reduced in the B6-C3^{D1115N}.C7$^{-/-}$ lines when compared to C3^{D1115N} controls.   Interestingly, C3 glomerular deposition increases in the kidney of B6-C3^{D1115N}.C7$^{-/-}$ mice, although this increased complement activation (deposition) does not result in clinical disease. Data that is identical to C5 deletion on this background and C5aR$^{-/-}$. No difference was observed in glomerular C9 deposition between controls and B6-C3^{D1115N}.C7$^{-/-}$ at 12 months of age. I hypothesise in the absence of C7, Protein S is unable to inhibit the polymerisation of C9, and we are detecting polymerised C9 rather than the lytic membrane attack complex.

The new model draws parallels again with the FH$^{R/R}$ mouse model of c-aHUS. They similarly saw an increase in glomerular C3 deposition in the FH$^{R/R}$.C6$^{-/-}$ and FH$^{R/R}$.C9$^{-/-}$ as the mice aged. In contrast to their findings though, I did not find features of a glomerular hypercellularity phenotype in the ageing animals. The FH$^{R/R}$.C6$^{-/-}$ animals were clearly more resistant to developing a renal TMA, as the ageing FH$^{R/R}$.C9$^{-/-}$ developed features of a renal disease beyond 20 weeks of age, suggesting that, both C5b-8 and C5b-9 contribute to disease. My C7 data supports that hypothesis in that disease is abolished in the absence of both C5b-8 and C5b-9. That said, they could not explain the persisting anaemia and thrombocytopenia in the FH$^{R/R}$.C6$^{-/-}$ mice. Whilst we see full haematological resolution in our B6.C3^{D1115N}.C7$^{-/-}$ animals. This reinforces that our model is a more faithful replication of c-aHUS as seen in man.

The data presented herein is supported by a previous study using a rat model to induce TMA through the administration of antibodies to the glomerular endothelial cells (GEC), leading to severe endothelial injury accompanied by platelet aggregation, fibrin deposition and

macrophage infiltration. These features were either absent or markedly reduced in C6 deficient rats, enabling them to surmise that C5b-9 played an integral role. Interestingly, akin to my mouse, the C6 deficient rats demonstrated glomerular C3 deposition but this did not translate into disease and the authors hypothesise this was due to the intact and undamaged endothelium (161).

Removing C7 prevents the activation of EC from C5b-8 and C5b-9, depleting the lytic and sublytic activity, thus attenuating glomerular EC activation from hyperfunctional C3 in the $C3^{D1115N}$ model of TMA. Binding of C7 to C5b6 forms a stable trimeric complex allowing it to become associated with the cell membrane (94). The addition of C8 to C5b-7 forms a tetrameric complex which promotes binding and polymerisation of C9, enabling it to induce its cytolytic activity upon the cell. Both, Clusterin and protein S preferentially bind C7 to regulate C5b-9. Clusterin prevents the insertion of C5b-7 into the cell membrane, whereas Protein S binds to C5b-7, inhibiting polymerisation of C9 (94). By preventing the formation of C5b-7 (through C7 depletion), it prevents the cytolytic effects of C5b-9 and the non-cytolytic effects of C5b-8.

The sublytic forms of C5b-8 & C5b-9 induces persistent stimulation of EC, through numerous pro thrombotic, pro inflammatory effects. Sublytic effects upon ECs requires the complex to insert into the membrane to signal the cell, thus by preventing insertion through C7 deficiency the sublytic effects are thwarted. C7 is the central portion of C5b-9 and is an important limiting factor (162), given its success in abolishing disease within my mouse model makes it an attractive therapeutic target.

Current C5 inhibition requires intravenous therapy, with a high target concentration, thus large drug doses are required to achieve therapeutic effect (163, 164). Not only that but the sheer cost of the drug restricts its testing and potential use in commoner complement mediated diseases. Finally, the presence of C5 polymorphisms leads to a failed therapeutic response to Eculizumab or Ravalizumab (165). C5 is abundant in plasma (~ 5% of total plasma protein) and is an acute phase reactant, thus there is an increased production and plasma concentration in response to infection and inflammation. So, for patients on Eculizumab who then develop and infection, the increased synthesis of C5 can lead to breakthrough haemolysis (81, 166). Interestingly, in the setting of intense complement activation, the less effective C5 inhibition is, suggesting that in this setting augmenting therapy may have limited benefit (166, 167). Targeting C7 may circumvent this. Plasma C7 levels are lower than C5, C7 is not an acute phase protein thus levels are stable in acute phase conditions so breakthrough is theoretically less likely to occur

(168) . Finally, given its stability, C7 lends itself to lower and less frequent drug doses which may be administered via alternative routes due to the lower plasma target concentration required (81, 82). C7 therapy would also enable C5a to function in its physiological role of host defence(169).

6.6 Strengths and limitations of work

My data clearly shows that the C7 deficiency in the $C3^{D1115N}$ mouse model of c-aHUS abolished disease, and by extension, therapeutic targeting of C7 may offer disease remission to patients. This would have the advantage over C5 inhibition as C5a would still be able to physiologically function as part of the immune response, i.e. in the stimulation of antigen presenting cells and C5a mediated neutrophil recruitment (170). However, MAC is essential to defending against meningococcal disease (171, 172)) and so an anti-C7 therapy would not mitigate against the risk of meningitis, as recognised with anti-C5 therapy (18). Additionally, there are difference between mouse and man with respect complement regulatory proteins in the kidney that may alter both short term and longer term outcomes and so clinical trials would be needed with these agents to make any concrete conclusions. That said, the data herein provides a valid rationale for such clinical studies, i.e. targeting/depleting C7 by monoclonal antibody therapy in patients whom develop a complement mediated aHUS.

6.7 Future work

To further substantiate my findings, therapeutic targeting of C7 using an anti-C7 antibody will consolidate our genetic deletion studies and are a necessary translational step. I also plan to use the anti-C7 antibody in the $B6.C3^{D1115N}.hC5aR1^{+/+}$ mice, to enable a seamless comparison of C5aR1 oral inhibitor vs anti-C7 therapy. Mechanistically, crossing the $B6.C3^{D1115N}$ onto a $B6.C8^{-/-}$ would allow us to determine the role of C5b-9 in the absence of C5b-8, ascertaining the effects of lytic and the possible contributions of sublytic C5b-8. A C8a deficient mouse is available from the IMPC (https://www.mousephenotype.org/data/genes/MGI:2668347) and wild type strains have also been reported to be C8 deficient (https://doi.org/10.1159/isbn.978-3-318-05411-8)(173).

Chapter7 Summary

Research into 'Haemolytic Uraemic syndrome' over the last two decades has seen a seismic revolution from understanding the basic pathogenesis into a gold standard therapy that has transformed patients' lives through reduction in morbidity and mortality. It is the truest story of bench to bedside medicine. The journey has also been transformative in the global complement research field, providing proof of concept of the utility and relative safety of complement inhibiting therapy, thus opening up and driving forward complement research in numerous diseases.

To date the majority of literature and pre-clinical studies focussed upon *CFH*. This followed the seminal study in 1998 by the Newcastle group identifying the role of *CFH* mutations and associated risk of c-aHUS(2). I sought to investigate the role of hyperfunctional C3. I began by purifying and modelling C3^{L1109V}, determining it to be a likely pathogenic variant through a lack of binding of FH SCR19-20. My work provided clear information to the National aHUS service and to the patient when the discussions arose around the withdrawal of Eculizumab and the relative risk of relapse. The C3^{L1109V} studies provided proof of concept that mutations clustering in C3d, which mirror *CFH* SCR19-20 pathogenic mutations, are equally pathogenic and provide rationale for their role in c-aHUS, illuminating the mechanism of disease.

So, I next took the C3^{D1115N} change from our local family based within Newcastle upon Tyne and modelled this C3 point mutation in a mouse model. I have clearly demonstrated the C3^{D1115N} mouse model faithfully replicates the human disease and is an incredibly useful pre-clinical model to dissect c-aHUS disease mechanisms and trial alternative complement inhibiting therapies. Due to the rarity of c-aHUS and the immense success of anti-C5 therapy (the gold standard) it is challenging to test developing agents in man given the high risks posed by possible treatment failure.

I took the C3^{D1115N} mouse and backcrossed onto a C5aR1$^{-/-}$ and C7$^{-/-}$ mice to dichotomise the contribution from the terminal pathway. With the advancement in oral C5aR1 inhibitors, this approach offers a tangible treatment option to patients that is significantly less burdensome than current therapy (Eculizumab/Ravalizumab IV infusion) and oral C5aR1 inhibition would significantly reduce the increased risk of meningococcal disease associated with complete terminal pathway blockade (18, 80). Whilst anti-C7 therapy remains within the preclinical stage, the rationale to understand the role of C5a and C5b-9 would lay the foundations for future translational treatment strategies.

Undoubtedly, my data clearly indicates that complete loss of C7 is superior over a longer period in the context of the functioning kidney. We saw no evidence of a renal TMA up to 12 months of age. That said, the mice still had a significant glomerular complement burden, with the longer-term effects of this (beyond 12 months) remaining unknown. C5aR1 deficiency clearly attenuated disease, with the renal limited TMA only identified on post mortem analysis in 6-12 month old mice. Whether this approach of inhibiting C5aR1 would be sufficient to induce disease remission in patients in the acute phase remains unknown. Based upon our studies we would favour targeting C7 and it is a natural refinement of anti-C5 therapy based upon its plausible favourable pharmacodynamics (81, 163).

Current literature describes the pro-thrombotic effects of both C5a and C5b-9 upon the endothelial cell, from which it is difficult to isolate their individual effects due to cross over activity.

In reality, divorcing the effects of C5b-9 from C5a is very difficult. We have attempted this with our Balb/c-C3^{D1115N}.C5aR1$^{-/-}$ and B6-C3^{D1115N}.C7$^{-/-}$, and whilst we have shown removal of C7 (and by extension C5b-8 and C5b-9) is superior to C5aR1 in that all histological evidence of disease is abolished, the exact mechanism through which this is achieved remains elusive.

I propose (based upon our data) that C5b-9 ignites a series of events that leads to activation of the endothelial cells and platelets culminating in the pathological process of TMA. C5a then amplifies the initial effects of C5b-9 leading to perpetual feedforward mechanisms of ongoing complement activation, endothelial cell activation, platelet activation and aggregation.

C5b-9 leads to the endothelial expression of tissue factor, which activates the extrinsic coagulation pathway (99). An increase in pro-thrombinase activity leads to the increased generation of thrombin that can then independently cleave C5 leading to further terminal pathway activation. Simultaneously, exocytosis of P-selectin and vWF factor onto the endothelial cell luminal surface leads to platelet activation and captures circulating vWF creating an adhesive thrombogenic scaffold. Next, expression of ICAM-1 and E-selectin in unison with TNF-alpha recruits inflammatory cells which C5a then amplifies, leading to additional activated neutrophils and ongoing pro-inflammatory infiltration. Additionally, expression of platelet activating factor, transforms resting platelets to activated platelets, leading to platelet leucocyte aggregates. Finally, C5b-9 leads to p-selectin translocation onto the platelet surface that provides a surface for ongoing AP activity and the release of C3, FB

and properdin that then provides a further source for ongoing complement activation. The release of prothrombotic micro particles, and production of C5a and C5b-9 from platelets themselves amplifies the ongoing vicious cycle. Collectively, all of these events culminate in activated platelets encountering a primed prothrombotic endothelial cell surface, resulting in a TMA.
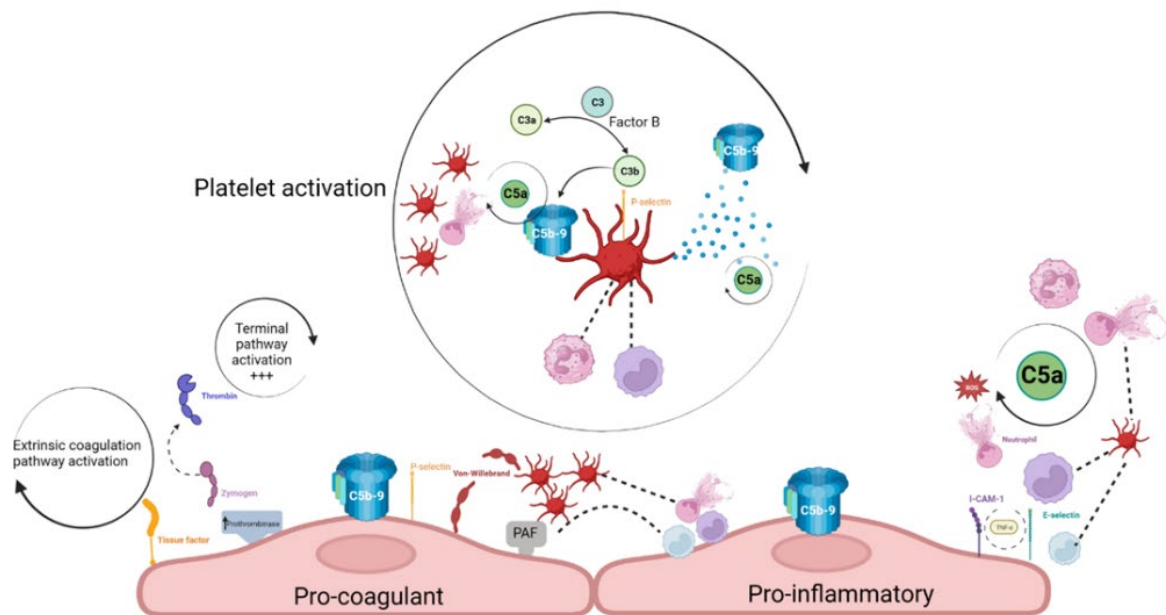
Figure 118 C5b-9 proposed mechanism for TMA induction

C5b-9 ignites a series of events that leads to activation of the endothelial cells and platelets culminating in the pathological process of TMA. C5a amplifies the effects of C5b-9 leading to a perpetual feedforward mechanisms of ongoing complement activation, endothelial cell activation and platelet activation and aggregation.

The induction of a renal TMA by C5b-9 is likely multifactorial and to succinctly summarise the above; under resting and homeostatic conditions, the microvascular endothelium surface expresses complement regulatory proteins providing a barrier from complement mediated attack, following activation of the endothelium it becomes a complement activating surface (103). Transforming from an anti-coagulant, anti-inflammatory, non-thrombogenic luminal surface to a pro-thrombotic and pro-inflammatory environment that are optimum conditions for sustenance for a TMA.

The terminal event of a TMA is microvascular endothelial cell injury, leading to thrombi formation, a MAHA and end organ failure. Whilst we recognise that a complement mediated

TMA benefits from complement inhibiting therapy, and through our data we have shown how we would refine this approach to targeting C7, it remains, alluring to explore the effects of targeting the terminal pathway in secondary TMA.

Can complement inhibiting therapy prove a useful adjunct to supportive treatment remains to be validated. An alternative approach could be to target end products invoked following the activation of the endothelium such as vWF, P selectin and tissue factor. My mouse model can enable us to evaluate the success of this approach in the face of an endothelium saturated by complement activation and insufficient regulation (174).

Extrapolating this concept further, allows us to hypothesise the effects of restoring endothelial homeostasis through both C5a and C5b-9 inhibitors and how that may transform their potential therapeutic application from an orphan disease (c-aHUS) to numerous vascular diseases where an activated endothelium participates in disease pathogenesis.

Indeed work is already underway using the B6.C3^{D1115N} mouse as a model of chronic AP dysregulation and chronic C3 activation. We are trialling the effect of altered diet and ageing to determine the potential mechanistic complement pathways involved in liver and eye disease; and testing complement agents designed to rebalance activation rather than exclusively and systemically terminating complement activation through gene therapy delivery.

I conclude that the data presented provides a key spoke in the wheel of the ongoing research into the role of the terminal pathway upon endothelial cell activation and TMA development.

Chapter8   References

1.   Kavanagh D, Goodship TH, Richards A. Atypical hemolytic uremic syndrome. Semin Nephrol. 2013;33(6):508-30.

2.   Warwicker P, Goodship TH, Donne RL, Pirson Y, Nicholls A, Ward RM, et al. Genetic studies into inherited and sporadic hemolytic uremic syndrome. Kidney Int. 1998;53(4):836-44.

3.   Brocklebank V, Wood KM, Kavanagh D. Thrombotic Microangiopathy and the Kidney. Clin J Am Soc Nephrol. 2018;13(2):300-17.

4.   Walsh PR, Johnson S. Treatment and management of children with haemolytic uraemic syndrome. Arch Dis Child. 2018;103(3):285-91.

5.   Schifferli A, von Vigier RO, Fontana M, Sparta G, Schmid H, Bianchetti MG, et al. Hemolytic-uremic syndrome in Switzerland: a nationwide surveillance 1997-2003. Eur J Pediatr. 2010;169(5):591-8.

6.   Jokiranta TS. HUS and atypical HUS. Blood. 2017;129(21):2847-56.

7.   Szilagyi A, Kiss N, Bereczki C, Talosi G, Racz K, Turi S, et al. The role of complement in Streptococcus pneumoniae-associated haemolytic uraemic syndrome. Nephrol Dial Transplant. 2013;28(9):2237-45.

8.   Allen U, Licht C. Pandemic H1N1 influenza A infection and (atypical) HUS--more than just another trigger? Pediatr Nephrol. 2011;26(1):3-5.

9.   Noris M, Caprioli J, Bresin E, Mossali C, Pianetti G, Gamba S, et al. Relative role of genetic complement abnormalities in sporadic and familial aHUS and their impact on clinical phenotype. Clin J Am Soc Nephrol. 2010;5(10):1844-59.

10.   Maga TK, Nishimura CJ, Weaver AE, Frees KL, Smith RJ. Mutations in alternative pathway complement proteins in American patients with atypical hemolytic uremic syndrome. Hum Mutat. 2010;31(6):E1445-60.

11.   Fremeaux-Bacchi V, Kemp EJ, Goodship JA, Dragon-Durey MA, Strain L, Loirat C, et al. The development of atypical haemolytic-uraemic syndrome is influenced by susceptibility factors in factor H and membrane cofactor protein: evidence from two independent cohorts. J Med Genet. 2005;42(11):852-6.

12.   Fremeaux-Bacchi V, Fakhouri F, Garnier A, Bienaime F, Dragon-Durey MA, Ngo S, et al. Genetics and outcome of atypical hemolytic uremic syndrome: a nationwide French series comparing children and adults. Clin J Am Soc Nephrol. 2013;8(4):554-62.

13.   Nester CM, Barbour T, de Cordoba SR, Dragon-Durey MA, Fremeaux-Bacchi V, Goodship THJ, et al. Atypical aHUS: State of the art. Molecular Immunology. 2015;67(1):31-42.

14.   Brocklebank V, Kavanagh D. Complement C5-inhibiting therapy for the thrombotic microangiopathies: accumulating evidence, but not a panacea. Clin Kidney J. 2017;10(5):600-24.

15.   Goodship TH, Cook HT, Fakhouri F, Fervenza FC, Fremeaux-Bacchi V, Kavanagh D, et al. Atypical hemolytic uremic syndrome and C3 glomerulopathy: conclusions from a "Kidney Disease: Improving Global Outcomes" (KDIGO) Controversies Conference. Kidney Int. 2017;91(3):539-51.

16.   Moake JL. Thrombotic microangiopathies. N Engl J Med. 2002;347(8):589-600.

17.   Legendre CM, Licht C, Muus P, Greenbaum LA, Babu S, Bedrosian C, et al. Terminal Complement Inhibitor Eculizumab in Atypical Hemolytic–Uremic Syndrome. New England Journal of Medicine. 2013;368(23):2169-81.

18.   Brocklebank V, Walsh PR, Smith-Jackson K, Hallam TM, Marchbank KJ, Wilson V, et al. Atypical haemolytic uraemic syndrome in the era of terminal complement inhibition- An observational cohort study. Blood. 2023.

19.   Glover EK, Smith-Jackson K, Brocklebank V, Wilson V, Walsh PR, Montgomery EK, et al. Assessing the Impact of Prophylactic Eculizumab on Renal Graft Survival in Atypical Hemolytic Uremic Syndrome. Transplantation. 2023;107(4):994-1003.

20.   Orth D, Khan AB, Naim A, Grif K, Brockmeyer J, Karch H, et al. Shiga toxin activates complement and binds factor H: evidence for an active role of complement in hemolytic uremic syndrome. J Immunol. 2009;182(10):6394-400.

21.   Lapeyraque AL, Malina M, Fremeaux-Bacchi V, Boppel T, Kirschfink M, Oualha M, et al. Eculizumab in severe Shiga-toxin-associated HUS. N Engl J Med. 2011;364(26):2561-3.

22.   Kielstein JT, Beutel G, Fleig S, Steinhoff J, Meyer TN, Hafer C, et al. Best supportive care and therapeutic plasma exchange with or without eculizumab in Shiga-toxin-producing E. coli O104:H4 induced haemolytic-uraemic syndrome: an analysis of the German STEC-HUS registry. Nephrol Dial Transplant. 2012;27(10):3807-15.

23.   Garnier A, Brochard K, Kwon T, Sellier-Leclerc AL, Lahoche A, Launay EA, et al. Efficacy and Safety of Eculizumab in Pediatric Patients Affected by Shiga Toxin-Related Hemolytic and Uremic Syndrome: A Randomized, Placebo-Controlled Trial. J Am Soc Nephrol. 2023;34(9):1561-73.

24.   Sim RB, Schwaeble W, Fujita T. Complement research in the 18th-21st centuries: Progress comes with new technology. Immunobiology. 2016;221(10):1037-45.

25.   Ricklin D, Hajishengallis G, Yang K, Lambris JD. Complement: a key system for immune surveillance and homeostasis. Nat Immunol. 2010;11(9):785-97.

26.   Noris M, Remuzzi G. Overview of complement activation and regulation. Semin Nephrol. 2013;33(6):479-92.

27.   Thurman JM, Kulik L, Orth H, Wong M, Renner B, Sargsyan SA, et al. Detection of complement activation using monoclonal antibodies against C3d. J Clin Invest. 2013;123(5):2218-30.

28.   Janssen BJ, Christodoulidou A, McCarthy A, Lambris JD, Gros P. Structure of C3b reveals conformational changes that underlie complement activity. Nature. 2006;444(7116):213-6.

29.   Zarantonello A, Revel M, Grunenwald A, Roumenina LT. C3-dependent effector functions of complement. Immunol Rev. 2023;313(1):120-38.

30.   Walport MJ. Complement. First of two parts. N Engl J Med. 2001;344(14):1058-66.

31.   Harboe M, Mollnes TE. The alternative complement pathway revisited. J Cell Mol Med. 2008;12(4):1074-84.

32.   Liszewski MK, Farries TC, Lublin DM, Rooney IA, Atkinson JP. Control of the complement system. Adv Immunol. 1996;61:201-83.

33.   Roumenina LT, Loirat C, Dragon-Durey MA, Halbwachs-Mecarelli L, Sautes-Fridman C, Fremeaux-Bacchi V. Alternative complement pathway assessment in patients with atypical HUS. J Immunol Methods. 2011;365(1-2):8-26.

34.   Kavanagh D, Goodship T. Genetics and complement in atypical HUS. Pediatr Nephrol. 2010;25(12):2431-42.

35.   Thurman JM, Holers VM. The central role of the alternative complement pathway in human disease. J Immunol. 2006;176(3):1305-10.

36.   Lachmann PJ. The amplification loop of the complement pathways. Adv Immunol. 2009;104:115-49.

37.   Harboe M, Ulvund G, Vien L, Fung M, Mollnes TE. The quantitative role of alternative pathway amplification in classical pathway induced terminal complement activation. Clin Exp Immunol. 2004;138(3):439-46.

38.   Zipfel PF, Heinen S, Jozsi M, Skerka C. Complement and diseases: defective alternative pathway control results in kidney and eye diseases. Mol Immunol. 2006;43(1-2):97-106.

39.   Ferreira VP, Pangburn MK, Cortes C. Complement control protein factor H: the good, the bad, and the inadequate. Mol Immunol. 2010;47(13):2187-97.

40.   Kopp A, Hebecker M, Svobodova E, Jozsi M. Factor h: a complement regulator in health and disease, and a mediator of cellular interactions. Biomolecules. 2012;2(1):46-75.

41.   Liszewski MK, Java A, Schramm EC, Atkinson JP. Complement Dysregulation and Disease: Insights from Contemporary Genetics. Annu Rev Pathol. 2017;12:25-52.

42.   Roth A, Duhrsen U. Treatment of paroxysmal nocturnal hemoglobinuria in the era of eculizumab. Eur J Haematol. 2011;87(6):473-9.

43.   Hillmen P, Young NS, Schubert J, Brodsky RA, Socie G, Muus P, et al. The complement inhibitor eculizumab in paroxysmal nocturnal hemoglobinuria. N Engl J Med. 2006;355(12):1233-43.

44.   Brodsky RA, Young NS, Antonioli E, Risitano AM, Schrezenmeier H, Schubert J, et al. Multicenter phase 3 study of the complement inhibitor eculizumab for the treatment of patients with paroxysmal nocturnal hemoglobinuria. Blood. 2008;111(4):1840-7.

45.   Hillmen P, Muus P, Duhrsen U, Risitano AM, Schubert J, Luzzatto L, et al. Effect of the complement inhibitor eculizumab on thromboembolism in patients with paroxysmal nocturnal hemoglobinuria. Blood. 2007;110(12):4123-8.

46.   Armento A, Ueffing M, Clark SJ. The complement system in age-related macular degeneration. Cell Mol Life Sci. 2021;78(10):4487-505.

47.   Atkinson JP, Liszewski MK, Richards A, Kavanagh D, Moulton EA. Hemolytic uremic syndrome: an example of insufficient complement regulation on self-tissue. Ann N Y Acad Sci. 2005;1056:144-52.

48.   Fang CJ, Richards A, Liszewski MK, Kavanagh D, Atkinson JP. Advances in understanding of pathogenesis of aHUS and HELLP. Br J Haematol. 2008;143(3):336-48.

49.   Kerr H, Richards A. Complement-mediated injury and protection of endothelium: lessons from atypical haemolytic uraemic syndrome. Immunobiology. 2012;217(2):195-203.

50.   de Jorge EG, Pickering MC. Atypical hemolytic uremic syndrome: telling the difference between H and Y. Kidney International. 2010;78(8):721-3.

51.   Rodriguez de Cordoba S, Hidalgo MS, Pinto S, Tortajada A. Genetics of atypical hemolytic uremic syndrome (aHUS). Semin Thromb Hemost. 2014;40(4):422-30.

52.   Lhotta K, Janecke AR, Scheiring J, Petzlberger B, Giner T, Fally V, et al. A Large Family with a Gain-of-Function Mutation of Complement C3 Predisposing to Atypical Hemolytic Uremic Syndrome, Microhematuria, Hypertension and Chronic Renal Failure. Clin J Am Soc Nephro. 2009;4(8):1356-62.

53.   Iqbal Z, Wood K, Carter V, Goodship TH, Brown AL, Sheerin NS. Thrombotic Microangiopathy as a Cause of Chronic Kidney Transplant Dysfunction: Case Report Demonstrating Successful Treatment with Eculizumab. Transpl P. 2015;47(7):2258-61.

54.   Pickering MC, de Jorge EG, Martinez-Barricarte R, Recalde S, Garcia-Layana A, Rose KL, et al. Spontaneous hemolytic uremic syndrome triggered by complement factor H lacking surface recognition domains. J Exp Med. 2007;204(6):1249-56.

55.   de Jorge EG, Macor P, Paixao-Cavalcante D, Rose KL, Tedesco F, Cook HT, et al. The development of atypical hemolytic uremic syndrome depends on complement C5. J Am Soc Nephrol. 2011;22(1):137-45.

56.   Ueda Y, Mohammed I, Song D, Gullipalli D, Zhou L, Sato S, et al. Murine systemic thrombophilia and hemolytic uremic syndrome from a factor H point mutation. Blood. 2017;129(9):1184-96.

57.   Ueda Y, Gullipalli D, Song WC. Modeling complement-driven diseases in transgenic mice: Values and limitations. Immunobiology. 2016;221(10):1080-90.

58.   Miwa T, Sato S, Zhou L, Gullipalli D, Wang Y, Song WC. Distinct mechanisms of anti-factor H autoantibody-induced kidney disease in wild-type and membrane regulator-deficient mice. Molecular Immunology. 2014;61(2):235-6.

59.   Fremeaux-Bacchi V, Miller EC, Liszewski MK, Strain L, Blouin J, Brown AL, et al. Mutations in complement C3 predispose to development of atypical hemolytic uremic syndrome. Blood. 2008;112(13):4948-52.

60.   Morgan HP, Schmidt CQ, Guariento M, Blaum BS, Gillespie D, Herbert AP, et al. Structural basis for engagement by complement factor H of C3b on a self surface. Nat Struct Mol Biol. 2011;18(4):463-70.

61.   Schramm EC, Roumenina LT, Rybkine T, Chauvet S, Vieira-Martins P, Hue C, et al. Mapping interactions between complement C3 and regulators using mutations in atypical hemolytic uremic syndrome. Blood. 2015;125(15):2359-69.

62.   Goicoechea de Jorge E, Harris CL, Esparza-Gordillo J, Carreras L, Arranz EA, Garrido CA, et al. Gain-of-function mutations in complement factor B are associated with atypical hemolytic uremic syndrome. Proc Natl Acad Sci U S A. 2007;104(1):240-5.

63.   Rondeau E, Scully M, Ariceta G, Barbour T, Cataland S, Heyne N, et al. The long-acting C5 inhibitor, Ravulizumab, is effective and safe in adult patients with atypical hemolytic uremic syndrome naive to complement inhibitor treatment. Kidney Int. 2020;97(6):1287-96.

64.   Howard JF, Jr., Utsugisawa K, Benatar M, Murai H, Barohn RJ, Illa I, et al. Safety and efficacy of eculizumab in anti-acetylcholine receptor antibody-positive refractory generalised myasthenia gravis (REGAIN): a phase 3, randomised, double-blind, placebo-controlled, multicentre study. Lancet Neurol. 2017;16(12):976-86.

65.   Muppidi S, Utsugisawa K, Benatar M, Murai H, Barohn RJ, Illa I, et al. Long-term safety and efficacy of eculizumab in generalized myasthenia gravis. Muscle Nerve. 2019;60(1):14-24.

66.   Pittock SJ, Berthele A, Fujihara K, Kim HJ, Levy M, Palace J, et al. Eculizumab in Aquaporin-4-Positive Neuromyelitis Optica Spectrum Disorder. N Engl J Med. 2019;381(7):614-25.

67.   Fakhouri F, Fila M, Hummel A, Ribes D, Sellier-Leclerc AL, Ville S, et al. Eculizumab discontinuation in children and adults with atypical hemolytic-uremic syndrome: a prospective multicenter study. Blood. 2021;137(18):2438-49.

68.   Bouwmeester RN, Duineveld C, Wijnsma KL, Bemelman FJ, van der Heijden JW, van Wijk JAE, et al. Early Eculizumab Withdrawal in Patients With Atypical Hemolytic Uremic Syndrome in Native Kidneys Is Safe and Cost-Effective: Results of the CUREiHUS Study. Kidney Int Rep. 2023;8(1):91-102.

69.   Dunn S, Brocklebank V, Bryant A, Carnell S, Chadwick TJ, Johnson S, et al. Safety and impact of eculizumab withdrawal in patients with atypical haemolytic uraemic syndrome: protocol for a multicentre, open-label, prospective, single-arm study. BMJ Open. 2022;12(9):e054536.

70.   Volokhina EB, Westra D, van der Velden TJ, van de Kar NC, Mollnes TE, van den Heuvel LP. Complement activation patterns in atypical haemolytic uraemic syndrome during acute phase and in remission. Clin Exp Immunol. 2015;181(2):306-13.

71.   Noris M, Galbusera M, Gastoldi S, Macor P, Banterla F, Bresin E, et al. Dynamics of complement activation in aHUS and how to monitor eculizumab therapy. Blood. 2014;124(11):1715-26.

72. Wehling C, Amon O, Bommer M, Hoppe B, Kentouche K, Schalk G, et al. Monitoring of complement activation biomarkers and eculizumab in complement-mediated renal disorders. Clin Exp Immunol. 2017;187(2):304-15.

73. Galbusera M, Noris M, Gastoldi S, Bresin E, Mele C, Breno M, et al. An Ex Vivo Test of Complement Activation on Endothelium for Individualized Eculizumab Therapy in Hemolytic Uremic Syndrome. Am J Kidney Dis. 2019;74(1):56-72.

74. Duineveld C, Bouwmeester RN, Wijnsma KL, Bemelman FJ, van der Heijden JW, Berger SP, et al. Eculizumab Rescue Therapy in Patients With Recurrent Atypical Hemolytic Uremic Syndrome After Kidney Transplantation. Kidney Int Rep. 2023;8(4):715-26.

75. Aiello S, Gastoldi S, Galbusera M, Ruggenenti P, Portalupi V, Rota S, et al. C5a and C5aR1 are key drivers of microvascular platelet aggregation in clinical entities spanning from aHUS to COVID-19. Blood Adv. 2022;6(3):866-81.

76. Stevens KH, Baas LM, van der Velden TJAM, Bouwmeester RN, van Dillen N, Dorresteijn EM, et al. Modeling complement activation on human glomerular microvascular endothelial cells. Frontiers in Immunology. 2023;14.

77. Anliker-Ort M, Dingemanse J, van den Anker J, Kaufmann P. Treatment of Rare Inflammatory Kidney Diseases: Drugs Targeting the Terminal Complement Pathway. Front Immunol. 2020;11:599417.

78. Morgan BP, Walters D, Serna M, Bubeck D. Terminal complexes of the complement system: new structural insights and their relevance to function. Immunol Rev. 2016;274(1):141-51.

79. Ward PA. The dark side of C5a in sepsis. Nat Rev Immunol. 2004;4(2):133-42.

80. Jayne DRW, Merkel PA, Bekker P. Avacopan for the Treatment of ANCA-Associated Vasculitis. Reply. N Engl J Med. 2021;384(21):e81.

81. Zelek WM, Morgan BP. Monoclonal Antibodies Capable of Inhibiting Complement Downstream of C5 in Multiple Species. Front Immunol. 2020;11:612402.

82. Lekova E, Zelek WM, Gower D, Spitzfaden C, Osuch IH, John-Morris E, et al. Discovery of functionally distinct anti-C7 monoclonal antibodies and stratification of anti-nicotinic AChR positive Myasthenia Gravis patients. Front Immunol. 2022;13:968206.

83. Manthey HD, Woodruff TM, Taylor SM, Monk PN. Complement component 5a (C5a). Int J Biochem Cell Biol. 2009;41(11):2114-7.

84. Mollnes TE, Brekke OL, Fung M, Fure H, Christiansen D, Bergseth G, et al. Essential role of the C5a receptor in

induced oxidative burst and phagocytosis revealed by a novel lepirudin-based human whole blood model of inflammation. Blood. 2002;100(5):1869-77.

85.   Sacks T, Moldow CF, Craddock PR, Bowers TK, Jacob HS. Oxygen radicals mediate endothelial cell damage by complement-stimulated granulocytes. An in vitro model of immune vascular damage. J Clin Invest. 1978;61(5):1161-7.

86.   Perianayagam MC, Balakrishnan VS, King AJ, Pereira BJ, Jaber BL. C5a delays apoptosis of human neutrophils by a phosphatidylinositol 3-kinase-signaling pathway. Kidney Int. 2002;61(2):456-63.

87.   Laudes IJ, Chu JC, Huber-Lang M, Guo RF, Riedemann NC, Sarma JV, et al. Expression and function of C5a receptor in mouse microvascular endothelial cells. J Immunol. 2002;169(10):5962-70.

88.   Jagels MA, Daffern PJ, Hugli TE. C3a and C5a enhance granulocyte adhesion to endothelial and epithelial cell monolayers: epithelial and endothelial priming is required for C3a-induced eosinophil adhesion. Immunopharmacology. 2000;46(3):209-22.

89.   Molad Y, Haines KA, Anderson DC, Buyon JP, Cronstein BN. Immunocomplexes stimulate different signalling events to chemoattractants in the neutrophil and regulate L-selectin and beta 2-integrin expression differently. Biochem J. 1994;299 (Pt 3)(Pt 3):881-7.

90.   Foreman KE, Vaporciyan AA, Bonish BK, Jones ML, Johnson KJ, Glovsky MM, et al. C5a-induced expression of P-selectin in endothelial cells. J Clin Invest. 1994;94(3):1147-55.

91.   Muhlfelder TW, Niemetz J, Kreutzer D, Beebe D, Ward PA, Rosenfeld SI. C5 chemotactic fragment induces leukocyte production of tissue factor activity: a link between complement and coagulation. J Clin Invest. 1979;63(1):147-50.

92.   Ikeda K, Nagasawa K, Horiuchi T, Tsuru T, Nishizaka H, Niho Y. C5a induces tissue factor activity on endothelial cells. Thromb Haemost. 1997;77(2):394-8.

93.   Ferrer-Lopez P, Renesto P, Schattner M, Bassot S, Laurent P, Chignard M. Activation of human platelets by C5a-stimulated neutrophils: a role for cathepsin G. Am J Physiol. 1990;258(6 Pt 1):C1100-7.

94.   Woodruff TM, Nandakumar KS, Tedesco F. Inhibiting the C5-C5a receptor axis. Mol Immunol. 2011;48(14):1631-42.

95.   Morgan BP, Boyd C, Bubeck D. Molecular cell biology of complement membrane attack. Semin Cell Dev Biol. 2017;72:124-32.

96.   Muller-Eberhard HJ. The membrane attack complex of complement. Annu Rev Immunol. 1986;4:503-28.

97.   Davies A, Lachmann PJ. Membrane defence against complement lysis: the structure and biological properties of CD59. Immunol Res. 1993;12(3):258-75.

98.   Morgan BP. The membrane attack complex as an inflammatory trigger. Immunobiology. 2016;221(6):747-51.

99.   Noris M, Galbusera M. The complement alternative pathway and hemostasis. Immunol Rev. 2023;313(1):139-61.

100.   Hattori R, Hamilton KK, McEver RP, Sims PJ. Complement proteins C5b-9 induce secretion of high molecular weight multimers of endothelial von Willebrand factor and translocation of granule membrane protein GMP-140 to the cell surface. J Biol Chem. 1989;264(15):9053-60.

101.   Kilgore KS, Shen JP, Miller BF, Ward PA, Warren JS. Enhancement by the complement membrane attack complex of tumor necrosis factor-alpha-induced endothelial cell expression of E-selectin and ICAM-1. J Immunol. 1995;155(3):1434-41.

102.   Kilgore KS, Flory CM, Miller BF, Evans VM, Warren JS. The membrane attack complex of complement induces interleukin-8 and monocyte chemoattractant protein-1 secretion from human umbilical vein endothelial cells. Am J Pathol. 1996;149(3):953-61.

103.   Roumenina LT, Rayes J, Frimat M, Fremeaux-Bacchi V. Endothelial cells: source, barrier, and target of defensive mediators. Immunol Rev. 2016;274(1):307-29.

104.   Benzaquen LR, Nicholson-Weller A, Halperin JA. Terminal complement proteins C5b-9 release basic fibroblast growth factor and platelet-derived growth factor from endothelial cells. J Exp Med. 1994;179(3):985-92.

105.   Tedesco F, Pausa M, Nardon E, Introna M, Mantovani A, Dobrina A. The cytolytically inactive terminal complement complex activates endothelial cells to express adhesion molecules and tissue factor procoagulant activity. J Exp Med. 1997;185(9):1619-27.

106.   Saadi S, Platt JL. Transient perturbation of endothelial integrity induced by natural antibodies and complement. J Exp Med. 1995;181(1):21-31.

107.   Bustos M, Coffman TM, Saadi S, Platt JL. Modulation of eicosanoid metabolism in endothelial cells in a xenograft model. Role of cyclooxygenase-2. J Clin Invest. 1997;100(5):1150-8.

108.   Hamilton KK, Hattori R, Esmon CT, Sims PJ. Complement proteins C5b-9 induce vesiculation of the endothelial plasma membrane and expose catalytic surface for assembly of the prothrombinase enzyme complex. J Biol Chem. 1990;265(7):3809-14.

109.   Polley MJ, Nachman R. The human complement system in thrombin-mediated platelet function. J Exp Med. 1978;147(6):1713-26.

110.   Heurich MmRM. Purification and Characterisation of Human and Mouse Complement C3. 2014.

111.   Vandenberg CW, Dijk HV, Capel PJA. Rapid Isolation and Characterization of Native Mouse Complement Component-C3 and Component-C5. Journal of Immunological Methods. 1989;122(1):73-8.

112.   Ingham KC. Precipitation of proteins with polyethylene glycol. Methods Enzymol. 1990;182:301-6.

113.   Spriestersbach A, Kubicek J, Schafer F, Block H, Maertens B. Purification of His-Tagged Proteins. Methods Enzymol. 2015;559:1-15.

114.   Fromell K, Adler A, Aman A, Manivel VA, Huang S, Duhrkop C, et al. Assessment of the Role of C3(H2O) in the Alternative Pathway. Front Immunol. 2020;11:530.

115.	Pangburn MK, Muller-Eberhard HJ. Relation of putative thioester bond in C3 to activation of the alternative pathway and the binding of C3b to biological targets of complement. J Exp Med. 1980;152(4):1102-14.

116.	Ekdahl KN, Mohlin C, Adler A, Åman A, Manivel VA, Sandholm K, et al. Is generation of C

(H

O) necessary for activation of the alternative pathway in real life? Molecular Immunology. 2019;114:353-61.

117.	Hallam TM, Cox TE, Smith-Jackson K, Brocklebank V, Baral AJ, Tzoumas N, et al. A novel method for real-time analysis of the complement C3b:FH:FI complex reveals dominant negative CFI variants in age-related macular degeneration. Front Immunol. 2022;13:1028760.

118.	Burkholder T, Foltz C, Karlsson E, Linton CG, Smith JM. Health Evaluation of Experimental Laboratory Mice. Curr Protoc Mouse Biol. 2012;2:145-65.

119.	Smith-Jackson K, Yang Y, Denton H, Pappworth IY, Cooke K, Barlow PN, et al. Hyperfunctional complement C3 promotes C5-dependent atypical hemolytic uremic syndrome in mice. J Clin Invest. 2019;129(3):1061-75.

120.	Hopken UE, Lu B, Gerard NP, Gerard C. The C5a chemoattractant receptor mediates mucosal defence to infection. Nature. 1996;383(6595):86-9.

121.	Richards A, Buddles MR, Donne RL, Kaplan BS, Kirk E, Venning MC, et al. Factor H mutations in hemolytic uremic syndrome cluster in exons 18-20, a domain important for host cell recognition. Am J Hum Genet. 2001;68(2):485-90.

122.	Schmidt CQ, Herbert AP, Kavanagh D, Gandy C, Fenton CJ, Blaum BS, et al. A new map of glycosaminoglycan and C3b binding sites on factor H. J Immunol. 2008;181(4):2610-9.

123.	Wong EKS, Hallam TM, Brocklebank V, Walsh PR, Smith-Jackson K, Shuttleworth VG, et al. Functional Characterization of Rare Genetic Variants in the N-Terminus of Complement Factor H in aHUS, C3G, and AMD. Front Immunol. 2020;11:602284.

124.	Kajander T, Lehtinen MJ, Hyvarinen S, Bhattacharjee A, Leung E, Isenman DE, et al. Dual interaction of factor H with C3d and glycosaminoglycans in host-nonhost discrimination by complement. Proc Natl Acad Sci U S A. 2011;108(7):2897-902.

125.	Roumenina LT, Frimat M, Miller EC, Provot F, Dragon-Durey MA, Bordereau P, et al. A prevalent C3 mutation in aHUS patients causes a direct C3 convertase gain of function. Blood. 2012;119(18):4182-91.

126.	Croset A, Delafosse L, Gaudry JP, Arod C, Glez L, Losberger C, et al. Differences in the glycosylation of recombinant proteins expressed in HEK and CHO cells. J Biotechnol. 2012;161(3):336-48.

127.   Schramm EC, Roumenina LT, Rybkine T, Chauvet S, Vieira-Martins P, Hue C, et al. Mapping interactions between complement C3 and regulators using mutations in atypical hemolytic uremic syndrome. Blood. 2015;125(15):2359-69.

128.   Xue XG, Wu J, Ricklin D, Forneris F, Di Crescenzio P, Schmidt CQ, et al. Regulator-dependent mechanisms of C3b processing by factor I allow differentiation of immune responses. Nat Struct Mol Biol. 2017;24(8):643-+.

129.   Molina H, Wong W, Kinoshita T, Brenner C, Foley S, Holers VM. Distinct Receptor and Regulatory Properties of Recombinant Mouse Complement Receptor-1 (Cr-1) and Crry, the 2 Genetic Homologs of Human Cr-1. Journal of Experimental Medicine. 1992;175(1):121-9.

130.   Kim YU, Kinoshita T, Molina H, Hourcade D, Seya T, Wagner LM, Holers VM. Mouse complement regulatory protein Crry/p65 uses the specific mechanisms of both human decay-accelerating factor and membrane cofactor protein. J Exp Med. 1995;181(1):151-9.

131.   Walsh MC, Bourcier T, Takahashi K, Shi L, Busche MN, Rother RP, et al. Mannose-binding lectin is a regulator of inflammation that accompanies myocardial ischemia and reperfusion injury. J Immunol. 2005;175(1):541-6.

132.   Busche MN, Stahl GL. Role of the complement components C5 and C3a in a mouse model of myocardial ischemia and reperfusion injury. Ger Med Sci. 2010;8.

133.   Pechtl IC, Kavanagh D, McIntosh N, Harris CL, Barlow PN. Disease-associated N-terminal complement factor H mutations perturb cofactor and decay-accelerating activities. J Biol Chem. 2011;286(13):11082-90.

134.   Nester CM, Barbour T, de Cordoba SR, Dragon-Durey MA, Fremeaux-Bacchi V, Goodship TH, et al. Atypical aHUS: State of the art. Mol Immunol. 2015;67(1):31-42.

135.   Pickering MC, Cook HT, Warren J, Bygrave AE, Moss J, Walport MJ, Botto M. Uncontrolled C3 activation causes membranoproliferative glomerulonephritis in mice deficient in complement factor H. Nat Genet. 2002;31(4):424-8.

136.   Lesher AM, Zhou L, Kimura Y, Sato S, Gullipalli D, Herbert AP, et al. Combination of factor H mutation and properdin deficiency causes severe C3 glomerulonephritis. J Am Soc Nephrol. 2013;24(1):53-65.

137.   Vernon KA, Ruseva MM, Cook HT, Botto M, Malik TH, Pickering MC. Partial Complement Factor H Deficiency Associates with C3 Glomerulopathy and Thrombotic Microangiopathy. J Am Soc Nephrol. 2016;27(5):1334-42.

138.   Ueda Y, Gullipalli D, Song WC. Modeling complement-driven diseases in transgenic mice: Values and limitations. Immunobiology. 2016;221(10):1080-90.

139.   Licht C, Greenbaum LA, Muus P, Babu S, Bedrosian CL, Cohen DJ, et al. Efficacy and safety of eculizumab in atypical hemolytic uremic syndrome from 2-year extensions of phase 2 studies. Kidney International. 2015;87(5):1061-73.

140.   Fakhouri F, Hourmant M, Campistol JM, Cataland SR, Espinosa M, Gaber AO, et al. Terminal Complement Inhibitor Eculizumab in Adult Patients With Atypical Hemolytic Uremic Syndrome: A Single-Arm, Open-Label Trial. Am J Kidney Dis. 2016;68(1):84-93.

141.   Greenbaum LA, Fila M, Ardissino G, Al-Akash SI, Evans J, Henning P, et al. Eculizumab is a safe and effective treatment in pediatric patients with atypical hemolytic uremic syndrome. Kidney International. 2016;89(3):701-11.

142.   Dutta S, Sengupta P. Men and mice: Relating their ages. Life Sci. 2016;152:244-8.

143.   Yang Y, Denton H, Davies OR, Smith-Jackson K, Kerr H, Herbert AP, et al. An Engineered Complement Factor H Construct for Treatment of C3 Glomerulopathy. J Am Soc Nephrol. 2018;29(6):1649-61.

144.   Ruseva MM, Peng T, Lasaro MA, Bouchard K, Liu-Chen S, Sun F, et al. Efficacy of Targeted Complement Inhibition in Experimental C3 Glomerulopathy. J Am Soc Nephrol. 2016;27(2):405-16.

145.   Bertram P, Akk AM, Zhou HF, Mitchell LM, Pham CT, Hourcade DE. Anti-mouse properdin TSR 5/6 monoclonal antibodies block complement alternative pathway-dependent pathogenesis. Monoclon Antib Immunodiagn Immunother. 2015;34(1):1-6.

146.   McNamara LA, Topaz N, Wang X, Hariri S, Fox L, MacNeil JR. High Risk for Invasive Meningococcal Disease Among Patients Receiving Eculizumab (Soliris) Despite Receipt of Meningococcal Vaccine. Am J Transplant. 2017;17(9):2481-4.

147.   Cullinan N, Gorman KM, Riordan M, Waldron M, Goodship TH, Awan A. Case report: Benefits and challenges of long-term eculizumab in atypical hemolytic uremic syndrome. Pediatrics. 2015;135(6):e1506-9.

148.   Vellanki VS, Bargman JM. Aspergillus Niger peritonitis in a peritoneal dialysis patient treated with eculizumab. Ren Fail. 2014;36(4):631-3.

149.   Benamu E, Montoya JG. Infections associated with the use of eculizumab: recommendations for prevention and prophylaxis. Curr Opin Infect Dis. 2016;29(4):319-29.

150.   Rabe M, Schaefer F. Non-Transgenic Mouse Models of Kidney Disease. Nephron. 2016;133(1):53-61.

151.   Ueda Y, Miwa T, Ito D, Kim H, Sato S, Gullipalli D, et al. Differential contribution of C5aR and C5b-9 pathways to renal thrombic microangiopathy and macrovascular thrombosis in mice carrying an atypical hemolytic syndrome-related factor H mutation. Kidney Int. 2019;96(1):67-79.

152.   Seshan SV, Franzke CW, Redecha P, Monestier M, Mackman N, Girardi G. Role of tissue factor in a mouse model of thrombotic microangiopathy induced by antiphospholipid antibodies. Blood. 2009;114(8):1675-83.

153.   Romay-Penabad Z, Liu XX, Montiel-Manzano G, Papalardo De Martinez E, Pierangeli SS. C5a receptor-deficient mice are protected from thrombophilia and endothelial cell activation induced by some antiphospholipid antibodies. Ann N Y Acad Sci. 2007;1108:554-66.

154. Kenawy HI, Boral I, Bevington A. Complement-Coagulation Cross-Talk: A Potential Mediator of the Physiological Activation of Complement by Low pH. Front Immunol. 2015;6:215.

155. Scola AM, Higginbottom A, Partridge LJ, Reid RC, Woodruff T, Taylor SM, et al. The role of the N-terminal domain of the complement fragment receptor C5L2 in ligand binding. J Biol Chem. 2007;282(6):3664-71.

156. Li R, Coulthard LG, Wu MC, Taylor SM, Woodruff TM. C5L2: a controversial receptor of complement anaphylatoxin, C5a. FASEB J. 2013;27(3):855-64.

157. Zhang T, Garstka MA, Li K. The Controversial C5a Receptor C5aR2: Its Role in Health and Disease. J Immunol Res. 2017;2017:8193932.

158. DiScipio RG, Chakravarti DN, Muller-Eberhard HJ, Fey GH. The structure of human complement component C7 and the C5b-7 complex. J Biol Chem. 1988;263(1):549-60.

159. Morgan BP. Complement membrane attack on nucleated cells: resistance, recovery and non-lethal effects. Biochem J. 1989;264(1):1-14.

160. Kilgore KS, Schmid E, Shanley TP, Flory CM, Maheswari V, Tramontini NL, et al. Sublytic concentrations of the membrane attack complex of complement induce endothelial interleukin-8 and monocyte chemoattractant protein-1 through nuclear factor-kappa B activation. Am J Pathol. 1997;150(6):2019-31.

161. Nangaku M, Alpers CE, Pippin J, Shankland SJ, Kurokawa K, Adler S, et al. Renal microvascular injury induced by antibody to glomerular endothelial cells is mediated by C5b-9. Kidney Int. 1997;52(6):1570-8.

162. Wurzner R. Modulation of complement membrane attack by local C7 synthesis. Clin Exp Immunol. 2000;121(1):8-10.

163. Lekova E, Zelek WM, Gower D, Spitzfaden C, Osuch IH, John-Morris E, et al. Discovery of functionally distinct anti-C7 monoclonal antibodies and stratification of anti-nicotinic AChR positive Myasthenia Gravis patients. Frontiers in Immunology. 2022;13.

164. Morgan BP, Harris CL. Complement, a target for therapy in inflammatory and degenerative diseases. Nat Rev Drug Discov. 2015;14(12):857-77.

165. Nishimura J, Yamamoto M, Hayashi S, Ohyashiki K, Ando K, Brodsky AL, et al. Genetic variants in C5 and poor response to eculizumab. N Engl J Med. 2014;370(7):632-9.

166. Harder MJ, Kuhn N, Schrezenmeier H, Hochsmann B, von Zabern I, Weinstock C, et al. Incomplete inhibition by eculizumab: mechanistic evidence for residual C5 activity during strong complement activation. Blood. 2017;129(8):970-80.

167. Harder MJ, Hochsmann B, Dopler A, Anliker M, Weinstock C, Skerra A, et al. Different Levels of Incomplete Terminal Pathway Inhibition by Eculizumab and the Clinical Response of PNH Patients. Front Immunol. 2019;10:1639.

168.   Wurzner R, Joysey VC, Lachmann PJ. Complement component C7. Assessment of in vivo synthesis after liver transplantation reveals that hepatocytes do not synthesize the majority of human C7. J Immunol. 1994;152(9):4624-9.

169.   Ghosh M, Rana S. The anaphylatoxin C5a: Structure, function, signaling, physiology, disease, and therapeutics. Int Immunopharmacol. 2023;118:110081.

170.   Klos A, Tenner AJ, Johswich KO, Ager RR, Reis ES, Köhl J. The role of the anaphylatoxins in health and disease. Molecular Immunology. 2009;46(14):2753-66.

171.   Rameix-Welti MA, Regnier CH, Bienaime F, Blouin J, Schifferli J, Fridman WH, et al. Hereditary complement C7 deficiency in nine families: subtotal C7 deficiency revisited. Eur J Immunol. 2007;37(5):1377-85.

172.   Wurzner R, Orren A, Lachmann PJ. Inherited deficiencies of the terminal components of human complement. Immunodefic Rev. 1992;3(2):123-47.

173.   Mohammed Y, Michaud SA, Petrosova H, Yang J, Ganguly M, Schibli D, et al. Proteotyping of knockout mouse strains reveals sex- and strain-specific signatures in blood plasma. NPJ Syst Biol Appl. 2021;7(1):25.

174.   Macor P, Durigutto P, Argenziano M, Smith-Jackson K, Capolla S, Di Leonardo V, et al. Plasminogen activator-coated nanobubbles targeting cellbound beta2-glycoprotein I as a novel thrombus-specific thrombolytic strategy. Haematologica. 2023;108(7):1861-72.

Chapter9　Publications arising from this work

Hyperfunctional complement C3 promotes C5-dependent atypical hemolytic uremic syndrome in mice

Kate Smith-Jackson,[1,2] Yi Yang,[1] Harriet Denton,[1] Isabel Y. Pappworth,[1] Katie Cooke,[1] Paul N. Barlow,[3] John P. Atkinson,[4] M. Kathryn Liszewski,[4] Matthew C. Pickering,[5] David Kavanagh,[1,2] H. Terence Cook,[5] and Kevin J. Marchbank[1,2]

[1]Institute of Cellular Medicine, Newcastle University, Newcastle upon Tyne, United Kingdom. [2]The National Renal Complement Therapeutics Centre (NRCTC), Newcastle upon Tyne Hospitals NHS Foundation Trust, Newcastle upon Tyne, United Kingdom. [3]Department of Chemistry, University of Edinburgh, Edinburgh, United Kingdom. [4]Division of Rheumatology, Washington University in St. Louis, St. Louis, Missouri, USA. [5]Department of Medicine, Imperial College London, London, United Kingdom.

Atypical hemolytic uremic syndrome (aHUS) is frequently associated in humans with loss-of-function mutations in complement-regulating proteins or gain-of-function mutations in complement-activating proteins. Thus, aHUS provides an archetypal complement-mediated disease with which to model new therapeutic strategies and treatments. Herein, we show that, when transferred to mice, an aHUS-associated gain-of-function change (D1115N) to the complement-activation protein C3 results in aHUS. Homozygous C3 p.D1115N (C3KI) mice developed spontaneous chronic thrombotic microangiopathy together with hematuria, thrombocytopenia, elevated creatinine, and evidence of hemolysis. Mice with active disease had reduced plasma C3 with C3 fragment and C9 deposition within the kidney. Therapeutic blockade or genetic deletion of C5, a protein downstream of C3 in the complement cascade, protected homozygous C3KI mice from thrombotic microangiopathy and aHUS. Thus, our data provide in vivo modeling evidence that gain-of-function changes in complement C3 drive aHUS. They also show that long-term C5 deficiency is not accompanied by development of other renal complications (such as C3 glomerulopathy) despite sustained dysregulation of C3. Our results suggest that this preclinical model will allow testing of novel complement inhibitors with the aim of developing precisely targeted therapeutics that could have application in many complement-mediated diseases.

Introduction

Our understanding and treatment of complement-mediated diseases has grown exponentially over the last 20 years. We now understand that complement plays an integral role in many autoimmune- and inflammation-based diseases or conditions (1). The identification of hyperactive complement as the primary driver in atypical hemolytic uremic syndrome (aHUS) (2) and its largely successful treatment using eculizumab (3, 4) has revealed the potential of anti-complement therapy in the treatment of many diseases, such as age-related macular degeneration (AMD), autoimmune disorders, and neurodegenerative conditions (5). However, eculizumab is not a panacea in AMD (6) or rheumatic diseases (7) or even in aHUS (8). Thus, there remains a need for better models of complement-mediated diseases to trial drugs and dissect the molecular pathways that are common among complement-mediated/associated diseases.

The complement system, consisting of more than 50 proteins, is integral to defense against pathogens and for maintenance of host homeostasis. It is considered the backbone of innate immunity, as it is critical in microbial killing, apoptotic cell clearance, and immune complex handling (9). Key complement proteins are activated in a stepwise manner through an enzymatic activation cascade that is regulated by an array of modulators (10). Activation can be achieved through one or more of the classical, lectin, and alternative pathways, all of which culminate in the cleavage of C3. Cleavage of C3 (185 kDa) into C3b (177 kDa) and C3a (8 kDa) is the central activating step of the complement cascade (11). C3 cleavage leads to deposition of C3b onto the surface of microbes (opsonization), release of the proinflammatory anaphylactic products C3a and C5a, and initiation of the terminal pathway, leading to the formation of the membrane attack complex (MAC) C5b-9 and cell lysis (12). Given the intricate nature of the complement cascade, many soluble and membrane-associated proteins function to regulate C3 activation (13). Together these protect healthy host cells and tissues from unwanted complement activation, while unprotected surfaces rapidly become coated in C3b molecules (1). Abnormalities in the complement system, derived by genetic or acquired means, are associated with a variety of pathologies (14).

aHUS is a renal disease that encompasses the clinical triad of microangiopathic hemolytic anaemia, thrombocytopenia, and acute renal failure (15). Dysregulation of the alternative pathway of the complement system at the cell or extracellular matrix surface is a major factor in susceptibility to aHUS (16). In particular,

an imbalance between the activators and regulators of the alternative pathway results in complement-mediated damage to the endothelium (17). Approximately 60% of individuals with aHUS have at-risk mutations in their complement genes (4). Mutations occur either in the genes encoding complement-regulating proteins such as factor H (FH), factor I (FI), and membrane cofactor protein (MCP) or in genes encoding complement-activation proteins (C3 and factor B [FB]) (18). In general, it has been observed that disease-linked mutations in regulators result in a loss of function, while disease-linked mutations in activators result in a gain of function (19). The most frequently mutated gene in aHUS patients is *CFH* (the gene encoding FH), occurring in 25% of sporadic cases, followed by mutations in *C3* (4%–11% of cases), in *CFI* (5%–10%), in *MCP* (5%–9%), and in *FB* (<4%) (20).

The nature of the genetic complement abnormality has a significant impact on the clinical phenotype. Those with mutations in *MCP* have the best prognosis (only 6% reach end-stage renal failure [ESRF]), while mutations in *CFH* have historically been associated with the worst prognosis, including earlier disease onset and higher risk of relapse (20). *CFH* mutations typically cluster in exons 22 and 23 of *CFH*, which encode the C-terminal short consensus repeats (SCRs; also referred to as complement control protein domains [CCPs]) 19–20 of FH (21, 22). This region is important for regulating C3b amplification on host cell and tissue surfaces, while the N-terminal region SCRs 1–4 are important for regulatory activity both in the fluid phase and on surfaces (21, 23). The functional significance of the SCRs 19–20 was elegantly illustrated through transgenic expression of an FH truncation protein that lacked the C-terminal 5 SCRs backcrossed onto FH-knockout mice (24). These mice spontaneously developed features mirroring aHUS in humans. This observation indicated that regulation in the fluid phase (preventing futile depletion of C3 in plasma) combined with dysregulation at the cell surface was pathogenic in aHUS. Further work confirmed the damage caused by downstream events in the complement cascade, since the phenotype could be rescued by breeding onto a *C5*-deficient background (25). We have known for some time that gain-of-function C3 mutations, clustering in the FH-binding interface of C3b, are associated with aHUS (26). Interestingly, mutations in *C3* have varied outcomes, with 63%–67% of adult patients progressing rapidly to ESRF and some *C3* mutations (including D1115N) resulting in chronic progression (27, 28), a renal prognosis similar to that seen with many *CFH* mutations (15). As SCRs 19–20 of FH bind to the thioester domain (TED) of C3b, it was expected that in vitro studies would confirm that recombinant human C3 proteins with mutations located in the TED (mature C3 p.D1093N, p.C1136W, p.Q1139K, p.A1072V) were defective in binding to FH (26, 29). This reduced binding affinity was proposed to cause reduced proteolytic inactivation and therefore enhanced complement activation in vivo. To date, however, no in vivo studies have examined C3 gain-of-function aHUS mutations. Consequently, a direct demonstration that these mutations cause aHUS has been lacking.

The historical work in animal models, coupled with the successful use of C5 inhibitors in aHUS patients, lays the foundation for our current understanding of the pathogenesis of aHUS (30). However, what is not yet known is the effects of long-term C5 inhibition in the presence of continued dysregulation of the alternative pathway (31). In theory, with time, patients on C5-inhibiting therapy could convert their phenotype from aHUS to a C3-mediated glomerular disease (e.g., complement 3 glomerulopathy [C3G]; refs. 32, 33) as opposed to a C5/terminal pathway–mediated disease. Lifelong C5 inhibition poses a significant immunosuppressive burden on the patient (34), particularly patients who have renal transplants and are already on triple immunosuppressive therapy (35). While previous (24) and existing mouse models based on FH functional deficit (36, 37) display some of the characteristic phenotypes/pathologies of aHUS, reflecting potential subsets of the disease, they do not entirely reproduce the clinical observations, i.e., disease induction required either nephrotoxic serum (36) or was driven by excessive coagulation/thrombosis (37).

Herein, we describe the transfer of human C3 gain-of-function aHUS-associated mutations to murine C3. Following in vitro characterization of these murine C3 mutants, we introduced a point mutation in murine *C3* (p.D1115N) in conditional knockin mice. C57BL/6 mice homozygous for C3 Asn1115 (C3KI) exhibit a spontaneous aggressive renal phenotype that is identical to aHUS as described in humans. Ex vivo analysis confirmed that failure to bind FH could explain the pathogenicity of this point mutant. C5 blockade protected C3KI mice from disease, and through long-term studies of C5 genetic deletion, we have shown that while increased C3 turnover continues through dysregulation of the alternative pathway, this does not evolve into a C3 glomerulopathy. Given that our model robustly recapitulates the clinical phenotype in humans, this allows us to translate our long-term studies in mice to humans — providing insight into the effects of chronic terminal pathway inhibition on the alternative pathway. This C3 gain-of-function mouse model of aHUS thus provides an opportunity for anti-complement drug testing.

Results

Natural history of a familial C3 Asn1115 mutation discovered in the NRCTC aHUS cohort. The C3 Asn1115 point mutation has been identified in 3 families, including in the NRCTC/Paris aHUS patient cohort (Figure 1A) (26). The patients are heterozygous for a missense mutation in *C3* (*C3* c.3343 G>A), corresponding to replacement of an aspartic acid with an asparagine at position 1115 of C3 (D1115N, Figure 1B; note this is D1093N in the mature protein) (15, 26, 28). The C3 Asn1115 variant has a substantial loss in binding to both MCP (CD46) and FH (26, 29), which we confirmed in additional surface plasmon resonance (SPR) analysis (Supplemental Figure 1; supplemental material available online with this article; https://doi.org/10.1172/JCI99296DS1). Despite almost complete loss of interaction with MCP, we hypothesized that the loss of interaction of the C-terminal region FH with the TED of this C3b (the cleaved, activated form of C3) variant, as illustrated in Figure 1B, would be important for selective recognition of a self-surface (38), which could be critical for the pathogenicity of the mutation. The chronological clinical parameters of creatinine and C3, FB, and FH of the family carrying the Asn1115 mutation are presented as available (Figure 1, C and D). One patient has a functioning renal transplant (28). This patient received the transplant before the era of preemptive eculizumab for kidney transplantation, and when graft function started to decline, a biopsy confirmed features of a chronic thrombot-
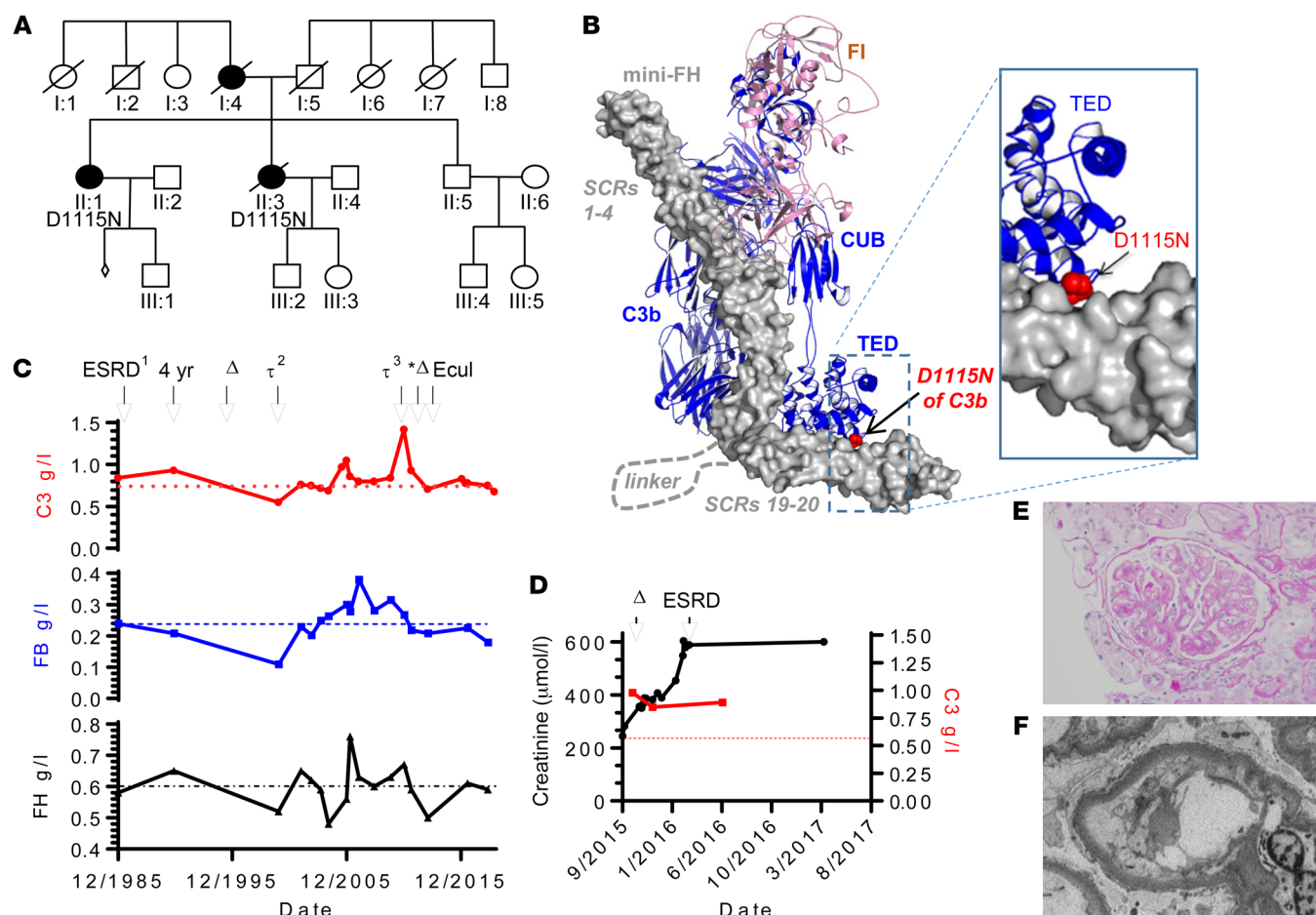
Figure 1. The NRCTC family heterozygous for C3 Asn1115 mutation. (**A**) Family pedigree showing affected individuals. (**B**) Location of the C3 mutation (D1115N) within the activated C3b fragment. The structure shown is the complex of human C3b, human FI, and mini-FH (SCRs 1–4 and SCRs 19–20, of human FH, connected by a poly-Gly linker) (5o32.pdb). C3b (blue) and FI (pink) are shown as cartoons, and mini-FH (gray) as a surface. The side chain atoms of C3b residue D1115 are shown as red spheres. CUB, complement C1r/C1s, Uegf, Bmp1. (**C**) Complement profile and renal events of II:1. Where available, C3 levels (top panel) with lower reference range (dotted line); FB levels (middle panel) with lower reference range (dashed line); and FH levels (bottom panel) with upper reference range (black dash-dotted line) are shown over more than 30 years. Associated clinical features are indicated above: ERSD and received first renal allograft, fourth year after transplant; Δ indicates declining graft function as a result of chronic allograft nephropathy; the second and third renal allografts are indicated by τ^2 and τ^3, respectively, with asterisk highlighting loss of third renal allograft to recurrent aHUS with increased creatinine and treatment with eculizumab (Ecul). (**D**) Where available, C3 and creatinine levels of individual II:3; C3 level in red (right y axis), and renal function in black; Δ indicates chronic TMA on biopsy followed by ESRD as indicated. (**E**) Representative H&E staining of II:3 showing double contouring (a feature of TMA); original magnification, ×40. (**F**) Electron micrograph from II:3 shows a capillary loop with detachment of the endothelium with accumulation of electron lucent material; original magnification, ×8000.

ic microangiopathy (TMA; Figure 1, E and F). In the context of low-grade hemolysis, eculizumab treatment was commenced for recurrent aHUS (Figure 1C). This was successful, with no further deterioration in allograft function to date (albeit chronic damage had already occurred prior to the use of eculizumab). Notably in this patient, FH plasma levels were found to be above the upper limits of the normal range for the majority of the time points analyzed, while FB levels were below the normal range (Figure 1C), providing evidence of increased alternative pathway activation.

Successful generation and functional testing of recombinant mouse C3 and several disease-associated mutants. Data generated in vitro with mutant human C3 molecules have suggested that some are resistant to control by FH (26, 29), but there has been no direct in vivo demonstration that mutations in C3, including those identified in the Newcastle patients, cause aHUS. To address this, we sought

to develop a new animal model. Initially, we needed to test the feasibility of transferring mutations in human C3 and their functional outcomes to murine C3. A pairwise sequence alignment confirmed that all mutated C3 residues identified in our earlier study (26) and several others identified later (29) were conserved in mouse C3, with the exception of R102 (Supplemental Figure 2A). Indeed, this pattern of residue conservation was noted across rat (P01026), bovine (Q2UVX4), pig (P01025), and guinea pig (P12387) C3 proteins (Supplemental Figure 2B). For ease of purification, we designed a cDNA construct to allow production of recombinant FLAG- and 7xHis-tagged murine C3 (NM_009778.3) in mammalian tissue culture (see Supplemental Methods and Supplemental Figure 3). After sequence confirmation of the recombinant mouse C3 (rmC3) construct, we used site-directed mutagenesis to generate 10 mutant rmC3 clones. These included 923ΔDG rmC3, based
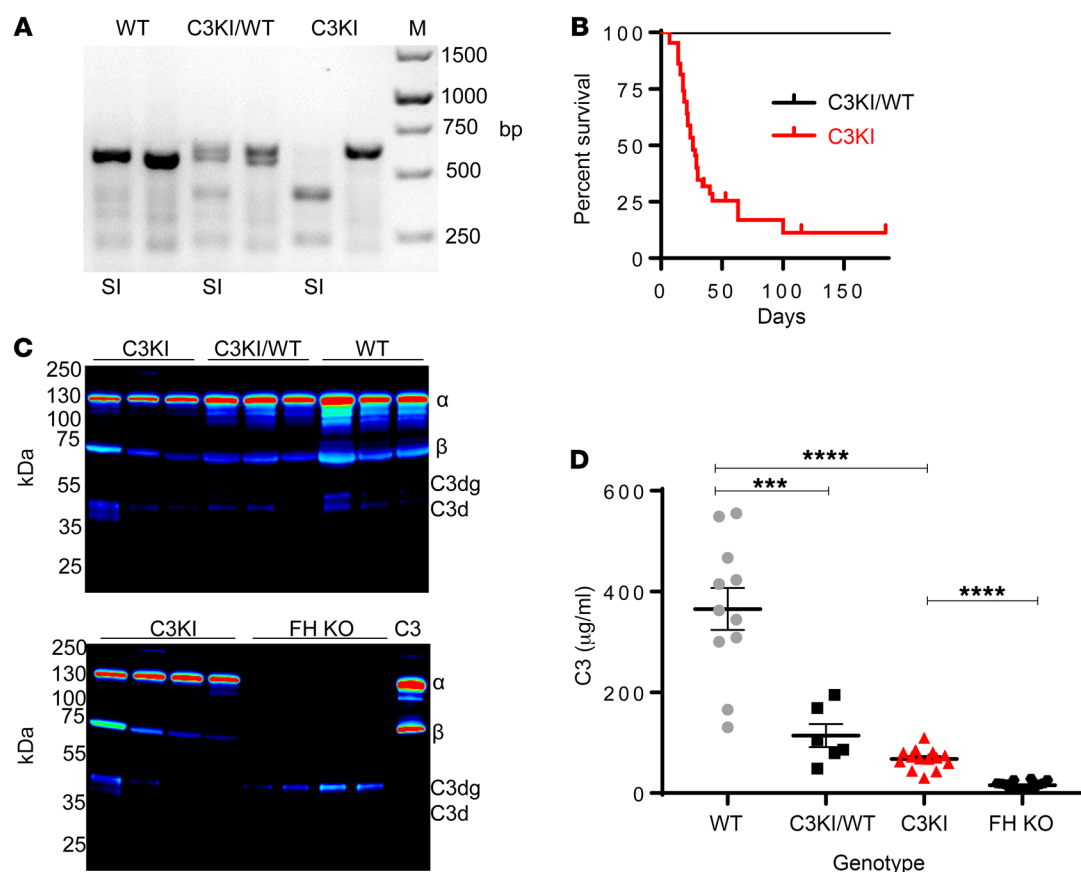
Figure 2. Initial characterization of C3KI mice. (A) A representative ethidium bromide–stained PCR gel illustrating genotyping of C3KI mice, with the SalI digest, as appropriate, indicated by SI below the gel. **(B)** Kaplan-Meier survival curve analysis of the first 44 C3KI and C3KI/WT littermates (F_1–F_3). Data for 44 WT littermates were identical to those for C3KI/WT. **(C)** Western blots of murine C3 derived from plasma (freshly collected into EDTA and run under reduced conditions) detected by goat anti–mouse C3 (MP Biomedicals). Mouse genotype is indicated above the lanes; each lane represents an individual mouse. Chemiluminescence image were captured using LI-COR Odyssey FC and displayed in pseudo-color. **(D)** Plasma murine C3 levels from 11 WT (gray circles), 6 knockin (KI)/WT (black squares), 15 KI (red triangles), and 16 FH-KO (black hexagons) mice were measured. Absorbance readings at 450 nm were converted to μg/ml using a standard curve based on purified mouse C3; mean ± SEM. ***$P < 0.001$ and ****$P < 0.0001$ using unpaired t test with Welch's correction.

on the previous findings of gain of function for this mutant associated with C3 glomerulopathy (Supplemental Figure 2C) (39). The recombinant proteins were purified to homogeneity using FLAG-tag affinity chromatography and examined by SDS-PAGE (Supplemental Figure 4). Using standard fluid-phase cofactor assays, we found evidence that rmC3b (Val1072) and rmC3b (Asn1115), in comparison to WT rmC3b, demonstrated clear resistance to proteolytic inactivation by FI (Supplemental Figure 4). Furthermore, using SPR (Biacore), several of our C3b mutants had reduced binding to "mini" murine FH (mini-FH; a construct containing the 2 key C3b-binding sites, i.e., SCRs 1–5 and SCRs 18–20 of murine FH), with rmC3(Asn1115) having one of the lowest-affinity interactions in this assay (Supplemental Figure 5). This is entirely consistent with loss of an important H-bonding interaction with Tyr1190 of FH as described by Morgan et al. (38). To explore the in vivo consequence of C3 gain-of-function changes, we next generated a conditional knockin mouse (C3KI) based on the Asn1115 change.

Development of the C3KI model. Possession of a form of C3b that cannot be recognized by FH is expected to be embryonically lethal (40). Thus, C3KI mice were generated using conditional knockin technologies (Ozgene; see Supplemental Figure 6). When these

mice were bred onto constitutive Cre-expressing mice (B6[Tm1Cre/Oz]), heterozygous (C3KI/WT) and homozygous (C3KI) mice were readily identified by genotype PCR (Figure 2A). Subsequent analysis of F_2 litters showed that proportions of specific genotypes were in line with expectations (20% WT versus 28% C3KI, with no influence on sex; Supplemental Figure 7A) from a normal Mendelian mode of inheritance, indicating that the D1115N mutation in C3 did not affect embryo survival in utero. At weaning (aged 18–21 days), many C3KI mice weighed less than their littermates (Supplemental Figure 7B), and by postpartum day 50 (P50) they exhibited significantly ($P < 0.0001$) higher mortality (Figure 2B). Analysis of plasma from C3KI/WT and C3KI mice showed the presence of intact mutant C3 protein and some evidence of C3 breakdown fragments, i.e., C3d, but not complete loss of intact C3 as observed in FH-deficient mice (Figure 2, C and D). See complete unedited blots in the supplemental material. Similar evidence was noted with respect to FB consumption (Supplemental Figure 7C). We suspect that C3b amplification is less well regulated, leading to an increased rate of conversion of C3 Asn1115 to C3b Asn1115 and low C3 levels (68 ± 5 μg/ml C3KI versus 365 ± 41 μg/ml for WT). However, the degree of C3 consumption/fragment generation was significantly lower than that seen in
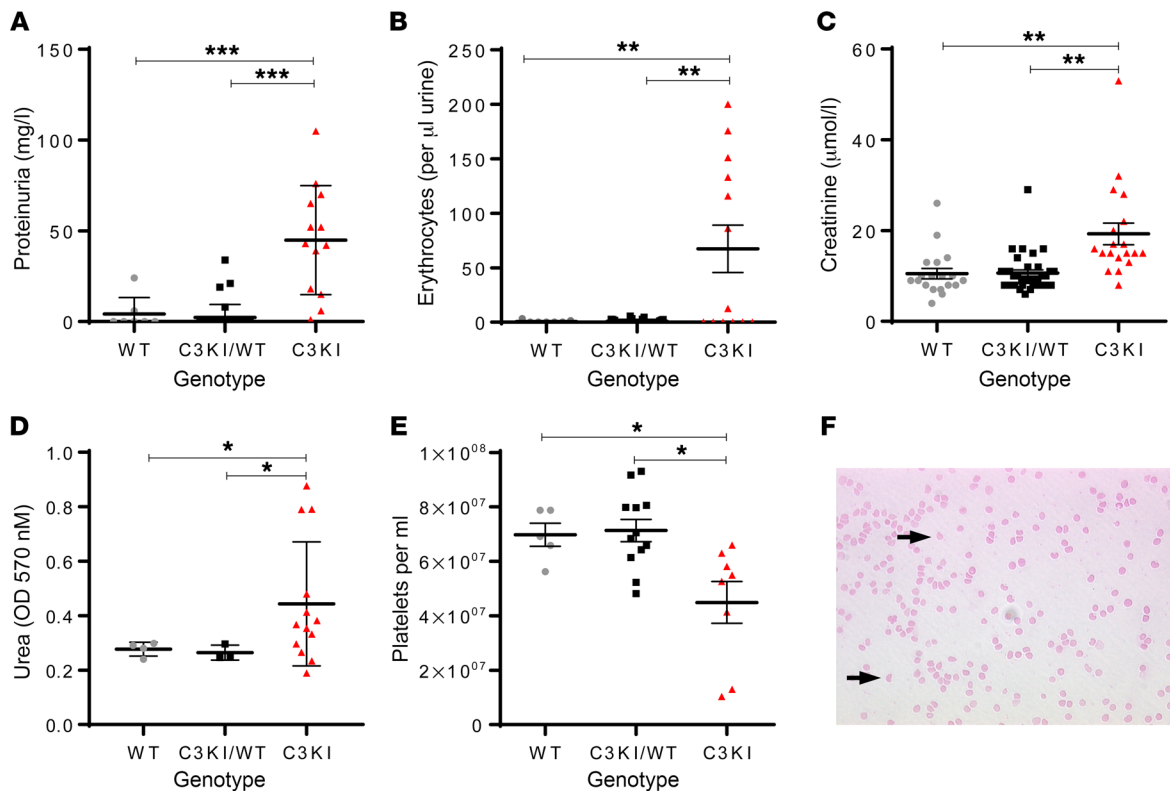
Figure 3. Further characterization of the C3KI mice. Where available, levels of proteinuria (**A**) and hematuria (**B**) were measured by Combistix (Siemens/Bayer) analysis of urine collected during routine handling. Results for 13 C3KI (triangles), 24 C3KI/WT (squares), and 8 WT (circles) mice, P14–P21, are shown. (**C**) Creatinine values obtained from the mouse plasma taken from 19 C3KI, 34 C3KI/WT heterozygous, and 19 WT mice, P14–P28, are shown. (**D**) Urea values obtained from plasma taken from 13 C3KI mice, 4 C3KI/WT, and 4 WT mice. (**E**) Platelet counts of 8 C3KI, 12 C3KI/WT, and 5 WT mice on P21. Absolute numbers were provided by use of cell count beads and flow cytometry. (**F**) A representative ($n = 8$, P21) Giemsa-stained blood film from a C3KI mouse showing schistocytes (indicated by black arrows), consistent with mechanical hemolysis of red blood cells. Original magnification ×40. *$P < 0.05$, **$P < 0.01$, ***$P < 0.005$ using unpaired t test with Welch's correction.

the FH-deficient mouse, where very little intact C3 was detectable in isolated plasma (15 ± 3 μg/ml; Figure 2, C and D) (36, 41).

Characterization of C3KI mice. Analysis of survival curves showed clearly that (homozygous) C3KI mice, but not (heterozygous) C3KI/WT mice, had a higher mortality than WT mice. We therefore decided to track C3KI mice from P7. C3KI mice were smaller than littermates at all stages of analysis, and many C3KI mice displayed heavy proteinuria and significant hematuria (Figure 3, A and B). Creatinine levels (reflecting renal impairment) were elevated in the majority of C3KI mice, but were highest in mice in the final stages of disease, as expected (Figure 3C). Additionally, urea levels, another surrogate marker of renal dysfunction, were elevated in the majority of C3KI mice (Figure 3D). Platelet counts were lower in C3KI mice, and very sick animals presented with severe thrombocytopenia (Figure 3E). Blood films from C3KI mice contained schistocytes, indicating fragmentation of red blood cells (Figure 3F). The presence of schistocytes coupled with the observation of thrombocytopenia are consistent with microangiopathic hemolytic anemia, a salient feature of aHUS.

TMA in C3KI mice. C3KI mice had renal disease, as evidenced by proteinuria, hematuria and elevated creatinine, and a proportion reached ESRF, requiring euthanasia. Periodic acid–Schiff (PAS) staining of kidney sections, from C3KI mice ranging from

14 to 28 days old, was consistent with histological features typical of a chronic TMA, including mesangiolysis (Figure 4A), followed by microaneurysm formation resulting from the dissolution of the mesangial matrix (Figure 4B) and double contouring of the glomerular basement membrane (Figure 4C). Electron microscopy confirmed endothelial injury with loss of fenestrations and subendothelial lucency (Figure 4D). Fibrin deposition within glomeruli was observed in C3KI mice, and occasionally, intravascular thromboses were identified (Supplemental Figure 7, D–I). Interestingly, we did not see any histological evidence of a TMA in the C3KI/WT mice (Supplemental Figure 8, A–C), MAHA (Supplemental Figure 8D), or kidney disease even after a year (Supplemental Figure 8E).

Complement dysregulation of C3KI. Having identified an aggressive renal disease in the C3KI mice, coupled with the histological analysis showing a TMA (in keeping with aHUS), we investigated the complement profile of the C3KI mice. Interestingly, plasma FH levels in C3KI mice were elevated (Figure 5A). This is consistent with a response to higher levels of complement activation or regulation (37). Additionally, plasma C5 levels were lower in C3KI mice (Figure 5B). Significant C3 fragment deposition was identified using immunofluorescence staining (Figure 5C). A granular staining pattern, largely confined to the mesangium and capillary walls of the glomerulus, was clearly evident in the C3KI
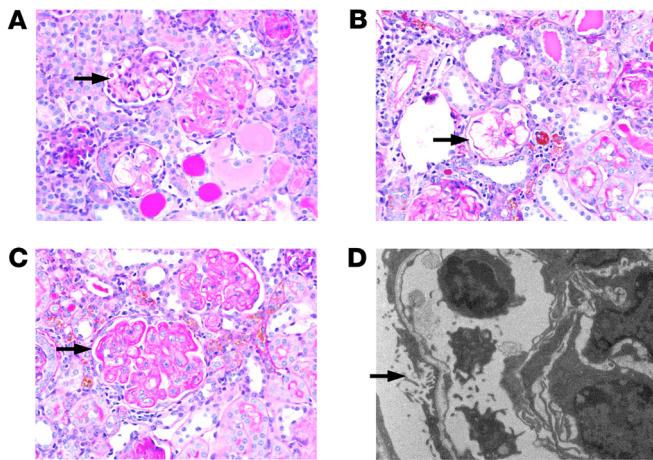
Figure 4. TMA in C3KI mice. PAS-stained sections from C3KI mice aged 14–28 days. Images are representative of the 8 C3KI mice examined. Arrows highlight key examples of the following: (**A**) Mesangiolysis in the glomerulus. (**B**) Microaneurysms of the glomerular capillaries following dissolution of the matrix after the mesangiolysis. (**C**) Double contouring of glomerular capillary walls, a key feature of chronic TMA. Original magnification in **A**–**C**, ×40. (**D**) Electron microscopy (original magnification, ×7900) showing subendothelial lucency, which is consistent with ischemic conditions precipitated by the TMA from a day 7 C3KI mouse.

mice. This was distinct from the C3KI/WT and WT littermates, in which tubulointerstitial staining was observed (which is normal in murine kidneys; refs. 24, 37). Detection of C9 (Figure 5D) in the glomeruli of C3KI mice, by immunofluorescence staining, suggested that terminal pathway activation and MAC deposition contribute to disease in the C3KI mice, as also happens during aHUS in humans. No glomerular C9 deposition was found in the kidney of C3KI/WT or WT mice (Figure 5D).

Molecular basis for complement dysregulation. Based on our work using rmC3 (Supplemental Figures 4 and 5), we expected C3 isolated from the blood of C3KI mice to have lower affinity, compared with WT murine C3, for FH. To confirm this, we isolated and purified C3 Asn1115 protein from knockin mice to homogeneity, and purified WT C3 as well as full-length FH from C57BL/6 mice. In addition, we generated recombinant mouse FH1–5, mouse Crry, and human FH19–20 (see Supplemental Methods for details). Using SPR, we measured the strength of the interaction between WT murine C3b or murine C3b Asn1115 (generated by incubation with human FB and FD; see Methods; 930 ± 10 RU amine coupled to a CM5 chip) and regulatory proteins or protein fragments. Full-length mouse serum–derived FH bound to WT C3 with an affinity (K_D) of 1.4 ± 0.13 μM, while it bound C3b Asn1115 with a K_D of 3.7 ± 0.25 μM (Figure 6A). Recombinant mouse FH1–5 bound to both WT C3b and C3b Asn1115 with essentially equivalent affinity (2.9 ± 0.24 μM and 3.1 ± 0.34 μM, respectively; Figure 6B). These values are broadly similar to the affinity of full-length mouse FH binding to C3b Asn1115, and hence, taken together, these SPR data suggest the almost complete loss of binding between mutant C3 and the C-terminus of FH. We confirmed this using SPR to measure the binding between human FH19–20 (42, 43) (the analyte) and various versions of mouse C3b. FH19–20 bound WT C3b with a K_D of 9.4 ± 1.2 μM (43), whereas it bound immobilized C3b Asn1115 with a much weaker K_D (saturation was not reached) of >17.4 (Figure 6C). Finally, as Crry is the major cell surface regulator of complement in the mouse, we also evaluated its binding to WT and mutant C3b and found that recombinant mouse Crry bound to WT C3b and C3b Asn1115 with essentially equivalent affinity (3.2 ± 0.03 μM and 3.5 ± 0.06 μM, respectively; Figure 6D). Finally, fluid-phase FI cofactor assays, with purified reagents, indicated that C3b Asn1115 was more resistant to cleavage by human FI (with murine FH as cofactor) than

WT murine C3b (Figure 6, E and F). These data are thus consistent with a mechanism whereby alternative pathway dysregulation in C3KI mice, arising from a perturbation of the binding site in C3b for the self/non-self–discriminatory C-terminal region of FH, is responsible for a TMA within the kidney and an aHUS-like phenotype in the mouse.

Reversing complement dysregulation in C3KI mice. The data presented above suggest that C3KI mice provide a unique model of complement-mediated disease that arises from a gain-of-function mutation rather than a loss-of-function change in complement regulators. The current gold standard treatment for complement-mediated aHUS in humans is eculizumab. We reasoned that treatment of C3KI mice with a C5-blocking mAb should protect them from developing aHUS.

Therefore, we injected P13–P30 C3KI mice with 50 μg/g BB5.1 (a C5-inhibiting mAb, with dosing based on previous studies; refs. 44, 45), for up to 2 weeks and compared them with C3KI mice dosed with isotype-control antibody (mouse IgG$_1$/ PBS). While 55% (6 of 11) of mice treated with the control antibody were removed from the study due to poor health, none of the mice treated with BB5.1 (0 of 8) succumbed to disease (Figure 7A). Failure to thrive, as indicated by low weight gain, was also partially reversed in BB5.1-treated mice compared with isotype controls (Supplemental Figure 9). Creatinine values were lower in the BB5.1 treatment arm, reflecting attenuation of renal injury, or else signs of renal recovery (Figure 7B). Platelet counts were significantly higher in the animals treated with BB5.1 (Figure 7C). C3 immunofluorescence appeared similar in both treatment arms, but C9 glomerular deposition was lower in the BB5.1 treatment arm (Figure 7D). Despite the marked clinical recovery in the BB5.1-treated cohort, histological analysis revealed only subtle improvement over the treatment period, with some persisting pathological features in both treated and control cohorts (Figure 7E). In general, an improvement in hematological outcomes for C3KI mice was achieved by C5 inhibition, consistent with a major role for the complement cascade in this mouse model of aHUS.

Genetic deficiency in C5 protects mice from all kidney disease. To further validate the model and provide translational insight into long-term C5 blockade, we backcrossed the C3KI onto the
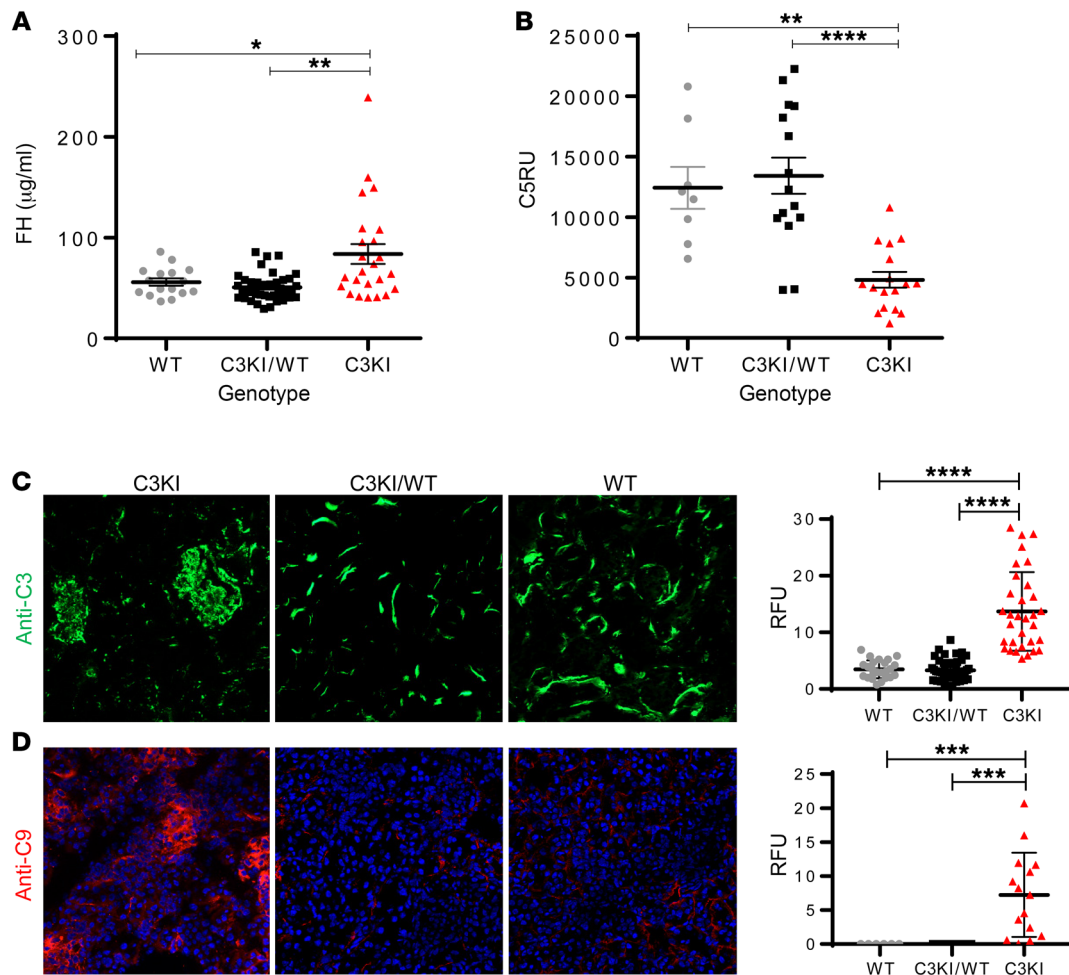
Figure 5. Complement dysregulation in C3KI mice. (**A**) Complement FH levels in mouse plasma isolated from 19 C3KI mice (triangles), 34 C3KI/WT (squares), and 19 WT (circle) mice, P14–28, were established using an in-house sandwich ELISA described in Methods. (**B**) C5 levels in mouse plasma isolated from 17 C3KI, 15 C3KI/WT, and 8 WT mice on P14–P28 were established using an in-house sandwich ELISA. Relative units were generated via a standard curve based on WT control serum. (**C**) Immunofluorescence of glomerular C3 deposition in C3KI, C3KI/WT, and WT kidneys (representative of $n = 10$ in each group). Images were taken on a Zeiss Axio Imager II. Original magnification, ×20. Densitometry analysis is shown to the right of the panels; relative fluorescence units from >25 image captures are indicated. (**D**) Glomerular C9 deposition in C3KI in comparison to background staining of WT. Original magnification ×20; >6 image captures shown in densitometry. *$P < 0.05$, **$P < 0.005$, ***$P < 0.001$, ****$P < 0.0001$ using unpaired t test with Welch's correction.

C5-deficient mice (C5KO). As expected there was 100% survival of the C3KI.C5KO mice. Two cohorts of mice were tracked and culled at 2 and 6 months, respectively. No evidence of proteinuria was detected in urine collected before mice were culled in either cohort (Figure 8A and Supplemental Figure 10A), and creatinine levels were similar to those in age- and littermate-matched controls (Figure 8B and Supplemental Figure 10B). Collectively, these observations indicate a lack of chronic kidney disease. Plasma C3 levels remained low in C3KI.C5KO mice (118 ± 6 μg/ml) (Supplemental Figure 10C). This was particularly evident in the 6-month-old animals (84 ± 8 μg/ml) when compared with C3KI mice (68 ± 8 μg/ml) or C5KO mice (281 ± 60 μg/ml) (Figure 8C). Nevertheless, levels of C3 in the C3KI.C5KO mice were significantly ($P < 0.0001$) higher than the levels reported in the FH-KO mice (current model of C3 glomerulopathy), where all the fluid-phase C3 had been consumed

(Figure 2C; ref. 41). As might be surmised from the low plasma C3 levels, glomerular C3 fragment deposition was still evident in both cohorts (Figure 8D and Supplemental Figure 10, D and E), while C9 staining was absent (Figure 8D, lower panels). The C3 fragment deposition in C3KI.C5KO mice did not appear to lead to morphological features of C3 glomerulopathy, as glomeruli appeared normal in the Martius scarlet blue– (MSB-) and PAS-stained sections (Figure 8, E and F, and Supplemental Figure 10, F–I). This was further validated using electron microscopy, whereby 6-month C3KI.C5KO mice showed healthy glomeruli and no evidence of electron-dense deposits (Figure 8G), similar to aged-matched WT (Figure 8H) and in contrast to 6-month FH-KO animals, which showed pathological features of C3 glomerulopathy (Supplemental Figure 10J). Peripheral blood smears showed no evidence of schistocytes in the C3KI.C5KO mice (Figure 8I and Supplemental Figure 10K).
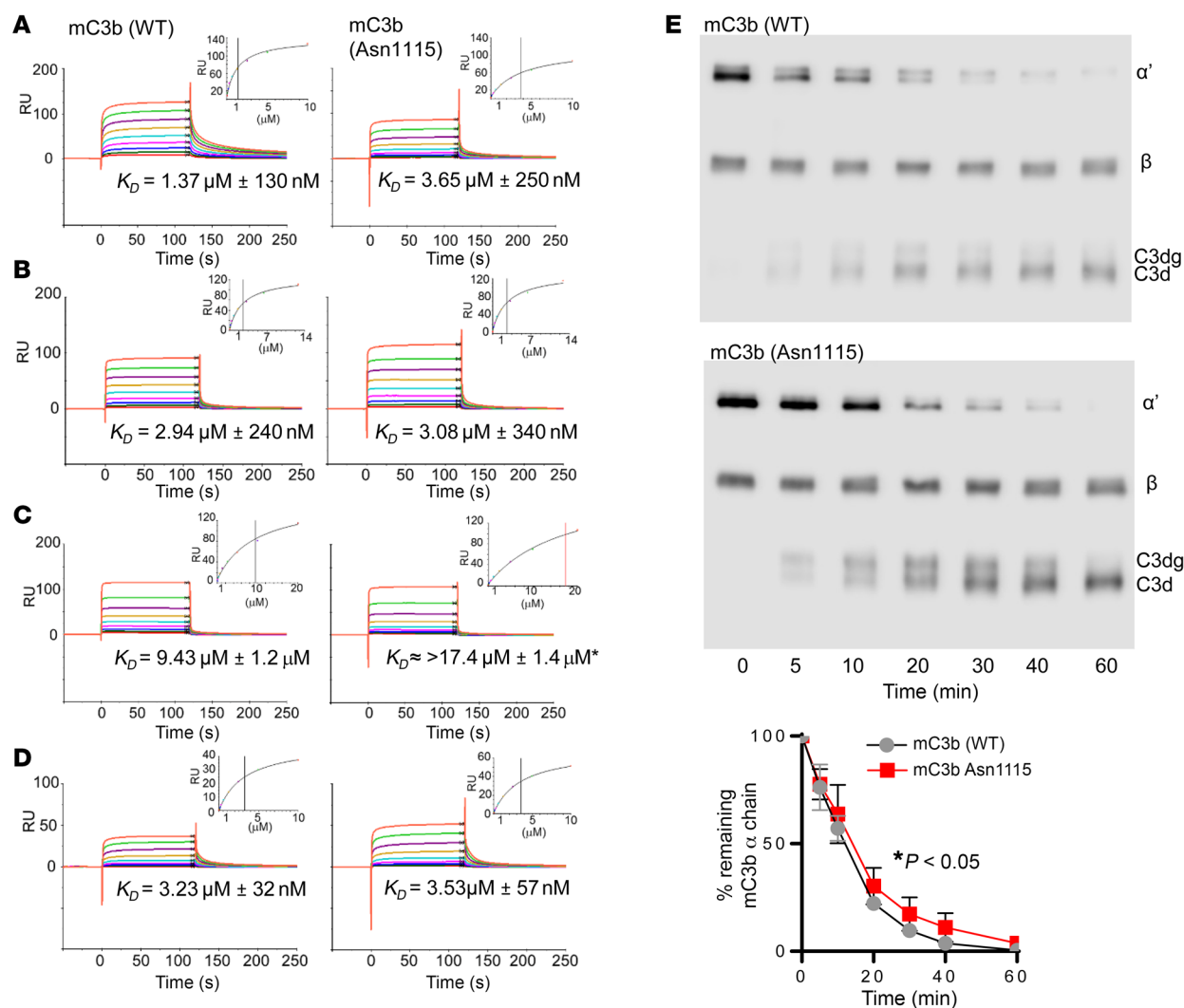
Figure 6. Molecular basis of complement dysregulation in C3KI mice. SPR analysis using mouse C3b derived from WT or C3KI mouse plasma. Mouse C3b was amine coupled to a CM5 biosensor chip (930 ± 10 RU). Doubly diluted concentration series of (**A**) purified murine FH (0 to 10 μM), (**B**) recombinant murine FH SCRs 1–5 (0 to 14.6 μM), (**C**) recombinant human FH SCRs 19-20 (0 to 20 μM), or (**D**) recombinant murine Crry SCRs 1–5 (0 to 10 μM) were flowed across the chip surface. The equilibrium dissociation constant K_D was calculated using a steady-state model in the Biacore evaluation package, indicated as the black vertical line. *At the concentration range assayed here, human FH19–20 was not able to achieve saturated binding on the C3b Asn1115 surface; thus, an underestimated K_D is indicated by the red vertical line. (**E**) Representative gels showing plasma-purified murine C3, as indicated, incubated with human FI and FH in a fluid phase cofactor activity assay, with densitometry analysis (Image Studio version 5.2) of intact α chain shown below; shown is the average of 3 experiments ± SEM with unpaired t test.

Discussion

This study demonstrates that transferring a disease-associated single-nucleotide substitution in *C3*, present in a family within the NRCTC aHUS cohort, to murine *C3* faithfully recapitulated the salient features of the human disease. Indeed, it could be argued that the resultant mouse model of aHUS, with respect to disease pathology, represents a more faithful animal model of aHUS-like disease than those generated to date (24, 36, 37), and this makes it particularly relevant for the testing of new anti-complement therapies. The data presented herein support the prevailing view that aHUS arises primarily due to deficient protection of host cellular and extracellular matrix surfaces from complement activation. This aHUS mouse model, based on a C3 gain-of-function amino acid substitution, offers opportunities to further dissect the precise role of complement and other factors that drive aHUS in

humans. The relative health of the heterozygous mice (C3KI/WT) despite markedly increased complement turnover also offers the potential to investigate how C3 activity shapes the progression of other complex genetic disorders, such as rheumatic and neurological conditions, including AMD. In short, the development of this precision, rapid, and spontaneous model of complement dysregulation, in conjunction with subsequent strategic backcrosses, has the potential to provide platforms to carry out preclinical testing of drugs (anti-complement in particular) for the treatment of patients with a wide variety of complement-mediated diseases.

FHΔSCR16–20–transgenic mice (24) established that deletion of the FH C-terminus and its self-surface-binding capabilities, combined with uncompromised FH N-terminus–mediated control of C3 depletion in fluid phase, allows development of an aHUS-like disease. This study was fully consistent with the discovery that most
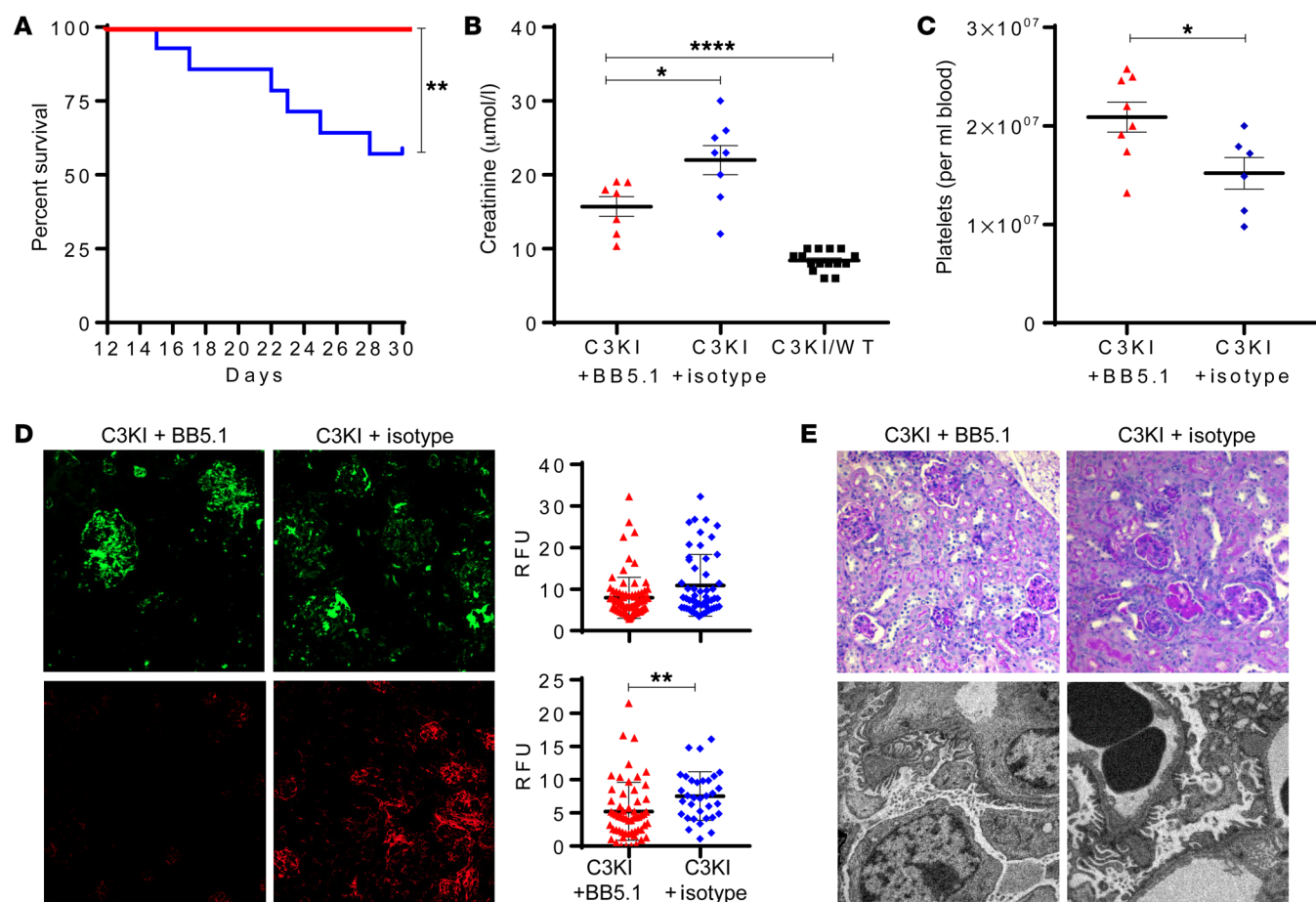
Figure 7. Treatment of the C3KI mice. (A) Kaplan-Meier survival curve analysis showing 100% survival in C3KI animals treated with BB5.1 ($n = 8$), in comparison to isotype control–treated animals ($n = 11$). **(B)** Where available, plasma creatinine values were analyzed. Shown are results for 7 C3KI mice treated with BB5.1 (C3KI + BB5.1, red triangles), 8 C3KI mice treated with isotype control antibody (C3KI + isotype, blue diamonds), and 15 untreated C3KI/WT mice (black squares). **(C)** Platelet counts of 8 C3KI mice treated with BB5.1 and 6 C3KI mice treated with isotype control antibody. Absolute numbers were provided by use of cell count beads and flow cytometry. **(D)** Frozen kidney sections were collected from C3KI mice treated with BB5.1 or isotype control antibody and stained for glomerular C3 (anti-C3, upper panels, original magnification, ×20) and C9 deposition (anti-C9, lower panels, original magnification, ×10). Images are representative of 5 images per animal analyzed. **(E)** Top panels: PAS-stained sections from C3KI mice treated with BB5.1 and IgG control. Histology demonstrates features of a TMA. Original magnification, ×20. Representative of 8 BB5.1-treated animals and 6 IgG control-treated animals. Bottom panels: Electron microscopy images of BB5.1-treated animals and IgG control showing foot process effacement and subtle areas of subendothelial lucency. Original magnification, ×5000 (BB5.1), ×6000 (IgG). Representative of 2 C3KI BB5.1-treated and 2 C3KI IgG control–treated mice. *$P < 0.05$, **$P < 0.005$, ****$P < 0.0001$ using unpaired t test with Welch's correction.

(although not all) disease-associated mutations in human FH cluster within SCRs 19–20, which are known to contain binding sites for C3d, the TED of C3b, and surface polyanions and to be crucial for distinguishing between self- and non-self-surfaces (46). Such a truncation of FH has, however, not been identified in humans.

In contrast, the present model derives from a single mutation in a murine gene that maps directly to the equivalent disease-linked mutation in humans (26). Our starting point was the discovery that mutations in human *C3* associated with aHUS encode amino acid substitutions that, in C3b, occur throughout the binding regions for FH, although there is a bias toward the region that binds to FH SCRs 19–20 (double the number found in the rest of C3), i.e., the TED of C3b. This clustering of aHUS-linked mutations in C3 is not as prominent as it is in FH, in which there is a "hot spot" of aHUS-linked mutations within SCRs 19–20 (4 times the number found in the rest of FH) (21, 29, 47). There is

accumulating evidence that mutations that affect the functional properties of C3/C3b are associated not just with aHUS but also with membranoproliferative glomerulonephritis (MPGN)/C3G (39, 48–50), and defining that link remains of keen interest.

While we initially surveyed in vitro the functions of multiple candidate mutations in recombinant human C3, we were drawn to D1115N, since it maps to the binding interface between the TED of C3b and SCRs 19–20 of FH (38) but also results in complete loss of MCP binding when MCP is coated on a solid surface such as a sensor chip or ELISA well (26, 29). Our own analysis with recombinant human proteins, in which WT or variant C3(H$_2$O) was attached to a CM5 Biacore chip and FH or MCP used as analyte, confirmed these findings (Supplemental Figure 1). Reduced FH binding was also observed in both the human and mouse proteins (Figure 6 and Supplemental Figures 1, 4, and 5). The clear affinity reductions observed in SPR studies of both recombinant
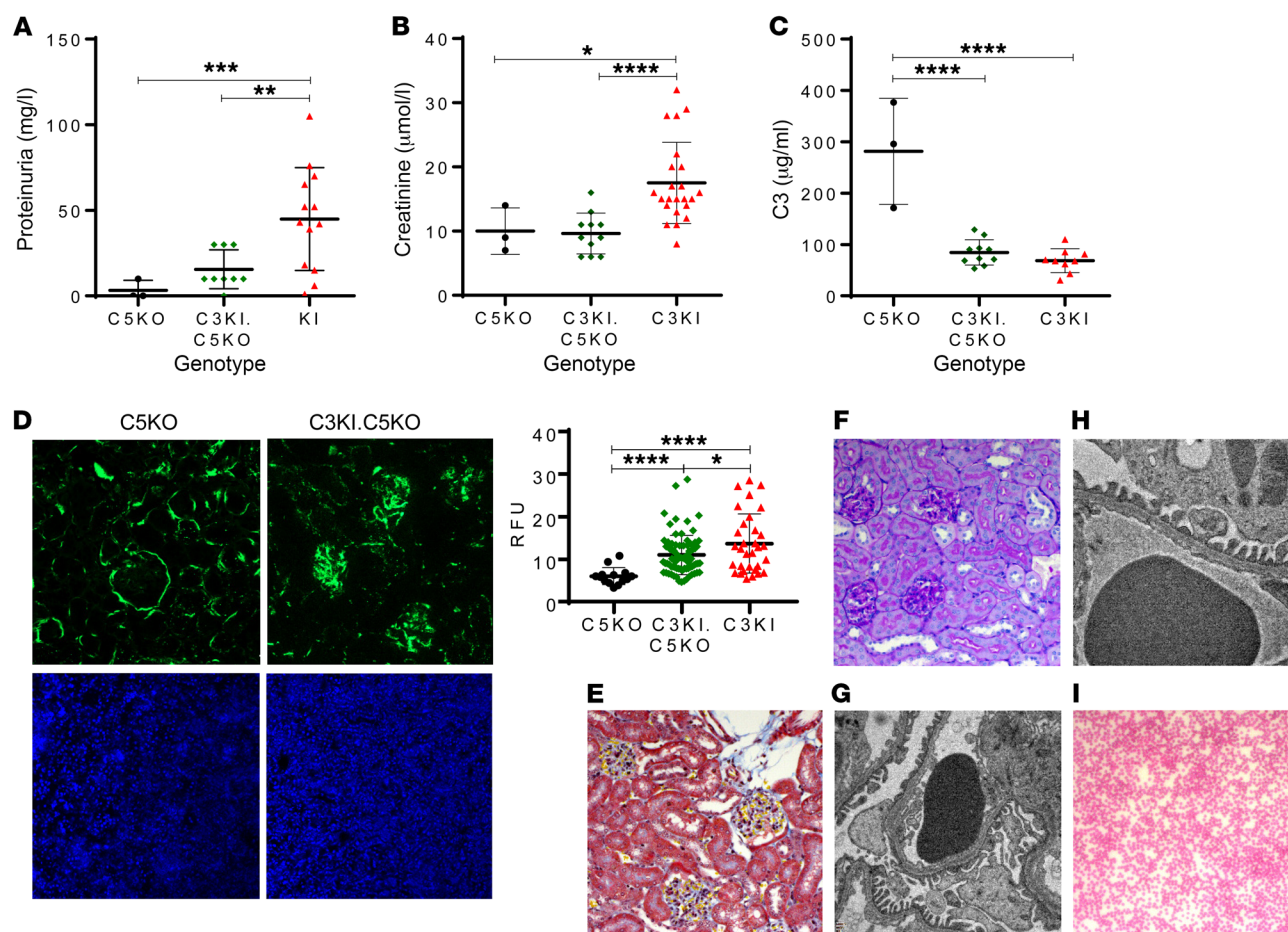
Figure 8. C3KI phenotype is rescued through genetic deletion of complement C5. (**A**) Proteinuria measurements of urine collected from 3 C5KO mice premortem (black circles) and, 9 C3KI.C5KO mice at 6 months of age (green diamonds) as well as, 12 C3KI mice on P21–P28 (red triangles). (**B**) Creatinine values obtained from 3 C5KO mice, 10 C3KI.C5KO mice at 6 months old, and 19 C3KI mice. (**C**) Plasma C3 levels. (**D**) Immunofluorescence of glomerular C3 deposition (upper panels; original magnification, ×20), with densitometry analysis of C3 deposition to the right, and with anti-C9 antibody (lower panels; original magnification, ×10). (**E**) MSB stain of C3KI.C5KO 6-month-old mice; original magnification, ×20 (representative of $n = 8$ examined). (**F**) PAS-stained sections of C3KI.C5KO 6-month-old mice showing normal glomeruli; original magnification, ×20 (representative of $n = 8$ examined). (**G**) Electron microscopy of a 6-month-old C3KI.C5KO mouse showing normal glomerular basement membrane and no evidence of dense deposits; original magnification, ×6000 (representative of $n = 4$ examined). (**H**) Electron microscopy of a 6-month-old WT mouse showing normal glomerular basement membranes; original magnification, ×10,000 (representative of $n = 4$ examined). (**I**) Diff-Quik–stained blood film of a C3KI.C5KO 6-month-old mouse showing no evidence of fragmented red blood cells; original magnification, ×10 (representative of $n = 8$ examined). *$P < 0.05$, **$P < 0.01$, ***$P < 0.001$, ****$P < 0.0001$. Unpaired t test (**C**) with Welch's correction (**A**, **B**, and **D**).

and ex vivo purified C3b Asn1115 are consistent with loss of an important C-terminal binding interaction but retention of the other FH (i.e., SCRs 1–5)-binding sites. Indeed, the affinity of full-length mouse FH binding to rmC3b Asn1115 was almost identical to that for recombinant mFH SCRs 1–5 alone (or mouse Crry), and the loss of binding for human FH SCRs 19–20 appears to confirm the mechanism (Figure 6), consistent with the studies by Morgan et al. (38). These data suggest that the D1115N substitution of murine C3b primarily perturbs interactions with the C-terminus of FH and hence the ability of C3b Asn1115 to be regulated by FH and FI. This is somewhat surprising, based on the deficit in MCP binding noted with this change (Supplemental Figure 1) (26, 29). However, it is clear that the mutation has only subtle effects, if any, on the interaction of mouse C3b with Crry or the N-terminus of FH. This likely reflects differences in the contact residues/ structures of mouse C3 in the context of Crry compared with

human C3 in the context of MCP, but it may give important information regarding the pathogenic burden of the loss of interaction with MCP versus FH. Clinically, MCP mutations rarely progress to end-stage renal disease (ESRD); this is in contrast to the poor renal prognosis associated with FH and C3 mutations (4, 15, 16). A failure of FH to engage fully with the TED is expected to be particularly detrimental to protection of host cell surfaces from excess complement activation. We also found evidence that C3b Asn1115 is marginally more resistant than WT C3b to fluid-phase FH- and FI-mediated cleavage (Figure 6E and Supplemental Figure 4). This, in concert with the MCP deficiency, apparently resulted in lower FB levels in one of the patients; in the mice, there was also evidence of increased FB consumption despite normal interaction with Crry (Figure 1 and Supplemental Figure 7C). Interestingly, we also detected an increase in FH levels in the plasma of C3KI mice. This suggests a compensatory upregulation

of *CFH* expression in an attempt to regulate the mutant C3b or that *CFH* expression can be modulated by the C3-driven inflammatory response. This observation is consistent with the mouse FH W1206R model of TMA, in which elevated FH levels were also observed (37). Notably, both NRCTC patients with the C3 Asn1115 mutation possessed plasma levels of FH above the normal range on the majority of readings, reaffirming the parallels of our model to human disease.

It is clear from previous work with transgenic mice that a more substantial plasma C3 depletion than that seen in the C3KI mice may lead to the alternative phenotype of MPGN/C3G (36, 41, 47). Moreover, normal fluid-phase regulation is preserved in all of the mouse models of aHUS reported to date (24, 37, 51). The phenotype we obtained is that of aHUS, as evidenced by the histological features of a renal TMA rather than C3G. We therefore infer that any enhanced resistance to fluid-phase cleavage by FI of C3b Asn1115 is not a major contributor to the disease-like symptoms observed in our model. Lower plasma C3 levels are seen in many aHUS humans with C3 mutations (26, 29). The lower C3 levels in our murine model are fully consistent with previously published mouse models of a TMA (24, 37).

Thus, we can conclude that in the C3KI mouse, once C3b Asn1115 is deposited on a surface, a positive feedback process can operate that is neither controllable by FH nor restricted by a shortage of C3. This leads to extensive C3b deposition and activation of the terminal pathway, as evidenced from our observation of C5 consumption coupled with glomerular C9 deposition (Figure 5, B and C). Thus, our data emphasize the delicate balance of complement regulation; disease develops when the balance is disturbed and the threshold of regulatory ability is breached. Our C3KI animals retain the C3 "resources" to overwhelm complement regulation at the cell surface despite plasma C3 levels being lower than those in their WT counterparts.

Our model of C3 convertase dysregulation has parallels with that in a study by the Song group, in which the aHUS-linked single amino acid substitution W1206R was transferred from human FH into murine FH (37). Homozygous FH W1206R mice developed a renal phenotype consistent with aHUS, but a subtantial proportion of animals also demonstrated an aggressive TMA, with notable thrombus found in multiple organs. Analysis of key organs in C3KI animals revealed no evidence of large thrombi or microthrombi, although we did not perform an exhaustive search. Across our study, 3 homozygous mice (of ~45 analyzed) showed symptoms consistent with stroke, but this was always in the clinical context of severe kidney failure and likely driven by hypertension. Thus, in these two models of aHUS, the mechanisms driving the fatal outcome likely differ substantially.

Given the successful use of C5 inhibition in aHUS patients (3, 35, 52–54) coupled with previous work showing that the disease is dependent on C5 (25), we sought to further validate our model through use of the murine C5 inhibitor BB5.1. As predicted, this rescued the phenotype, with 100% survival in C3KI mice at 30 days postpartum. While C3 fragment deposition in the kidney of BB5.1-treated mice appeared unchanged, there was a reduction in glomerular C9 deposition. This suggests that C5a and/or MAC are critical to the endothelial dysfunction and subsequent development of a TMA. Unfortunately, our analysis of kidney morphol-

ogy in the treated animals was not as unequivocal, as it showed that renal pathology remained. However, it is likely that more time is necessary to allow for full histological recovery. Therefore, we reasoned that extending our treatment study (mirroring clinical management) would lead to histological improvement, given the dramatic clinical improvement observed in the treatment cohort; thus, a pragmatic extension to this work was then to analyze the long-term effects of C5 blockade using the C5-knockout animals.

Eculizumab has revolutionized the treatment of patients with aHUS; however, we do not yet know nor will we know for some time what the long-term effects of this drug will be in our patient population. While inhibition at the level of C5 arrests disease, it does not target the effect of a persisting dysregulated alternative pathway and subsequent upregulation of C3. This is a vital question to answer, as it translates to all complement mutations associated with aHUS and could directly affect longevity of treatment. It has been hypothesized that over time patients on C5-inhibiting therapy may revert to a C3G due to sustained C3 activation. Our 6-month mouse cohort provides us with what we believe to be the clearest evidence to date that long-term C5 inhibition is unlikely to result in an alternative complement-mediated renal disease, despite the presence of deposited C3 within the glomeruli. Six months of age in a mouse is the equivalent of 20 human years (55); thus, our data highlight that C5 blockade in patients for this time frame will be unlikely to lead to an alternative disease process.

Our results suggest that the present C3 gain-of-function mouse model of aHUS will allow evaluation of various complement-inhibiting therapies, for instance, targeting the ability of C5aR antagonists to reverse disease (56). This would allow the dissection of the independent roles of C5a and MAC in the pathogenesis of disease with a clarity not achievable by other currently available models. Furthermore, the C3 gain-of-function model offers the potential to assess therapies targeting the alternative pathway directly, such as homodimeric minimal FH (57), CR2-FH (58), and anti-properdin (59), in what we believe to be the most realistic model of complement genetic alterations to date. One major aim of our studies is to help test therapeutics that can mitigate the increased risk of infections posed by long-term use of eculizumab (34, 60–62).

We have shown that the C3KI mouse mirrors the aHUS clinical phenotype. A similar complement profile, i.e., low C3 levels and elevated FH levels in plasma, was seen in both patients and mice. Highly similar histological and biochemical phenotypes further underline the extent to which this model recapitulates the clinical phenotype in humans. Interestingly, in mice only homozygotes developed spontaneous disease early in life, while patients are heterozygous for C3 Asn1115. This is consistent with the notion that the genetic change predisposes to the human disease, but an environmental trigger is needed for development of the disease (15, 20, 63). We tracked our C3KI/WT mice for 12 months, and to date there is no evidence that the animals developed disease, consistent with the environmental trigger hypothesis. While the absence of disease in the heterozygotes could be seen as a limitation of this study, we would argue that they represent a model to identify the factors beyond uncontrolled complement activation that drive aHUS, i.e., the C3KI/WT mice can be used to investigate a range of potential environmental and dietary triggers that can precipitate aHUS. Col-

lectively, our spontaneous and likely inducible model will enable testing of a variety of complement-inhibiting therapies, and importantly, testing of withdrawal of therapy and remission monitoring. This has the potential to culminate in a wealth of translational data that will directly inform future clinical trials and targeted therapies, with the overall aim of outcome of improving outcome in patients with complement-mediated diseases.

In summary, our mouse model of aHUS, engineered by using a single point mutation in C3, recapitulates the clinical phenotype found in humans. This C3 mutation results in systemic complement activation and endothelial dysfunction, culminating in a renal TMA. Our model provides the opportunity to investigate the roles played by various players downstream of C3 activation and is a test bed for future complement therapeutics. Developing a therapy to restore complement homeostasis would, in addition, be transferable to several other endothelial damage–mediated diseases for which therapy remains an unmet clinical need.

Methods

Mice

B6.C3$^{Tm1(D1115N)Oz/NCL}$ (C3KI) mice were generated using standard knockin technology by Ozgene (see Supplemental Figure 5) and backcrossed onto constitutive Cre recombinase–expressing mice (B6^{OZCre}; Ozgene) or constitutive FLPe recombinase–transgene mice (B6^{OzFlpe}; Ozgene). These F$_1$ C3KI/CRE mice were shipped to Newcastle and intercrossed to provide homozygous C3KI mice. Genotyping of C3KI mice was performed by PCR on digested ear notch tissue using the following strategy devised by Ozgene. Primer pairs 5′-CCTTCTCTTTCTGGAATTTGCCTG-3′ and 5′-CTTTGGTGACCCTGTCTGTTCC-3′ were used in 30 cycles of PCR (58°C annealing temperature), generating a 574-bp product in the case of native C3 and a 633-bp product for the knocked-in sequence. The 633-bp product was digested into fragments of 402 bp and 231 bp by incubating with restriction enzyme SpeI. Using a 2% agarose gel, amplicons were separated sufficiently to allow identification of WT or the C3KI gene carriers. The presence of the Cre recombinase gene was detected through use of the following PCR primers: 5′-ATTTACGGCGCTAAGGATGACTC-3′ and 5′-TTACACCTGTTCAATTCCCCTG-3′, which generated a 680-bp amplicon in 30 cycles of PCR (58°C annealing temperature) (designed at Ozgene). FH-knockout mice (FH-KO, ref. 41) were generated by our research team. C3KI mice were backcrossed onto the previously described C5-deficient mice (C5KO; via Matthew Pickering) (25). In brief, C3KI/WT were crossed with C5KO mice. Pups were then all C5KO/WT, and those that were also C3KI/WT were crossed with C5KO mice. Pups from this cross were screened by PCR using DBA primers: 5′-CACGATAATGGGAGTCATCTG-CG-3′ and 5′-AAGTTGGAGTGTGGTCTTTGGGCC-3′, followed by a HindIII digest to distinguish between WT, +/–, and –/– genotypes. Pups that were C3KI/WT.C5KO were then crossed to produce C3KI.C5KO mice.

Protein purification

Murine C3 from plasma. Mouse C3 for biochemical analysis was purified from mouse plasma according to the method of Van den Berg et al. (64). Briefly, 10 ml mouse serum was precipitated using polyethylene glycol (PEG) followed by application onto a Mono Q anion-exchange column (GE, HR5/5) and gel filtration chromatography using a HiLoad 16/600 Superdex 200 pg column. WT and mutant mouse C3 protein (C3 Asn1115) concentrations were calculated by measuring absorbance at 280 nm using an extinction coefficient of 183,033 and a molecular weight of 186.48 kDa as determined from the mature WT amino acid sequence (see Supplemental Figure 2A) using the ExPASy ProtParam tool. Reducing and nonreducing SDS-PAGE gels were used to provide evidence of homogeneity.

Mouse FH. Murine FH was purified from 20 ml mouse serum using a previously generated mAb (2A5, anti-mouse FH, a gift from Claire Harris, Newcastle University) affinity chromatography resin using an ÄKTA Start (GE), followed by gel filtration chromatography on HiLoad 16/600 Superdex 200 pg column.

SDS-PAGE and Western blotting

Gels with the appropriate percentage of acrylamide were freshly prepared for each SDS-PAGE run. Samples containing recombinant or plasma-derived C3 were run under both nonreducing and reducing conditions. Protein bands were either stained using Coomassie blue or were transferred to nitrocellulose. The nitrocellulose was blocked in 5% w/v nonfat milk in PBS overnight at 4°C, then exposed to a polyclonal goat anti–mouse C3 antibody–HRP (1:10,000; catalog 55557, lot 06803, MP Biomedicals). After extensive washing in 0.01% v/v Tween in PBS, the nitrocellulose was then developed using Bio-Rad Clarity Western ECL substrate, followed by detection/analysis on the Odyssey FC imaging system (LI-COR).

Fluid-phase cofactor activity assays

See Supplemental Methods.

SPR

All experiments were conducted on a BIAcore S200. Each version of murine C3 was converted to C3b, via incubation with purified human FB and FD (at molar concentrations 50 and 1000 times less, respectively, than that of C3) at 37°C in PBS supplemented with 1 mM MgCl$_2$ for 1 hour. The incubated samples were gel filtrated using a Superdex 200 10/300 GL column; C3b-containing fractions were pooled and concentrated. Each version of murine C3b (i.e., WT C3b and C3b Asn1115) was immobilized (930 ± 10 RU) on separate flow cells of a CM5 chip using standard amine coupling. A 2-fold dilution series of purified murine FH (10 to 0 μM), recombinant murine FH SCRs 1–5 (14.6 to 0 μM), recombinant human FH SCRs 19–20 (20 to 0 μM), or recombinant murine Crry SCRs 1–5 (10 to 0 μM) was made in HBST buffer (10 mM HEPES, 150 mM NaCl, and 0.005% Tween-20, pH 7.4) and flowed across either chip surface in the same buffer. All analytes were injected in duplicate (30 μl/minutes for 200 seconds), followed by running buffer for 300 seconds and a regeneration phase involving injection of regeneration buffer (10 mM sodium acetate, 1 M NaCl, pH 4.5) for 60 seconds. The equilibrium dissociation constant, K_D, and standard error were calculated using the steady-state model in BIAcore S200 Evaluation Software.

ELISA

Murine C3. To determine mouse C3 levels, mAb 11H9 (recognizing both intact C3 and its cleaved products C3b, iC3b, C3d, and C3dg; catalog HM1045, Hycult Biotech via Cambridge Bioscience) was

coated on each well of a Nunc MaxiSorp flat-bottom ELISA plate (20 ng/well) to capture mouse C3. Then 50 μl of a 1:800-diluted sample was applied for analysis. Bound C3 was detected through use of an HRP-conjugated goat polyclonal anti–mouse C3 antibody (1:25,000, catalog 55557, lot 06803, MP Biomedicals). This dilution biases the assay to detect bound intact C3. The ELISA was developed with TMB. The C3 concentrations were interpreted based on a standard curve generated using purified WT mouse C3 and interpolated using Graph-Pad Prism software.

FH. To measure FH present in mouse plasma, ELISA plates (Nunc) were coated with monoclonal anti-FH (2A5) at 1 μg/ml. After overnight incubation at 4°C, plates were blocked with 1% w/v BSA at room temperature for 1 hour. After washing, plates were incubated with diluted mouse plasma (1:1000) for 1 hour at room temperature. Plates were washed and then incubated with sheep anti–mouse FH (1:5000, Abcam Ab8842) for 1 hour at room temperature and then detected by adding donkey anti-sheep HRP-conjugated antibody (1:5000, 713-035-147, lot 125113, Jackson ImmunoResearch Laboratories Inc. via Stratech Scientific) for 1 hour at room temperature. A standard curve was compiled using the known concentration of purified mouse CFH.

C5. To measure C5 present in mouse plasma, ELISA plates were coated with 1 μg/ml BB5.1 (anti-C5, catalog HM1073, Hycult Biotech via Cambridge Biosciences). After overnight incubation at 4°C, plates were blocked with 1% w/v BSA at room temperature for 1 hour and then washed. Plates were then incubated with diluted mouse plasma (1:1000) for 1 hour, washed, and then incubated with goat anti–human C5 (1:1000, Quidel A306, 073139). Plates were then incubated with donkey anti-goat HRP-conjugated antibody (1:5000, 705-036-147, lot 124700 Jackson ImmunoResearch Laboratories Inc. via Stratech Scientific). After a final wash, the plate was developed with TMB. Samples were standardized to WT control.

Assessment of murine renal function and hematological parameters

Plasma creatinine was measured by collecting plasma by cardiac puncture into EDTA and subsequently measured on a Cobas 602 analyzer in the Newcastle Hospitals NHS laboratories. Plasma urea was measured using a urea assay kit (MAK006, Sigma-Aldrich). Mouse urine was collected and measured for hematuria and proteinuria using Hema-Combistix (Siemens/Bayer). Platelet analysis was performed by flow cytometry. Briefly, 10 μl EDTA-blood was mixed with 400 μl red cell lysis buffer (Sigma-Aldrich) and incubated for 10 minutes at room temperature. An aliquot of 5 μl was then transferred to 1 ml flow buffer (PBS containing 5% w/v BSA, 1 mM EDTA, 0.1% w/v Na azide) and washed at 1000 *g* for 5 minutes, 3 times, and resuspended in 200 μl flow buffer containing 1:400 CD41-FITC, 1:800 CD61-PE, and 1:800 CD62P- BV421 (catalog 553848, 553347, and 564289, respectively, BD Biosciences). Samples were incubated for an hour on ice in the dark before washing 3 times with 3 ml flow buffer (1000 *g* for 5 minutes). Finally, samples were resuspended in 250 μl of 1% w/v paraformaldehyde/flow buffer with 25 μl Count-Bright beads (i.e., 2.5×10^4 beads per tube; Invitrogen). Data were collected using a FACSCanto flow cytometer and analyzed on FCS Express, version 6 (De Novo Software). Alternatively, platelets were analyzed by using an improved Neubauer hemocytometer through addition of 25 μl of the red cell lysed solution (as above) and allowing the sample to settle for 10 minutes before counting as per the manufacturer's instructions.

Histological analysis

Light microscopy. Kidneys were harvested and fixed in 10% buffered formalin solution. Following fixation, the tissues were embedded in paraffin, then cut in 3-μm sections. Sections were stained with PAS reagent, then examined by light microscopy. Newcastle Hospitals NHS pathology laboratories stained for fibrin using a standard MSB stain protocol. Sections were blinded to avoid interpreter bias.

Immunofluorescence. Mouse kidneys were snap-frozen in isopentane (pre-cooled in liquid nitrogen) and stored at –80°C in individual containers. Five-micrometer cyrosections from mouse kidneys were mounted on a Shandon ColorFrost Plus microscope slide (Thermo Fisher Scientific), before fixing in acetone and stored in –80°C. The thawed tissue sections were blocked for an hour with 60 μl of 20% (v/v) goat serum in PBS, then detected with 60 μl FITC-conjugated goat polyclonal anti–mouse C3 antibody (catalog 0855500, MP Biomedicals, 1:100). After repeated washing with PBS, the tissue sections were stained with DAPI (catalog H-1200, Vector Laboratories) and covered with glass coverslips. Fluorescence images were taken at ×10 or ×20 magnification utilizing a Zeiss Axio Imager II.

For C9 immunofluorescence, sections were blocked with rabbit and goat serum, followed by rat anti–mouse CD16/CD32 Fc block (catalog 553141, BD Pharmingen 1:100) in 2% w/v BSA in PBS for 1 hour at room temperature. After washing, sections were incubated with rabbit anti–rat C9 (1:75, a gift from B.P. Morgan, Cardiff University, Cardiff, United Kingdom) overnight at 4°C. The next day, sections were washed, then incubated with goat anti-rabbit Alexa Fluor 594 (1:100, catalog A-11012, Abcam). Finally, the sections were washed, mounted in DAPI, and imaged as above. Immunofluorescence images were analyzed in ImageJ (NIH) and expressed as relative fluorescence units (RFU).

Electron microscopy. Small pieces of cortical tissue (1 mm³) were fixed in 2% w/v glutaraldehyde in 0.1 M cacodylate buffer, post-fixed in osmium tetroxide, dehydrated in a graded series of acetone, and embedded in Taab epoxy resin. Ultrathin sections (70 nm) were picked up on copper grids, stained with uranyl acetate and lead citrate, and examined using a Philips CM100 transmission electron microscope (EM Research Services, Newcastle University).

Availability of data and materials. The C3KI conditional/constitutive mouse and recombinant mouse C3 plasmid/protein are available through a material transfer agreement (MTA) with Newcastle University.

Statistics

Data were analyzed using GraphPad Prism 7.00 for Windows (GraphPad Software). Densitometry was carried out using Image studio version 5.2 (LI-COR). Groups were compared at each time point using 1- or 2-way ANOVA with Bonferroni's multiple-comparisons test as indicated. A *P* value less than 0.05 was considered significant; *$P < 0.05$, **$P < 0.01$, ***$P < 0.0005$. Student's *t* test was 2-tailed, and data are shown as mean ± SEM.

Study approval

All animal experiments were approved by the ethics committee of the Comparative Biology Centre of Newcastle University and performed under the United Kingdom's Home Office granted license PD86B3678. The clinical study involving subjects from the NRCTC was approved by the Northern and Yorkshire Multi-Centre Research Ethics Committee, and informed consent obtained in accordance with the Declaration of Helsinki.

Address correspondence to: Kevin Marchbank, Institute of Cellular Medicine, Newcastle University, 3rd Floor William Leech Building, The Medical School, Framlington Place, Newcastle upon Tyne, NE2 4HH, United Kingdom. Phone: 0191.2085598; Email: Kevin.Marchbank@Newcastle.ac.uk.

1. Ricklin D, Lambris JD. Complement in immune and inflammatory disorders: therapeutic interventions. *J Immunol*. 2013;190(8):3839–3847.

2. Warwicker P, et al. Genetic studies into inherited and sporadic hemolytic uremic syndrome. *Kidney Int*. 1998;53(4):836–844.

3. Licht C, et al. Efficacy and safety of eculizumab in atypical hemolytic uremic syndrome from 2-year extensions of phase 2 studies. *Kidney Int*. 2015;87(5):1061–1073.

4. Nester CM, et al. Atypical aHUS: state of the art. *Mol Immunol*. 2015;67(1):31–42.

5. Ricklin D, Mastellos DC, Reis ES, Lambris JD. The renaissance of complement therapeutics. *Nat Rev Nephrol*. 2018;14(1):26–47.

6. Yehoshua Z, et al. Systemic complement inhibition with eculizumab for geographic atrophy in age-related macular degeneration: the COMPLETE study. *Ophthalmology*. 2014;121(3):693–701.

7. Trouw LA, Pickering MC, Blom AM. The complement system as a potential therapeutic target in rheumatic disease. *Nat Rev Rheumatol*. 2017;13(9):538–547.

8. Wong EKS, Kavanagh D. Diseases of complement dysregulation-an overview. *Semin Immunopathol*. 2018;40(1):49–64.

9. Walport MJ. Complement. First of two parts. *N Engl J Med*. 2001;344(14):1058–1066.

10. Sarma JV, Ward PA. The complement system. *Cell Tissue Res*. 2011;343(1):227–235.

11. Thurman JM, et al. Detection of complement activation using monoclonal antibodies against C3d. *J Clin Invest*. 2013;123(5):2218–2230.

12. Noris M, Remuzzi G. Overview of complement activation and regulation. *Semin Nephrol*. 2013;33(6):479–492.

13. Liszewski MK, Farries TC, Lublin DM, Rooney IA, Atkinson JP. Control of the complement system. *Adv Immunol*. 1996;61:201–283.

14. Liszewski MK, Java A, Schramm EC, Atkinson JP. Complement dysregulation and disease: insights from contemporary genetics. *Annu Rev Pathol*. 2017;12:25–52.

15. Kavanagh D, Goodship TH, Richards A. Atypical hemolytic uremic syndrome. *Semin Nephrol*. 2013;33(6):508–530.

16. Atkinson JP, Liszewski MK, Richards A, Kavanagh D, Moulton EA. Hemolytic uremic syndrome: an example of insufficient complement regulation on self-tissue. *Ann N Y Acad Sci*. 2005;1056:144–152.

17. Fang CJ, Richards A, Liszewski MK, Kavanagh D, Atkinson JP. Advances in understanding of pathogenesis of aHUS and HELLP. *Br J Haematol*. 2008;143(3):336–348.

18. Noris M, Remuzzi G. Atypical hemolytic-uremic syndrome. *N Engl J Med*. 2009;361(17):1676–1687.

19. Goicoechea de Jorge E, Pickering MC. Atypical hemolytic uremic syndrome: telling the difference between H and Y. *Kidney Int*. 2010;78(8):721–723.

20. Rodríguez de Córdoba S, Hidalgo MS, Pinto S, Tortajada A. Genetics of atypical hemolytic uremic syndrome (aHUS). *Semin Thromb Hemost*. 2014;40(4):422–430.

21. Richards A, et al. Factor H mutations in hemolytic uremic syndrome cluster in exons 18-20, a domain important for host cell recognition. *Am J Hum Genet*. 2001;68(2):485–490.

22. Pérez-Caballero D, et al. Clustering of missense mutations in the C-terminal region of factor H in atypical hemolytic uremic syndrome. *Am J Hum Genet*. 2001;68(2):478–484.

23. Sánchez-Corral P, et al. Structural and functional characterization of factor H mutations associated with atypical hemolytic uremic syndrome. *Am J Hum Genet*. 2002;71(6):1285–1295.

24. Pickering MC, et al. Spontaneous hemolytic uremic syndrome triggered by complement factor H lacking surface recognition domains. *J Exp Med*. 2007;204(6):1249–1256.

25. de Jorge EG, et al. The development of atypical hemolytic uremic syndrome depends on complement C5. *J Am Soc Nephrol*. 2011;22(1):137–145.

26. Frémeaux-Bacchi V, et al. Mutations in complement C3 predispose to development of atypical hemolytic uremic syndrome. *Blood*. 2008;112(13):4948–4952.

27. Lhotta K, et al. A large family with a gain-of-function mutation of complement C3 predisposing to atypical hemolytic uremic syndrome, microhematuria, hypertension and chronic renal failure. *Clin J Am Soc Nephrol*. 2009;4(8):1356–1362.

28. Iqbal Z, Wood K, Carter V, Goodship TH, Brown AL, Sheerin NS. Thrombotic microangiopathy as a cause of chronic kidney transplant dysfunction: case report demonstrating successful treatment with eculizumab. *Transplant Proc*. 2015;47(7):2258–2261.

29. Schramm EC, et al. Mapping interactions between complement C3 and regulators using mutations in atypical hemolytic uremic syndrome. *Blood*. 2015;125(15):2359–2369.

30. Fremeaux-Bacchi V. Treatment of atypical uraemic syndrome in the era of eculizumab. *Clin Kidney J*. 2012;5(1):4–6.

31. Hayes W, Tschumi S, Ling SC, Feber J, Kirschfink M, Licht C. Eculizumab hepatotoxicity in pediatric aHUS. *Pediatr Nephrol*. 2015;30(5):775–781.

32. Manenti L, et al. Atypical haemolytic uraemic syndrome with underlying glomerulopathies. A case series and a review of the literature. *Nephrol Dial Transplant*. 2013;28(9):2246–2259.

33. Boyer O, et al. Complement factor H deficiency and posttransplantation glomerulonephritis with isolated C3 deposits. *Am J Kidney Dis*. 2008;51(4):671–677.

34. McNamara LA, Topaz N, Wang X, Hariri S, Fox L, MacNeil JR. High risk for invasive meningococcal disease among patients receiving eculizumab (soliris) despite receipt of meningococcal vaccine. *Am J Transplant*. 2017;17(9):2481–2484.

35. Brocklebank V, Kavanagh D. Complement C5-inhibiting therapy for the thrombotic microangiopathies: accumulating evidence, but not a panacea. *Clin Kidney J*. 2017;10(5):600–624.

36. Vernon KA, Ruseva MM, Cook HT, Botto M, Malik TH, Pickering MC. Partial complement factor H deficiency associates with C3 glomeru-

lopathy and thrombotic microangiopathy. *J Am Soc Nephrol*. 2016;27(5):1334–1342.

37. Ueda Y, et al. Murine systemic thrombophilia and hemolytic uremic syndrome from a factor H point mutation. *Blood*. 2017;129(9):1184–1196.

38. Morgan HP, et al. Structural basis for engagement by complement factor H of C3b on a self surface. *Nat Struct Mol Biol*. 2011;18(4):463–470.

39. Martínez-Barricarte R, et al. Human C3 mutation reveals a mechanism of dense deposit disease pathogenesis and provides insights into complement activation and regulation. *J Clin Invest*. 2010;120(10):3702–3712.

40. Xu C, Mao D, Holers VM, Palanca B, Cheng AM, Molina H. A critical role for murine complement regulator crry in fetomaternal tolerance. *Science*. 2000;287(5452):498–501.

41. Pickering MC, et al. Uncontrolled C3 activation causes membranoproliferative glomerulonephritis in mice deficient in complement factor H. *Nat Genet*. 2002;31(4):424–428.

42. Nichols EM, et al. An extended mini-complement factor H molecule ameliorates experimental C3 glomerulopathy. *Kidney Int*. 2015;88(6):1314–1322.

43. Ferreira VP, et al. The binding of factor H to a complex of physiological polyanions and C3b on cells is impaired in atypical hemolytic uremic syndrome. *J Immunol*. 2009;182(11):7009–7018.

44. Walsh MC, et al. Mannose-binding lectin is a regulator of inflammation that accompanies myocardial ischemia and reperfusion injury. *J Immunol*. 2005;175(1):541–546.

45. Busche MN, Stahl GL. Role of the complement components C5 and C3a in a mouse model of myocardial ischemia and reperfusion injury. *Ger Med Sci*. 2010;8:Doc20.

46. Pechtl IC, Kavanagh D, McIntosh N, Harris CL, Barlow PN. Disease-associated N-terminal complement factor H mutations perturb cofactor and decay-accelerating activities. *J Biol Chem*. 2011;286(13):11082–11090.

47. Lesher AM, et al. Combination of factor H mutation and properdin deficiency causes severe C3 glomerulonephritis. *J Am Soc Nephrol*. 2013;24(1):53–65.

48. Chauvet S, et al. A familial C3GN secondary to defective c3 regulation by complement receptor 1 and complement factor H. *J Am Soc Nephrol*. 2016;27(6):1665–1677.

49. Bu F, et al. High-throughput genetic testing for thrombotic microangiopathies and C3 glomerulopathies. *J Am Soc Nephrol*. 2016;27(4):1245–1253.

50. Iatropoulos P, et al. Complement gene variants determine the risk of immunoglobulin-associated MPGN and C3 glomerulopathy and predict long-term renal outcome. *Mol Immunol*. 2016;71:131–142.

51. Ueda Y, Gullipalli D, Song WC. Modeling complement-driven diseases in transgenic mice: values and limitations. *Immunobiology*. 2016;221(10):1080–1090.

52. Legendre CM, et al. Terminal complement inhibitor eculizumab in atypical hemolytic-uremic syndrome. *N Engl J Med*. 2013;368(23):2169–2181.

53. Fakhouri F, et al. Terminal complement inhibitor eculizumab in adult patients with atypical hemolytic uremic syndrome: a single-arm, open-label trial. *Am J Kidney Dis*. 2016;68(1):84–93.

54. Greenbaum LA, et al. Eculizumab is a safe and effective treatment in pediatric patients with atypical hemolytic uremic syndrome. *Kidney Int*. 2016;89(3):701–711.

55. Dutta S, Sengupta P. Men and mice: relating their ages. *Life Sci*. 2016;152:244–248.

56. Xiao H, et al. C5a receptor (CD88) blockade protects against MPO-ANCA GN. *J Am Soc Nephrol*. 2014;25(2):225–231.

57. Yang Y, et al. An Engineered complement factor H construct for treatment of C3 glomerulopathy. *J Am Soc Nephrol*. 2018;29(6):1649–1661.

58. Ruseva MM, et al. Efficacy of targeted complement inhibition in experimental C3 glomerulopathy. *J Am Soc Nephrol*. 2016;27(2):405–416.

59. Bertram P, Akk AM, Zhou HF, Mitchell LM, Pham CT, Hourcade DE. Anti-mouse properdin TSR 5/6 monoclonal antibodies block complement alternative pathway-dependent pathogenesis. *Monoclon Antib Immunodiagn Immunother*. 2015;34(1):1–6.

60. Cullinan N, Gorman KM, Riordan M, Waldron M, Goodship TH, Awan A. Case report: benefits and challenges of long-term eculizumab in atypical hemolytic uremic syndrome. *Pediatrics*. 2015;135(6):e1506–e1509.

61. Vellanki VS, Bargman JM. Aspergillus Niger peritonitis in a peritoneal dialysis patient treated with eculizumab. *Ren Fail*. 2014;36(4):631–633.

62. Benamu E, Montoya JG. Infections associated with the use of eculizumab: recommendations for prevention and prophylaxis. *Curr Opin Infect Dis*. 2016;29(4):319–329.

63. Goodship TH, et al. Atypical hemolytic uremic syndrome and C3 glomerulopathy: conclusions from a "Kidney Disease: Improving Global Outcomes" (KDIGO) Controversies Conference. *Kidney Int*. 2017;91(3):539–551.

64. Van den Berg CW, Van Dijk H, Capel PJ. Rapid isolation and characterization of native mouse complement components C3 and C5. *J Immunol Methods*. 1989;122(1):73–78.

Plasminogen activator-coated nanobubbles targeting cell-bound β2-glycoprotein I as a novel thrombus-specific thrombolytic strategy

Paolo Macor,[1] Paolo Durigutto,[2] Monica Argenziano,[3] Kate Smith-Jackson,[4] Sara Capolla,[5] Valeria Di Leonardo,[1] Kevin Marchbank,[4] Valerio Stefano Tolva,[6] Fabrizio Semeraro,[7] Concetta T. Ammollo,[7] Mario Colucci,[7] Roberta Cavalli,[3] Pierluigi Meroni[2] and Francesco Tedesco[2]

[1]Department of Life Sciences, University of Trieste, Trieste, Italy; [2]Istituto Auxologico Italiano, IRCCS, Laboratory of Immuno-Rheumatology, Milan, Italy; [3]Department of Scienza e Tecnologia del Farmaco, University of Turin, Turin, Italy; [4]Translational and Clinical Research Institute, Faculty of Medical Sciences, Newcastle University, Newcastle, UK; [5]Experimental and Clinical Pharmacology Unit, C.R.O.-IRCCS, Aviano, Italy; [6]Struttura Complessa di Chirurgia Vascolare, ASST GOM Niguarda. Milano, Italy and [7]Dipartimento di Scienze Biomediche e Oncologia Umana, Università degli Studi di Bari Aldo Moro, Bari, Italy

Abstract

β2-glycoprotein I (β2-GPI) is a serum protein widely recognized as the main target of antibodies present in patients with antiphospholipid syndrome (APS). β2-GPI binds to activated endothelial cells, platelets and leukocytes, key players in thrombus formation. We developed a new targeted thrombolytic agent consisting of nanobubbles (NB) coated with recombinant tissue plasminogen activator (rtPA) and a recombinant antibody specific for cell-bound β2-GPI. The therapeutic efficacy of targeted NB was evaluated *in vitro*, using platelet-rich blood clots, and *in vivo* in three different animal models: i) thrombosis developed in a rat model of APS; ii) ferric chloride-induced mesenteric thrombosis in rats, and iii) thrombotic microangiopathy in a mouse model of atypical hemolytic uremic syndrome (C3-gain-of-function mice). Targeted NB bound preferentially to platelets and leukocytes within thrombi and to endothelial cells through β2-GPI expressed on activated cells. *In vitro*, rtPA-targeted NB (rtPA-tNB) induced greater lysis of platelet-rich blood clots than untargeted NB. In a rat model of APS, administration of rtPA-tNB caused rapid dissolution of thrombi and, unlike soluble rtPA that induced transient thrombolysis, prevented new thrombus formation. In a rat model of ferric chloride triggered thrombosis, rtPA-tNB, but not untargeted NB and free rtPA, induced rapid and persistent recanalization of occluded vessels. Finally, treatment of C3-gain-of-function mice with rtPA-tNB, that target β2-GPI deposited in kidney glomeruli, decreased fibrin deposition, and improved urinalysis data with a greater efficiency than untargeted NB. Our findings suggest that targeting cell-bound β2-GPI may represent an efficient and thrombus-specific thrombolytic strategy in both APS-related and APS-unrelated thrombotic conditions.

Introduction

Antiphospholipid syndrome (APS) is an autoimmune disease characterized by antibody-mediated vascular thrombosis and adverse pregnancy outcomes including fetal loss, pre-eclampsia, preterm delivery, and intrauterine growth restriction.[1,2] Vascular thrombosis is a serious and often recurrent medical condition that affects relatively young individuals with important social and clinical implications.[3,4] Vessel occlusion by blood clots is the most common clinical manifestation observed in a 10-year prospective study of 1,000 APS patients followed in various University Hospitals in Europe.[5] Although thrombi may potentially form in all arteries and veins of the vascular tree, clinical observation of APS patients has revealed 40% localization in certain districts of the circulatory system, that are responsible for stroke, myocardial infarction, deep vein thrombosis, pulmonary embolism, and other less frequent vascular manifestations.[5]

Evidence collected from clinical studies and animal models of APS has documented the critical role played by antibodies to β2-glycoprotein I (β2-GPI) in thrombus formation. Medium-to-high-titer antibodies are detected in APS patients with increased risk of thrombosis and are listed among the classification criteria for the diagnosis of the disease.[6] β2-GPI is a five-domain serum protein now recognized to be the main target of antiphospholipid antibodies. Four domains (DI-IV) are composed of short consensus repeats of approximately 60 amino acids shared with other members of the complement (C) con-

trol protein family, while the fifth domain contains a phospholipid binding site that interacts with the membrane of various cell types involved in thrombus formation including endothelial cells, platelets, and leukocytes.[7,8] The binding of β2-GPI to endothelial cells requires cell priming with LPS, as documented by the analysis of the *in vivo* protein biodistribution in mice,[9] and may also be induced by proinflammatory and physical stimuli such as surgery.[10] An epitope exposed in the open form of β2-GPI on the N-terminal DI is the preferential target of the pathogenic antibodies that induce thrombus formation.[11] The critical role played by the C system in this process is supported by the finding that vascular thrombosis, caused by passive administration of patients' antibodies or a monoclonal antibody to DI in an animal model of APS, is not observed in C-deficient animals or in animals receiving a non-C fixing antibody.[11,12] Despite the beneficial effect of long-term anticoagulation with vitamin K antagonists, recurrent thrombosis has been reported in 30-40% of high-risk patients with triple APL positivity[5] and remains a problem to be solved. Resolution of thrombi formed in carotid and cerebral arteries, and less frequently in coronary arteries, that cause serious clinical consequences including death, still represents an unmet clinical need. Thrombolytic agents administered to dissolve thrombi and surgical intervention aimed at removing blood clots in medium-large arteries in a limited number of patients unresponsive to pharmacologic treatment are the therapies currently used to control thrombosis in APS patients. However, despite the beneficial effect observed in patients treated with recombinant tissue plasminogen activator (rtPA), this therapy has significant limitations in safety and efficacy.[13] Bleeding is a serious side effect frequently observed in patients with ischemic stroke receiving rtPA and can be reduced, but not abolished, using a lower dose of the drug. Moreover, the rapid clearance of rtPA from the circulation, the relative resistance of large vessels to recanalization and the modest response observed in approximately 40% of patients with small vessel occlusions represent additional limitations of the thrombolytic therapy.[14-16]

The aim of this work was to devise a strategy to selectively deliver rtPA at sites of vessel-occluding thrombi in an attempt to reduce the systemic side effects of the thrombolytic therapy and to make the treatment more effective. The therapeutic approach was based on the administration of polymer-shelled nanobubbles (NB) conjugated with rtPA and a recombinant antibody specific for β2-GPI bound to activated endothelial cells lining the occluded vessel, and to activated platelets and leukocytes that accumulate within the thrombus. Moreover, considering that β2-GPI binds to these cells independently of antiphospholipid antibodies, we investigated whether this type of engineered NB had also a beneficial effect in thrombosis models unrelated to APS.

Methods

Nanobubbles preparation and characterization
NB with a perfluoropentane core and a chitosan shell were prepared by tuning a method previously reported[17] and used at the final concentration of 4×10^{11} NB/mL saline. Further details are available in the *Online Supplementary Appendix*.

Patients' sera
Serum samples were obtained from five APS patients with medium-high titer antibodies to the DI domain of β2-GPI after obtaining informed consent and were previously shown to induce clot formation in rats.[18] The ethical committee of Istituto Auxologico Italiano approved the study.

Human thrombi
Three patients aged 60-72 years with clinical atherosclerotic disease, undergoing thrombectomy for thrombotic occlusion of descending thoracic aorta, popliteal or femoral arteries gave written informed consent to use surgically removed thrombi for research purposes. *In vitro* clots were prepared from freshly collected citrated human blood by the addition of thromboplastin and $CaCl_2$. Two different types of clots were generated: i) blood clots prepared under static conditions,[19] referred to as platelet-poor clots, and ii) blood clots prepared under flowing conditions (Chandler loop),[20] that have been shown to resemble arterial thrombi, and referred to as platelet-rich clots. Patient's thrombi and *in vitro*-generated clots (prepared from 3 different donors) were fixed for 24 hours in 10% buffered formalin, snap-frozen and embedded in OCT medium (Diagnostic Division; Miles Inc).

Immunofluorescence analysis
Patients' thrombi, *in vitro* blood clots and kidneys from C3 gain-of-function (GOF) mice were examined by immunofluorescence as detailed in the *Online Supplementary Appendix*.

In vitro fibrinolytic and thrombolytic assays
The fibrinolytic and thrombolytic activities of rtPA-coated NB were estimated as previously reported.[20,21] Further details are available in the *Online Supplementary Appendix*.

Animal models
Experimental thrombosis models were established in male Wistar rats (270-290 g) kept under standard conditions in the Animal House of the University of Trieste, Italy, and in C3 GOF mice at Newcastle University, UK. The *in vivo* procedures were performed in compliance with the guidelines of European (86/609/EEC) and Italian (Legislative Decree 116/92) laws and were approved by the Italian Ministry of University and Research (Prot. N°

910/2018PR, rat models) and by the ethics committee of the Comparative Biology Center of Newcastle University (United Kingdom's Home Office granted license PD86B3678, mice model). The study was conducted in accordance with the Declaration of Helsinki.

Antiphospolipid syndrome model

We used a previously published model of APS.[12] Further details are available in the *Online Supplementary Appendix*.

Ferric chloride-induced thrombosis

The experiments were carried out according to Li *et al.*,[22] in anesthetized rats following an incision made through the abdominal wall to exteriorize the ileal mesentery.[23] Further details are available in the *Online Supplementary Appendix*.

C3 gain-of-function mouse model of atypical hemolytic uremic syndrome

The C3 GOF mouse model of atypical hemolytic uremic syndrome (aHUS) has been previously published.[24] Further details are available in the *Online Supplementary Appendix*.

Nanobubbles distribution in rat

In vivo biodistribution studies were performed in two anesthetized rats per group that received an intraperitoneal injection of LPS followed by either tNB conjugated with 3 nmol of cyanine 5.5 or saline and euthanized 2 hours later. The organs were analyzed *ex vivo* by IVIS Lumina III (PerkinElmer, Milan, Italy).[25,26]

Statistical analysis

Data are presented as mean ± standard deviation. Difference between groups was assessed by one-way analysis of variance (ANOVA) followed by Student-Newman-Keuls test for pairwise comparisons. Survival estimates were calculated according to Kaplan-Meier and compared with the log rank test. A two-sided *P* value of 0.05 was considered significant. Statistical analyses were done with GraphPad Prism 9 (San Diego, CA).

Results

Expression of β2-GPI on thrombi

In the initial experiments, we sought to determine whether β2-GPI may represent a potentially valuable target for antibody-coated thrombolytic NB. For this purpose, we searched for the presence of β2-GPI in the thrombi surgically removed from three patients with arterial thrombotic occlusions (Figure 1A) or *in vitro*-formed blood clots with different composition (Figure 1B). Staining of patient's

thrombus sections with antibodies to β2-GPI and to either fibrin or CD9 (to detect platelets and leukocytes) revealed co-localization of β2-GPI with platelets and leukocytes but not with fibrin. Deposits of β2-GPI on nucleated cells were also observed by nuclear staining with DAPI (Figure 1A). The preferential deposition of β2-GPI on platelets and nucleated cells was confirmed by the more intense staining of *in vitro* clots formed under flow conditions (Chandler thrombi), which resemble platelet-rich arterial thrombi, as compared to platelet-poor clots generated under static conditions (Figure 1B).

Preparation and targeting properties of nanobubble formulations

A recombinant scFv-Fc miniantibody (MBB2) containing the hinge-CH2-CH3 domains of human IgG1 engineered from scFv isolated from phage display library was selected to functionalize the NB as ligand for bound β2-GPI.[11] In order to avoid C activation by the MBB2/β2-GPI complex, a CH2-deleted variant of MBB2 (MBB2ΔCH2) was conjugated to NB via a covalent bond. Transmission electron microscopy (TEM) analysis of the NB showed no difference in the morphology of targeted and untargeted NB (Figure 2A). Likewise, the two types of NB had a similar size with an average diameter of 363.5±10.6 nm for the untargeted NB and 359±12.5 nm for the targeted NB and both the polydispersity index, a measure of particle size distribution, and the Z potential, an indicator of particle charge, were within the same range (Figure 2B).

Analysis of NB interaction with thrombi revealed a significant binding of MBB2ΔCH2-coated NB that was inhibited by 10-fold excess soluble MBB2ΔCH2, but not by an unrelated recombinant antibody,[27,28] preincubated with the clot section (Figure 2C), supporting the targeting specificity for β2-GPI. Search for binding of tNB was extended to thrombi induced *in vivo* by patients' sera containing antibodies to β2-GPI. Rhodamine 6G was administered to anesthetized rat to stain platelets and leukocytes prior to infusion of antibodies to β2-GPI. Targeted or control NB loaded with coumarin 6 were infused immediately after formation of thrombi in mesenteric microvessels. Analysis of NB distribution in rats revealed selective co-localization of tNB and platelets/leukocytes in blood clots while untargeted NB were practically undetectable (Figure 2D; *Online Supplementary Videos S1* and *S2*).

Preparation and evaluation of *in vitro* thrombolytic activity of rtPA-coated nanobubbles

In order to selectively deliver the thrombolytic agent at site of thrombi and avoid its release into the circulation, rtPA was covalently conjugated to the NB shell exploiting two binding methods. The fibrinolytic activity of the two types of rtPA-coated NB was investigated by a turbidimetric clot lysis assay in which the NB were added to plasma

prior to clot formation. As shown in *Online Supplementary Figure S1*, type B rtPA-NB (carbodiimide-mediated amide bond) displayed a concentration-dependent fibrinolytic activity, which was comparable to that of soluble rtPA, whereas type A rtPA-NB (amino-reductive reaction) were inactive at all tested concentrations. Based on these results, type B rtPA-NBs coated with MBB2ΔCH2 (rtPA-tNB) or untargeted (rtPA-NB) were used for all the *in vitro* and *in vivo* experiments.

The physico-chemical properties of rtPA-tNB, including the size, the polydispersity index and the Z potential, were essentially similar to those observed with rtPA-NB (Figure 3A). The encapsulation efficiency, expressed as percentage amount of rtPA loaded on NB / total amount of rtPA, was over 90% and the loading capacity, expressed as percentage amount of rtPA loaded / total weight of NB, was about 3.5%. These data did not change when rtPA was loaded on tNB. The amount of rtPA bound to NB stored at 4°C was quantified and functionally evaluated at different time points and found to be stable for up to 6 months. The *in vitro* thrombolytic activity of targeted and untargeted rtPA-NB was investigated in a model consisting of platelet-rich blood clots bathed in autologous plasma. Upon addition of the fibrinolytic agent to the plasma surrounding the clot, the degree of lysis by targeted NB was greater than that of untargeted NB and was comparable to that of soluble rtPA (Figure 3B). The thrombolytic activity of untargeted rtPA-NB can be most likely attributed to the static conditions of the *in vitro* clot lysis and to the continued presence of the thrombolytic agent in the plasma surrounding the clot.

Effect of targeted nanobubbles on thrombi in the rat model of antiphospholipid syndrome

In order to investigate the thrombolytic effect of rtPA-tNB in the rat model of APS, NB were infused intravenously
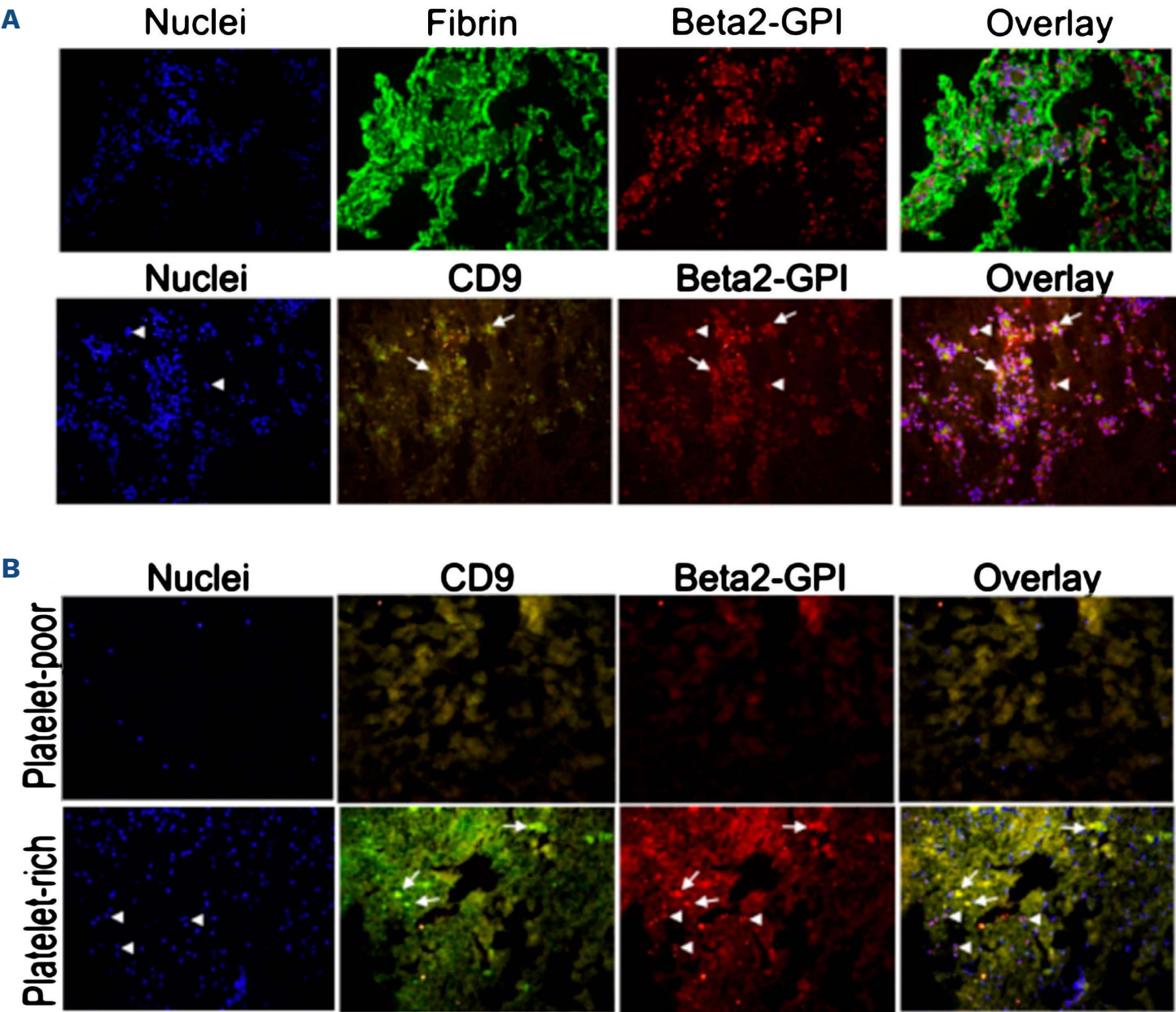
Figure 1. Detection of β2-GPI on thrombi by immunofluorescence analysis. Clot sections were double stained with rabbit antibody to β2 glycoprotein 1 (β2-GPI) and either antibody to fibrin or to CD9, to investigate the localization of β2-GPI on fibrin, platelets and leukocytes. DAPI was used to stain cell nuclei. The thrombi were obtained from 2 different sources: (A) 3 patients undergoing surgical thrombectomy; (B) *in vitro* blood clots generated under static (platelet-poor) or flow (platelet-rich) conditions (see Methods for additional details). Representative images of thrombus section from 1 patient showing absence of co-staining of β2-GPI and fibrin. Arrows highlight the co-localization of β2-GPI with CD9-positive structures and arrowheads show the co-localization of β2-GPI with DAPI-positive nucleated cells.

after thrombus formation, approximately 30 minutes (min) after the injection of antibodies to β2-GPI, and the presence and size of rhodamine 6G-stained thrombi in mesenteric vessels were monitored over time. Administration of rtPA-tNB caused thrombolysis within 1 min (*Online Supplementary Video S3*) as opposed to the less rapid dissolution of thrombi caused by soluble rtPA (*Online Supplementary Video S4*), whereas untargeted rtPA-NB were ineffective (*Online Supplementary Video S5*). The dissolution of the thrombi, obtained with rtPA-tNB and soluble rtPA, was confirmed by quantitative analysis of rhodamine 6G intensity staining (Figure 4A). A point to emphasize is that the dose of rtPA bound to NB was 10 times lower than that of the soluble rtPA. Moreover, as shown in Figure 4A and *Online Supplementary Video S3* and *S4*, sol-

uble rtPA exhibited a transient thrombolytic effect that lasted less than 3 min and was followed by the formation of new thrombi. Conversely, rtPA-tNB induced fast thrombolysis and prevented the formation of new thrombi during the 90-minute observation period (Figure 4A). Untargeted rtPA-NB failed to lyse the thrombi at all time points (Figure 4A; *Online Supplementary Video S5*). We further analyzed the efficacy of rtPA-tNB on blood vessels occlusion by evaluating the number of vessels with markedly reduced or absent blood flow. The results presented in Figure 4B show that treatment with rtPA-tNB resulted in vascular recanalization and restoration of blood flow in over 80% of occluded vessels whereas both rtPA and rtPA-NB were ineffective.

The endothelium of the mesenteric vessels examined at

	Average diameter ± SD (nm)	Polydispersity index ± SD	Z potential ± SD (mV)	MBB2dCH2 (mg/mL)
tNB	359 ± 12.5	0.122 ± 0.003	+ 29.67± 2.05	0.1
NB	364 ± 10.6	0.116 ± 0.004	+ 31.44 ± 2.11	-
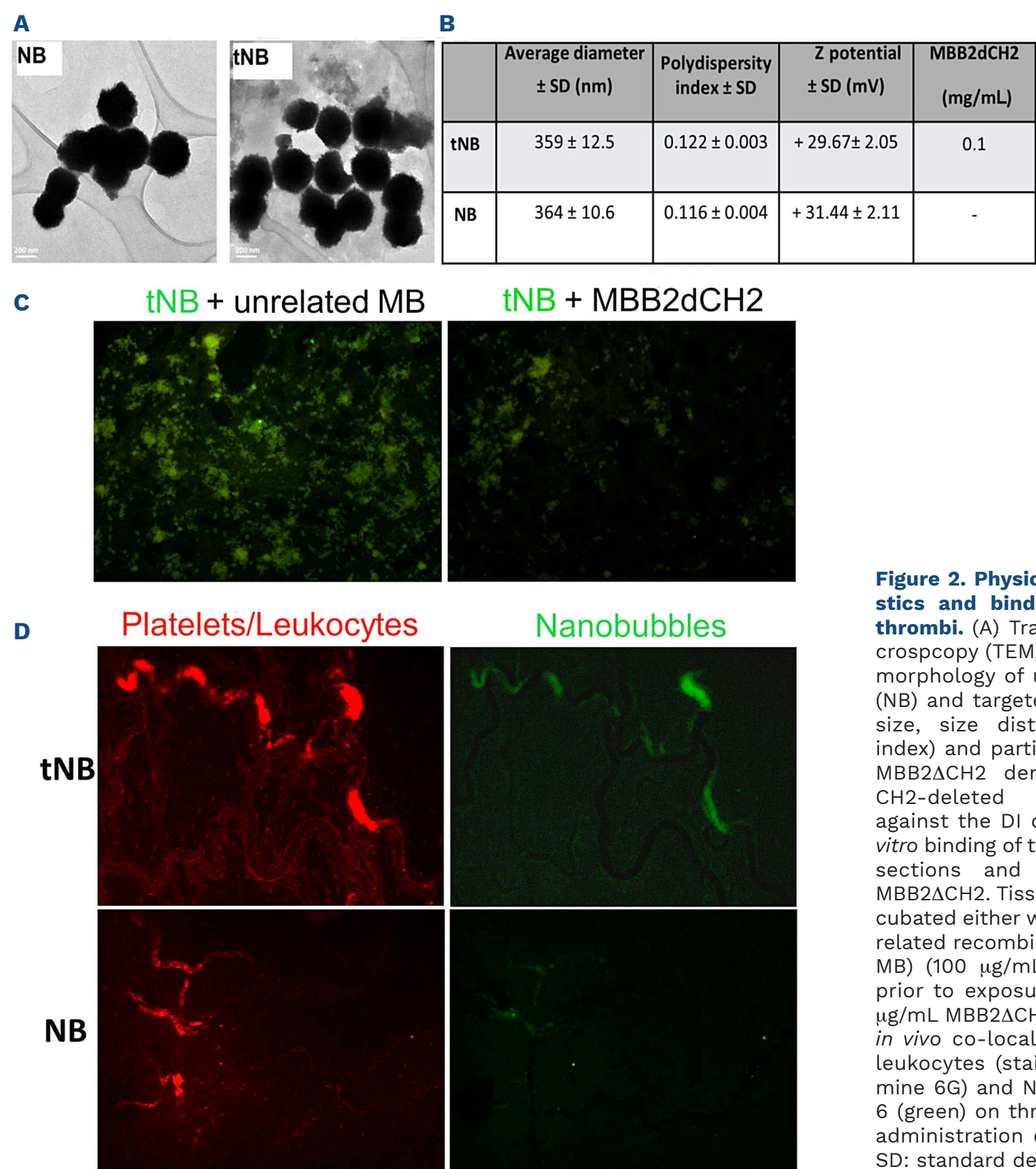
Figure 2. Physico-chemical characteristics and binding of nanobubbles to thrombi. (A) Transmission electron microspcopy (TEM) images showing similar morphology of untargeted nanobubbles (NB) and targeted NB (tNB); (B) average size, size distribution (polydispersity index) and particle charge (Z potential); MBB2ΔCH2 denotes the recombinant CH2-deleted scFv-Fc miniantibody against the DI domain of β2-GPI. (C) *In vitro* binding of tNB to patient's thrombus sections and inhibition by soluble MBB2ΔCH2. Tissue sections were pre-incubated either with MBB2ΔCH2 or an unrelated recombinant antibody (unrelated MB) (100 μg/mL) for 15 minutes (min) prior to exposure to tNB containing 10 μg/mL MBB2ΔCH2 for further 60 min; (D) *in vivo* co-localization of platelets and leukocytes (stained in red with rhodamine 6G) and NB loaded with coumarin 6 (green) on thrombi induced in rats by administration of antibodies to β2-GPI. SD: standard deviation.

the end of the experiment was still covered by tNB indicating a stable interaction of β2-GPI with endothelial cells (Figure 5). This finding might explain the prolonged profibrinolytic effect observed after administration of rtPA-tNB. No sign of vascular leakage, assessed by extravascular diffusion of free rhodamine 6G, or blood extravasation was seen in the ileal mesentery of rats treated with rtPA-tNB throughout the experimental procedure despite the micro-traumas caused by the tissue manipulation during the mesentery exteriorization from the abdominal cavity to petri dishes for the intravital microscopy analysis.

It is important to underline that only a small percentage of the infused tNB localized in the thrombi while a large proportion was cleared by the liver and, to a lesser extent, by the lung (*Online Supplementary Figure S2*).

Effect of targeted nanobubbles on ferric chloride thrombosis

Having found that β2-GPI was expressed on thrombi independently of the presence of antibodies to this protein, we sought to determine whether rtPA-tNB may also be effective in lysing blood clots induced by ferric chloride (FeCl$_3$) applied to the rat mesentery. As in the case of APS, the NB were infused soon after thrombus formation, which occurred within 10 min after removal of the chemical compound applied to the mesentery. Unlike rtPA and untargeted NB, rtPA-tNB localized at the thrombus site (Figure 6A) and induced rapid and persistent thrombolysis (*Online Supplementary Video S6 to S8*). The greater effi-

cacy of rtPA-tNB was also confirmed by the substantial decrease in the percentage of occluded vessels that was not seen using either soluble rtPA or untargeted rtPA-NB (Figure 6B).

Effect of targeted nanobubbles on the C3 gain-of-function murine model of atypical hemolytic uremic syndrome

Immunofluorescence analysis confirmed that both β2-GPI and fibrin were co-localized within the glomeruli and renal vessels (*Online Supplementary Figure S3*), thus proving the rationale to test the *in vivo* therapeutic effect of rtPA-tNB. Mice exhibiting active disease (evidenced through an active urinary sediment) were randomized into three groups receiving saline, rtPA-NB or rtPA-tNB. As predicted, a modest reduction in fibrin deposition with rtPA-NB treatment was observed due to the thrombolytic effects of rtPA. However, rtPA-tNB, which enabled targeted therapy due to the addition of antibodies to β2-GPI, significantly attenuated fibrin deposition within the glomeruli when compared to untreated animals and rtPA-NB-treated animals (Figure 7A and B).

Survival analysis showed that C3 GOF mice treated with rtPA-tNB had reduced mortality in comparison to saline-treated or rtPA-NB-treated animals (*Online Supplementary Figure S4A*); the difference, however, did not reach statistical significance because of the small number of animals. Urinalysis data are shown in the *Online Supplementary Figure S4B to D*. Saline group exhibit persisting hematuria,

A

Sample	Average diameter ± SD (nm)	PDI ± SD	Z potential ± SD (mV)	NB concentration (10^{11}/mL)	MBB2dCH2 (mg/mL)	rtPA (mg/mL)
rtPA-tNB	356.7 ± 9.5	0.123 ± 0.003	+ 28.65 ± 1.22	4	0.1	0.1
rtPA-NB	360.2 ± 12.3	0.125 ± 0.002	+ 29.03 ± 0.87	4,1	-	0.1

B
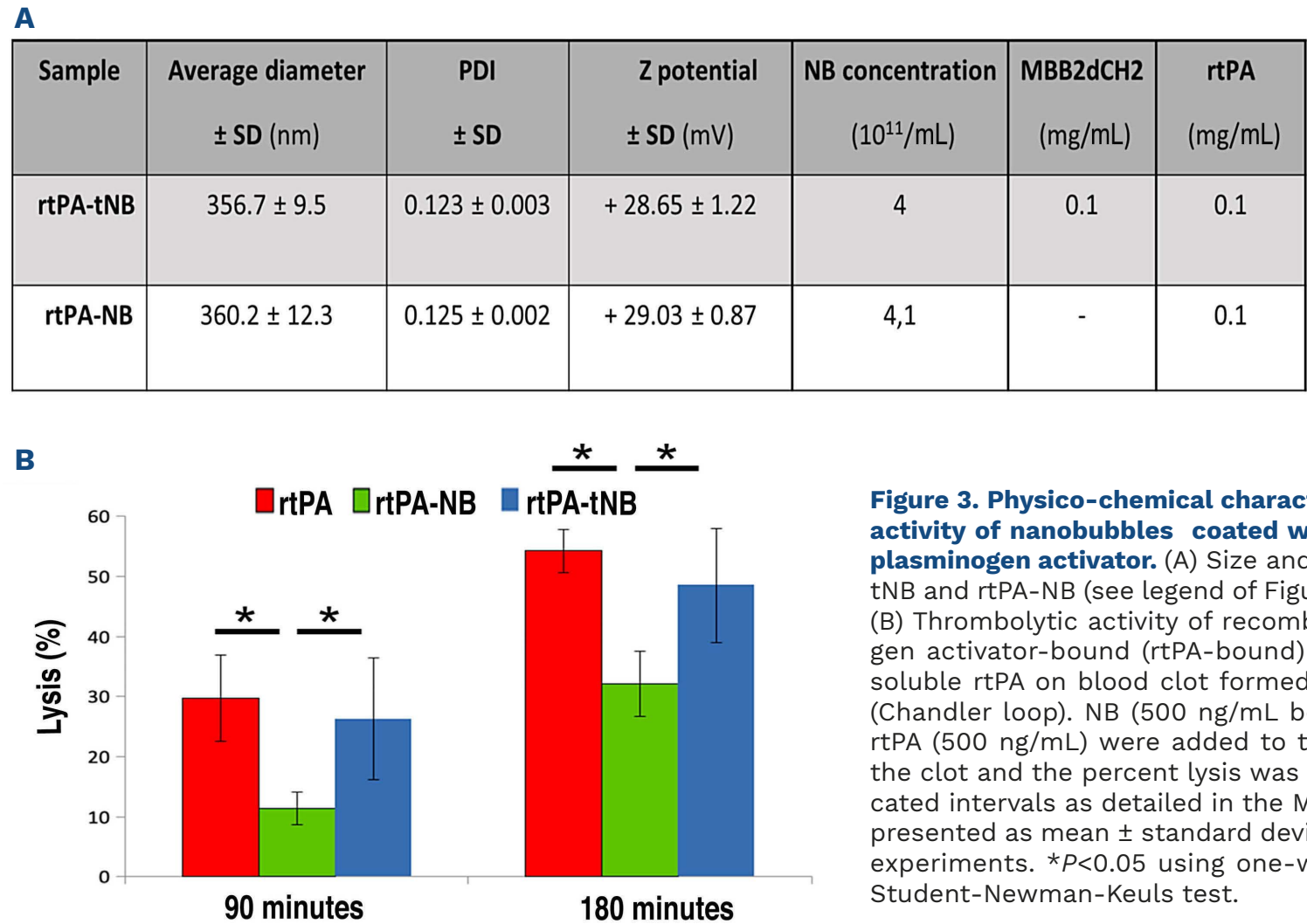
Figure 3. Physico-chemical characteristics and functional activity of nanobubbles coated with recombinant tissue plasminogen activator. (A) Size and characteristics of rtPA-tNB and rtPA-NB (see legend of Figure 2 for further details). (B) Thrombolytic activity of recombinant tissue plasminogen activator-bound (rtPA-bound) nanobubbles (NB) and soluble rtPA on blood clot formed under flow conditions (Chandler loop). NB (500 ng/mL bound rtPA) and soluble rtPA (500 ng/mL) were added to the plasma surrounding the clot and the percent lysis was determined at the indicated intervals as detailed in the Methods. The results are presented as mean ± standard deviation (SD) of 3 different experiments. *$P<0.05$ using one-way ANOVA followed by Student-Newman-Keuls test.
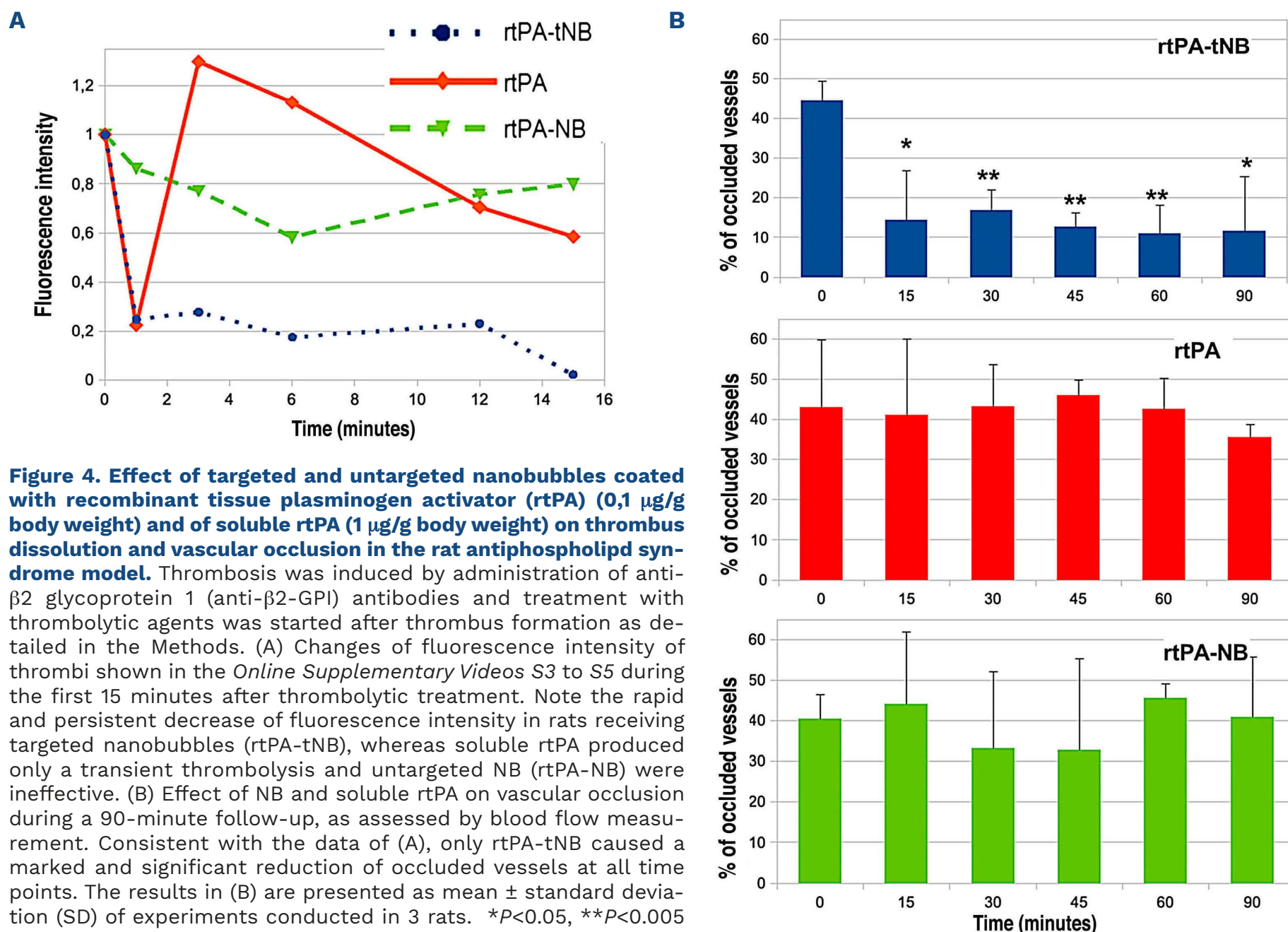
Figure 4. Effect of targeted and untargeted nanobubbles coated with recombinant tissue plasminogen activator (rtPA) (0,1 µg/g body weight) and of soluble rtPA (1 µg/g body weight) on thrombus dissolution and vascular occlusion in the rat antiphospholipid syndrome model. Thrombosis was induced by administration of anti-β2 glycoprotein 1 (anti-β2-GPI) antibodies and treatment with thrombolytic agents was started after thrombus formation as detailed in the Methods. (A) Changes of fluorescence intensity of thrombi shown in the *Online Supplementary Videos S3* to *S5* during the first 15 minutes after thrombolytic treatment. Note the rapid and persistent decrease of fluorescence intensity in rats receiving targeted nanobubbles (rtPA-tNB), whereas soluble rtPA produced only a transient thrombolysis and untargeted NB (rtPA-NB) were ineffective. (B) Effect of NB and soluble rtPA on vascular occlusion during a 90-minute follow-up, as assessed by blood flow measurement. Consistent with the data of (A), only rtPA-tNB caused a marked and significant reduction of occluded vessels at all time points. The results in (B) are presented as mean ± standard deviation (SD) of experiments conducted in 3 rats. *$P<0.05$, **$P<0.005$ using one-way ANOVA followed by Student-Newman-Keuls test.

which reached clinical end point in five of six mice (*Online Supplementary Figure S4D*). In contrast, three of the five animals receiving rtPA-tNB showed improvement in hematuria after the second dose of the thrombolytic agent.

Discussion

Nanoparticles are being developed as a novel therapeutic tool to deliver a sufficient amount of thrombolytic drugs to vessel-occluding thrombi and to reduce and possibly avoid serious side effects associated with the administration of soluble drugs. This therapeutic approach can be made more effective by coating NB with ligands that bind with reasonably good affinity to target molecules expressed on blood clots. The data presented here provide evidence that rtPA-coated NB targeting cell-bound β2-GPI clear occluded vessels and re-establish blood flow in APS and non-APS thrombosis models.

Chitosan-shelled NB employed in this study have been largely used thanks to their stability, biocompatibility, low immunogenicity and biodegradability and have been adopted in different biomedical and pharmaceutical fields.[29,30] The good biocompatibility of NB is related to their components, such as chitosan and phospholipids, that are biodegradable, safe and admitted by the Regulatory Agencies Food and Drug Administration and European Medicines Agency. Indeed, chitosan-shelled NB have previously been shown to be non-cytotoxic on different cell lines and no signs of acute toxicity was observed after intravenous or intradermal administration in animal models.[31-33] The approximately 400 nm size of the NB has the advantage of preventing or markedly reducing their renal excretion and their distribution is favored by the physical property of soft particles.[34] An additional advantage of the polymer-shelled NB is to be easily modified by covalently binding antibodies, aptamers, peptides and small molecules that allow selective *in vivo* localization.[33,35] Equally important is the characteristic of the NB to be filled with safe and biologically inert gases or vaporizable compounds such as perfluorocarbons, sulfur hexafluoride, air and carbon dioxide, enabling them to be good ultrasound reflectors and to be used as an ultrasound imaging probe to localize thrombi and monitor their *in vivo* dissolution.[36]
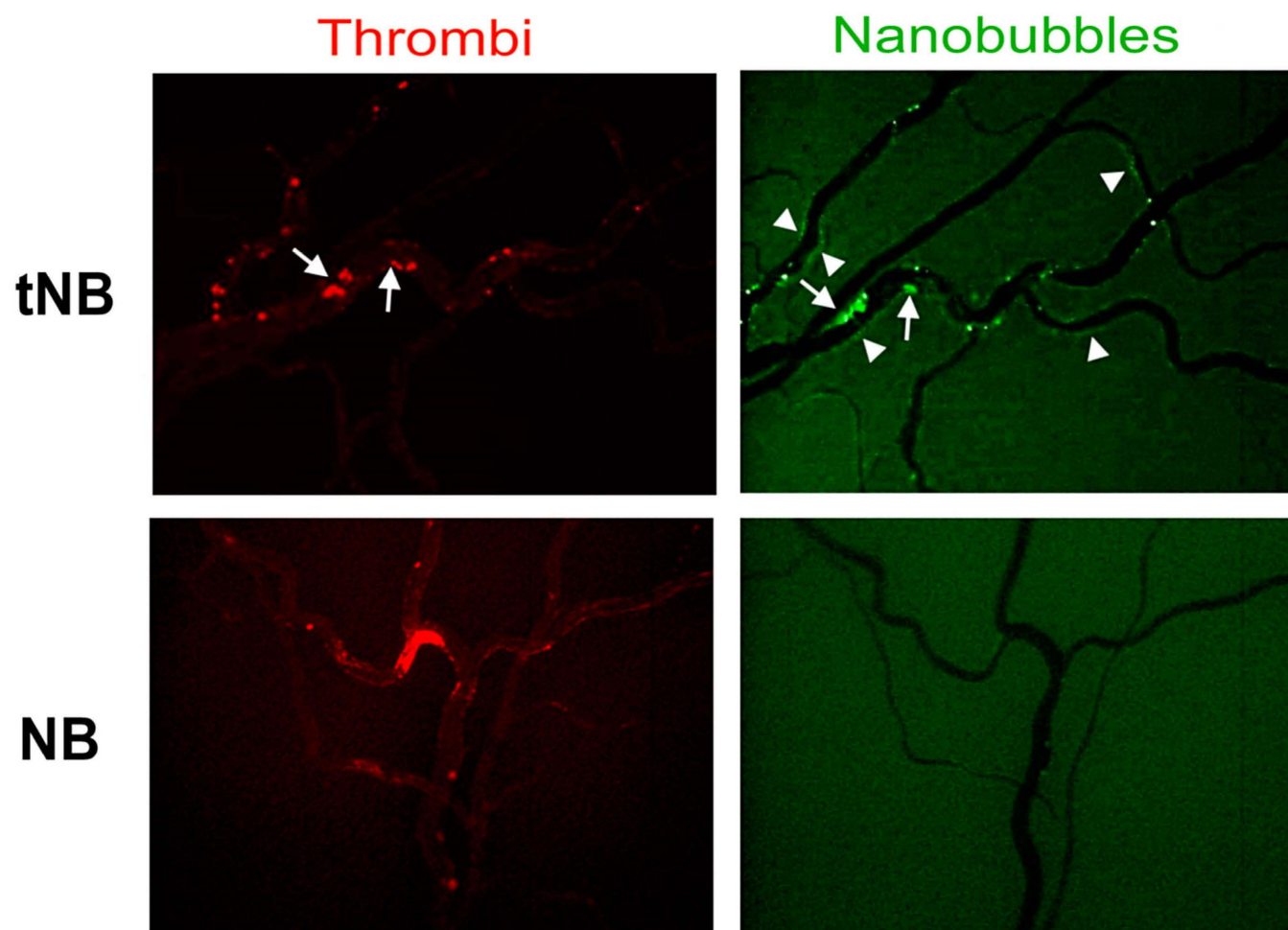
Figure 5. Localization of targeted nanobubbles on endothelium and vascular thrombi during thrombolytic treatment in a rat model of antiphospolipid syndrome. Thrombus formation and nanobubble (NB) deposits were followed by intravital microscopy and the images were collected 90 minutes after injection of NB. Residual intravascular thrombi are visualized in red by *in vivo* staining with rhodamine 6G and NB loaded with coumarin 6 in green. Arrows show the co-localization of rtPA-tNB and residual vascular thrombi and arrowheads highlight the localization of rtPA-tNB on activated endothelium. Note the absence of untargeted NB and the presence of occluded vessels in rtPA-NB-treated animal. TNB: targeted NB; rtPA: recombinant tissue plasminogen activator.

Platelets and fibrin, being the major components of vascular thrombi, have been investigated as potential targets for the local delivery of nanoparticles coated with thrombolytic agents. Monoclonal antibodies and peptides reacting with fibrin have proven successful for the selective delivery of nanoparticles to thrombi for theranostic purposes.[37,38] Satisfactory results have also been obtained targeting the platelets with a monoclonal antibody to the GPIIb/IIIa receptor expressed on both quiescent and activated platelets.[39] Unfortunately, treatment with this antibody is often associated with bleeding, which can be markedly reduced by targeting the platelets with a single-chain fragment variable that binds the activated form of GPIIb/IIIa.[40] Thrombus dissolution with minimal hemorrhagic risk has also been induced by microbubbles loaded with thrombolytic agents and targeted to blood clots by the arginine-glycine-aspartic acid-serine peptide.[41] However, this therapeutic approach has the limitation of having been tested on thrombi induced by either chemical or physical vascular injury, but not in models relevant to human diseases. We addressed this issue by selecting β2-GPI as a target for the delivery of rtPA-coated NB to APS and non-APS thrombi. The advantage of β2-GPI over other targets is to interact with different cells involved in throm-bus formation including platelets, endothelial cells and leukocytes. These cells express several receptors for β2-GPI such as ApoER2, Toll-like receptors 2 and 4, annexin A2, glycoprotein Ibα, and LRP8,[42] though their *in vivo* relevance in the procoagulant effect of anti-β2-GPI antibodies in APS patients remains to be established. The endothelium is an important target of β2-GPI and represents the initial site of clot formation triggered by the interaction of antibodies with cell-bound β2-GPI. It is important to emphasize that binding of β2-GPI to endothelial cells requires cell activation by LPS and possibly proinflammatory cytokines, and is independent of antibodies.[9] This is consistent with the finding reported here that β2-GPI is localized on both renal vascular endothelium and glomeruli of a mouse model of aHUS in the absence of specific antibodies. Activation seems to be also required for the binding of β2-GPI to platelets, as suggested by the detection of this molecule on platelets incubated with thrombin receptor-activating peptide, but not on resting platelets.[43] This observation is supported by our data showing that β2-GPI is expressed in platelet-rich thrombi such as human arterial thrombi or *in vitro* formed platelet-rich blood clots (Chandler thrombi). However, platelets do not seem to be the only target of β2-GPI
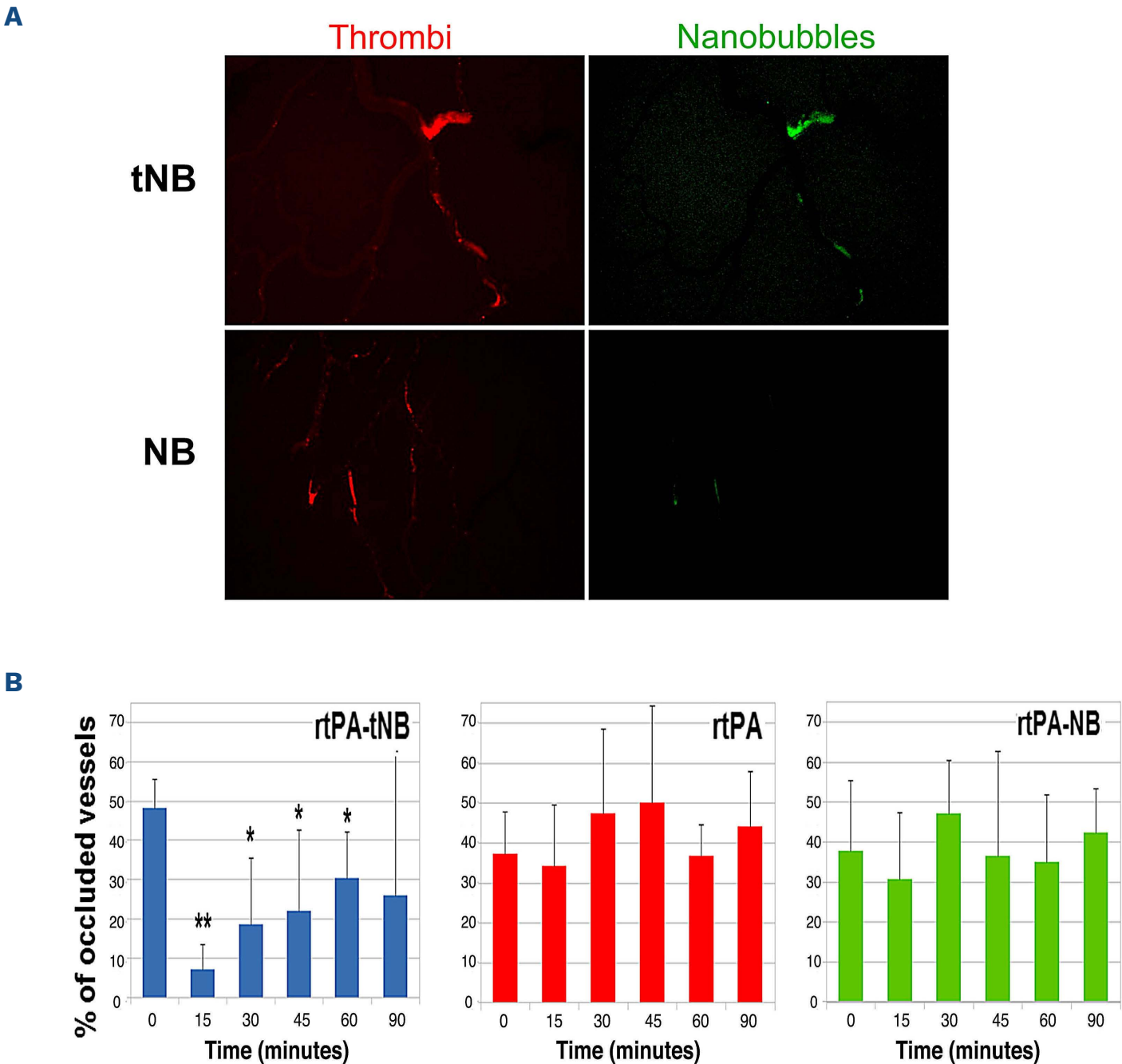
Figure 6. Localization of targeted and untargeted nonobubbles (tNB and NB) (without recombinant tissue plasminogen activator [rtPA]) on vascular thrombi induced by ferric chloride and effect of rtPA-NB, rtPA-tNB and soluble rtPA on vascular thrombotic occlusion. (A) Intravascular thrombi are visualized in red by *in vivo* staining with rhodamine 6G and in green by coumarin 6-loaded targeted nanobubbles (tNB). The images were collected 30 minutes after injection of NB. Note the absence of thrombus green staining in rats that received untargeted NB. (B) Time course of vascular occlusion after treatment with rtPA-coated tNB or untargeted NB (0,2 μg/g body weight) or soluble recombinant tissue plasminogen activator (rtPA) (2 ρg/g body weight), as assessed by intravascular microscopy analysis. A significant reduction in the number of occluded vessels was seen in rats treated with targeted NB (rtPA-tNB) but not in those treated with untargeted NB or soluble rtPA. The results are presented as mean ± standard deviation of experiments conducted in 3 rats. *P<0.05, **P< 0.005 using one-way ANOVA followed by Student-Newman-Keuls test.

in thrombi as positive staining was seen in thrombus-associated nucleated cells, which include monocytes and neutrophils, known to be involved in thrombogenesis by expressing and/or releasing tissue factor and neutrophil extracellular traps.[44]

The rtPA-coated tNB induced faster dissolution (within 1 min) of thrombi in the mesenteric microcirculation in the rat model of APS than soluble rtPA, whereas untargeted rtPA-NB were ineffective. These results clearly indicate that targeted NB are able to deliver rtPA to blood clots localized in large arteries as well as in microvessels of various organs observed in the classic APS, and in the more severe catastrophic APS. The *in vivo* effect of rtPA was transient because rethrombosis occurred within a few min and

persisted for the whole observation period. On the contrary, administration of targeted NB prevented the formation of new thrombi despite the presence of circulating thrombus-inducing antibodies to β2-GPI. This protection against rethrombosis is most likely due to the binding of rtPA-bearing tNB to β2-GPI deposited on the endothelium at sites of vascular thrombi, thereby creating a profibrinolytic shield. Moreover, the fast and persistent recanalization of occluded vessels by targeted NB was achieved with a dose of rtPA that was 10-fold lower than that of soluble rtPA, which is expected to significantly reduce the bleeding risk as suggested by our failure to detect bleeding in the ileal mesentery during the *in vivo* experiments. This greater efficiency can be explained by the reduced dispersion and the selec-

tive delivery of the thrombolytic agent bound to NB at sites of thrombus formation. One possible indication of this therapeutic approach in the clinical setting might be APS patients undergoing vascular surgery, who are known to be at high risk of rethrombosis as a result of β2-GPI deposition on activated endothelium followed by the binding of pathogenic antibodies and C activation.[10]

Another important finding of this work is the ability of targeted NB to lyse thrombi in non-APS models such as ferric chloride-induced thrombosis[45-47] and the more clinically relevant atypical hemolytic uremic syndrome in C3 GOF mice that manifests with hematuria, proteinuria, high creatinine level, hemolysis, fibrin deposition in the glomeruli and occasional intravascular thromboses. As anticipated by our previous observations that chemical and physical stimuli can promote β2-GPI deposition on endothelial cells,[10,12] it was not surprising to discover that the tNB were able to dissolve blood clots formed in vessels where the local application of ferric chloride leads to activation of endothelial cells and binding of β2-GPI. Our data also show that thrombotic microangiopathy (TMA) observed in the C3 GOF mouse model of aHUS is a predisposing condition for the deposition of β2-GPI on endothelial cells of glomeruli. The role of bound β2-GPI is to focalize the delivery of rtPA-coated NB at sites of fibrin clots where they induce fibrin dissolution. The successful reduction of fibrin deposition within the microvasculature of the glomeruli in C3 GOF mice suggests this therapy could be a useful adjunct in the treatment of thrombotic microangiopathies. For C-mediated TMA, a C-inhibiting therapy will still be required to extinguish the disease process through restoring C regulation. However, restoration of C regulation takes time and thus a fast-acting prophylactic treatment with targeted fibrinolytic NB could reduce the fibrin burden within the glomeruli, thereby attenuating renal ischemic injury and thus end organ damage. This targeted therapy could be extended to patients with secondary TMA to reduce ischemic injury in the interim, whilst the precipitating factor of the TMA is identified and subsequently removed. Collectively, any reduction in end organ damage will translate to improved clinical outcomes.

In conclusion, rtPA-coated polymer-shelled NB targeted to β2-GPI expressed on activated endothelial cells, platelets and leukocytes have been shown to be effective in dissolving thrombi and prevent rethrombosis in rat models of APS and ferric chloride thrombosis, as well as in removing fibrin deposits in the kidneys of mice that develop aHUS. Targeting cell-bound β2-GPI may represent an efficient and safe strategy to selectively deliver a fibrinolytic agent at sites of thrombotic vessel occlusion as well as at sites at risk of developing thrombosis such as injured vascular districts, where activated endothelial cells, along with activated platelets and leukocytes adhering to their surface, might promote a strong thrombogenic environment.
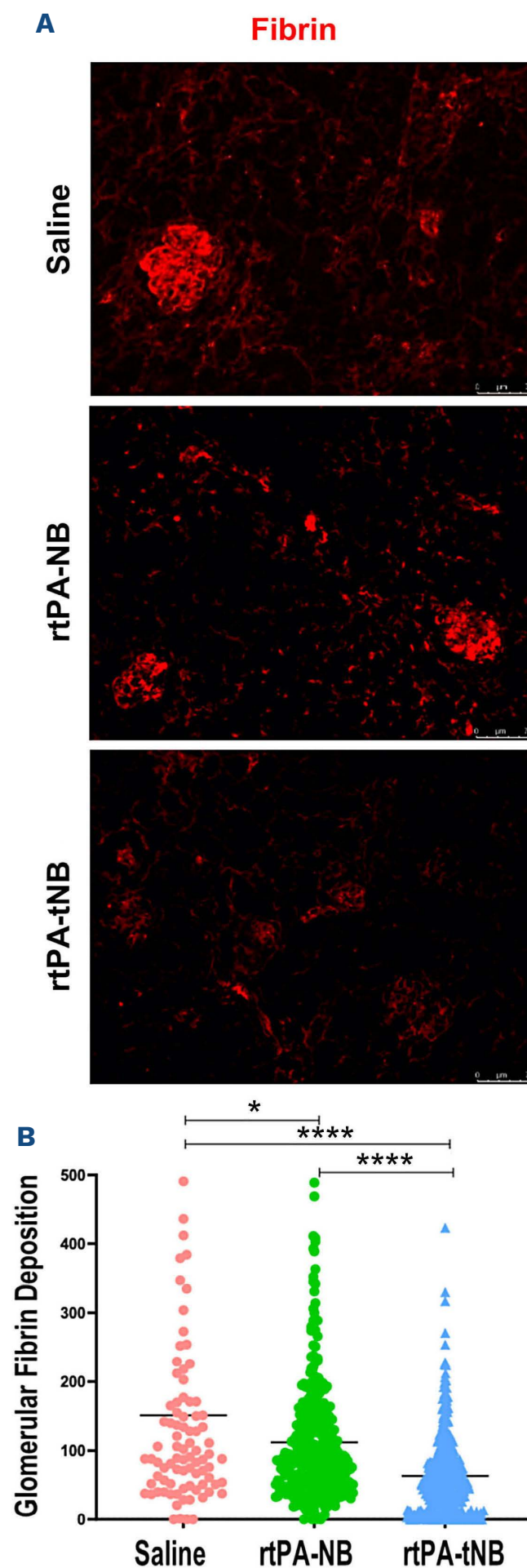
Figure 7. Recombinant tissue plasminogen activator targeted nanobubbles dissolve clots in the C3 gain-of function mouse model of atypical hemolytic uremic syndrome. (A) Representative image of glomerular fibrin deposition in saline-treated atypical hemolytic uremic syndrome (aHUS) mice (n=3), aHUS mice treated with rtPA-NB, (0,5 µg/g body weight; n=6) or aHUS mice treated with recombinant tissue plasminogen activator targeted nanobubbles (rtPA-tNB) (0,5 µg/g body weight; n=5). (B) Densitometry analysis of glomerular fibrin deposition, 87 glomeruli scored in saline-treated C3 gain of function (GOF), 358 glomeruli scored in rtPA-NB, 459 scored in rtPA-tNB. *P<0.05, **P<0.005, ***P<0.0001 using one-way ANOVA followed by Student-Newman-Keuls test.

References

1. Meroni PL, Borghi MO, Grossi C, Chighizola CB, Durigutto P, Tedesco F. Obstetric and vascular antiphospholipid syndrome: same antibodies but different diseases? Nat Rev Rheumatol. 2018;14(7):433-440.
2. Meroni PL, Borghi MO, Raschi E, Tedesco F. Pathogenesis of antiphospholipid syndrome: understanding the antibodies. Nat Rev Rheumatol. 2011;7(6):330-339.
3. Garcia D, Erkan D. Diagnosis and management of the antiphospholipid syndrome. N Engl J Med. 2018;379(13):1290-1291.
4. Sciascia S, Sanna G, Murru V, Roccatello D, Khamashta MA, Bertolaccini ML. The global anti-phospholipid syndrome score in primary APS. Rheumatology (Oxford). 2015;54(1):134-138.
5. Cervera R, Serrano R, Pons-Estel GJ, et al. Morbidity and mortality in the antiphospholipid syndrome during a 10-year period: a multicentre prospective study of 1000 patients. Ann Rheum Dis. 2015;74(6):1011-1018.
6. Miyakis S, Lockshin MD, Atsumi T, et al. International consensus statement on an update of the classification criteria for definite antiphospholipid syndrome (APS). J Thromb Haemost. 2006;4(2):295-306.
7. de Groot PG, Urbanus RT. The significance of autoantibodies against beta2-glycoprotein I. Blood. 2012;120(2):266-274.
8. Giannakopoulos B, Krilis SA. The pathogenesis of the antiphospholipid syndrome. N Engl J Med. 2013;368(11):1033-1044.
9. Agostinis C, Biffi S, Garrovo C, et al. In vivo distribution of beta2 glycoprotein I under various pathophysiologic conditions. Blood. 2011;118(15):4231-4238.
10. Meroni PL, Macor P, Durigutto P, et al. Complement activation in antiphospholipid syndrome and its inhibition to prevent rethrombosis after arterial surgery. Blood. 2016;127(3):365-367.
11. Agostinis C, Durigutto P, Sblattero D, et al. A non-complement-fixing antibody to beta2 glycoprotein I as a novel therapy for antiphospholipid syndrome. Blood. 2014;123(22):3478-3487.
12. Fischetti F, Durigutto P, Pellis V, et al. Thrombus formation induced by antibodies to beta2-glycoprotein I is complement dependent and requires a priming factor. Blood. 2005;106(7):2340-2346.
13. Thiebaut AM, Gauberti M, Ali C, et al. The role of plasminogen activators in stroke treatment: fibrinolysis and beyond. Lancet Neurol. 2018;17(12):1121-1132.
14. Campbell BC. Thrombolysis and thrombectomy for acute ischemic stroke: strengths and synergies. Semin Thromb Hemost. 2017;43(2):185-190.
15. Rabinstein AA. Update on treatment of acute ischemic stroke. Continuum (Minneap Minn). 2020;26(2):268-286.
16. Waqas M, Kuo CC, Dossani RH, et al. Mechanical thrombectomy versus intravenous thrombolysis for distal large-vessel occlusion: a systematic review and meta-analysis of observational studies. Neurosurg Focus. 2021;51(1):E5.
17. Cavalli R, Bisazza A, Trotta M, et al. New chitosan nanobubbles for ultrasound-mediated gene delivery: preparation and in vitro characterization. Int J Nanomedicine. 2012;7(1):3309-3318.
18. Durigutto P, Grossi C, Borghi MO, et al. New insight into antiphospholipid syndrome: antibodies to beta2glycoprotein I-domain 5 fail to induce thrombi in rats. Haematologica. 2019;104(4):819-826.
19. Colucci M, Scopece S, Gelato AV, Dimonte D, Semeraro N. In vitro clot lysis as a potential indicator of thrombus resistance to fibrinolysis - study in healthy subjects and correlation with blood fibrinolytic parameters. Thromb Haemost. 1997;77(4):725-729.
20. Mutch NJ, Moore NR, Mattsson C, Jonasson H, Green AR, Booth NA. The use of the Chandler loop to examine the interaction potential of NXY-059 on the thrombolytic properties of rtPA on human thrombi in vitro. Br J Pharmacol. 2008;153(1):124-131.
21. Colucci M, Binetti BM, Tripodi A, Chantarangkul V, Semeraro N. Hyperprothrombinemia associated with prothrombin G20210A mutation inhibits plasma fibrinolysis through a TAFI-mediated mechanism. Blood. 2004;103(6):2157-2161.
22. Li W, Nieman M, Sen Gupta A. Ferric chloride-induced murine thrombosis Models. J Vis Exp. 2016;(115):1-12.
23. Dobrina A, Pausa M, Fischetti F, et al. Cytolytically inactive terminal complement complex causes transendothelial migration of polymorphonuclear leukocytes in vitro and in vivo. Blood. 2002;99(1):185-192.
24. Smith-Jackson K, Yang Y, Denton H, et al. Hyperfunctional complement C3 promotes C5-dependent atypical hemolytic uremic syndrome in mice. J Clin Invest. 2019;129(3):1061-1075.
25. Capolla S, Mezzaroba N, Zorzet S, et al. A new approach for the treatment of CLL using chlorambucil/hydroxychloroquine-loaded anti-CD20 nanoparticles. Nano Research. 2016;9:537-548.
26. Colombo F, Durigutto P, De Maso L, et al. Targeting CD34(+) cells of the inflamed synovial endothelium by guided nanoparticles for the treatment of rheumatoid arthritis. J Autoimmun. 2019;103(2019):102288-102301.
27. Macor P, Secco E, Mezzaroba N, et al. Bispecific antibodies targeting tumor-associated antigens and neutralizing

complement regulators increase the efficacy of antibody-based immunotherapy in mice. Leukemia. 2015;29(2):406-414.

28. Mezzaroba N, Zorzet S, Secco E, et al. New potential therapeutic approach for the treatment of B-cell malignancies using chlorambucil/hydroxychloroquine-loaded anti-CD20 nanoparticles. PLoS One. 2013;8(9):E74216.

29. Cavalli R, Argenziano M, Vigna E, et al. Preparation and in vitro characterization of chitosan nanobubbles as theranostic agents. Colloids Surf B Biointerfaces. 2015;129(1):39-46.

30. Xing Z, Wang J, Ke H, et al. The fabrication of novel nanobubble ultrasound contrast agent for potential tumor imaging. Nanotechnology. 2010;21(14):145607-145615.

31. Argenziano M, Occhipinti S, Scomparin A, et al. Exploring chitosan-shelled nanobubbles to improve HER2 + immunotherapy via dendritic cell targeting. Drug Deliv Transl Res. 2022;12(8):2007-2018.

32. Marano F, Frairia R, Rinella L, et al. Combining doxorubicin-nanobubbles and shockwaves for anaplastic thyroid cancer treatment: preclinical study in a xenograft mouse model. Endocr Relat Cancer. 2017;24(6):275-286.

33. Shen S, Li Y, Xiao Y, et al. Folate-conjugated nanobubbles selectively target and kill cancer cells via ultrasound-triggered intracellular explosion. Biomaterials. 2018;181(1):293-306.

34. Cavalli R, Bisazza A, Lembo D. Micro- and nanobubbles: a versatile non-viral platform for gene delivery. Int J Pharm. 2013;456(2):437-445.

35. Brown T. Design thinking. Harv Bus Rev. 2008;86(6):84-92.

36. Cavalli R, Soster M, Argenziano M. Nanobubbles: a promising efficient tool for therapeutic delivery. Ther Deliv. 2016;7(2):117-138.

37. McCarthy JR, Patel P, Botnaru I, Haghayeghi P, Weissleder R, Jaffer FA. Multimodal nanoagents for the detection of intravascular thrombi. Bioconjug Chem. 2009;20(6):1251-1255.

38. Marsh JN, Hu G, Scott MJ, et al. A fibrin-specific thrombolytic nanomedicine approach to acute ischemic stroke. Nanomedicine (Lond). 2011;6(4):605-615.

39. Alonso A, Dempfle CE, Della Martina A, et al. In vivo clot lysis of human thrombus with intravenous abciximab immunobubbles and ultrasound. Thromb Res. 2009;124(1):70-74.

40. Wang X, Palasubramaniam J, Gkanatsas Y, et al. Towards effective and safe thrombolysis and thromboprophylaxis: preclinical testing of a novel antibody-targeted recombinant plasminogen activator directed against activated platelets. Circ Res. 2014;114(7):1083-1093.

41. Hua X, Zhou L, Liu P, et al. In vivo thrombolysis with targeted microbubbles loading tissue plasminogen activator in a rabbit femoral artery thrombus model. J Thromb Thrombolysis. 2014;38(1):57-64.

42. Del Papa N, Sheng YH, Raschi E, et al. Human beta 2-glycoprotein I binds to endothelial cells through a cluster of lysine residues that are critical for anionic phospholipid binding and offers epitopes for anti-beta 2-glycoprotein I antibodies. J Immunol. 1998;160(11):5572-5578.

43. Lonati PA, Scavone M, Gerosa M, et al. Blood cell-bound C4d as a marker of complement activation in patients with the antiphospholipid Syndrome. Front Immunol. 2019;10(1):773-781.

44. Shantsila E, Lip GY. The role of monocytes in thrombotic disorders. Insights from tissue factor, monocyte-platelet aggregates and novel mechanisms. Thromb Haemost. 2009;102(5):916-924.

45. McCarthy JR, Sazonova IY, Erdem SS, et al. Multifunctional nanoagent for thrombus-targeted fibrinolytic therapy. Nanomedicine (Lond). 2012;7(7):1017-1028.

46. Schwarz M, Meade G, Stoll P, et al. Conformation-specific blockade of the integrin GPIIb/IIIa: a novel antiplatelet strategy that selectively targets activated platelets. Circ Res. 2006;99(1):25-33.

47. Wang X, Gkanatsas Y, Palasubramaniam J, et al. Thrombus-targeted theranostic microbubbles: a new technology towards concurrent rapid ultrasound diagnosis and bleeding-free fibrinolytic treatment of thrombosis. Theranostics. 2016;6(5):726-738.

Visual abstract
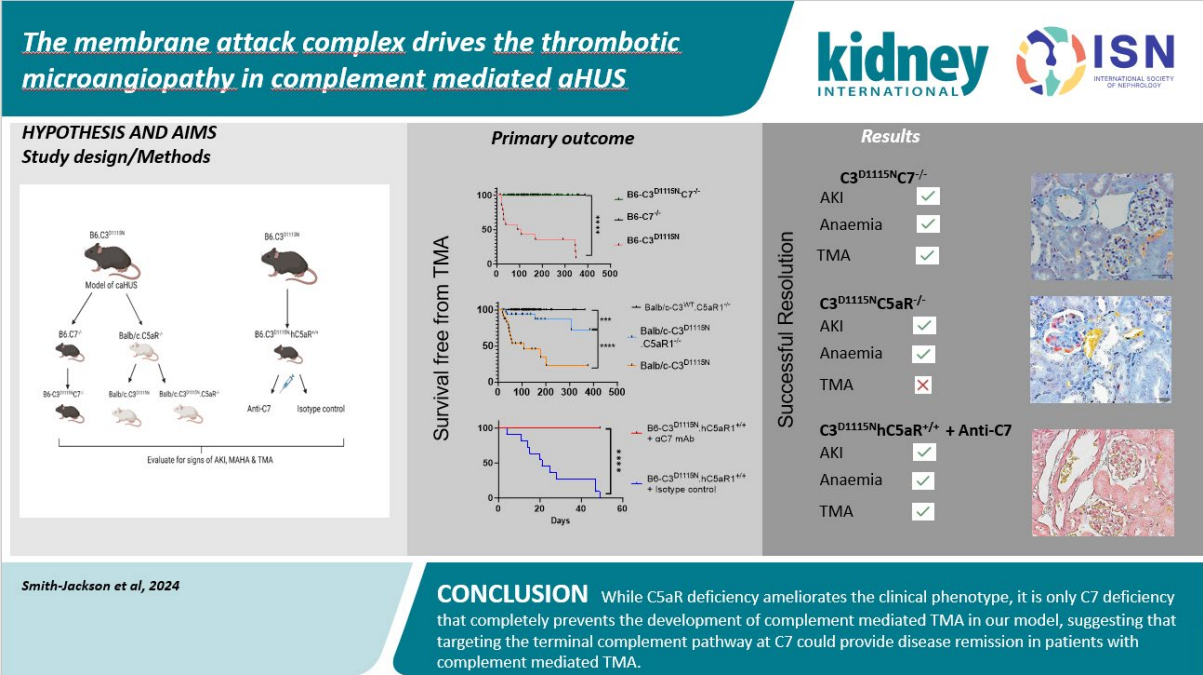
The membrane attack complex drives the thrombotic microangiopathy in complement mediated aHUS.

Kate Smith-Jackson [1,2], Patrick Walsh[1,2], Wioleta M. Zelek[3], Thomas Hoyler[4], Marianne M. Martinic[4], Gemma Thompson[1,2], Beth Gibson[1,2], Chloe Connelly[1,2], Isabel Pappworth[1,2], Mark J. Murphy[4], David Kavanagh[1,2], Kevin J. Marchbank[1,2]

[1].Complement Therapeutics Research Group, Newcastle University Translational and Clinical Research Institute, The Medical School, Newcastle-upon-Tyne, UK.

[2]. National Renal Complement Therapeutics Centre, The Royal Victoria Infirmary, Newcastle-upon-Tyne, UK.

[3]. UK Dementia Research Institute Cardiff and Division of Infection and Immunity, School of Medicine, Cardiff University, Cardiff, Wales, UK

[4].Idorsia Pharmaceuticals Ltd, Hegenheimermattweg 91, 4123 Allschwil, Switzerland.

Abstract

The C3^{D1115N} mouse, engineered around a gain of function point mutation in C3 associated with complement mediated atypical haemolytic uraemic syndrome (aHUS) in man, recapitulates the clinical disease. Backcrossing our model onto C7 deficient and C5aR1 deficient mice enabled us to further determine the roles of the C5a-C5aR1 axis and C5b-9 (the membrane attack complex) on kidney disease. C7 deficiency completely abolished both clinical and histological evidence of disease. We found that removing *C5aR1* (CD88) attenuated the risk of developing clinical disease, but mice could still develop a thrombotic microangiopathy (TMA). Therapeutic inhibition consolidated our genetic findings, showing that both anti-C7 therapy and an oral C5aR1 antagonist when used before evidence of significant renal injury, prevented mice from succumbing to disease. However, there was ongoing histological disease within mice treated with the C5aR1 antagonist. Our data suggest that both C5aR1 and C7 play a role in the development of the conditions required for renal TMA. While disrupting the C5a-C5aR1 axis is beneficial, our genetic and therapeutic studies showed that a renal TMA can still develop and ultimately our data confirms that the membrane attack complex (MAC) is required to develop renal TMA. Thus, as well as the requirement for alternative pathway dysregulation, local generation of MAC within the kidney is also critical to drive disease pathology in complement mediated aHUS.

Key words: aHUS, MAC, TMA, Complement, Therapy, C3 GOF.

Translational statement

Whilst loss of C5aR1 ameliorates clinical disease, C7 deficiency prevents the development of complement mediated TMA, suggesting that preferentially targeting the terminal complement pathway at C7 could provide disease remission in patients with complement mediated thrombotic microangiopathy, while leaving the C5a-C5aR1 axis available to aid the patient in dealing with infections.

Introduction

The introduction of complement inhibition into clinical practice has revolutionised the treatment of patients with complement mediated aHUS; C5 inhibition reduces the incidence of end stage renal disease (ESRD) and enables successful transplantation in those who have reached ESRD (1-4). As complement therapeutics evolve, targeted agents are progressing through pre-clinical and clinical trials. Refining complement inhibiting therapy has the potential advantages of easier administration, reducing the immunosuppressive burden and enabling wider access to medication through reduction in costs. Successfully adopting a refined treatment approach requires a detailed understanding of the pathogenesis. In aHUS, the importance of C5a or C5b-9 in driving complement mediated thrombotic microangiopathy (TMA, the histological process resulting in the clinical disease) remains to be fully elucidated. Current literature is conflicting; a mouse model engineered around a complement factor H (*CFH*) mutation found no benefit of C5aR1 deficiency upon renal TMA formation, whereas a model induced by antiphospholipid antibodies found the C5a-C5aR axis critical to disease development (5, 6). Thus, understanding the contributions of C5a-C5aR and C5b-9 on disease development may help guide future treatment strategies for both existing and novel drugs which target the complement system. Given the rarity of complement mediated aHUS coupled with the mortality and morbidity associated with treatment failure, pre-clinical models offer an invaluable translational insight and test bed to ascertain if there is a clinical rationale to justify change from the current gold standard of treatment. We used the C3^{D1115N} mouse model of complement mediated TMA (7), to determine the role of C5a-C5aR1 axis and C5b-9 upon disease.

Methods

Mice

B6-C3^{D1115N} mice were maintained in house and were genotyped as previously described (7). RRID:IMSR_JAX:006845 (*C5ar1^{tm1Cge}* or Balb/c-*C5aR1$^{-/-}$*) and RRID:MMRRC_042133-MU (C57BL/6N-C7$^{em1(IMPC)J}$/J or B6-C7$^{-/-}$) were purchased from the Jackson Laboratory (JAX Lab, Bar Harbour, Maine, USA) (8). B6-C3^{D1115N} were backcrossed for 4 generations onto either the Balb/c-C5aR1$^{-/-}$ or B6-C7$^{-/-}$ background, respectively. Resulting mice, heterozygous for C3^{D1115N}, were then intercrossed to produce the homozygous Balb/c-C3^{D1115N}.*C5aR1$^{-/-}$* and B6-C3^{D1115N}.C7$^{-/-}$ lines, respectively. Additionally, Balb/c-C3^{D1115N}.*C5aR1$^{-/-}$* mice were subsequently backcrossed onto wild type Balb/c to produce a Balb/c-C3^{D1115N}(.C5aR1$^{+/+}$) line. Genotyping for C5aR1 deficiency was performed by PCR following methods provided by the JAX lab (https://www.jax.org/Protocol?stockNumber=006845&protocolID=23815). Deletion of the C7 gene was monitored by PCR using Primer pairs 5'- ATG GCT CTT CCT CTC ATC TCC-3, 5'- CTG CAG CTC TCT GAA TGA AAG T-3, 30 cycles (annealing 64.8^{0}C), generating 415bp (WT) and 168bp (C7KO). A humanized C5aR1 receptor knock in mouse was generated by Cyagen Biosciences (under contract from Idorsia; B6.C5aR1$^{tm2(hC5aR1)Idor}$) and this was crossed onto the C3^{D1115N} background for 4 generations producing C3^{D1115N}.hC5aR1$^{+/+}$ mice. Power calculations were used to guide N in experiments at outset based on previous survival curves or variation in complement deposition in the kidney (7). All animal experiments were approved by the animal welfare and ethics review board (AWERB) of Newcastle University and the UK Home office under the auspices of animal procedure licences PD86B3678 and PP2560803. The ARRIVE reporting guidelines were used(9).

C5aR1 inhibition

We tested the ability of the oral C5aR1 antagonist ACT-1014-6470 (10) to protect mice from disease. Mice were placed on diet, ad libitum from weaning, containing ACT-1014-6470 (with estimated dosing being calculated to 45mg/day (i.e. 20g mouse eating ~ 3g of diet daily)) or a matched diet without the

drug for 8 weeks with daily health checks. Any mice reaching predefined clinical scores for renal disease or general welfare concerns were euthanised during the study, with the remaining culled at the end of the study where blood and tissue was harvested as described below.

Anti-C7 inhibition

Within 24 hours of weaning, $C3^{D1115N}.hC5aR^{+/+}$ homozygote animals were treated with either anti-C7 mAb (73D1 provided by Dr W Zelek) or $IgG_{2a,k}$ isotype control (cultured in sterile conditions in house from ECACC hybridoma 2:D12) (40mg/kg) via intraperitoneal injections every 7 days for 8 weeks. Mice underwent daily health checks, any mice breaching the predefined clinical scores for renal disease or general welfare were euthanised and tissue collected as above.

Mouse clinical monitoring and terminal blood analysis

Mice were monitored daily (weighing and urinalysis - Combistix™, Siemens) from weaning, reducing to weekly from 2 months of age, in the absence of detectable clinical disease. Mice reaching clinical end point, as defined by welfare constraints agreed with AWERB were euthanised and tissues harvested. Due to the restraints of clinical monitoring blinding was not practical in these experiments. Mice that remained clinically well were culled in aged cohorts at 3, 6 and 12 months of age. Where possible, blood was collected using cardiac puncture under terminal anaesthesia into pre-coated lithium heparin syringes (in many cases mice were found in crisis, with insufficient blood volume/hemodynamic pressure to allow blood draw during terminal cardiac puncture). Where available, possible, blood urea nitrogen (BUN) and Haemoglobin (Hb) measurements were obtained using an ISTAT analyser with a CHEM 8+ cartridge, following manufacturer's instructions (Abbott Laboratories LTD).

Flow cytometry for Reticulocyte and Platelet count

To measure reticulocyte or platelets, 10μl of heparinised blood was mixed with 1ml of PBS control or 1ml BD Reticulocyte agent (BD Retic-Count ™, BD Bioscience) for 30 minutes at room temperature or

to 400µl of FACS Flow buffer (PBS containing 5% w/v BSA, 1 mM EDTA, 0.1% w/v Na azide, plus 1ul purified Rat Anti-Mouse CD41 clone MWReg30 BD Bioscience) for one hour on ice, respectively. Platelet count was established using the method previously described (7). Samples were immediately analysed on a FACS symphony (BD Biosciences, Oxford, UK). An example of this analysis is shown in supplementary figure 1.

Histology analysis

Kidneys were harvested, fixed in 10% formalin then processed and embedded in paraffin. 4µM sections were then cut and stained for with Periodic Acid Schiff and Martius Scarlet Blue then imaged on an Olympus X microscope. Thrombotic microangiopathy is a histological pattern of injury with no current standardised scoring system within clinical practice to enable quantification of injury, therefore, kidney sections were reviewed, and TMA was ascribed to be present or absent.

Immunofluorescence

Methods for C3 and C9 staining are essentially as previously described (7), with minor modification. Briefly, kidneys embedded in OCT were frozen on dry ice. In addition to C3 and C9, fibrinogen was also analysed. After fixation, sections were, permeabilised with triton-X, and rabbit serum used as blocking serum for fibrinogen staining. For fibrinogen, slides were incubated with sheep anti-human fibrinogen 1:100, followed by rabbit anti-sheep Alexa 597 (Abcam, 1:200). Slides underwent repetitive washing in PBS and then imaged after being mounted in DAPI mounting medium. Fluorescence images were taken at x20 on Leica DM2000 LED using a Leica DFC 7000 T camera. Densitometry analysis of glomerular complement deposition was performed using image J. This is presented as mean glomerular intensity (average pixel intensity on the grey scale in this area). A minimum of 10 glomeruli were scored for each mouse.

Immunohistochemistry

For F4/80 (Macrophage) and Ly6-G (Neutrophil) staining, frozen sections were fixed in acetone then blocked in 3% hydrogen peroxide. After repetitive washing, sections were blocked in 20% normal goat

serum then incubated with recombinant rabbit anti-mouse F4/80 (Abcam, 1:100) or rat anti-mouse Ly6-G 9 (R&D systems, 1:50) followed by goat anti-rabbit HRP (Abcam, 1:200) or goat anti-rat HRP (Abcam,1:200) for Ly6-G. Following further washing, sections were incubated with DAB, counterstained with Meyers haemotoxylin and then dehydrated through graded alcohols and mounted in DPX. Images were then taken on an Olympus X microscope at x20 and analysed using a freely available macro plug-in for image J (Immunohistochemistry (IHC) Image Analysis Toolbox, open source available online).

Statistical analysis

All statistical analysis were undertaken using GraphPad prism v9.0. Mantel-Cox was used for survival analysis. For statistical test between two or more groups, a test of normality (Kolmogorov-Smirnov) was undertaken, and when met, an unpaired students T test was performed. If unmet, then a Mann-Whitney test used. Welch's correction was applied if two groups were not assumed to have the same SD. Two-way ANOVA with Tukey's multiple comparison test was used to establish significance between groups and across time. A P value <0.5 was taken as statistically significant. P values are identified as follow, ns = non-significant, * = p <0.05, ** = p<0.01, *** = p<0.005, **** = p<0.0001. Data is shown as Mean ±SEM.

Results

C7 deficiency prevents renal TMA in the B6-C3^{D1115N} animal model.

We have previously demonstrated that B6-C3^{D1115N} mice develop a spontaneous TMA associated with significant microangiopathic haemolytic anaemia (MAHA) culminating in the death of greater than 50% of animals within the first 10 weeks of life, which could be rescued via C5 deficiency (7). The work of the group of Song demonstrated that C6 and C9 were important for a renal TMA to develop while disrupting C5a - C5aR1 signalling had little effect (5). Therefore, we sought to corroborate the importance of the MAC in our B6-C3^{D1115N} model of complement mediated TMA through cross to a C7 deficient background. Over a period of 12 months, all 20 B6-C3^{D1115N}.C7$^{-/-}$ mice survived in contrast to a contemporaneous cohort of B6-C3^{D1115N} animals, where only 6 mice survived and only 2 out of 14 mice survived TMA free (figure 1). Post-mortem histology of kidney collected at various time points revealed no evidence of TMA in B6-C3^{D1115N}.C7$^{-/-}$ kidneys, compared to significant evidence of TMA in B6-C3^{D1115N} controls (with 4/6 surviving mice having evidence of TMA after histological examination at end point, figure 2). The data suggests C7 (and C5b-9) is essential for the development of a complement mediated TMA in this model.   Blood urea nitrogen (BUN), haemoglobin (Hb) levels, reticulocyte- and platelet counts were all comparable to heathy baseline controls in the C7 deficient C3^{D1115N} animals (figure 3) in keeping with no MAHA and the absence of TMA. Surviving B6-C3^{D1115N} with TMA (purple symbols) versus those without (blue symbols) had higher BUN on average, correlating with disease, although this was not reflected in the Hb levels. However, B6-C3^{D1115N} mice that required sacrifice (red symbols) uniformly had significantly worse kidney function and lower Hb than surviving B6-C3^{D1115N} (Figure 3). The fibrin deposition seen in TMA (5) is significantly reduced in the B6-C3^{D1115N}.C7$^{-/-}$ mice when compared to C3^{D1115N} controls (figure 4, B,D,F,H). However, levels of C3 glomerular deposition increase in the kidney of B6-C3^{D1115N}.C7$^{-/-}$ mice with age (figure 4, A, C,E,G,), but this is not accompanied with any evidence of

MAHA, haematuria, proteinuria or increased BUN levels(Figure 2 & 3). This finding is entirely consistent to that seen in aged matched C3^{D1115N} mice with a C5 deletion (supplementary figure 2). As expected, no evidence of MAC (C7 deposits, supplementary figure 3 C) were noted in the glomerulus of these mice. However, unexpectedly an increased expression of native C9, which may be aggregated or polymerised (see supplementary figure 3) was detected but given C9 can be detected in glomeruli of healthy 12 month old B6.C3^{WT}.C7$^{-/-}$ mice (Supplementary figure 3 I) the increased C9 staining is not overtly pathogenic.

C5aR1 deficiency reduces TMA development in a Balb/c-C3^{D1115N} model.

To investigate the role of the C5aR1-C5a axis in pathogenesis, we next crossed the mice to a C5aR1 deficient line on the Balb/c background (while not allowing for seamless comparison between the arms of this study, this was a choice of necessity at the time, recognising this is a study limitation). The Balb/c.C3^{D1115N} line that was generated as a strain specific control demonstrated spontaneous renal TMA, with MAHA, proving the transfer of the D1115N change in C3 to the Balb/c background would drive clinical disease irrespective of background genetic variation (see Supplementary figure 4).

Despite, Balb/c-C3^{D1115N}.C5aR1$^{-/-}$ mice showing a significant survival benefit (27 out of 34 survived) versus Balb/c-C3^{D1115N} animals, 4/34 animals in the ageing Balb/c-C3^{D1115N}.C5aR1$^{-/-}$ cohort died as a result of renal TMA (Figure 5 B I&II). The remaining 3 deaths had an alternative cause of death i.e. bad teeth or litter runt, they could not be attributed to renal disease as they had clear urinalysis and no histological evidence of disease. In an additional attempt to help explain the death of the remaining 3 animals, the Balb/c-C3^{D1115N}.C5aR1$^{-/-}$ underwent a further comprehensive histological review of brain, lung, heart, liver, spleen and bone marrow at Charles River research animal diagnostics but no significant pathology was identified (data not shown). Postmortem histological analysis of the Balb/c-C3^{D1115N}.C5aR1$^{-/-}$ surviving mice (at prescribed end point), showed 3/7 of the mice taken at the 6-month cull and a further 3/5 taken in the 12-month cull showed

histological evidence of TMA (figure 6 E-H). No mice (n =15) taken in the 3-month cull showed evidence of TMA.

Surviving Balb/c-C3^{D1115N}.C5aR1$^{-/-}$ show improved clinical parameters.

In the Balb/c-C3^{D1115N}.C5aR1$^{-/-}$ mice that remained clinically well until their allotted end point, we found no biochemical evidence of an impaired renal function as determined by normal BUN levels compared to age matched controls (Figure 7 A). Furthermore, haemoglobin levels, platelet- and reticulocyte counts were within normal limits (Figure 7, B-D). These results come with the caveat that in mice that succumbed to TMA and died acutely i.e. 4/34, no blood was available for real time analysis of renal function or MAHA parameters and so these results are inevitably skewed towards surviving mice. The fact that some mice with histological evidence of TMA (figure 6) had essentially normal levels of BUN may highlight that there has been renal recovery, and we are visualising a historical TMA injury, which is not affecting renal excretory function at our defined end point and only becomes evidence on post mortem review. Consequently, this suggests that removal of C5a-C5aR1 axis can attenuate the disease process.

C5aR1 deficiency reduces C9 and fibrin in Balb/c-C3^{D1115N} kidney.

The evidence that C5aR1 deficiency attenuates the disease process is further substantiated through the significant reduction in fibrin deposits in the glomeruli of Balb/c-C3^{D1115N}.C5aR1$^{-/-}$ mice (figure 8 C,F,I,L,O). Similar to what was observed in the B6-C3^{D1115N}.C7$^{-/-}$ mice, C3 glomerular deposits were increased in Balb/c-C3^{D1115N}.C5aR1$^{-/-}$ mice over time (Figure 8, A,D,G,J,M).

Pharmacological blockade of C5aR1 or C7 attenuates disease and provides a clear survival benefit.

To determine if pharmacological blockade of C5aR1 or an anti-C7 mAb attenuates the disease process (mitigating against the strain difference of the Balb/c.C5aR$^{-/-}$ mice thus allowing seamless comparison), we used an oral C5aR1 antagonist (ACT-1014-6470) (10) or a weekly intraperitoneal injection of an anti-C7 mAb (11). To use the oral C5aR1 agent, which is only active on the human receptor, humanized C5aR1 mice were generated in which mouse C5aR1 was replaced with human C5aR1. After intercross and generation of a new C3^{D1115N}.hC5aR1$^{+/+}$ double knock-in line, we carried out standard analysis to confirm that the phenotype remained unchanged in the C3^{D1115N}.hC5aR1$^{+/+}$ line. As expected, key features of a renal TMA were readily identified, validating the humanised model for therapeutic testing (figure 9, A-F).

Mice receiving the C5aR1 antagonist ACT-1014-6470 (~45mg/per day) after weaning (for 8 weeks via diet) showed 100% survival compared to only 35% survival for C3^{D1115N}.hC5aR1$^{+/+}$ mice on a normal diet (figure 9, A). However, there was evidence of renal disease (25ery/ul haem for at least 2 consecutive days) in 3 mice on the oral treatment (figure 9 B) with 6/12 animals exhibiting post-mortem histological evidence of TMA at the end of the study. Although there was histological evidence of a TMA the mice did not meet criteria necessitating euthanasia within the study duration. Indeed, only the 3 mice with renal disease detected by urine analysis showed a slight elevation in BUN levels in the treatment group (normal range 20 – 36 mg/dl, figure 9, G), reflecting improved renal function across the treatment cohort. When assessing markers of MAHA, normal parameters were observed in the mice receiving the C5aR1 antagonist, except for platelet numbers, which remained low in some of the treated animals (figure 9, H-J). The slightly elevated BUN and marginally lower platelets numbers in some treated mice compared to control may reflect the fact that we also found a spectrum of histological disease (figure 9 K-N). These findings are not surprising and mimic those seen in the Balb/c-C3^{D1115N}.C5aR1$^{-/-}$ strain where genetic knockout of C5aR1 did not prevent a TMA. Similarly, and as expected, 100% survival was achieved with anti-C7 mAb treatment compared to the isotype control

(figure 10 A). One mouse was removed from the treatment study for analysis due to post-mortem finding that the kidney was hydronephrotic. There was no evidence of haematuria in any other mice on anti-C7 mAb treatment. Whilst the isotype control conferred survival protection (figure 10 A; Supplemental figure 5), the rate of renal injury was similar across the studies, with all mice on isotype control demonstrating significant and sustained haematuria (figure 10 B). This was mirrored on histological analysis with 100% of the isotype control mice showing postmortem histological evidence of TMA, including glomeruli fibrin deposition with mesangiolysis, microaneurysm formation and intra-arterial thrombi (Figure 10, I, J). The anti-C7 mAb treatment resulted in lower BUN and higher haemoglobin levels compared to the isotype treated B6-C3^{D1115N}.hC5aR$^{+/+}$ (Figure 10 C &E). A clear difference in the reticulocyte count was observed between the anti-C7 mAb and isotype control groups (figure 10 D). However, despite some improvement in platelet counts these were still significantly lower than the WT control. Overall, anti-C7 mAb treatment improved the majority of haematological parameters. Analysis of MSB stained sections confirmed no evidence of TMA in 7/8 animals treated with anti-C7 mAb (Figure 10 G, H). One animal in the anti-C7 mAb therapy group was found to have glomerular sclerosis, although endpoint BUN was in the normal range.

Attenuation of inflammatory infiltration in the absence of C5aR1 or C7 in the C3^{D1115N} mice.

Our data to date has shown that the complement mediated TMA within the mice is initiated and driven by C5b-9; evidenced by the complete abolishment of clinical and histological disease in the B6-C3^{D1115N}.C7$^{-/-}$ cohorts. Renal TMA is associated with endothelial cell damage and immune cell infiltrates (12). To investigate for the presence of neutrophils and macrophages in the kidneys of both C7 and C5aR1 deficient animals, kidneys were stained with anti-Ly6-G (neutrophils) and anti-F4/80 (macrophages) (figure 11). In C7 deficient animals, inflammatory cell infiltrates were significantly reduced compared to B6-C3^{D1115N} mice and remained equivalent to negative control animals at each time point analysed (figure 11A-H). We see a similar reduction in staining of F4/80 and Ly6-G when examining the Balb/c-C3^{D1115N}.C5aR1$^{-/-}$ at 6 months of age (the time point when histological evidence of disease emerges on post-mortem review) (figure 11, I,J,M,N,L,P). However, at 12 months,

neutrophil infiltrate in a proportion of the Balb/c-C3^{D1115N}.C5aR1$^{-/-}$ mice is similar to that observed in Balb/c-C3^{D1115N} mice.

Discussion

The C3^{D1115N} mouse model of aHUS recapitulates the clinical phenotype both on the C57BL/6 (7) and Balb/c strain (supplementary figure 4), proving the D1115N change in C3 to be robust and reproducible in generating spontaneous complement mediated aHUS, independent of the influence of background genetic traits in these mouse strains (13). C7 deficiency protected C3^{D1115N} mice from developing a renal TMA and MAHA up to 12 months of age, with 0% disease penetrance compared to 85% in the B6-C3^{D1115N} mice. Therefore, we demonstrate C5b-9 to be central in initiating renal TMA *in vivo* under normal conditions and that C5a/C5aR1 amplifies the effects of C5b-9 (Figure 12). This is suggested by the observations that although *C5aR1* deficiency (removal of the C5a –C5aR axis) clearly attenuates disease, it does not totally abolish TMA. Despite the subtle reduction in the penetrance of histological disease observed in the Balbc-C3^{D1115N} (75% compared to 85% in the B6-C3^{D1115N} strain) which had no effect on overall mortality from TMA, we still identified histological disease in a proportion of the Balbc-C3^{D1115N}.C5aR$^{-/-}$. Pharmacological inhibition on the B6 background through either a C5aR1 antagonist or anti-C7 mAb further substantiated our genetic findings, particularly when suppression of renal disease (measured by active urinary sediment and histological injury) is also accounted for. The data herein also suggests that MAC driven inflammation is recruiting neutrophils in the absence of C5aR1 signalling, and this, over time, may contribute to TMA. We propose that whilst C5b-9 initiates disease, C5a mediated signalling amplifies these igniting effects, culminating in a positive feedforward loop, with potentiated complement activation and endothelial cell activation. By removing C5a signalling through the absence of C5aR1 there is a reduction in complement induced inflammation, reducing inflammatory infiltrate, which translates into an attenuated disease process within the kidney (figure 12).

Our findings share some similarities with a previously published mouse model of renal thrombotic microangiopathy, a factor H point mutation (W1206R, FH[R/R]) (5). In this model, C6 and C9 deficiency significantly improved survival and diminished renal TMA, suggesting C5b-9 contributed significantly to renal TMA. However, we did not see any significant proteinuria (beyond control levels) in the aging B6.C3[D1115N].C7^{-/-} mice, suggesting despite increasing levels of deposited C3, this was tolerated, which was not the case in the C6 deficient FH[R/R] mouse. Furthermore, the Song group found no survival benefit with C5aR1 gene deficiency in the FH[R/R] model, and that the renal TMA persisted (5). In addition to this, neither C6, C9, nor C5aR1 deficiency rescued the haemolytic anaemia or resolved the thrombocytopenia (although there was a variety of levels across mice). In both C3[D1115N] and FH[R/R] mice, there is markedly reduced complement regulation by FH at cell surfaces, consequently there is significant consumption of C3 (to 25% vs 50% of normal levels, respectively) and C5 (to 33% vs 52% of normal levels, respectively) (7,8), but it is important to highlight the significant difference in the FH[R/R] model to our C3[D1115N] model. The FH[R/R] mice develop widespread macrovascular thromboses in multiple organs, which is not typical of the clinical syndrome in man, and this may link to "non-canonical or non-complement" roles that FH is reported to play in coagulation (14) and in cell activation (via competition with FHR proteins(15)) that could be more significantly disrupted by a loss of function FH molecule. Interestingly, while C5aR1 deficiency rescued the macrovascular thromboses it did not resolve thrombocytopenia in FH[R/R] mice, which in all likelihood reflects MAC driven TMA in the kidney. The haemolytic anaemia in the C3[D1115N] mice is rescued through *C7* and *C5aR1* deficiency reflecting the restoration of health to the glomerular endothelium. The protective effects of *C5aR1* deficiency on the glomerular endothelium in C3[D1115N] mice mirror that seen in an alternative immune complex mouse model of TMA induced by antiphospholipid antibodies where deficiency improved pathological and clinical features of disease. *C5aR1* deficiency undoubtedly protects C3[D1115N] mice from renal TMA in a manner akin to the APL model. Another modifier we were unable to explore is the role of the C5L2 receptor. The specific role of this receptor remains controversial, but C5adesArg (less potent form of C5a) retains high affinity to it, so may exert some

effects (16). The C3a/C3aR axis can be both inflammatory and anti-inflammatory in renal tissue depending on the context of the injury (17) and with the potential increased C3 deposition in the C5aR1 deficient mice this may also provide some additional signalling that was not as pronounced in the FH[R/R] mice and is protective in our model. These changes may in sum provide an explanation for the difference between the FH[R/R] and C3[D1115N] models with respect to the effectiveness of deficient C5aR1 signalling in slowing disease progression.

Our genetic data demonstrates that whilst blockade of C7 prevents a TMA, a C5aR antagonist may ameliorate disease; this is clearly the case in C3[D1115N].hC5aR1^{+/+} mice receiving the C5aR1 antagonist orally from weaning. There was no statistical difference in BUN, haemoglobin, reticulocytes and platelets, i.e. no evidence of a MAHA was detected between the treated and WT control (figure 9 G-J), mirroring the protective effects of the *C5aR1* deficiency in younger mice. However, despite the survival advantage conferred by C5aR1 inhibition (i.e. 100% survival while on the drug) the pathological features of TMA could still be readily seen in 50% of mice on treatment. We have previously demonstrated in this model that some mice develop early features of TMA by day 7 post-partum (7) and in this study mice could only be treated from weaning (post-partum day 21-24). Thus, some of the features seen in these mice could be due to sub clinical damage prior to treatment however the development of TMA in the genetic knockout of C5aR1 indicates that blockade at this level is insufficient to prevent TMA. That ACT-1014-6470 treatment mirrored the effects of genetic knockdown of C5aR1 suggests effective target engagement, albeit in a model dependent on the membrane attack complex with only a minor amplifying effect of C5a after disease initiation. Consequently, as genetic deletion of C7 in this model, and C6, C9 in the FHR/R model (5), indicate that targeting MAC is superior to targeting C5aR1. Pharmacological inhibition with anti-C7 mAb consolidated this hypothesis and provides translational evidence that pharmacological inhibition of C7 may prove to be a more efficacious treatment for disease remission in man, given that there was a greater level of renal injury (evidenced through an active urinary sediment and histological evidence of disease) on oral C5aR1 blockade compared to anti-C7 mAb.

Notably, isotype control also had a therapeutic effect (Supplemental figure 5), possibly a mixture of plasma expansion and mild complement depletion, and inhibition of monocytes and macrophage activation, correlating with the previously described protective effects of IVIg (18). However, histological evidence of a TMA was identified in all mice receiving the isotype control.

From current literature, it is difficult to tease apart the specific individual roles of C5b-9 and C5a upon glomerular endothelial cell (EC) activation, given their individual capability to induce a pro thrombotic environment (19). C5a and C5b-9 can alter the thrombotic phenotype of the glomerular EC; triggering exocytosis of von Willebrand factor (vWF) and p-selectin from weibal palade bodies(20, 21), triggering the coagulation system through stimulating an increase in expression of tissue factor, which supports formation of the prothombinase complex further potentiating platelet aggregation and modifying vascular tone (22, 23). Further, C5b-9 induces expression of adhesion molecules and platelet activation factor (24) and C5a appears to reduce endothelial expression of thrombomodulin, increase vessel permeability and induce platelet-leucocyte aggregates (20). In addition to endothelial cell dysfunction, complement activation can also activate platelets. Activated platelets are, in turn, a source of complement. C5b-9 acts as a platelet agonist, releasing pro-coagulant particles and vWF with simultaneous translocation of p-selectin to the platelet surface (25-27). C5a potentiates the activation of platelets. This activated platelet surface provides a scaffold for initiation of the alternative pathway, which is further enhanced when properdin becomes bound (28). An alteration in the thrombotic phenotype of the EC coupled with activated platelets creates a hypercoaguable endothelial luminal environment, providing optimum conditions for a continuing renal TMA (see figure 12).

Removing C7 prevents the activation of EC from C5b-9, thus attenuating glomerular EC activation from hyperfunctional C3 in the C3^{D1115N} model of TMA. Binding of C7 to C5b6 forms a stable trimeric complex allowing it to become associated with the cell membrane (22). The addition of C8 to C5b-7 forms a tetrameric complex which promotes binding and polymerisation of C9, enabling it to induce its

cytolytic activity upon the cell. Both, Clusterin and protein S preferentially bind C7 to regulate C5b-9. Clusterin prevents the insertion of C5b-7 into the cell membrane, whereas protein S binds to C5b-7, inhibiting polymerisation of C9 (22). The lytic and sublytic effects upon ECs requires the complex to insert into the membrane to signal the cell, thus by preventing insertion through C7 deficiency the effects are thwarted. C7 is the central portion of C5b-9 and is an important limiting factor (29), given the success of C7 deletion in abolishing disease within our mouse model, makes C7 an attractive therapeutic target. Current C5 inhibition requires continuous intravenous therapy, with a high target concentration, thus large drug doses are required to achieve therapeutic effect (30). Targeting C7 could circumvent this whilst also enabling C5a to function in its physiological roles.

Limitations.

There is an obvious limitation when comparing two different strains of mice, i.e. B6.C3^{D1115N} and the Balb/c C3^{D1115N}, which was due to the available strains of mice i.e. difficulties transporting mice during the COVID-19 pandemic. However, we believe the therapeutic inhibition of targeting both C7 and C5aR1 on the same genetic background (i.e.B6-C3^{D1115N}.hC5aR$^{+/+}$) substantiates our genetic data. There is a smaller limitation in that the anti-C7 mAb study was run after completion of the C5aR1 antagonist study rather than contemporaneously due to operations constraints and it is possible, genetic or environmental modifiers may have changed between the studies despite mice being maintained in a heterozygous C3$^{+/N}$ background and in the same facility. Another intrinsic limitation is that fully reflective haematological analysis is dependent on mice being euthanised in a controlled manner at endpoint rather than succumbing to disease when researchers were not on site and therefore at certain points in the study, due to inaccessibility to the facilities (during the COVID pandemic), opportunities to collect the samples as we would have liked was not afforded to us. This will skew certain read outs towards normal when they would be expected to be more severely affected and limited the scope of analysis in certain cohorts.

In Summary

The C3^{D1115N} mouse model of aHUS faithfully recapitulates the clinical manifestations of complement mediated aHUS. Examination of *C7* and *C5aR1* deficiency over 12 months demonstrates that whilst loss of either is protective there is a clear added survival benefit with C7 deficiency across time, i.e. MAC is essential for generation of TMA while C5aR signalling provides a potentiating effect.

The data suggests C5b-9 in the kidney plays an essential role as the trigger and driver of pathogenesis upon activating of the complement system in the context of complement mediated aHUS.

This work offers key insights into disease mechanisms and as to future pharmacological targets in complement mediated aHUS. Future preclinical work will be required to establish if therapeutic

inhibition at more advanced stages of disease (where haematuria and proteinuria are established) will induce remission in mice prior to clinical trials.

Disclosure statement.

References

1. Legendre CM, Licht C, Muus P, Greenbaum LA, Babu S, Bedrosian C, et al. Terminal complement inhibitor eculizumab in atypical hemolytic-uremic syndrome. *N Engl J Med.* 2013;368(23):2169-81.

2. Rondeau E, Scully M, Ariceta G, Barbour T, Cataland S, Heyne N, et al. The long-acting C5 inhibitor, Ravulizumab, is effective and safe in adult patients with atypical hemolytic uremic syndrome naive to complement inhibitor treatment. *Kidney Int.* 2020;97(6):1287-96.

3. Glover EK, Smith-Jackson K, Brocklebank V, Wilson V, Walsh PR, Montgomery EK, et al. Assessing the Impact of Prophylactic Eculizumab on Renal Graft Survival in Atypical Hemolytic Uremic Syndrome. *Transplantation.* 2023;107(4):994-1003.

4. Brocklebank V, Walsh PR, Smith-Jackson K, Hallam TM, Marchbank KJ, Wilson V, et al. Atypical hemolytic uremic syndrome in the era of terminal complement inhibition: an observational cohort study. *Blood.* 2023;142(16):1371-86.

5. Ueda Y, Miwa T, Ito D, Kim H, Sato S, Gullipalli D, et al. Differential contribution of C5aR and C5b-9 pathways to renal thrombic microangiopathy and macrovascular thrombosis in mice carrying an atypical hemolytic syndrome-related factor H mutation. *Kidney Int.* 2019;96(1):67-79.

6. Seshan SV, Franzke CW, Redecha P, Monestier M, Mackman N, and Girardi G. Role of tissue factor in a mouse model of thrombotic microangiopathy induced by antiphospholipid antibodies. *Blood.* 2009;114(8):1675-83.

7. Smith-Jackson K, Yang Y, Denton H, Pappworth IY, Cooke K, Barlow PN, et al. Hyperfunctional complement C3 promotes C5-dependent atypical hemolytic uremic syndrome in mice. *J Clin Invest.* 2019;129(3):1061-75.

8. Hopken UE, Lu B, Gerard NP, and Gerard C. The C5a chemoattractant receptor mediates mucosal defence to infection. *Nature.* 1996;383(6595):86-9.

9. Percie du Sert N, Ahluwalia A, Alam S, Avey MT, Baker M, Browne WJ, et al. Reporting animal research: Explanation and elaboration for the ARRIVE guidelines 2.0. *PLoS Biol.* 2020;18(7):e3000411.

10. Ort M, Dingemanse J, Hsin CH, Richard M, Huehn E, Sabattini G, et al. First-in-human study with ACT-1014-6470, a novel oral complement factor 5a receptor 1 (C5aR1) antagonist, supported by pharmacokinetic predictions from animals to patients. *Basic Clin Pharmacol Toxicol.* 2022;131(2):114-28.

11. Zelek WM, and Morgan BP. Monoclonal Antibodies Capable of Inhibiting Complement Downstream of C5 in Multiple Species. *Frontiers in Immunology.* 2020;11.

12. Genest DS, Patriquin CJ, Licht C, John R, and Reich HN. Renal Thrombotic Microangiopathy: A Review. *Am J Kidney Dis.* 2023;81(5):591-605.

13. Rabe M, and Schaefer F. Non-Transgenic Mouse Models of Kidney Disease. *Nephron.* 2016;133(1):53-61.

14. Heurich M, and McCluskey G. Complement and coagulation crosstalk - Factor H in the spotlight. *Immunobiology.* 2023;228(6):152707.

15. Kopp A, Hebecker M, Svobodová E, and Józsi M. Factor h: a complement regulator in health and disease, and a mediator of cellular interactions. *Biomolecules.* 2012;2(1):46-75.
16. Scola AM, Higginbottom A, Partridge LJ, Reid RC, Woodruff T, Taylor SM, et al. The role of the N-terminal domain of the complement fragment receptor C5L2 in ligand binding. *J Biol Chem.* 2007;282(6):3664-71.
17. Gao S, Cui Z, and Zhao MH. The Complement C3a and C3a Receptor Pathway in Kidney Diseases. *Front Immunol.* 2020;11:1875.
18. Jefferson JA, Suga SI, Kim YG, Pippin J, Gordon KL, Johnson RJ, et al. Intravenous immunoglobulin protects against experimental thrombotic microangiopathy. *Kidney Int.* 2001;60(3):1018-25.
19. Schmidt CQ, Schrezenmeier H, and Kavanagh D. Complement and the prothrombotic state. *Blood.* 2022;139(13):1954-72.
20. Noris M, and Remuzzi G. Terminal complement effectors in atypical hemolytic uremic syndrome: C5a, C5b-9, or a bit of both? *Kidney Int.* 2019;96(1):13-5.
21. Noris M, and Galbusera M. The complement alternative pathway and hemostasis. *Immunol Rev.* 2023;313(1):139-61.
22. Woodruff TM, Nandakumar KS, and Tedesco F. Inhibiting the C5-C5a receptor axis. *Mol Immunol.* 2011;48(14):1631-42.
23. Ikeda K, Nagasawa K, Horiuchi T, Tsuru T, Nishizaka H, and Niho Y. C5a induces tissue factor activity on endothelial cells. *Thromb Haemost.* 1997;77(2):394-8.
24. Hamilton KK, Hattori R, Esmon CT, and Sims PJ. Complement proteins C5b-9 induce vesiculation of the endothelial plasma membrane and expose catalytic surface for assembly of the prothrombinase enzyme complex. *J Biol Chem.* 1990;265(7):3809-14.
25. Polley MJ, and Nachman RL. Human platelet activation by C3a and C3a des-arg. *J Exp Med.* 1983;158(2):603-15.
26. Polley MJ, and Nachman R. The human complement system in thrombin-mediated platelet function. *J Exp Med.* 1978;147(6):1713-26.
27. Hattori R, Hamilton KK, McEver RP, and Sims PJ. Complement proteins C5b-9 induce secretion of high molecular weight multimers of endothelial von Willebrand factor and translocation of granule membrane protein GMP-140 to the cell surface. *J Biol Chem.* 1989;264(15):9053-60.
28. Saggu G, Cortes C, Emch HN, Ramirez G, Worth RG, and Ferreira VP. Identification of a novel mode of complement activation on stimulated platelets mediated by properdin and C3(H2O). *J Immunol.* 2013;190(12):6457-67.
29. Wurzner R. Modulation of complement membrane attack by local C7 synthesis. *Clin Exp Immunol.* 2000;121(1):8-10.
30. Lekova E, Zelek WM, Gower D, Spitzfaden C, Osuch IH, John-Morris E, et al. Discovery of functionally distinct anti-C7 monoclonal antibodies and stratification of anti-nicotinic AChR positive Myasthenia Gravis patients. *Frontiers in Immunology.* 2022;13.

Acknowledgement

Data sharing statement.

All data are presented in the article. There are no genetic, proteomic, or transcriptomic data and no specific codes or algorithms, etc., in this article.

Authorship Contributions

KJM & KSJ conceived, carried out, wrote, edited and funded the study. PW developed the reticulocyte and platelet count assays and assisted with data collection, IYP, GT, CC and BG collected data, and edited the manuscript. WZ provided the anti-C7 mAb and edited the manuscript. TH, MMM and MJM provided C5aR antagonist and hC5aR animals and edited the manuscript. DK provided supervision, critical analysis and edited the manuscript.

Legends

Figure 1- 100% survival free from renal TMA in the B6.C3^{D1115N}.C7$^{-/-}$

B6.C3^{D1115N}.C7$^{-/-}$ animals were monitored for renal disease (proteinuria/haematuria) from post-partum d15 until they reached 3 (n=7), 6 (n=6) and 12 (n=7) months of age. No animals succumbed to disease and no TMA was detected on histological examination, as per B6-C7-/- control animals at 3 (n=3), 6 (n=4) and 12 (n=6) months of age. However, 8 out of 14 B6.C3^{D1115N} animals succumbed to TMA during the study and a further 4 were found to have TMA on histological analysis at end point (denoted by the sharp drop in 'survival free from TMA' at one year). Mantel-Cox test was used to establish significance. **** $p<0.0001$.

Figure 2- C7 deficiency prevents renal thrombotic microangiopathy in the B6-C3^{D1115N} mice.

Representative Periodic-Acid-Shiff stained (A,C,E,G) and Martius scarlet blue stained sections (B,D,F,H) of B6-C3^{D1115N} and B6-C3^{D1115N} C7 $^{-/-}$ at 3, 6 and 12 months of age. B6-C3^{D1115N} animals (~2 month) (A) show segmental sclerosis (as indicated by *), mesangiolysis (as indicated by arrow) (B) and glomerular fibrin deposition (indicated by * and arrow); collectively these are features of TMA. Normal glomeruli seen in the B6-C3^{D1115N}.C7$^{-/-}$ at 3 months (C, D), 6 months (E, F), and 12 months (G, H) of age. (I, J) are representative images of B6-C3^{WT}.C7$^{-/-}$ 12 months of age showing normal glomeruli.

Figure 3- C7 deficiency protects against renal injury and MAHA

Where available, mouse blood was analysed via iSTAT and flow cytometry, see methods. Lower BUN levels and corrected haemoglobin were seen in the B6-C3^{D1115N}.C7$^{-/-}$ cohorts when compared to the B6-C3$^{D1115N.}$ controls. The control group is further sub-divided by symbol colour – red = culled due to health concerns in study, purple = survived to 1 year but had TMA on histological analysis while blue = mice that survived and did not have evidence of TMA **(A-B).** Normalisation of reticulocyte was

achieved through C7$^{-/-}$ deficiency in the 3 & 6 -month cohort and data from the one available sample suggest this remains the case at 12 months **(C)**. Resolution of thrombocytopenia was observed in the B6-C3^{D1115N}.C7$^{-/-}$ when compared to the B6-C3^{D1115N} **(D).** Two-way ANOVA with Tukey's multiple comparison test was used to establish significance between groups of mice and across time. Only significant results between the multiple comparison are shown, with * = p <0.05, ** = p<0.01, *** = p<0.005, **** = p<0.0001. Values from individual mice are represented by dots, with Mean ± SEM illustrated.

Figure 4- C7 deficiency and the glomerular complement burden in the B6.C3^{D1115N} mice

Representative immunofluorescence images of C3 (A,C,E,G) and fibrin (B,D,F,H) deposition in the B6-C3^{D1115N} and B6-C3^{D1115N}.C7$^{-/-}$ mice taken on a Leica DM200 at 20x magnification. The exposure time was kept constant for the individual fluorophores. (I, J) Images were saved as LIF files then opened as 8 BIT images in image J and the region of interest (glomerulus) was demarcated, then mean glomerular intensity for this area was calculated within the software. Values from individual glomeruli are represented by dots, with Mean ± SEM illustrated. Two-way ANOVA with Tukey's multiple comparison test was used to establish significance between groups and across time. Only significant results between the multiple comparison are illustrated, with ** = p<0.01, *** = p<0.005, **** = p<0.0001.

Figure 5- Survival free from TMA is considerably improved on the Balb/c-C3^{D1115N}.C5aR1$^{-/-}$ background

(A) 7 animals in the Balb/c-C3^{D1115N}.C5aR1$^{-/-}$ cohort (n=34) were euthanised due to health concerns and histological evidence of TMA was identified in 4 of the animals. 13 of the Balb/c-C3^{D1115N} mice succumbed to TMA out of 24. (B) I & II, MSB stains of two of the BALB/c-C3^{D1115N} mice that were culled

due to health concern and found to have TMA on histological analysis. Mantel-Cox test was used to establish significance. ***, p<0.005; ****, p<0.0001.

Figure 6. Renal limited TMA detected in ageing Balb/c-C3^{D1115N}.C5aR1 $^{-/-}$.

Balb/c.C3^{D1115N}.C5aR1$^{-/-}$ were clinically monitored from post-partum d15 and culled in 3 (n= 15), 6 (n=7) and 12 month (n=5) cohorts. (A) & (B) Representative images of Balb/c-C3^{D1115N} (2-3 month old) showing histological features of TMA. Post-mortem histological evidence of TMA was detected in Balb/c-C3^{D1115N}.C5aR1$^{-/-}$ mice in the 6 (n= 3/7) and 12 (n= 3/5) month cohorts evidenced through PAS and MSB stained sections (E, F, G, H). In (E), * shows mesangiolysis, (F) * Illustrates fibrin deposition, (G) * shows microaneurysm formation and (H) the arrow is highlighting the thrombus. (I, J) are representative images of Balb/c-C3^{WT}.C5aR1$^{-/-}$ at 12 months of age showing normal glomeruli. Light microscopy images were taken on the Olympus SC 50 at 20x magnification. Images were then exported as TIFF files.

Figure 7. TMA is not detectable on clinical parameters.

Lower BUN levels and corrected haemoglobin were seen in the Balb/c-C3^{D1115N}.C5aR1$^{-/-}$ cohorts when compared to the Balb/c-C3^{D1115N} controls **(A, B)**. Resolution of thrombocytopenia was observed in Balb/c-C3^{D1115N}.C5aR1$^{-/-}$ when compared to the Balb/c-C3^{D1115N} **(C)**. Normalisation of reticulocyte count was achieved through C5aR1 deficiency **(D)**. Insufficient blood was available from the Balb/c-C3^{D1115N}.C5aR1$^{-/-}$ that succumbed to TMA to obtain measurements in these animals. Two-way ANOVA with Tukey's multiple comparison test was used to establish significance between groups and across time. Only significant results between the multiple comparison are illustrated, with * = p <0.05, ** = p<0.01, *** = p<0.005, **** = p<0.0001.

Figure 8. Attenuation of glomerular complement deposition in the Balb/c-C3^{D1115N}.C5aR1$^{-/-}$

An initial reduction in glomerular C3 is observed in the Balb/c-C3^{D1115N}.C5aR1$^{-/-}$ 3 month cohort (A,D,M), with no change compared to controls at 6 months (A,G,M), followed by an increase in glomerular C3 deposition at 12 months of age (A,J,M). Glomerular C9 deposition is reduced in all aged cohorts of the Balb/c-C3^{D1115N}.C5aR1$^{-/-}$ animals (B,E,H,K,N). Similarly, glomerular fibrin deposition is reduced in all aged cohorts of the Balb/c.C3^{D1115N}.C5aR1$^{-/-}$ animals (C,F,I,L,O). A minimum number of 10 glomeruli were scored from each mouse. Immunofluorescence images were taken on the Leica DM200 at 20x magnification at room temperature using FITC (C3), Alexa 546 (C9) & Alexa 594 for fibrin. The exposure time was kept constant for the individual fluorophores. Images were saved as LIF files then opened as 8 BIT images in image J. Region of interest (glomerulus) was demarcated then the mean glomerular intensity for this area calculated by the software. (**M-O**). Two-way ANOVA with Tukey's multiple comparison test was used to establish significance between groups and across time. Only significant results between the multiple comparison are illustrated, with * = p <0.05, ** = p<0.01, *** = p<0.005, **** = p<0.0001.

Figure 9. Oral C5aR1 inhibition in B6-C3^{D1115N}.hC5aR1$^{+/+}$ mice provides a clear survival benefit and prevents development of clinical disease.

(A). Survival analysis shows B6-C3^{D1115N}.hC5aR1$^{+/+}$ mice succumb to a spontaneous renal TMA in a similar fashion to the B6-C3^{D1115N} parent strain – confirming full function of the hC5aR1 knock-in gene. The data also demonstrates that early therapeutic treatment of B6-C3^{D1115N}.hC5aR1$^{+/+}$ mice with ACT-1014-6470 (C5aR1 inhibitor) via diet is highly effective. (B) Oral hC5aR1 antagonism does not completely prevent renal disease in the mice, i.e. at least two consecutive days 25ery/ul of haematuria

was detected in 3 mice, an indication of renal TMA and an additional 3 mice were found to have renal TMA on histological analysis after cull. Mantel-Cox was used to establish significance. (C,D,E) PAS stained sections showing histological features of TMA (*including double contouring and mesangiolysis) of C3^{D1115N}.hC5aR1 confirming the phenotype following the introduction of the hC5aR1. (F). MSB stain showing fibrin clot in a vessel in the C3^{D1115N}.hC5aR1$^{+/+}$ mouse. N=4 examined. (G). Blood urea nitrogen (plasma marker of kidney impairment) levels collected during terminal bleeds at the end of the study. (H) Mice receiving the C5aR inhibitor have higher levels of haemoglobin compared to untreated controls. (I). Reduced reticulocytosis in treated mice. (J). Improved platelet counts in treated mice. Two-way ANOVA was used for statistical analysis in Graphpad. Data shown as mean ± SEM. Only significant results between the multiple comparison are illustrated, * p <0.05, ** p<0.01, *** p<0.005, **** p<0.0001. Note that as around 50% of B6.C3^{D1115N}.hC5aR$^{+/+}$ died before we were able to collect blood the data in F thru I is skewed to surviving mice, indeed 2 mice show little or no evidence of disease at endpoint. (K-N), Histological analysis of C3^{D1115N}.hC5aR1$^{+/+}$ after 8 weeks of C5aR1 antagonist containing diet. Stained sections showing varied histology in the mice who received the C5aR1 inhibitor treatment, TMA was identified in 6/12 mice treated with a range of TMA. i.e. (K) Thrombi, (L) mesangiolysis/double contouring, (M) mesangiolysis and (N) fibrin deposits.

Figure 10. Prophylactic use of an anti-C7 mAb ameliorates disease in B6-C3^{D1115N}.hC5aR1$^{+/+}$ mice.

(A). Prophylactic treatment of B6-C3^{D1115N}.hC5aR1$^{+/+}$ mice with anti-C7 (7) via weekly I.P. injection from weaning confers 100% protection from disease. The isotype control is also protective (See supplementary figure 4), although (B) does not completely prevent renal TMA (2 or more consecutive days of 25ery/ul haematuria) in the mice. Mantel-Cox was used to establish significance. (C). Blood urea nitrogen levels collected during terminal bleeds at the end of the study. (D) Reduced reticulocytosis in treated mice. (E) Haemoglobin levels in treated animals are not significantly different to WT mice. (F) Improved platelet counts in treated mice. (C, D, F) Two-way ANOVA with Welch's

correction or (E) Kruskal-Wallis was used for statistical analysis using Graphpad. Data shown as mean ± SEM. Only significant results between the multiple comparison are illustrated, * p <0.05, ** p<0.01, *** p<0.005, **** p<0.0001. Note, that one anti-C7 mAb treated B6.C3^{D1115N}.hC5aR$^{+/+}$ was removed from analysis in B-F due to a hydronephrotic kidney and one isotype control mouse was found dead. (G-J), Histological analysis of C3^{D1115N}.hC5aR1$^{+/+}$ after 8 weeks of anti-C7 mAb therapy. no evidence of TMA in 7/8 animals treated with anti-C7 treatment using MSB Staining, representative glomeruli from two different mice treated with the anti-C7 mAb are shown with normal glomeruli (G, H). All isotype control mice showed histological evidence of ongoing TMA including glomeruli fibrin deposition with mesangiolysis and microaneurysm formation (I) as well as an intra-arterial thrombi (J).

Figure 11. Attenuation of inflammatory infiltration in the absence of C5a or C7 in the C3^{D1115N} mice.

Positive F4/80 and Ly6-G staining is seen in both the B6-C3^{D1115N} (A, E), and Balb/c-C3^{D1115N} (I, M) mice. Reduced F4/80 and Ly6-G staining is seen in both the B6-C3$^{D1115N.}$C7$^{-/-}$ (B, F) and the Balb/c-C3$^{D1115N.}$ C5aR1$^{-/-}$ at 6 months (J,N) or 12 months, with the exception of Neutrophils in the Balb/c-C3$^{D1115N.}$ C5aR1$^{-/-}$ mice (O,P), where some mice showed similar infiltrate to the Balb/c-C3^{D1115N} mice. No difference in staining was noted when deficient mice were compared to their wild type controls - B6-C3$^{wt.}$C7$^{-/-}$ (D,H) and Balb/c-C3$^{WT.}$C5aR1$^{-/-}$ (L,P). Light microscopy images were taken on the Olympus SC 50 at 20x magnification. Images were then exported as TIFF files. Two-way ANOVA with Tukey's multiple comparison test was used to establish significance between groups and across time. Only significant results between the multiple comparison are illustrated, with * = p <0.05, ** = p<0.01, *** = p<0.005, **** = p<0.0001.

Figure 12. Proposed mechanisms for C5b-9 driven TMA.

C5b-9 ignites a series of events that leads to activation of the endothelial cells and platelets culminating in the pathological process of TMA. C5a amplifies the effects of C5b-9 leading to a feedforward mechanisms of ongoing complement activation, endothelial cell activation and platelet activation and aggregation. C5b-9 leads to the endothelial expression of tissue factor which activates the extrinsic pathway. An increase in pro-thrombinase activity leads to the increased generation of thrombin which can then independently cleave C5 leading to further terminal pathway activation. Exocytosis of P-selectin and vWF factor onto the endothelial cell surface leads to platelet activation and captures circulating vWF creating an adhesive scaffold upon the endothelial cell surface. Expression of platelet activating factor, transforms resting platelets to activated platelets, which then leads to platelet leucocyte aggregates. Expression of ICAM-1 and E-selectin in unison with TNF-alpha recruits inflammatory cells which C5a then amplifies, leading to additional activated neutrophils. C5b-9 leads to p-selectin translocation onto the platelet surface which provides a surface for ongoing AP activity and the release of C3, FB and properdin which then provides a further source for ongoing complement activation. The release of prothrombotic microparticles, C5a and C5b-9 release from platelets then amplifies the ongoing vicious cycle. All these events culminate in activated platelets encountering a primed prothrombotic endothelial cell surface, resulting in a TMA.

Figure 1

Figure 2

B6-C3^D1115N

B6-C3^D1115N . C7^-/-
3 months

B6-C3^D1115N . C7^-/-
6 months

B6-C3^D1115N . C7^-/-
12 months

B6-C3^wt . C7^-/-
12 months

Figure 3

Figure 4

Anti C3

Anti Fibrin

B6-C3^{D1115N}

**B6-C3^{D1115N}.C7^{-/-}
3 months**

**B6-C3^{D1115N}.C7^{-/-}
6 months**

**B6-C3^{D1115N}.C7^{-/-}
12 months**

Figure 5

Figure 6

Balb/c-C3^{D1115N}

Balb/c-C3^{D1115N}. C5aR1 $^{-/-}$
3 months

Balb/c-C3^{D1115N}. C5aR1 $^{-/-}$
6 months

Balb/c-C3^{D1115N}. C5aR1 $^{-/-}$
12 months

Balb/c-C3^{wt}. C5aR1 $^{-/-}$
12 months
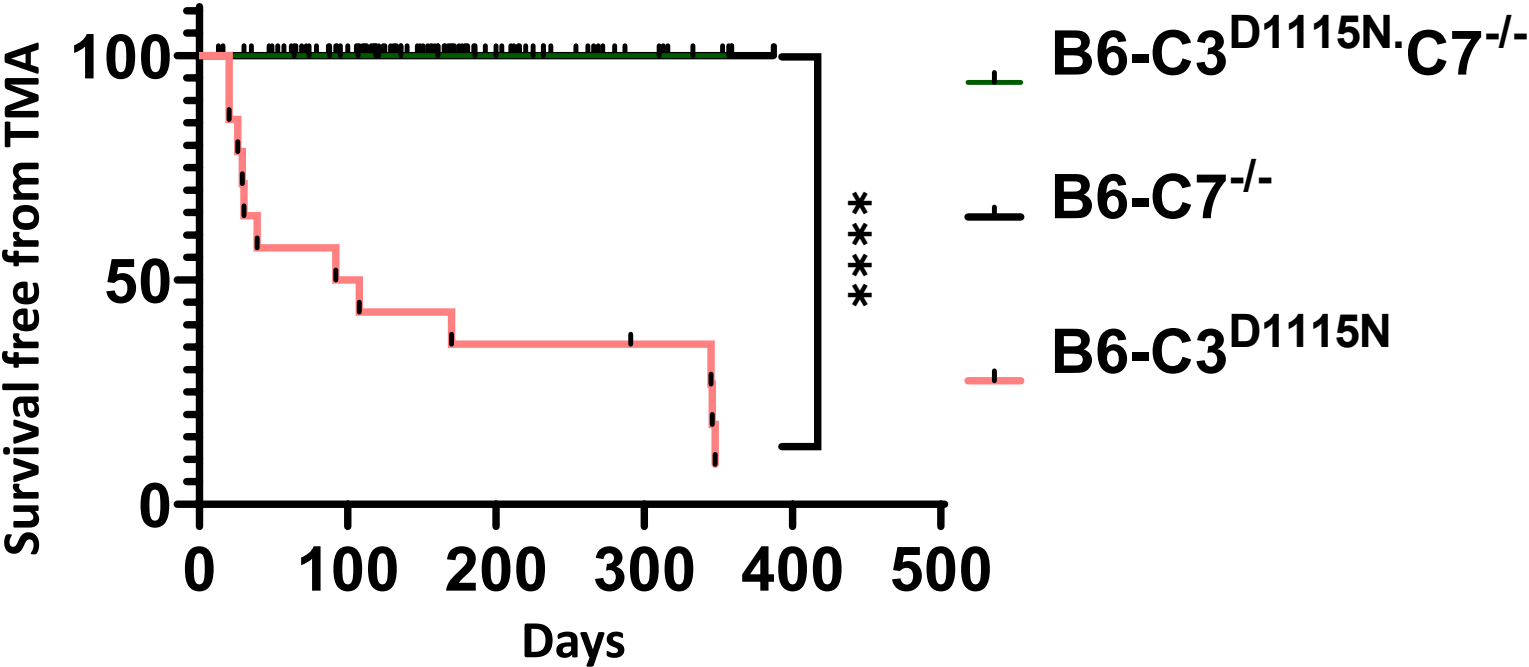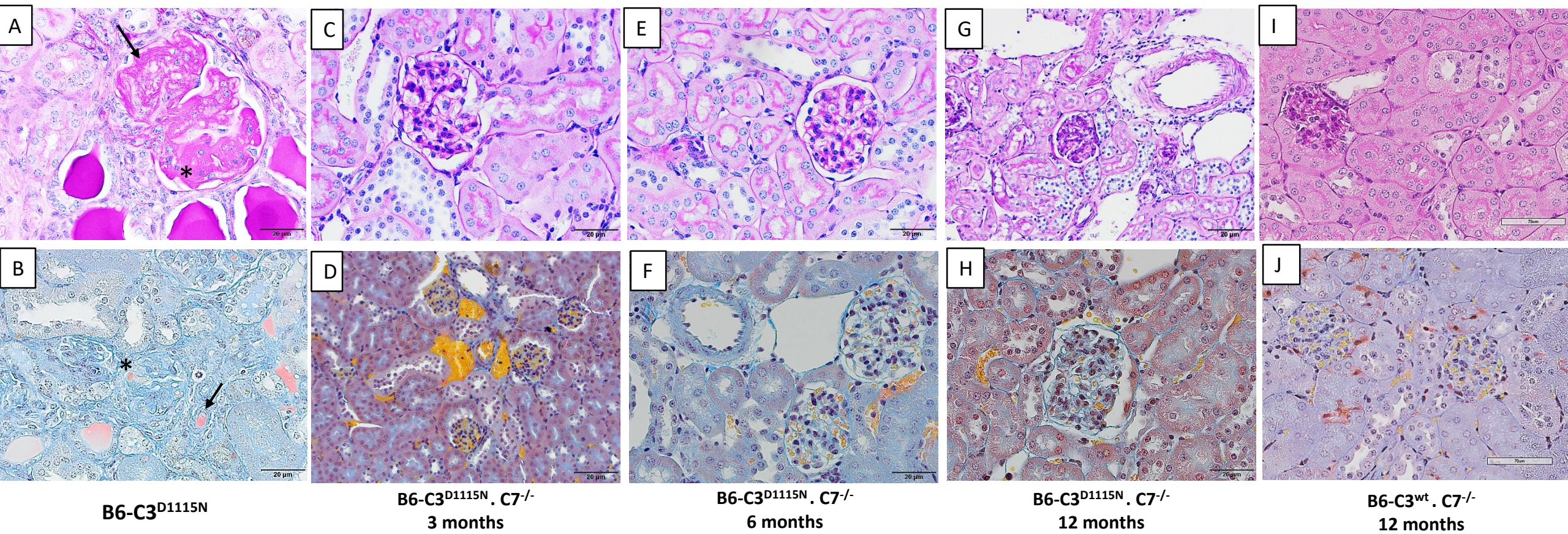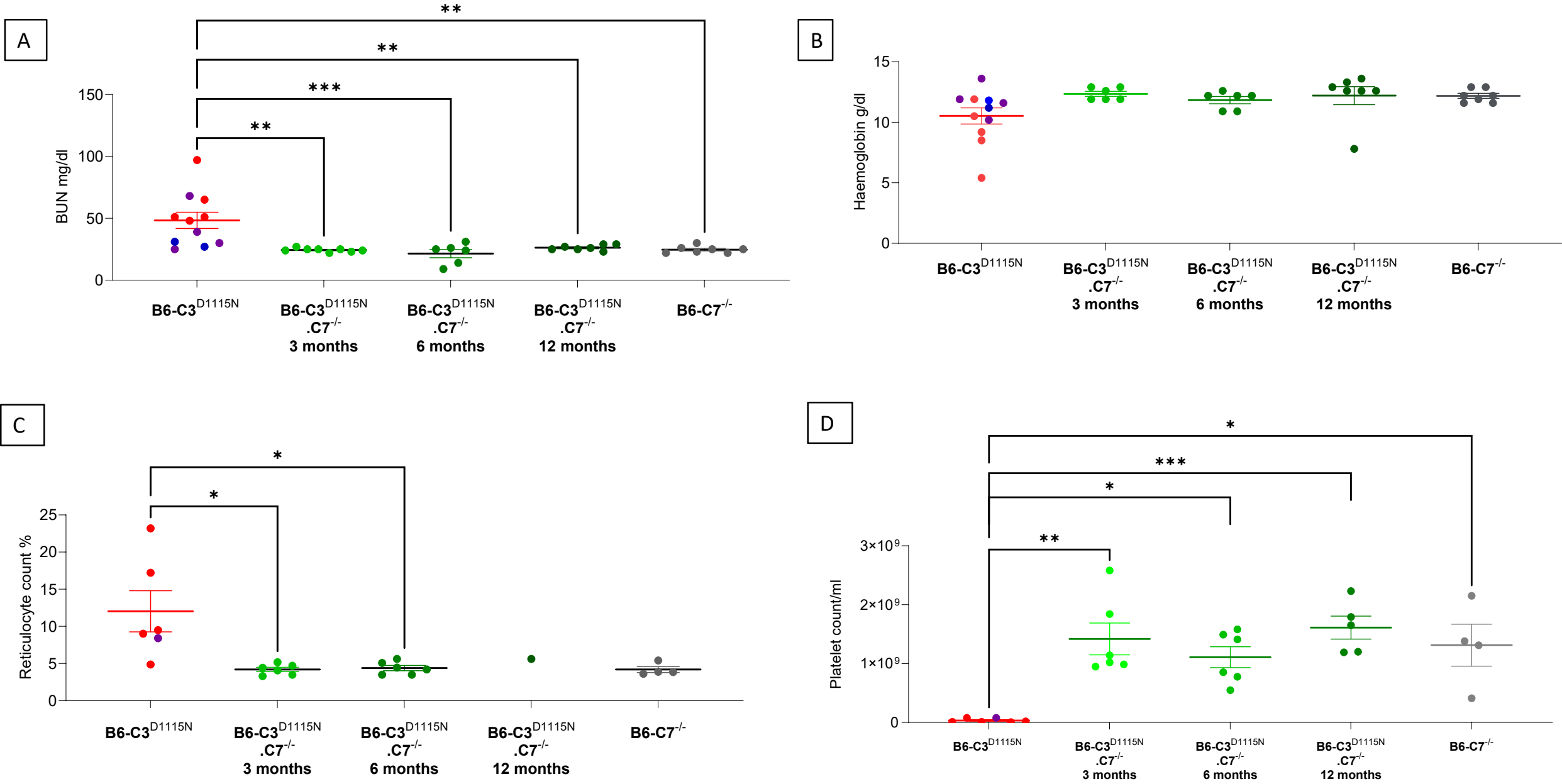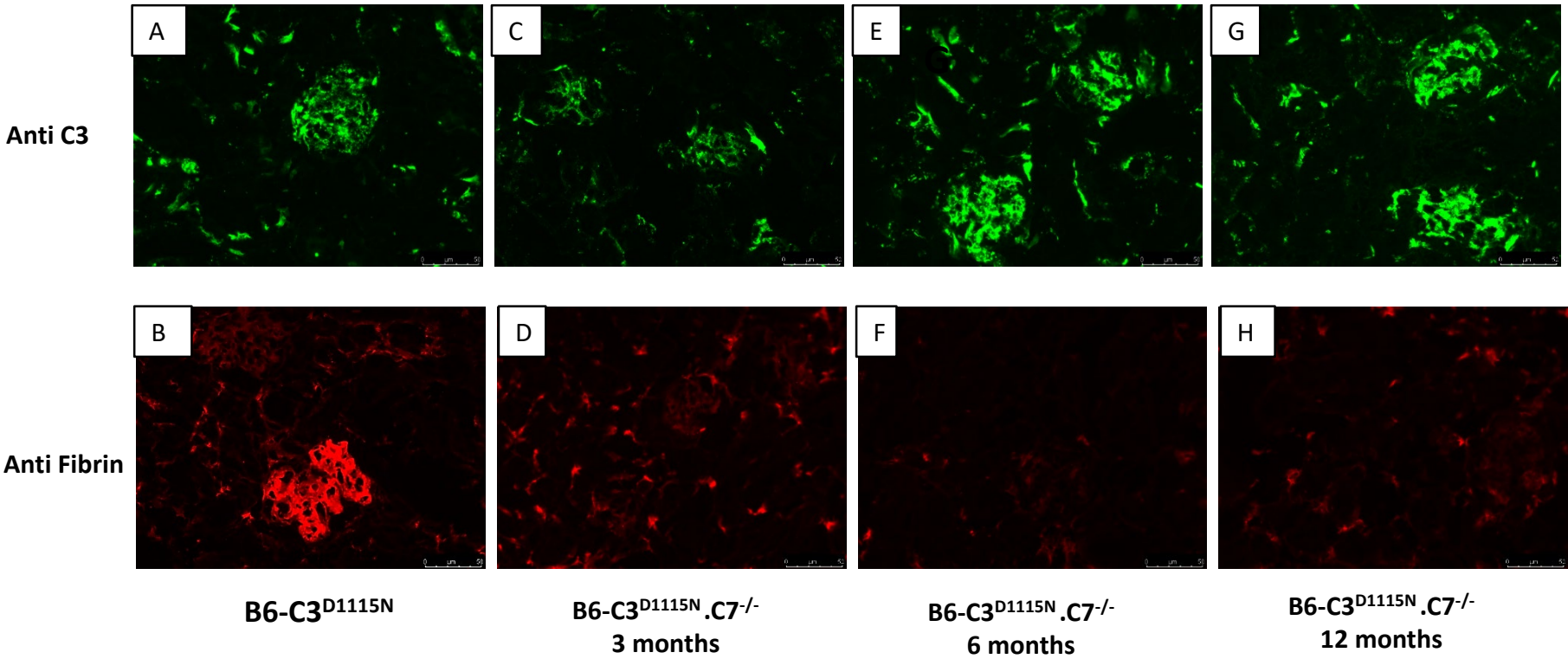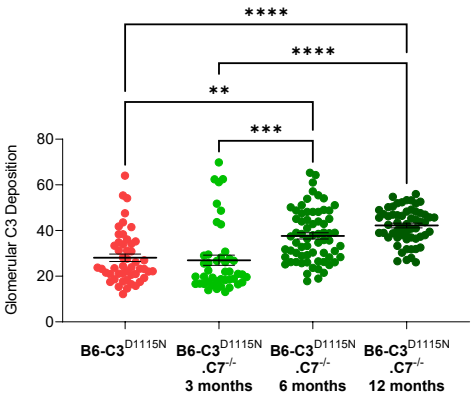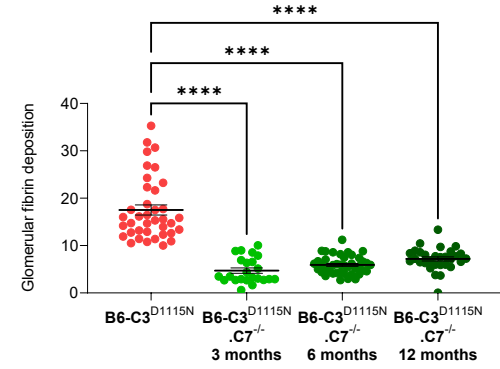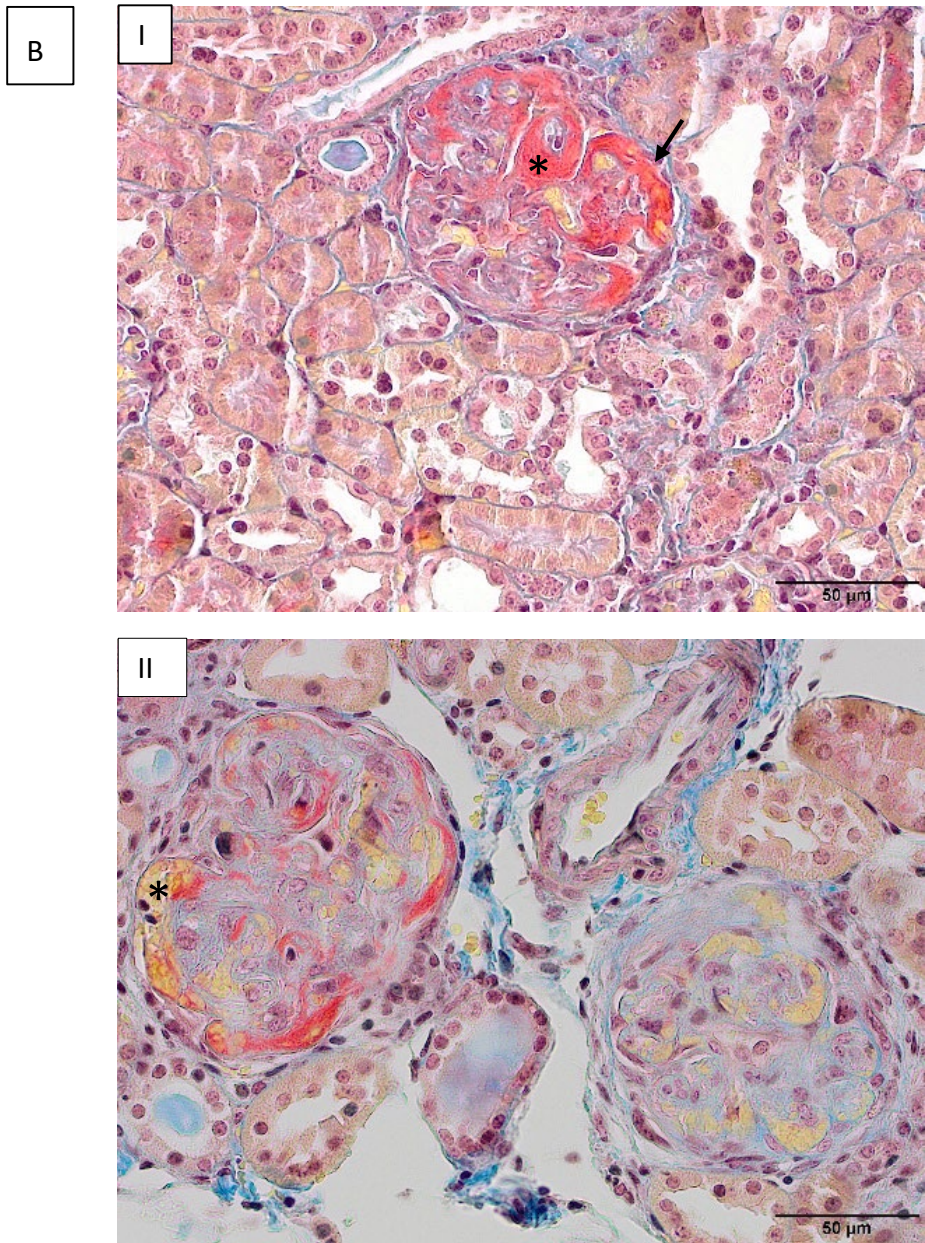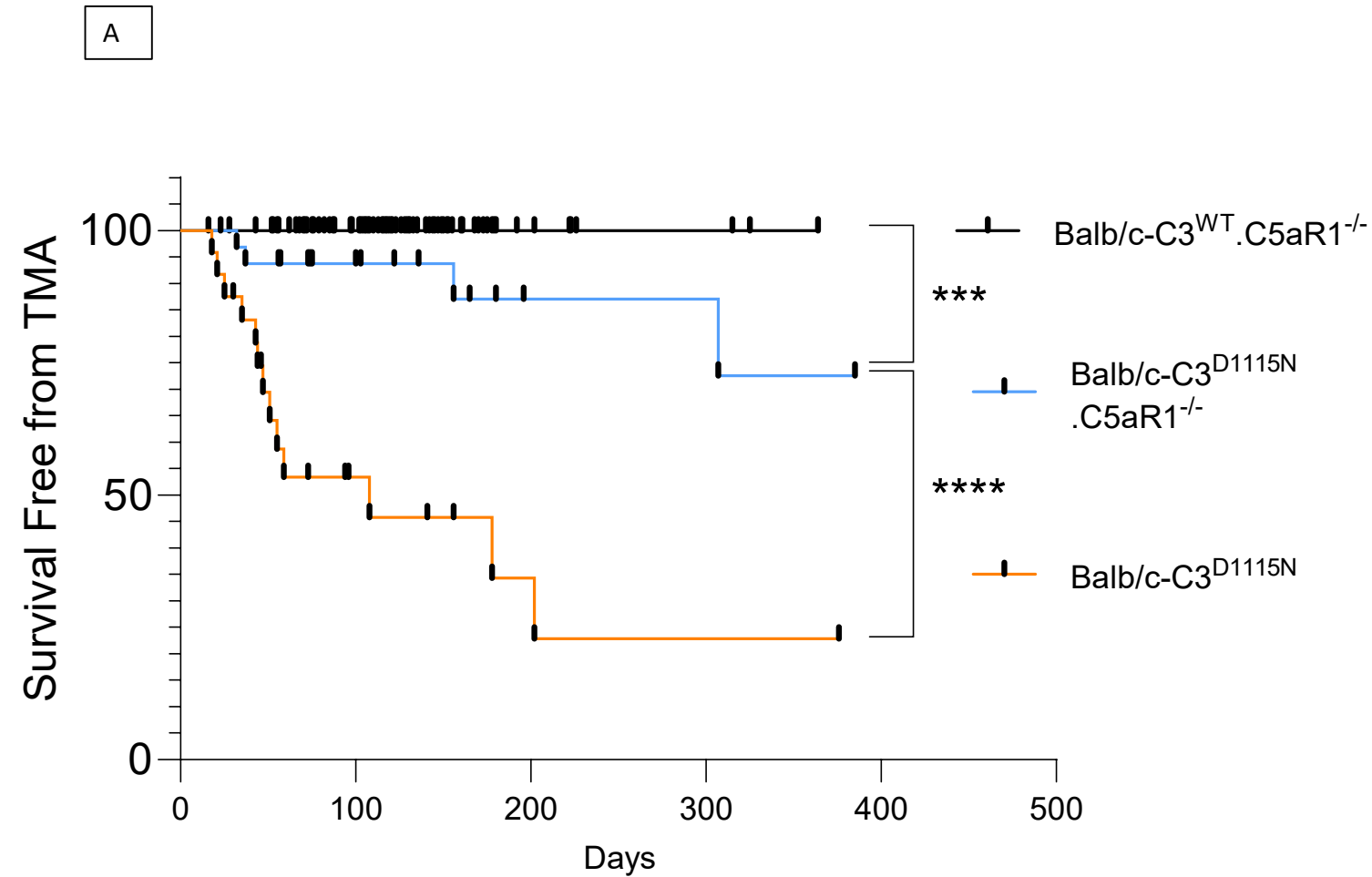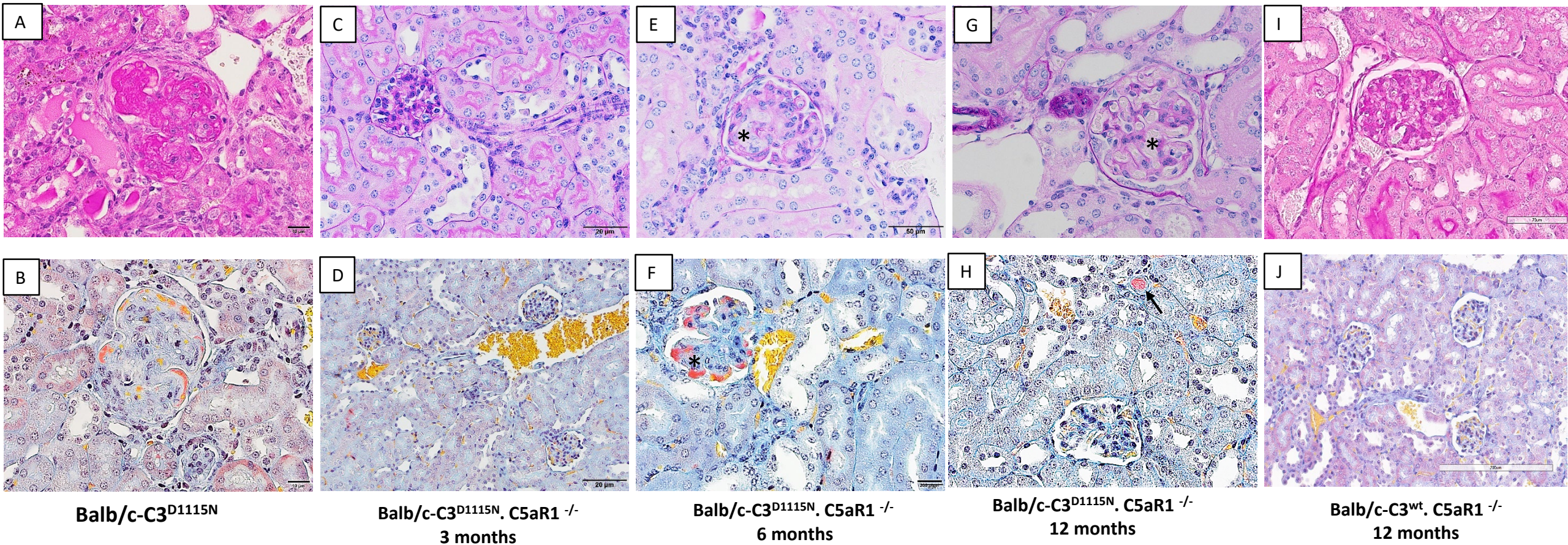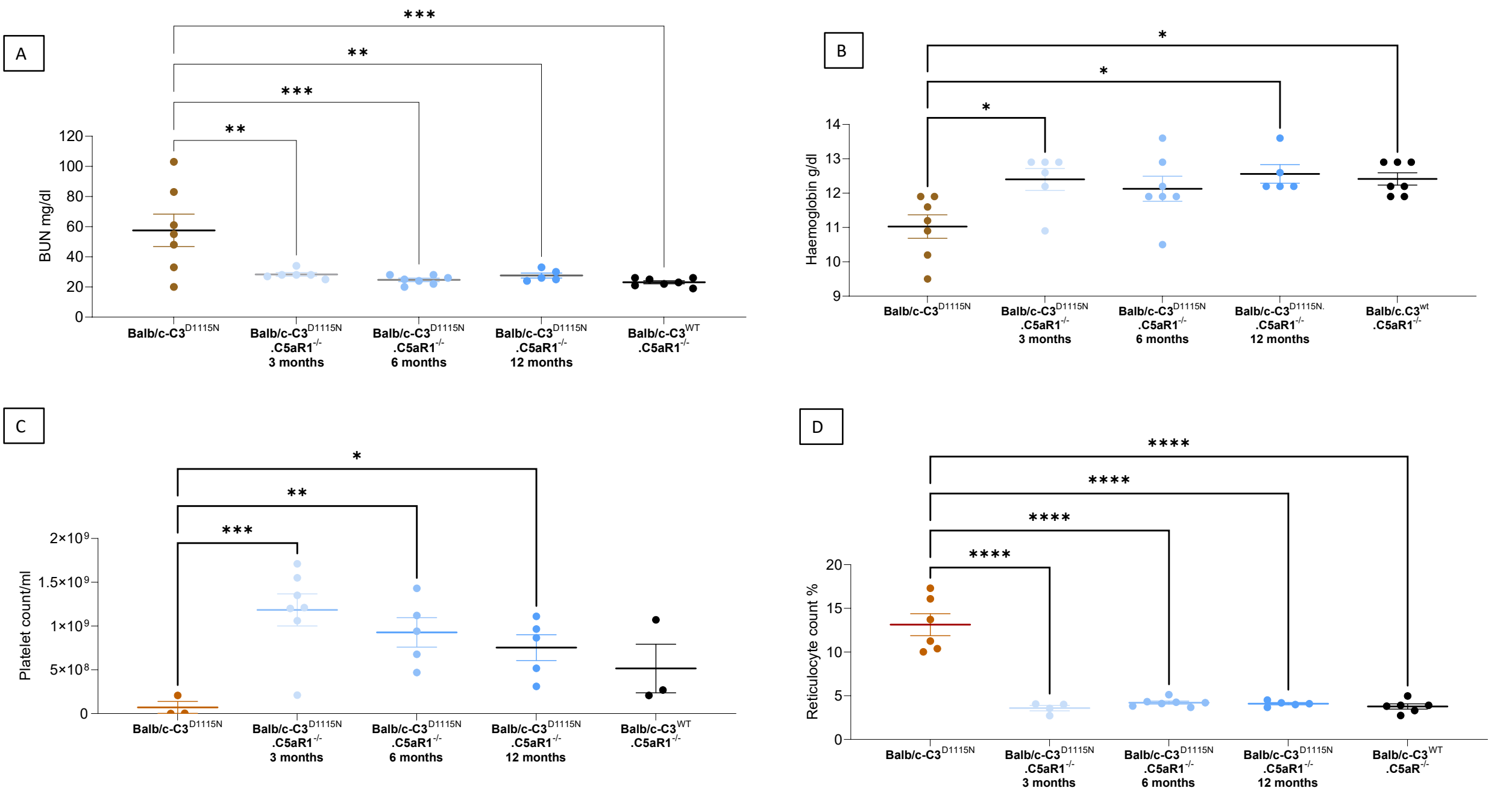
Figure 7
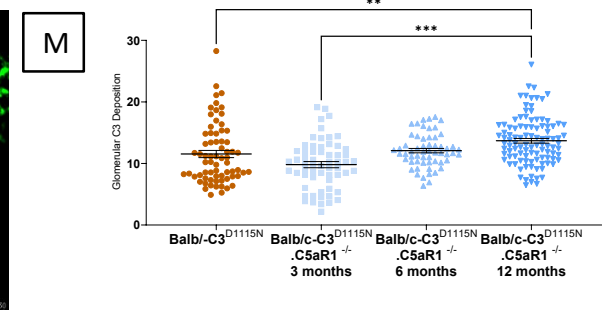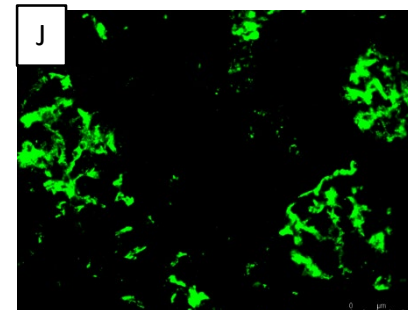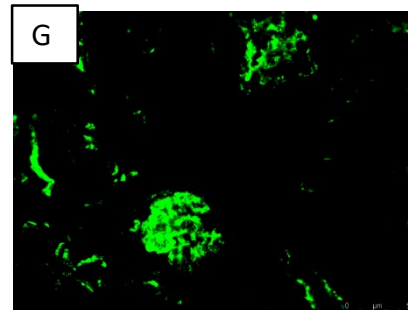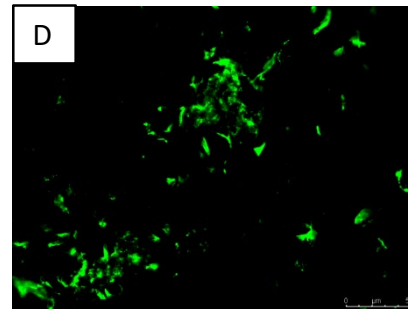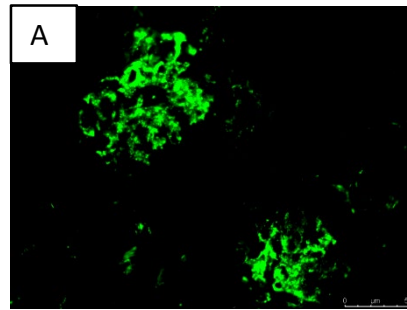
Figure 8

Anti C3

Anti C9
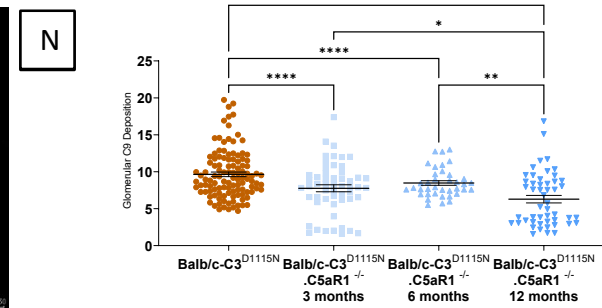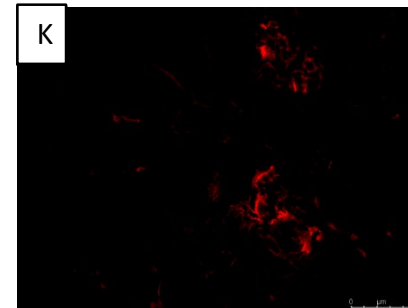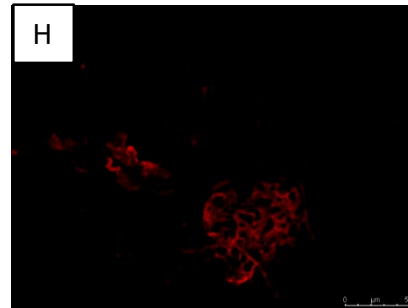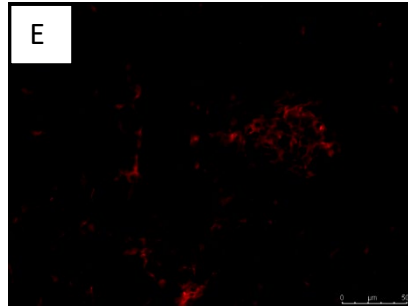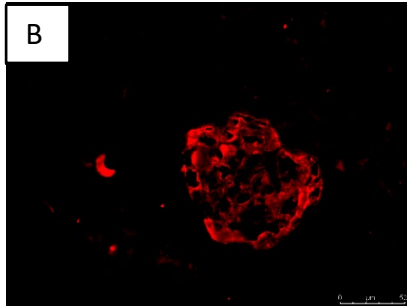
Anti Fibrin
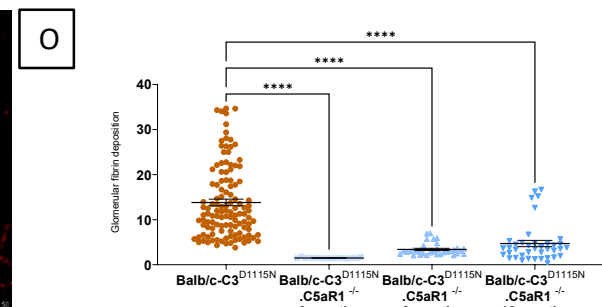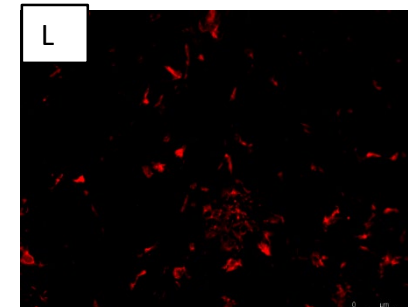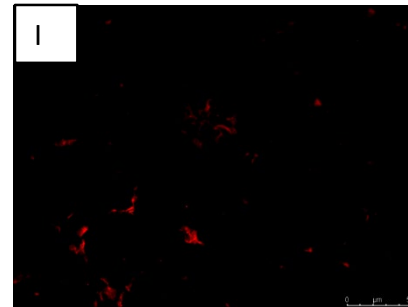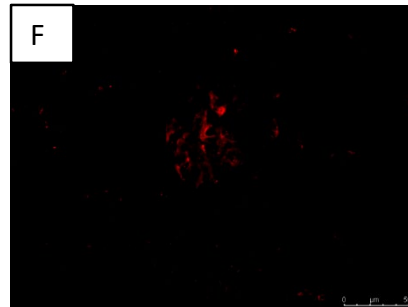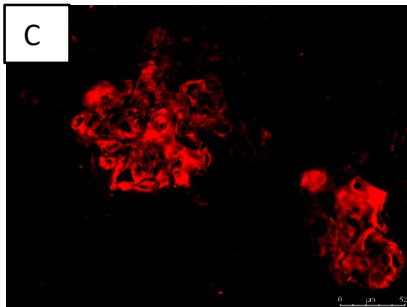
Balb/c-C3^{D1115N}

Balb/c-C3^{D1115N}
.C5aR1$^{-/-}$
3 months

Balb/c-C3^{D1115N}
.C5aR1$^{-/-}$
6 months

Balb/c-C3^{D1115N}
.C5aR1$^{-/-}$
12 months

Figure 9
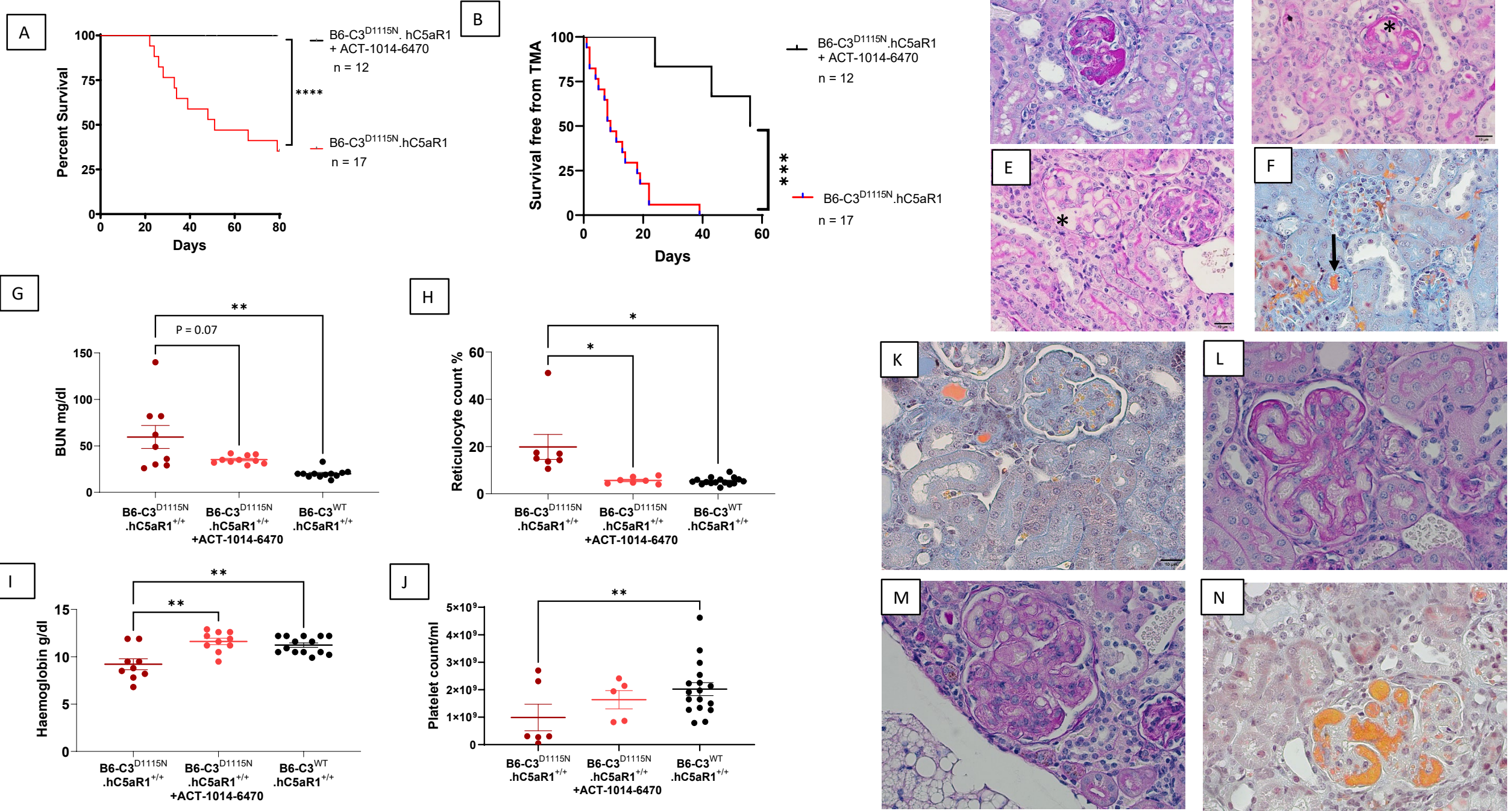
Figure 10
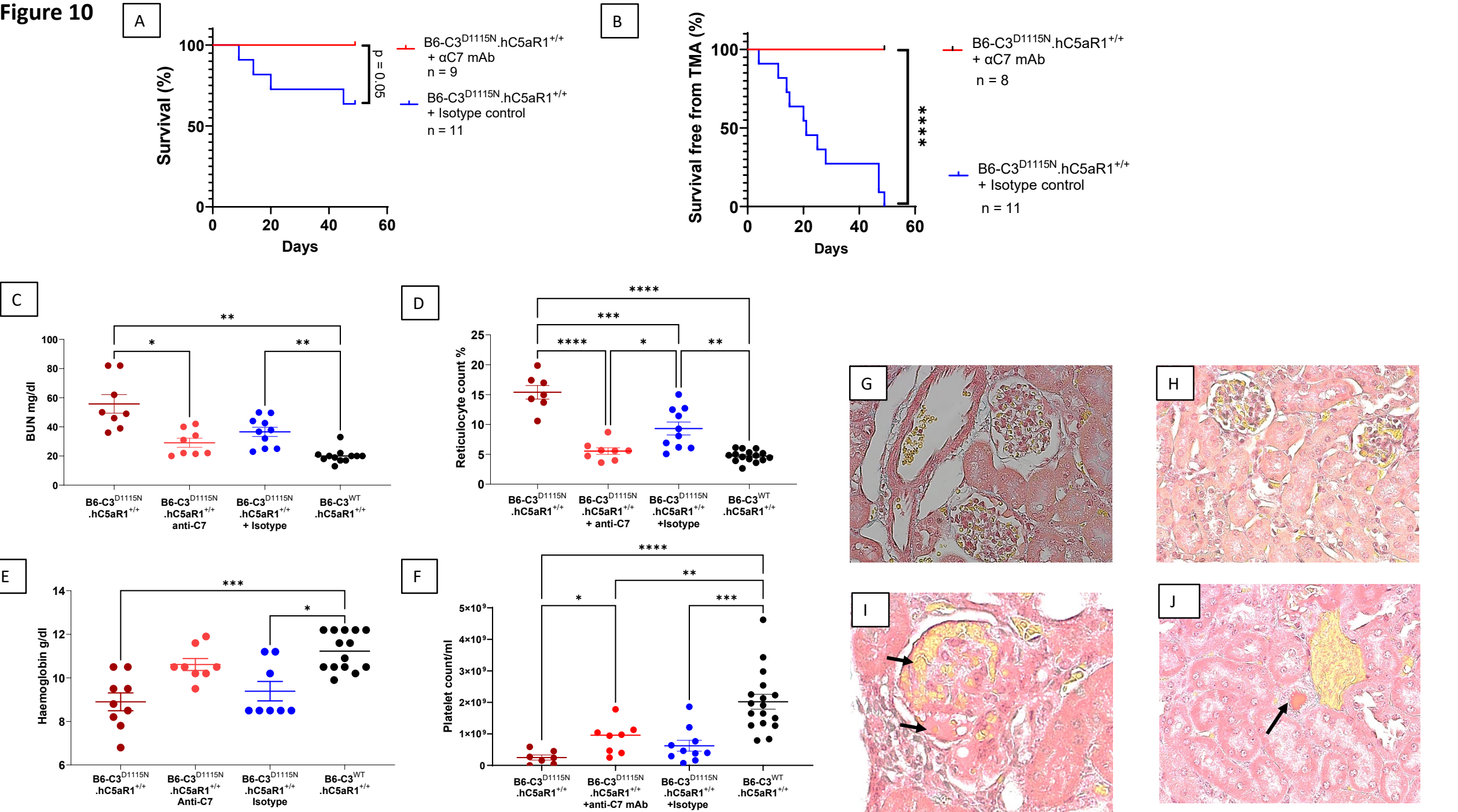
Figure 11

Macrophage staining Anti-F4/80

Neutrophil infiltration Anti Ly6-G

Macrophage staining Anti-F4/80
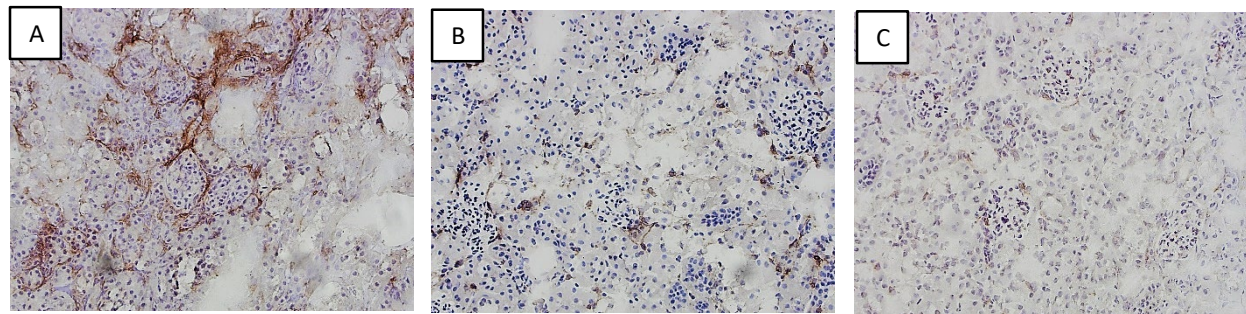
Neutrophil infiltration Anti Ly6-G
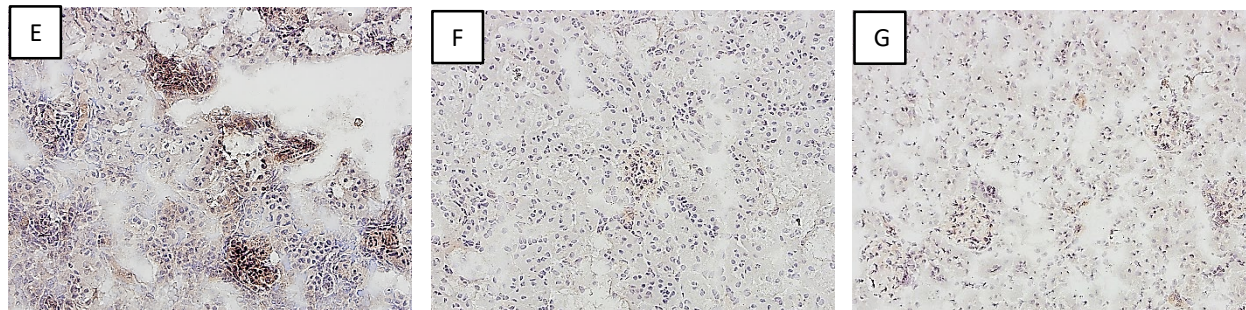
B6-C3^{D1115N}

B6-C3^{D1115N} . C7$^{-/-}$ 6 months

B6-C3^{wt} . C7$^{-/-}$ 12 months
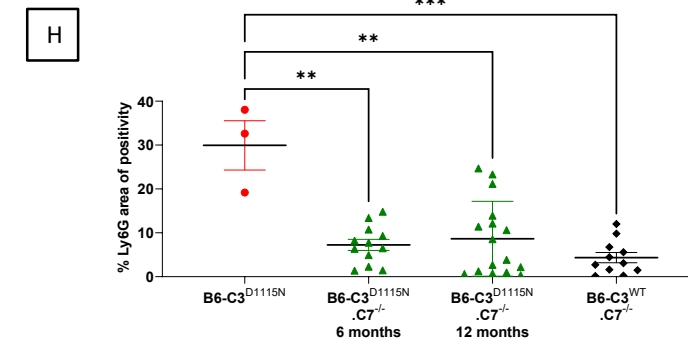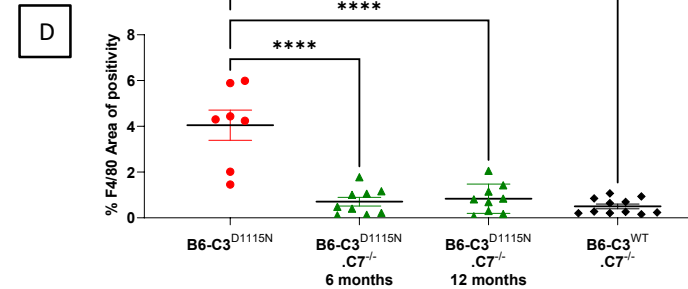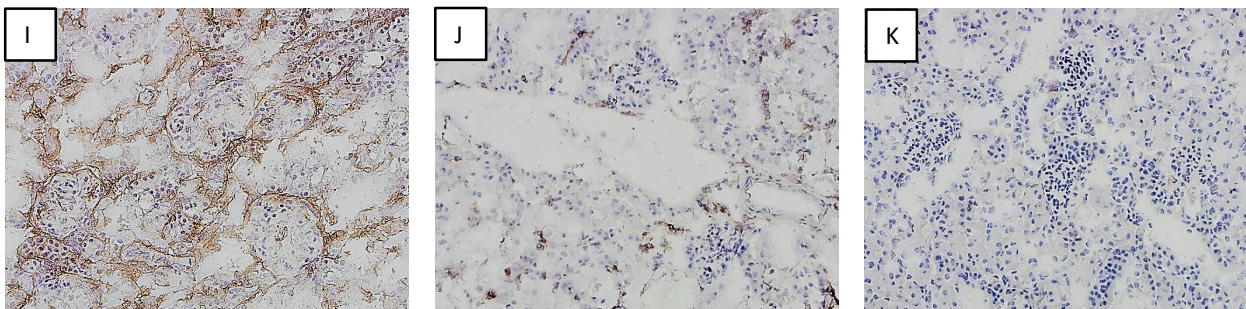
Balb/c-C3^{D1115N}

Balb/c-C3^{D1115N}. C5aR1$^{-/-}$ 6 months

Balb/c-C3^{wt}. C5aR1$^{-/-}$ 12 months

Figure 12

INVITED REVIEW
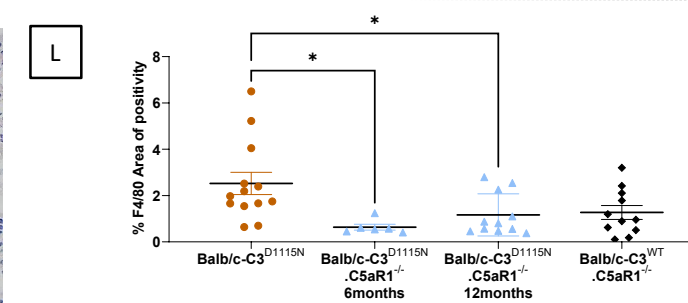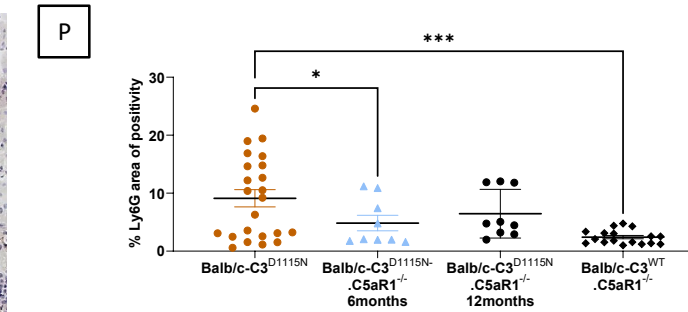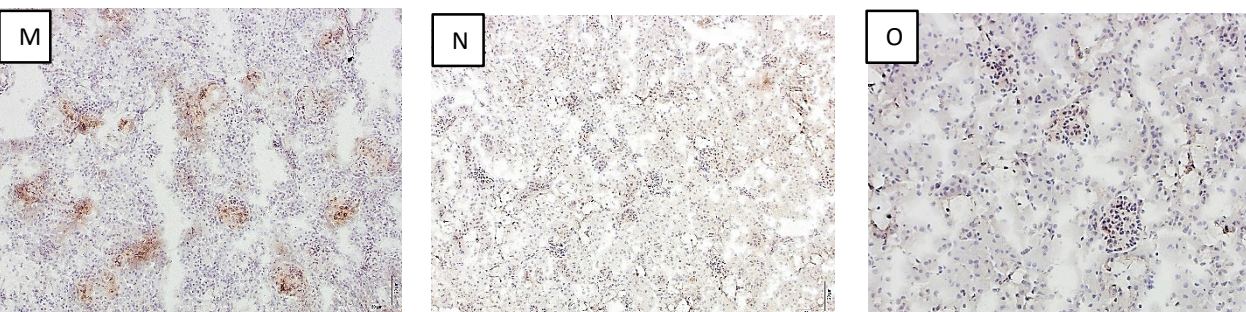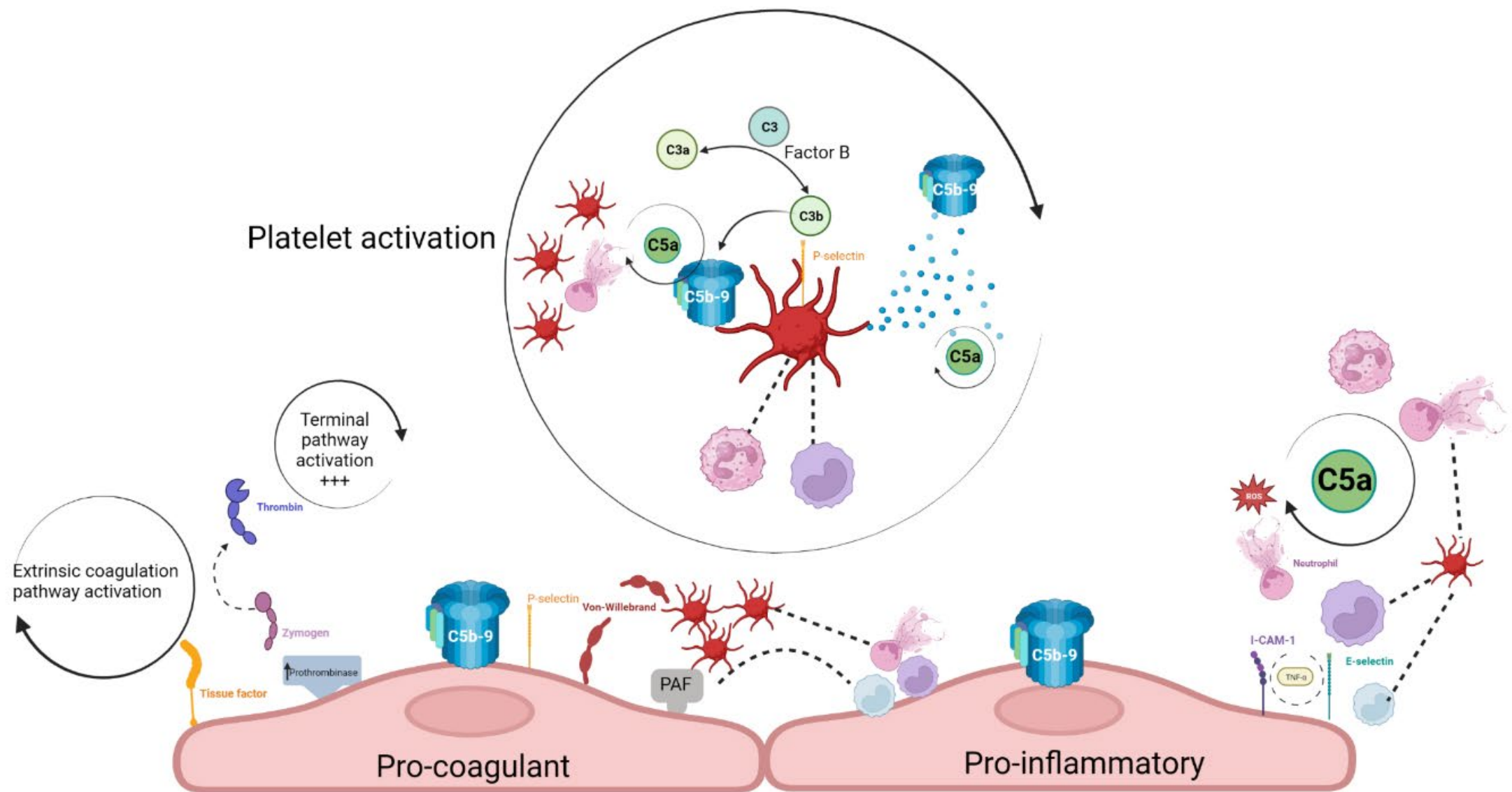
Alternative pathway activation in pregnancy, a measured amount "complements" a successful pregnancy, too much results in adverse events

Kate Smith-Jackson[1,2] | Richard Alexander Harrison[3]

[1]Complement Therapeutics Research Group, Translational and Clinical Research Institute, Faculty of Medical Science, Newcastle University, Newcastle-upon-Tyne, UK

[2]The National Renal Complement Therapeutics Centre (NRCTC), Newcastle-upon-Tyne Hospitals NHS Foundation Trust, Newcastle-upon-Tyne, UK

[3]Institute of Infection and Immunity, School of Medicine, Cardiff University, Cardiff, UK

Correspondence

Kate Smith-Jackson, Complement Therapeutics Research Group, Translational and Clinical Research Institute, Faculty of Medical Sciences, Newcastle University, 3rd Floor, William Leech Building, Framlington Place, Newcastle-upon-Tyne NE2 4HH, UK.
Email: kate.smith-jackson@newcastle.ac.uk

Summary

During pregnancy, the maternal host must adapt in order to enable growth of the fetus. These changes affect all organ systems and are designed both to protect the fetus and to minimize risk to the mother. One of the most prominent adaptations involves the immune system. The semi-allogenic fetoplacental unit has non-self components and must be protected against attack from the host. This requires both attenuation of adaptive immunity and protection from innate immune defense mechanisms. One of the key innate immune players is complement, and it is important that the fetoplacental unit is not identified as non-self and subjected to complement attack. Adaptation of the complement response must, however, be managed in such a way that maternal protection against infection is not compromised. As the complement system also plays a significant facilitating role in many of the stages of a normal pregnancy, it is also important that any necessary adaptation to accommodate the semi-allogenic aspects of the fetoplacental unit does not compromise this. In this review, both the physiological role of the alternative pathway of complement in facilitating a normal pregnancy, and its detrimental participation in pregnancy-specific disorders, are discussed.

KEYWORDS

complement, obesity, pre-eclampsia, pregnancy

1 | INTRODUCTION

Pregnancy leads to profound maternal physiological and metabolic changes. These are required to accommodate and nurture the developing fetus, and affect all organ systems.[1] In a normal pregnancy, these orchestrated multisystem changes enable successful delivery of a healthy baby and minimize the risks associated with pregnancy to the mother. However, pregnant women with pre-existing health conditions are at increased risk of adverse events in pregnancy. These can arise either indirectly, following decompensation of their underlying disease, or directly, from a collection of pregnancy-specific disorders; women with no underlying premorbidity are at risk of developing pregnancy-specific disorders due to the "stress" test of pregnancy.[2] The effects of adverse events in the mother are not limited to the pregnancy, they impact upon a woman's risk of developing disease in later life. Similarly, infants that are exposed to adverse events in utero have increased risk of developing vascular dysfunction in later life. Maternal morbidity and mortality remain a significant healthcare concern across the globe[3]; thus, understanding, identification, and treatment of adverse events in pregnancy is of vital public health importance.

The immune system undergoes profound changes in order to tolerate the semi-allogeneic feto-placental unit. These changes are required both for engraftment and for the fetus to thrive within the maternal environment. Adaptations in the immune system prevent rejection of the engrafted unit while simultaneously protecting both mother and fetus from microbial attack. Maternal immune tolerance is achieved through several adapted immune mechanisms. For example, attenuation of adaptive immunity through the generation of an immunologically privileged environment within the maternal decidua prevents access of maternal T- and B cells to fetal tissue.[4] The villous trophoblasts, which encase the placental villi providing nutrient exchange, lack major histocompatibility (MHC) molecules, enabling them to escape immunological detection.[5] The extravillous trophoblast cells (EVT), which invade the uterine lining, express unique MHC molecules; these limit their recognition by T cells, but still enable them to act as major ligands for natural killer (NK) cells and macrophages.[5] Uterine NK cells (uNK) and macrophages are the predominant immune cell populations within the decidua and myometrium, and participate in trophoblast invasion through pro-angiogenic activity.[4,6,7] Additionally, the placenta expresses high levels of indoleamine 2,3-dioxygenase (IDO). IDO activity protects the developing fetus from maternal T cell responses.[8] Together, these measures provide an effective modification of adaptive immunity within the fetoplacental environment such that both the host and the fetus remain protected.

The situation with respect to complement is different. The complement system plays an integral role in normal pregnancy, from fertilization to parturition. Any adaptation to prevent identification of the fetoplacental unit, and the fetus, as non-self, must simultaneously permit complement to play its essential role in normal pregnancy and to continue to provide host defense against infection.

Women with active autoimmune conditions are more vulnerable to adverse events in pregnancy,[9] and the fine balance that the immune system has to maintain in pregnancy is illustrated by disorders in which it is sensitized. This is evidenced, for example, in pre-eclampsia. Pre-eclampsia is a multisystem disorder classically defined by new onset of hypertension coupled with the presence of additional endothelial dysfunction, and carries significant risk not just for the mother, both during pregnancy and in later life, but also for the fetus.[10] The incidence of pre-eclampsia is increased in women with risk factors for chronic inflammation (eg obesity), also with a preponderance for women with autoimmune diseases, such as antiphospholipid syndrome (APS) and systemic lupus erythematosus (SLE), and dysregulated complement activation appears to provide a major effector mechanism.

While there are many immune-related mechanisms at play in both normal pregnancy and in pregnancy-associated disorders, in this review, we confine ourselves primarily to discussion of the role of the AP in facilitating a normal pregnancy, and its participation in the inflammatory-mediated injury of pregnancy-specific disorders.

2 | THE ROLE OF COMPLEMENT ACTIVATION IN NORMAL PREGNANCY

2.1 | Conception

It is quite clear that complement does not play an essential role in conception; mice deficient in complement components, particularly, in the context of this review, C3 and Factor B (FB), remain fertile. However, there are considerable data that support a facilitatory role for components of the system. During conception, capacitated spermatozoa bind to the zona pellucida (ZP) of the oocyte and trigger the acrosome reaction (AR). This exocytosis event releases the acrosomal contents and exposes membrane cofactor protein (MCP, CD46), located on the inner acrosomal membrane of the sperm, to the reproductive tract environment.[11] While CD46 exists as multiple isoforms, with individual isoform expression determined by the tissue or cell type, it should be noted that the isoform of CD46 expressed on the acrosomal membrane is unique to spermatozoa, suggestive of a highly specific role.[12,13]

It has been shown that acrosin, an acrosomal protease released during the AR, can cleave C3 to generate a C3b-like molecule. This nascent C3b has the transient ability to bind covalently to adjacent surfaces, including both the acrosomal and the ovum plasma membranes. Subsequent interactions, either between C3b bound to the ovum and CD46 expressed on the spermatozoa, or between C3b and/or its degradation product iC3b and complement receptors (CR1, CD35; CR3, CD11b/CD18) on the ovum, has been proposed to facilitate fusion of the sperm with the oocyte.[11] In the same study, it was noted that subsaturating concentrations of C3b promote penetration and that saturating C3b inhibits these interactions. One possible rationale for this is that dead or damaged spermatozoa are more strongly complement-activating than

healthy spermatozoa, and therefore more likely to produce saturating amounts of C3b, thus enhancing fertilization by healthy spermatozoa.

A more recent study confirmed, in part, these observations, and supported the facilitated fusion hypothesis.[14] In this study, using sera depleted of specific components, it was shown that C3 activation could be initiated in a CRP-C1q-C2-dependent pathway, and that activation was amplified through the C3 feedback loop. C3b deposited on the inner acrosomal membrane could be converted to iC3b by Factor I (FI) using Factor H (FH), but not MCP, as a cofactor. Interestingly, activation of the terminal pathway (TP) was not seen. This strengthens the hypothesis that iC3b can act as a ligand to facilitate fertilization through enhancing sperm–egg interactions. In their conclusion, the authors suggested that complement activation is precise and measured when compared to non-specific activation by foreign antigens, with fragment deposition targeted to a precise cellular location (the acrosomal inner membrane), and tightly controlled, such that a restricted amount of C3b/iC3b is deposited.[14]

2.2 | Pre-implantation

Once fertilized, and prior to implantation of the blastocyst in the maternal decidua of the uterus, the rapidly dividing zygote migrates down the fallopian tube and into the uterus. Mucosal secretions in the fallopian tube and uterus contain all of the components required to mount a complement attack.[15] Thus, during this passage, which takes around 9 days in humans, the semi-allogeneic fertilized egg or blastocyst may be subject to complement attack. A study using cryopreserved human embryos has shown that mucosal complement can target healthy embryos prior to implantation, evidenced by deposition of C1q and activation fragments of C3 (C3b/iC3b and C3d) on the blastomere membrane.[16] The embryos also expressed the membrane-bound regulators CD46, CD55 and CD59 on their surface, and recruited the soluble regulators FH and C4bp. Efficient protection of the embryo surface was demonstrated both by the absence of C5 on blastomere membranes (C5 deposition was confined to the ZP, the extracellular matrix that surrounds the blastomere membrane) and the observation that C3 fragment deposition was primarily as C3d, the inactive limit degradation product of surface-bound C3b.[16] Interestingly, C5 deposition was identified in the ZP but not on the blastomere membrane. The ZP also contained FH but not membrane-bound regulators or C4bp. This suggests that the ZP may be a site of concentrated complement attack, with AP activation/amplification playing a prominent part. Based on these observations, the authors hypothesized that one role of the ZP might be to protect the inner embryo from complement attack, providing a protective shield that diverts activation products away from the blastomere membrane.

This protection must be achieved without compromising pre-implantation pregnancy-specific roles of complement. C3 is synthesized and secreted into the reproductive tract by the embryo, oviduct epithelial cells, and the endometrium. The rate of synthesis follows a cyclical pattern, with highest production during estrus.[17–19] Activation of this to C3b, and the subsequent FI-mediated breakdown of this to iC3b, plays an embryotrophic role as the embryo develops, presumably through an interaction with CR3, which is expressed by the embryo, with iC3b the most potent embryotrophic ligand.[20,21] This in vitro work is further validated in mice that are deficient in C3. These have smaller blastocytes, suggesting a growth compromise in the absence of C3.[21,22]

Additionally, complement plays a role in the successful decidualization of the endometrium prior to implantation. Decidualization results in the transformation of uterine stromal cells into decidual stromal cells (DSC). DSC possess unique properties that induce immunological, hormonal, and vascular changes, creating a maternal decidual layer that enables the blastocyte to implant, and the trophoblasts to invade, and leading ultimately to the successful establishment of a functioning placenta.[23,24] Studies in non-human primates treated with human chorionic gonadotrophin (hCG) showed upregulation of endometrial expression of C3, with a specific increase identified within the uterine stromal tissue. Similar results were obtained in human endometrial tissue in response to hCG, with an increase in C3 mRNA and protein expression, again confined to the stromal tissue. Thus, the embryo, through its release of hCG, is able to communicate and signal to the endometrium, leading to an upregulation of C3 within the uterine stromal compartment, suggesting a role for C3 within the decidual immune environment. An increase in complement activation is also met with an increase in CD55 (decay accelerating factor; DAF) expression within the uterine luminal epithelium, underlying the need for balanced control of complement activation during decidualization.[25,26]

C1q is expressed in the decidual endothelial cells and synthesized locally by EVT. Specifically during pregnancy, C1q acts in a physiological manner to support the adhesion of the endovascular trophoblasts to the uterine endothelium during the remodeling of the spiral arteries. Additionally, EVT secrete C1q that binds to extracellular matrix proteins within the decidua, which the EVT use to further their invasion of the decidua. In vivo studies using the C1q deficient pregnant mice have shown an impaired labyrinth development and vessel remodeling, illustrating, the importance presence of C1q for the successful formation of the murine placenta.[27,28]

These essential roles of an intact complement system in the reproductive tract in early pregnancy highlight the stringent need for adaptation of the embryo to survive in an otherwise hostile environment. Without these adaptations, the embryo would not survive, and pregnancy would be terminated. In addition to the complement-specific processes outlined above, additional protection against an immune attack on the developing embryo may be provided by immunological priming.[29] Constituents of seminal fluid influence the maternal cellular response; postmating, there is an expansion of lymphocyte populations, with pronounced homing of these to the site of implantation. It has been hypothesized that this may facilitate maternal tolerance of the embryo.

2.3 | Implantation and placental development

As the blastocyte progresses along the reproductive tract, the uterine endometrium undergoes a transformation, generating the maternal decidua, the structure in which the blastocyte implants. Extravillous trophoblasts migrate through the maternal deciduas towards the spiral arteries, with extensive remodeling of these transforming them into high flow, low resistance vessels (see Figure 1). This remodeling is necessary to ensure that the growing fetus receives the blood flow and nourishment that it needs (reviewed in[30]). Implantation of the blastocyte into the maternal decidua occurs at around 9 days postcoitus (dpc) for humans and 4 dpc for mice (see Figure 2) and rats.[15] Both mice and humans form a hemochorial placenta. In this, maternal blood passes through vascular spaces lined with fetal trophoblasts (syncytiotrophoblast) forming the vascular barrier. The syncytiotrophoblast is a multinucleated syncytium with a microvillous brush border that covers the entire length of the chorionic placental villi. The apical membrane is in direct contact with the maternal blood and the basal membrane in contact with the fetal blood vessels; it facilitates transport to the fetus through transcytosis.[31]

Animal models have proved invaluable in developing our understanding of the role of complement in blastocyte implantation and placental development. As stated above, iC3b is embryotrophic
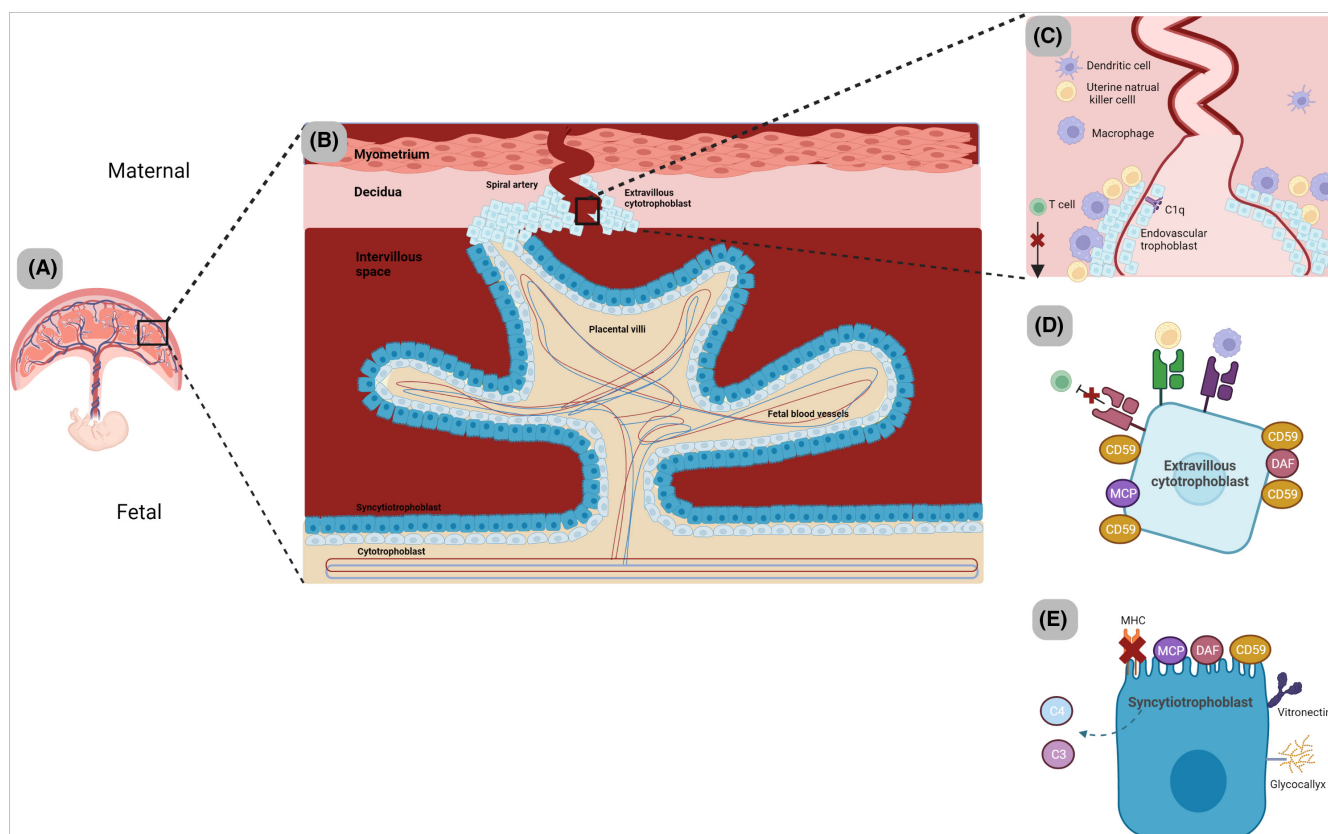
FIGURE 1 Maternal-fetal interface. (A) The human hemochorial placenta. (B) A placental villous is formed by a double cell layer of syncytiotrophoblasts (in direct contact with maternal blood) and cytotrophoblasts directly beneath. Fetal blood vessels and fetal macrophages remain housed within the villus. Extravillous trophoblasts (EVTs) depart from the tip of the placental villi and migrate into the maternal decidua, providing anchorage of the villi to the uterine wall. (C) In response, uterine natural killer cells (uNK) are recruited, which promote blastocyte implantation and provide support for the continued EVT migration through the release of cytokines promoting angiogenic activity. The EVT invade the spiral arteries (now termed endovascular trophoblasts), and in union with the uNK remodel the spiral arteries, replacing the vessels inner lining (characterized by loss of smooth muscle cells). This remodeling creates a dilated vessel that has "High flow" and "low resistance" conditions, optimizing blood flow to the placenta. C1q is locally produced from the decidual endothelial cells on the inner side of spiral arteries and from the endovascular trophopblasts. This physiological response appears to provide a functional scaffold between the two cells. The maternal decidua also houses macrophages and T cells. Macrophages restrict T cell activity through the release of IDO and phagocytose apoptotic EVT, as well as contributing to remodeling. (D) The Extravillous trophoblast express unique MHC molecules, which disguises them from T cells, while simultaneously acting as a major ligand for uterine natural killer cells and macrophages. They preferentially express CD59 to protect from lytic attack. (E) The Syncytiotrophoblasts are in direct contact with maternal blood and act as the site of nutrient, gas and waste exchange between the mother and developing fetus. They are immunological undetectable given the absence of any MHC molecules. A thick glycocalyx layer provides further shelter against immunological attack. MCP, DAF, CD59 are all expressed to protect the cell layer from maternal complement attack. Further reinforcement is provided by binding of vitronectin (soluble inhibitor from maternal blood) to prevent C5b-9 assembly. They have also been shown to be a source of locally produced C3 and C4. Cytotrophoblasts express MCP and CD59 to protect from any complement spill over from the syncytiotrophoblast layer.
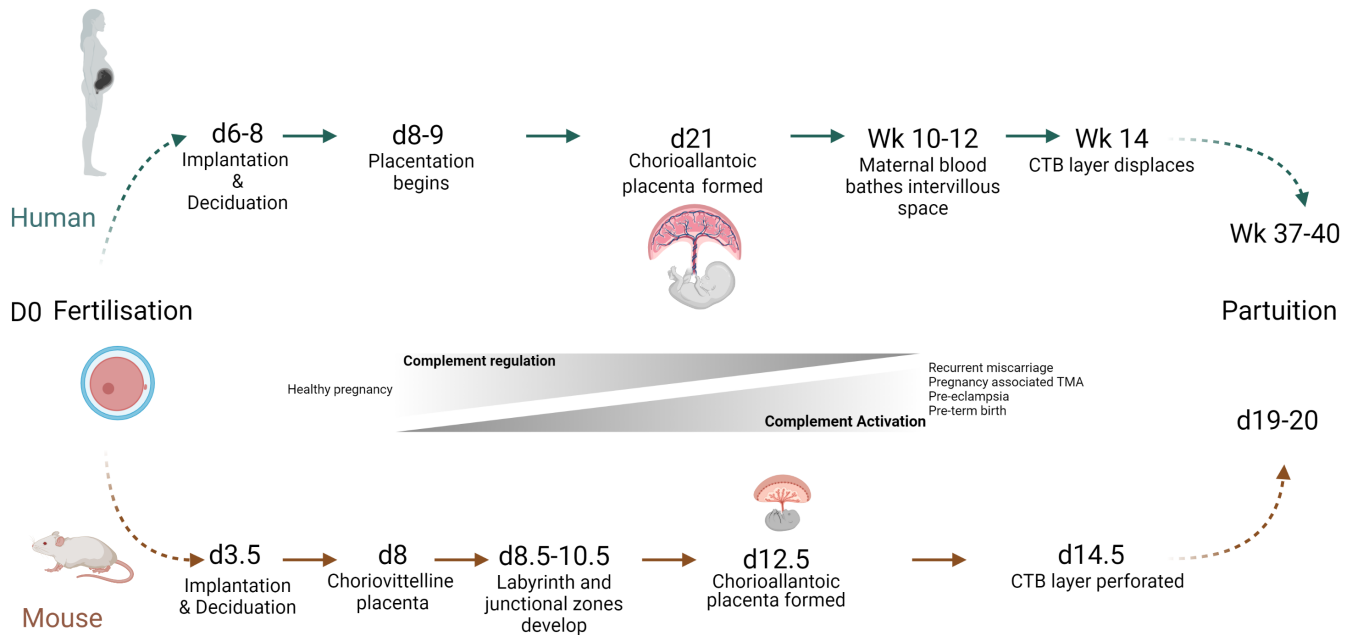
FIGURE 2 Pregnancy milestones in human and mouse. Humans and mice both form a hemochorial placenta (maternal blood is in direct contact with the chorion). In humans, maternal blood bathes the intervillous space toward the end of the first trimester. In contrast, mice form a primitive placenta (choriovitelline), followed by the definitive (chorioallantoic) placenta around day 11–12.5 postcoitus. In structural contrast to the villous tree formed in the human placenta, mice form a highly interconnected maze-like structure of chorionic villi which is termed the labyrinth. The labyrinth is supported by the spongiotrophoblast layer (not present in humans). The labyrinth comprises of two layers of syncytiotrophoblasts (SYN) overlaid by a layer of cytotrophobasts (CTB) which directly contact maternal blood. Maternal blood accesses the outermost SYN layer once the CTB layer is perforated (around day 14 postcoitus). Achieving each successive pregnancy milestone requires adequate complement regulation, complement dysregulation and increased activation has been shown to be involved with adverse events in pregnancy.

and likely contributes to embryo growth and development before the placenta is fully established.[15,22] Additionally, *C3−/−* mice have a normal number of implantation sites, but an increase in resorptions occurs around 15 dpc, suggesting that C3 is particularly important for placental development rather than implantation.[15,22] While CD55 and CD46 are heavily expressed in the human placenta, regulating both classical pathway (CP) and AP activation of C3, neither CD55 nor CD46 is expressed in the murine embryo or trophoblast.[32] In rodents, a novel membrane-bound protein, Crry, replaces CD55 and CD46 in the placenta.[33] It regulates deposition of activated C3, combining CD55- and CD46-like regulatory activities,[34] and is highly expressed on the trophoblast cells of wildtype mice at 7.5 dpc.[35] Seminal work using the Crry−/− mouse showed the importance of AP regulation for successful maintenance of a normal pregnancy in mice, with Crry knockout leading to embryonic lethality at 10.5 dpc.[35] In these mice, maximal C3b deposition was seen at 7.5 dpc; this was accompanied by the presence of neutrophils around the trophoblast cells, and preceded death by 3 days. In the same study, the authors further showed that maternal C3 was primarily responsible, with backcrossing onto maternal *C3−/−* mice rescuing the phenotype and preventing the neutrophil influx.[35] In follow-up work, the same group demonstrated that backcrossing *Crry−/−* mice onto *C4−/−* mice or B cell deficient mice did not rescue the phenotype, thus neither antibody nor CP activation is involved in embryonic lethality. Similarly, embryonic lethality of *Crry−/−* pups

was still observed in the setting of either neutrophil depletion or backcrossing with C5 deficient mice. (While the backcross with C5-deficient mice did result in rescue of a small minority of pups [5%], a primary dependence of lethality on C3 activation products remains, with C5 activation playing, at most, a minor role.) By contrast, backcrossing the *Crry−/−* mice with *FB−/−* mice rescued the lethality phenotype, with viable *Crry−/−* pups produced. Neither increased C3b deposition nor neutrophil infiltration was observed in this double knockout mice.[36] From this, the authors concluded that unregulated activation of the AP triggers C3-dependent neutrophil infiltration of the trophoblast and impaired feto-maternal tolerance, leading ultimately to fetal demise.[36] The virtually total dependence of the embryonic lethality phenotype on C3, but not downstream effector arms of complement, suggests that there is either a C3a/C3aR- or an iC3b/CR3-driven, or a mixture of both, mechanism at play. Dual perfusion of the placenta, and thus independence of the fetus on the embryonic yolk sac for nutrition, is achieved in Crry-sufficient mice at 9.5 dpc. The timing of fetal lethality in *Crry−/−* animals is consistent with a failure in development of the allatonic placental vessels, resulting in impaired vascular supply to the developing fetus at a critical time when its source of nutrients is transitioning from the yolk sac to the placenta.[36]

Work using the *CMAS−/−* mouse has further validated the essential need for complement regulation to enable fetal survival.[37] Mammalian cells are coated in a dense layer of glycans (the

glycocalyx), with sialic acid occupying the outermost position in the bulk of the glycocalyx glycans.[38] *CMAS−/−* mice lack the sia-activation enzyme (CMP-sialic acid synthase [CMAS]), and, as a consequence, the glycocalyx glycans are not sialylated. Sialylation has a major impact on the functioning of glycans, being able to dampen immune responses (reviewed in[39]), and functioning as a ligand for FH and enabling recognition between self and non-self.[40] Trophoblasts from wildtype embryos are extensively sialylated. The absence of sialylated glycans following genetic deletion of CMAS resulted in embryonic lethality at 9.5 dpc,[37] with complement activation on trophoblasts. As with *Crry−/−* mice, complement activation was accompanied by an influx of maternal neutrophils at the fetal-maternal interface, leading to impaired fetal growth and subsequent demise. Lethality could be rescued by depletion of maternal C3, at 8.5 dpc, through injection of cobra venom factor (a tool compound for systemic C3 depletion). This prevented C3 deposition and infiltration of maternal neutrophils.[37] Neither C1q nor C4d were detected in immunohistochemical staining of the embryo, indicating that there was no significant role of CP or lectin pathway (LP) in complement activation. By contrast, an increase in properdin staining was seen, consistent with AP activation. While C3a (and C5a) are chemoattractants for neutrophils, suggesting a possible role for neutrophils in lethality, antibody-induced depletion of neutrophils did not rescue *CMAS−/−* embryos. These data demonstrate that neutrophil recruitment is a secondary effect following excess complement activation by the AP,[37] and that sialylation is crucial for human trophoblasts protection from maternal complement attack. Recruitment of FH requires the presence of sialylated glycans; thus, in the absence of sialylation, a lack of FH likely contributes to hyperactivation of C3.

In support of this, mutations in FH that affect the sialic acid recognition site have been associated with atypical hemolytic uremic syndrome (aHUS, a rare kidney disease also consequent on dysregulation of the AP),[41] and genes encoding enzymes involved in sialic acid synthesis and processing have been reported to be differentially regulated in the placenta of women who develop pre-eclampsia (see later).[42,43]

What is particularly interesting from the above mouse studies is that complement-dependent embryonic lethality appears to be driven almost entirely by activation (C3a/C3b) and degradation (iC3b) products of C3. Neither neutrophils nor C5 activation products (C5a; C5b-9, the membrane attack complex of complement [MAC]) appear to play a significant role, and this has implications for possible treatments for recurrent early pregnancy loss. It also appears likely that, in the mouse, surface-bound FH alone cannot give sufficient protection. While it is not clear why this should be so, one possibility is that FH has a location-specific role, which is insufficient to protect the fetus.

Collating the above data, derived mainly from pregnancy studies in mouse models, it is clear that, appropriately regulated, the AP plays an integral role in facilitating successful blastocyte implantation within the maternal decidua, in engraftment, and in establishing a functioning placenta. C1q, C4, C5, C6, C9 are all found in the placenta and in the decidual spiral arteries,[44,45] trophoblast cell lines

have been shown to synthesize C3 and C4, and it is logical that the placenta possesses an intact complement system to provide immune defense against pathogens.[46] In order to protect the allogeneic fetus, activation within the reproductive tract requires tightly regulated control of the system, and the placenta normally achieves this through the high expression of CD55, CD46 and CD59 on EVT throughout the gestation period,[7] as well as through the recruitment of FH to cell membranes. If regulation fails, the fetus comes under attack from maternal C3, with pregnancy failure the likely outcome.

2.4 | Circulating complement during pregnancy

Multiple studies have confirmed that pregnant women have an increase in the plasma concentrations of circulating complement proteins and anaphylatoxins when compared to non-pregnant controls.[47–49]

In a recent longitudinal study of complement and complement activation products in pregnant and non-pregnant women, He et al. evaluated plasma samples taken from the 1st to 3rd trimesters. While <30% of the cohort had three or more samples from which to assess the impact of increased gestation time on complement,[50] they were able to determine that C3 and C4 increased gradually throughout pregnancy. Levels of C1q, C5a, and sC5b-9 were similar to non-pregnant women in the 1st and 2nd trimesters. FB and FH rose during the 1st and 2nd trimesters and then remained stable during the 3rd trimester. An increase in FB seen during the 1st trimester is compatible with enhanced activation potential and the involvement of the AP in placental formation. The concomitant increase in FH levels, and the relative abundance of FH in the 2nd and 3rd trimesters of normal pregnancy, highlight the need for a balanced regulatory response to avoid excessive systemic activation of the AP while, at the same time, permitting local C3-dependent mechanisms required to maintain a normal pregnancy.

C3a in the 2nd and 3rd trimester, and C5a in 3rd trimester, were higher in pregnant women, with sC5b-9 remaining unchanged. Collectively, and primarily assessed through the presence of the anaphylatoxins in the maternal circulation, this illustrates that there is systemic activation of the complement system in the 2nd and 3rd trimesters of normal pregnancy. (Given the concentrations of complement proteins in plasma, anaphylatoxin levels are likely to give a more accurate assessment of activation than variations in native protein concentrations.) Comparison of C3a, C4a, and C5a levels were indicative that not all C3a was generated after C4 activation; thus, the AP was likely to be involved.[48]

Supportive data for increased hemolytic activity in pregnancy come from observations of pregnant women with aHUS or paroxysmal nocturnal hemoglobinuria (PNH). Following the introduction of complement inhibiting therapy (eculizumab, an anti-C5 monoclonal antibody that prevents C5 activation), pregnant women were often found to require increased dosing.[51]

Increased complement activation in pregnancy is likely a normal physiological response consequent on increased placental cellular

debris. Enhanced maternal synthetic function may be a normal physiological response to increased consumption, required to maintain effective host protection against infection. Complement homeostasis is key to achieving successful pregnancy milestones, and if this is disrupted adverse events leading to the development of pregnancy-specific disorders can arise.

3 | PREGNANCY DISORDERS

3.1 | Pregnancy-associated thrombotic microangiopathy

Atypical hemolytic uremic syndrome (aHUS) is a rare kidney disease consequent on AP dysregulation, histologically defined through the presence of a thrombotic microangiopathy (TMA) in the kidney, accompanied with the clinical triad of thrombocytopenia, microangiopathic hemolytic anemia and acute kidney injury.[52] The majority of aHUS patients carry mutations in proteins of the AP, resulting in its defective regulation. Autoantibodies, primarily those directed against the C-terminal domains of FH, are also associated with the disease. Many of these autoantibodies block sialic acid-dependent recruitment of FH to the cell surface, and hence augmentation of CD55- and CD46-downregulation of AP amplification. What is noteworthy in aHUS is that mutations and autoantibodies are predisposing factors for aHUS, and an additional trigger is required for disease to develop.[53–55] Additionally, while aHUS represents an archetypal AP disease, successful therapy with eculizumab (an anti-C5 monoclonal antibody) identifies C5 activation products (C5a, C5b-9) as key effector molecules.[56]

Pregnancy-associated aHUS (p-aHUS) comes under the umbrella of complement-mediated aHUS, sharing similar disease severity and frequency of mutations in complement genes.[57] A large cohort study, incorporating national registries from France, England, and Italy, showed that while p-aHUS commonly presents in the first pregnancy (58%) and within the postpartum period (76%),[57] the risk is not significantly lower in subsequent pregnancies. It was hypothesized that cases occurred in the postpartum phase as delivery of the placenta removes the enhanced regulatory capacity of CD55 that the placenta provides. This, coupled with complement activation following parturition, for example through infection and/or bleeding, may provide the trigger that breaches the regulatory capacity of the AP, leading to the clinical manifestation of aHUS. The study found that two thirds of p-aHUS women required dialysis, with more than 50% reaching end-stage renal disease (ESRD).[57] In this context, it should be noted that the data were collated over four decades, with most cases from the pre-eculizumab era. A more recent study, in the era of eculizumab, showed significant improvement in renal outcomes in women with aHUS triggered in pregnancy.[58,59] However, even today, affected women will experience an acute aHUS episode before anti-C5 therapy can be introduced.

In the combined registry study discussed above, an AP-relevant variant complement protein was detected in 56% of the registry patients, with FH variants being the most abundant; this mirrors the picture seen in complement-mediated aHUS cohorts.[60,61] Around 70%–75% of the women had no personal or family history of aHUS and thus could not be identified as being "at risk." Patients with complement protein variants had more severe outcomes than those in which no variant protein could be identified. The risk of recurrence of aHUS in a subsequent pregnancy is about 25%, and women should be informed of this.[62]

While the hypothesis discussed above, that p-aHUS is consequent on a decrease in AP regulatory capacity combined with an increased challenge, makes theoretical sense, there is little directly supportive data, and the precise mechanism(s) by which pregnancy triggers aHUS remains unknown. One possibility is that the gravid endothelium, and its altered imbalance of angiogenic factors, may make it more vulnerable to complement activation. Further work investigating the differences between the gravid- and non-gravid endothelium and its ability to control AP activation are needed for rational preventative and treatment strategies to be developed.

3.2 | Preterm birth

Spontaneous preterm birth (birth between $20^{0/7}$ and $36^{+6/7}$) is one of the leading causes of perinatal morbidity and mortality worldwide, with approximately 11% of neonates across the world being born prematurely.[63] Not only is there an increased rate of neonatal and infant mortality in preterm births, an increase in all-cause mortality accompanies the child into adolescence.[64] Surviving infants are at increased risk of impaired development, behavioral problems, and long-term general health morbidities such as cardiometabolic disease in adulthood.[65] Given these long-term health consequences can transcend for decades, preterm birth (PTB) is an important public health issue.

Multiple risk factors that can identify vulnerable women with a predisposition to PTB have been defined or proposed. One possible player is complement, and the studies that implicate a causative role for complement in preterm birth are discussed below.

3.2.1 | Murine studies

Inducible mouse models of PTB include vaginal administration of a low-dose endotoxin (LPS) or of a progesterone antagonist (RU486), both of which lead to cervical ripening and PTB.[66,67] In both models, increased cervical deposition of C3 was observed; this was accompanied by macrophage infiltration into the cervix. While, in the mouse, the mechanism responsible for cervical C3 deposition is not understood, an increase in serum levels of the anaphylatoxins C3a and C5a, when compared to gestational age-matched controls, was also noted. An increase in plasma C5a correlated with an increase in cervical matrix-metalloproteinase 9 (MMP-9) activity, collagen breakdown, and cervical remodeling. In vitro studies with murine macrophages showed that MMP-9 release was triggered by C5a.[7,66]

Consistent with this, mice deficient in C5aR did not show an increase in MMP-9, did not undergo cervical remodeling, nor was premature delivery seen following either LPS or RU486 administration. Progesterone administration also prevented C5a-induced activation of macrophages and reduced PTB in mice.[66] Importantly, no local C3 deposition on the cervix, nor evidence of systemic activation of complement in maternal plasma, was identified in mice that delivered at term, indicating that complement activation does not play a role in normal parturition.

3.2.2 | Human studies

PTB is associated with intrauterine infection and inflammation. A recent study by Chan et al. has hypothesized a mechanistic role for complement in microbial-driven inflammation and PTB. The longitudinal study analyzed vaginal microbiota and cervicovaginal fluid, finding, an increase in C3b and C5a in women who delivered preterm. An increase in C3b and C5 were in response to a specific vaginal microbial composition and could be positively correlated with pro-inflammatory cytokines, providing a link between the microbial environment, complement and PTB.[68]

An early study investigated possible markers of intrauterine infection in amniotic fluid obtained by amniocentesis of women in preterm labor, and found that C3 levels gave the best correlation with infection. This study was performed in women with singleton pregnancies, with amniocentesis performed between 23 and 35 weeks gestation, and found that the culture positive group had higher C3 than the culture negative group.[69] A number of related studies, all supportive of Elimian et al.,[69] have subsequently been published. Women with preterm labor associated with intrauterine infection were found to have higher amniotic fluid levels of C3a, C4a and C5a than women with preterm labor in the absence of infection.[70] The same study found that elevated maternal plasma levels of C5a were also associated with PTB with accompanying intra-amniotic infection (IAI), whereas maternal plasma levels of C5a in PTB without IAI, and in those who delivered at term, were not elevated.[70] A follow-up study by the same group showed that spontaneous labor at term is not associated with changes in amniotic fluid of any of the anaphylatoxins.[71] Indeed, women with spontaneous labor at term had lower median maternal plasma C5a concentrations when compared to women at term not in labor (no difference was identified in C3a and C4a).[70] All of this suggests that complement activation fragments could be biomarkers to detect subclinical intrauterine infection. However, their use, is unlikely to change clinical practice due to the practical limitations of obtaining appropriate samples.

Of particular relevance to this review, the activation fragment of FB, Bb, has also been measured in amniotic fluid, with the finding of higher median concentration of Bb in pregnancies complicated with IAI, irrespective of membrane status.[72] This implies that the host response against IAI infection involves AP activation. Interestingly, a significant relationship was also found between elevated plasma levels of Bb in early pregnancy and spontaneous preterm birth. Plasma levels of Bb in the first trimester of pregnancy were predictive of PTB at less than 34 weeks' gestation (but not of PTB between 34 and 37 weeks).[73] One interpretation of this finding is that Bb is generated during an early infection-related inflammatory event, precipitates changes that lead to PTB, but that the infection remains occult until the onset of preterm labor.

3.2.3 | Therapeutic approaches to PTB

The above data suggest a number of possible approaches that could be evaluated for prevention of PTB. The mouse data suggest that both a C5aR antagonist and progesterone might be efficacious.[66] Until now, no C5aR antagonist has been evaluated, but clinical trials have examined the efficacy of daily vaginal progesterone or weekly intramuscular 17-alpha hydroxyprogesterone caproate (17-OHPC) administration to prevent PTB and associated neonatal adverse outcomes, with conflicting results.[74-79] A recent systemic review and meta-analysis found that vaginal progesterone reduced the risk for PTB before 34 weeks' gestation and reduced neonatal outcomes in high-risk singleton pregnancies,[80] and vaginal progesterone is now recommended by the UK National Institute for Health and Care Excellence (NICE) to prevent early miscarriage.

3.3 | Pre-eclampsia

Pre-eclampsia is a serious complication of pregnancy, occurring in 2%–8% of pregnancies, and manifesting as a pregnancy-induced onset of hypertension, renal dysfunction, and a myriad of other complications. Untreated, it has serious implications for the health of both mother and fetus.[81] It has been proposed that pre-eclampsia develops as a two-stage process. Stage 1 occurs early in the first trimester, with failed remodeling of the maternal spiral arterioles; this leads to placental Ischemia.[82] Stage 2 occurs later in pregnancy. In healthy pregnancy, the fetoplacental unit produces the pro-angiogenic factors vascular endothelial growth factor (VEGF) and placenta growth factor (PIGF). However, once the placental is functionally established, it produces soluble fms-like tyrosine kinase 1 (sFLT-1), an anti-angiogenic factor which sequesters free VEGF and modulates its activity, rendering both VEGF and PIGF inactive.[83] A delicate balance is required between pro- and antiangiogenic factors for maintenance of a healthy placenta.[84] In pre-eclampsia, with advancing gestational age (second and third trimesters), this balance is disrupted (Stage 2), and favors the release of sFLT-1 and other antiangiogenic factors. These spillover into the maternal circulation, leading to multi-organ maternal endothelial cell dysfunction, organ injury, and the clinical manifestations of pre-eclampsia.[82] Interestingly, the kidney again appears particularly susceptible with hypertension and proteinuria being cardinal features.[82]

Over the last two decades, both animal models and human studies have suggested a role of complement in the pathogenesis of pre-eclampsia. However, what has been difficult to establish is

whether complement activation might play a central role in the disease mechanism, or whether it is simply a secondary response to immune dysregulation of placental angiogenesis. Human studies have been confounded by sample size, methodology, disease severity, and gestational age.

3.3.1 | Insights into animal models

Given the remit of this review we will focus on studies that implicate the AP in pre-eclampsia pathogenesis; animal models of the classical (*C1q−/−*) and lectin (*MBL-A−/−*) pathways will not be discussed.

The BPH/5 (blood pressure high/5) mouse is a spontaneous model of abnormal placental development, and recapitulates much of the clinical phenotype of pre-eclampsia.[85–87] It has been proposed that complement activation provides an initiation mechanism for the development of pre-eclampsia as abnormal placentation can be reversed by inhibiting complement activation at the maternal fetal interface.[86] To investigate this, the effects of two fusion proteins, CR2-Crry and CR2-FH, designed to provide targeted complement inhibition at the cell surface, were investigated. The CR2 (complement receptor 2) component targets the fusion proteins to sites of C3 (C3b, iC3b, and C3d) deposition, Crry and FH provide the complement regulatory function. CR2-Crry inhibits the classical, lectin and alternative pathways, in comparison with CR2-FH that specifically inhibits AP activation. At the doses used in these studies, the fusion proteins had only minimal effect on systemic complement activity, with preferential targeting to sites with localized complement activation. The constructs remained in situ and functionally active for prolonged periods. Both inhibitors prevented fetal loss and growth restriction in the BPH/5 mice. Increased placental weight and normalized placental spiral artery morphology were achieved with CR2-Crry treatment, but not in mice treated with CR2-FH,[86] suggesting that, while the AP plays a role in this early stage of placentation, activation of other pathways is also important. Increased placental VEGF concentrations were achieved with both agents. Complement activation at the maternal-fetal interface leads to neutrophil recruitment, elevated local tumor necrosis factor-alpha (TNF-α), reduced VEGF, abnormal placentation, and fetal demise. The above data suggest that complement activation, and the ensuing neutrophil infiltration into the placenta, triggers abnormal spiral artery remodeling and angiogenic dysregulation.[86]

In an inducible rat model of placental insufficiency (reduced uterine placental perfusion through surgical manipulation), hypertensive rats had decreased circulating C3 and increased circulating C3a, showing that complement, specifically C3, activation had occurred.[88] Soluble complement receptor 1 (sCR1) is a synthetic form of CR1 lacking its transmembrane domain, and an inhibitor of the CP, LP, and AP C3 and C5 convertases. Administration of sCR1 in this rat model inhibited complement activation, with reduced circulating C3a and a reduction in mean arterial pressure (MAP).[88] While VEGF was reduced in hypertensive rats, sCR1 inhibition of complement activation had no effect on this.[88] In further evaluation of potential

mediators of pre-eclampsia-like effects, administration of both C3aR and C5aR antagonists was shown to inhibit the increase in MAP, with both antagonists being equivocal. Surprisingly, combination therapy failed to augment their effects. However, only the C5aR antagonist was able to attenuate endothelial dysfunction, suggesting that C3a and C5a have specific immunological roles in contributing to placental ischemia.[89] In agreement with sCR1 data, neither antagonist affected VEGF levels.[89] Thus, complement activation leading to placental ischemia-induced hypertension was independent of VEGF in this inducible model.

The difficulties of interpreting animal models of pre-eclampsia are illustrated in a further mouse model. Mating of two mouse strains, CBA/J×DBA/2, reproduces features of pre-eclampsia with proteinuria, renal impairment (elevated BUN), glomerular fibrin deposition and glomerular endotheliosis.[90] A single dose of CR2-Crry at 5 dpc prevented development of proteinuria and glomerular endotheliosis.[90] However, in contrast to the inducible rat model, an increase in C5a levels was associated with disruption to the balance of angiogenic factors, with elevated C5a correlating with reduced VEGF and increased sFLT-1. This argues for a role for C5a in the induction of anti-angiogenic factor release from the inflamed and ischemic placenta.[91]

In a different approach, the effect of injection of IgG from normotensive or pre-eclamptic pregnant women into pregnant C57BL/6 mice was examined. IgG was purified from the blood of pre-eclamptic women with severe disease (gestational age 32 weeks) and from women with uncomplicated normotensive pregnancies (gestational age 36 weeks), and injected into pregnant mice at 13 and 14 dpc, followed by euthanasia at 18 dpc. Histological features of placental distress were identified in the mice injected with IgG from pre-eclamptic women, but not in mice injected with IgG from normotensive women. Pre-eclamptic women have agonistic autoantibodies to the angiotensin II type 1 (AT1) receptor, and in this study, it was demonstrated that C3 deposition in placentas of mice injected with IgG from pre-eclamptic women correlated with AT1 receptor activation.[92] While the mechanism by which AT1 receptor activation induces C3 activation is not known, it seems clear that C3 activation plays an important role in initiating events that lead to pre-eclampsia. Blockade of the C3aR with a C3aR antagonist, SB290157, reduced hypertension and proteinuria in the mice, prevented intrauterine growth reduction (IUGR), and reduced sFLT1, demonstrating a role for C3aR signaling in impaired placental angiogenesis.[92]

3.3.2 | Complement activation within the placenta

Early studies identified increased C3 and C9 deposition in pre-eclamptic placentas when compared to normotensive controls.[44,93] However, a more recent study comparing early onset (<34 weeks of gestation; 7 subjects) vs. late onset pre-eclampsia (5 subjects) vs. normotensive controls (10 subjects) failed to find supportive data for this; activated C4 deposition, an indicator of CP and/or LP activation, was abundant, but no difference in C3b/IC3b/C3d or C9

deposition was seen between the groups.[94] In the same study, abundant amounts of the membrane-bound regulators CD55, CD46, and CD59 were found, both in pre-eclamptic placenta and healthy controls. There was, however, an irregular distribution of C4bp and FH in pre-eclamptic placenta,[94] suggesting possible structure-specific regulatory control needs.

In a separate study, a significant increase in mRNA expression of CD55 and CD59 in pre-eclamptic placenta was observed.[95] This, coupled with diffuse placental C4d deposition associated with a significantly lower gestational age at delivery, is suggestive of excessive CP activation and an altered need for a compensatory increase in membrane protection in the pre-eclamptic placenta. Interestingly, in this study, no difference in staining for properdin between pre-eclamptic and normotensive placentas was seen, possibly indicative of a minimal role for the AP in complement-mediated events.

A reduction in C3aR mRNA and protein expression in placental tissue of severe early onset pre-eclamptic women compared with preterm normotensive control pregnancies has also been reported.[96] This reduction in C3aR expression suggests impairment in C3a-mediated effector mechanisms, seemingly at odds with the data reported by Wang et al.,[92] who concluded that C3a drove pre-eclampsia. Variable results have also been obtained with analysis of C5aR expression, with no change,[96] elevated,[97] or reduced[98] expression in pre-eclamptic placentas. In vitro work has also shown C5a is able to disrupt the angiogenic balance within the placenta, with C5a stimulated trophoblasts increasing expression of sflt-1 and decreasing PlGF.[97]

No clear picture, other than that complement activation, and its probable aberrant regulation, plays a role in the development of pre-eclampsia, emerges from the above data. Certainly, there is no clear evidence pointing to a role of the AP. It should, however, be noted that the above studies were of small cohorts, and made at different pre-eclamptic stages, and the large spectrum of disease seen in pre-eclampsia may account for the conflicting data.

3.3.3 | Complement activation in the maternal circulation

A pivotal prospective study by Lynch et al., of 701 pregnant women, identified Bb as a biomarker for women at increased risk of pre-eclampsia. Women with elevated plasma levels of Bb before the 20th week of pregnancy were three times more likely to develop pre-eclampsia than those with normal levels of Bb at the same time point.[99] In a follow-up study, plasma Bb levels were measured longitudinally during pregnancy (up to three samples/pregnancy). Of the 552 evaluable pregnancies, 28 (5%) developed pre-eclampsia; these were compared with randomly selected normotensive pregnancies from the same population. The study found that Bb levels were highest, in both normotensive and pre-eclampsia subjects, in early pregnancy, with a gradual decline up to the time of parturition. While the initial plasma level of Bb varied with gestational age at blood draw, a significant trend to increased Bb levels between

10 and 21 weeks was found in women who subsequently developed pre-eclampsia when compared to women who remained normotensive during pregnancy. No relationship between Bb levels in later pregnancy and pre-eclampsia was identified.[100]

This was confirmed by Derzsy et al., who looked at complement protein levels at a late gestational stage, and found that pre-eclamptic (n = 60; gestational age at blood draw 36 weeks) pregnancies had higher CRP, C4d, C3a, and sC5b9, and lower C3, when compared to healthy pregnant controls (n = 60; gestational age at blood draw 37 weeks). When both pregnancy groups were compared with healthy non-pregnant controls, FH levels were also found to be higher, and C1inh levels lower, in pregnancy, with or without pre-eclampsia. No difference in plasma Bb (or C4bp) levels between the pregnancy groups, or between these and healthy non-pregnant women, was observed at this late stage in pregnancy.[49] In further analysis of complement protein plasma levels in these groups, Derzsy et al. also noted that pre-eclamptic pregnancies with intrauterine growth restriction (IUGR) had higher sC5b-9 than those without IUGR. Taken together, these data suggest that in late pregnancy there is elevated activation of complement, probably through both the CP and the LP, but that only C5b-9 generation is exacerbated in some cases of pre-eclampsia.

Ma et al. found an increase in maternal C5a in women with pre-eclampsia, and this positively correlated with maternal blood pressure and arterial stiffness.[97] These results were echoed in further studies showing an increase in maternal circulating C5a in pre-eclamptic women compared with normotensive controls.[101–103] Soto et al. measured C3a, C4a, and C5a plasma levels in normotensive and pre-eclampsia pregnancies and found that pre-eclampsia was associated with increased plasma concentration of C5a (but not C3a or C4a). They also compared complement anaphylatoxin levels in small for gestational age (SGA) pregnancies, with or without pre-eclampsia, with the surprising finding that whereas SGA associated with pre-eclampsia was associated with elevated C5a levels, SGA alone was not.[104] Pre-eclampsia associated with IUGR indicates placental insufficiency, thus terminal complement activation may be consequent on debris generated by the failing placenta. Systemic complement activation in late pregnancy may therefore simply reflect a pro-inflammatory environment in the placenta and the sequelae of maternal endothelial dysfunction, that is, an association with, rather than causation of, IUGR. A lack of consistent association between plasma C3a levels and pre-eclampsia has also been noted by others.[102]

While pre-eclampsia is almost invariably associated with elevated maternal plasma C5a, the data with sC5b-9 are less consistent. As noted above, Derzsy et al. found elevated sC5b-9 levels in late stage pregnancies with pre-eclampsia, and especially with pre-eclampsia associated with IUGR.[49] By contrast, Haeger et al., in a longitudinal study of 685 primiparous women followed throughout pregnancy, only found an increase in sC5b-9 in women with HELLP syndrome at delivery.[103] (HELLP -Hemolysis, Elevated Liver enzymes, Low Platelet syndrome is a serious blood clotting complication of pregnancy, which, while usually occurring at delivery, can occur earlier

in pregnancy.) Lynch et al. conducted a secondary analysis to see if sC5b-9 could be used as an independent predictor of pre-eclampsia at 10–15 weeks' gestation, but no difference was identified in early pregnancy among women who later develop pre-eclampsia when compared to normotensive pregnant controls.[105] Burwick et al. looked at sC5b-9 levels in women with severe pre-eclampsia, comparing these with controls with pre-existing chronic hypertension and to healthy controls, both matched by parity and by gestation age (±2 weeks). They found an increase in urinary excretion of sC5b-9 which correlated with elevated sflt-1 (anti-angiogenic) and suppression of PlGF and VEGF (pro-angiogenic) factors in plasma,[106] but no association between plasma sC5b-9 and the same angiogenic factors. Additionally, while plasma levels of sC5b-9 were increased in cases of severe pre-eclampsia when compared to healthy controls, there was no difference between the pre-eclampsia and chronic hypertension group.[107]

While it is difficult to extrapolate plasma protein levels with local activation events, elevated plasma C5a is consistently seen in pre-eclampsia. This association does not define C5 activation as causative of pre-eclampsia, but a causative association would be consistent with in vitro work that has shown that C5a induces monocytes to produce sFLT-1 (soluble VEGF receptor 1) which then sequesters VEGF. This was confirmed with in vivo data showing that the complement system regulates VEGF activity, and that a deficiency of free VEGF induced by high levels of sflt-1 leads to abnormal placental development.[91]

A surprising, but potentially important, finding arising from evaluation of complement activation products as markers for pre-eclampsia is that urine, rather than plasma, might provide a better biomarker source material.[106]

What also appears clear from evaluation of complement activation products in pre-eclampsia is that it is early (first trimester) complement activation, and particularly FB activation, that is predictive of pre-eclampsia later in pregnancy. It also points intriguingly to the possible involvement of the AP in the defective placentation that leads subsequently to pre-eclampsia.

3.3.4 | Genetic studies

It has been hypothesized that polymorphisms in complement genes may be linked to adverse pregnancy outcomes. The PROMISSE study looked at 250 pregnant women with a diagnosis of SLE and/or APS; this population have an increased risk of developing pre-eclampsia, and it was hypothesized they might have an impaired ability to regulate complement activation. In this study, of 250 pregnancies, *CD46*, *CFI*, and *CFH* genes were sequenced.[108] These proteins are regulators of C3 activation. Of these 250 pregnancies, 40 developed pre-eclampsia, and, of these, seven (17%) were found to be heterozygous for a variant previously identified as a risk variant for aHUS. Five risk variants of CD46 or FI and one novel CD46 variant were identified. While these proteins are involved in regulation of both CP and AP C3 convertases, the fact that aHUS is clearly a disease of dysregulated

AP activation[109–111] enabled the authors to conclude that the AP amplification loop plays a role in susceptibility to pre-eclampsia.[108] That said, no FH risk variants were identified, and of the three regulators investigated, only FH is AP-restricted. What is also notable in this study is that in 83% of the pre-eclamptic women, no AP risk variant was identified. It is possible that some carried risk variants in genes not evaluated, but, at first sight, it would seem that only a minority of women who went on to develop pre-eclampsia had a clearly definable complement-dependent risk, suggesting a high degree of complexity in determinants of the condition. It should also be noted that this study was conducted in women with an underlying autoimmune condition that predisposes them to complement activation.

In contrast to the above findings, Lokki et al. sequenced the CD46 exome in 95 Finnish women, and found no association between CD46 risk variants and severe pre-eclampsia.[112] The two studies are not equivalent in view of the autoimmune status of the PROMISSE population and ethnic differences between the two groups, but this divergence in findings demonstrates the need for further work to replicate (and extend) evaluation in a group without underlying autoimmune disease, and who will likely have a higher threshold for developing pre-eclampsia.

A recent study has suggested the possibility of a pregnancy-specific complotype predisposing women to development of pre-eclampsia. In this study, *CFH*, *C3*, and *CD46* genes were sequenced. A novel approach in this study was to focus on fetal, not maternal, *CD46*, and hence introduce consideration of the allogeneic nature of the fetal-placental interface. The allelic frequencies of two SNPs in fetal *CD46* were elevated in pre-eclampsia pregnancies when compared with normotensive pregnancies. These, combined with allelic variants of *C3* and *CFH*, allowed complotypes defining susceptibility to pre-eclampsia to be defined. What was also noteworthy in this study was that the rare CD46 risk alleles are associated with decreased CD46 expression. Consistent with defective regulation of C3 activation, C4, C3, and C5b-9 deposition on the placenta was significantly higher in pre-eclamptic vs. normotensive pregnancies.[113]

3.3.5 | Long-term sequalae of pre-eclampsia

Pre-eclampsia is primarily a disease of the endothelium, and women who suffer from pre-eclampsia have a greater risk of cardiovascular disease in later life. Large population-based studies have shown an increased risk of ischemic heart disease, hypertension, thromboembolic events, and type 2 diabetes (T2DM). The severity of pre-eclampsia dictates the severity of cardiovascular disease developing in later life.[114] Cardiovascular disease is the leading cause of death in women, so there is a vital need to understand how pre-eclampsia leads to persisting endothelial damage. Is it causally associated with postpartum vascular remodeling,[115] or does it unmask women with a pre-disposition who have failed the "stress test" of pregnancy? There is a paucity of data investigating the role of complement on long-term vascular remodeling following pre-eclampsia. It has been shown that hypoxia-induced perivascular inflammation is

—WILEY⊥

complement-dependent, and that AP activation plays a critical role in this.[116] Recent in vitro work has demonstrated higher AP activation and C3a generation by human glomerular vascular endothelial cells (GMVECs) compared with brain microvascular endothelial cells (BMVECs),[117] showing that not all endothelial cells are equivalent. One avenue that deserves further evaluation in pre-eclampsia is the role that the AP has in postpartum vascular remodeling[118] in different tissues.

3.3.6 | Treatments for pre-eclampsia

As outlined in this section, there is a plethora of evidence pointing to dysregulation of complement activation, and particularly of C5 activation, in the inflammatory-mediated injury of pre-eclampsia. Eculizumab, a monoclonal antibody inhibitor of C5 activation, has been highly successful in the treatment of PNH and aHUS. While both are AP-driven diseases, the major effector arm of both conditions requires C5 activation. The latter similarity with pre-eclampsia suggests that pre-eclampsia might be effectively treated by anti-C5 therapy. The very narrow species-specificity of eculizumab precludes preclinical evaluation in a pharmacodynamically relevant species, and hence, no preclinical reproductive and developmental safety evaluation has been possible.[119] However, continuation of treatment during pregnancy of patients with PNH and aHUS has shown an acceptable safety profile for the drug during pregnancy.[62,120] Additionally, despite eculizumab binding to the Fc receptor, and being found in one third of cord blood samples, it does not accumulate in fetal plasma. The newborn's complement activity remains within the normal range despite C5 activation in the mother being adequately blocked,[121] even though increased dosage might be required during pregnancy because of increased C5 synthesis and a higher distribution volume.[62] Importantly, eculizumab does not appear to transfer to the newborn via breastmilk.[120] A number of reports of the successful treatment of pre-eclampsia with eculizumab have been published.[122,123] However, there are also an increasing number of reports of pregnancy hypertension syndromes (including pre-eclampsia) in aHUS despite adequate complement blockade with an anti-C5 therapy, so it is unlikely that eculizumab therapy will be a panacea for pre-eclampsia.

Aspirin is the therapy proven to reduce the incidence of preterm pre-eclampsia, and there is a rationale for this.[124] A recent study examining hepatocyte nuclear transcription factors (HNF), found that HNF4α positively regulated expression of C3 and FB. Both were significantly downregulated in transgenic placentas by aspirin treatment in a mouse model of severe pre-eclampsia induced by feto-placental overexpression of human transcription factor STOX1A.[125]

Heparin has therapeutic effects beyond anticoagulation. Unfractionated or low-molecular-weight heparin prevented complement activation and adverse obstetric complication in a mouse model of APS. This effect was distinct from its anticoagulation properties as alternative anticoagulants did not replicate the protective effects.[126] Clinical trials with heparin have also shown inconsistent results in pre-eclampsia. Collating evidence through systematic reviews and meta-analyses has failed to provide a consensus; it is likely that the heterogeneity of the condition explains the conflicting data. Women who present with severe early onset disease, identified within the index pregnancy using a combination of placental and cardiovascular assessment, may identify a cohort whom would benefit from the protective vascular effects of heparin, but further clinical studies are required to assess this.[127]

It is also worth noting that none of the above therapies are preventative of disease, but treat disease once it occurs. Any early preventative treatment would have to be introduced early in pregnancy, and for this, a highly reliable diagnostic of early disruption to placentation would be required.

3.4 | Obesity and adverse effects of pregnancy

Pregnancy is associated with a physiological state of inflammation and insulin resistance, which is further amplified in women who are overweight.[128] Obesity is a known risk factor for pre-eclampsia, with a higher incidence of pre-eclampsia in women who are obese.[128] Weight loss preceding pregnancy reduces the risk of pre-eclampsia.[129] Obesity also increases neonatal adverse events including macrosomia (large for gestational age) and congenital defects.[130] Obesity is the expansion of adipose tissue, and complement components, particularly C3, FB and Factor D (FD),[131,132] can be synthesized by adipose tissue. Of particular relevance here, the primary site of FD synthesis is adipose tissue, and its role in adipose tissue metabolism (as adipsin) has long been recognized.[133] An increase in local concentrations of C3, FB, and FD is known to promote local complement activation.[134] Possibly even more relevant, elevated FD levels result in increased AP activation.[135] Complement activity is increased with obesity, positively correlating with BMI and decreasing with weight loss.[84] In mice, an increase in C3 is found in the adipose tissue before and during pregnancy as well as at the maternal fetal interface; this is reduced following calorie restriction, implying that dietary intervention could influence the propensity of immune dysregulation during pregnancy.[84,136] C3aR is highly expressed in adipose tissue and, in mice, with increased expression when they are placed onto a high fat diet.[137] In mice, maternal obesity has been shown to directly alter the placental transcriptome during development.[138] Women with increased concentrations of Bb and C3a combined with obesity were more likely to develop pre-eclampsia.[105,128]

In addition to its value in investigating the mechanism of pre-eclampsia, the BPH/5 mouse model is useful in study of the effects of obesity on complement activation. The female BPH/5 is obese with borderline hypertension but an absence of renal disease. Pregnancy exacerbates the model, female mice developing a superimposed pre-eclampsia.[136] Adult females also show hyperphagia and hyperleptinaemia with signs of leptin (an appetite-suppressing hormone) resistance. Interestingly, males are not obese and do not mirror the cardiometabolic phenotype of their female counterparts.[136] Following blastocyte implantation, and prior to decidualization and

placentation, BPH/5 mice have reduced macrophage but increased T lymphocyte infiltration within the maternal decidua, and reduced IL-10 levels, indicating an aberrant maternal immune response.[139] At 7.5 dpc complement gene upregulation (*C3* and *CFB*) in BPH/5 mice corresponds to peak decidualization.[85] An increase in placental C3 mRNA expression is detected with increased deposition of C3 and C9 at 10.5 dpc localized to the trophoblast giant cell layer. Increased mRNA expression of VEGF-α at 5.5 dpc preceded complement activation; this correlated with abnormal placental vasculaturisation, and culminated in downregulation of pro-angiogenic genes and an increase in levels of the anti-angiogenic factor, sFLT-1, at 10 dpc.[85] Thus, early local altered expression of VEGF-related genes and abnormal decidual vasculaturisation preceded Sflt-1 upregulation and increased complement deposition. Abnormal decidual angiogenesis, with associated complement activation, appears to contribute to altered trophoblast invasion and subsequent poor placentation of the BPH/5 mouse.[85]

Visceral white adipose tissue (WAT) contains inflammatory mediators, including complement factors, that, particularly when adjacent to the female reproductive tract, may contribute to angiogenic imbalance and pre-eclampsia.[84] Using the BPH/5 mouse model, investigators sought to determine whether reversal of maternal obesity through calorie restriction lowered inflammation in adipose tissue, and if this improved placental development. C3 and FB (but not FD) mRNA expression is increased in the reproductive WAT of non-pregnant BPH/5 females when compared with a matched cohort of calorie-restricted mice, showing that the reproductive WAT may be a source of complement components. As calorie restriction was successful in reducing mRNA expression of C3 and FB in the reproductive WAT of non-pregnant females, it was thought that reducing obesity could attenuate the inflammatory milieu in the reproductive WAT. BPH/5 mice were therefore calorie-restricted for 2 weeks prior to, and for the first seven days of, pregnancy. This attenuated C3 gene expression, but not that of FB or FD expression, at the implantation site.[140]

Calorie restriction during pregnancy also restored VEGF and PIGF mRNA levels at the implantation site in the BPH/5 mouse.[140] While interpretation of the above data is complex, it appears that maternal reproductive WAT is a source of increased C3 during pregnancy, especially at the maternal-fetal interface, and that reducing maternal weight, and hence C3 (from which antiangiogenic factors are produced) in adipose tissue, may assist in improving the angiogenic balance in the BPH/5 mice.

Correa et al. compared immunological and metabolic blood components during the first half of pregnancy in women who began a pregnancy under normal healthy conditions with those who had risk factors for obstetric complications, including obesity.[141] Pregnancy outcomes, ranging from pre-eclampsia to SGA deliveries, were significantly higher in pregnancies initiated in women with risk factors. While no changes in AP-specific proteins (Bb, FD) were observed, elevated CRP, C4, and C3a were seen in the at risk group, implying CP and/or LP activation.[141] It has been suggested that higher CRP levels may have an impact on the regulatory activity of FH, impairing

its ability to clear apoptotic cells.[101] CRP binds to FH SCRs 7 and 8–11 in a calcium dependent manner.[142] These sites are distinct from C3b binding sites; CRP preserves the ability of FH to enable FI-mediated cleavage of C3b, and it has therefore been proposed that it might target functionally active FH to injured self-tissue, restricting excess complement attack in tissues without affecting AP activity against invading microbes in the blood.[142] In the context of pregnancy in obese and other at risk populations, it is possible that CRP-dependent sequestering of FH might constitute a maternal response that offers some protection against complement attack on the placenta.

3.5 | Gestational diabetes

Gestational diabetes (GDM), in which pregnant women with no known history of diabetes develop chronic hyperglycemia, is one of the most common complications of pregnancy. GDM can lead to serious maternal and fetal complications. While it typically resolves upon delivery, it is associated with T2DM and cardiovascular disease in later life. It also increases the risk of future obesity, cardiovascular disease, T2DM and GDMs in the infant (reviewed in Ref. [143]).

In normal pregnancy, a state of insulin resistance develops to facilitate the delivery of glucose to the placenta, supporting the growing fetus. GDM arises during pregnancy due to impaired β cell function on a background of chronic insulin resistance; low-grade inflammation has been involved in the pathogenesis of insulin resistance. In T2DM, activation of the AP may participate in development of a chronic inflammation and insulin resistance state. *CFB* gene expression is higher in the omentum tissue, with a positive correlation with BMI and fasting glucose,[144] and higher circulating levels of FB (and properdin) have been identified in T2DM patients and their first-degree relatives compared with a healthy control group.[145,146] These data point directly to a role of FB, and hence the AP, in the development of GDM. As GDM is considered a precursor for T2DM, it is plausible to hypothesize a role of the AP in the pathogenesis of T2DM as well.

Work in a rat model of spontaneous hypertension (exhibits hypertension, insulin resistance and dyslipidemia, features of metabolic syndrome) showed that knocking out the *CFB* gene improved glucose tolerance and insulin sensitivity, with redistribution of visceral to subcutaneous fat. This suggests an important role, at least in the rodent, for FB in development of metabolic syndrome,[147] yet another risk factor for diabetes. Additionally, a reduced blood pressure, increased ejection fraction, and reduced left ventricular mass was seen in the *CFB* knockout, implying a wider role in cardiovascular disease.

While studies linking GDM to complement activation are limited in number, one has shown that higher levels of circulating Bb between 11 and 17 weeks of gestation are associated with an increased risk of developing GDM.[148] FH levels are also increased in patients with T2DM and plasma levels of FH are negatively associated with insulin sensitivity,[144] suggesting an increased regulatory

—WILEY 311

requirement in these conditions. In a follow-up nested case control study of 397 pregnant women, the same group analyzed FH levels in women who had GDM, comparing them with non-GDM controls, finding FH levels to be higher in GDM. FH levels were not, however, independently associated with GDM.[149]

Screening and identifying women with GDM enables early treatment to reduce maternal and fetal morbidity. A secondary analysis from the pregnancy exercise and nutrition research study (PEARS) found that the maternal C3 levels were predictive of not just GDM, but also pregnancy-induced hypertension and pre-eclampsia.[150] Associations were, however, weak, and it is difficult to draw any firm conclusions from them.

Low levels of CD59, the membrane-bound inhibitor of the complement membrane attack complex, are shed into blood. Hyperglycemia results in a non-enzymatic glycation of CD59, which inactivates the inhibitor. The plasma level of glycated CD59 has been investigated as a potential early diagnostic biomarker of GDM (at <20 weeks' gestation), with promising results. Soluble glycated CD59 has also been associated with LGA infants.[151] Glycation and inactivation of placental CD59 may result in increased complement-mediated placental damage by the membrane attack complex, potentially contributing to the multiple complications seen in women with GDM.[152]

4 | ROLE OF ALTERNATIVE PATHWAY AND THE INCREASED OBSTETRIC BURDEN IN WOMEN WITH UNDERLYING SYSTEMIC AUTOIMMUNE DISEASES

In the previous sections, we have discussed the potential role of complement in the development of pregnancy-specific disorders. We will conclude with discussion of the role of complement, and specifically of the AP, in women with underlying conditions who are at increased risk of complement-related disorders because of an autoimmune disease, focusing on SLE and APS. These conditions disproportionately affect women of childbearing age, placing them at increased risk of obstetric complication during their pregnancies.

4.1 | SLE

SLE is a complex multisystem autoimmune disease. Complement activation by immune complexes formed in the fluid phase and at the tissue level following interaction of autoantibodies with their target antigen leads to the clinical manifestations.[153] Complement activation in SLE leads to a reduction in circulating C3, C4, and C1q, reflecting consumption, with a concomitant increase in split products that correlates with disease activity. Pregnancies in patients with SLE are regarded as high risk due to an increase risk of disease flaring coupled with high risk of adverse pregnancy outcome. Pregnant women with SLE have an increased risk of pregnancy loss, PTB, IUGR, and premature rupture of membranes, with an increase in pre-eclampsia

if their disease is active (13–35% compared with 5%–8% in the general population).[154] Despite this, improvements in maternal mortality and reduction in fetal mortality have been achieved over the last two decades.[155] Risk factors for poor pregnancy outcome include hypertension, secondary antiphospholipid syndrome and lupus nephritis. A large systematic review found that one-quarter of pregnancies were unsuccessful, with 39.4% preterm births within the live birth cohort. Active lupus nephritis increases the risk of adverse pregnancy outcomes[156]; a history of lupus nephritis is associated with a threefold increased risk of renal flare during pregnancy.

In an early paper, Buyon et al. showed that the AP was activated in disease flares in pregnant women with SLE, and that this was associated with a lowered CH50.[157] What was especially interesting in this study was that elevated Ba levels were also seen in pre-eclampsia, indicative of AP involvement, but that these were not associated with a low CH50, indicating differences in the triggers for complement activation. Consistent with this, and much later, analysis of complement activation products in the PROMISSE cohort showed that Bb and sC5b-9 detected in the circulation in early gestation identified women whom later developed an adverse outcome.[158]

Analysis of placentas from antiphospholipid antibody (aPL)-negative SLE patients has found evidence of increased complement deposition of C4d and C5b-9 in syncytiotrophoblasts and extravillous trophoblasts when compared to healthy control placentas.[159] Lupus anticoagulant was associated with adverse pregnancy outcomes after the first trimester, but no association was seen with anticardiolipin antibodies.[160–162]

4.2 | APS

APS is characterized by thrombosis and recurrent pregnancy loss accompanied with detectable antiphospholipid antibodies (aPL). It is the leading cause of recurrent pregnancy loss. In women with a history of obstetric APS, the current recommended treatment is with low-dose aspirin and low-molecular-weight heparin.[163] In a large European Registry study, the outcomes of pregnancies in 1000 women were analyzed. Miscarriage was recorded in 38.6% of the pregnancies, pre-eclampsia in 18.1%, and IUGR in 16.1%. However, in those women who received the recommended treatment, a live birth rate of 85% was recorded. This fell to 72.4% in women receiving either aspirin or low molecular weight heparin, but not on the recommended schedule, and to 49.6% in women receiving no treatment. 15.2% of patients on recommended treatment remained refractory.[164]

It should be noted that, since the initiation of the European Registry study, hydroxychloroquine (HCQ), a disease-modifying antirheumatic drug (DMARD) also used as an antimalarial, has been introduced in the treatment of pregnant women with APS, with some success, and this may impact on the outcomes reported above. HCQ appears to have been introduced based on anecdotal data, with little understanding of its mechanism of action. In investigating this,

Bertolaccini et al. demonstrated that it prevented complement activation in vivo and in vitro, with lower C5a levels and reduced placental insufficiency with HCQ-treatment in a mouse model of APS.[165] Similarly, HCQ lowered C5a levels in pregnant women with APS. HCQ appears safe to both mother and fetus, and these mouse studies suggest that a possible mechanism of action is blockade of complement (C5) activation, consistent with data reported in earlier sections suggesting that C5 activation early in pregnancy might adversely impact placentation.

Antiphospholipid (aPL) antibodies activate a plethora of immune cells, monocytes, neutrophils, platelets, and endothelial cells; this culminates in inflammation and thrombosis. Branch et al. showed that passive infusion of IgG from patients with aPL increased the rate of fetal resorption in pregnant mice, illustrating the pathogenic role of the antibody in fetal loss.[166] Holers et al. showed that C3 activation was required for aPL-induced fetal loss and growth restriction. Pregnant mice were injected with human IgG containing aPL antibodies at 8 and 12 dpc. The animals were then euthanized on day 15 and found to have an increased incidence of fetal resorption (40%) and reduced fetal weights compared with control mice.[167] Mice treated with a C3 convertase inhibitor (Crry-Ig) or mice deficient in C3 did not experience fetal loss or fetal growth retardation,[167] confirming that complement activation is the major mechanism of aPL mediated tissue injury. Follow on work from Girardi et al. using the same model showed that while C4 deficient mice were protected from fetal injury, FB was required for fetal death, confirming a critical role for the AP in the induction of fetal loss.[168] Confirmation of this came from the use of a novel anti-murine FB monoclonal antibody that inhibited AP activation. Mice treated with the antibody had significant protection from AP activation, and reduced fetal resorption, decidual inflammation, and decidual complement activation.[169]

Further analysis of the effector mechanism showed that the C5a-C5aR axis and C5a-dependent recruitment of neutrophils were key mediators of fetal injury. Both C5aR deficiency and C5aR antagonist administration were protective.[168] Key sequelae to C5a production are that neutrophils are attracted into the deciduas, endothelial cells are stimulated to produce monocyte chemoattractant protein-1, and monocytes express tissue factor. The culmination of these (and other related events) is trophoblastic injury and fetal loss. The pathogenicity of C5a, and its potent ability to induce prothrombotic conditions within the deciduas, was confirmed when it was shown that C6 deficient mice had a similar rate of pregnancy loss as wildtype mice,[170] and therefore that the consequences of C5b-9 generation are insignificant in this model.

Collating studies using murine models of APS shows that aPL-induced tissue damage is mediated through complement activation. While amplification via the AP is critical, induction appears to be through the CP, culminating with C5a as the dominant driver of disease pathology. Heparin has been shown to attenuate inflammatory responses through multiple interactions with complement proteins including inhibition of C1q binding to immune complexes, inhibition of C4 activation, and blockade of the C3 convertase in the amplification loop and the formation of MAC.[126] Heparin, at sub-anticoagulant

doses, prevented obstetric complications by blocking CP activation at the decidual tissue.[126] Combination therapy with heparin and a FB inhibitor and/or a C5aR antagonist might therefore provide a therapeutic strategy to explore in the treatment of refractory obstetric APS (but see cautionary note below).

The above conclusions regarding the role of complement are all derived from animal model studies, and it is important that corroborative data in human pregnancies be evaluated. An increase in deposition of C4d and C3b on human APS-placentas when compared with healthy pregnancy controls has been found.[171] This was apparent even if the disease was clinically senescent with no adverse features. Surprisingly, there was a decrease in C5b-9 deposition; the reason for this is not understood.[171] In a separate study, complement activation products were identified in all placentae examined, with C1q, C4 and C3 detected on the decidual endothelium vessels at sites of IgG and IgM deposition, whereas C5b-9 showed a predominance for a subendothelial distribution.[172] Complement deposition was also found on surface of syncytiotrophoblasts with additional distribution of C5b-9 on intervillous fibrin deposits, and C3 deposition on the endothelium of villous vessels.[172] Interestingly, this occurred despite treatment with low-dose aspirin and heparin. One conclusion from this study was that the anticomplement effects of heparin seen in the murine model are not replicated in humans.[172]

In the above study, complement deposition was found in all APS placenta, even in women who had a live birth. Antiphospholipid antibodies bind to endothelial cells, inducing activation through upregulation of ICAM, VCAM, E-selectin, and tissue factor. This, coupled with platelet activation by C3a, C5a and C5b-9, results in a prothrombotic environment.[173] It has been suggested that these events overwhelm the complement regulatory capacity of placental CD55, CD46, and CD59, leading to Ischemia and tissue injury.[173]

When comparing circulating complement levels during pregnancy, some multicenter case–controlled studies in pregnant women with APS have shown that lower C3 and C4 at baseline and at the end of pregnancy was significantly correlated with poor pregnancy outcome.[174–176] This, however, has not been a universal finding; while one group identified lower levels of C3 and C4 in each trimester in APS pregnancies when compared with healthy women, this was not associated with adverse pregnancy outcome.[177] Despite these inconsistencies, hypocomplementaemia is still considered a prognostic factor for adverse pregnancy outcomes in APS patients.[178]

A significant increase in levels and frequencies of FH autoantibodies has also been reported in patients with APS when compared to matched controls, higher in secondary APS than in primary APS. (Secondary APS is APS that occurs on top of a pre-existing condition, most commonly SLE.) This study also reported that the presence of FH autoantibodies was associated with venous thrombosis.[179] Given our current understanding of the role that surface-recruitment of FH plays in regulation of AP activation on host cells (discussed earlier), autoantibodies to the C-terminal region of FH that block this recruitment might be expected to exacerbate any APL-antibody effect, further disturbing the orchestrated interplay between complement and the clotting cascade. The evidence linking anti-FH antibodies

to aHUS is compelling, with thrombosis in both aHUS and APS resulting from activation of the endothelium, which generates a pro-thrombotic phenotype. Supportive of this is the observation that FH levels are lower in APS than in healthy controls.[180] As yet, no systematic evaluation of the role of autoantibodies to FH in obstetric APS has been published, but one would be warranted, if only to identify women at increased risk of obstetric complications.

In addition to adverse pregnancy outcomes such as miscarriage and compromised fetal development, pregnancy can trigger catastrophic APS (CAPS). Case reports have shown clinical benefit with eculizumab administration both in CAPS[181,182] and in a patient at high risk of developing CAPS,[183] and a clinical trial is underway to evaluate eculizumab for CAPS following renal transplantation (NCT01029587). Together, animal studies and observations in women provide a strong case for a causative role for AP activation in adverse pregnancy outcomes in APS, and provide a strong rationale for clinical evaluation of AP inhibitors, at least in refractory APS if not in all APS pregnancies.

5 | CONCLUSIONS

A successful pregnancy requires a measured amount of complement activation. Dysregulation of the AP undoubtedly contributes to the obstetric burden of adverse events in pregnancy. Events that take place in early pregnancy, detected by the AP activation fragment Bb, are predictive of adverse events arising at a later gestation. Dysregulated AP activation plays a clear role in APS-related adverse obstetric events. Future research should focus on how we can harness this information to detect clinically-quiescent disease before it leads to detrimental health effects to mother and infant. Identification of this subgroup of women in whom there is an established event in early pregnancy may inform treatment which, in future, might include complement-directed therapeutics.

Research is also needed into the fourth trimester of pregnancy; the postpartum phase and beyond. The complications of pregnancy-specific conditions dictate a woman's future health risk and exploring the role of the AP on postpartum vascular remodeling may provide insightful data relevant to attenuation of a woman's postobstetric cardiovascular risk, thus improving womens' global health.

CONFLICT OF INTEREST
KSJ none to declare. RAH is the owner and director of RAH Pharma Consulting Ltd. He also was employed by Novartis Pharma AG from 2001 to 2013, and between 2013 and 2022 held various consultancy agreements with Novartis.

DATA AVAILABILITY STATEMENT
Data sharing not applicable to this article as no datasets were generated or analysed during the current study.

GLOSSARY

Term	Definition
Zygote	Fertilized egg following union of a female ovum with a male sperm
Blastocyte	A group of dividing cells formed by a fertilized oocyte which then develops into an embryo
Decidua	Maternal component of maternal-fetal interface. It only exists during pregnancy and comes from the endometrial lining of the uterus. Following labor, the decidua is shed, and only rebuilds if a subsequent pregnancy happens
Decidualization	Describes the functional and morphological changes that occur within the endometrium, enabling the blastocyte to implant and the placenta to develop
Extravillous cytotrophoblasts	The extravillous trophoblasts (EVT) depart from the tip of the placental villi and migrate into the maternal decidua, providing anchorage of the villi to the uterine wall. The EVT invade the spiral arteries (now termed endovascular trophoblast) and in union with the uNK remodel the spiral arteries
Placental villi	Houses the fetal blood vessels and comprises of the syncytiotrophoblast and cytotrophoblast layers. The villi are in direct contact with maternal blood enabling nutrient and gas exchange, they form "finger like" projections (chorionic villi)
Syncytiotrophoblasts	Outer syncytial layer of the trophoblast (fetal origin) that invades uterine wall forming outermost fetal component of placenta. Formed from the fusion of two or more of the underlying cytotrophoblasts (hence multinucleated cells). The syncytiotrophoblasts are the major cellular barrier between the fetal compartment and maternal blood
Cytotrophoblasts	Reside directly underneath the syncytiotrophoblasts. They are undifferentiated mononucleated cells in the chorionic villi and differentiate into either syncytiotrophoblasts or extravillous cytotrophoblasts

Term	Definition
Semi-allogenic feto-placental unit	The placenta and developing fetus as a unit, deriving, half of its genetics from the mother and the other half inherited from the father
Uterine natural killer cells	Natural killer cells within the decidua that have a distinct phenotype compared to peripheral blood natural killer cells
Zona pellucida	The extracellular matrix surrounding the blastomere membrane
Decidual stromal cells	The main cellular component of maternal decidual layer
Haemochoiral placenta	A placenta where maternal blood comes into direct contact with the fetal chorion (the outermost fetal membrane)
Pre-eclampsia	Pregnancy-specific condition defined by hypertension with accompanying maternal organ dysfunction
HELLP syndrome	A pregnancy-specific condition characterized with Hemolysis, elevated liver enzyme and low platelets, considered a severe variant of pre-eclampsia
Preterm birth	Birth of neonate between $20^{0/7}$–$36^{+6/7}$ weeks' gestation

ORCID

Kate Smith-Jackson https://orcid.org/0000-0003-4735-0836
Richard Alexander Harrison https://orcid.org/0000-0002-2408-6043

REFERENCES

1. Soma-Pillay P, Nelson-Piercy C, Tolppanen H, Mebazaa A. Physiological changes in pregnancy. *Cardiovasc J Afr*. 2016;27(2):89-94.
2. Facca TA, Mastroianni-Kirsztajn G, Sabino ARP, et al. Pregnancy as an early stress test for cardiovascular and kidney disease diagnosis. *Pregnancy Hypertens*. 2018;12:169-173.
3. Hirshberg A, Srinivas SK. Epidemiology of maternal morbidity and mortality. *Semin Perinatol*. 2017;41(6):332-337.
4. Zhao H, Kalish F, Schulz S, Yang Y, Wong RJ, Stevenson DK. Unique roles of infiltrating myeloid cells in the murine uterus during early to midpregnancy. *J Immunol*. 2015;194(8):3713-3722.
5. Male V. Medawar and the immunological paradox of pregnancy: in context. *Oxford Open Immunol*. 2020;2(1):iqaa006.
6. Moffett A, Colucci F. Uterine NK cells: active regulators at the maternal-fetal interface. *J Clin Invest*. 2014;124(5):1872-1879.
7. Girardi G. Complement activation, a threat to pregnancy. *Semin Immunopathol*. 2018;40(1):103-111.
8. Mellor AL, Chandler P, Lee GK, et al. Indoleamine 2,3-dioxygenase, immunosuppression and pregnancy. *J Reprod Immunol*. 2002;57(1–2):143-150.
9. Borchers AT, Naguwa SM, Keen CL, Gershwin ME. The implications of autoimmunity and pregnancy. *J Autoimmun*. 2010;34(3):J287-J299.
10. Turbeville HR, Sasser JM. Preeclampsia beyond pregnancy: long-term consequences for mother and child. *Am J Physiol Renal Physiol*. 2020;318(6):F1315-F1326.
11. Anderson DJ, Abbott AF, Jack RM. The role of complement component C3b and its receptors in sperm-oocyte interaction. *Proc Natl Acad Sci USA*. 1993;90(21):10051-10055.
12. Cervoni F, Oglesby TJ, Adams EM, et al. Identification and characterization of membrane cofactor protein of human spermatozoa. *J Immunol*. 1992;148(5):1431-1437.
13. Riley RC, Kemper C, Leung M, et al. Characterization of human membrane cofactor protein (MCP; CD46) on spermatozoa. *Mol Reprod Dev*. 2002;62(4):534-546.
14. Riley-Vargas RC, Lanzendorf S, Atkinson JP. Targeted and restricted complement activation on acrosome-reacted spermatozoa. *J Clin Invest*. 2005;115(5):1241-1249.
15. Girardi G, Lingo JJ, Fleming SD, Regal JF. Essential role of complement in pregnancy: from implantation to parturition and beyond. *Front Immunol*. 2020;11:1681.
16. Reichhardt MP, Lundin K, Lokki AI, et al. Complement in human pre-implantation embryos: attack and defense. *Front Immunol*. 2019;10:2234.
17. Li SH, Huang HL, Chen YH. Ovarian steroid-regulated synthesis and secretion of complement C3 and factor B in mouse endometrium during the natural estrous cycle and pregnancy period. *Biol Reprod*. 2002;66(2):322-332.
18. Brown EO, Sundstrom SA, Komm BS, Yi Z, Teuscher C, Richard Lyttle C. Progesterone regulation of estradiol-induced rat uterine secretory protein, complement C3. *Biol Reprod*. 1990;42(4):713-719.
19. Hasty LA, Lambris JD, Lessey BA, Pruksananonda K, Lyttle CR. Hormonal regulation of complement components and receptors throughout the menstrual cycle. *Am J Obstet Gynecol*. 1994;170(Pt 1):168-175.
20. Tse PK, Lee YL, Chow WN, Luk JMC, Lee KF, Yeung WSB. Preimplantation embryos cooperate with oviductal cells to produce embryotrophic inactivated complement-3b. *Endocrinology*. 2008;149(3):1268-1276.
21. Lee YL, Lee KF, Xu JS, et al. The embryotrophic activity of oviductal cell-derived complement C3b and iC3b, a novel function of complement protein in reproduction. *J Biol Chem*. 2004;279(13):12763-12768.
22. Chow WN, Lee YL, Wong PC, Chung MK, Lee KF, Yeung WSB. Complement 3 deficiency impairs early pregnancy in mice. *Mol Reprod Dev*. 2009;76(7):647-655.
23. Dunn CL, Kelly RW, Critchley HO. Decidualization of the human endometrial stromal cell: an enigmatic transformation. *Reprod Biomed Online*. 2003;7(2):151-161.
24. Ramathal CY, Bagchi IC, Taylor RN, Bagchi M. Endometrial decidualization: of mice and men. *Semin Reprod Med*. 2010;28(1):17-26.
25. Sherwin JR, Sharkey AM, Cameo P, et al. Identification of novel genes regulated by chorionic gonadotropin in baboon endometrium during the window of implantation. *Endocrinology*. 2007;148(2):618-626.
26. Palomino WA, Argandona F, Azua R, et al. Complement C3 and decay-accelerating factor expression levels are modulated by human chorionic gonadotropin in endometrial compartments during the implantation window. *Reprod Sci*. 2013;20(9):1103-1110.
27. Bulla R, Agostinis C, Bossi F, et al. Decidual endothelial cells express surface-bound C1q as a molecular bridge between endovascular trophoblast and decidual endothelium. *Mol Immunol*. 2008;45(9):2629-2640.
28. Agostinis C, Bulla R, Tripodo C, et al. An alternative role of C1q in cell migration and tissue remodeling: contribution to trophoblast invasion and placental development. *J Immunol*. 2010;185(7):4420-4429.
29. Johansson M, Bromfield JJ, Jasper MJ, Robertson SA. Semen activates the female immune response during early pregnancy in mice. *Immunology*. 2004;112(2):290-300.

30. Lyall F. Priming and remodelling of human placental bed spiral arteries during pregnancy—a review. *Placenta*. 2005;26(suppl A):S31-S36.

31. Fuchs R, Ellinger I. Endocytic and transcytotic processes in villous syncytiotrophoblast: role in nutrient transport to the human fetus. *Traffic*. 2004;5(10):725-738.

32. Tsujimura A, Shida K, Kitamura M, et al. Molecular cloning of a murine homologue of membrane cofactor protein (CD46): preferential expression in testicular germ cells. *Biochem J*. 1998;330(Pt 1):163-168.

33. Molina H. The murine complement regulator Crry: new insights into the immunobiology of complement regulation. *Cell Mol Life Sci*. 2002;59(2):220-229.

34. Kim YU, Kinoshita T, Molina H, et al. Mouse complement regulatory protein Crry/p65 uses the specific mechanisms of both human decay-accelerating factor and membrane cofactor protein. *J Exp Med*. 1995;181(1):151-159.

35. Xu C, Mao D, Holers VM, Palanca B, Cheng AM, Molina H. A critical role for murine complement regulator crry in fetomaternal tolerance. *Science*. 2000;287(5452):498-501.

36. Mao DL, Wu XB, Deppong C, et al. Negligible role of antibodies and C5 in pregnancy loss associated exclusively with C3-dependent mechanisms through complement alternative pathway. *Immunity*. 2003;19(6):813-822.

37. Abeln M, Albers I, Peters-Bernard U, et al. Sialic acid is a critical fetal defense against maternal complement attack. *J Clin Investig*. 2019;129(1):422-436.

38. Mockl L. The emerging role of the mammalian glycocalyx in functional membrane organization and immune system regulation. *Front Cell Dev Biol*. 2020;8:253.

39. Bull C, den Brok MH, Adema GJ. Sweet escape: sialic acids in tumor immune evasion. *Biochim Biophys Acta*. 2014;1846(1):238-246.

40. Blaum BS, Hannan JP, Herbert AP, Kavanagh D, Uhrín D, Stehle T. Structural basis for sialic acid-mediated self-recognition by complement factor H. *Nat Chem Biol*. 2015;11(1):77-82.

41. Richards A, Buddles MR, Donne RL, et al. Factor H mutations in hemolytic uremic syndrome cluster in exons 18-20, a domain important for host cell recognition. *Am J Hum Genet*. 2001;68(2):485-490.

42. Winn VD, Gormley M, Paquet AC, et al. Severe preeclampsia-related changes in gene expression at the maternal-fetal interface include sialic acid-binding immunoglobulin-like lectin-6 and papp-alysin-2. *Endocrinology*. 2009;150(1):452-462.

43. Tsai S, Hardison NE, James AH, et al. Transcriptional profiling of human placentas from pregnancies complicated by preeclampsia reveals disregulation of sialic acid acetylesterase and immune signalling pathways. *Placenta*. 2011;32(2):175-182.

44. Sinha D, Wells M, Faulk WP. Immunological studies of human placentae: complement components in pre-eclamptic chorionic villi. *Clin Exp Immunol*. 1984;56(1):175-184.

45. Girardi G, Bulla R, Salmon JE, Tedesco F. The complement system in the pathophysiology of pregnancy. *Mol Immunol*. 2006;43(1–2):68-77.

46. Bulla R, Bossi F, Agostinis C, et al. Complement production by trophoblast cells at the feto-maternal interface. *J Reprod Immunol*. 2009;82(2):119-125.

47. Tedder RS, Nelson M, Eisen V. Effects on serum complement of normal and pre-eclamptic pregnancy and of oral contraceptives. *Br J Exp Pathol*. 1975;56(5):389-395.

48. Richani K, Soto E, Romero R, et al. Normal pregnancy is characterized by systemic activation of the complement system. *J Matern Fetal Neonatal Med*. 2005;17(4):239-245.

49. Derzsy Z, Prohaszka Z, Rigo J Jr, et al. Activation of the complement system in normal pregnancy and preeclampsia. *Mol Immunol*. 2010;47(7–8):1500-1506.

50. He YD, Xu BN, Song D, et al. Normal range of complement components during pregnancy: a prospective study. *Am J Reprod Immunol*. 2020;83(2):e13202.

51. Alashkar F, Saner FH, Vance C, et al. Pregnancy in classical paroxysmal nocturnal hemoglobinuria and aplastic anemia-paroxysmal nocturnal hemoglobinuria: a high-risk constellation. *Front Med (Lausanne)*. 2020;7:543372.

52. Brocklebank V, Wood KM, Kavanagh D. Thrombotic microangiopathy and the kidney. *Clin J Am Soc Nephro*. 2018;13(2):300-317.

53. Kavanagh D, Goodship TH, Richards A. Atypical hemolytic uremic syndrome. *Semin Nephrol*. 2013;33(6):508-530.

54. Esparza-Gordillo J, de Jorge EG, Garrido CA, et al. Insights into hemolytic uremic syndrome: segregation of three independent predisposition factors in a large, multiple affected pedigree. *Mol Immunol*. 2006;43(11):1769-1775.

55. Moore I, Strain L, Pappworth I, et al. Association of factor H autoantibodies with deletions of CFHR1, CFHR3, CFHR4, and with mutations in CFH, CFI, CD46, and C3 in patients with atypical hemolytic uremic syndrome. *Blood*. 2010;115(2):379-387.

56. Legendre CM, Licht C, Muus P, et al. Terminal complement inhibitor eculizumab in atypical hemolytic-uremic syndrome. *N Engl J Med*. 2013;368(23):2169-2181.

57. Bruel A, Kavanagh D, Noris M, et al. Hemolytic uremic syndrome in pregnancy and postpartum. *Clin J Am Soc Nephrol*. 2017;12(8):1237-1247.

58. Fakhouri F, Scully M, Ardissino G, al-Dakkak I, Miller B, Rondeau E. Pregnancy-triggered atypical hemolytic uremic syndrome (aHUS): a global aHUS registry analysis. *J Nephrol*. 2021;34(5):1581-1590.

59. Huerta A, Arjona E, Portoles J, et al. A retrospective study of pregnancy-associated atypical hemolytic uremic syndrome. *Kidney Int*. 2018;93(2):450-459.

60. Fremeaux-Bacchi V, Fakhouri F, Garnier A, et al. Genetics and outcome of atypical hemolytic uremic syndrome: a nationwide French series comparing children and adults. *Clin J Am Soc Nephrol*. 2013;8(4):554-562.

61. Kavanagh D, Richards A, Atkinson J. Complement regulatory genes and hemolytic uremic syndromes. *Annu Rev Med*. 2008;59:293-309.

62. Fakhouri F, Scully M, Provot F, et al. Management of thrombotic microangiopathy in pregnancy and postpartum: report from an international working group. *Blood*. 2020;136(19):2103-2117.

63. Glover AV, Manuck TA. Screening for spontaneous preterm birth and resultant therapies to reduce neonatal morbidity and mortality: a review. *Semin Fetal Neonatal Med*. 2018;23(2):126-132.

64. Watkins WJ, Kotecha SJ, Kotecha S. All-cause mortality of low birthweight infants in infancy, childhood, and adolescence: population study of England and Wales. *PLoS Med*. 2016;13(5):e1002018.

65. Markopoulou P, Papanikolaou E, Analytis A, et al. Preterm birth as a risk factor for metabolic syndrome and cardiovascular disease in adult life: a systematic review and meta-analysis. *J Pediatr*. 2019;210:69-80.e5.

66. Gonzalez JM, Franzke CW, Yang F, Romero R, Girardi G. Complement activation triggers metalloproteinases release inducing cervical remodeling and preterm birth in mice. *Am J Pathol*. 2011;179(2):838-849.

67. Denison FC, Riley SC, Elliott CL, Kelly RW, Calder AA, Critchley HO. The effect of mifepristone administration on leukocyte populations, matrix metalloproteinases and inflammatory mediators in the first trimester cervix. *Mol Hum Reprod*. 2000;6(6):541-548.

68. Chan D, Bennett PR, Lee YS, et al. Microbial-driven preterm labour involves crosstalk between the innate and adaptive immune response. *Nat Commun*. 2022;13(1):975.

69. Elimian A, Figueroa R, Canterino J, Verma U, Aguero-Rosenfeld M, Tejani N. Amniotic fluid complement C3 as a marker of intra-amniotic infection. *Obstet Gynecol*. 1998;92(1):72-76.

70. Soto E, Romero R, Richani K, et al. Anaphylatoxins in preterm and term labor. *J Perinat Med*. 2005;33(4):306-313.

71. Soto E, Romero R, Richani K, et al. Evidence for complement activation in the amniotic fluid of women with spontaneous preterm labor and intra-amniotic infection. *J Matern Fetal Neonatal Med*. 2009;22(11):983-992.

72. Vaisbuch E, Romero R, Erez O, et al. Fragment Bb in amniotic fluid: evidence for complement activation by the alternative pathway in women with intra-amniotic infection/inflammation. *J Matern Fetal Neonatal Med*. 2009;22(10):905-916.

73. Lynch AM, Gibbs RS, Murphy JR, et al. Complement activation fragment bb in early pregnancy and spontaneous preterm birth. *Am J Obstet Gynecol*. 2008;199(4):354.e1-8.

74. Norman JE, OPPTIMUM co-authors. Vaginal progesterone prophylaxis for preterm birth—author's reply. *Lancet*. 2016;388(10050):1160.

75. Meis PJ, Klebanoff M, Thom E, et al. Prevention of recurrent preterm delivery by 17 alpha-hydroxyprogesterone caproate. *N Engl J Med*. 2003;348(24):2379-2385.

76. da Fonseca EB, Bittar RE, Carvalho MH, et al. Prophylactic administration of progesterone by vaginal suppository to reduce the incidence of spontaneous preterm birth in women at increased risk: a randomized placebo-controlled double-blind study. *Am J Obstet Gynecol*. 2003;188(2):419-424.

77. Hassan SS, Romero R, Vidyadhari D, et al. Vaginal progesterone reduces the rate of preterm birth in women with a sonographic short cervix: a multicenter, randomized, double-blind, placebo-controlled trial. *Ultrasound Obstet Gynecol*. 2011;38(1):18-31.

78. Dodd JM, Jones L, Flenady V, Cincotta R, Crowther CA, Cochrane Pregnancy and Childbirth Group. Prenatal administration of progesterone for preventing preterm birth in women considered to be at risk of preterm birth. *Cochrane Database Syst Rev*. 2013;7:CD004947.

79. Blackwell SC, Gyamfi-Bannerman C, Biggio JR Jr, et al. 17-OHPC to prevent recurrent preterm birth in singleton gestations (PROLONG study): a multicenter, international, randomized double-blind trial. *Am J Perinatol*. 2020;37(2):127-136.

80. EPPPIC Group. Evaluating progestogens for preventing preterm birth international collaborative (EPPPIC): meta-analysis of individual participant data from randomised controlled trials. *Lancet*. 2021;397(10280):1183-1194.

81. Ghulmiyyah L, Sibai B. Maternal mortality from preeclampsia/eclampsia. *Semin Perinatol*. 2012;36(1):56-59.

82. Rana S, Lemoine E, Granger J, et al. Preeclampsia pathophysiology, challenges, and perspectives. *Circ Res*. 2019;124(7):1094-1112.

83. Lynch AM, Salmon JE. Dysregulated complement activation as a common pathway of injury in preeclampsia and other pregnancy complications. *Placenta*. 2010;31(7):561-567.

84. Olson KN, Redman LM, Sones JL. Obesity "complements" preeclampsia. *Physiol Genomics*. 2019;51(3):73-76.

85. Sones JL, Merriam AA, Seffens A, et al. Angiogenic factor imbalance precedes complement deposition in placentae of the BPH/5 model of preeclampsia. *FASEB J*. 2018;32(5):2574-2586.

86. Gelber SE, Brent E, Redecha P, et al. Prevention of defective placentation and pregnancy loss by blocking innate immune pathways in a syngeneic model of placental insufficiency. *J Immunol*. 2015;195(3):1129-1138.

87. Davisson RL, Hoffmann DS, Butz GM, et al. Discovery of a spontaneous genetic mouse model of preeclampsia. *Hypertension*. 2002;39(Pt 2):337-342.

88. Lillegard KE, Johnson AC, Lojovich SJ, et al. Complement activation is critical for placental ischemia-induced hypertension in the rat. *Mol Immunol*. 2013;56(1–2):91-97.

89. Lillegard KE, Loeks-Johnson AC, Opacich JW, et al. Differential effects of complement activation products c3a and c5a on cardiovascular function in hypertensive pregnant rats. *J Pharmacol Exp Ther*. 2014;351(2):344-351.

90. Qing X, Redecha PB, Burmeister MA, et al. Targeted inhibition of complement activation prevents features of preeclampsia in mice. *Kidney Int*. 2011;79(3):331-339.

91. Girardi G, Yarilin D, Thurman JM, Holers VM, Salmon JE. Complement activation induces dysregulation of angiogenic factors and causes fetal rejection and growth restriction. *J Exp Med*. 2006;203(9):2165-2175.

92. Wang W, Irani RA, Zhang Y, et al. Autoantibody-mediated complement C3a receptor activation contributes to the pathogenesis of preeclampsia. *Hypertension*. 2012;60(3):712-721.

93. Tedesco F, Radillo O, Candussi G, et al. Immunohistochemical detection of terminal complement complex and S protein in normal and pre-eclamptic placentae. *Clin Exp Immunol*. 1990;80(2):236-240.

94. Lokki AI, Heikkinen-Eloranta J, Jarva H, et al. Complement activation and regulation in preeclamptic placenta. *Front Immunol*. 2014;5:312.

95. Buurma A, Cohen D, Veraar K, et al. Preeclampsia is characterized by placental complement dysregulation. *Hypertension*. 2012;60(5):1332-1337.

96. Lim R, Lappas M. Decreased expression of complement 3a receptor (C3aR) in human placentas from severe preeclamptic pregnancies. *Eur J Obstet Gynecol Reprod Biol*. 2012;165(2):194-198.

97. Ma Y, Kong LR, Ge Q, et al. Complement 5a-mediated trophoblasts dysfunction is involved in the development of pre-eclampsia. *J Cell Mol Med*. 2018;22(2):1034-1046.

98. Ye Y, Kong Y, Zhang Y. Complement split products C3a/C5a and receptors: are they regulated by circulating angiotensin II type 1 receptor autoantibody in severe preeclampsia? *Gynecol Obstet Invest*. 2016;81(1):28-33.

99. Lynch AM, Murphy JR, Byers T, et al. Alternative complement pathway activation fragment bb in early pregnancy as a predictor of preeclampsia. *Am J Obstet Gynecol*. 2008;198(4):385.e1-9.

100. Lynch AM, Wagner BD, Giclas PC, West NA, Gibbs RS, Holers VM. The relationship of longitudinal levels of complement bb during pregnancy with preeclampsia. *Am J Reprod Immunol*. 2016;75(2):104-111.

101. Haeger M, Unander M, Norder-Hansson B, Tylman M, Bengtsson A. Complement, neutrophil, and macrophage activation in women with severe preeclampsia and the syndrome of hemolysis, elevated liver enzymes, and low platelet count. *Obstet Gynecol*. 1992;79(1):19-26.

102. Denny KJ, Coulthard LG, Finnell RH, et al. Elevated complement factor C5a in maternal and umbilical cord plasma in preeclampsia. *J Reprod Immunol*. 2013;97(2):211-216.

103. Haeger M, Unander M, Bengtsson A. Complement activation in relation to development of preeclampsia. *Obstet Gynecol*. 1991;78(1):46-49.

104. Soto E, Romero R, Richani K, et al. Preeclampsia and pregnancies with small-for-gestational age neonates have different profiles of complement split products. *J Matern Fetal Neonatal Med*. 2010;23(7):646-657.

105. Lynch AM, Murphy JR, Gibbs RS, et al. The interrelationship of complement-activation fragments and angiogenesis-related factors in early pregnancy and their association with pre-eclampsia. *BJOG*. 2010;117(4):456-462.

106. Guseh SH, Feinberg BB, Dawood HY, Yamamoto HS, Fichorova RN, Burwick RM. Urinary excretion of C5b-9 is associated with the anti-angiogenic state in severe preeclampsia. *Am J Reprod Immunol*. 2015;73(5):437-444.

107. Burwick RM, Fichorova RN, Dawood HY, Yamamoto HS, Feinberg BB. Urinary excretion of C5b-9 in severe preeclampsia: tipping the balance of complement activation in pregnancy. *Hypertension*. 2013;62(6):1040-1045.

108. Salmon JE, Heuser C, Triebwasser M, et al. Mutations in complement regulatory proteins predispose to preeclampsia: a genetic analysis of the PROMISSE cohort. *PLoS Med.* 2011;8(3):e1001013.

109. Warwicker P, Goodship THJ, Donne RL, et al. Genetic studies into inherited and sporadic hemolytic uremic syndrome. *Kidney Int.* 1998;53(4):836-844.

110. Ferreira VP, Herbert AP, Cortes C, et al. The binding of factor H to a complex of physiological polyanions and C3b on cells is impaired in atypical hemolytic uremic syndrome. *J Immunol.* 2009;182(11):7009-7018.

111. Atkinson JP, Liszewski MK, Richards A, et al. Hemolytic uremic syndrome: an example of insufficient complement regulation on self-tissue. *Ann N Y Acad Sci.* 2005;1056:144-152.

112. Lokki AI, Aalto-Viljakainen T, Meri S, Laivuori H, FINNPEC. Genetic analysis of membrane cofactor protein (CD46) of the complement system in women with and without preeclamptic pregnancies. *PLoS ONE.* 2015;10(2):e0117840.

113. Banadakoppa M, Balakrishnan M, Yallampalli C. Common variants of fetal and maternal complement genes in preeclampsia: pregnancy specific complotype. *Sci Rep.* 2020;10(1):4811.

114. Bokslag A, van Weissenbruch M, Mol BW, de Groot CJM. Preeclampsia; short and long-term consequences for mother and neonate. *Early Hum Dev.* 2016;102:47-50.

115. Hong K, Kim SH, Cha DH, Park HJ. Defective uteroplacental vascular remodeling in preeclampsia: key molecular factors leading to long term cardiovascular disease. *Int J Mol Sci.* 2021;22(20):11202.

116. Frid MG, Thurman JM, Hansen KC, Maron BA, Stenmark KR. Inflammation, immunity, and vascular remodeling in pulmonary hypertension; evidence for complement involvement? *Glob Cardiol Sci Pract.* 2020;2020(1):e202001.

117. Sartain SE, Turner NA, Moake JL. Brain microvascular endothelial cells exhibit lower activation of the alternative complement pathway than glomerular microvascular endothelial cells. *J Biol Chem.* 2018;293(19):7195-7208.

118. Hertle E, Arts IC, van der Kallen CJ, et al. The alternative complement pathway is longitudinally associated with adverse cardiovascular outcomes. The CODAM study. *Thromb Haemost.* 2016;115(2):446-457.

119. Schatz-Jakobsen JA, Zhang Y, Johnson K, Neill A, Sheridan D, Andersen GR. Structural basis for eculizumab-mediated inhibition of the complement terminal pathway. *J Immunol.* 2016;197(1):337-344.

120. Kelly RJ, Hochsmann B, Szer J, et al. Eculizumab in pregnant patients with paroxysmal nocturnal hemoglobinuria. *N Engl J Med.* 2015;373(11):1032-1039.

121. Hallstensen RF, Bergseth G, Foss S, et al. Eculizumab treatment during pregnancy does not affect the complement system activity of the newborn. *Immunobiology.* 2015;220(4):452-459.

122. Burwick RM, Feinberg BB. Eculizumab for the treatment of preeclampsia/HELLP syndrome. *Placenta.* 2013;34(2):201-203.

123. Elabd H, Elkholi M, Steinberg L, et al. Eculizumab, a novel potential treatment for acute kidney injury associated with preeclampsia/HELLP syndrome. *BMJ Case Rep.* 2019;12(9):e228709.

124. Rolnik DL, Wright D, Poon LC, et al. Aspirin versus placebo in pregnancies at high risk for preterm preeclampsia. *N Engl J Med.* 2017;377(7):613-622.

125. Ducat A, Vargas A, Doridot L, et al. Low-dose aspirin protective effects are correlated with deregulation of HNF factor expression in the preeclamptic placentas from mice and humans. *Cell Death Discov.* 2019;5:94.

126. Girardi G, Redecha P, Salmon JE. Heparin prevents antiphospholipid antibody-induced fetal loss by inhibiting complement activation. *Nat Med.* 2004;10(11):1222-1226.

127. McLaughlin K, Scholten RR, Parker JD, Ferrazzi E, Kingdom JCP. Low molecular weight heparin for the prevention of severe preeclampsia: where next? *Br J Clin Pharmacol.* 2018;84(4):673-678.

128. Lynch AM, Eckel RH, Murphy JR, et al. Prepregnancy obesity and complement system activation in early pregnancy and the subsequent development of preeclampsia. *Am J Obstet Gynecol.* 2012;206(5):428.e1-8.

129. Galazis N, Docheva N, Simillis C, Nicolaides KH. Maternal and neonatal outcomes in women undergoing bariatric surgery: a systematic review and meta-analysis. *Eur J Obstet Gynecol Reprod Biol.* 2014;181:45-53.

130. Yogev Y, Catalano PM. Pregnancy and obesity. *Obstet Gynecol Clin North Am.* 2009;36(2):285-300.

131. Vlaicu SI, Tatomir A, Boodhoo D, Vesa S, Mircea PA, Rus H. The role of complement system in adipose tissue-related inflammation. *Immunol Res.* 2016;64(3):653-664.

132. Pattrick M, Luckett J, Yue L, Stover C. Dual role of complement in adipose tissue. *Mol Immunol.* 2009;46(5):755-760.

133. White RT, Damm D, Hancock N, et al. Human adipsin is identical to complement factor-D and is expressed at high-levels in adipose-tissue. *J Biol Chem.* 1992;267(13):9210-9213.

134. Nydegger UE, Fearon DT, Austen KF. The modulation of the alternative pathway of complement in C2-deficient human serum by changes in concentration of the component and control proteins. *J Immunol.* 1978;120(4):1404-1408.

135. Zhang YZ, Keenan A, Dai DF, et al. C3(H$_2$O) prevents rescue of complement-mediated C3 glomerulopathy in Cfh(−/−) Cfd(−/−) mice. *JCI Insight.* 2020;5(9):e135758.

136. Sones JL, Yarborough CC, O'Besso V, Lemenze A, Douglas NC. Genotypic analysis of the female BPH/5 mouse, a model of superimposed preeclampsia. *PLoS ONE.* 2021;16(7):e0253453.

137. Mamane Y, Chung Chan C, Lavallee G, et al. The C3a anaphylatoxin receptor is a key mediator of insulin resistance and functions by modulating adipose tissue macrophage infiltration and activation. *Diabetes.* 2009;58(9):2006-2017.

138. Stuart TJ, O'Neill K, Condon D, et al. Diet-induced obesity alters the maternal metabolome and early placenta transcriptome and decreases placenta vascularity in the mouse. *Biol Reprod.* 2018;98(6):795-809.

139. Heyward CY, Sones JL, Lob HE, et al. The decidua of preeclamptic-like BPH/5 mice exhibits an exaggerated inflammatory response during early pregnancy. *J Reprod Immunol.* 2017;120:27-33.

140. Olson KN, Reijnders D, Gomes VCL, et al. Complement in reproductive white adipose tissue characterizes the obese preeclamptic-like BPH/5 mouse prior to and during pregnancy. *Biology (Basel).* 2020;9(9):304.

141. Correa N, Arbildi P, Rosano S, et al. Predictive value of blood measurement of complement system proteins and metabolic components for early detection of obstetric complications linked to poor placental function. *Placenta.* 2020;101:45-48.

142. Jarva H, Jokiranta TS, Hellwage J, et al. Regulation of complement activation by C-reactive protein: targeting the complement inhibitory activity of factor H by an interaction with short consensus repeat domains 7 and 8–11. *J Immunol.* 1999;163(7):3957-3962.

143. Plows JF, Stanley JL, Baker PN, Reynolds C, Vickers M. The pathophysiology of gestational diabetes mellitus. *Int J Mol Sci.* 2018;19(11):3342.

144. Moreno-Navarrete JM, Martinez-Barricarte R, Catalan V, et al. Complement factor H is expressed in adipose tissue in association with insulin resistance. *Diabetes.* 2010;59(1):200-209.

145. Somani R, Richardson VR, Standeven KF, Grant PJ, Carter AM. Elevated properdin and enhanced complement activation in first-degree relatives of south Asian subjects with type 2 diabetes. *Diabetes Care.* 2012;35(4):894-899.

146. Fujita T, Hemmi S, Kajiwara M, et al. Complement-mediated chronic inflammation is associated with diabetic microvascular complication. *Diabetes Metab Res Rev.* 2013;29(3):220-226.

147. Coan PM, Barrier M, Alfazema N, et al. Complement factor B is a determinant of both metabolic and cardiovascular features of metabolic syndrome. *Hypertension.* 2017;70:624-633.

148. Shen Y, Li J, Tian H, et al. High level of complement factor Ba within first prenatal test of gestation increases the risk of subsequent gestational diabetes: a propensity score-matched study. *Gynecol Endocrinol.* 2022;38(2):158-163.

149. Li J, Shen Y, Tian H, et al. The role of complement factor H in gestational diabetes mellitus and pregnancy. *BMC Pregnancy Childbirth.* 2021;21(1):562.

150. Kennelly MA, Killeen SL, Phillips CM, et al. Maternal C3 complement and C-reactive protein and pregnancy and fetal outcomes: a secondary analysis of the PEARS RCT-an mHealth-supported, lifestyle intervention among pregnant women with overweight and obesity. *Cytokine.* 2022;149:155748.

151. Ma D, Luque-Fernandez MA, Bogdanet D, et al. Plasma glycated CD59 predicts early gestational diabetes and large for gestational age newborns. *J Clin Endocrinol Metab.* 2020;105(4):e1033-e1040.

152. Bogdanet D, O'Shea PM, Halperin J, Dunne F. Plasma glycated CD59 (gCD59), a novel biomarker for the diagnosis, management and follow up of women with gestational diabetes (GDM)—protocol for prospective cohort study. *BMC Pregnancy Childbirth.* 2020;20(1):412.

153. Chighizola CB, Lonati PA, Trespidi L, Meroni PL, Tedesco F. The complement system in the pathophysiology of pregnancy and in systemic autoimmune rheumatic diseases during pregnancy. *Front Immunol.* 2020;11:2084.

154. Skorpen CG, Lydersen S, Gilboe IM, et al. Influence of disease activity and medications on offspring birth weight, pre-eclampsia and preterm birth in systemic lupus erythematosus: a population-based study. *Ann Rheum Dis.* 2018;77(2):264-269.

155. Mehta B, Luo Y, Xu J, et al. Trends in maternal and fetal outcomes among pregnant women with systemic lupus erythematosus in the United States: a cross-sectional analysis. *Ann Intern Med.* 2019;171(3):164-171.

156. Smyth A, Oliveira GH, Lahr BD, et al. A systematic review and meta-analysis of pregnancy outcomes in patients with systemic lupus erythematosus and lupus nephritis. *Clin J Am Soc Nephrol.* 2010;5(11):2060-2068.

157. Barnett AH, Mijovic C, Fletcher J, et al. Low plasma C4 concentrations: association with microangiopathy in insulin dependent diabetes. *Br Med J (Clin Res Ed).* 1984;289(6450):943-945.

158. Kim MY, Guerra MM, Kaplowitz E, et al. Complement activation predicts adverse pregnancy outcome in patients with systemic lupus erythematosus and/or antiphospholipid antibodies. *Ann Rheum Dis.* 2018;77(4):549-555.

159. Matrai CE, Rand JH, Baergen RN. Absence of distinct Immunohistochemical distribution of annexin A5, C3b, C4d, and C5b-9 in placentas from patients with antiphospholipid antibodies, preeclampsia, and systemic lupus erythematosus. *Pediatr Dev Pathol.* 2019;22(5):431-439.

160. Yelnik CM, Laskin CA, Porter TF, et al. Lupus anticoagulant is the main predictor of adverse pregnancy outcomes in aPL-positive patients: validation of PROMISSE study results. *Lupus Sci Med.* 2016;3(1):e000131.

161. Mankee A, Petri M, Magder LS. Lupus anticoagulant, disease activity and low complement in the first trimester are predictive of pregnancy loss. *Lupus Sci Med.* 2015;2(1):e000095.

162. Lockshin MD, Kim M, Laskin CA, et al. Prediction of adverse pregnancy outcome by the presence of lupus anticoagulant, but not anticardiolipin antibody, in patients with antiphospholipid antibodies. *Arthritis Rheum.* 2012;64(7):2311-2318.

163. Tektonidou MG, Andreoli L, Limper M, et al. EULAR recommendations for the management of antiphospholipid syndrome in adults. *Ann Rheum Dis.* 2019;78(10):1296-1304.

164. Alijotas-Reig J, Esteve-Valverde E, Ferrer-Oliveras R, et al. The European Registry on Obstetric Antiphospholipid Syndrome (EUROAPS): a survey of 1000 consecutive cases. *Autoimmun Rev.* 2019;18(4):406-414.

165. Bertolaccini ML, Contento G, Lennen R, et al. Complement inhibition by hydroxychloroquine prevents placental and fetal brain abnormalities in antiphospholipid syndrome. *J Autoimmun.* 2016;75:30-38.

166. Branch DW, Dudley DJ, Mitchell MD, et al. Immunoglobulin G fractions from patients with antiphospholipid antibodies cause fetal death in BALB/c mice: a model for autoimmune fetal loss. *Am J Obstet Gynecol.* 1990;163(Pt 1):210-216.

167. Holers VM, Girardi G, Mo L, et al. Complement C3 activation is required for antiphospholipid antibody-induced fetal loss. *J Exp Med.* 2002;195(2):211-220.

168. Girardi G, Berman J, Redecha P, et al. Complement C5a receptors and neutrophils mediate fetal injury in the antiphospholipid syndrome. *J Clin Invest.* 2003;112(11):1644-1654.

169. Thurman JM, Kraus DM, Girardi G, et al. A novel inhibitor of the alternative complement pathway prevents antiphospholipid antibody-induced pregnancy loss in mice. *Mol Immunol.* 2005;42(1):87-97.

170. Redecha P, Tilley R, Tencati M, et al. Tissue factor: a link between C5a and neutrophil activation in antiphospholipid antibody induced fetal injury. *Blood.* 2007;110(7):2423-2431.

171. Shamonki JM, Salmon JE, Hyjek E, et al. Excessive complement activation is associated with placental injury in patients with antiphospholipid antibodies. *Am J Obstet Gynecol.* 2007;196(2):167.e1-5.

172. Tedesco F, Borghi MO, Gerosa M, et al. Pathogenic role of complement in antiphospholipid syndrome and therapeutic implications. *Front Immunol.* 2018;9:1388.

173. De Carolis S, Botta A, Santucci S, et al. Predictors of pregnancy outcome in antiphospholipid syndrome: a review. *Clin Rev Allerg Immu.* 2010;38(2–3):116-124.

174. Ruffatti A, Tonello M, Visentin MS, et al. Risk factors for pregnancy failure in patients with anti-phospholipid syndrome treated with conventional therapies: a multicentre, case-control study. *Rheumatology (Oxford).* 2011;50(9):1684-1689.

175. De Carolis S, Botta A, Santucci S, et al. Complementemia and obstetric outcome in pregnancy with antiphospholipid syndrome. *Lupus.* 2012;21(7):776-778.

176. Deguchi M, Yamada H, Sugiura-Ogasawara M, et al. Factors associated with adverse pregnancy outcomes in women with antiphospholipid syndrome: a multicenter study. *J Reprod Immunol.* 2017;122:21-27.

177. Reggia R, Ziglioli T, Andreoli L, et al. Primary anti-phospholipid syndrome: any role for serum complement levels in predicting pregnancy complications? *Rheumatology (Oxford).* 2012;51(12):2186-2190.

178. Tabacco S, Giannini A, Garufi C, et al. Complementemia in pregnancies with antiphospholipid syndrome. *Lupus.* 2019;28(13):1503-1509.

179. Zadura AF, Memon AA, Stojanovich L, et al. Factor H autoantibodies in patients with antiphospholipid syndrome and thrombosis. *J Rheumatol.* 2015;42(10):1786-1793.

180. Nakamura H, Oku K, Ogata Y, et al. Alternative pathway activation due to low level of complement factor H in primary antiphospholipid syndrome. *Thromb Res.* 2018;164:63-68.

181. Rovere-Querini P, Canti V, Erra R, et al. Eculizumab in a pregnant patient with laboratory onset of catastrophic antiphospholipid syndrome: a case report. *Medicine (Baltimore).* 2018;97(40):e12584.

182. Barratt-Due A, Floisand Y, Orrem HL, et al. Complement activation is a crucial pathogenic factor in catastrophic antiphospholipid syndrome. *Rheumatology.* 2016;55(7):1337-1340.

183. Gustavsen A, Skattum L, Bergseth G, et al. Effect on mother and child of eculizumab given before caesarean section in a patient with severe antiphospholipid syndrome: a case report. *Medicine (Baltimore).* 2017;96(11):e6338.